ulm university universität
uulm

Theory of the Free-Electron Laser: From Classical to Quantum

Dissertation
zur Erlangung des Doktorgrades
Dr. rer. nat.
der Fakultät für Naturwissenschaften
der Universität Ulm

Vorgelegt von:
Peter Kling
aus
Günzburg

2017

Dekan:	Prof. Dr. Peter Dürre
Erstgutachter:	Prof. Dr. Wolfgang P. Schleich
Zweitgutachter:	Prof. Dr. Peter Reineker
Tag der Promotion:	15.11.2017

Zusammenfassung

Alle bisherigen Realisierungen eines Freie-Elektronen-Lasers (FELs) können allein durch klassische Physik beschrieben werden. In dieser Arbeit hingegen befassen wir uns mit einem Parameterbereich, in dem Quanteneffekte wichtig werden. Wenn der diskrete Rückstoß, den ein Elektron durch die Streuung an den Feldern erfährt, die bestimmende Größe der Dynamik darstellt, sprechen wir vom 'Quanten Regime' oder von einem 'Quanten FEL'. In diesem Grenzfall besetzen die Elektronen nur zwei resonante Impulszustände.
Ziel dieser Arbeit ist es dabei, sowohl den Übergangsbereich zwischen klassischer Physik und Quantenmechanik im FEL zu beleuchten, als auch bisherige Modelle für den extremen Quantenbereich zu erweitern und dessen Eigenschaften mit denen des klassischen Grenzfalls zu vergleichen.
Neben einem hohen Rückstoß benötigen wir eine sehr schmale Impulsverteilung der Elektronen, um Quanteneffekte im FEL beobachten zu können. Um diese Aussagen zu beweisen, verwenden wir zwei verschiedene Ansätze: Im Heisenberg Bild wird deutlich, dass die diskrete Dynamik der Elektronen ihre Ursache in den nichtvertauschenden Orts- und Impulsoperatoren hat, während der Ansatz im Phasenraum mit Hilfe der Wignerfunktion am besten dazu geeignet ist, den Einfluss der Impulsbreite zu untersuchen.
Um die Resultate für die statistischen Eigenschaften des ausgesandten Lichts eines Quanten FELs besser einordnen zu können, müssen wir erst die entsprechenden Merkmale eines klassischen FEls kennen und dafür ein Modell entwickeln, in dem sowohl die Elektronen als auch das Lichtfeld quantisiert sind. Durch Verwendung der Wignerfunktion und Vernachlässigung des Rückstoßes leiten wir eine Fokker–Planck–Gleichung her, die sowohl den Drift als auch die Diffusion der Laseramplitude beschreibt. Damit sind wir in der Lage, Ausdrücke für die Photonenstatistik im stationären Zustand sowie für die intrinsische Linienbreite eines klassischen FELs herzuleiten, die im Einklang mit bestehender Literatur stehen.
Erhöhen wir nun den Rückstoß, erreichen wir schließlich das Quanten Regime des FELs, in dem die Dynamik der Elektronen durch ein Zwei-Niveau-Verhalten charakterisiert wird. Wir beweisen dieses Verhalten durch asymptotisches Lösen der Schrödingergleichung, wobei wir, die vom Rückstoß verursachten, schnellen Oszillationen vernachlässigen. Unsere Methode gibt uns dabei die Möglichkeit, die zu Grunde liegenden Prozesse zu erkennen und erbringt den Beweis, dass Mehr-Photonen-Prozesse sowie nicht-resonante Übergänge im Quanten FEL unterdrückt sind.
Um die Strahlungseigenschaften des Quanten FELs zu berechnen, benutzen wir die Fock-Darstellung der reduzierten Dichtematrix für das Laserfeld und machen von Standardmethoden aus der Lasertheorie Gebrauch. Wir finden unter anderem, dass die Photonenstatistik im Quanten Regime schmäler ist als im klassichen Bereich und somit der Poisson-Verteilung eines kohärenten Zustandes näher kommt.
Die wichtigste Leistung dieser Arbeit besteht jedoch darin, das bisherige Einzel-Elektron-Modell auf die kollektive Wechselwirkung von vielen Elektronen mit dem Laserfeld zu

verallgemeinern. Trotz experimenteller Schwierigkeiten, hinsichtlich der Impulsverteilung des Elektronenstrahls und der benötigten Länge des Undulators, zeigen wir damit die Möglichkeit auf, einen Quanten FEL in einem Parameterbereich zu betreiben, in dem ein einzelner Durchgang von Elektronen ausreicht um eine hohe Verstärkung spontan emittierter Strahlung zu erreichen. Dies ist vor allem dann wichtig, wenn wir uns in einem Bereich des Spektrums, zum Beispiel dem Röntgenbereich, befinden, in dem keine hochwertigen Resonatoren zur Verfügung stehen, um die Strahlung über mehrere Durchgänge von Elektronen zu speichern. Wir finden für diesen Parameterbereich ein exponentielles Wachstum der Laserintensität, das jedoch sättigt, wenn jedes Elektron maximal ein Photon ausgesandt hat im Gegensatz zu den Mehr-Photonen Prozessen im klassischen FEL.

Contents

List of Figures

1 Introduction

Since the advent of quantum mechanics in the early 20th century there is an ongoing quest to observe quantum effects in experiments. This search was successful for several kinds of physical systems: atomic physics, solid state physics, or the interaction between matter waves and light, to name only a few of them.
In the field of free-electron lasers (FELs), however, classical physics is sufficient to explain all important mechanisms of an experiment. Hence, the FEL is broadely viewed as the prime example of a classical laser [1]. On the other hand, since quantum mechanics is the more fundamental theory we expect that the range of parameters accessible to current experiments is just one extreme limit. By going to a different regime we, indeed, should observe quantum effects. The realization of this 'quantum regime' or 'Quantum FEL' [2, 3, 4] would lead to the very remarkable situation that an FEL as *huge* facility consisting of a large accelerator and a long undulator displays properties inherent to the *microscopic* world described by quantum physics.
In this thesis we theoretically study the transition from the classical to the quantum regime of an FEL. In short, we enter the quantum regime when the quantum mechanical recoil, which the electron experiences during interaction, dominates the dynamics leading to a discrete momentum ladder in contrast to the continuous trajectories in the classical regime. In the extreme quantum limit the electron even occupies just *two* resonant momentum levels. This reduction to only a few discrete levels quite naturally establishes the connection of the Quantum FEL to an atomic laser.

1.1 Historical overview

In order to put this thesis into a broader context we briefly review in the following the history of FEL theory with a particular emphasis on the quantum regime and quantum mechanical models. Before it was discovered that the FEL can be described as a classical device its properties were primarily derived by means of quantum electrodynamics [5] by John M. J. Madey in 1971 who was inspired by stimulated inverse Compton scattering in astrophysics [6]. However, in the course of Madey's calculations the Planck constant $\hbar$ dropped out of the equations and one was left with completely classical expressions. The resulting confusion whether the FEL is classical or quantum was resolved when in 1976 the first models, which solely relied on classical physics, explained the gain mechanism of the FEL. While the approach of Hopf *et al.* [7] was based on a distribution function for the electrons in phase space, William Colson [8] considered the motion of each electron for which he derived the famous FEL pendulum equation.
Nevertheless, quantum mechanics did not completely vanish from FEL theory. The quantum mechanical models of the FEL [9, 10, 11] established in the 1980s investigated the emergence of the *classical limit* of the FEL from a *quantum point of view*. Moreover, by quantizing the electron motion as well as the laser field, genuine quantum mechanical properties of the light

field like the photon statistics [12, 13] or the intrinsic linewidth [14, 15, 16] were derived. In addition, the existence of a quantum regime was appreciated [9, 17, 18] which was, however, far beyond the experimental possibilities at that time.
Parallel to the emergence of quantum models for the FEL there was a development in FEL theory which had a larger effect on the experimental situation: the high-gain theory [19, 20, 21]. While earlier models considered the effective interaction of a *single electron* with the laser mode in analogy to standard laser theory [22], the high-gain theory treated the collective interaction of *many* electrons with the laser field. Due to the small intensity change in the single-electron model one had to use a resonator to store the field in *many passages* of electron bunches. In contrast, the many-electron approach leads to an exponential growth of the laser intensity in a *single passage* of electrons through a very long undulator. Hence, it became possible to operate an FEL in parts of the spectrum, where no high-quality mirrors are available. More than 20 years after its appearance the high-gain theory thus has led to the first lasing of an X-ray FEL [23, 24].
With a decrease of wavelength the quantum mechanical recoil, which is proportional to the product of $\hbar$ and of the wave number, increases. Hence, the successful construction of X-ray FELs made the quantum regime more feasible in experiments. Therefore, in the beginning of the new millenium novel theoretical approaches [2, 3, 25] towards a Quantum FEL were developed. These models considered the high-gain regime and predicted enhanced properties of the emitted radiation when compared to its classical counterpart [25].
In Ref. [25], for example, first the full set of the dynamical equations for the FEL was solved before the quantum and the classical regime were identified as two extreme limits. On the other hand, in our approach in Refs. [4, 26, 27, 28, 29, 30, 31], which is the starting point of the present thesis, we have first considered directly a limit in the equations of motion, where only two levels of the momentum ladder are occupied, which is our definition of a Quantum FEL [4]. Then, we have solved the simplified set of equations. By this procedure, we have established the connection to the Jaynes-Cummings model [32] which describes the interaction of a two-level atom with a quantized field mode.

1.2 Goals & results

In the present thesis we do not just follow the goal to refine and to extend the theory of the quantum regime of the FEL put forward in Refs. [4, 26, 27], but we also try to gain fundamental understanding of the transition from classical to quantum. Moreover, we want to compare the properties of a Quantum FEL with the ones of its classical counterpart in order to deduce consequences for possible experiments. These goals quite naturally serves as a guideline for this thesis: we start by reviewing the classical FEL theory, then we study the transition regime between classical and quantum, before we finally enter the deep quantum regime.
Quantum effects in the FEL emerge due to the discreteness of momentum states in contrast to the continuum of momenta in the classical case. This discreteness is induced by a high value of the quantum mechanical recoil of the electrons interacting with the fields. However, a high recoil is not the only constraint: the momentum spread of the electron beam has to be small enough for quantum effects not be washed out. Guided by these intuitions we calculate explicit expressions for quantum corrections to the classical regime of the FEL verifying our

assumptions. Moreover, we identify the classical limit from a quantum point of view: a small recoil and a 'classical initial state' [33] for the electrons which is characterized by a relatively broad momentum spread.

In order to classify the quantum statistical properties of the radiation from a Quantum FEL we first have to know the corresponding properties of a classical FEL. With the help of our insights gained in investigating the emergence of quantum effects we develop a fully-quantized description of the FEL in the classical regime and derive a Fokker–Planck equation [34] for the dynamics of the laser field. Within this novel and intuitive approach we study the photon statistics and the linewidth of the FEL radiation and are able to rederive the results of Refs. [13, 14, 15, 16, 35].

Since the deep quantum regime of the FEL is defined as the limit, where the electron occupies just two momentum levels, we employ standard methods [22] from laser theory to derive the properties of the FEL radiation in this regime. A comparison to the corresponding quantities from the classical regime reveals, for example, that the photon statistics of a Quantum FEL is narrowed, a fact that we identify as a pure quantum effect.

The main result of this thesis, however, is the extension of our model for the Quantum FEL from a single-electron theory to a many-electron model. This generalization is necessary to understand the high-gain regime and, thus, to eventually construct an X-ray Quantum FEL without the need of a resonator in this part of the spectrum. For the many-electron case we identify the quantum regime as the *collective* interaction of many 'two-level electrons' with the radiation field. Similar to the classical high-gain regime we obtain exponential gain for short times and saturation for longer times. While the classical FEL is characterized by multiphoton processes each electron in the Quantum FEL maximally emits only one photon.

1.3 Outline

This thesis is structured in the following way: We begin our investigations in Chap. 2 with a review of the classical FEL theory. After summarizing the basic scheme of an FEL we establish the connection of the FEL to Lamb's classical laser [1] and rederive the pendulum equation [8] for the electron dynamics. In addition, we give an extensive overview of the various gain regimes of an FEL and discuss their emergence and properties.

In Chap. 3 we study the transition from classical to quantum in the FEL by calculating quantum corrections to the classical limit. In an illustrative approach [4] which compares classical trajectories with discrete quantum levels we deduce two conditions for quantum effects to emerge: (i) a high value for the quantum mechanical recoil and (ii) a small momentum spread of the electron beam. We proceed by explicitly calculating quantum corrections to the classical gain with the help of two different methods: first we solve the quantized pendulum equation in the Heisenberg picture before we consider the dynamics of the Wigner function for an electron in the FEL. By employing the Heisenberg picture it becomes most obvious that the nonzero commutator of position and momentum for the electrons is responsible for deviations from the classical theory. The Wigner function approach, on the other hand, reveals that for the 'true classical limit', besides a small recoil, the preparation of a 'classical' initial state [33] is of utmost importance, that is we require a broad momentum spread in accordance with our expectation from the illustrative model.

We then extend the semiclassical model for the Wigner function in Chap. 3 to a fully quantized theory for the FEL in Chap. 4, that is the electron motion *and* the laser field are quantized. By considering the small-recoil limit and by eliminating the electron variables we derive a Fokker–Planck equation [34] for the laser field of a classical FEL in an oscillator configuration. Thus, we are in the position to derive explicit expressions for the steady-state photon statistics and the intrinsic linewidth of such a device. Besides establishing the connection to existing literature on the radiation properties of an FEL [13, 14, 15, 16, 35] the results of this chapter serve as a reference when we later on compare the Quantum FEL to its classical counterpart. After considering the classical limit as well as the transition regime between classical and quantum we discuss the quantum regime of the FEL in Chap. 5. Based on the asymptotic method of averaging [36] we derive in analogy to Ref. [4] two conditions for the operation of a Quantum FEL: On one hand we require a small value for the quantum parameter α, which is connected to a high value of the quantum mechanical recoil, and on the other hand we demand for a small momentum spread of the electron beam in analogy to our discussions in Chap. 3. Moreover, we define [4] the quantum regime as the limit, where only two resonant momenta of the electrons are relevant for the dynamics leading to Rabi oscillations. In addition, we study higher orders of the asymptotic expansion as well as other resonances beyond the fundamental two-level system and observe that the corresponding multiphoton processes are suppressed in the deep quantum regime, where single-photon transitions prevail. In contrast to the approach in Ref. [4], we apply here a slightly different variant of the method of averaging which is in operator form [37]. This procedure helps us to gain understanding of the underlying processes.

The definition of the Quantum FEL as a two-level system enables us to calculate in Chap. 6 the radiation properties of a low-gain Quantum FEL oscillator in analogy to the theory for a one-atom maser [38, 39, 40]. By employing the photon number representation we derive explicit expressions for gain, steady-state photon statistics, and intrinsic linewidth. Despite difficulties for the experimental realization, regarding undulator length and electron energy, we deduce that the realization of a Quantum FEL oscillator would lead to a narrowed photon statistics and thus to smaller intensity fluctuations compared to its classical counterpart. In contrast to the self-amplified spontaneous emission (SASE) mode, considered in Refs. [2, 3], the linewidth of an FEL oscillator is not narrowing when we enter the quantum regime. Additionally, we study the effects of a nonzero momentum spread on the radiation properties of a Quantum FEL and find novel conditions for the efficient operation of such a device.

Up to this point we have just considered a single-electron approach which yields a low-gain theory for the FEL. In Chap. 7, however, we apply the ideas and concepts developed so far in this thesis to a many-electron model leading to a description of the high-gain Quantum FEL. For short times we observe an exponential growth of the laser intensity starting from zero which is necessary to realize a Quantum SASE FEL. In this context, we establish the connection of our approach and the model in Ref. [3]. Moreover, we study the dynamics for longer times and obtain that at saturation each electron has emitted on average approximately one photon.

We conclude the main body of this thesis in Chap. 8 by summarizing our results and giving an outlook on possible extensions to expand our theory on the Quantum FEL. In order to keep this thesis self-contained we add several appendices which explain our methods and calculations in more detail.

2 The Classical Theory of the FEL

In this introductory chapter we review the classical theory of the FEL. For this purpose, we first collect the main components of such a device and discuss the basic properties of the radiation distinguishing an FEL from other radiation sources. To understand why the FEL really constitutes a laser we review the concept of a classical laser as introduced in Ref. [1] and compare the interaction in the FEL with this model. At the end of this chapter we provide an overview of the different regimes of FEL operation.

2.1 What is an FEL?

A truly free electron cannot emit radiation [41] – this would violate energy-momentum conservation. However, if the motion of the electron is modified by a uniform or periodic structure emission of radiation can become possible. Thus, it would be more precise to speak of 'quasifree electrons' [9].

There exist several possible realizations of a radiation source employing quasifree electrons: Čerenkov radiation [42, 43], the Smith-Purcell effect [44], or the cyclotron-resonance maser [45], to name only a few of them.

However, in this thesis we focus on one particular device: the free-electron laser (FEL) as proposed in Ref. [5] and experimentally realized first in Ref. [46]. In the case of the FEL a highly relativistic electron beam travels through an alternating array of magnets, called 'wiggler' or 'undulator'. This scheme is shown in Fig. 2.1. Due to Lorentz force the electrons oscillate (or 'wiggle') transversely to the wiggler axis and as accelerated charges they emit radiation. We note, that the energy for the radiation does not come from the static magnetic field of the wiggler but from the longitudinal motion of the electron. A fraction of the longitudinal motion converts into a transverse one which creates the radiation.

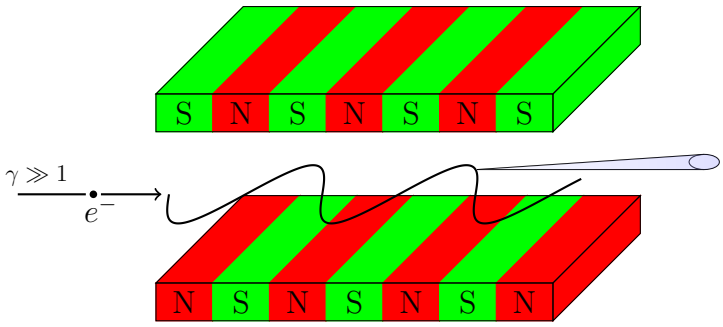

Figure 2.1: Basic components of an FEL: Relativistic electrons travel through the wiggler, that is an array of alternating magnets. Due to Lorentz force the electrons oscillate and thus emit radiation in forward direction.

The main feature why the FEL is such interesting for many applications in material and life science is its wide tunability up to the X-ray regime of the electromagnetic spectrum. This is a purely relativistic effect which arises since the electrons are accelerated to a velocity v close to the speed of light c before they enter the wiggler.
For highly relativistic electrons, where $\beta \equiv v/c \lesssim 1$, the relativistic factor

$$\gamma \equiv \frac{1}{\sqrt{1-\beta^2}}\,, \tag{2.1}$$

which characterizes the dimensionless kinetic energy of the electrons, becomes very large, that is $\gamma \gg 1$. Suppose that the periodicity of the wiggler (the distance between two subsequent poles of the same direction) is given by the length λ_W. In the rest frame of the electron λ_W transforms due to length contraction to $\lambda'_\mathrm{W} = \lambda_\mathrm{W}/\gamma$. In this frame of reference the electrons oscillate perpendicular to the wiggler axis and emit radiation with the wavelength λ_L of their excitation, that is $\lambda'_L = \lambda'_\mathrm{W}$. When we go back to the lab frame we have take the Doppler shift of this wavelength into account yielding $\lambda_\mathrm{L} \cong \lambda'_\mathrm{L}/(2\gamma)$. Combining all transformations and factors we finally obtain the wavelength [47, 48]

$$\lambda_\mathrm{L} = \frac{\lambda_\mathrm{W}}{2\gamma^2} \tag{2.2}$$

of the radiation in the FEL which becomes shorter for increasing electron energies. Hence, we are in the position to produce *short-wavelength* radiation from the *long-'wavelength'* structure of the wiggler – with the cost of building large electron accelerators to achieve relativistic electron energies.
Moreover, to produce a high gain in the FEL the electrons have to pass through many periods of the wiggler [48]. Due to the relatively long periodicity λ_W of the magnets in the wiggler, one has to build a very long wiggler to get many periods. For example, the X-ray FEL FLASH1 at DESY in Hamburg operates with a wiggler that is 27 m long with a periodicity of 27.3 mm [49].
At least this last problem could be overcome by the development of the so-called 'Compton laser' [50]. This device basically uses the same scheme as the usual FEL with the difference that the magnetostatic wiggler is replaced by a counterpropagating laser or microwave field. This 'optical undulator' or 'laser wiggler' has of course a much smaller wavelength than the magnetostatic one which would reduce the wiggler length by some orders of magnitude.
On the theory side there is no essential difference between the laser wiggler or the magnetostatic one, since in the rest frame of the electron both kinds of wigglers can be modeled as a counterpropagating electromagnetic wave. The main difference arises for the resonance condition Eq. (2.2) in the laboratory frame. The first Lorentz transformation from the lab to the co-moving frame has to be replaced by the Doppler shift $\lambda'_\mathrm{W} \cong \lambda_\mathrm{W}/(2\gamma)$ and at the end we arrive at $\lambda_\mathrm{L} = \lambda_\mathrm{W}/(4\gamma^2)$ [51].
In the experiment, however, an FEL with a laser wiggler is not achieved yet due to higher requirements for the quality of the electron beam and the laser beam. Nevertheless, there is a high amount of research on this topic [52] since it would be a huge step towards a table-top FEL.
We emphasize that the resonance condition as written down in Eq. (2.2) is not the full story. In a more extensive approach [48], which includes the transverse motion of the electron, one

obtains the relation

$$\lambda_{\mathrm{L}} = \frac{\lambda_{\mathrm{W}}}{2\gamma^2}(1 + a_0^2) \tag{2.3}$$

where a_0 is the dimensionless wiggler parameter [48] characterizing the strength of the wiggler field. Thus, besides the periodicity of the wiggler λ_{W} and the kinetic energy γ of the electrons, we have by changing the strength of the wiggler field a third possibility to tune the wavelength of the FEL radiation.

In addition to the wide tunability, there is a second feature of the radiation that stands out: it is mainly directed in forward direction. In its rest frame the electron emits radiation in an isotropic way. However, this symmetric radiation pattern changes to a cone which is directed into the forward direction if we transform to the laboratory frame. The opening angle of this cone is proportional to $1/\gamma$ and thus decreases with higher electron energies [48]. Hence, this focusing in the FEL is also a relativistic effect.

An FEL can be operated in three different modes [48]: The first possibility is given by an amplifier where a seeded laser wave is amplified by the FEL interaction. Secondly, one can build an FEL oscillator where the spontaneously emitted radiation is amplified with the help of a resonator which stores the radiation during *many passages* of electron bunches in the wiggler. The third option is given by the so-called SASE ('self-amplified spontaneous emission') mode. In a SASE FEL, the spontaneous emission is amplified in a *single pass* trough a very long wiggler making a resonator unnecessary. This mode of operation is up to now the only possibility to build an X-ray FEL due to the lack of mirrors in the X-ray regime [48].

Talking of amplification and resonators is quite naturally in the context of lasers. However, why should the interaction of light and matter in the FEL be considered suitable for a laser?

2.2 FEL as classical laser

In this section we discuss the concept of a classical laser as introduced in Ref. [1], where the interaction between a beam of particles, modeled as classical anharmonic oscillators, with a single mode of the electromagnetic field is considered. We compare this model to the FEL interaction which is characterized by the equation of motion for a classical pendulum.

2.2.1 Lamb's classical laser

The term LASER stands for 'light amplification of stimulated emission of radiation'. From the viewpoint of quantum electrodynamics (QED) the emission of radiation is explained with the help of the photon picture. According to QED the stimulated emission of a photon into an initially occupied mode, that is the stimulating field, is more likely than the emission into an empty mode and in this way the incident field is amplified [22, 40, 53].

In contrast, the dynamics of an FEL is purely classical and quite naturally the question arises, if such a device really constitutes a laser. However, this question can be answered positively by recognizing that the energy gain of an electromagnetic field due to its interaction with an electrical charge or current can be understood by classical electrodynamics – without any need for photons [54]. This fact even becomes more pronounced when we consider semiclassical

laser-theory [22, 55, 56], which investigates the interaction of two-level atoms with a classical electromagnetic field, and correctly predicts many properties of a laser.

The FEL even goes a step further: whereas the two-level atoms in ordinary laser theory [22] have to be treated quantum mechanically, in FEL theory, both, the field and the electron dynamics can be understood by classical physics alone. Already in 1972 M. Borenstein and W. E Lamb jr. discovered the possibility of a 'classical laser' [1] by showing that the the interaction of anharmonic oscillators with an electromagnetic field can give rise to an amplification of this field. In this section we briefly review this theory and in this way we introduce many concepts and arguments which we need for a large part of the whole thesis.

The dynamics of the electromagnetic field is given by Maxwell's equations [41]. However, we can equivalently employ a Hamiltonian formalism, where the Hamiltonian of the electromagnetic field is given by its energy [40]

$$H_{\text{Field}} = \int \mathrm{d}^3x \left[\frac{\varepsilon_0}{2} \boldsymbol{E}^2(\boldsymbol{x}, t) + \frac{\mu_0}{2} \boldsymbol{H}^2(\boldsymbol{x}, t) \right] \tag{2.4}$$

with $\boldsymbol{E}$ denoting the electric and $\boldsymbol{H}$ the magnetic field, while ε_0 represents the vacuum permittivity and μ_0 the vacuum permeability, which are fundamentally related to the speed of light c via $c^{-2} = \varepsilon_0 \mu_0$ [40].

We can interpret the Hamiltonian, Eq. (2.4), as a sum of infinitely many oscillators [40]

$$H_{\text{Field}} = \sum_j \nu_j a_j^* a_j \tag{2.5}$$

for the radiation field in a cavity. The jth oscillator, represented by the complex amplitude a_j, gives the jth mode of the electromagnetic field. The dynamics of the field then has to be calculated from the Hamiltonian equations of motion

$$\dot{a}_j = -i \frac{\partial H_{\text{Field}}}{\partial a_j^*} , \tag{2.6}$$

where a_j and a_j^* represent conjugate variables. Although the interpretation of the field as sum of harmonic oscillators is strictly speaking only valid for the field in a cavity, this approach is also often suitable for situations in free space when we make the slowly varying amplitude and phase approximation [57].

In our situation of interest we restrict ourselves to a single mode of the radiation field with the Hamiltonian $H_{\text{L}} \equiv \nu a_{\text{L}}^* a_{\text{L}}$, that is the laser mode. The electric field of this mode reads in terms of the complex amplitude a_{L} [40]

$$\boldsymbol{E}(\boldsymbol{x}) = \mathcal{E} u(\boldsymbol{x}) \left(a_{\text{L}} + a_{\text{L}}^* \right) \boldsymbol{e}_x . \tag{2.7}$$

The field is directed parallel to the x-axis and is characterized by the mode function $u(\boldsymbol{x})$ and the amplitude $\mathcal{E}$.

The dipole interaction of a particle with the electric charge $-e$ and the field is given by the interaction Hamiltonian

$$H_{\text{int}} = -e\boldsymbol{x} \cdot \boldsymbol{E}(\boldsymbol{x}) . \tag{2.8}$$

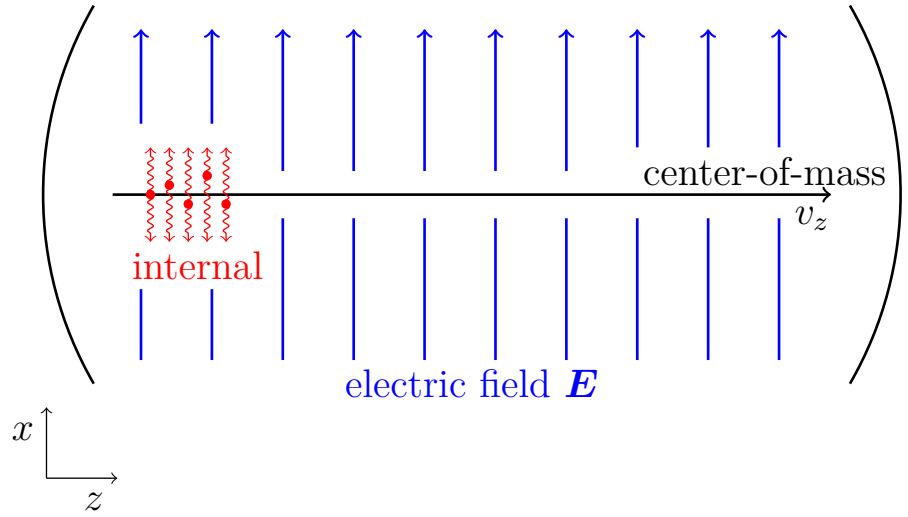

Figure 2.2: Scheme of a 'classical laser' according to Ref. [1]. A beam of particles is injected into a resonator with a center-of-mass motion which is perpendicular to the electric field $\boldsymbol{E}$ in the cavity. The internal motion of a particle is modeled as the one of a classical anharmonic oscillator and couples to the radiation field via dipole interaction according to Eq. (2.9).

This form is analogous to the formulation in terms of the vector potential $\boldsymbol{A}$ and gives us the term $\boldsymbol{p} \cdot \boldsymbol{A}$ which corresponds to $\boldsymbol{x} \cdot \boldsymbol{E}$ and which arises from squaring the momentum of the particle $\boldsymbol{p}$ coupled to the vector potential $(\boldsymbol{p} - e\boldsymbol{A})^2$. The additional term that goes with $\boldsymbol{A}^2$ is neglected here, but later becomes important, when we treat the FEL.

By considering just a single mode, Eq. (2.7), of the electric field $\boldsymbol{E}$ for the interaction, Eq. (2.8), we of course neglect the effect that the charged particle, which is accelerated, produces a field with a broad spectrum and interacts with this field. This self-interaction would lead to damping and we could take this effect into account by introducing a damping constant for the equation of motion of the particle [58].

Following the lines of Ref. [1] we model classical particles as oscillators and inject them into a cavity perpendicular to the electric field $\boldsymbol{E}$, that is the z-direction. We assume that the oscillation occurs in x-direction, that is the direction of their excitation $\boldsymbol{E}$, while their center-of-mass motion is in z-direction, see Fig. 2.2, and stays approximately unaffected by the interaction. If the amplitude of the oscillations in z-direction is small we assume that the mode function is only a function of z, $u(\boldsymbol{r}) \cong u(z)$, and since the center-of-mass motion approximately decouples from the internal degree of freedom, we neglect it for our considerations.

The interaction Hamiltonian for a single particle then reads

$$H_{\text{int}} = -e\mathcal{E}u(z)\left(a_{\text{L}} + a_{\text{L}}^*\right)x \tag{2.9}$$

which translates for N anharmonic oscillators into the total Hamiltonian

$$H = \nu\left|a_{\text{L}}\right|^2 + \sum_{j=1}^{N}\left[\frac{p_j^2}{2} + \frac{\omega^2}{2}\left(x_j^2 - \frac{\lambda^2}{12}x_j^4\right)\right] + g\sqrt{2\omega}\left(a_{\text{L}} + a_{\text{L}}^*\right)\sum_{j=1}^{N}x_j\,, \tag{2.10}$$

where the x_j and p_j give the position and conjugate momentum, respectively, for the oscillators which should be characterized by the same frequency ω. The coupling strength is denoted by g and its explicit form is chosen because of convenience while λ characterizes the anharmonicity of the oscillators.
The time evolution of the laser field is given by

$$\begin{aligned} \dot{a}_\mathrm{L} &= -i\frac{\partial H}{\partial a_\mathrm{L}^*} \\ &= -i\nu a_\mathrm{L} + igN\sqrt{2\omega}\,\langle x\rangle\ , \end{aligned} \tag{2.11}$$

where we have introduced the average position $\langle x\rangle \equiv N^{-1}\sum_{j=1}^{N} x_j$ of all oscillators. The canonical equations for a particle lead to the equation of motion

$$\ddot{x}_j + \omega^2\left(x_j - \frac{\lambda^2}{6}x_j^3\right) = -g\sqrt{2\omega}\,(a_\mathrm{L} + a_\mathrm{L}^*) \tag{2.12}$$

for a driven anharmonic oscillator which is known as the Duffing equation [59, 60].
The particles enter the cavity at different times at the same position and interact with the field during the time T. Alternatively, we can interpret this situation such that the oscillators enter the cavity at the same time t and possess different initial phases giving rise to the initial condition $x_j(t) = x_0\cos\theta_j^{(\mathrm{in})}$. We assume uniformly distributed phases $\theta_j^{(\mathrm{in})}$ while the initial amplitude x_0 should be the same for every oscillator.
We consider the dynamics of the system at a time $\bar{t}$ during the interaction of the oscillators with the laser field, that is $t \le \bar{t} < t+T$. Following the procedure of Ref. [1] we could directly solve Eqs. (2.11) and (2.12). However, in order to clarify the calculations, we pursue an equivalent but slightly different approach. For this purpose, we perform the transformation

$$b_j \equiv \sqrt{\frac{\omega}{2}}\left(x_j + \frac{i}{\omega}p_j\right) \tag{2.13}$$

which describes the complex amplitude of the jth oscillator subject to the initial condition $b_j(t) = \sqrt{\frac{\omega}{2}}A^{(\mathrm{in})}\,\mathrm{e}^{-i\theta_j^{(\mathrm{in})}}$.
Inserting Eq. (2.13) into Eqs. (2.11) and (2.12) yields

$$\begin{aligned} \dot{b}_j &= -i\omega b_j + i\frac{\lambda^2}{24}\,(b+b^*)^3 + ig\,(a_\mathrm{L} + a_\mathrm{L}^*) \\ \dot{a}_\mathrm{L} &= -i\nu a_\mathrm{L} + igN\,\langle b + b^*\rangle \end{aligned} \tag{2.14}$$

for the dynamics of the system.
Resonant processes are fundamental for many fields in physics and in particular for lasers. We assume that considerable energy transfer happens only close to resonance, that is for ω being close to the driving frequency ν. Hence, we make the second transformation

$$\begin{cases} b_j \equiv \mathrm{e}^{-i\nu(\bar{t}-t)}\,B_j \\ a_\mathrm{L} \equiv \mathrm{e}^{-i\nu(\bar{t}-t)}\,A_\mathrm{L}\,, \end{cases} \tag{2.15}$$

where we have made sure that the transformed quantities coincide with the original ones at the beginning of the interaction at $\bar{t} = t$. Transforming Eq. (2.14) according the prescription, Eq. (2.15), leads to terms which are independent of time as well as to contributions which are oscillating with $\pm 2\nu$ and multiples of it, that is $2(2\nu)$.

In this context, we introduce the important concept that rapid oscillations are averaged out during the interaction and can be neglected, which often is refered to as a rotating-wave approximation [40]. For the nearly resonant case, where the detuning $\Delta \equiv \omega - \nu$ is small, that is $\Delta \ll \omega + \nu \cong 2\nu$, we disregard rapidly varying contributions and just keep time-independent terms. Hence, we arrive at

$$\begin{aligned} \dot{B}_j &= -i\left(\Delta - \frac{\lambda^2}{8}|B_j|^2\right) B_j - igA_\mathrm{L} \\ \dot{A}_\mathrm{L} &= -igN\left\langle B\right\rangle \ , \end{aligned} \tag{2.16}$$

for the dynamics of the system.

In the further course of this thesis neglecting rapidly varying terms often plays an important role and we justify this kind of approximation by an asymptotic expansion, which is known as 'method of averaging' [36, 59]. The rotating-wave approximation can be understood by noticing that the integration of the differential equations would bring the frequency 2ν into the denominator [40]. Thus, these rapid oscillations only yield small contributions to the solution scaling with $1/(2\nu)$.

Additionally to a small detuning we also require a small coupling g between the field and the oscillators to employ the rotating-wave approximation. Later on we show that the applicability of this approximation depends on the ratio of the coupling strength to the large frequency scale, which in our example is given by $g/(2\nu)$. This parameter has to be much smaller than unity to ensure that an asymptotic expansion converges and the rapidly varying terms really are suppressed.

The solution of Eq. (2.16) would boil down to the diagonalization of an $(N+1) \times (N+1)$ matrix. However, we apply another approximation which is commonly used in laser theory and significantly reduces our calculational effort: We assume that the change of the laser field during the interaction is small, that is $A_\mathrm{L}(\bar{t}) \cong A_\mathrm{L}(t) = \text{const}$. Thus, we solve the equation of motion for the oscillators for a constant driving and insert the result for the oscillators into the equation of motion for the laser field. By doing so we effectively arrive at a single-particle theory, since the interaction between the oscillators, mediated by the laser field, vanishes and the equations decouple. In ordinary laser theory this procedure often is called 'adiabatic elimination of atomic variables' [56] while the FEL literature [48] identifies this limit of a nearly constant field as the 'low-gain regime'.

Similar to Ref. [1] we write the complex amplitude of the oscillator $B_j = \rho_j \, \mathrm{e}^{-i\theta}$ in terms of modulus ρ_j and phase θ_j the dynamics of which are described by

$$\begin{cases} \dot{\rho}_j &= g|A_\mathrm{L}| \sin\left(\theta_j - \varphi\right) \\ \dot{\theta}_j &= \Delta - \frac{\lambda^2}{8}\rho_j^2 + \frac{g|A_\mathrm{L}|}{\rho_j} \cos\left(\theta_j - \varphi\right) \end{cases} \tag{2.17}$$

which follows from Eq. (2.16). Moreover, we have introduced the polar representation of the amplitude of the laser field $A_\mathrm{L} \equiv |A_\mathrm{L}|\,\mathrm{e}^{-i\varphi}$. We note that the gain of the field

$$G \equiv \frac{|A_\mathrm{L}(t+T)| - |A_\mathrm{L}(t)|}{|A_\mathrm{L}(t)|} \tag{2.18}$$

is defined as the relative change of the modulus $|A_\mathrm{L}|$ during the interaction.
However, even by performing the low-gain approximation of a constant laser field A_L we cannot solve Eq. (2.17) in an analytic way. Hence, we restrict ourselves to the case, where the laser field can be considered as a small perturbation for the dynamics of the electrons, and we solve Eq. (2.17) perturbatively in powers of $|A_\mathrm{L}|$ [1]. This regime is known as the small-signal regime and should not be confused with the low-gain approximation which still allows for a strong laser signal $|A_\mathrm{L}|$.
By setting $g|A_\mathrm{L}| = 0$ in Eq. (2.17) we obtain the zeroth-order solution

$$B_j^{(0)} = \sqrt{\frac{\omega}{2}} x_0\,\mathrm{e}^{-i\theta_j^{(\mathrm{in})}}\,\mathrm{e}^{-i\tilde{\Delta}(\bar{t}-t)}\,, \tag{2.19}$$

where we have defined $\tilde{\Delta} \equiv \Delta - \dfrac{\lambda^2}{16} x_0^2 \omega$. This solution of the free Duffing equation is well-known in the literature [59].
To calculate the gain we have to average over the initial phases $\theta_j^{(in)}$ according to Eq. (2.18). Since these initial phases are distributed uniformly the mean value $\langle \mathrm{e}^{-i\theta^{(\mathrm{in})}} \rangle = 0$ vanishes and thus the zeroth-order solution, Eq. (2.19), does not contribute to a change of the laser field. However, when we consider the first order in $g|A_\mathrm{L}|$ we encounter terms of the form of $\langle \mathrm{e}^{-i\theta^{(\mathrm{in})}}\,\mathrm{e}^{+i\theta^{(\mathrm{in})}} \rangle = 1$ which are responsible for the gain in the laser. These arguments which are based on a uniform distribution of phases are important for the FEL as well and we use similar arguments throughout a large part of this thesis.
We write the first-order solution for B_j as

$$B_j^{(1)} = \mathrm{e}^{-i\theta_j^{(\mathrm{in})}}\,\mathrm{e}^{-i\tilde{\Delta}(\bar{t}-t)} \left(\rho_j^{(1)} - i\theta_j^{(1)} \rho^{(\mathrm{in})} \right), \tag{2.20}$$

where we have expanded the phase factor $\mathrm{e}^{-i\theta^{(1)}}$ to first order in $\theta^{(1)}$. Moreover, the contribution $\rho_j^{(1)}$ of the modulus

$$\rho_j^{(1)} = \rho^{(+)}\,\mathrm{e}^{+i(\theta_j^{(\mathrm{in})} - \varphi)} + \rho^{(-)}\,\mathrm{e}^{-i(\theta^{(\mathrm{in})} - \varphi)} \tag{2.21}$$

constitutes a sum of a term $\rho^{(+)}$ with positive and one $\rho^{(-)}$ with negative phase factor. An analogue distinction can be made for the phase $\theta^{(1)}$ which splits into $\theta^{(+)}$ and $\theta^{(-)}$. With the help of Eqs. (2.18) and (2.20) we obtain the expression

$$G = \frac{gN}{|A_\mathrm{L}(t)|} \int_t^{t+T} \mathrm{d}\bar{t}\,\mathrm{Im}\left\{ \mathrm{e}^{-i\tilde{\Delta}(\bar{t}-t)} \left[\rho^{(+)} - i\theta^{(+)} \rho^{(\mathrm{in})} \right] \right\} \tag{2.22}$$

for the gain where we have already averaged over the initial phases by keeping just terms which are independent of $\theta_j^{(\mathrm{in})}$.

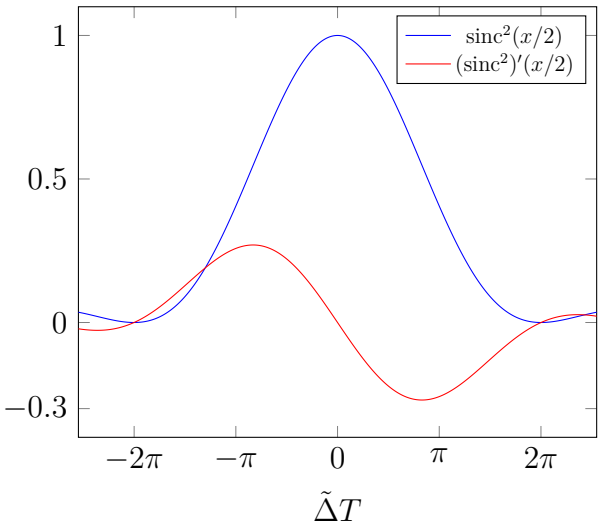

Figure 2.3: The two contributions $\mathrm{sinc}^2(\tilde{\Delta}T/2)$ (blue lines) and $\partial \mathrm{sinc}^2(x/2)/\partial x\big|_{x=\tilde{\Delta}T}$ (red line) for the gain of the classical laser, Eq. (2.24), as functions of the detuning parameter $\tilde{\Delta}T$. For nonzero values of the anharmonicity d, for example $d = 1$, the second contribution can exceed the first one for certain ranges of $\tilde{\Delta}T$. In such a case we obtain positive gain according to Eq. (2.24) and thus the radiation field is amplified.

We have to solve

$$\begin{cases} \dot{\rho}^{(+)} &= \frac{g|A_\mathrm{L}|}{2i}\, \mathrm{e}^{i\tilde{\Delta}(\bar{t}-t)} \\ \dot{\theta}^{(+)} &= -\frac{\lambda^2}{4}\rho^{(\mathrm{in})}\rho^{(+)} + \frac{g|A_\mathrm{L}|}{2\rho^{(\mathrm{in})}}\, \mathrm{e}^{i\tilde{\Delta}(\bar{t}-t)} \end{cases} \tag{2.23}$$

and finally arrive with the help of Eq. (2.22) at [1]

$$G = \frac{(gT)^2 N}{2}\left[-\mathrm{sinc}^2\left(\frac{\tilde{\Delta}T}{2}\right) + d\,\frac{\partial}{\partial x}\mathrm{sinc}^2\left(\frac{x}{2}\right)\bigg|_{x=\tilde{\Delta}T}\right] \tag{2.24}$$

which is the gain of the 'classical laser' in the low-gain small-signal regime. Here, we have defined the parameter

$$d \equiv \frac{\lambda^2 x_0^2}{16}(\omega T) \tag{2.25}$$

in analogy to Ref. [1].
We emphasize that for the case of harmonic oscillators instead anharmonic ones, that is $d \to 0$ and $\tilde{\Delta} \to \Delta$ in Eq. (2.24), we never obtain a positive gain and hence there is no amplification. However, for a nonzero value of d the gain can become positive as illustrated in Fig. 2.3. In this case, we do observe amplification of the radiation field, justifying the term 'laser'.
We note that this identification of a classical laser is just based on the possibility of amplifying a field mode and not on the coherence properties of the radiation. In order to discuss these properties the quantization of the electromagnetic field becomes necessary in analogy to ordinary laser theory [22]. Hence, it might be possible that our system of consideration does not possess the coherence of an ordinary laser. If we define a laser by the possibility of amplification *and* its coherence properties the classical laser thus is not necessarily a laser.

2.2.2 The FEL pendulum equation

In this section we investigate the classical dynamics of an FEL and discuss similarities and differences to Lamb's 'classical laser' which we have studied in the preceding section. Starting from first principles we derive the pendulum equation for the electron dynamics [8, 48] and the equation of motion for the laser field.

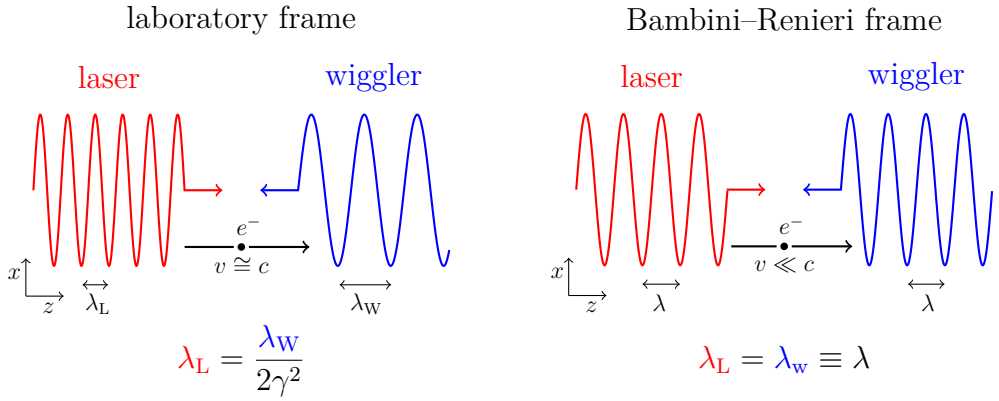

Figure 2.4: Transition from the laboratory frame (left) to the co-moving Bambini–Renieri frame. In the lab frame the electron travels close to the speed of light c. The wavelength λ_L in this frame is connected to the periodicity λ_W of the wiggler and to the relativistic factor γ of the electron via the resonance condition, Eq. (2.2). In contrast, the motion of an electron close to resonance in the Bambini–Renieri frame is nonrelativistic while λ_L and λ_W coincide. The two modes constitute a standing wave in this frame of reference.

For this purpose, we consider an approach in the co-moving Bambini–Renieri frame [61]. This frame of reference is defined by the condition that the wave numbers of the laser k_L and the wiggler k_W coincide, that is $k_\mathrm{L} = k_\mathrm{W} \equiv k$, which is illustrated in Fig. 2.4. Thus, the electron effectively interacts with a standing light field. Moreover, this model has the advantage that the motion of an electron close to resonance is always nonrelativistic which considerably simplifies our theoretical investigations. A detailed treatment of the Lorentz transformation from the laboratory to the Bambini–Renieri frame and the derivation of the FEL Hamiltonian in this frame can be found in App. A.
The nonrelativistic Hamiltonian of N free electrons, characterized their positions $\boldsymbol{x}_j$, momenta $\boldsymbol{p}_j$, and mass m, interacting with the radiation field is given by [41]

$$H = \sum_{j=1}^{N} \frac{\left[\boldsymbol{p}_j - \boldsymbol{A}(z_j, t)\right]^2}{2m} \,. \tag{2.26}$$

We assume that the radiation field consists of two counterpropagating plane waves, where the laser field copropagates with while the wiggler field counterpropagates towards the electron. The total vector potential $\boldsymbol{A}$ depends only on z, that is the direction along the wiggler axis, and not on the transverse directions x, y. Hence, the Hamiltonian is also independent of these variables, $H \neq H(x, y)$, and by means of the Hamiltonian equations of motion the transverse

momentum is constant and even vanishes if we inject the electrons parallel to the wiggler axis, that is $p_x = p_y = \text{const} \equiv 0$.

Finally, we arrive at a one-dimensional theory for the position z and the conjugate momentum $p \equiv p_z$. If we write down explicitly the square in Eq. (2.26), we furthermore find that the term $\boldsymbol{p} \cdot \boldsymbol{A} = 0$ is zero because the vector potential $\boldsymbol{A}$ is transversal. In contrast to the anharmonic oscillators treated in the preceding section, or two-level atoms [40], the interaction in the FEL is not characterized by the $\boldsymbol{x} \cdot \boldsymbol{E}$(or equivalently $\boldsymbol{p} \cdot \boldsymbol{A}$) term but by the contribution arising from $\boldsymbol{A}^2$. We emphasize that the explicit time-dependency of the vector potentials comes from the fact that we have already included the dynamics of the free field, that is of the Hamiltonian of Eq. (2.4).

The explicit form of the vector potentials of the laser $\boldsymbol{A}_\mathrm{L}$ and the wiggler $\boldsymbol{A}_\mathrm{W}$ then reads

$$\boldsymbol{A}_\mathrm{L}(z,t) = \mathcal{A}_\mathrm{L} \left(a_\mathrm{L}(t) \boldsymbol{e}\, \mathrm{e}^{-i\omega t + ikz} + a_\mathrm{L}^*(t) \boldsymbol{e}^*\, \mathrm{e}^{i\omega t - ikz} \right) \tag{2.27}$$

and

$$\boldsymbol{A}_\mathrm{W}(z,t) = \tilde{\mathcal{A}}_\mathrm{W} \left(\boldsymbol{e}\, \mathrm{e}^{-i\omega t - ikz} + \boldsymbol{e}^*\, \mathrm{e}^{i\omega t + ikz} \right) , \tag{2.28}$$

respectively which we have modeled as two counterpropagating plane waves with the amplitudes $\mathcal{A}_\mathrm{L}$ and $\tilde{\mathcal{A}}_\mathrm{W}$, respectively. These two modes are characterized by the same frequency ω and wave number k and both are circularly polarized with $\boldsymbol{e} \cdot \boldsymbol{e}^* = 1$ and $\boldsymbol{e}^2 = \boldsymbol{e}^{*2} = 0$. Since the wiggler field is very strong we assume that it is constant during the interaction, while the dynamics of the laser field is described by the dimensionless amplitude $a(t)$ and its complex conjugate $a^*(t)$.

The total vector potential

$$\boldsymbol{A} = \boldsymbol{A}_\mathrm{L} + \boldsymbol{A}_\mathrm{W} \tag{2.29}$$

is the sum of the laser and the wiggler field and we obtain three contributions to the $\boldsymbol{A}^2$ potential, namely $\boldsymbol{A}_\mathrm{L}^2$, $\boldsymbol{A}_\mathrm{W}^2$ and the cross term $2\boldsymbol{A}_\mathrm{L} \cdot \boldsymbol{A}_\mathrm{W}$.

We neglect the effect of $\boldsymbol{A}_\mathrm{L}^2$ since $\boldsymbol{A}_\mathrm{L}^2 \ll \boldsymbol{A}_\mathrm{W}^2$ and we effectively incorporate $\boldsymbol{A}_\mathrm{W}^2$ into the mass m of the electron (see App. A). Thus, the relevant term for the FEL interaction is given by the cross term and we obtain the Hamiltonian

$$H = \sum_{j=1}^{N} \frac{p_j^2}{2m} + \frac{e^2}{m} \sum_{j=1}^{N} \boldsymbol{A}_\mathrm{L}(z_j,t) \cdot \boldsymbol{A}_\mathrm{W}(z_j,t) \, . \tag{2.30}$$

With the explicit expressions for the vector potential, Eqs. (2.27) and (2.28) we arrive at [61]

$$H = \sum_{j=1}^{N} \frac{p_j^2}{2m} + \frac{U_0}{2} \left(a_\mathrm{L} \sum_{j=1}^{N} \mathrm{e}^{i2kz_j} + a_\mathrm{L}^* \sum_{j=1}^{N} \mathrm{e}^{-i2kz_j} \right) , \tag{2.31}$$

where

$$U_0 \equiv \frac{e^2 \mathcal{A}_\mathrm{L} \tilde{\mathcal{A}}_\mathrm{W}}{m} \tag{2.32}$$

is defined as the height of the potential. We note that the potential in Eq. (2.31) is independent of time. This feature emerges since we have chosen circular polarization for the laser and the wiggler field. However, even for another choice of polarization we would effectively obtain the

Hamiltonian in Eq. (2.26) because the additional contributions give rise to rapid oscillations which are suppressed.
The dynamics of the electron is dictated by the Hamiltonian equations of motion

$$\begin{cases} \dot{z}_j &= \frac{\partial H}{\partial p_j} = p_j \\ \dot{p}_j &= -\frac{\partial H}{\partial z_j} = \frac{2kU_0}{2i}\left(a_\mathrm{L}\,\mathrm{e}^{i2kz_j} - a_\mathrm{L}^*\,\mathrm{e}^{-i2kz_j}\right) . \end{cases} \tag{2.33}$$

Four our investigations it is convenient to introduce the dimensionless variables

$$\begin{cases} \tau &\equiv \frac{t}{T} \\ \theta_j &\equiv 2kz_j \\ \wp_j &\equiv \frac{2kT}{m} p_j \\ \kappa &\equiv \frac{(2kT)^2 U_0}{m} , \end{cases} \tag{2.34}$$

where θ is known as the ponderomotive phase and $\wp$ denotes the Doppler parameter. Moreover, we write the amplitude $a_\mathrm{L} \equiv |a_\mathrm{L}|\,\mathrm{e}^{-i\varphi}$ of the laser field in terms of its modulus $|a_\mathrm{L}|$ and its phase φ and arrive at

$$\begin{cases} \dot{\theta}_j &= \wp_j \\ \dot{\wp}_j &= \frac{\kappa}{2i}\left(a_\mathrm{L}\,\mathrm{e}^{i\theta_j} - a_\mathrm{L}^*\,\mathrm{e}^{-i\theta_j}\right) = \kappa|a_\mathrm{L}|\sin\left(\theta_j - \varphi\right) \end{cases} \tag{2.35}$$

which are the equations of motion of Eq. (2.33) in a dimensionless form.
By differentiating $\dot{\theta}_j$ with respect to time τ we observe that the relations in Eq. (2.35) are equivalent to

$$\ddot{\theta}_j = \kappa|a_\mathrm{L}|\sin\left(\theta_j - \varphi\right) \tag{2.36}$$

which describes the motion of a mathematical pendulum, and therefore Eq. (2.36) is known as pendulum equation for the FEL [8].
Hence, we finally observed that like Lamb's 'classical laser' the dynamics of an electron in the FEL is given by the equation of motion of an anharmonic oscillator, a fact which becomes even more clear if we expand the sine in Eq. (2.36) yielding $\sin\theta \cong \theta - \theta^3/(3!)$.
However, the situation of the FEL is still different from the one described in the preceding section: while in the 'classical laser' the field couples only to the position x of the oscillator, in the FEL the laser amplitude appears as a factor in the total potential making the FEL similar to a parametric amplifier. This difference clearly arises from the corresponding kind of interaction: in the 'classical laser' the laser field interacts via $\boldsymbol{x}\cdot\boldsymbol{E}$ with the *internal* degree of the oscillator, whereas the interaction in the FEL is characterized by the $\boldsymbol{A}^2$ term and the *external motion* of the electron.
The dynamics of the laser field is given by the Hamiltonian equation of motion, Eq. (2.6), with the FEL Hamiltonian, Eq. (2.31), yielding, Eq. (A.37),

$$\dot{a}_\mathrm{L} = -igT\sum_{j=1}^{N}\mathrm{e}^{-i\theta_j} \tag{2.37}$$

which could also be derived with the help of Maxwell's equations describing the laser and wiggler field coupled to an electron current [62]. We note that that the coupling constant g

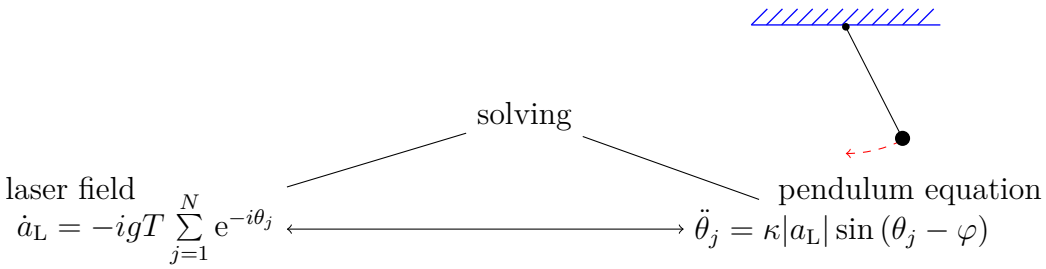

Figure 2.5: Scheme of a self-contained model for the FEL: for the dynamics of an electron we have to solve the pendulum equation, Eq. (2.36), which depends on the amplitude a_L of the laser. The time evolution of $|a_\mathrm{L}|$ is given by Eq. (2.37), which in turn depends on the dimensionless positions θ_j of the electrons.

has the dimension of a frequency and is proportional to the potential height U_0. Its specific form depends on the way how we define $\mathcal{A}_\mathrm{L}$ and a_L. In this thesis we always employ a scaling where $\mathcal{A}_\mathrm{L}$ describes the amplitude of the vacuum field [40] which is best suited when we later on consider a quantized laser field. When we exclusively deal with the classical regime another scaling of the variables would be more reasonable, for example the 'universal scaling' for the classical high-gain FEL introduced in Ref. [21]. However, when we compare the quantum with the classical regime our approach turns out to be useful.
In order to decide whether the FEL really is a laser with positive gain we have to solve the pendulum equation Eq. (2.36) for the electrons and the equations of motion, Eq. (2.37), for the laser field in a self-contained manner which is illustrated in Fig. 2.5. In this context, we have to distinguish between different gain regimes which is the topic of the following section.

2.3 The different regimes of FEL operation

There exist several different limits of the FEL dynamics leading to different expressions for the gain of the laser field. In the following we discuss this range covering the transition from a low to a high gain as well as the distinction between the small-signal limit and a saturated FEL. Moreover, we briefly study the influence of the 'slippage' of the radiation over the electrons and we discuss the distinction of a 'Compton' and a 'Raman' FEL.

2.3.1 Madey gain: low gain and small signal

We begin our investigations concerning the different regimes of FEL operation with the one that started it all: the low-gain FEL in the small-signal limit [5]. To avoid confusion we emphasize that 'low-gain' means something different than 'small-signal'.
In the low-gain FEL the gain of the field, that is its relative energy change during a *single passage* of an electron bunch through the wiggler, is smaller than unity. Hence, the interaction of a single bunch of electrons with the wiggler is not sufficient to operate a laser. However, if we place the wiggler inside a resonator and subsequently send many bunches of electrons through the wiggler, we observe a considerable amplification [48] and eventually steady state. This device is sometimes called 'FEL oscillator' [48].

We enter the low-gain regime by assuming that the amplitude of the laser field a_L at a time $\bar{\tau}$ during the interaction with a single electron bunch, with $\tau \leq \bar{\tau} < \tau + 1$, has not changed appreciable from its value at time τ when the electrons have entered the wiggler. This means that the electrons do not notice a change of the laser field, that is $a_\mathrm{L}(\bar{\tau}) \cong a_\mathrm{L}(\tau) = \text{const}$ while they are traveling through the wiggler. Thus, the equations of motion for the electrons in the bunch, Eq. (2.36), decouple. This way we arrive at a single-electron theory which is no longer justified for a high-gain FEL. This latter regime is characterized by a large interaction time and a many-electron theory as we discuss later in this chapter.
Not just the amplitude $|a_\mathrm{L}| = \text{const}$, is approximately constant for the electron dynamics in a single pass but also the phase $\varphi \cong \text{const}$. Hence, without loss of generality we set the phase equal to zero and arrive from Eq. (2.36) at the single-particle pendulum equation

$$\ddot{\theta}_j = \kappa |a_\mathrm{L}| \sin\theta_j \tag{2.38}$$

for an electron and from Eq. (2.37) at the equation of motion

$$\frac{\mathrm{d}}{\mathrm{d}\bar{\tau}} |a_\mathrm{L}| = -gTN \langle \sin\theta \rangle \tag{2.39}$$

for the modulus of the field amplitude.
When we compare Eq. (2.38) with Eq. (2.39) and use the relation $\dot{\wp} = \ddot{\theta}$ for the dimensionless momentum and position of an electron, we realize that the change of the laser field is proportional to the change of mean momentum of the electrons. Hence, we easily derive the relation

$$G \propto -\left(\langle \wp \rangle - \langle \wp \rangle_{(\mathrm{in})} \right) \tag{2.40}$$

of the laser gain and the change of the mean momentum. If the electrons on average lose momentum, the laser field is amplified.
As mentioned above we have to distinguish between the expressions 'low-gain' and 'small-signal'. Talking of a small signal means that the interaction time T is relatively short and thus saturation effects can be neglected or are just included in lowest order. Analogously to ordinary laser theory [22] we find in the low-gain regime of the FEL a linear small-signal gain, that is G is independent of $|a_\mathrm{L}|$. Later on in this chapter we also observe a small-signal regime for the high-gain FEL where the gain per pass grows exponentially with the interaction time T.
There are basically two equivalent approaches towards the dynamics of an FEL: either we follow each electron and solve the pendulum equation, Eq. (2.38), or we consider a distribution function in phase space the dynamics of which is given by a Vlasov equation. We first present the former approach [8, 63] and solve the pendulum equation in the low-gain small-signal limit.

Pendulum equation

Formally, we enter the small-signal regime by treating the laser field as a small perturbation to the motion of the electron, Eq. (2.38), [51] which is valid for $\kappa|a_\mathrm{L}| \ll 1$.
Setting $\kappa|a_\mathrm{L}| = 0$ in Eq. (2.38) we easily obtain the zeroth-order solution

$$\theta_j^{(0)} = \theta_j^{(\mathrm{in})} + \wp_j^{(\mathrm{in})} (\bar{\tau} - \tau) \tag{2.41}$$

which simply describes the free motion of an electron with the initial phase $\theta_j^{(\mathrm{in})}$ and the initial momentum $\wp_j^{(\mathrm{in})}$. We use this solution for the calculation of the average in Eq. (2.39) leading to vanishing terms $\langle \sin\theta^{(\mathrm{in})}\rangle = \langle \cos\theta^{(\mathrm{in})}\rangle = 0$ and hence $\langle \sin\theta^{(0)}\rangle = 0$, where we have assumed that the initial phases $\theta_j^{(\mathrm{in})}$ are uniformly distributed. Thus, there is no gain in zeroth order.

To calculate the next higher order of our perturbative expansion we insert the free solution, Eq. (2.41) into the pendulum equation, Eq. (2.38), that is

$$\ddot{\theta}_j = \kappa |a_\mathrm{L}| \sin\theta^{(0)} \,. \tag{2.42}$$

Straightforward algebra yields the expression

$$\theta_j^{(1)} = \kappa |a_\mathrm{L}| \frac{1}{\wp_j^{(\mathrm{in})2}} \left\{ \wp_j^{(\mathrm{in})} (\bar{\tau} - \tau) \cos\theta_j^{(\mathrm{in})} + \sin\theta_j^{(\mathrm{in})} - \sin\left[\theta_j^{(\mathrm{in})} + \wp_j^{(\mathrm{in})} (\bar{\tau} - \tau)\right] \right\} \tag{2.43}$$

as first-order perturbation to the free motion of the electron due to the interaction with the laser field.

With the help of elementary trigonometric identities and a Taylor expansion we obtain

$$\sin\left(\theta^{(0)} + \theta^{(1)}\right) \cong \sin\theta^{(0)} + \theta^{(1)} \cos\theta^{(0)} \,. \tag{2.44}$$

The second term in Eq. (2.44) is the first-order contribution to $\sin\theta$ and we have to form its expectation value with respect to the initial phases and momenta to calculate the gain according to Eq. (2.39). In contrast to the procedure in zeroth order, we encounter terms with $\cos^2\theta_j^{(\mathrm{in})} = \frac{1}{2} + \frac{1}{2}\cos 2\theta_j^{(\mathrm{in})}$ leading to a nonzero expectation value $\langle \cos^2\theta^{(\mathrm{in})}\rangle = \frac{1}{2}$. On the other hand terms going with $\sin\theta_j^{(\mathrm{in})} \cos\theta^{(\mathrm{in})} = \frac{1}{2}\sin 2\theta_j^{(\mathrm{in})}$ give no contribution, that is $\langle \sin\theta^{(\mathrm{in})} \cos\theta^{(\mathrm{in})}\rangle = 0$.

We assume that each electron initially possesses the same momentum $\wp_j^{(\mathrm{in})} = \bar{\wp}$ and arrive by means of Eqs. (2.39) and (2.44) at

$$G = -gTN\kappa \frac{1}{2\bar{\wp}^2} \int_\tau^{\tau+1} \mathrm{d}\bar{\tau} \left\{ \bar{\wp} (\bar{\tau} - \tau) \cos\left[\bar{\wp}(\bar{\tau} - \tau)\right] - \sin\left[\bar{\wp}(\bar{\tau} - \tau)\right] \right\} \tag{2.45}$$

for the gain of the laser field according to the definition in Eq. (2.18).

The final integration with respect to time yields the famous Madey gain [5, 51, 48]

$$\begin{aligned} G &= gTN\kappa \frac{1 - \cos\bar{\wp} - \frac{\bar{\wp}}{2}\sin\bar{\wp}}{\bar{\wp}^3} \\ &= -\frac{gTN\kappa}{4} \frac{\partial}{\partial\wp} \mathrm{sinc}^2 \frac{\wp}{2} \Big|_{\wp=\bar{\wp}} \end{aligned} \tag{2.46}$$

in the low-gain small signal regime which is shown in Fig. 2.6. We note that this gain function is point-symmetric with respect to the origin and basically adopts positive values for positive values of the initial Doppler parameter $\bar{\wp}$ while being negative for $\bar{\wp} < 0$. While the gain

vanishes at $\bar{\varphi} = 0$, it is maximized at $\bar{\varphi} \cong \pi$. That is why we define $\bar{\varphi} = \pi$ as resonance for the FEL in the low-gain small-signal limit.

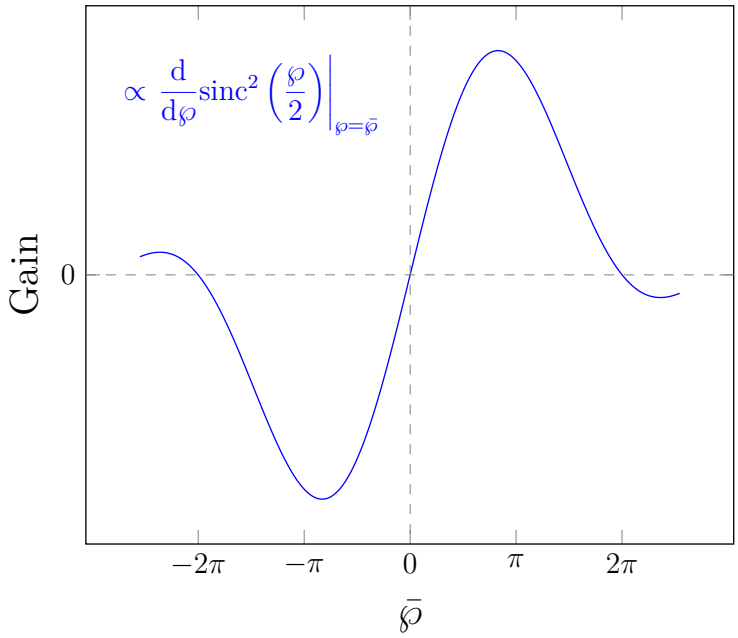

Figure 2.6: Gain of a low-gain small-signal FEL as a function of the initial dimensionless momentum $\bar{\varphi} \equiv 2k\bar{p}T/m$ according to Eq. (2.46). The odd function reaches its maximum at the positive momentum $\bar{\varphi} \cong \pi$ and vanishes for $\bar{\varphi} = 0$.

Of course, we could have also used Eq. (2.40) by calculating the average change of electron momentum and equating it with the laser gain. A perturbative treatment in second order [51] would have given the same result as in Eq. (2.46).

Not just the modulus $|a_\mathrm{L}|$ of the field amplitude changes during interaction but also its phase φ which is known as phase pulling [22, 55]. Taking the imaginary part of the equation of motion for a_L, Eq. (2.37), we find the relation

$$\dot{\varphi} = \frac{gTN}{|a_\mathrm{L}|} \langle \cos(\theta) \rangle \tag{2.47}$$

for the dynamics of the laser phase during a passage of electrons. After inserting the perturbative solution $\theta^{(1)}$, Eq. (2.43), into Eq. (2.47), integrating over time from t to $t+T$, and averaging over the initial phases we arrive at

$$\varphi(t+T) - \varphi(t) \cong gTN\kappa \frac{\sin\bar{\varphi} - (\bar{\varphi}/2)(1+\cos\bar{\varphi})}{\bar{\varphi}^3} \tag{2.48}$$

for the change of the laser phase after interacting with the electrons. We note that this expression is zero when we consider resonance, $\bar{\varphi} = \pi$, in analogy to standard laser theory [22]. However, for higher orders in $\kappa|a_\mathrm{L}|$ the change of the phase is nonzero at resonance, as we show in Chap. 4, and which stands in contrast to an ordinary laser [22].

Distribution function

The first approach towards the FEL which is exclusively based on classical physics was developed by Hopf *et al.* [7] and relies on distribution functions in phase space. We sketch this approach in the following, since we use elements of it later on in this thesis, when we study the classical-quantum transition by means of the Wigner distribution function in the next chapter.

The equation of motion for the distribution function $f(\theta, \wp; \bar{\tau})$ for classical particles, subject to the pendulum equation Eq. (2.38), is given by the collisionless Boltzmann – or Vlasov – equation [64]

$$\left(\frac{\partial}{\partial\bar{\tau}} + \wp\frac{\partial}{\partial\theta}\right) f(\theta, \wp; \bar{\tau}) = -\kappa|a_\mathrm{L}| \sin\theta \frac{\partial}{\partial\wp} f(\theta, \wp; \bar{\tau}) \,, \tag{2.49}$$

where the right-hand side emerges since we have had to form the derivative of the cosine potential with respect to the phase, that is $\partial \cos\theta/\partial\theta = -\sin\theta$.

The dynamics of the laser field still is given by Eq. (2.39), but we have to rewrite this relation in terms of the distribution function $f(\theta, \wp; \bar{\tau})$ yielding

$$\begin{aligned} \frac{\partial}{\partial\bar{\tau}}|a_\mathrm{L}| &= -gTN \langle\sin\theta\rangle \\ &= -gTN \int_0^{2\pi} \mathrm{d}\theta \int \mathrm{d}\wp \sin\theta f(\theta, \wp; \bar{\tau}) \,. \end{aligned} \tag{2.50}$$

The electrons are again uniformly distributed in the θ-direction, but now we assume an arbitrary distribution function $g(\wp)$ for the electron momentum. This way, we distinguish between a cold and a warm electron beam depending on the width $\Delta\wp$ of $g(\wp)$. The total phase space distribution function at the initial time τ reads $f(\theta, \wp; \tau) = \dfrac{1}{2\pi} g(\wp)$ and we have to solve Eq. (2.49) with respect to this initial condition.

Since we consider the low-gain small-signal regime we treat Eq. (2.49) in a perturbative manner. The distribution function of a free particle is simply given by making the displacement $\theta \to \theta - \wp(\bar{\tau} - \tau)$ according to the unperturbed trajectory of a single particle. Thus, the zeroth-order solution of Eq. (2.49) reads

$$f^{(0)}(\theta, \wp; \bar{\tau}) = f(\theta - \wp(\bar{\tau} - \tau); \tau) = \frac{1}{2\pi} g(\wp) \tag{2.51}$$

which reduces to the initial distribution function, because the electrons initially are distributed uniformly in θ-direction. Again, we obtain that the zeroth-order solution does not contribute to the gain and therefore we have to go to the next higher order.

In first order, Eq. (2.49) translates to

$$\left(\frac{\partial}{\partial\bar{\tau}} + \wp\frac{\partial}{\partial\theta}\right) f^{(1)}(\theta, \wp; \bar{\tau}) = -\kappa|a_\mathrm{L}| \sin\theta \frac{\partial}{\partial\wp} f^{(0)}(\theta, \wp; \bar{\tau}) \,. \tag{2.52}$$

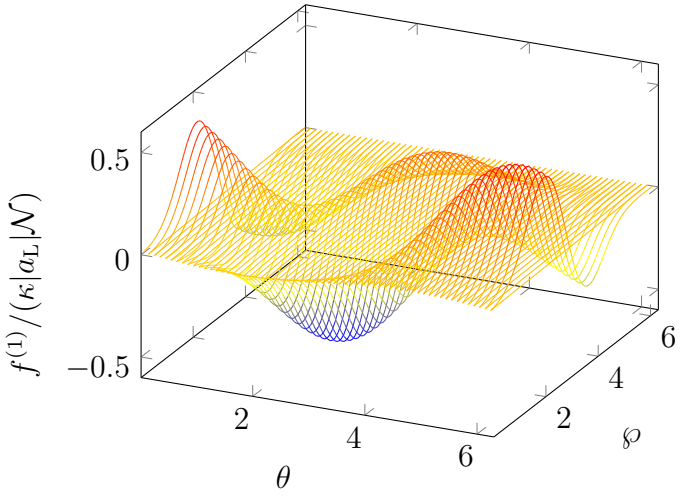

Figure 2.7: First-order correction $f^{(1)}$ to the classical distribution function at time $\bar{\tau} = \tau + 1$, according to Eq. (2.56), as a function of the ponderomotive phase θ and the Doppler parameter $\wp$ for an initial momentum distribution $g(\wp)$ which is a Gaussian with the mean value $\bar{\wp} = \pi$ and variance $\Delta\wp = 1$. The function is normalized by the small parameter $\kappa|a_L|$ and the normalization constant $\mathcal{N}$ of $g(\wp)$. We observe modulations of the distribution function in θ- as well as in $\wp$-direction. We emphasize that only these corrections take on negative values while the total distribution function $f^{(0)} + f^{(1)}$ is always positive if we choose $\kappa|a_L|$ small enough.

This inhomogeneous differential equation can be solved with the help of Green's function $G_{\text{free}}(\theta, \bar{\tau}; \theta', \tau')$ and the formal solution reads

$$f^{(1)}(\theta, \wp; \bar{\tau}) = -\kappa|a_L| \int_{\tau}^{\bar{\tau}} \mathrm{d}\tau' \int \mathrm{d}\theta' G_{\text{free}}(\theta, \bar{\tau}; \theta', \tau') \sin\theta' \frac{\partial}{\partial \wp} f^{(0)}(\theta', \wp; \tau') \,, \tag{2.53}$$

where the Green's function for the Boltzmann equation of a free particle has to be calculated from

$$\left(\frac{\partial}{\partial \tau} + \wp \frac{\partial}{\partial \theta} \right) G_{\text{free}}(\theta, \tau) = \delta(\theta)\delta(\tau) \,. \tag{2.54}$$

Inserting the explicit expression for G_{free} [65]

$$G_{\text{free}}(\theta, \bar{\tau}; \theta', \tau') = \delta(\theta - \theta' - \wp(\bar{\tau} - \tau')) \tag{2.55}$$

into Eq. (2.53), evaluating the delta function by the integration over θ' and performing the integration over time τ' brings us to

$$f^{(1)}(\theta, \wp; \bar{\tau}) = -\kappa|a_L| \frac{\cos\left[\theta - \wp(\bar{\tau} - \tau)\right] - \cos\theta}{\wp} \frac{1}{2\pi} \frac{\partial}{\partial \wp} g(\wp) \tag{2.56}$$

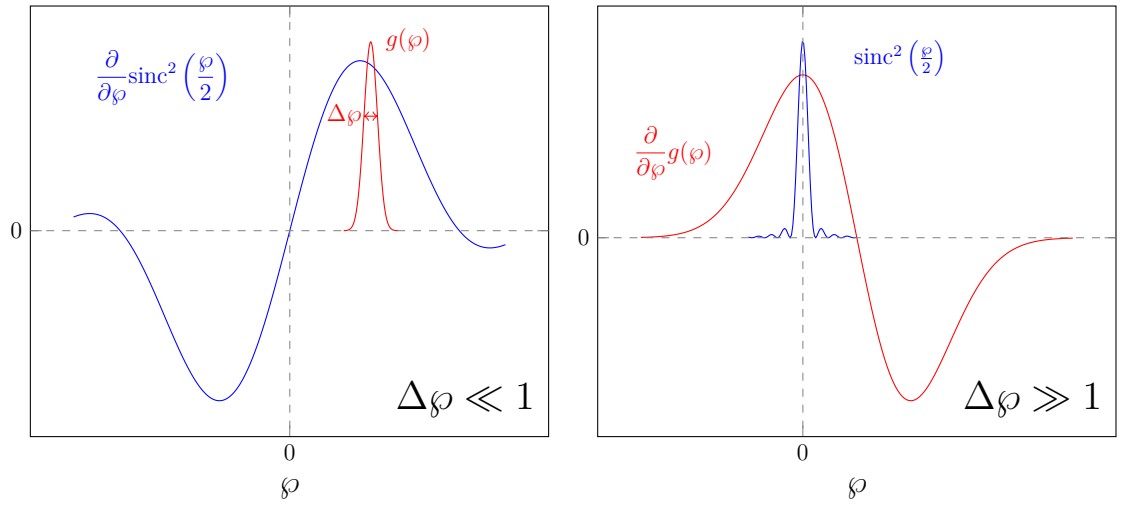

Figure 2.8: Comparison of a cold (left) and a warm (right) electron beam. For a small momentum spread $\Delta\wp \ll 1$ the distribution function acts like a delta function in Eq. (2.58) and we easily evaluate the integral of $\partial\mathrm{sinc}^2(\wp/2)/(\partial\wp)$. In contrast, for $\Delta\wp \gg 1$ the sinc^2-function behaves like a delta function for $\partial g/(\partial\wp)$ in Eq. (2.58).

which is shown in Fig. 2.7. Due to the motion in the potential modulations of the distribution function in position as well as in momentum have emerged which stand in contrast to the uniform position distribution prior to interaction.

We calculate the gain of the laser field, Eq. (2.18), by integrating Eq. (2.50) with respect to time $\bar{\tau}$ and obtain

$$G = -gTN\kappa \int_{\tau}^{\tau+1} \mathrm{d}\bar{\tau} \int_{0}^{2\pi} \mathrm{d}\theta \int \mathrm{d}\wp \sin\theta \, \frac{\cos\left[\theta - \wp(\bar{\tau}-\tau)\right] - \cos\theta}{\wp} \frac{1}{2\pi} g(\wp)\,, \tag{2.57}$$

where the averaging over the phase θ is performed by noting that the terms which include $\langle \sin\theta \sin\theta \rangle_{\theta^{(\mathrm{in})}} = 1/2$ give the only nonzero contribution while the terms with $\langle \sin\theta \cos\theta \rangle_{\theta^{(\mathrm{in})}} = 0$ vanish.

Hence, we are left with the expression

$$\begin{aligned} G &= \frac{gTN\kappa}{2} \int_{\tau}^{\tau+1} \mathrm{d}\bar{\tau} \int \mathrm{d}\wp \frac{\sin\left[\wp(\bar{\tau}-\tau)\right]}{\wp} \frac{\partial}{\partial\wp} g(\wp) \\ &= \frac{gTN\kappa}{4} \int \mathrm{d}\wp \, \mathrm{sinc}^2\left(\frac{\wp}{2}\right) \frac{\partial}{\partial\wp} g(\wp)\,, \end{aligned} \tag{2.58}$$

where we have explicitly performed the integration with respect to time in the second step.

So far, we have only considered the situation of a monoenergetic electron beam. However, in the experimental situation, the electron accelerator always produces an electron beam with a nonzero momentum width $\Delta\wp$. As we show later in this thesis this fact is of utmost importance in order to observe quantum effects in the FEL.

Our current approach is only justified in the limit of $\Delta\wp \ll 1$ which we define as the 'cold beam' limit. In this case $g(\wp)$ acts like a delta function, $g(\wp) \cong \delta(\wp - \bar{\wp})$, in the integral of Eq. (2.58), as can be seen from Fig. 2.8, and we arrive at the same result for the gain as before, that is

$$G = -\frac{gTN\kappa}{4}\frac{\partial}{\partial\wp}\mathrm{sinc}^2\left(\frac{\wp}{2}\right)|_{\wp=\bar{\wp}}\,, \tag{2.59}$$

where we have integrated by parts, have applied trigonometric identities and have used the fact that the momentum distribution function vanishes at infinity, that is $g(\wp \to \pm\infty) = 0$.

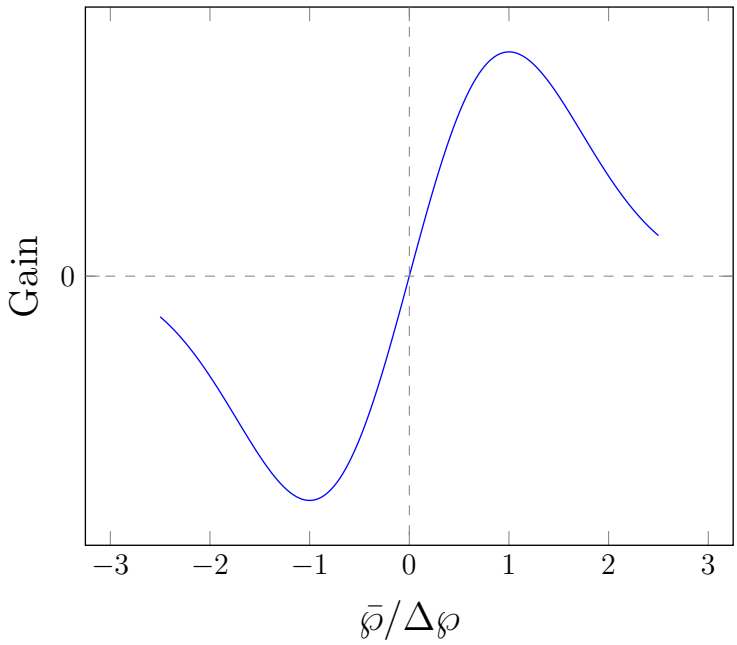

Figure 2.9: Gain of the low-gain small-signal FEL, Eq. (2.60), for a warm electron beam as a function of mean momentum $\bar{\wp}$ of the initial distribution $g(\wp)$ given by a Gaussian. The extreme values for the gain are located at $\bar{\wp} = \pm\Delta\wp$.

The other extreme limit is the one of a 'warm beam', where we have a broad momentum distribution with $\Delta\wp \gg 1$. In this case the function $\mathrm{sinc}^2(x/2)$ can be approximated by a delta function [51], that is $\mathrm{sinc}^2(\wp/2) \cong \delta(\wp - \bar{\wp})$, in Eq. (2.58) (see Fig. 2.8) and we obtain

$$G = \frac{gTN\kappa}{2}\frac{\partial g(\wp)}{\partial\wp}|_{\wp=0} \tag{2.60}$$

which is drawn in Fig. 2.9 for a Gaussian distribution $g(\wp)$. At first sight, the form of this curve is very similar to the one of the cold beam limit in Fig. 2.6. However, the maximum and minimum gain occur at $\bar{\wp} = \Delta\wp$ and $\bar{\wp} = -\Delta\wp$, respectively, instead of $\bar{\wp} \cong \pm\pi$ for a cold beam.

In conclusion, we have illustrated how two different approaches, that is (i) following the trajectories of each electron and (ii) considering the distribution function for an ensemble of electrons lead to the same result for the gain, Eq. (2.46), of the low-gain FEL in the small-signal limit. Moreover, we have identified two different limits of this gain regime depending on the momentum spread $\Delta\wp$ of the electrons.

2.3.2 Saturated low-gain regime

In the small-signal regime the field acts like a small perturbation on the dynamics of the electrons. When we increase the interaction time or the field strength this assumption is not justified any longer. The electrons follow a periodic motion and at a certain time they do not emit but *absorb* radiation from the field [57] and saturation of the field occurs. That is why this regime is often referred to as 'saturated FEL' [51, 66].
According to Ref. [51] we interpret this situation such that the energy of the electrons is much smaller than the height of the standing wave potential and the main contributions to the change of the field come from the electrons close to the wells of the cosine potential. Therefore, we perform the transformation

$$\theta_j \equiv \psi_j + \pi \tag{2.61}$$

shifting the origin of our coordinate to such a well. For a large potential height we make a Taylor approximation of the potential and arrive from Eq. (2.38) at the equation of motion

$$\ddot{\psi}_j = -\mu \sin\psi_j \cong -\mu\psi\left(1 - \frac{1}{6}\psi_j^2\right) \tag{2.62}$$

for an electron which is analogous to an anharmonic oscillator. In Eq. (2.62) we have defined the saturation parameter $\mu \equiv \sqrt{\kappa|a_\mathrm{L}|}$ which is large, that is $\mu \gg 1$, in the limit of a saturated FEL [51].
With the help of the transformations $b_j \equiv (2\mu)^{-1/2}(\psi_j + (i/\mu)\wp_j)$ and $b = B\,\mathrm{e}^{-i\mu(\bar{\tau}-\tau)}$ in analogy to our procedure for the classical laser in Sec. 2.2.1 we arrive at the relation

$$\dot{B}_j = \frac{i}{8}|B_j|^2 B_j\,, \tag{2.63}$$

where we have neglected rapidly varying contributions.
Similar to Eq. (2.19) the solution of Eq. (2.63) is given by $B_j = B_j^{(\mathrm{in})}\,\mathrm{e}^{i|B_j^{(\mathrm{in})}|^2(\bar{\tau}-\tau)/8}$ and the back transformation to the initial variables yields the expression

$$\wp_j = -\mu\psi_j^{(\mathrm{in})}\sin\left(\mu - \frac{\bar{\wp}^2}{16} - \mu\frac{\theta_j^{(\mathrm{in})2}}{16}\right) + \bar{\wp}\cos\left(\frac{\bar{\wp}^2}{16} - \mu\frac{\theta_j^{(\mathrm{in})2}}{16}\right) \tag{2.64}$$

for the momentum of an electron right at the end of the interaction, where we have assumed that the initial momentum is the same for all electrons, that is $\wp_j^{(\mathrm{in})} = \bar{\wp}$ while the initial phases $\psi_j^{(\mathrm{in})}$ are uniformly distributed.
In order to calculate the gain we employ Eq. (2.40) and equate the change of the laser field with the change of the average momentum of the electrons. By averaging over the initial phases we find the nonzero contributions [67]

$$\frac{1}{2\pi}\int_{-\infty}^{\infty}\mathrm{d}\theta^{(\mathrm{in})}\sin\left(\mu\frac{\theta^{(\mathrm{in})2}}{16}\right) = \frac{1}{2\pi}\int_{-\infty}^{\infty}\mathrm{d}\theta^{(\mathrm{in})}\cos\left(\mu\frac{\theta^{(\mathrm{in})2}}{16}\right) = \sqrt{\frac{2}{\pi\mu}}\,, \tag{2.65}$$

where we have extended the limits of integration to minus and plus infinity.

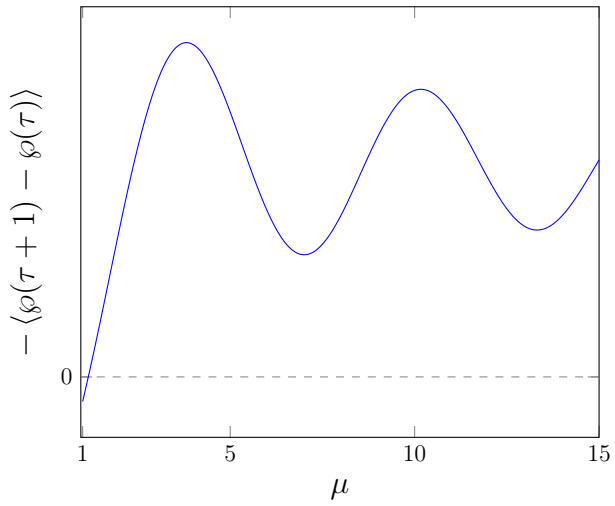

Figure 2.10: Change of the average momentum of the electrons as function of the saturation parameter $\mu \equiv \sqrt{\kappa|a_{\mathrm{L}}|}$ in the saturated regime, Eq. (2.67), that is $\mu \gg 1$. Indeed, the growth of the energy transfer to the field saturates and we obtain oscillations.

With the help of Eqs. (2.18) and (2.40) we arrive at

$$G = -\frac{gTN}{\mu^2|a_{\mathrm{L}}|}\left\langle \wp(\tau+1)-\wp(\tau)\right\rangle \tag{2.66}$$

and by employing the identity $\sqrt{2}\cos(\alpha-\pi/4) = \sin\alpha + \cos\alpha$ we finally obtain the expression [51]

$$G = -\frac{gTN}{\mu^2|a_{\mathrm{L}}|}\bar{\wp}\left\{1-\frac{2}{\sqrt{\pi\mu}}\cos\left[\mu\left(1-\frac{\bar{\wp}^2}{16\mu^2}\right)-\frac{\pi}{4}\right]\right\} \tag{2.67}$$

for the saturated gain of the classical FEL in the low-gain regime. The average change of electron momentum is drawn in Fig. 2.10 as a function of the saturation parameter μ. Indeed, for increasing values of μ the energy transfer to the field saturates and eventually shows an oscillatory behavior.
In accordance to Ref. [51] we estimate the magnitude of G in the saturated regime by setting $\bar{\wp} = \mu$ and neglecting the oscillatory part of Eq. (2.67). Hence, we obtain

$$G \cong \frac{gTN}{\sqrt{\kappa}|a_{\mathrm{L}}|^{3/2}} \tag{2.68}$$

which decreases for increasing magnitudes of the field amplitude.

2.3.3 High-gain FEL: the many-electron model

Up to now we have thoroughly discussed the low-gain regime for the FEL. However, many FELs in experiment are operating in a different limit: the high-gain regime [19, 20, 21, 68, 69, 70]. Additionally, to achieve the SASE mode, and thus to build X-ray FELs [23], one *has* to consider the high-gain case.

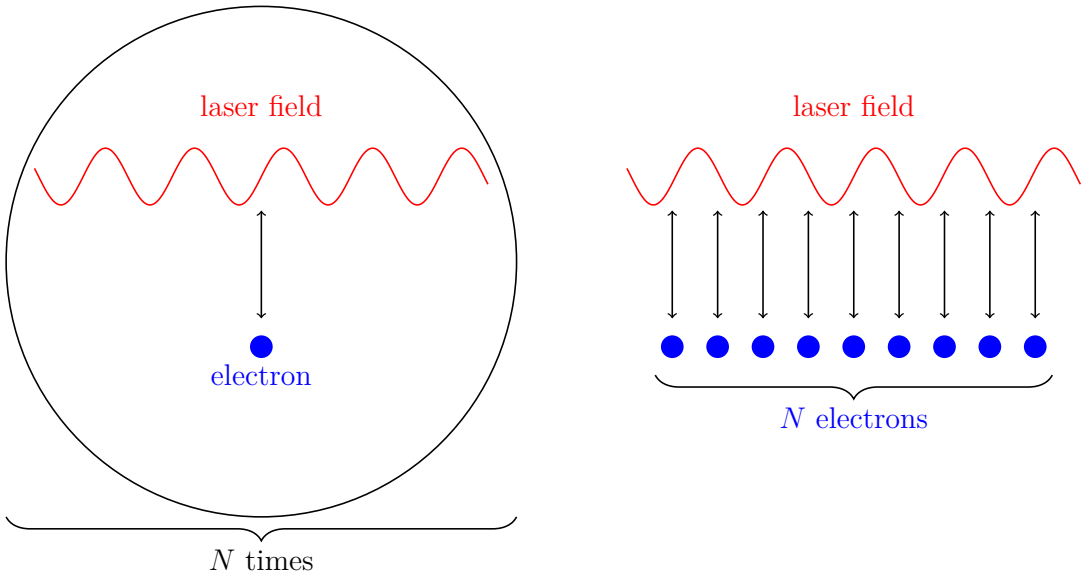

Figure 2.11: Difference between the single-electron limit (left) for the low-gain FEL and the many-electron model (right) for the high-gain regime. In the former case we just consider the interaction between a single electron with the laser field and multiply the result with the number N of electrons in the bunch. In contrast, the many-particle theory describes the *collective* interaction of all N electrons with the laser field. Hence, the motion of an electron is affected by the dynamics of all other electrons via the laser field. We emphasize that this collective effect must not be confused with the effect of space charge due to the Coulomb force between the electrons which is neglected here.

From the theoretical viewpoint the main difference between a high and a low gain is that for a high-gain FEL a many-electron theory is mandatory. The change of the laser field during the interaction of a single electron bunch is not negligible any longer and this change of the field couples to the motion of the electrons making a self-consistent approach necessary. So to say the electrons interact via the laser field with each other, which is depicted in Fig. 2.11.

We emphasize that the collective effect described here is different from the effect of space charge, that is the Coulomb force between the electrons, which is a direct interaction of the electrons. For high densities we have to include this effect and find a slightly different behavior. Therefore, one distinguishes between the 'Compton regime', without any space charge effects, and the 'Raman regime', which includes these effects [62, 71]. For the time being we concentrate on the Compton regime.

To reduce our calculational effort we first make a Galilei transformation into a frame of reference which moves with the initial average velocity of the electrons, in dimensionless variables given by $\bar{\wp}$. Thus, by following the prescription

$$\begin{cases} \theta_j & \to \theta_j - \bar{\wp}\tau \\ \wp_j & \to \wp_j - \bar{\wp} \\ a_\mathrm{L} & \to a_\mathrm{L}\, \mathrm{e}^{i\bar{\wp}\tau} \end{cases} \tag{2.69}$$

Eqs. (2.35) and (2.37) transform to

$$\begin{aligned} \dot{\theta}_j &= \wp_j \\ \dot{\wp}_j &= -\frac{\kappa}{2i}\left(a_\mathrm{L}\, \mathrm{e}^{i\theta_j} - a_\mathrm{L}^*\, \mathrm{e}^{-i\theta_j}\right) \\ \dot{a}_\mathrm{L} &= -igTN\left\langle \mathrm{e}^{-i\theta}\right\rangle + i\bar{\wp}\, a_\mathrm{L} \end{aligned} \tag{2.70}$$

which have to be solved self-consistently.

To make connection with the theory of the high-gain Quantum FEL, presented later in this thesis, we follow the approach of *collective variables* introduced in Refs. [21, 72]. We define

$$\begin{cases} B & \equiv \left\langle \mathrm{e}^{-i\theta}\right\rangle \\ P & \equiv \left\langle \wp\, \mathrm{e}^{-i\theta}\right\rangle \end{cases} \tag{2.71}$$

and by means of Eq. (2.70) we arrive at

$$\begin{aligned} \dot{B} &= -iP \\ \dot{P} &= -\frac{\kappa}{2i}a_\mathrm{L} + \frac{\kappa}{2i}a_\mathrm{L}^*\left\langle \mathrm{e}^{-i2\theta}\right\rangle - i\left\langle \wp^2\, \mathrm{e}^{-i\theta}\right\rangle \\ \dot{a}_\mathrm{L} &= i\bar{\wp}\, a_\mathrm{L} - igTNB \end{aligned} \tag{2.72}$$

which has the disadvantage of not being a closed set of equations making it impossible to find an analytic solution for the whole range of parameters.

Small-signal regime

Just as for the low-gain case, we investigate specific limits of the interaction. If we consider the small-signal limit, we make the approximation that the change of the variables during the interaction is small, that is

$$\begin{cases} \theta_j & \cong \theta_j^{(\mathrm{in})} + \delta\theta_j \\ \wp_j & \cong \delta\wp_j \\ a_\mathrm{L} & \cong \delta a_\mathrm{L} \end{cases} \tag{2.73}$$

where $\delta\theta_j$, $\delta\wp_j$ δa_L are first-order quantities. We assume that the initial amplitude of the laser field is small. Thus, in contrast to the low-gain case, the gain during a single pass of electrons can reach comparable high values.

The collective variables, introduced in Eq. (2.71), then reduce to

$$\begin{cases} B & \cong \langle -i\delta\theta\, \mathrm{e}^{-i\theta^{(\mathrm{in})}} \rangle \equiv \delta B \\ P & \cong \langle \delta\wp\, \mathrm{e}^{-i\theta^{(\mathrm{in})}} \rangle \equiv \delta P\,, \end{cases} \tag{2.74}$$

where we have inserted the small-signal approximation, Eq. (2.73), expanded the exponential $\mathrm{e}^{-i\delta\theta_j}$ to first order in $\delta\theta_j$, have taken into account that $\langle \mathrm{e}^{-\theta^{(\mathrm{in})}} \rangle = 0$ and have neglected terms with $\delta\wp_j\delta\theta_j$.

Hence, the equations of motion for the collective variables, Eq. (2.72), read in this approximation

$$i\frac{\mathrm{d}}{\mathrm{d}\tau}\begin{pmatrix} \delta B \\ \delta P \\ \delta a_\mathrm{L} \end{pmatrix} = \begin{pmatrix} 0 & 1 & 0 \\ 0 & 0 & \kappa/2 \\ gTN & 0 & -\bar{\wp} \end{pmatrix} \cdot \begin{pmatrix} \delta B \\ \delta P \\ \delta a_\mathrm{L} \end{pmatrix}\,, \tag{2.75}$$

where we have again neglected second order terms and have encountered vanishing terms like $\langle \mathrm{e}^{-2i\theta^{(\mathrm{in})}} \rangle$.

We finally arrived at a linearized set of differential equations which can easily be solved with the ansatz $\sim \mathrm{e}^{-i\lambda\tau}$ yielding the characteristic equation [21]

$$\lambda^2(\lambda + \bar{\wp}) - \frac{gTN\kappa}{2} = 0\,. \tag{2.76}$$

This cubic equation has three solutions, and for a certain range of values of $\bar{\wp}$ two of them possess a nonzero imaginary part. This imaginary part occurs in both solutions with a different sign and the positive one is responsible for an exponential growing field $\sim \mathrm{e}^{|\mathrm{Im}\lambda|}$.

The positive imaginary part of λ depending on the initial momentum $\bar{\wp}$ is shown in Figure 2.12 and we identify this curve as the gain function of the high-gain FEL. We observe that $|\mathrm{Im}\lambda|$ reaches its maximum at $\bar{\wp} = 0$ and thus there the gain is also maximized. This stands in strong contrast to the low-gain regime, where the largest gain is achieved at $\bar{\wp} \cong \pi$ and even vanishes at $\bar{\wp} = 0$. Hence, we clearly identify here a substantive difference between the single-particle and the many-particle approach.

For $\bar{\wp} = 0$, which we define as the resonance for the high-gain FEL, Eq. (2.76) simplifies and we find the analytic solution

$$\mathrm{Im}\lambda = \pm\frac{\sqrt{3}}{2}\left(\frac{gTN\kappa}{2}\right)^{1/3} \tag{2.77}$$

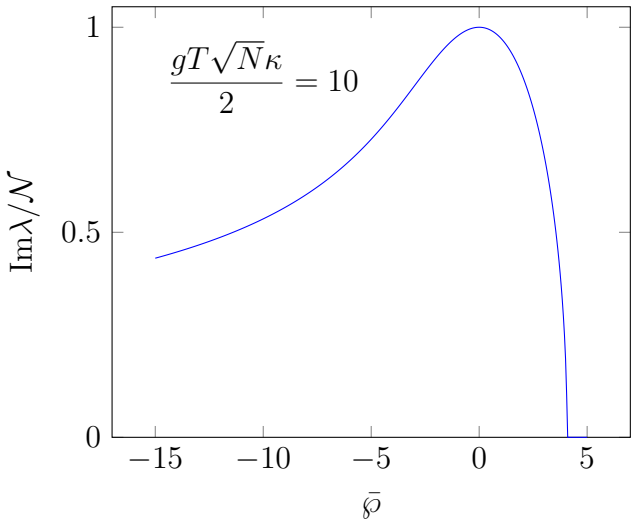

Figure 2.12: Normalized modulus of Imλ as a function of the initial Doppler parameter $\bar{\wp} \equiv 2k\bar{p}T/m$. We interpret this curve as gain function of the high-gain FEL since a nonzero value of Imλ is responsible for exponential gain. In contrast to the low-gain small signal case, Eq. (2.46), the gain is maximized at $\bar{\wp} = 0$. For the numerical solution of the characteristic equation, Eq. (2.76), we have assumed $gT\sqrt{N}\kappa/2 = 10$.

for the increment of the gain.

It is often convenient to rewrite the gain in terms of the position $z \approx ct$ of the electrons instead of the time $\tau \equiv t/T$. By this procedure we arrive at the form $\mathrm{e}^{z/L_\mathrm{g}}$ of the intensity growth, where the gain length

$$L_g \equiv c\left(\frac{2m}{(2k)^2 gNU_0}\right)^{1/3} \tag{2.78}$$

is a measure of how quick the laser field is amplified in the wiggler. We recognize that the gain length scales with $N^{-1/3}$. Thus, if we increase for a fixed wiggler length L the number N of electrons the gain of the FEL also increases, which we would expect from intuition.

According to Refs. [21, 48] the exponential gain in the high-gain regime reduces to the linear Madey gain for a short interaction time, yielding the condition

$$L \ll L_g \tag{2.79}$$

for the length L of the wiggler. This constraint, thus, defines the range of validity for the low-gain approximation.

We have studied the high-gain FEL within an approach [21] based on collective variables. However, we could have also employed a model [48] in phase space, where the electron dynamics is dictated by a Vlasov equation. Both approaches lead to equivalent results, that is the cubic equation Eq. (2.76), just like in the low-gain, small-signal limit.

Saturation

Similar to the low-gain case, at some point the laser field saturates. After a couple of gain lengths the exponential growth vanishes and the laser intensity stays more ore less constant [48]. For a growing laser field the height of the potential also increases. As a result, the electrons follow a self-organization process and accumulate in the wells of this potential, an effect which is known as microbunching [48]

To estimate the field intensity at saturation we assume that the electrons are perfectly bunched at the potential wells, that is at $\theta = \pi, 3\pi, 5\pi, ...$, leading to $B = -1$ in Eq. (2.72) for the 'bunching factor' [70], defined in Eq. (2.71). Estimating the growth of the field amplitude a_{L} with the rate λ in the linearized regime, that is $\dot{a}_{\mathrm{L}} \cong -i\lambda a_{\mathrm{L}}$, we arrive at [48]

$$\lambda a_{\mathrm{L}} = -gTN\,. \tag{2.80}$$

Thus, we obtain

$$|a_{\mathrm{L}}^{\mathrm{sat}}|^2 \cong \left(\frac{2mg^2}{(2k)^2 U_0}\right)^{2/3} N^{4/3} \tag{2.81}$$

for the dimensionless intensity of the field at saturation which scales with $N^{4/3}$. According to Ref. [73] the saturation sets in at $L_{\mathrm{sat}} \cong 4\pi\sqrt{3}L_g$ if the laser has started from vacuum.

Self-amplified spontaneous emission

For radiation in the X-ray regime there do not exist suitable mirrors to build cavities. Moreover, it is difficult to realize a suitable seeding field which could be amplified by the FEL [48]. That is why the realization of X-ray FELs in experiment [23] relies on the concept of self-amplified spontaneous emission (SASE) [21, 68, 74, 75, 76].

In this mode of operation the laser field starts from vacuum due to spontaneous emission or density fluctuations in the electron beam [48]. Since no cavity is present this radiation has to be considerably amplified in a single passage of the electrons through a long wiggler, that is the high-gain regime.

Instead of a perfectly uniform distribution of the electrons along the wiggler axis one has to consider randomly distributed electrons [70]. Indeed, the electron beam has to be modeled such that the initial mean value of B is zero, that is $\langle B(0)\rangle = 0$, but not the second moment, which gives $\langle B\rangle = 1/N$, where the average is over all possible ensembles. Since randomness is of major importance for a SASE FEL the emitted radiation shows a chaotic behavior with a noisy and spiky spectrum [48, 75, 76].

In this context, we also mention the effect of slippage [62, 75, 77] of the radiation field over the electrons. This slippage occurs since light is always faster than the electrons moving at a velocity $v \lesssim c$ and hence the light pulse slips ahead with the distance of $N_W\lambda_{\mathrm{L}}$ in comparison to the electrons, where N_{W} is the number of wiggler periods. To obtain this effect in the equations of motion for the electron and the laser field we have to consider a relativistic theory and replace the total time derivative by [62]

$$\frac{\mathrm{d}}{\mathrm{d}t} \to \frac{\partial}{\partial t} + \bar{v}\frac{\partial}{\partial z} \tag{2.82}$$

for the electron positions z_j and momenta p_j, respectively, where we have introduced the mean velocity $\bar{v}$ in the z-direction while we have to apply

$$\frac{\mathrm{d}}{\mathrm{d}t} \to \frac{\partial}{\partial t} + c\frac{\partial}{\partial z} \tag{2.83}$$

for the dynamics of the amplitude a_L of the laser field.

According to Ref. [75] we have to distinguish between a long and a short electron bunch due to the influence of slippage. For this purpose, the authors of Ref. [75] defined the 'cooperation length' $L_\mathrm{c} \equiv (\lambda_\mathrm{L}/\lambda_\mathrm{W})L_\mathrm{g}$ which has to be compared with the length L_b of the bunch. For a long bunch, that is $L_\mathrm{b} \gg L_\mathrm{c}$, the exponential gain, discussed in the preceding section, is observed which is not the case for the opposite limit $L_\mathrm{b} \ll L_\mathrm{c}$ [75]. However, even for a long bunch the slippage leads to fluctuations of the intensity and spikes in the spectrum [75].

2.3.4 Raman regime: effect of space charge

So far, we have neglected the Coulomb interaction between the electrons in the beam. However, when the density of the electron beam is high enough this effect becomes relevant [20, 62, 71, 78, 79, 80]. In the high-density limit we obtain another regime of FEL operation, which is sometimes called the 'Raman regime' to contrast it from the small-density case which is known as 'Compton regime' [62].

An important quantity which we have to introduce in this context is the plasma frequency for the electron beam [64]

$$\omega_\mathrm{p}^2 \equiv \frac{e^2}{\varepsilon_0 m} n_\mathrm{e} \tag{2.84}$$

which depends on the electron density $n_\mathrm{e} \equiv N/V$ of the electrons in the bunch.

For the investigation of the Raman regime an approach [20, 48] using the Vlasov equation is best suited. The resulting characteristic equation for the high-gain small-signal regime reads [20]

$$(\lambda - \omega_\mathrm{p} T)\,(\lambda + \omega_\mathrm{p} T)\left(\lambda + \bar{\wp} - \frac{\omega_\mathrm{p}^2 T}{2ck}\right) = \frac{gTN\kappa}{2} \tag{2.85}$$

which reduces to the one of the Compton regime when we let $\omega_\mathrm{p} \to 0$. The gain length in the Raman limit can be estimated [20] by

$$L_g^\mathrm{ram} = (2\sqrt{3})^{3/2}\sqrt{\frac{\omega_\mathrm{p}}{c}}\left(L_g^\mathrm{com}\right)^{3/2}, \tag{2.86}$$

where we have added the superscripts ram and com to distinguish Raman and Compton regime, with L_g^com given by Eq. (2.78).

For an X-ray FEL the effect of space charge usually is not of importance [48] and it thus operates in the Compton regime. According to Ref. [48] neglecting Coulomb interaction is justified when the condition

$$k_\mathrm{p} \ll \frac{1}{L_g^\mathrm{com}} \tag{2.87}$$

is satisfied. The parameter

$$k_p \equiv \frac{1}{\gamma_0 c}\omega_{\mathrm{p}}^* \tag{2.88}$$

is defined in the laboratory frame, where the expression for the plasma frequency $\omega_{\mathrm{p}}^* \equiv \sqrt{n_{\mathrm{e}}e^2/(\varepsilon_0\gamma_0 m_0)}$ differs from the one, Eq. (2.84), in the co-moving frame by the factor $\gamma_0^{-1/2}$ due to relativistic length contraction.

3 The Quantum–Classical Transition Illustrated by the FEL Gain

In the preceding chapter we have studied in detail the classical theory of the FEL which is sufficient to describe all operating devices. However, since quantum mechanics is the more fundamental theory we expect that the range of validity of classical physics is just an extreme limit of the FEL interaction and that at some point quantum effects have to appear.
We first discuss this transition from classical to quantum in an illustrative approach in phase space [4] which compares classical trajectories with discrete momentum steps due to Compton scattering. This procedure allows us to identify the important parameters for quantum effects to emerge. In this context we demand (i) for a high value of the quantum mechanical recoil the electron experiences due to the scattering with the wiggler and the laser field and (ii) for a small momentum spread of the electron beam.
In the following discussion we restrict ourselves to the gain of the laser field and thus consider a semiclassical approach where the electrons are quantized and the field is treated classically in analogy to semi-classical laser theory [22, 55]. To calculate the gain including quantum corrections we employ two different methods, that is (i) solving the quantized pendulum equation in the Heisenberg picture and (ii) studying the dynamics of the Wigner distribution function [40] for the electron in analogy to the classical distribution function in phase space. Since we just consider the low-gain small-signal limit we are allowed to treat the dynamics in a perturbative manner according to the preceding chapter. The results of these calculations justify the predictions of our heuristic approach, namely, that we require, both, a high recoil *and* a small momentum spread in order to obtain quantum effects in the FEL.

3.1 Classical trajectories vs. Compton scattering

Before we investigate the transition from classical to quantum in the FEL in a rigorous manner and explicitly calculate the quantum corrections to the classical gain, we try to understand this transition from a heuristic description in phase space. This discussion is already presented in Ref. [4].
On a microscopic level the interaction in the FEL can be described as 'stimulated Compton scattering' [50]. Either a wiggler photon with momentum $\hbar k_{\mathrm{W}}$ is annihilated by the electron and a laser photon with $\hbar k_{\mathrm{L}}$ is created ('emission') while the electron is decelerated or the opposite process occurs and a laser photon is annihilated ('absorption'). Both processes are shown in Fig. 3.1.
Whether emission or absorption, in any case the change of the electron momentum is given by the quantum mechanical recoil

$$q \equiv \hbar(k_{\mathrm{L}} + k_{\mathrm{W}}) = 2\hbar k\,, \tag{3.1}$$

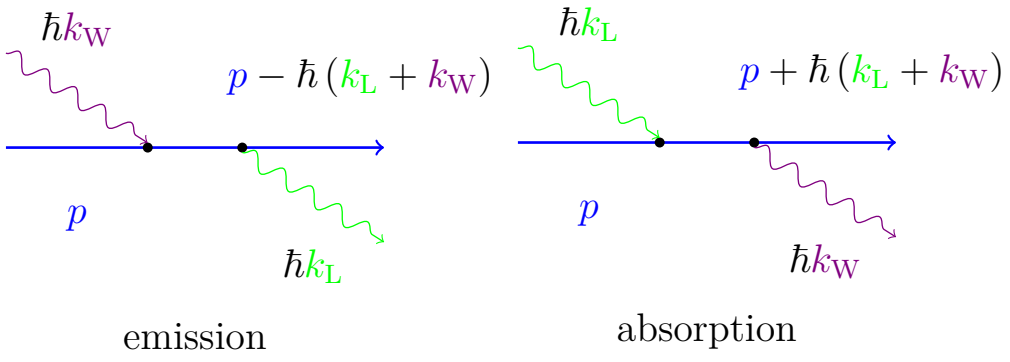

Figure 3.1: Discrete momentum steps of the electron in the FEL: a wiggler photon with momentum $\hbar k_\mathrm{W}$ is annihilated and a laser photon is created, that is 'emission', with the electron decelerating by a momentum recoil of $\hbar(k_\mathrm{L} + k_\mathrm{W})$ (left) and the opposite process, that is 'absorption', where the electron gains the momentum $\hbar(k_\mathrm{L} + k_\mathrm{W})$.

where the second equality holds only true in the Bambini–Renieri frame, or by an integer multiple of q. Hence, we expect a discrete momentum ladder to characterize the dynamics of the electron in the FEL.

However, in the preceding chapter we have understood the gain mechanism in the FEL completely in terms of classical physics and have described the electron motion by smooth trajectories. How can we connect this classical approach with the discrete momentum steps due to Compton scattering?

We answer this question by realizing that for the classical FEL the recoil q has to be *small* and thus we obtain a continuum of momentum levels yielding the effectively continuous trajectories as shown on the left-hand side of Fig. 3.2. During the interaction with the wiggler each electron emits or absorbs many laser photons [51, 81] and hence the change of the momentum occurs on a classical scale.

In contrast, for quantum effects to be visible the recoil q has to be very *large* and in the deep quantum regime it even has to be the dominating momentum scale. This situation is shown on the right-hand side of Fig. 3.2 where we obtain discrete momentum steps instead of classical trajectories [4]. Moreover, we deduce that in this case, where quantum effects become relevant, each electron emits or absorbs just a few photons.

We quantify our statement of a small or a large recoil by considering the magnitude of the Doppler parameter $\wp \equiv 2kpT/m$, defined in Eq. (2.34) as typical scale for the FEL dynamics. When we set $p = \hbar k$ in the definition for $\wp$ we arrive at the parameter $\omega_\mathrm{r} T$ where we have introduced the recoil frequency

$$\omega_\mathrm{r} \equiv \frac{2\hbar k^2}{m} = \frac{1}{\hbar}\frac{q^2}{2m} \tag{3.2}$$

which is the energy $q^2/(2m)$ associated to the recoil divided by $\hbar$. Since $\omega_\mathrm{r} T$ is proportional to $\hbar$ we expect that for $\omega_\mathrm{r} T \ll 1$ the classical description of the FEL is valid while for increasing recoil, that is $\omega_\mathrm{r} T \sim \mathcal{O}(1)$, quantum effects start to emerge. This parameter $\omega_\mathrm{r} T$ was already found in Ref. [35] by solving the Schrödinger equation and identifying the classical and the quantum limit of the FEL.

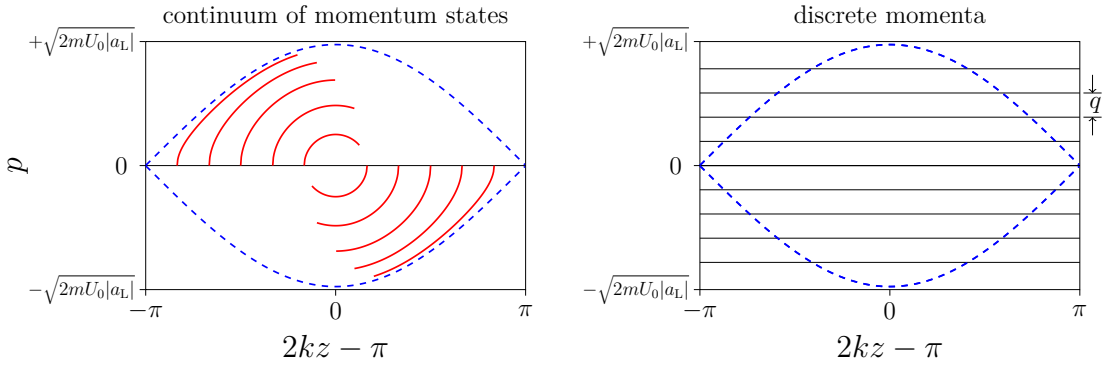

Figure 3.2: Dynamics of the electron in phase space (z, p) for the classical (left) and quantum regime (right) of the FEL: in the classical limit the recoil q, Eq. (3.1), is small and the electron follows continuous trajectories. In contrast, the electron momentum changes by discrete steps, separated by q, when quantum mechanics become relevant, that is for increasing values of q. The separatrix which divides bounded from unbounded motion is indicated by the blue line and spans from $-\sqrt{2mU_0|a_L|}$ to $+\sqrt{2mU_0|a_L|}$ along the momentum axis. This figure is adapted from Ref. [4].

When we even assume that the recoil is the dominating momentum scale and we enter the quantum regime we have to compare q with the typical scale of the classical dynamics in the FEL. From Fig. 3.2 we identify this quantity with the help of the separatrix which is the border between bounded and unbounded motion. The maximum momentum that is covered by the separatrix is given by $\sqrt{2mU_0|a_L|}$, which depends on the potential height $U_0|a_L|$ of the ponderomotive potential.

Hence, we define the ratio of the potential height and of the recoil energy $q^2/2m$ as the quantum parameter

$$\alpha \equiv \frac{U_0|a_L|/2}{q^2/2m} \tag{3.3}$$

in accordance with Ref. [4]. For $\alpha \ll 1$ we expect to be in the deep quantum regime, where classical physics does not matter any more.

It is convenient to rewrite the quantum parameter

$$\alpha \equiv \frac{g\sqrt{n}}{\omega_r} \tag{3.4}$$

in terms of two frequencies, where we have defined the coupling strength $g \equiv U_0/\hbar$, have identified the amplitude $|a_L|$ as the square root $\sqrt{n}$ of the photon number n, or dimensionless intensity, of the laser field and have employed the definition of the recoil frequency, Eq. (3.2). This form of the quantum parameter, Eq. (3.4), is also found in Chap. 5 of this thesis by a rigorous quantum mechanical approach. We note that this quantity, moreover, is analogous to the parameter $\bar{\rho}$ in Ref. [3] as discussed in Ref. [4].

However, just increasing the recoil q is not the full story. A second condition to observe quantum effects for the FEL emerges when we consider the initial state of the electron beam.

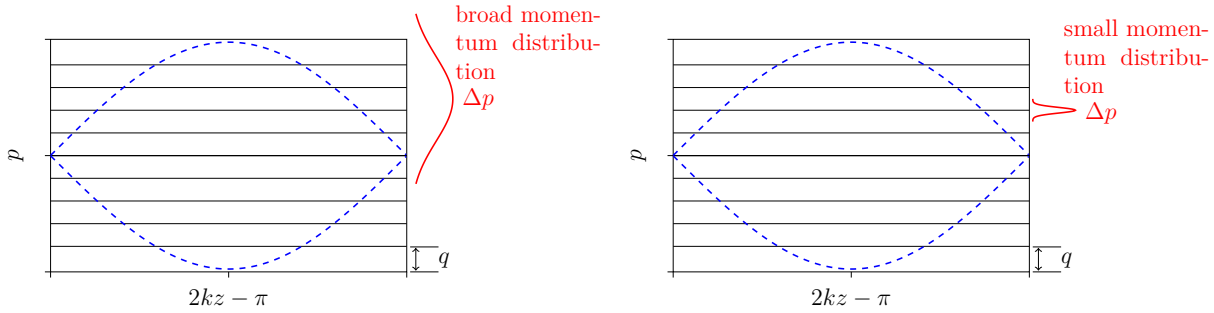

Figure 3.3: The phase space (z, p) describing the electron motion in the FEL in the regime of high recoil q. In this limit the dynamics is given by a discrete momentum ladder with steps separated by q. When the width Δp of the initial momentum distribution of the electron covers many steps of the ladder (left) there are no quantum effects. Hence, we require a width Δp (right) which is smaller than a single step q, Eq. (3.5), to observe quantum effects in the FEL dynamics.

An electron bunch always possesses an energy spread when it leaves the accelerator which in our model translates to a momentum distribution with a nonzero width Δp.
When we assume that this width is large and covers many steps of the momentum ladder, the situation on the left-hand side of Fig. 3.3 emerges. In this case, we argue that the large width prevents the emergence of quantum effects since the discreteness of the momenta is 'washed out' [4].
Hence, to observe quantum effects we demand that the width Δp of the initial momentum distribution is confined to a single step of the momentum ladder characterized by the recoil q and is shown on the right-hand side of Fig. 3.3. Thus, we require

$$\Delta p < q \tag{3.5}$$

to observe quantum effects in the FEL in analogy to Ref. [4]. We note that the upper limit for the momentum spread in Eq. (3.5) is the most difficult obstacle to obtain quantum effects for the FEL in an experiment, at least in our one-dimensional model.
We emphasize that we have made use of the concept of photons in the discussion about Compton scattering just because it is very intuitive, but for the description of quantum effects in the FEL it is not necessary at all. It is even wrong to think that quantum mechanics arises in the FEL due to the properties of a quantized *light field*: it is the *electron* dynamics in which the transition from classical to quantum physics becomes apparent.
In contrast to the classical position z and momentum p of an electron, the quantum mechanical operators $\hat{z}$ and $\hat{p}$, respectively, do not commute. It is the commutation relation $[\hat{z}, \hat{p}] = i\hbar$ for these operators that leads to quantum effects. We prove this statement in the later course of this chapter when we compute the quantum corrections to the classical gain formula. The quantized version of the single-electron Hamiltonian, Eq. (2.31), then reads

$$\hat{H} = \frac{\hat{p}^2}{2m} + \frac{U_0}{2}\left(a_\mathrm{L}\,\mathrm{e}^{i2k\hat{z}} + a_\mathrm{L}^*\,\mathrm{e}^{-i2k\hat{z}}\right) \tag{3.6}$$

which describes a semiclassical model since the laser field is not quantized.

When we investigate the action of the Hamiltonian, Eq. (3.6), on a quantum mechanical state we observe terms of the form

$$\mathrm{e}^{\pm i2k\hat{z}}\,|p\rangle = \int \mathrm{d}z\,\langle z|p\rangle\,\mathrm{e}^{\pm i2kz}\,|z\rangle\ , \tag{3.7}$$

where we have expanded the momentum eigenstate $|p\rangle$ with eigenvalue p in terms of the position eigenstates $|z\rangle$ satisfying $\hat{z}\,|z\rangle = z\,|z\rangle$. Since momentum in position representation constitutes a plane wave, that is $\langle z|p\rangle \sim \mathrm{e}^{izp}$ [40], we obtain the relation [82]

$$\mathrm{e}^{\pm i2k\hat{z}}\,|p\rangle = |p \pm q\rangle\ . \tag{3.8}$$

This means that the operator $\mathrm{e}^{\pm i2k\hat{z}}$ shifts the momentum of the eigenstate $|p\rangle$ by the discrete recoil $\pm q \equiv \pm 2\hbar k$ and thus we identify $\mathrm{e}^{\pm i2k\hat{z}/\hbar}$ as a momentum-shift operator. Applying this operator many times yields a change of total momentum which constitutes an *integer* multiple of q.
Hence, we have obtained the discrete momentum ladder which we have already introduced by hand in terms of energy-momentum conservation for Compton scattering. However, in Eq. (3.6) the radiation field is classical and we do not require the 'picture' of a photon to understand the discrete dynamics of the electron in the FEL. Instead, the motion of the electron has to be quantized to observe quantum effects.

3.2 Quantum corrections: Heisenberg picture

In the preceding section we have discussed the transition from classical to quantum from a rather heuristic or graphical point of view. Now, we derive explicit expressions for the corrections to the classical gain when we leave the classical regime and quantum effects are not negligible any longer. On the one hand we want to illuminate further the classical–quantum transition in the FEL and on the other hand we try to find the conditions and the explicit form of quantum corrections which are important for a possible experimental verification.
The first method to achieve this goal stands in close analogy to the solution of the pendulum equation, Eq. (2.38), in Chap. 2 where we have considered the individual trajectories of the electrons to calculate the FEL classical gain, Eq. (2.46), in the low-gain, small-signal regime. In the Heisenberg picture of quantum mechanics position $\hat{z}$ and momentum $\hat{p}$ are time-dependent operators instead of simple numbers. After solving the Heisenberg equations of motion for these operators, in analogy to the Hamiltonian equations of motion for classical variables, we use the resulting time-dependent expression to calculate expectation values with respect to the initial state of the system.

3.2.1 Baker–Campbell–Hausdorff theorem

The main difference between classical variables and quantum mechanical operators is, that latter ones in general do not commute with each other. That is for example the case for position $\hat{z}$ and momentum $\hat{p}$ which fulfill the commutation relation

$$[\hat{z}, \hat{p}] = i\hbar\,. \tag{3.9}$$

This fundamental identity includes the Planck constant $\hbar$ and is responsible for quantum effects in the FEL [13] as we prove in the following. We again emphasize that it is the quantized motion of the electron that brings us closer to the quantum regime and not the laser field which is classical in the current discussion.

In our approach we restrict ourselves to the low-gain regime that is why we consider the single-electron Hamiltonian $\hat{H}$ in its quantized form of Eq. (3.6). This Hamiltonian dictates the dynamics of an arbitrary operator $\hat{\mathcal{O}}$ via the Heisenberg equation of motion

$$i\hbar\frac{\mathrm{d}}{\mathrm{d}t}\hat{\mathcal{O}} = \left[\hat{\mathcal{O}}, \hat{H}\right] \tag{3.10}$$

which is the analogue to the Schrödinger equation in the Schrödinger picture, where one considers time-dependent states and time-independent operators.

From the equation of motion, Eq. (3.10), and the Hamiltonian, Eq. (3.6), we obtain the quantum analogue of the pendulum equation, Eq. (2.36),

$$\frac{\mathrm{d}^2}{\mathrm{d}\tau^2}\,\hat{\theta} = \frac{\kappa|a_\mathrm{L}|}{2}\left(\mathrm{e}^{i\hat{\theta}} - \mathrm{e}^{-i\hat{\theta}}\right) . \tag{3.11}$$

In close analogy with the classical definition, Eq. (2.34), we have introduced the dimensionless operators $\hat{\theta} \equiv 2k\hat{z}$ for the ponderomotive phase and $\hat{\wp} \equiv (2kT\hat{p})/m$ for the Doppler parameter. In this scaling the fundamental commutation relation, Eq. (3.9), translates to

$$\left[\hat{\theta}, \hat{\wp}\right] = i2\omega_\mathrm{r}T\,, \tag{3.12}$$

after employing the definition Eq. (3.2) of the recoil frequency ω_r.

In accordance with Eq. (2.37) the dynamics of the modulus $|a_\mathrm{L}|$ of the laser field amplitude is prescribed by the relation

$$\frac{\mathrm{d}}{\mathrm{d}\tau}|a_\mathrm{L}| = -\frac{gTN}{2}\left\langle \mathrm{e}^{i\hat{\theta}} - \mathrm{e}^{-i\hat{\theta}}\right\rangle . \tag{3.13}$$

On the right-hand side we calculate the expectation values of the quantum mechanical operators $\mathrm{e}^{i\hat{\theta}}$ and $\mathrm{e}^{-i\hat{\theta}}$. In the low-gain regime the field amplitude $|a_\mathrm{L}|$ in the pendulum equation, Eq. (3.11), is considered as constant. Thus, we first solve the pendulum equation for $\hat{\theta}$ and insert the result into Eq. (3.13) which is then simply integrated with respect to time, analogously to the classical procedure presented in Chap. 2. Moreover, we assume that the initial state of the electron is given by the momentum eigenstate $|\bar{p}\rangle$ which gives us a uniform distribution in z-direction but a sharp value of the momentum at $p = \bar{p}$.

We restrict ourselves to the small-signal regime. Hence, we identify the right-hand side of the pendulum equation, Eq. (3.11), as a small perturbation to the free motion

$$\hat{\theta}^{(0)} = \hat{\theta}^{(\mathrm{in})} + \hat{\wp}^{(\mathrm{in})}\tau \tag{3.14}$$

of the electron and similar to the classical case, Chap. 2, we use a perturbative expansion of $\hat{\theta}$ which reads

$$\hat{\theta} = \hat{\theta}^{(0)} + \hat{\theta}^{(1)} + \hat{\theta}^{(2)} + \dots . \tag{3.15}$$

Of course, this expansion is only valid for a small coupling $\kappa|a_\mathrm{L}|$. Moreover, the quantum corrections which are quantified by the parameter $\omega_\mathrm{r}T$ according to Eq. (3.12) are small but not negligible any more. That is why we assume that the coupling and the quantum corrections are of the same order, that is $\kappa|a_\mathrm{L}| \sim \omega_\mathrm{r}T$.

We omit the details of the perturbative expansion and refer the reader to App. B where this lengthy and cumbersome calculation is presented in all its 'beauty'. Here, we just shortly illuminate in which way the quantum corrections to the classical gain emerge.

In contrast to ordinary numbers, we cannot easily separate an exponential of the sum $\hat{A}+\hat{B}$ of two operators, but instead we have to pay attention to the Baker–Campbell–Hausdorff theorem [82]

$$\mathrm{e}^{\hat{A}+\hat{B}} = \mathrm{e}^{\hat{A}}\,\mathrm{e}^{\hat{B}}\,\mathrm{e}^{-\frac{1}{2}\left[\hat{A},\hat{B}\right]}\,\mathrm{e}^{\frac{1}{6}\left(2\left[\hat{B},\left[\hat{A},\hat{B}\right]\right]+\left[\hat{A},\left[\hat{A},\hat{B}\right]\right]\right)}\,\ldots\,, \tag{3.16}$$

where $\hat{A}$ and $\hat{B}$ denote two arbitrary operators.

In our perturbative calculation we very quickly get contact to such exponentials. For example, when we insert the zeroth-order solution from Eq. (3.14) into Eq. (3.11) we obtain terms like

$$\mathrm{e}^{i\hat{\theta}^{(\mathrm{in})}+i\hat{\wp}^{(\mathrm{in})}\tau} = \mathrm{e}^{i\hat{\theta}^{(\mathrm{in})}}\,\mathrm{e}^{i\hat{\wp}^{(\mathrm{in})}\tau}\,\mathrm{e}^{i\omega_\mathrm{r}T\tau} \tag{3.17}$$

according to Eq. (3.16). Since the commutator, Eq. (3.12), of $\hat{\theta}$ and $\hat{\wp}$ yields a c-number all nested commutators vanish resulting in the relatively simple form of Eq. (3.17). Moreover, for a small value of $\omega_\mathrm{r}T$ we arrive at the expression

$$\mathrm{e}^{i\hat{\theta}^{(\mathrm{in})}+i\hat{\wp}^{(\mathrm{in})}\tau} \cong \mathrm{e}^{i\hat{\theta}^{(\mathrm{in})}}\,\mathrm{e}^{i\hat{\wp}^{(\mathrm{in})}\tau}\left(1+i\omega_\mathrm{r}T\tau-\frac{1}{2}(\omega_\mathrm{r}T)^2\tau^2+\ldots\right), \tag{3.18}$$

where we have expanded the exponential $\mathrm{e}^{i\omega_\mathrm{r}T\tau}$ in powers of $\omega_\mathrm{r}T$.

Hence, we have found terms with $\omega_\mathrm{r}T$ in Eq. (3.18) which are the first contributions for the quantum corrections to the classical FEL. In the further course of our perturbative solution of the pendulum equation, Eq. (3.11), we obtain more such contributions, like for example $[\hat{\theta}^{(0)},\hat{\theta}^{(1)}]$ or $[\hat{\theta}^{(0)},[\hat{\theta}^{(0)},\hat{\theta}^{(1)}]]$ which all scale with powers of $\omega_\mathrm{r}T$. Moreover, when we compute expectation values it is convenient to order the operators in a specific way which also causes terms depending on $\omega_\mathrm{r}T$.

In conclusion, we have shown that the commutation relation, Eq. (3.9), between position operator $\hat{z}$ and momentum operator $\hat{p}$ of the electron is responsible for quantum effects in the FEL. This fact appears in our perturbative solution in the Heisenberg picture in form of the Baker–Campbell–Hausdorff relation, Eq. (3.16).

3.2.2 Gain including quantum corrections

In App. B we derive the expression

$$|a_\mathrm{L}(T)| - |a_\mathrm{L}(0)| = \left(G^{(1)}_\mathrm{cl} - G^{(3)}_\mathrm{cl}|a_\mathrm{L}|^2 + G^{(3)}_\mathrm{qm}\right)|a_\mathrm{L}| \tag{3.19}$$

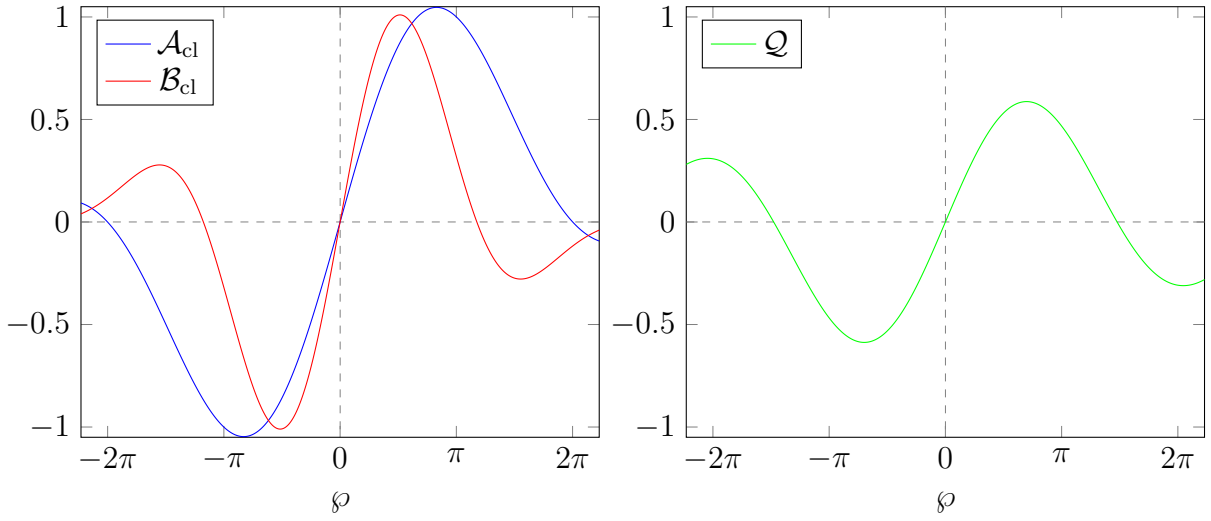

Figure 3.4: Characteristic functions $\mathcal{A}_{\mathrm{cl}}$, Eq. (3.21), and $\mathcal{B}_{\mathrm{cl}}$, Eq. (3.23), for the classical gain in the low-gain small-signal regime in first and third order, respectively, and $\mathcal{Q}$, Eq. (3.25), for the quantum corrections, all depending on the Doppler parameter $\wp$.

for the change of the laser field in the FEL including the lowest-order quantum corrections. Here, we have introduced the classical linear gain, Eq. (B.59),

$$G_{\mathrm{cl}}^{(1)} = gTN\kappa\frac{2}{\pi^3}\mathcal{A}_{\mathrm{cl}}(\bar{\wp}) \tag{3.20}$$

with the characteristic function, Eq. (B.60),

$$\mathcal{A}_{\mathrm{cl}}(\wp) \equiv \frac{\pi^3}{2}\frac{1-\cos\wp-\frac{\wp}{2}\sin\wp}{\wp^3} \tag{3.21}$$

which simply represents the Madey gain, Eq. (2.46). Moreover, we have included the third-order contribution, Eq. (B.62),

$$G_{\mathrm{cl}}^{(3)} = \frac{gTN}{4\pi^5}\kappa^3\mathcal{B}_{\mathrm{cl}}(\bar{\wp}) \tag{3.22}$$

together with, Eq. (B.63),

$$\begin{aligned}\mathcal{B}_{\mathrm{cl}}(\wp) \equiv \frac{\pi^5}{\wp^7}\Bigg(&\frac{9}{2}\cos 2\wp + 12\cos\wp - \frac{33}{2} + \frac{11}{4}\wp\sin 2\wp + \frac{53}{4}\wp\sin\wp \\ &-\frac{\wp^2}{2}\cos 2\wp - \frac{13}{4}\wp^2\cos\wp - \frac{\wp^2}{4}\sin\wp\Bigg)\end{aligned} \tag{3.23}$$

of the classical result [43]. Due to the negative sign in front of this term and the proportionality to $|a_{\mathrm{L}}|^2$ in Eq. (3.19) we identify $G_{\mathrm{cl}}^{(3)}$ as the self-saturation coefficient for the classical FEL

in analogy to an ordinary laser [22]. This term is necessary to obtain steady state in an oscillator configuration as we discuss in detail in Chap. 4.

In addition to these classical contributions, we observe the expression, Eq. (B.72),

$$G_{\mathrm{qm}}^{(3)} = -(\omega_{\mathrm{r}}T)^2 \frac{2gTN}{\pi^5} \kappa \mathcal{Q}(\bar{\wp}) \tag{3.24}$$

characterized by, Eq. (B.73),

$$\mathcal{Q}(\wp) \equiv \frac{\pi^5}{4\wp^5} \left(4\cos\wp - 4 + 3\wp\sin\wp - \wp^2\cos\wp - \frac{\wp^3}{6}\sin\wp \right) \tag{3.25}$$

which represents the lowest-order quantum correction to the classical gain in the low-gain small-signal regime.

By inspecting Eqs. (3.20) and (3.22) we can relax the condition $\kappa|a_{\mathrm{L}}| \ll 1$ for the small-signal regime. The comparison of the third-order classical term with the first-order one leads us to

$$\frac{G_{\mathrm{cl}}^{(3)}}{G_{\mathrm{cl}}^{(1)}} \sim \frac{\kappa^2|a_{\mathrm{L}}|^2}{8\pi^2} \,. \tag{3.26}$$

Thus, we obtain the condition

$$\kappa|a_{\mathrm{L}}| \ll 2\sqrt{2}\pi \tag{3.27}$$

which follows when we demand that the ratio in Eq. (3.26) is much smaller than unity in order to truncate our asymptotic expansion. In analogy, by considering the ratio

$$\frac{G_{\mathrm{qm}}^{(3)}}{G_{\mathrm{cl}}^{(1)}} \sim \left(\frac{\omega_{\mathrm{r}}T}{\pi} \right)^2 \tag{3.28}$$

of classical gain in first order, Eq. (3.20), and of the lowest-order quantum correction, Eq. (3.24), we deduce the second constraint

$$\omega_{\mathrm{r}}T \ll \pi \tag{3.29}$$

for the validity of our perturbative approach.

In Fig. 3.5 we have drawn the change of the field amplitude $|a_{\mathrm{L}}|$ as a function of the initial Doppler parameter $\bar{\wp}$, according to Eq. (3.19), in comparison to the classical limit $\omega_{\mathrm{r}}T = 0$. For increasing values of $\omega_{\mathrm{r}}T$ the maximum gain decreases and the positions of the extreme values are shifted outwards.

We emphasize that this result for the classical gain and its quantum corrections is not new [17, 83]. Even the first article by Madey [5] towards the FEL in principle contained this result. In the following we sketch the basic approach of these references.

With the help of first-order perturbation theory for the Schrödinger equation one obtains the probabilities $P_{+1} \propto \mathrm{sinc}^2(\wp/2 - \omega_{\mathrm{r}}T)$ and $P_{-1} \propto \mathrm{sinc}^2(\wp/2 + \omega_{\mathrm{r}}T)$ for single-photon emission and single-photon absorption, respectively. The difference of emission and absorption

$$G \propto \frac{1}{2\omega_{\mathrm{r}}T} \left[\mathrm{sinc}^2\left(\frac{\wp}{2} - \omega_{\mathrm{r}}T \right) - \mathrm{sinc}^2\left(\frac{\wp}{2} + \omega_{\mathrm{r}}T \right) \right] \tag{3.30}$$

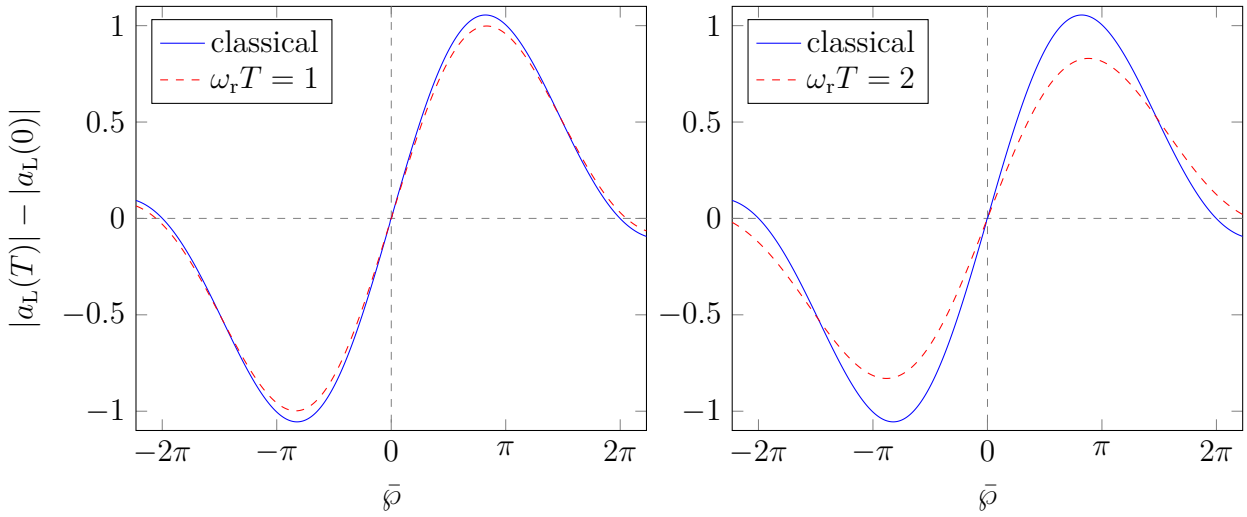

Figure 3.5: Change of the laser field amplitude $|a_L|$, according to Eq. (3.19), in a low-gain small-signal FEL as a function of the initial momentum $\bar{\wp}$. We compare the classical limit (blue line), where $\omega_r T = 0$, with the case, where Eq. (3.19) includes the lowest-order quantum corrections (red, dashed line) for $\omega_r T = 1$ (left side) and $\omega_r T = 2$ (right side), respectively. We observe that for increasing values of $\omega_r T$ the positions of minimum and maximum are slightly shifted to the left and to the right, respectively, while the magnitude of the gain decreases.

can be interpreted as the gain of the FEL [17]. When $\omega_r T$ is small we are allowed to perform a Taylor expansion

$$G \propto -\frac{\partial}{\partial \wp}\mathrm{sinc}^2\left(\frac{\wp}{2}\right) - \frac{(\omega_r T)^2}{3!}\frac{\partial^3}{\partial \wp^3}\mathrm{sinc}^2\left(\frac{\wp}{2}\right)\ldots, \tag{3.31}$$

where the first term is proportional to the linear gain $G_{\mathrm{cl}}^{(1)}$ in the classical regime, according to Eq. (2.46). By calculating the third derivative in Eq. (3.31) we further obtain the expression

$$\frac{1}{3!}\frac{\partial^3}{\partial \wp^3}\mathrm{sinc}^2\left(\frac{\wp}{2}\right) = \frac{8}{\pi^5}\mathcal{Q}(\wp) \tag{3.32}$$

for the quantum corrections which is analogous to our result in Eq. (3.25).
However, as was stressed for example in Ref. [81], this procedure of employing standard perturbation theory is only valid when just *single-photon* transitions occur and the corresponding asymptotic expansion is allowed for $gT\sqrt{n} \ll 1$. In the classical regime of the FEL, however, *multiphoton* processes are dominant [81]. In contrast, in our approach we overcome this problematic interpretation of single-photon transitions and the small parameter of the asymptotic expansion is given by $\kappa|a_L|$. Instead, we identify the fact that position and momentum of an electron do not commute in quantum mechanics as the origin of quantum effects in the FEL which finally appear as quantum corrections to the classical trajectories. Hence, our model gives a reasonable interpretation for quantum effects as well as for the classical limit of the FEL. Alternatively, one can regard the situation from the point of view

of Ref. [83]: despite the fact that the asymptotic expansion for the wave function cannot be truncated when multiphoton processes are of relevance we are allowed to cut off the corresponding expression for the gain and it mathematically gives the correct result.

3.3 Quantum corrections: Wigner function

We now present our second technique to obtain quantum corrections to the classical gain in the FEL: a method based on the Wigner distribution function. First, we discuss the properties of this function and introduce the Quantum Liouville equation which governs the dynamics of the Wigner function for the example of the FEL. We proceed by perturbatively solving the Quantum Liouville equation in analogy to our approach in Chap. 2 for the classical distribution function. Finally, we derive explicit expressions for quantum corrections for a cold and a warm electron beam, respectively, and we obtain that these corrections are suppressed when the momentum spread Δp of the electron beam increases. Finally, we investigate realistically modeled electron beams as well as the scattering of wave packets.

3.3.1 Wigner function and Quantum Liouville equation

Contrarily to the Heisenberg picture the operators in the Schrödinger picture are independent of time and the dynamics of the system is described by the state vector $|\Psi(t)\rangle$. In a more general formulation of quantum mechanics, where we have to take into account the insufficient information the observer possesses about the preparation of the quantum state, we have to consider the density operator $\hat{\rho}(t)$ [40, 82].
The dynamics of $\hat{\rho}(t)$ follows from the von Neumann equation [82]

$$i\hbar\frac{\mathrm{d}}{\mathrm{d}t}\hat{\rho}(t) = \left[\hat{H}, \hat{\rho}(t)\right] \tag{3.33}$$

which is basically the extension of the Schrödinger equation to the concept of a density-operator. We form the expectation value [82] for an observable $\hat{\mathcal{O}}$

$$\langle\hat{\mathcal{O}}(t)\rangle = \mathrm{Tr}\left\{\hat{\rho}(t)\hat{\mathcal{O}}\right\} \tag{3.34}$$

by taking the trace of the product of density operator and observable.
Similar to the Heisenberg equation of motion, Eq. (3.10), the von Neumann equation, Eq. (3.33), is an operator equation. Hence, when we solve Eq. (3.33) we have to pay attention to the ordering of the involved operators in every single step of the calculations. However, there exist several techniques to order the operators correctly from the beginning where we transform the operator equation to an equation which only contains ordinary c-numbers [82]. The c-number equivalent of the density operator $\hat{\rho}$ is given by so-called quasi-probability functions. Besides the Glauber–Sudarshan P-function [84] and the Husimi–Kano Q-function [85] we can cast the density operator into a third kind of representation: the Wigner function [33, 40, 86]. Like the other two examples of distribution functions it is defined as a Fourier transform [82]

$$W(z,p;t) \equiv \int\mathrm{d}\xi \int\mathrm{d}\zeta\, \mathrm{e}^{-iz\xi}\, \mathrm{e}^{-ip\zeta}\, \chi_{\hat{\rho}}(\xi,\zeta;t) \tag{3.35}$$

of a specific characteristic function

$$\chi_{\hat{\rho}}(\xi,\zeta;t) \equiv \mathrm{Tr}\left\{\mathrm{e}^{i\xi\hat{z}+i\zeta\hat{p}}\,\hat{\rho}\right\}\,, \tag{3.36}$$

where we have introduced the real parameters ξ and ζ. The arguments z and p of the Wigner function are c-number versions of the position $\hat{z}$ and momentum operator $\hat{p}$ and hence we interpret $W(z,p;t)$ as phase-space distribution function which hints a similarity to the classical distribution function $f(z,p;t)$ introduced in Chap. 2. However, the interpretation as a probability distribution is not fully correct since the Wigner function can take on negative values [40] in contrast to its classical counterpart. We note that the operator ordering occurs in the definition, Eq. (3.36), of the characteristic function $\chi_{\hat{\rho}}(\xi,\zeta;t)$ and is also known as Wigner–Weyl ordering [33].

The expectation value of an observable $\hat{\mathcal{O}}$ has to be calculated from

$$\langle\hat{\mathcal{O}}(t)\rangle = \int\mathrm{d}z\int\mathrm{d}p\,\tilde{\mathcal{O}}(z,p)W(z,p;t)\,, \tag{3.37}$$

with

$$\tilde{\mathcal{O}}(z,p;t) \equiv \int\mathrm{d}\xi\int\mathrm{d}\zeta\,\mathrm{e}^{-iz\xi}\,\mathrm{e}^{-ip\zeta}\,\chi_{\hat{\mathcal{O}}}(\xi,\zeta;t) \tag{3.38}$$

denoting the Wigner–Weyl transform of $\hat{\mathcal{O}}$, where we have defined the characteristic function

$$\chi_{\hat{\mathcal{O}}}(\xi,\zeta;t) \equiv \mathrm{Tr}\left\{\mathrm{e}^{i\xi\hat{z}+i\zeta\hat{p}}\,\hat{\mathcal{O}}\right\} \tag{3.39}$$

in analogy to Eq. (3.36).

With the help of the von Neumann equation, Eq. (3.33), and the FEL Hamiltonian, Eq. (3.6), we are in the position to derive the equation of motion for the Wigner function defined in Eqs. (3.35) and (3.36). We omit here the explicit derivation and refer to App. C.1. There, we obtain

$$\left(\frac{\partial}{\partial t}+\frac{p}{m}\frac{\partial}{\partial z}\right)W(z,p;t) = -\frac{2kU_0|a_\mathrm{L}|}{q}\sin 2kz\,[W(z,p+q/2;t)-W(z,p-q/2;t)] \tag{3.40}$$

which is the Quantum Liouville equation for the FEL. In Refs. [25, 87, 88] an analogous equation for the FEL dynamics was considered. However, these references are about the high-gain regime and the Wigner function for the electrons there emerges from a collective field operator approximated as classical field in analogy to Ref. [89].

Before we proceed we rewrite Eq. (3.40) in our usual dimensionless scaling, Eq. (2.34), which yields

$$\left(\frac{\partial}{\partial\tau}+\wp\frac{\partial}{\partial\theta}\right)W(\theta,\wp;\tau) = -\kappa|a_\mathrm{L}|\sin\theta\frac{1}{2\omega_\mathrm{r}T}\left[W(\theta,\wp+\omega_\mathrm{r}T;\tau)-W(\theta,\wp-\omega_\mathrm{r}T;\tau)\right]\,. \tag{3.41}$$

The right-hand side of Eq. (3.41) consists of the difference of two Wigner functions where the argument corresponding to the momentum $\wp$ is displaced by $\wp+\omega_\mathrm{r}T$ and by $\wp-\omega_\mathrm{r}T$, respectively. When we perform a Taylor expansion of these functions around $\wp$ in powers of $\omega_\mathrm{r}T$ we obtain that all even derivatives vanish, due to the minus sign, and Eq. (3.41)

transforms to

$$\left(\frac{\partial}{\partial\tau}+\wp\frac{\partial}{\partial\theta}\right)W(\theta,\wp;\tau)=-\kappa|a_{\mathrm{L}}|\sin\theta\sum_{m=0}^{\infty}\frac{(\omega_{\mathrm{r}}T)^{2m}}{(2m+1)!}\frac{\partial^{2m+1}}{\partial\wp^{2m+1}}W(\theta,\wp;\tau)\,. \tag{3.42}$$

Now, we find the most important similarity to the classical formulation in terms of the distribution function $f(\theta,\wp;\tau)$: by neglecting all terms with derivatives higher than first order, similar to the procedure in Ref. [87], we obtain that no term with $\omega_{\mathrm{r}}T$, that is with $\hbar$, is present and we arrive at

$$\left(\frac{\partial}{\partial\tau}+\wp\frac{\partial}{\partial\theta}\right)W(\theta,\wp;\tau)=-\kappa|a_{\mathrm{L}}|\sin\theta\frac{\partial}{\partial\wp}W(\theta,\wp;\tau)\,, \tag{3.43}$$

which is equivalent to the Boltzmann equation, Eq. (2.49), for the classical distribution function f.

Moreover, we show in the course of the following calculations that higher-order terms are responsible for the quantum corrections to the gain. However, we emphasize that the transition from quantum mechanics to classical physics in terms of the Wigner function is more subtle than simply performing the limit $\omega_{\mathrm{r}}T\to 0$: Due to the derivatives with respect to $\wp$ terms including $\hbar$ can appear in the denominator and eventually we are not allowed to cut off the series [33].

The dynamics of the laser field is given by

$$\frac{\partial}{\partial\tau}|a_{\mathrm{L}}|=-gTN\left\langle\sin\theta(\tau)\right\rangle=-gTN\int\mathrm{d}\theta\int\mathrm{d}\wp\sin\theta\,W(\theta,\wp;\tau)\,, \tag{3.44}$$

where we have written Eq. (3.13) in terms of the Wigner function according to the prescription Eq. (3.37) for expectation values. The simple transformation of $\sin\hat{\theta}$ to $\sin\theta$ in the Wigner–Weyl representation arises since this function depends only on $\hat{z}$ and not on $\hat{p}$. A more involved ordering procedure would become necessary for combinations of $\hat{z}$ and $\hat{p}$.

3.3.2 Perturbative solution

By restricting ourselves to the low-gain small-signal regime we are allowed to apply perturbation theory to solve the Quantum Liouville equation in analogy to the classical case in Chap. 2. The structure of Eq. (3.42) is given by

$$\mathcal{L}_0W=\mathcal{L}_1W\,, \tag{3.45}$$

where $\mathcal{L}_0$ includes the contribution from the kinetic energy of the electron and hence describes its free motion, while $\mathcal{L}_1$ represents the perturbation due to the cosine potential.

We assume that the state of the electron initially is described by

$$W(\theta,\wp;0)=\frac{1}{2\pi}g(\wp) \tag{3.46}$$

which means that the electron is again uniformly distributed in z-direction, but in contrast to our calculations in the Heisenberg picture the distribution of momenta is given by the

function $g(\wp)$ which possesses an arbitrary width $\Delta_\wp$. This feature of the initial Wigner function, Eq. (3.46), becomes crucial when we investigate the difference between a cold and a warm electron beam.

We expand the solution of Eq. (3.42)

$$W = W^{(0)} + W^{(1)} + W^{(2)} + ... \tag{3.47}$$

and insert this expansion order by order into Eq. (3.42) which yields

$$\mathcal{L}_0 W^{(n)} = \mathcal{L}_1 W^{(n-1)} \tag{3.48}$$

for $n > 0$. According to Chap. 2 we obtain in zeroth order, that is $\mathcal{L}_0 W_0 = 0$, the solution

$$W(\theta, \wp; \tau)^{(0)} = W(\theta - \wp\tau, \wp; 0) = \frac{1}{2\pi} g(\wp)\,, \tag{3.49}$$

which is identical to the initial Wigner function $W(\theta, \wp; 0)$ since it is independent of θ according to Eq. (3.46).

The equation of first order reads

$$\mathcal{L}_0 W^{(1)} = \mathcal{L}^{(1)} W^{(0)} \tag{3.50}$$

which has the formal solution

$$W^{(1)}(\theta, \wp; \tau) = -\kappa |a_\mathrm{L}| \left(\int \mathrm{d}\tau' \int \mathrm{d}\theta' G_\mathrm{free}(\theta, \tau; \theta', \tau') \sin\theta \right) \sum_{m=0}^{\infty} \frac{(\omega_\mathrm{r} T)^{2m}}{(2m+1)!} \left(\frac{\partial^{2m+1}}{\partial \wp^{2m+1}} \frac{1}{2\pi} g(\wp) \right), \tag{3.51}$$

where we have inserted $W^{(0)}$ from Eq. (3.49) and have used the Green's function G_free, Eq. (2.55), for the free motion to solve the inhomogeneous differential equation. We emphasize that the zeroth-order solution from Eq. (3.49) is independent of θ and τ and we can put it outside of the integral. Hence, our procedure is analogous to the classical case and we straightforwardly arrive at the expression

$$W^{(1)}(\theta, \wp; \tau) = -\kappa |a_\mathrm{L}| \frac{\cos(\theta - \wp\tau) - \cos\theta}{\wp} \sum_{m=0}^{\infty} \frac{(\omega_\mathrm{r} T)^{2m}}{(2m+1)!} \left(\frac{\partial^{2m+1}}{\partial \wp^{2m+1}} \frac{1}{2\pi} g(\wp) \right), \tag{3.52}$$

where we have recalled the explicit form of the Green's function G_free, Eq. (2.55), and have performed the integrations over θ' and τ' in analogy to the computations in Chap. 2.

In the following we illuminate why just setting $\omega_\mathrm{r} T$ to zero in Eq. (3.52) is *not* the correct classical limit for the Wigner function, although it naively gives the result for the classical distribution function from Eq. (2.56). Besides a small recoil the preparation of the initial state is of utmost importance to observe the classical limit for the dynamics.

We assume that the initial momentum distribution $g(\wp)$ is given by the Gaussian

$$g(\wp) = \frac{1}{\sqrt{2\pi}\Delta_\wp} \mathrm{e}^{-\frac{(\wp - \bar{\wp})^2}{2\Delta_\wp^2}} \tag{3.53}$$

described by its mean value $\bar{\wp}$ and its variance $\Delta_\wp$. The nth derivative of a Gaussian with respect to the argument x

$$\frac{\partial^n}{\partial x^n}\,\mathrm{e}^{-x^2} = (-1)^n H_n(x)\,\mathrm{e}^{-x^2} \tag{3.54}$$

is proportional to the nth Hermite polynomial $H_n(x)$ [90]. Thus, for a Gaussian distribution, Eq. (3.53), the Wigner function can be cast into the form

$$W(\theta,\wp;\tau) = \left[1 + \kappa|a_\mathrm{L}|\frac{\cos(\theta-\wp\tau)-\cos\theta}{\wp}\left(\sum_{m=0}^{\infty}\frac{H_{2m+1}(\frac{\wp-\bar{\wp}}{\sqrt{2}\Delta_\wp})}{(2m+1)!}\frac{(\omega_\mathrm{r}T)^{2m}}{(\sqrt{2}\Delta_\wp)^{2m+1}}\right)\right]\frac{1}{2\pi}g(\wp) \tag{3.55}$$

which is equivalent to

$$W(\theta,\wp;\tau) = \left\{1 + \kappa|a_\mathrm{L}|\frac{\cos(\theta-\wp\tau)-\cos\theta}{\wp}\,\mathrm{e}^{-\frac{(\omega_\mathrm{r}T)^2}{2\Delta_\wp{}^2}}\,\frac{1}{\omega_\mathrm{r}T}\sinh\left[\frac{\omega_\mathrm{r}T}{\Delta_\wp{}^2}(\wp-\bar{\wp})\right]\right\}\frac{1}{2\pi}g(\wp)\,. \tag{3.56}$$

In the second step we have used a fundamental identity for Hermite polynomials [90]. We would also find this expression for W when we are using the Quantum Liouville equation in the form of Eq. (3.41) instead of Eq. (3.42). By inspection of Eq. (3.56) we obtain that the first-order term is proportional to the difference $g(\wp+\omega_\mathrm{r}T) - g(\wp-\omega_\mathrm{r}T)$ of the initial momentum distribution shifted by $+\omega_\mathrm{r}T$ and by $-\omega_\mathrm{r}T$, respectively, in analogy to Eq. (3.41). However, for our following procedure the form of the Liouville equation given in Eq. (3.42) is more suitable.

For $\omega_\mathrm{r}T \to 0$ we would naively expect that the quasi-probability function W, Eq. (3.55), reduces to the classical distribution function f from Eq. (2.56). We compare both functions in Fig. 3.6, where we have chosen the parameters $\tau = 1$, $\bar{\wp} = \pi$, $\Delta_\wp = 0.05$ and $\omega_\mathrm{r}T = 0.1$. We obtain that our expectation is not true: the classical and the quantum mechanical result significantly differ.

As already mentioned this discrepancy arises since due to the derivatives with respect to $\wp$ in Eq. (3.42) terms, which eventually can be small, appear in the denominator and in general we cannot cut off the series. We can illuminate this statement when we write down the first two terms of the expansion in Eq. (3.55) in the following way

$$W^{(1)}(\theta,\wp;\tau) \cong \kappa|a_\mathrm{L}|\frac{\cos(\theta-\wp\tau)-\cos\theta}{\wp\Delta_\wp}\left[H_1\left(\frac{\wp-\bar{\wp}}{\sqrt{2}\Delta_\wp}\right) + \frac{1}{12}\left(\frac{\omega_\mathrm{r}T}{\Delta_\wp}\right)^2 H_3\left(\frac{\wp-\bar{\wp}}{\sqrt{2}\Delta_\wp}\right)\right]\frac{g(\wp)}{2\pi}\,. \tag{3.57}$$

The first contribution is independent of $\hbar$ and we identify it as the classical result, Eq. (2.56). The second term, however, scales quadratic with the parameter $\omega_\mathrm{r}T/\Delta_\wp = \hbar k/\Delta p$ where we have recalled the definitions Eqs. (3.2), (2.34) and (3.1) of the recoil frequency ω_r, the Doppler phase $\wp$ and the recoil q, respectively.

Hence, the classical result, Eq. (2.56), is only obtained from the quantum mechanical one, when the initial momentum spread Δp is much larger than the recoil $q/2$. For example, by assuming that the initial momentum is given by $\wp = \bar{\wp} + \Delta_\wp$ we find with the help of the explicit expressions [90] of the Hermite polynomials, H_1 and H_3, the condition $\omega_\mathrm{r}T/\Delta_\wp \ll \sqrt{3}$ to cut off the expansion in Eq. (3.55) after the first term. Moreover, we require $\kappa|a_\mathrm{L}|/\Delta_\wp \ll 1$ for the perturbation theory to be valid.

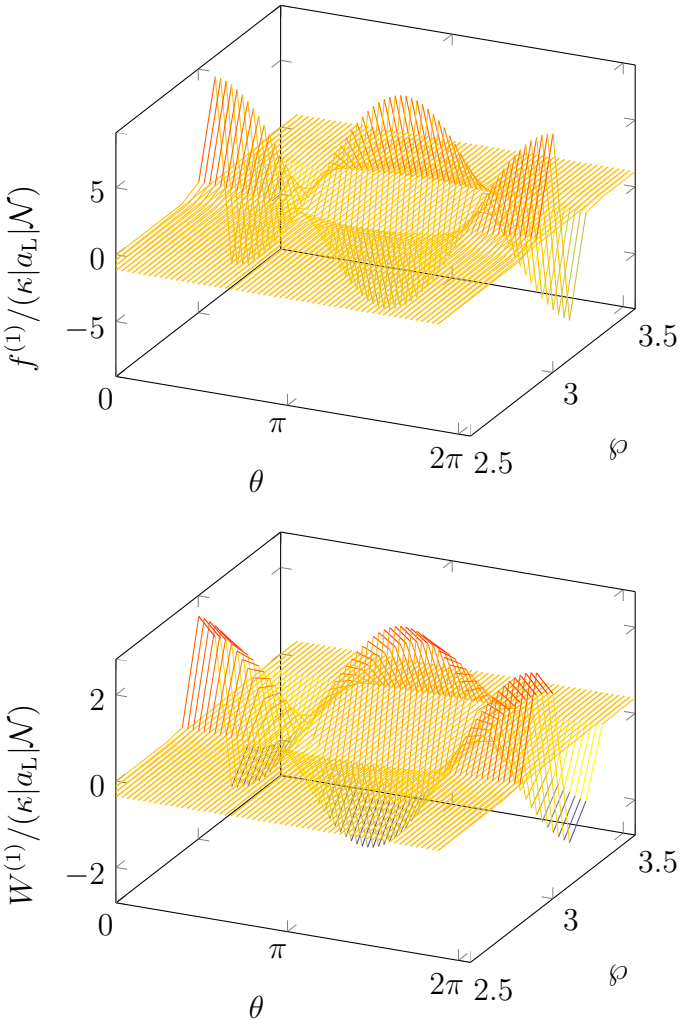

Figure 3.6: Comparison of the first-order corrections $f^{(1)}$, Eq. (2.56), and $W^{(1)}$, Eq. (3.56), of the classical distribution function (above) and of the Wigner function (below), respectively, in phase space $(\theta, \wp)$ where θ denotes the dimensionless position and $\wp$ the dimensionless momentum of the electron. For our choice of parameters, that is for $\tau = 1$, $\bar{\wp} = \pi$, $\Delta_\wp = 0.05$ and $\omega_r T = 0.1$, the functions show a different behavior which stands in contrast to the naive assumption that the Quantum Liouville equation, Eq. (3.42), reduces to the classical Boltzmann equation, Eq. (3.43), by neglecting the higher-order derivatives for $\omega_r T \to 0$. These derivatives with respect to $\wp$ bring powers of the initial momentum spread Δp into the denominator and since Δp is of the order of the recoil $\hbar k$, that is $\hbar k/\Delta p = 2$, we are not allowed to cut off the series in Eq. (3.43).

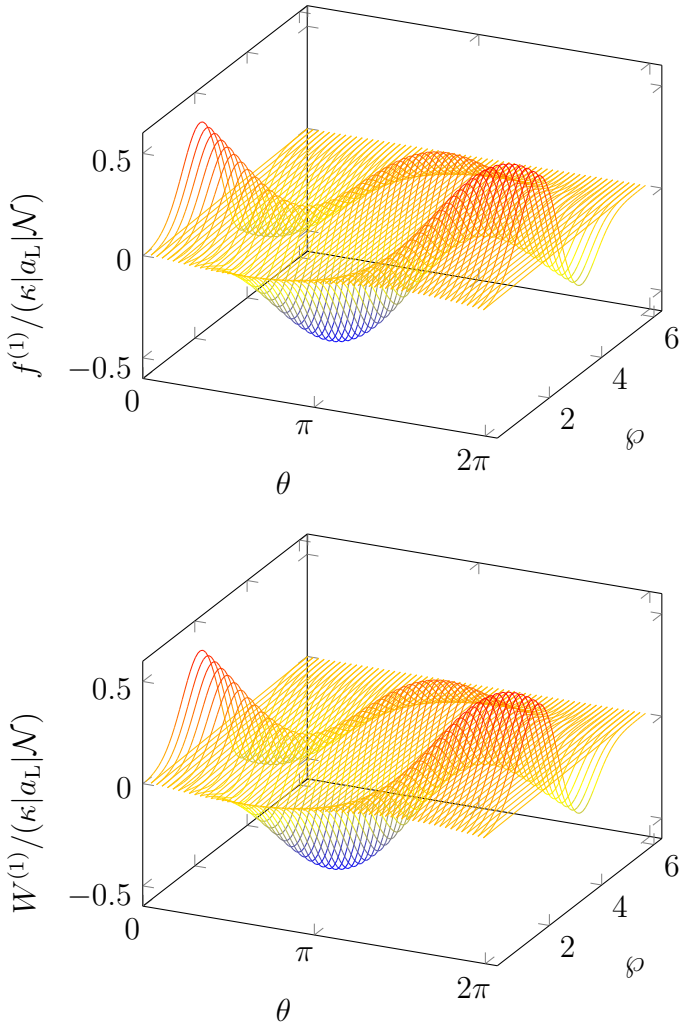

Figure 3.7: Comparison of the first-order corrections $f^{(1)}$, Eq. (2.56), and $W^{(1)}$, Eq. (3.56), of the classical distribution function (above) and of the Wigner function (below), respectively, in phase space $(\theta, \wp)$, where θ denotes the dimensionless position and $\wp$ the dimensionless momentum of the electron. In contrast to Fig. 3.6 both functions agree when we choose the parameters $\tau = 1$, $\bar{\wp} = \pi$, $\Delta_\wp = 1$ and $\omega_r T = 0.1$. Since $\hbar k/\Delta p = 0.1$ is small we are allowed to neglect the higher derivatives in Eq. (3.42) in accordance with Eq. (3.57). We identify this situation as the 'true classical limit' of the FEL.

Indeed, when we plot in Fig. 3.7 $W^{(1)}$ from Eq. (3.55) and $f^{(1)}$ from Eq. (2.56) for the parameters $\tau = 1$, $\bar{\wp} = \pi$, $\Delta\wp = 1$ and $\omega_\mathrm{r}T = 0.1$ both curves match since the ratio of recoil $\hbar k$ and momentum spread Δp is very small, that is $\hbar k/\Delta p = 0.1$.
Hence, we obtain the classical limit [33, 91] for the Wigner function when the terms with $\hbar$ are small *and* when the initial state is classical as well, that is the width Δp of the momentum distribution is large compared to the recoil. We call this situation the 'true classical limit' of the FEL.
However, ultimately we are not interested in the explicit form of the Wigner function but in the gain of the FEL which has to be calculated from the expectation value $\langle \sin\theta \rangle$ in Eq. (3.44). Thus, we first consider the full series in Eq. (3.52) and form $\langle \sin\theta \rangle$ before we investigate how the classical limit emerges for the gain.

3.3.3 Quantum corrections for cold and warm electron beam

To compute the gain of the laser field we insert the perturbative expansion of the Wigner function into the equation of motion, Eq. (3.44). While the zeroth-order term $W^{(0)}$ does not contribute to the gain since it is independent of θ we obtain in first order

$$\langle \sin\theta \rangle = -\frac{\kappa|a_\mathrm{L}|}{2} \int \mathrm{d}\wp \frac{\sin \wp\tau}{\wp} \sum_{m=0}^{\infty} \frac{(\omega_\mathrm{r}T)^{2m}}{(2m+1)!} \frac{\partial^{2m+1}}{\partial \wp^{2m+1}} g(\wp)\,, \tag{3.58}$$

where we have used the explicit expression, Eq. (3.52), for $W^{(1)}$.
By integrating from 0 to 1 with respect to time τ we find the relation

$$G = \frac{1}{4} gTN\kappa \sum_{m=0}^{\infty} \frac{(\omega_\mathrm{r}T)^{2m}}{(2m+1)!} \int \mathrm{d}\wp\, \mathrm{sinc}^2\left(\frac{\wp}{2}\right) \frac{\partial^{2m+1} g(\wp)}{\partial \wp^{2m+1}} \tag{3.59}$$

for the gain G, Eq. (2.18). In the following we investigate this relation in the limits of a cold and a warm electron beam, respectively.

Cold beam

In the cold-beam case we consider a very sharp momentum distribution $g(\wp)$ characterized by a small width, that is $\Delta\wp \ll 1$, allowing us to make the approximation $g(\wp) \cong \delta(\wp - \bar{\wp})$. By integrating the expression in Eq. (3.59) by parts we obtain

$$G = -\frac{1}{4} gTN\kappa \sum_{m=0}^{\infty} \frac{(\omega_\mathrm{r}T)^{2m}}{(2m+1)!} \int \mathrm{d}\wp \left[\frac{\partial^{2m+1}}{\partial \wp^{2m+1}} \mathrm{sinc}^2\left(\frac{\wp}{2}\right)\right] g(\wp)\,, \tag{3.60}$$

where we have assumed that $g(\wp)$ and its derivatives vanish for $\wp \to \pm\infty$. In the next step we approximate $g(\wp)$ as delta function which yields the result

$$G = -\frac{1}{4} gTN\kappa \sum_{m=0}^{\infty} \frac{(\omega_\mathrm{r}T)^{2m}}{(2m+1)!} \frac{\partial^{2m+1}}{\partial \wp^{2m+1}} \mathrm{sinc}^2\left(\frac{\wp}{2}\right)\Bigg|_{\wp=\bar{\wp}} \tag{3.61}$$

after evaluating the integral over $\wp$.

By shifting the derivatives from $g(\wp)$ to the sinc^2 function we get rid of any $\Delta\wp$ in the denominator which for example becomes apparent by comparing Eq. (3.61) with Eq. (3.57). Hence, we obtain the classical limit for a cold electron beam even for $\Delta p \to 0$, where the ratio $q/\Delta p$ becomes very large. Here, the quantum corrections indeed scale with powers of $\omega_\mathrm{r} T$, even when we are outside the true classical limit for the Wigner function.

We note that the expression in Eq. (3.61) corresponds to the Taylor expansion of the difference, Eq. (3.31), of the two shifted sinc^2 functions from standard-perturbation theory. However, our approach does not rely on single-photon processes but is rather a generalization of the solution of the classical Boltzmann equation in Chap. 2.

The lowest-order corrections to the classical gain are obtained when we consider just the first two terms of the series, Eq. (3.61), yielding

$$G \cong -\frac{1}{4}\kappa g T N \left(\frac{\partial}{\partial \wp} \mathrm{sinc}^2\left(\frac{\wp}{2}\right)\bigg|_{\wp=\bar{\wp}} + \frac{(\omega_\mathrm{r} T)^2}{6} \frac{\partial^3}{\partial \wp^3} \mathrm{sinc}^2\left(\frac{\wp}{2}\right)\bigg|_{\wp=\bar{\wp}} \right) \tag{3.62}$$

or equivalently

$$G = \frac{2}{\pi^3}\kappa g T N \left(\mathcal{A}(\bar{\wp}) - \left(\frac{\omega_\mathrm{r} T}{\pi}\right)^2 \mathcal{Q}(\bar{\wp}) \right) , \tag{3.63}$$

where we have recalled the definitions Eqs. (3.21) and (3.25) for $\mathcal{A}$ and $\mathcal{Q}$, respectively.

Hence, we have found the same results as in the preceding section, where we have considered operators in the Heisenberg picture, at least for linear gain. That is not surprising since, both, the Wigner function and the Heisenberg picture are equivalent descriptions of quantum mechanics. However, the calculational effort for the Wigner function is much smaller and we find the result in a straightforward way in contrast to the cumbersome computations for the Heisenberg picture in App. B. This difference arises since for the Wigner function we have ordered the operators *from the beginning* in a suitable way and have derived an equation of motion, Eq. (3.42), for a c-number. On the other side, we have had to take care of the ordering of the operators in *every single step* of the calculation in the Heisenberg picture.

In the cold-beam limit the quantum corrections scale with powers of $\omega_\mathrm{r} T$, according to Eq. (3.61), and they are independent of the momentum spread $\Delta\wp$. To be in this limit we require $\Delta\wp \ll 1$ which we rewrite to

$$\Delta p \ll \frac{q}{2\omega_\mathrm{r} T} . \tag{3.64}$$

In the classical regime where $\omega_\mathrm{r} T \ll 1$ it is not difficult to satisfy this constraint.

However, when we consider the transition regime between classical and quantum physics we assume that the quantum corrections are moderate, that is $\omega_\mathrm{r} T = \mathcal{O}(1)$. Hence, we obtain from Eq. (3.64) the relation

$$\Delta p \ll q \tag{3.65}$$

which is analogous to the condition in Eq. (3.5) from the heuristic approach in Sec. 3.1. We emphasize that Eq. (3.65) only makes a statement about the validity of the cold-beam limit. In order to verify whether a large momentum width Δp really suppresses quantum corrections we have to go beyond this limit.

Warm beam

The opposite limit to a sharp momentum distribution is given by a very broad one with $\Delta\wp \gg 1$, that is a warm electron beam. For this case we cannot approximate $g(\wp)$ by a Delta function but instead the sinc^2 function in Eq. (3.59), that is

$$\mathrm{sinc}^2\left(\frac{\wp}{2}\right) \approx \delta(\wp)\,. \tag{3.66}$$

Hence, the integration over $\wp$ in Eq. (3.59) yields

$$G = \frac{1}{4}\kappa g T N \sum_{m=0}^{\infty} \frac{(\omega_\mathrm{r} T)^{2m}}{(2m+1)!} \left.\frac{\partial^{2m+1} g(\wp)}{\partial \wp^{2m+1}}\right|_{\wp=0}\,, \tag{3.67}$$

where in contrast to Eq. (3.61) the derivatives with respect to $\wp$ are applied now on $g(\wp)$.
To obtain an explicit expression for the gain in the warm-beam case we assume that the momentum distribution $g(\wp)$ is a Gaussian of the form of Eq. (3.53). When we insert this distribution into Eq. (3.67) we arrive at

$$G = \frac{1}{4}\kappa g T N \left(\sum_{m=0}^{\infty} \frac{(\omega_\mathrm{r} T)^{2m}}{(2m+1)!} \frac{H_{2m+1}\left(\frac{\bar\wp}{\sqrt{2}\Delta\wp}\right)}{(\sqrt{2}\Delta\wp)^{2m+1}}\right) g(\wp)\,, \tag{3.68}$$

where we have used Eq. (3.54) to calculate the derivatives of the Gaussian in terms of the Hermite polynomials H_n.
We are interested in the limit where quantum corrections to the classical gain are moderate. That is why we, similar to the cold beam case, consider just the first two terms of the series in Eq. (3.68) yielding

$$G = \frac{1}{4}\kappa g T N \left[H_1\left(\frac{\bar\wp}{\sqrt{2}\Delta\wp}\right) + \frac{1}{12}\left(\frac{\omega_\mathrm{r} T}{\Delta\wp}\right)^2 H_3\left(\frac{\bar\wp}{\sqrt{2}\Delta\wp}\right)\right] g(\wp) \tag{3.69}$$

which is shown in Fig. 3.8 for $\Delta\wp = 10$. We observe that for $\omega_\mathrm{r} T = 3$ the quantum effects are negligible since they are suppressed by the large momentum spread due to $\hbar k/\Delta p = 0.3$. This result differs from the cold beam case, where already $\omega_\mathrm{r} T = 2$ leads to noticeable quantum corrections according to Fig. 3.5. However, increasing $\omega_\mathrm{r} T$ to $\omega_\mathrm{r} T = 7$ effects the gain since $\hbar k/\Delta p = 0.7$. Similar to a cold beam we observe a decrease of the maximum gain and a shift of the positions for maximum and minimum to the right and to the left, respectively.
Indeed, the procedure of cutting off the series in Eq. (3.67) is justified for

$$\frac{\omega_\mathrm{r} T}{\Delta\wp} = \frac{q/2}{\Delta p} \ll \sqrt{3}\,, \tag{3.70}$$

where we have used the explicit expressions [90] for H_1 and H_3 at $\bar\wp = \Delta\wp$. Hence, the quantum corrections scale with powers of the ratio of recoil q and momentum spread Δp.
The inequality, Eq. (3.70), stands of course in contrast to the cold-beam case, where due to Eq. (3.65) Δp has to be much smaller than the recoil q. However, when we demand for moderate quantum corrections in the transition regime, Δp and q have to be of the same

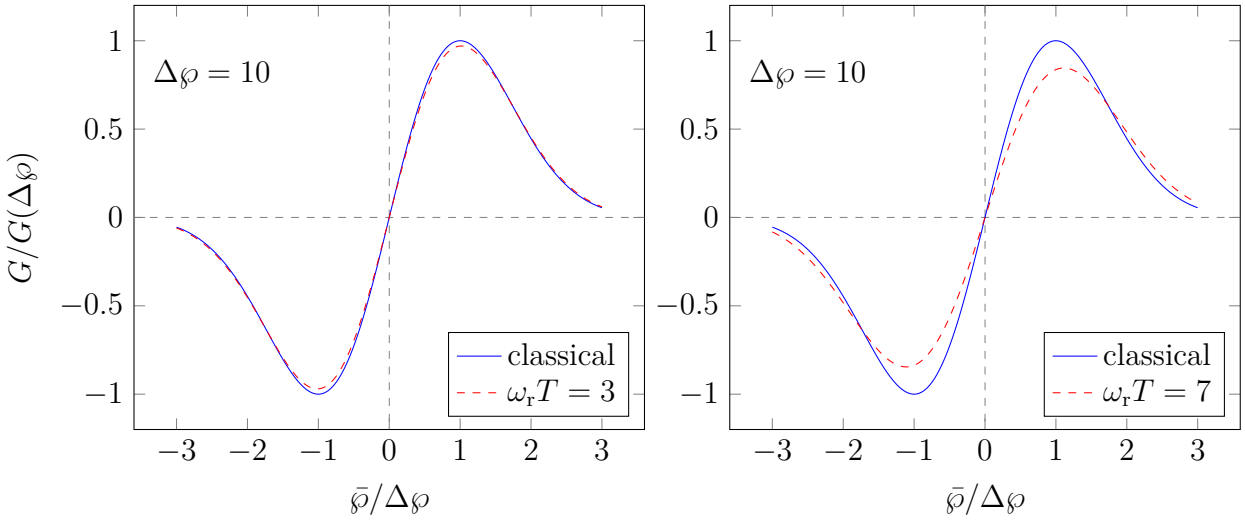

Figure 3.8: Quantum corrections for a warm electron beam in the low-gain, small-signal regime: we have drawn the gain G, Eq. (3.69), including quantum corrections as a function of the mean value $\bar{\wp}$ of the initial momentum distribution $g(\wp)$, Eq. (3.53), characterized by the width $\Delta_\wp = 10$. For $\omega_r T = 3$ (left side), leading to $\hbar k/\Delta p = 0.3$, we only observe very small corrections (red, dashed curve) to the classical gain, Eq. (2.60) (bue line). However, for $\omega_r T = 7$ (right side), that is $\hbar k/\Delta p = 0.7$, quantum effects lead to a shift of the positions of the maximum and minimum to the right and to the left, respectively, while the height of this curve decreases.

order of magnitude, that is $q \lesssim \Delta p$. Otherwise, for increasing Δp the quantum corrections in Eq. (3.69) are strongly suppressed and the classical limit, Eq. (2.60), is obtained.
In conclusion, in both limiting cases, that is a cold and a warm electron beam, we require a narrow momentum distribution the width Δp of which has to be of the order of the quantum mechanical recoil q.

3.3.4 Realistic model for electron beam & wave packets

Up to now we have characterized the electron beam prior to interaction as a uniform distribution in position space and an arbitrary, for example Gaussian, distribution $g(\wp)$ in momentum space. In recent years, however, there was a rising interest [92, 93] in modeling a more realistic electron beam as well as in including effects due to the interpretation of electrons as wave packets. In the following, we shortly study these topics from a phase-space point of view employing the Wigner function formalism.
In analogy to Ref. [93] we consider a Gaussian wave packet

$$|\Psi_{\tilde{z},\tilde{p}}(0)\rangle = \frac{1}{\left(\sqrt{2\pi}\Delta p_\mathrm{q}\right)^{1/2}} \int \mathrm{d}p' \; \mathrm{e}^{ip'\tilde{z}/\hbar} \exp\left[-\frac{(p'-\tilde{p})^2}{4\Delta p_\mathrm{q}^2}\right] |p'\rangle \tag{3.71}$$

in momentum representation for the initial state of the electron which is characterized by the mean values for position and momentum, $\tilde{z}$ and $\tilde{p}$, respectively, and the standard deviation Δp_q in momentum space.
According to Ref. [40] the Wigner function, Eq. (3.35), can equivalently be defined by

$$W_{\tilde{z},\tilde{p}}(z,p;0) \equiv \frac{1}{2\pi\hbar} \int \mathrm{d}\xi \; \mathrm{e}^{-ip\xi/\hbar} \langle z+\xi/2|\Psi_{\tilde{z},\tilde{p}}(0)\rangle \langle \Psi_{\tilde{z},\tilde{p}}(0)|z-\xi/2\rangle \;, \tag{3.72}$$

where we have assumed the pure state described by the state vector in Eq. (3.71) instead of an arbitrary density operator $\hat{\rho}$. With the help of Eqs. (3.71) and (3.72) as well as the relation

$$\langle z \pm \xi/2|p\rangle = \frac{1}{\sqrt{2\pi\hbar}} \, \mathrm{e}^{ip(z\pm\xi/2)/\hbar} \tag{3.73}$$

we obtain the Wigner function

$$W_{\tilde{z},\tilde{p}}(z,p;0) = \frac{1}{\pi\hbar} \exp\left[-\frac{(z-\tilde{z})^2}{2\Delta z_\mathrm{q}^2}\right] \exp\left[-\frac{(p-\tilde{p})^2}{2\Delta p_\mathrm{q}^2}\right] \tag{3.74}$$

corresponding to the state $|\Psi_{\tilde{z},\tilde{p}}(0)\rangle$ which represents the product of a Gaussian in position space and one in momentum space. Here, we have introduced the width

$$\Delta z_\mathrm{q} \equiv \frac{\hbar}{2\Delta p_\mathrm{q}} \tag{3.75}$$

of the wave packet in z-direction which follows from Eqs. (3.71) and (3.72). We note that $\Delta z_\mathrm{q} \Delta p_\mathrm{q} = \hbar/2$ which is the minimum phase space volume a quantum state can occupy according to the Heisenberg uncertainty principle. Therefore, we identify this state, Eq. (3.71), as minimum uncertainty wave packet [82].

However, besides the intrinsic uncertainty due to the widths Δp_{q} and Δz_{q} of the wave packet, Eq. (3.71), the electrons have a statistical classical uncertainty when they leave the accelerator. In analogy to our previous procedure we assume that the mean value $\tilde{z}$ of the initial state, Eq. (3.71), is uniformly distributed along a certain length L when we model a realistic beam of electrons. Moreover, the mean momenta $\tilde{p}$ of the electron wave packet should be distributed according to the Gaussian

$$f_{\mathrm{cl}}(\tilde{p};\bar{p}) \equiv \frac{1}{\sqrt{2\pi}\Delta p_{\mathrm{cl}}} \exp\left[-\frac{(\tilde{p}-\bar{p})^2}{2\Delta p_{\mathrm{cl}}^2}\right] \tag{3.76}$$

which is characterized by the mean value $\bar{p}$ and the 'classical' standard deviation Δp_{cl}.

Hence, the Wigner function of this statistical mixture has to be calculated via the prescription

$$W(z,p;0) \equiv \frac{1}{L}\int \mathrm{d}\tilde{z} \int \mathrm{d}\tilde{p}\, f_{\mathrm{cl}}(\bar{p};\tilde{p}) W_{\tilde{z},\tilde{p}}(z,p;0) \tag{3.77}$$

which yields

$$W(z,p;0) = \frac{1}{\sqrt{2\pi}\Delta p L} \exp\left[-\frac{(p-\bar{p})^2}{2\Delta p^2}\right] \tag{3.78}$$

after using fundamental relations for Gaussian integrals [67]. We observe that $W(z,p;0)$ is independent of position z while it constitutes a Gaussian in momentum space. We note that the construction of a 'classical' state from a wave packet in Ref. [33] and, moreover, the initial Wigner function, Eq. (3.46), of our previous procedure is analogous to the expression in Eq. (3.78).

However, we can now identify the single contributions to the total variance

$$\Delta p \equiv \sqrt{\Delta p_{\mathrm{q}}^2 + \Delta p_{\mathrm{cl}}^2} \tag{3.79}$$

in analogy to Ref. [93] as (i) the width Δp_{q} of the wave packet and (ii) the momentum spread Δp_{cl} due to statistical uncertainty.

To obtain quantum effects in the FEL we require

$$\sqrt{\Delta p_{\mathrm{q}}^2 + \Delta p_{\mathrm{cl}}^2} \ll \hbar k \tag{3.80}$$

according to the preceding section. When we assume that, in principle, the classical statistical uncertainty can be reduced to zero we still have to pay attention to Δp_{q} as a lower bound for the momentum spread leading to the constraint $\Delta p_{\mathrm{q}} \ll \hbar k$. We note that it is not clear how large the width of an electron wave packet is when the electron leaves the accelerator. To make statements about this magnitude we would have to develop a complete theory for the electron dynamics in the accelerator.

In Ref. [93] an additional drift region between accelerator and the interaction region was considered. This assumption leads to the evolved Wigner function

$$W(z,p;t_{\mathrm{D}}) = W\left(z-\frac{p}{m}t_{\mathrm{D}},p;0\right) = \frac{1}{\pi\hbar}\exp\left\{-\frac{\left[z-\left(\tilde{z}+\frac{p}{m}t_{\mathrm{D}}\right)\right]^2}{2\Delta z_{\mathrm{q}}^2}\right\}\exp\left[-\frac{(p-\tilde{p})^2}{2\Delta p_{\mathrm{q}}^2}\right] \tag{3.81}$$

corresponding to the unperturbed dynamics during the time t_D in which the electron travels through the drift region. While the width of the distribution in position space spreads, according to the relation

$$\Delta z_\mathrm{q}(t) = \sqrt{\Delta z_\mathrm{q}^2 + \left(\frac{\Delta p_\mathrm{q}}{m} t_\mathrm{D}\right)^2}\,, \tag{3.82}$$

the corresponding width Δp for the momentum does not change. Hence, the uncertainty $\Delta z_\mathrm{q}(t)\Delta p_\mathrm{q}$ of position and momentum in Eq. (3.81) is increased in comparison to its minimum value in Eq. (3.71). However, since in the statistical mixture in Eq. (3.77) we have to integrate over $\tilde{z}$ and since Δp does not change due to the free evolution, the drift region does not have an influence on the result for the statistical mixture in Eqs. (3.78) and (3.79).

However, it is still to be discussed under which conditions the assumption of a uniform distribution in position space is justified and when we have to consider the wave packet nature of the electrons. In Ref. [93] the time evolution of such a wave packet was calculated for a Smith–Purcell FEL and it was found that under certain circumstances effects of using a wave packet can emerge. To study this topic we therefore apply our perturbative treatment of the Quantum Liouville equation in the following to the initial Wigner function, Eq. (3.71), for a minimum uncertainty wave packet.

A crucial difference between a localized wave packet and a uniform distribution for the positions already emerges in zeroth order of our perturbative expansion of the Wigner function. The corresponding contribution

$$W^{(0)}(\theta, \wp; \tau) = W(\theta - \wp\tau, \wp; 0) = \frac{1}{2\pi\omega_\mathrm{r} T} \exp\left\{-\frac{\left[\theta - \left(\tilde{\theta} + \wp\tau\right)\right]^2}{2\Delta\theta_\mathrm{q}^2}\right\} \exp\left[-\frac{(\wp - \tilde{\wp})^2}{2\Delta\wp_\mathrm{q}^2}\right], \tag{3.83}$$

where we have recalled our usual dimensionless variables from Eq. (2.34), now depends on θ in contrast to Eq. (3.49) for a uniform distribution. Hence, we observe a nonzero mean value when we perform the averaging over positions. With the help of Eq. (3.83) we obtain the expression

$$|a(T)| - |a(0)| \cong -gTN\, \mathrm{e}^{-\Delta\theta_q^2/2}\, \frac{\cos\tilde{\theta} - \cos\left(\tilde{\theta} + \tilde{\wp}\right)}{\tilde{\wp}} \tag{3.84}$$

for the change of the laser field, where we have applied relations for Gaussian integrals as well as fundamental trigonometric identities [67]. Moreover, we have assumed a cold electron beam, that is $\Delta\wp_\mathrm{q} \ll 1$, leading to a Delta function $g(\wp) \cong \delta(\wp - \tilde{\wp})$ for the initial momentum distribution.

When we the position uncertainty is also very small, that is $\Delta\theta_\mathrm{q} \to 0$ in Eq. (3.84), we arrive at

$$|a(T)| - |a(0)| \cong -gTN\, \frac{\cos\tilde{\theta} - \cos\left(\tilde{\theta} + \tilde{\wp}\right)}{\tilde{\wp}}\,. \tag{3.85}$$

This expression equals the classical result emerging from the point-particle limit given by the initial distribution $W(\theta, \wp, 0) = \delta(\theta - \tilde{\theta})\delta(\wp - \tilde{\wp})$. On the other hand, the plane-wave limit $\Delta\theta_\mathrm{q} \to \infty$ leads to a vanishing value for the change of the field amplitude.

In order to obtain explicit effects due to the wave-packet nature of the electrons we thus require that $\Delta\theta_\mathrm{q} \sim \mathcal{O}(1)$. Since we consider a minimum uncertainty wave packet we arrive at

the condition

$$\Delta\theta_{\mathrm{q}} = \frac{\omega_{\mathrm{r}} T}{\Delta\wp_{\mathrm{q}}} = \frac{\hbar k}{\Delta p} \sim \mathcal{O}(1)\,, \tag{3.86}$$

that is the recoil has to be of the order of the momentum spread. Since we consider a cold electron beam $\Delta\wp_{\mathrm{q}} \ll 1$ we also demand for $\omega_{\mathrm{r}} T \ll 1$. Further decreasing the recoil down to $\hbar k \ll \Delta p$, however, suppresses this effect and gives rise to the classical result Eq. (3.85).
We note that the change of the field amplitude in Eq. (3.84) is independent of the initial amplitude and hence we cannot identify stimulated emission as the origin of this change. In order to observe effects corresponding to stimulated emission we would have to consider higher orders of our perturbative approach in powers of $\kappa|a_{\mathrm{L}}|$. Moreover, the result in Eq. (3.84), indeed, reduces to the correct point-particle limit, Eq. (3.85) , for $\Delta\theta_{\mathrm{q}} \to 0$ and $\Delta p_{\mathrm{q}} \to 0$ in contrast to the results of Ref. [93].

3.4 Summary

In this chapter we have discussed the transition from classical to quantum for the FEL dynamics. First, we have employed an illustrative model to deduce the two conditions for quantum effects to emerge which are given by (i) a large quantum mechanical recoil, that is $\omega_{\mathrm{r}} T \sim \mathcal{O}(1)$ or $\omega_{\mathrm{r}} T > 1$ with the recoil frequency ω_{r} defined in Eq. (3.2), and (ii) a small momentum spread Δp of the electron beam for which we require $\Delta p \ll \hbar k$. Moreover, we have discussed that the quantized motion of the electron, leading to a discrete momentum ladder, is responsible for quantum effects in the FEL and not quantum mechanical properties of the laser field.
In order to obtain explicit expressions for quantum corrections to the classical FEL gain we have employed an approach based on the Heisenberg picture as well as one in phase space in terms of the Wigner function. Needless to say, both procedures give analogous results. Moreover, we arrive at expressions analogous to the ones due to standard perturbation theory for the Schrödinger equation of Ref. [83]. However, in contrast to this model we do not obtain the contradiction to describe multiphoton processes by single-photon probabilities, but instead we identify the nonzero commutator of position and momentum of the electron as the origin for quantum effects.
In analogy to the classical–quantum transition for arbitrary systems in Ref. [33] we have discovered that the classical limit of the Wigner function only emerges for a ‘classical’ initial state with a broad momentum spread illustrated in Figs. 3.6 and 3.7. Moreover, we have investigated the limits of a cold, Fig. 3.5, and a warm electron beam, Fig. 3.8, and have rigorously proved our assumption that a large momentum spread suppresses quantum effects. At the end of the chapter we have briefly discussed the topic of realistically modeling electron beams and the influence of wave packets. These topics where brought up in Refs. [92, 93] and we have established the connection of our model to these articles. In this context, we propose that our approach in terms of the Wigner function is well-suited to study the time evolution of an electron-wave packet in the FEL.

4 Quantum Statistical Properties of the FEL Radiation in the Classical Regime

So far, we have only considered the gain of an FEL in a classical and in a semiclassical approach, respectively. However, in order to study the statistical properties of the radiation, we also have to quantize the laser field and by this procedure we arrive at a fully-quantized model of the FEL dynamics. In this context, we derive the steady-state photon statistics and the intrinsic linewidth of a low-gain, small-signal FEL oscillator in the classical regime within a novel approach based on the ideas developed in the preceding chapter for the Wigner distribution function. Later on in this thesis we use the results of this chapter as reference when we study the corresponding statistical features of a Quantum FEL.
In order to bring our model into a broader context and distinguish it from other approaches we first review the existing literature on a quantum theory for the FEL with emphasis on the resulting statistical properties of the radiation. We then study the FEL dynamics in the classical limit by employing the Wigner representation for the combined system of electron and laser field and by expanding the Wigner function in powers of the quantum mechanical recoil in close analogy to the procedure presented in the preceding chapter. After eliminating the electron variables we obtain a Fokker–Planck equation for the laser field and thus are in the position to calculate the steady-state photon statistics and the intrinsic linewidth in analogy to standard laser theory [22, 34, 56, 82, 94, 95].

4.1 Review of existing literature

There exist many approaches regarding a quantum theory for an FEL in the classical regime. Important to mention in this context are the contributions of M. Fedorov and J. McIver [51, 81, 96]. These authors were the first to point out [96] that the multiphoton processes in the FEL cannot be described by standard perturbation theory which only covers single-photon transitions. Moreover, they calculated the saturated gain, Eq. (2.67), by solving an effective Schrödinger equation with an anharmonic potential in analogy to the classical theory of the saturated FEL [51]. However, their model did not include a quantized laser field and thus it is not suitable to derive quantum statistical properties of the radiation.
Furhter crucial contributions to the quantum theory of the FEL came from W. Becker and coworkers [12, 14, 35, 97, 98, 99, 100, 101]. In their first approach [97] based on a perturbative treatment of the Dirac equation the authors also assumed a classical laser field and therefore only could determine the gain of an FEL. Another semiclassical model [98] described the FEL interaction by a Klein–Gordon equation coupled to two classical field modes giving rise to a Mathieu equation similar to Ref. [102].
In the following years more sophisticated approaches were developed which did include quantum mechanical effects of the radiation. For example in Ref. [99] the time evolution of a quantized laser field coupled to a classical and fixed current of electrons was calculated. The

momentum change of an electron by multiples of the recoil was put in by hand with the help of energy-momentum conservation.
A more rigorous treatment was presented in Refs. [12, 101] in terms of the time evolution due to a fully quantized Hamiltonian $\hat{H}_{\mathrm{I}}(t)$ in the interaction picture. The dynamics of the FEL was solved with the help of a so-called 'first-order recoil approximation'. In this technique the time-evolution operator

$$U(T/2;-T/2)=\mathcal{T}\left\{\exp\left[-\frac{i}{\hbar}\int\limits_{-T/2}^{T/2}\mathrm{d}t\,\hat{H}_{\mathrm{I}}(t)\right]\right\}, \tag{4.1}$$

with $\mathcal{T}$ as the time-ordering operator, is expanded linearly in momentum $\hat{p}$

$$U(T/2;-T/2)\cong U(T/2;-T/2)|_{p=p_0}+(\hat{p}-p_0)\,\frac{\partial}{\partial p}\,U(T/2;-T/2)|_{p=p_0} \tag{4.2}$$

around a c-number p_0. This expansion has to be performed such that the operator ordering is correct. The authors of Refs. [12] considered the effects of a single pass of the electrons on the laser field which initially is characterized by a Fock state. They deduced from their results that the FEL cannot preserve a coherent state when gain is not negligible.
The first theoretical models that considered an FEL oscillator were developed by J. Gea-Banacloche. In Ref. [83] standard perturbation theory and the photon number representation were employed to derive properties of the radiation although perturbation theory does not include multiphoton processes. Moreover, the same author presented in Ref. [13] an approach which uses conditional probabilities and the classical equations of motion for the electrons to derive a Fokker–Planck-like equation. According to this article the variance in the photon number at steady state is larger than for an ordinary laser, that is the photon distribution of an FEL is always much broader than the Poissonian of a coherent state. This result was later confirmed [35] in terms of the first-order recoil approximation, where it was deduced that the steady-state photon distribution is broadened as one goes deeper into the classical regime.
Another quantity of considerable interest was the intrinsic linewidth of an FEL. In Ref. [14] the first calculation for the linewidth in the spirit of standard laser theory [22] was presented which was based on the photon number representation and the first-order recoil approximation. An illustrative approach which focused on the phase diffusion of the complex field amplitude a_{L} was pursued in Ref. [15]. The result of these references was that the linewidth of the FEL is basically a classical quantity without any appearance of the Planck constant $\hbar$.
All of the mentioned quantum models of the FEL either used the photon number representation or incorporated quantum effects into a classical theory by hand. In contrast, M. Orszag considered the Glauber–Sudarshan P-representation [84] and derived in Ref. [16] a Fokker–Planck equation. However, within this approach perturbation theory was employed and just fluctuations were treated while drift terms were neglected. Thus, the theory in Ref. [16] does not include gain and self saturation. Indeed, the resulting expression for the linewidth equals the one of Refs. [14, 15], but the model cannot make a statement about the steady-state photon number.
The novel approach which we present in the following is based on the Wigner representation of the combined system of electron and laser field. After neglecting small recoil contributions in accordance with the results of the preceding chapter we eliminate the electron variables by

a perturbative calculation. However, this procedure differs from the ordinary perturbation theory for the Schrödinger equation which in lowest order describes single-photon transitions. Our perturbative approach is rather analogous to the solution of the classical Boltzmann equation for the electrons described in Chap. 2.
This way, we derive a Fokker–Planck equation for the Wigner function of the laser field which in contrast to Ref. [16] includes drift as well as fluctuations. We obtain analogous results for the steady-state solution and for the intrinsic linewidth as in the mentioned references, however, without the tedious calculations of the first-order recoil approximation or the inclusion of quantum effects by hand.

4.2 Wigner representation for electron and laser field

In this section we derive the equation of motion for the quasiprobability function of the combined system of electron and radiation field for the classical FEL in analogy to the theory of an ordinary laser in Refs. [56, 103, 104]. For this purpose, we employ the Wigner representation [40, 82] for the density operator.
In contrast to the semi-classical approach of the preceding chapter, we now consider the fully quantized Hamiltonian, Eq. (A.45),

$$\hat{H} = \frac{\hat{p}^2}{2m} + \hbar g \left(\hat{a}_\mathrm{L}\, \mathrm{e}^{i2k\hat{z}} + \hat{a}_\mathrm{L}^\dagger\, \mathrm{e}^{-i2k\hat{z}} \right) \tag{4.3}$$

for a single electron, $N = 1$. The photon annihilation $\hat{a}_\mathrm{L}$ and creation operator $\hat{a}_\mathrm{L}^\dagger$ satisfy the commutation relation $\left[\hat{a}_\mathrm{L}, \hat{a}_\mathrm{L}^\dagger\right] = 1$ and we have made the identification $U_0 \equiv 2\hbar g$.
In the preceding chapter we have introduced the Wigner function for the electron. We now generalize this representation of the density operator $\hat{\rho}$ for the *combined* system of electron and laser field and arrive at [56]

$$W(z,p,\alpha,\alpha^*;t) \equiv \int\!\mathrm{d}\xi \int\!\mathrm{d}\zeta \int\!\mathrm{d}\beta \int\!\mathrm{d}\beta^*\, \mathrm{e}^{-iz\xi}\, \mathrm{e}^{-ip\zeta}\, \mathrm{e}^{-i\alpha\beta}\, \mathrm{e}^{-i\alpha^*\beta^*}\, \chi_{\hat{\rho}}(\xi,\zeta,\beta,\beta^*;t)\,, \tag{4.4}$$

where

$$\chi_{\hat{\rho}}(\xi,\zeta,\beta,\beta^*;t) \equiv \mathrm{Tr}\left\{ \mathrm{e}^{i\xi\hat{z}+i\zeta\hat{p}}\, \mathrm{e}^{i\beta\hat{a}_\mathrm{L}+i\beta^*\hat{a}_\mathrm{L}^\dagger}\, \hat{\rho}(t) \right\} \tag{4.5}$$

denotes the Wigner characteristic function. Moreover, z and p correspond to the position and momentum of the electron, respectively, and α as well as α^* describe the complex amplitudes of the laser field.
The expectation value of an observable $\hat{\mathcal{O}}$ has to be calculated from the integral

$$\langle\hat{\mathcal{O}}\rangle = \int\!\mathrm{d}z \int\!\mathrm{d}p \int\!\mathrm{d}^2\alpha\, \tilde{\mathcal{O}}(z,p,\alpha,\alpha^*) W(z,p,\alpha,\alpha^*;t) \tag{4.6}$$

with the Wigner–Weyl transform [33, 82]

$$\tilde{\mathcal{O}}(z,p,\alpha,\alpha^*) \equiv \int\!\mathrm{d}\xi \int\!\mathrm{d}\zeta \int\!\mathrm{d}\beta \int\!\mathrm{d}\beta^*\, \mathrm{e}^{-iz\xi}\, \mathrm{e}^{-ip\zeta}\, \mathrm{e}^{-i\alpha\beta}\, \mathrm{e}^{-i\alpha^*\beta^*}\, \chi_{\hat{\mathcal{O}}}(\xi,\zeta,\beta,\beta^*) \tag{4.7}$$

of $\hat{\mathcal{O}}$ where $\chi_{\hat{\mathcal{O}}}$ is defined in analogy to $\chi_{\hat{\rho}}$ in Eq. (4.5) with $\hat{\rho}$ replaced by $\hat{\mathcal{O}}$.

Starting from the equation of motion, Eq. (3.33), for the density operator with the Hamiltonian of Eq. (4.3) we derive with the help of the definitions Eqs. (4.4) and (4.5) the corresponding equation of motion for the Wigner function. This derivation which is presented in detail in App. C.2 yields, Eq. (C.30),

$$\begin{aligned}\left(\frac{\partial}{\partial t}+\frac{p}{m}\frac{\partial}{\partial z}\right)W(z,p,\alpha,\alpha^*;t) = \\ -\frac{1}{i}\frac{2k\hbar g}{2\hbar k}\left(\alpha\,\mathrm{e}^{i2kz}-\alpha^*\,\mathrm{e}^{-i2kz}\right)\left[W(z,p+\hbar k,\alpha,\alpha^*;t)-W(z,p-\hbar k,\alpha,\alpha^*;t)\right] \\ +\frac{1}{2i}\frac{2k\hbar g}{2\hbar k}\left(\frac{\partial}{\partial\alpha^*}\,\mathrm{e}^{i2kz}-\frac{\partial}{\partial\alpha}\,\mathrm{e}^{-i2kz}\right)\left[W(z,p+\hbar k,\alpha,\alpha^*;t)+W(z,p-\hbar k,\alpha,\alpha^*;t)\right]\end{aligned} \tag{4.8}$$

which is similar to the equation of motion, Eq. (3.41), in the semi-classical model. It includes, however, additional terms proportional to the derivatives with respect to α and α^*, respectively.

For the classical regime of the FEL it is sufficient to keep only the contributions which scale with the lowest power of $\hbar$ according to our procedure in Chap. 3. Hence, we expand

$$W(z,p\pm\hbar k,\alpha,\alpha^*;t)\cong W(z,p,\alpha,\alpha^*;t)\pm\hbar k\frac{\partial}{\partial p}W(z,p,\alpha,\alpha^*;t)+... \tag{4.9}$$

in powers of $\hbar k$. We emphasize that this approximation is not valid in general since, due to the derivatives with respect to momentum, the quantum corrections to the classical distribution function are not always negligible in accordance to our discussion regarding the semi-classical model. However, our main interest lies in the dynamics of the laser field and we proceed by eliminating the variables for the electron from the equations. For this purpose, we average over positions and momenta of the electrons just as in the semi-classical calculation of the gain in Chap. 3. Integration by parts would convince us that the quantum corrections are also negligible for small momentum widths.

Alternatively, we could take the view that in the 'true classical limit' the width Δp is larger than the quantum mechanical recoil, that is $\Delta p \gg \hbar k$. Then, according to the preceding chapter, we are always allowed to neglect contributions of higher orders in $\hbar k$. In addition to the classical regime, we consider a cold electron beam with $\Delta p \ll m/2kT$ and thus arrive at the constraint

$$\hbar k \ll \Delta p \ll \frac{1}{\omega_\mathrm{r} T}\,\hbar k \tag{4.10}$$

for the initial momentum spread. Here, we have recalled the definition, Eq. (3.2), of the recoil frequency ω_r. Since we consider the classical limit, where $\omega_\mathrm{r} T \ll 1$, the condition in Eq. (4.10)can be easily satisfied.

By keeping only the lowest-order terms of the expansion, Eq. (4.9), we finally obtain the equation of motion

$$\left(\frac{\partial}{\partial\tau}+\wp\frac{\partial}{\partial\theta}\right)W(\theta,\wp,\alpha,\alpha^*;\tau)=-\frac{1}{2i}\kappa\left[\alpha\,\mathrm{e}^{i\theta}-\alpha^*\,\mathrm{e}^{-i\theta}\right]\frac{\partial}{\partial\wp}W(\theta,\wp,\alpha,\alpha^*;\tau)$$
$$+\frac{1}{2i}\frac{\kappa}{2}\left[\frac{1}{\omega_\mathrm{r}T}\frac{\partial}{\partial\alpha^*}\,\mathrm{e}^{i\theta}-\frac{1}{\omega_\mathrm{r}T}\frac{\partial}{\partial\alpha}\,\mathrm{e}^{-i\theta}\right]W(\theta,\wp,\alpha,\alpha^*;\tau) \tag{4.11}$$

for the Wigner function of the classical FEL in terms of the dimensionless variables

$$\begin{cases}\tau & \equiv\frac{t}{T}\\ \theta & \equiv 2kz\\ \wp & \equiv\frac{2kT}{m}p\\ \kappa & \equiv\frac{2(2kT)^2}{m}\hbar g\\ \omega_\mathrm{r}T & \equiv\frac{2kT}{m}\hbar k\end{cases} \tag{4.12}$$

introduced in Eq. (2.34). We note the relation $\kappa=4(\omega_\mathrm{r}T)(gT)$ from the definition, Eq. (3.2), of the recoil frequency.
The inspection of Eq. (4.11) further reveals that the dynamics of W is governed by three different contributions: While the left-hand side of Eq. (4.11) describes the free motion of the electron, the right-hand side includes the interaction between electron and laser field. The first term on the right-hand side, proportional to the derivative with respect to the momentum $\wp$ of the electron, corresponds to the classical Boltzmann equation, Eq. (2.49), for the electron distribution. The second term, however, is an addition and includes derivatives with respect to the field amplitudes α and α^*, respectively, but no derivative with respect to $\wp$.

4.3 Fokker–Planck equation

Our main focus lies on the properties of the radiation from a classical FEL. For this reason we eliminate the variables θ and $\wp$ for the electron dynamics in the time evolution, Eq. (4.11), of the system and keep only the dependency on the amplitudes α and α^* of the laser field. For this purpose, we employ perturbation theory in analogy to the treatment of the classical Boltzmann equation in Chap. 2. This procedure restricts us to the small-signal limit. By going to fourth order and including cavity losses we are able to derive a Fokker–Planck equation for the reduced Wigner function

$$W_\mathrm{L}(\alpha,\alpha;\tau)\equiv\int\mathrm{d}\theta\int\mathrm{d}\wp\,W(\theta,\wp,\alpha,\alpha^*;\tau) \tag{4.13}$$

for the laser field, which incorporates gain and self saturation as well as quantum mechanical fluctuations in analogy to standard laser theory [22, 56, 94, 103, 104]
Let us consider the time $\bar{t}$ which is during the interaction of an electron bunch with the laser, that is $t<\bar{t}\leq t+T$ which translates to $\tau<\bar{\tau}<\tau+1$ for the dimensionless time $\bar{\tau}$. At the beginning of the interaction at time τ the electron and the laser field should be uncorrelated,

that is

$$W(\theta, \wp, \alpha, \alpha^*; \tau) = W_{\mathrm{el}}(\theta, \wp; \tau) W_{\mathrm{L}}(\alpha, \alpha^*; \tau)\,. \tag{4.14}$$

Moreover, we assume that the phases θ of the electrons in a single bunch are uniformly distributed prior to interaction, giving rise to

$$W_{\mathrm{el}}(\theta, \wp; \tau) = \frac{1}{2\pi} g(\wp)\,, \tag{4.15}$$

where $g(\wp)$ denotes the initial momentum distribution. This distribution can for example be described by a Gaussian

$$g(\wp) = \frac{1}{\sqrt{2\pi}\Delta_\wp}\, \mathrm{e}^{-\frac{(\wp-\bar{\wp})^2}{2\Delta_\wp^2}} \tag{4.16}$$

with expectation value $\bar{\wp}$ and standard deviation $\Delta_\wp$. In the following we always consider a cold electron beam, that is $g(\wp) \cong \delta(\wp - \bar{\wp})$ which corresponds to a small width $\Delta_\wp \to 0$ in momentum space.

The equation of motion, Eq. (4.11), for the total system possesses the structure

$$\mathcal{L}_0 W = \mathcal{L}_1 W\,, \tag{4.17}$$

where the operator $\mathcal{L}_0$ gives the free motion of the electron while $\mathcal{L}_1$ describes the interaction between electron and field. In the small-signal regime, $\kappa|\alpha| \ll 1$, we interpret $\mathcal{L}_1$ as perturbation and thus expand the Wigner function

$$W \cong W^{(0)} + W^{(1)} + W^{(2)} + ... \tag{4.18}$$

in an asymptotic series. Hence, we arrive at the equations

$$\begin{cases} \mathcal{L}_0 W^{(0)} & = 0 \\ \mathcal{L}_0 W^{(n)} & = \mathcal{L}_1 W^{(n-1)} \quad \text{for} \;\; n > 0 \end{cases} \tag{4.19}$$

which we have to solve order by order.

The elimination procedure is presented in detail in App. C.3. We just sketch here the basic ideas of these lengthy calculations. The free solution of Eq. (4.19) is given by $W^{(0)} = W(\theta - \wp\bar{\tau}, \wp, \alpha, \alpha^*; \tau)$ which reduces to the initial function $W^{(0)} = W(\theta, \wp, \alpha, \alpha^*; \tau)$ for our case, Eq. (4.15), of a uniform distribution of the phases θ.

Since the first-order solution $W^{(1)}$, Eq. (C.47), contains only terms proportional to $\mathrm{e}^{\pm i\theta}$ the averaging over θ in Eq. (4.13) yields a vanishing result. In second order, however, we obtain terms which are independent of θ due to products of the form $\mathrm{e}^{\pm i\theta}\,\mathrm{e}^{\mp i\theta} = 1$. The perturbative solution, Eq. (4.19), and elimination of electron variables according to Eq. (4.13) then leads to contributions which are proportional to $\partial/(\partial\alpha)\alpha W_{\mathrm{L}}$ and to $\partial/(\partial\alpha^*)\alpha^* W_{\mathrm{L}}$ as well as to a term with $\partial^2/(\partial\alpha\partial\alpha^*)W_L$, as described in Eqs. (C.53) and (C.59), respectively. The former ones correspond to drift while the latter one is responsible for fluctuations.

To obtain saturation we have to go to the fourth order [22] of the asymptotic expansion in Eq. (4.18). In accordance with Ref. [22] we just consider contributions proportional to $(\partial/\partial\alpha)|\alpha|^2\alpha$ and its conjugate conjugate which correspond to drift in the Fokker–Planck equation. In conclusion, the elimination procedure results in an explicit expression, Eq. (C.85),

for the change of the Wigner function $W_{\mathrm{L}}(\alpha,\alpha^*;\tau+1)-W_{\mathrm{L}}(\alpha,\alpha^*;\tau)$ of the laser field due to the interaction with a single electron in fourth order of our perturbative approach.
However, when we describe an FEL oscillator we have to consider many passages of electron bunches and, moreover, we have to include cavity losses. Hence, the dynamics of the laser oscillator occurs on a longer time scale than the interaction of a single electron bunch. In order to derive an equation of motion for the laser field we separate the dynamics into two parts yielding

$$\frac{\partial}{\partial t}W_{\mathrm{L}}(\alpha,\alpha^*;t)=\left(\frac{\partial}{\partial t}W_{\mathrm{L}}(\alpha,\alpha^*;t)\right)_{\mathrm{int}}+\left(\frac{\partial}{\partial t}W_{\mathrm{L}}(\alpha,\alpha^*;t)\right)_{\mathrm{loss}}, \tag{4.20}$$

where the first contribution emerges from the interaction of the electrons with the field while the second one is due to cavity losses.
For the interaction term we employ the concept of a 'coarse-grained derivative' in analogy to Ref. [22] and arrive at

$$\left(\frac{\partial}{\partial t}W_{\mathrm{L}}(\alpha,\alpha^*;t)\right)_{\mathrm{int}}\cong\frac{N}{\tau_{\mathrm{inj}}}\left(W_{\mathrm{L}}(\alpha,\alpha^*;\tau+1)-W_{\mathrm{L}}(\alpha,\alpha^*;\tau)\right), \tag{4.21}$$

that is, we have approximated the continuous change of W_{L} in time with the discrete one due to a single passage of electrons. For this purpose, we have introduced the injection time τ_{inj} which denotes the time interval between the injection of two subsequent electron bunches. Moreover, we have multiplied the change of W_{L} due to a single electron with the number N of electrons in a single bunch to model the interaction with the whole bunch. This procedure is justified when we consider the low-gain regime of the FEL, where the equations of motion decouple resulting in a single-electron model for the interaction as described in Chap. 2.
Cavity losses, on the other hand, are responsible for a dynamics of the form [22, 56]

$$\left(\frac{\partial}{\partial t}W_{\mathrm{L}}(\alpha,\alpha^*;t)\right)_{\mathrm{loss}}=\frac{\omega_{\mathrm{L}}}{2Q}\left(\frac{\partial}{\partial\alpha}\alpha+\frac{\partial}{\partial\alpha^*}\alpha^*\right)W_{\mathrm{L}}(\alpha,\alpha^*;t)+\frac{\omega_{\mathrm{L}}}{2Q}\frac{\partial^2}{\partial\alpha\partial\alpha^*}W_{\mathrm{L}}(\alpha,\alpha^*;t), \tag{4.22}$$

where Q denotes the quality of the cavity. The derivation of Eq. (4.22) can be found in App. C.4.
Combining the contribution for interaction, Eqs. (4.21) and (C.85), with the damping term Eq. (4.22) in accordance with Eq. (4.20) we finally arrive at the equation of motion

$$\begin{aligned}\frac{\partial}{\partial t}W_{\mathrm{L}}(\alpha,\alpha^*;t)=&-\frac{\partial}{\partial\alpha}\left\{\left[\left(\frac{G_{\mathrm{cl}}^{(1)}}{\tau_{\mathrm{inj}}}-\frac{\omega_{\mathrm{L}}}{2Q}\right)-\frac{G_{\mathrm{cl}}^{(3)}}{\tau_{\mathrm{inj}}}|\alpha|^2\right]\alpha+\frac{i}{\tau_{\mathrm{inj}}}\left(M_{\mathrm{cl}}^{(1)}+M_{\mathrm{cl}}^{(3)}|\alpha|^2\right)\alpha\right\}\\&\times W_{\mathrm{L}}(\alpha,\alpha^*;t)+\mathrm{c.c.}+\left(\frac{\delta n^{\mathrm{sp}}}{\tau_{\mathrm{inj}}}+\frac{\omega_{\mathrm{L}}}{2Q}\right)\frac{\partial^2}{\partial\alpha\partial\alpha^*}W_{\mathrm{L}}(\alpha,\alpha^*;t)\end{aligned} \tag{4.23}$$

for the reduced Wigner function W_{L} of the laser field, which is analogous to a Fokker–Planck equation [34].
In Eq. (4.23) we have defined the coefficients

$$G_{\mathrm{cl}}^{(1)}\equiv\frac{2gTN\kappa}{\pi^3}\mathcal{A}_{\mathrm{cl}}(\bar{\varphi}), \tag{4.24}$$

$$G_{\mathrm{cl}}^{(3)} \equiv \frac{gTN\kappa^3}{4\pi^5}\mathcal{B}_{\mathrm{cl}}(\bar{\wp})\,, \tag{4.25}$$

$$M_{\mathrm{cl}}^{(1)} \equiv \frac{gTN\kappa}{6}\mathcal{M}_{\mathrm{cl}}(\bar{\wp})\,, \tag{4.26}$$

$$M_{\mathrm{cl}}^{(3)} \equiv \frac{gTN\kappa^3}{2\pi^6}\mathcal{R}_{\mathrm{cl}}(\bar{\wp}) \tag{4.27}$$

and

$$\delta n^{\mathrm{sp}} \equiv (gT)^2 N\mathcal{S}(\bar{\wp})\,, \tag{4.28}$$

according to Eqs. (C.54), (C.81), (C.55), (C.82) and (C.60), respectively, where $\bar{\wp}$ is the mean value of the momentum distribution $g(\wp)$ for the electrons in the cold beam limit, that is $g(\wp) = \delta(\wp - \bar{\wp})$.

Moreover, we have introduced the corresponding characteristic functions

$$\mathcal{A}_{\mathrm{cl}}(\wp) \equiv \frac{\pi^3}{2}\frac{1-\cos\wp-(\wp/2)\sin\wp}{\wp^3}\,, \tag{4.29}$$

$$\begin{aligned}\mathcal{B}_{\mathrm{cl}}(\wp) \equiv \frac{\pi^5}{\wp^7}\Bigg(&\frac{9}{2}\cos 2\wp + 12\cos\wp - \frac{33}{2} + \frac{11}{4}\wp\sin 2\wp + \frac{53}{4}\wp\sin\wp \\ &-\frac{\wp^2}{2}\cos 2\wp - \frac{13}{4}\wp^2\cos\wp - \frac{\wp^3}{4}\sin\wp\Bigg)\,,\end{aligned} \tag{4.30}$$

$$\mathcal{M}_{\mathrm{cl}}(\wp) \equiv 12\,\frac{\sin\wp-(\wp/2)(1+\cos\wp)}{\wp^3}\,, \tag{4.31}$$

$$\begin{aligned}\mathcal{R}_{\mathrm{cl}}(\wp) \equiv \frac{\pi^6}{2\wp^7}\Bigg(&\frac{9}{2}\sin 2\wp + \frac{27}{2}\sin\wp - \frac{25}{4}\wp - \frac{11}{4}\wp\cos 2\wp - \frac{27}{2}\wp\cos\wp \\ &-\frac{\wp^2}{2}\sin 2\wp - \frac{13}{4}\wp^2\sin\wp + \frac{\wp^3}{4}\cos\wp\Bigg)\end{aligned} \tag{4.32}$$

and

$$\mathcal{S}(\wp) \equiv 2\frac{1-\cos\wp}{\wp^2} = \mathrm{sinc}^2\left(\frac{\wp}{2}\right) \tag{4.33}$$

in accordance with Eqs. (C.56), (C.83), (C.57), (C.84) and (C.61), respectively.

The meaning of the individual terms in the Fokker–Planck equation, Eq. (4.23), becomes most evident when we transform to the polar representation, $\alpha = \varrho\,\mathrm{e}^{-i\varphi}$, where the amplitude α is characterized by the modulus ϱ and the phase φ. Hence, we obtain

$$\begin{aligned}\frac{\partial}{\partial t}W_{\mathrm{L}}(\varrho,\varphi;t) = &-\frac{1}{\varrho}\frac{\partial}{\partial\varrho}\left[\left(\frac{G_{\mathrm{cl}}^{(1)}}{\tau_{\mathrm{inj}}} - \frac{\omega_{\mathrm{L}}}{2Q}\right)\varrho^2 - \frac{G_{\mathrm{cl}}^{(3)}}{\tau_{\mathrm{inj}}}\varrho^4\right]W_{\mathrm{L}}(\varrho,\varphi;t) \\ &+\frac{1}{4}\left(\frac{n^{\mathrm{sp}}}{\tau_{\mathrm{inj}}} + \frac{\omega_{\mathrm{L}}}{2Q}\right)\frac{1}{\varrho}\frac{\partial}{\partial\varrho}\left(\varrho\frac{\partial}{\partial\varrho}W_{\mathrm{L}}(\varrho,\varphi;t)\right) \\ &+\frac{1}{\tau_{\mathrm{inj}}}\left(M_{\mathrm{cl}}^{(1)} + M_{\mathrm{cl}}^{(3)}\varrho^2\right)\frac{\partial}{\partial\varphi}W_{\mathrm{L}}(\varrho,\varphi;t) + \frac{1}{4}\left(\frac{n^{\mathrm{sp}}}{\tau_{\mathrm{inj}}} + \frac{\omega_{\mathrm{L}}}{2Q}\right)\frac{1}{\varrho^2}\frac{\partial^2}{\partial\varphi^2}W_{\mathrm{L}}(\varrho,\varphi;t)\end{aligned} \tag{4.34}$$

for the dynamics of W_{L}.

The first line in Eq. (4.34) describes the drift of the modulus ϱ of the field amplitude. We note that the coefficients $G_{\mathrm{cl}}^{(1)}$ and $G_{\mathrm{cl}}^{(3)}$ are given by the linear gain, Eq. (3.20), and the self saturation, Eq. (3.22), respectively, of the classical FEL. We could have derived this contribution of Eq. (4.34) from

$$\dot{\varrho} = \left(\frac{G_{\mathrm{cl}}^{(1)}}{\tau_{\mathrm{inj}}} - \frac{\omega_{\mathrm{L}}}{2Q} \right) \varrho - \frac{G_{\mathrm{cl}}^{(3)}}{\tau_{\mathrm{inj}}} \varrho^3 \tag{4.35}$$

which is the classical equation of motion for ϱ including the coarse-grained derivative and cavity losses ω_{L}/Q.

Similarly, the first term of the third line in Eq. (4.34) causes a drift of the phase φ, that is mode pulling. The coefficient $M_{\mathrm{cl}}^{(1)}$ was derived in Chap. 2, Eq. (2.48), by perturbatively solving the pendulum equation, Eq. (2.36). In a similar way we would have found the expression $M_{\mathrm{cl}}^{(3)}$ by considering higher orders of this perturbative solution.

More interesting for the statistical properties of the radiation field are the diffusion terms of Eq. (4.34). While the fluctuations of the modulus in the second line are crucial for the variance of the steady-state distribution, the phase diffusion given by the second term of the third line leads to a finite linewidth. In analogy to standard laser theory [22] we identify spontaneous emission into the laser mode as the reason for these fluctuations. However, we must not confuse this effect with spontaneous emission into the reservoir of infinitely many modes of the radiation field. This latter effect is responsible for a decay of the momentum states of the electron and is considered in Ref. [27] for the quantum regime of the FEL.

Our interpretation of the fluctuations can be justified with the help of the so-called 'recoilless approximation' [35] to estimate the number δn^{sp} of spontaneously emitted photons for the FEL. This rather hand-waving procedure yields the same result as the rigorous approach in the framework of the Fokker–Planck equation, Eq. (4.23).

To estimate the contribution from spontaneous emission we assume that the electron dynamics in the Heisenberg picture is given by

$$\hat{\theta}(\bar{\tau}) = \hat{\theta}^{(\mathrm{in})} + \hat{\wp}^{(\mathrm{in})}(\bar{\tau} - \tau) \tag{4.36}$$

which corresponds to a free time evolution of the phase $\hat{\theta}$ which is determined by the initial operators $\hat{\theta}^{(\mathrm{in})}$ and $\hat{\wp}^{(\mathrm{in})}$ for for position and momentum, respectively. Moreover, we have assumed the initial state $|p\rangle$ [35] for the electron, that is a momentum eigenstate with momentum p.

On the other hand, we obtain the Heisenberg equation of motion

$$\frac{\mathrm{d}}{\mathrm{d}\bar{\tau}} \hat{a}_{\mathrm{L}} = -igT\, \mathrm{e}^{-i\hat{\theta}^{(\mathrm{in})}}\, \mathrm{e}^{-i\hat{\wp}^{(\mathrm{in})}(\bar{\tau}-\tau)} \tag{4.37}$$

for $\hat{a}_{\mathrm{L}}$ with the Hamiltonain, Eq. (4.3), where we have already inserted Eq. (4.36) and have neglected all terms arising from the commutator of $\hat{\theta}^{(\mathrm{in})}$ and $\hat{\wp}^{(\mathrm{in})}$. By integrating Eq. (4.37) over time $\bar{\tau}$ it is straightforward to derive the mean number

$$\delta n^{\mathrm{sp}} \equiv \langle \hat{n}(\tau + 1) \rangle - \langle \hat{n}(\tau) \rangle = N g^2 T^2 \mathrm{sinc}^2(\wp/2) \tag{4.38}$$

of spontaneously emitted photons for N electrons. In this derivation we have made use of $\langle p|\, \mathrm{e}^{\pm i\hat{\theta}^{(\mathrm{in})}}\, |p\rangle = 0$ and have neglected all recoil corrections. Moreover, we emphasize that the result Eq. (4.38) is only prominent when we do not consider the contributions from stimulated emission which scale with the initial photon number $n \gg 1$. We note that the recoilless approximation in Ref. [35] is based on solving the Schrödinger equation for the state vector while our derivation is based on the Heisenberg picture. However, both approaches lead to equivalent results.

In Fig. 4.1 we have drawn the characteristic functions $\mathcal{A}_{\mathrm{cl}}$, Eq. (4.29), $\mathcal{B}_{\mathrm{cl}}$, Eq. (4.30), $\mathcal{M}_{\mathrm{cl}}$, Eq. (4.31), and $\mathcal{R}_{\mathrm{cl}}$, Eq. (4.32), corresponding to linear gain, self saturation, first-order and third-order mode pulling, respectively, as functions of the Doppler parameter $\wp$. While $\mathcal{A}_{\mathrm{cl}}$ and $\mathcal{B}_{\mathrm{cl}}$, which correspond to a change of the modulus, are odd functions, $\mathcal{M}_{\mathrm{cl}}$ and $\mathcal{R}_{\mathrm{cl}}$, which are responsible for a change of the phase, are even functions. Moreover, we obtain that $\mathcal{M}_{\mathrm{cl}}$ vanishes for resonance $\wp = \pi$. In contrast, the higher-order term $\mathcal{R}_{\mathrm{cl}}$ yields a nonzero contribution at $\wp = \pi$.

Before we proceed to calculate the steady-state distribution of the laser field we note that an inspection of the Fokker–Planck equation, Eq. (4.34), justifies our procedure to consider drift terms up to fourth order while keeping fluctuation terms only up to second order. The second-order contribution to the drift, corresponding to linear gain, is reduced by cavity losses and we have to go to fourth order in order to eventually obtain steady state. The fluctuations in second order, however, are not reduced by losses and we consider only the leading term.

4.4 Steady-state solution

A Fokker–Planck equation of the form of Eq. (4.34) allows for an analytic solution [56] when we consider steady state, that is

$$\frac{\partial}{\partial t} W_{\mathrm{L}}^{(ss)}(\varrho, \varphi) = 0\,. \tag{4.39}$$

Moreover, we assume, according to Ref. [56], that

$$\frac{\partial}{\partial \varphi} W_{\mathrm{L}}^{(ss)}(\varrho, \varphi) = 0 \tag{4.40}$$

which means that for steady state the probability for the field to be described by any phase φ is uniform.

With the assumptions Eqs. (4.39) and (4.40) the Fokker–Planck equation, Eq. (4.34), takes the form

$$\frac{\partial}{\partial \varrho}\left\{\left[\left(G_{\mathrm{cl}}^{(1)} - \frac{\omega_{\mathrm{L}}\tau_{\mathrm{inj}}}{2Q}\right)\varrho^2 - G_{\mathrm{cl}}^{(3)}\varrho^4\right] W_{\mathrm{L}}(\varrho)\right\} = \frac{1}{4}\left(\delta n^{\mathrm{sp}} + \frac{\omega_{\mathrm{L}}\tau_{\mathrm{inj}}}{2Q}\right)\frac{\partial}{\partial \varrho}\left(\varrho\frac{\partial W_{\mathrm{L}}(\varrho)}{\partial \varrho}\right) \tag{4.41}$$

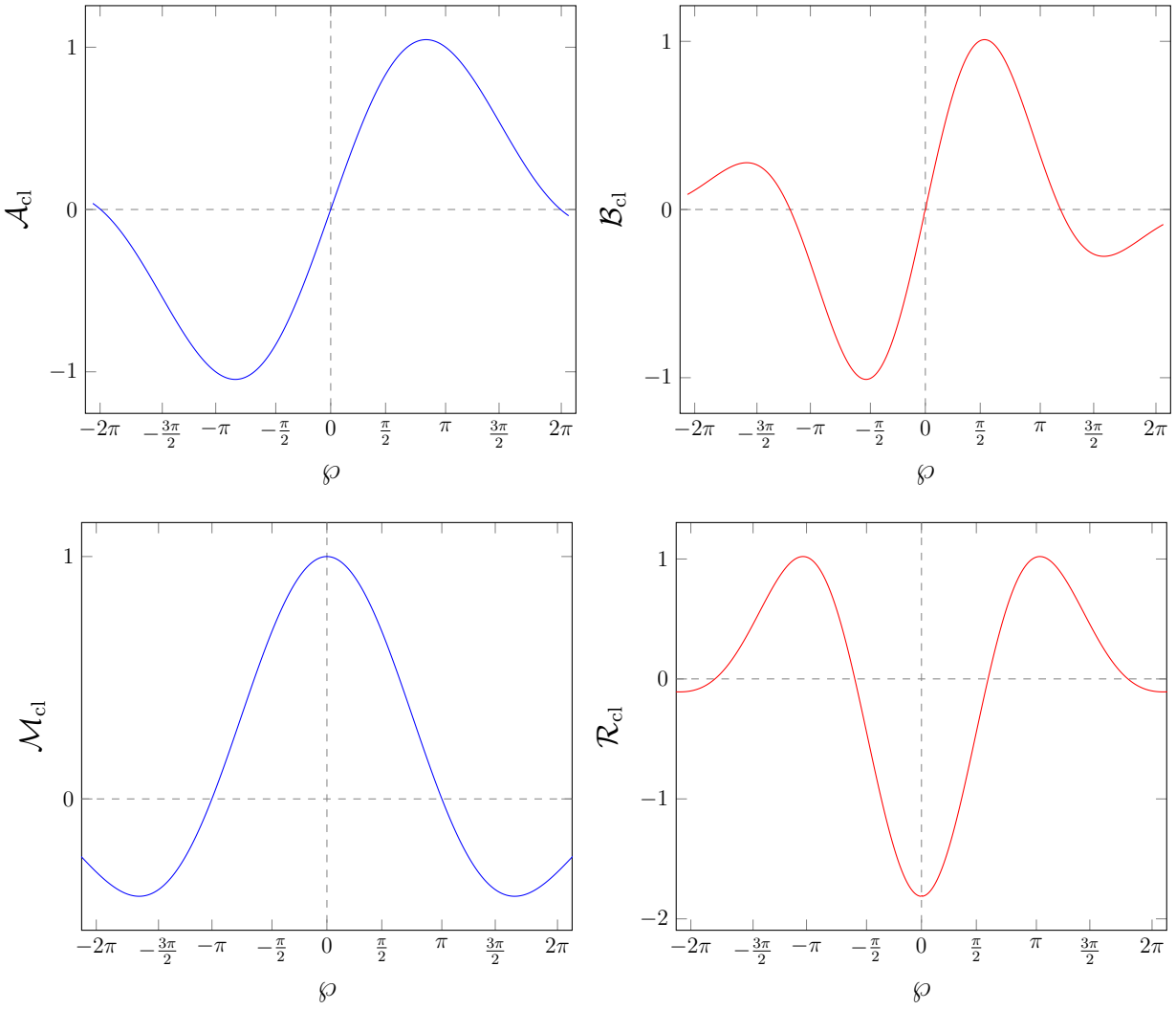

Figure 4.1: Characteristic functions $\mathcal{A}_{\mathrm{cl}}$, Eq. (4.29), $\mathcal{B}_{\mathrm{cl}}$, Eq. (4.30), $\mathcal{M}_{\mathrm{cl}}$, Eq. (4.31), and $\mathcal{R}_{\mathrm{cl}}$, Eq. (4.32), for linear gain, self saturation, first-order and third-order mode pulling, respectively, all as functions of the Doppler parameter $\wp$. While $\mathcal{A}_{\mathrm{cl}}$ and $\mathcal{B}_{\mathrm{cl}}$ are odd functions $\mathcal{M}_{\mathrm{cl}}$ and $\mathcal{R}_{\mathrm{cl}}$ are even. In contrast to $\mathcal{M}_{\mathrm{cl}}$, $\mathcal{R}_{\mathrm{cl}}$ has a nonzero value at resonance $\wp = \pi$

which only depends on the modulus ϱ. By integrating both sides of Eq. (4.41) with respect to ϱ we arrive at

$$\frac{\partial W_{\mathrm{L}}(\varrho)}{\partial \varrho} = \left\{ \frac{\left(G_{\mathrm{cl}}^{(1)} - \frac{\omega_{\mathrm{L}}\tau_{\mathrm{inj}}}{2Q}\right)\varrho - G_{\mathrm{cl}}^{(3)}\varrho^3}{\frac{1}{4}\left(\delta n^{\mathrm{sp}} + \frac{\omega_{\mathrm{L}}\tau_{\mathrm{inj}}}{2Q}\right)} \right\} W_{\mathrm{L}}(\varrho) \tag{4.42}$$

which is an ordinary differential equation of first order.

The solution of Eq. (4.42) in terms of the dimensionless intensity $n \equiv |\alpha|^2 = \varrho^2$, which we can identify as number of photons, is represented by the Gaussian

$$W_{\mathrm{L}}^{\mathrm{ss}}(n) = \frac{\mathcal{N}}{2\pi} \exp\left[-\frac{(n - n_{\mathrm{cl}}^{\mathrm{ss}})^2}{2\Delta n_{\mathrm{cl}}^2}\right] \tag{4.43}$$

for positive n as drawn in Fig. 4.2. The mean value of this distribution is given by

$$n_{\mathrm{cl}}^{\mathrm{ss}} = \frac{G_{\mathrm{cl}}^{(1)} - \frac{\omega_{\mathrm{L}}\tau_{\mathrm{inj}}}{2Q}}{G_{\mathrm{cl}}^{(3)}} \equiv \epsilon \frac{G_{\mathrm{cl}}^{(1)}}{G_{\mathrm{cl}}^{(3)}} \tag{4.44}$$

while

$$\Delta n_{\mathrm{cl}}^2 = \frac{\delta n^{\mathrm{sp}} + \frac{\omega_{\mathrm{L}}\tau_{\mathrm{inj}}}{2Q}}{2G_{\mathrm{cl}}^{(3)}} \tag{4.45}$$

denotes its variance. The normalization constant $\mathcal{N}$ has to be chosen such that the the integral over n and φ equals to unity, that is the constraint

$$\int_0^{2\pi} \mathrm{d}\varphi \int_0^{\infty} \mathrm{d}n\, W_{\mathrm{L}}^{(\mathrm{ss})}(n) = 1 \tag{4.46}$$

has to be satisfied.

4.4.1 Mean value

In order to obtain a nonzero mean value of the distribution, linear gain has to overcome the losses which we define as threshold of a laser [22]. That is why we write

$$n_{\mathrm{cl}}^{\mathrm{ss}} = \epsilon \frac{G_{\mathrm{cl}}^{(1)}}{G_{\mathrm{cl}}^{(3)}} \tag{4.47}$$

in terms of the relative deviation

$$\epsilon \equiv \frac{G_{\mathrm{cl}}^{(1)} - \frac{\omega_{\mathrm{L}}\tau_{\mathrm{inj}}}{2Q}}{G_{\mathrm{cl}}^{(1)}} \tag{4.48}$$

from threshold. To be above threshold we require $0 < \epsilon < 1$.

For the interpretation of $n_{\mathrm{cl}}^{\mathrm{ss}}$ as mean photon number we calculate the expectation value of the number operator $\hat{n} = \hat{a}_{\mathrm{L}}^{\dagger}\hat{a}_{\mathrm{L}}$, according to the prescription in Eq. (4.6). We note that the

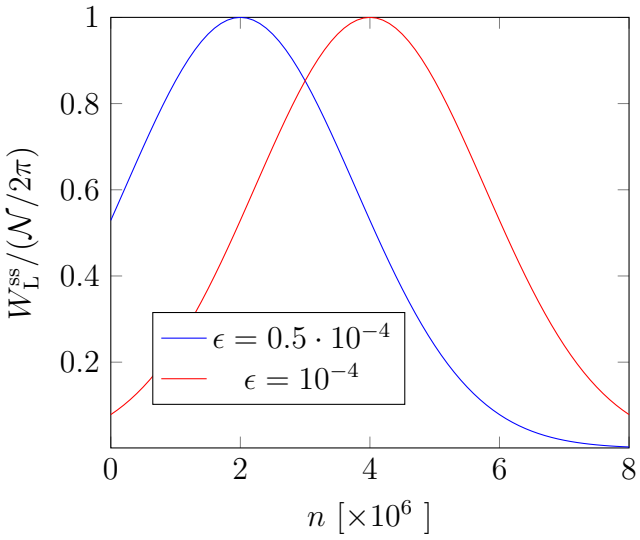

Figure 4.2: Steady-state Wigner distribution $W_{\mathrm{L}}^{\mathrm{ss}}$, Eq. (4.43), for the laser field of a classical FEL in the low-gain small-signal regime at resonance $\wp = \pi$ as function of the photon number n. We have compared the situations for two different values of the relative deviation ϵ, Eq. (4.48), from threshold, that is $\epsilon = 0.5 \cdot 10^{-4}$ (blue line) and $\epsilon = 10^{-4}$ (red line). We have chosen the parameters $gT = \sqrt{\pi^3/8} \cdot 10^{-3}$ and $\omega_{\mathrm{r}} T = 0.01$ which lead in both cases to $G_{\mathrm{cl}}^{(1)} = 0.1$, according to Eq. (4.24) with $N = 10^9$, while Eq. (4.52) yields $n_{\mathrm{cl}}^{\mathrm{ss}} = 2 \cdot 10^6$ and $n_{\mathrm{cl}}^{\mathrm{ss}} = 4 \cdot 10^6$, respectively. The small-signal approximation is justified as $\kappa\sqrt{n_{\mathrm{cl}}^{\mathrm{ss}}} \cong 0.056$ and $\kappa\sqrt{n_{\mathrm{cl}}^{\mathrm{ss}}} \cong 0.08$, respectively. Close to threshold the left wing of the Gaussian is cut off.

Wigner–Weyl representation, Eq. (4.7), of $\hat{n}$ is given by

$$\tilde{n} = |\alpha|^2 - \frac{1}{2} \tag{4.49}$$

which emerges by ordering the operators in a symmetric way [82], that is

$$\hat{n} = \frac{1}{2}(\hat{a}_{\mathrm{L}}^{\dagger}\hat{a}_{\mathrm{L}} + \hat{a}_{\mathrm{L}}\hat{a}_{\mathrm{L}}^{\dagger}) - \frac{1}{2} \tag{4.50}$$

and replacing the operators $\hat{a}_{\mathrm{L}}$ and $\hat{a}_{\mathrm{L}}^{\dagger}$ by the complex numbers α and α^*, respectively.

Hence, we have to compute the integral

$$\langle\hat{n}\rangle_{\mathrm{cl}}^{\mathrm{ss}} = 2\pi \int_0^{\infty} \mathrm{d}n \, \left(n - \frac{1}{2}\right) W_{\mathrm{L}}^{\mathrm{ss}}(n) \cong n_{\mathrm{cl}}^{\mathrm{ss}} - \frac{1}{2}\,, \tag{4.51}$$

where we have assumed that the FEL operates well above threshold. This way we are allowed to extend the lower limit of integration to $-\infty$ since in this case the left wing of the Gaussian is not cut off according to the red curve in Fig. 4.2. For $n_{\mathrm{cl}}^{\mathrm{ss}} \gg 1$ we neglect the term $1/2$ in Eq. (4.51) and the expectation value of $\hat{n}_{\mathrm{L}}$ indeed equals the number $n_{\mathrm{cl}}^{\mathrm{ss}}$.

We estimate the magnitude of the mean steady-state intensity by considering resonance, that is $\wp = \pi$, where $\mathcal{A}_{\mathrm{cl}} = 1$ and $\mathcal{B}_{\mathrm{cl}} \cong 1/\pi$. Inserting Eqs. (4.24) and (4.25) into Eq. (4.47) we obtain the expression

$$\langle\hat{n}\rangle_{\mathrm{cl}}^{\mathrm{ss}} \cong \epsilon \, \frac{1}{(\omega_{\mathrm{r}}T)^2} \frac{\pi^3/2}{(gT)^2} \tag{4.52}$$

for the mean photon number. This expression is just valid in the small-signal regime, defined by $\kappa\sqrt{n_{\mathrm{cl}}^{\mathrm{ss}}} \ll 1$ which translates with $\kappa = 4(\omega_{\mathrm{r}}T)(gt)$ to the necessary condition $\epsilon \ll 1$ for the deviation from threshold.

We note that the mean photon number scales with $\hbar^{-1}$ according to Eq. (4.52). However, this is no contradiction to the assumption of the classical regime of the FEL where the intensity can be derived from the classical equation of motion, Eq. (4.35). Instead of the photon number we have to consider the intensity, defined by [13]

$$I_{\mathrm{cl}}^{\mathrm{ss}} \equiv 2\varepsilon_0\omega_{\mathrm{L}}^2 c\mathcal{A}_{\mathrm{L}}^2 \, \langle\hat{n}\rangle_{\mathrm{cl}}^{\mathrm{ss}} = \frac{\hbar\omega_{\mathrm{L}}}{V} \, \langle\hat{n}\rangle_{\mathrm{cl}}^{\mathrm{ss}}\,, \tag{4.53}$$

where $\hbar$ in the denominator of $\langle\hat{n}\rangle_{\mathrm{cl}}^{\mathrm{ss}}$ cancels with the factor $\hbar\omega_{\mathrm{L}}$. In terms of the laboratory frame we obtain the expression, Tab. A.1,

$$I_{\mathrm{cl}}^{\mathrm{ss}} = \frac{\epsilon}{32} \frac{\gamma_0^2 m_0 c^3}{a_0^2 N_{\mathrm{W}}^4 \lambda_{\mathrm{W}}^2 r_{\mathrm{e}}}\,, \tag{4.54}$$

where we have made use of the transformation properties derived in App. A. Moreover, we have introduced the number $N_{\mathrm{W}} \equiv L/\lambda_{\mathrm{W}}$ of periods of the wiggler and have employed the definitions Eqs. (A.30) and (A.51) of the dimensionless wiggler parameter a_0 and the classical electron radius r_{e}, respectively. Indeed, $I_{\mathrm{cl}}^{\mathrm{ss}}$ is independent of $\hbar$.

4.4.2 Variance

Up to now, we have only considered the mean value of the steady-state distribution, Eq. (4.43). However, to characterize the statistical behavior of the laser field we require knowledge of the variance

$$\langle \Delta\hat{n}^2 \rangle \equiv \langle \hat{n}^2 \rangle - \langle \hat{n} \rangle^2 \tag{4.55}$$

of the photon number. For this purpose, we first write $\hat{n}^2$ in a symmetrical ordered way yielding

$$\begin{aligned} \hat{n}^2 = \frac{1}{6}\left(\hat{a}_\mathrm{L}^\dagger\hat{a}_\mathrm{L}^\dagger\hat{a}_\mathrm{L}\hat{a}_\mathrm{L} + \hat{a}_\mathrm{L}^\dagger\hat{a}_\mathrm{L}\hat{a}_\mathrm{L}^\dagger\hat{a}_\mathrm{L} + \hat{a}_\mathrm{L}^\dagger\hat{a}_\mathrm{L}\hat{a}_\mathrm{L}\hat{a}_\mathrm{L}^\dagger + \hat{a}_\mathrm{L}\hat{a}_\mathrm{L}^\dagger\hat{a}_\mathrm{L}^\dagger\hat{a}_\mathrm{L} + \hat{a}_\mathrm{L}\hat{a}_\mathrm{L}^\dagger\hat{a}_\mathrm{L}\hat{a}_\mathrm{L}^\dagger + \hat{a}_\mathrm{L}\hat{a}_\mathrm{L}\hat{a}_\mathrm{L}^\dagger\hat{a}_\mathrm{L}^\dagger\right) \\ -\frac{1}{2}\left(\hat{a}_\mathrm{L}^\dagger\hat{a}_\mathrm{L} + \hat{a}_\mathrm{L}\hat{a}_\mathrm{L}^\dagger\right), \end{aligned} \tag{4.56}$$

where we have employed the commutation relation $\left[\hat{a}_\mathrm{L}, \hat{a}_\mathrm{L}^\dagger\right] = 1$ for the operators of the laser mode. By replacing $\hat{a}_\mathrm{L}$ and $\hat{a}_\mathrm{L}^\dagger$ by the complex numbers α and α^*, respectively, we arrive at the expression

$$\widetilde{n^2} = |\alpha|^4 - |\alpha|^2 \tag{4.57}$$

for the Wigner–Weyl transform of $\hat{n}^2$.

We calculate the variance, Eq. (4.55), of the photon number according to the prescription in Eq. (4.6) and obtain

$$\langle \Delta\hat{n}^2 \rangle_\mathrm{cl}^\mathrm{ss} = 2\pi \int_0^\infty \mathrm{d}n \, \left(n^2 - n_\mathrm{cl}^{\mathrm{ss}2}\right) W_\mathrm{L}^\mathrm{ss}(n) - \frac{1}{4}\,. \tag{4.58}$$

Here, we have used the Wigner–Weyl representation, Eq. (4.57), of $\hat{n}^2$ as well as the result for $\langle \hat{n} \rangle$, Eq. (4.51). The integral in Eq. (4.58) results in the variance Δn_cl^2 of the Gaussian, Eq. (4.43), when we assume that the FEL operates well above threshold in analogy to our procedure for $\langle \hat{n} \rangle_\mathrm{cl}^\mathrm{ss}$, Eq. (4.51). Finally, we arrive at the expression

$$\langle \Delta\hat{n}^2 \rangle_\mathrm{cl}^\mathrm{ss} = \Delta n_\mathrm{cl}^2 - \frac{1}{4} \tag{4.59}$$

for the variance of the photon number in the classical regime of the FEL with Δn_cl^2 defined in Eq. (4.45). We note that in the derivation which led to Eq. (4.58) it was crucial to keep the contribution of 1/2 in Eq. (4.51). The cross term which arises by squaring $\langle \hat{n} \rangle_\mathrm{cl}^\mathrm{ss}$ cancels with the term due to $|\alpha|^2$ in the Wigner–Weyl transform, Eq. (4.57), of $\hat{n}^2$ and we are left with the expression in Eq. (4.58) .

To classify our result, Eq. (4.59), for the variance of the photon number in a classical FEL we compare it to the situation of a coherent state which is characterized by a Poisson distribution. For this purpose, we define the normalized variance [40]

$$\sigma^2 \equiv \frac{\langle \Delta\hat{n}^2 \rangle}{\langle \hat{n} \rangle} \tag{4.60}$$

as the ratio of variance and mean value. In the case of a Poisson distribution σ^2 equals unity, $\sigma^2 = 1$. We speak of a sub-Poissonian behavior when $\sigma^2 < 1$ and of a super-Poissonian statistics in the opposite case, $\sigma^2 > 1$.

For the radiation of a classical FEL we obtain the normalized variance

$$\sigma_{\mathrm{cl}}^2 \cong \frac{1}{2\epsilon}\left[\frac{\delta n^{\mathrm{sp}}}{G_{\mathrm{cl}}^{(1)}} + (1-\epsilon)\right], \tag{4.61}$$

where we have used the definitions Eqs. (4.47) and (4.48) of the steady-state photon number $n_{\mathrm{cl}}^{\mathrm{ss}}$ and the relative deviation from threshold ϵ, respectively. Moreover, we have made the approximations $\langle\hat{n}\rangle_{\mathrm{cl}}^{\mathrm{ss}} \cong n_{\mathrm{cl}}^{\mathrm{ss}}$ as well as $\langle\Delta\hat{n}^2\rangle_{\mathrm{cl}}^{\mathrm{ss}} \cong \Delta n_{\mathrm{cl}}^2$.

When we estimate δn^{sp} and G_{cl} by their values at resonance $\wp \cong \pi$ we arrive at

$$\frac{\delta n^{\mathrm{sp}}}{G_{\mathrm{cl}}^{(1)}} \cong \frac{\pi}{2}\frac{1}{\omega_{\mathrm{r}}T} \gg 1 \tag{4.62}$$

after using the relations $\mathcal{A}_{\mathrm{cl}} = 1$ and $\mathcal{S} = 4/\pi^2$. We identify the expression in Eq. (4.62) as the leading term of Eq. (4.61) since it is much larger than unity. Hence, we obtain the expression

$$\sigma_{\mathrm{cl}}^2 \cong \frac{\pi}{4\epsilon}\frac{1}{\omega_{\mathrm{r}}T} \gg 1 \tag{4.63}$$

for the magnitude of the normalized variance.

Since we require $\epsilon \ll 1$ for the small-signal limit and $\omega_{\mathrm{r}}T \ll 1$ for the classical regime the normalized variance σ_{cl}^2 is much larger than unity according to Eq. (4.63). Thus, the statistics of a classical FEL displays a super-Poissonian behavior similar to an ordinary laser [22, 105] in the small-signal limit. However, in contrast to the ordinary laser where σ^2 scales with ϵ^{-1} the distribution of a classical FEL is additionally broadened by the factor $(\omega_{\mathrm{r}}T)^{-1} \gg 1$.

This effect of a super-Poissonian photon statistics for the FEL was also derived in Refs. [13, 35] employing different approaches. In Ref. [35] the lower bound

$$\langle\Delta\hat{n}^2\rangle_{\mathrm{cl}}^{\mathrm{ss}} \geq \frac{1}{\omega_{\mathrm{r}}T}\langle\hat{n}\rangle_{\mathrm{cl}}^{\mathrm{ss}} \tag{4.64}$$

for the variance was derived with the help of the first-order recoil approximation of the time-evolution operator. Here, the inequality sign already takes into account the broadening due to ϵ^{-1}, that is due to the deviation from threshold. We note that Eq. (4.64) agrees very well with our result, Eq. (4.63), besides a numerical factor of $\pi/4$ which, however, is close to unity.

Similarly, in Ref. [13] an expression for the photon-number variance in the small-signal limit was derived which is analogous to Eq. (4.45). As mentioned in Sec. 4.1 the model of Ref. [13] is based on classical equations of motion for the electron and a conditional probability for the laser field. However, the approach in Ref. [13] is not restricted to the small-signal regime. A numerical analysis reveals that the statistical behavior of the FEL radiation at steady state is always super-Poissonian even when we enter the strong-signal regime. This behavior stands in contrast to the ordinary laser which approaches the Poissonian statistics of a coherent state for an increasing signal [22].

We emphasize that our results are valid for an FEL oscillator at steady state. In Ref. [100] it was reported that the FEL shows a sub-Poissonian behavior when we consider a single passage of electrons in the negative gain regime, that is $\wp < 0$. However, in the case of negative gain no steady state emerges and it is questionable to talk about a laser when there is no amplification. In principle, we can also study this effect with our approach when we consider $\wp < 0$ for the perturbative solution of W_{L} and a suitable initial state.

4.5 Linewidth

In contrast to the steady-state photon statistics which relies on the *modulus* ϱ of the field amplitude α, the linewidth of a laser emerges due to fluctuations in the *phase* φ [22, 82]. Far above threshold the Wigner distribution W_{L} is stabilized at steady state and we treat $|\alpha|^2 = n_{\mathrm{cl}}^{\mathrm{ss}} \cong \text{const}$ as a constant. Hence, the Fokker–Planck equation, Eq. (4.34), reduces to

$$\frac{\partial}{\partial t} W_{\mathrm{L}}(\varphi; t) = A_{\varphi} \frac{\partial}{\partial \varphi} W_{\mathrm{L}}(\varphi; t) + \frac{1}{2} D_{\mathrm{cl}} \frac{\partial^2}{\partial \varphi^2} W_{\mathrm{L}}(\varphi; t)\,, \tag{4.65}$$

with

$$A_{\varphi} \equiv \frac{M_{\mathrm{cl}}^{(3)}}{\tau_{\mathrm{inj}}} n_{\mathrm{cl}}^{\mathrm{ss}} \tag{4.66}$$

denoting the drift coefficient for the phase. We note that this form, Eq. (4.66), arises since we consider resonance, where $\wp = \pi$ and therefore $M_{\mathrm{cl}}^{(1)} = 0$. Thus, we have to go to the next higher order, that is $M_{\mathrm{cl}}^{(3)}$. Moreover, we have introduced in Eq. (4.65) the quantity

$$D_{\mathrm{cl}} \equiv \frac{1}{2\tau_{\mathrm{inj}}} \frac{1}{n_{\mathrm{cl}}^{\mathrm{ss}}} \left[\delta n^{\mathrm{sp}} + \frac{\omega_{\mathrm{L}} \tau_{\mathrm{inj}}}{2Q} \right] \tag{4.67}$$

which is the Diffusion constant for the phase.

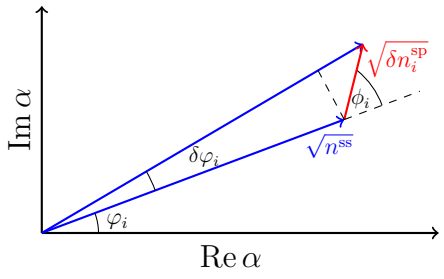

Figure 4.3: Real part $\mathrm{Re}\,\alpha$ and imaginary part $\mathrm{Im}\,\alpha$ of the amplitude $\alpha = \sqrt{n^{\mathrm{ss}}}\,\mathrm{e}^{-i\varphi}$ (blue line) of the laser field. Spontaneous emission leads in a single emission event to a change of α of $\delta\alpha^{(i)} = \sqrt{\delta n_i^{\mathrm{sp}}}\,\mathrm{e}^{-i\phi_i}$ (red line). At steady state the modulus $\sqrt{n^{\mathrm{ss}}}$ is approximately constant, while φ varies in each step from φ_i to $\delta\varphi_i$ resulting in a diffusion [15] of the phase.

We can understand the form of the diffusion constant in Eq. (4.67) with the help of an illustrative description following the lines of Ref. [15]. According to Fig. 4.3 the phase φ of

the amplitude $\alpha = \sqrt{n_{\mathrm{ss}}}\,\mathrm{e}^{-i\varphi}$ of the radiation field undergoes a diffusive process, while the modulus $\varrho \cong \sqrt{n^{\mathrm{ss}}}$ is stabilized at its value at steady state, when we consider a situation well above threshold [22].

Spontaneous emission leads in the ith step to a change of the amplitude by $\delta\alpha = \sqrt{\delta n_{\mathrm{i}}^{\mathrm{sp}}}\,\mathrm{e}^{-i\phi_i}$ where δn_i^{sp} denotes the number of spontaneously emitted photons per event. The change $\delta\varphi_i$ of the phase can be deduced with the help of simple geometry from Fig. 4.3 and we arrive at

$$\delta\varphi_i = \sqrt{\frac{\delta n_i^{\mathrm{sp}}}{n^{\mathrm{ss}}}}\,\sin\phi_i\,, \tag{4.68}$$

where we have approximated $\tan\delta\varphi_i \cong \delta\varphi_i$ for a small angle φ_i, which is justified when the steady-state photon number n^{ss} is approximately constant.

The diffusion constant [15]

$$D \equiv \frac{1}{\tau_{\mathrm{inj}}}\,\langle\delta\varphi^2\rangle \tag{4.69}$$

is defined as the average of the phase fluctuations multiplied by the rate $1/\tau_{\mathrm{inj}}$ of injected electron bunches. With the help of the identity $\sin^2\phi = 1/2(1-\cos 2\phi)$ we obtain the relation

$$\langle\delta\varphi^2\rangle = \frac{\langle\delta n^{\mathrm{sp}}\rangle}{n_{\mathrm{ss}}}\,\underbrace{\langle\sin^2\phi\rangle}_{=1/2} \tag{4.70}$$

for these fluctuations. Moreover, we have assumed that the photon number and the phase evolve independently from each other according to Ref. [15].

Hence, we finally arrive at the expression

$$D = \frac{1}{\tau_{\mathrm{inj}}}\frac{\delta n^{\mathrm{sp}}}{2n_{\mathrm{ss}}} \tag{4.71}$$

for the diffusion constant with the abbreviation $\delta n^{\mathrm{sp}} \equiv \langle\delta n^{\mathrm{sp}}\rangle$. This relation, Eq. (4.71), for the diffusion constant is rather general and applies for any laser oscillator. The properties of the FEL explicitly enter in form of the number $\langle\delta n^{\mathrm{sp}}\rangle$ of spontaneously emitted photons, Eq. (4.28), and through the steady-state photon number $n_{\mathrm{cl}}^{\mathrm{ss}}$ in Eq. (4.44). The comparison to Eq. (4.67) reveals that we have neglected in the derivation of Eq. (4.71) the influence of cavity losses on the diffusion.

In analogy to standard laser theory [22] we identify the diffusion constant $D_{\mathrm{cl}}^{\mathrm{ss}}$, Eq. (4.67), as the linewidth of the FEL in the classical regime. In the following, we prove this statement by following the lines of Ref. [82]. For this purpose, we consider the correlation function

$$\langle\hat{a}_{\mathrm{L}}^{\dagger}(t+\Delta t)\hat{a}_{\mathrm{L}}(t)\rangle \cong n_{\mathrm{cl}}^{\mathrm{ss}}\,\mathrm{e}^{i\omega_{\mathrm{L}}\Delta t}\int_0^{2\pi}\mathrm{d}\varphi\int_0^{2\pi}\mathrm{d}\varphi_0\;\mathrm{e}^{i(\varphi-\varphi_0)}\,W_{\mathrm{L}}(\varphi,t+\Delta t;\varphi_0,t)W_{\mathrm{L}}^{\mathrm{ss}}(\varphi_0) \tag{4.72}$$

for $\hat{a}_{\mathrm{L}}$ in a time interval Δt. To write $n_{\mathrm{cl}}^{\mathrm{ss}}$ outside of the integral we have assumed that the modulus $\varrho \cong \sqrt{n_{\mathrm{cl}}^{\mathrm{ss}}}$ is constant in the interval Δt. The expression in Eq. (4.72) describes the fluctuation of the phase φ at time $t+\Delta t$ with respect to an initial phase φ_0 at time t,

characterized by the distribution $W_{\mathrm{L}}^{\mathrm{ss}}$, with $W_{\mathrm{L}}(\varphi, t+\Delta t; \varphi_0, t)$ denoting the propagator for the Fokker–Planck equation, Eq. (4.65).

According to the preceding section the distribution of phases at steady state is uniform, Eq. (4.40), yielding the expression

$$W_{\mathrm{L}}^{\mathrm{ss}}(\varphi_0) = \frac{1}{2\pi} \tag{4.73}$$

which is independent of φ_0. The propagator, on the other hand, is given by [82]

$$W_{\mathrm{L}}(\varphi, t+\Delta t; \varphi_0, t) = \frac{1}{2\pi} \sum_{n=-\infty}^{\infty} \mathrm{e}^{in(\varphi-\varphi_0)}\, \mathrm{e}^{inA_\varphi \Delta t}\, \mathrm{e}^{-n^2 D \Delta t/2} \tag{4.74}$$

which is derived in App. C.5 by solving the Fokker–Planck equation, Eq. (4.65), under the condition that the propagator reduces to a delta function, that is $W_{\mathrm{L}}(\varphi, t+\Delta t; \varphi_0, t) \to \delta(\varphi - \varphi_0)$, for $\Delta t \to 0$.

By inserting Eqs. (4.73) and (4.74) into Eq. (4.72) and by making use of the identity

$$\frac{1}{2\pi} \int_0^{2\pi} \mathrm{d}\varphi'\, \mathrm{e}^{i(n+1)\varphi'} = \delta_{n,-1} \tag{4.75}$$

we obtain the expression

$$\langle \hat{a}_{\mathrm{L}}^\dagger(t+\Delta t) \hat{a}_{\mathrm{L}}(t) \rangle \cong n_{\mathrm{cl}}^{\mathrm{ss}}\, \mathrm{e}^{i(\omega_{\mathrm{L}} - A_\varphi)\Delta t}\, \mathrm{e}^{-\frac{D_{\mathrm{cl}} \Delta t}{2}} \tag{4.76}$$

for the correlation function of $\hat{a}_{\mathrm{L}}$. The Fourier transform of Eq. (4.76) yields the spectrum of the field which is a Lorentzian characterized by the width D_{cl} [22]. That is why we identify D_{cl} as the linewidth of a classical FEL. Moreover, we find a small shift of the central frequency ω_{L} due to a nonzero value of A_φ.

We emphasize that our result, Eq. (4.67), for the linewidth of the FEL in the classical regime is in accordance with the results of Refs. [14, 15, 16]. To study D_{cl} more closely we first note that in the small-signal limit, $\epsilon \ll 1$, the losses are of the same order of magnitude as the linear gain, that is $(\omega_{\mathrm{L}} \tau_{\mathrm{inj}})/(2Q) \sim G_{\mathrm{cl}}^{(1)}$. The ratio of gain $G_{\mathrm{cl}}^{(1)}$ and number δn^{sp} of spontaneously emitted photons, Eq. (4.28),

$$\frac{G_{\mathrm{cl}}^{(1)}}{\delta n^{\mathrm{sp}}} \cong \frac{2\omega_{\mathrm{r}} T}{\pi} \ll 1 \tag{4.77}$$

is very small in the classical regime $\omega_{\mathrm{r}} T \ll 1$ which was also appreciated in Ref. [14]. Hence, we are allowed to neglect the contribution due to losses in Eq. (4.67) and are left with the expression

$$D_{\mathrm{cl}} \cong \frac{1}{2\tau_{\mathrm{inj}}} \frac{\delta n^{\mathrm{sp}}}{n_{\mathrm{cl}}^{\mathrm{ss}}} \tag{4.78}$$

for the laser linewidth.

To estimate the magnitude of D_{cl} we consider resonance, that is $\wp = \pi$, where $\delta n^{\mathrm{sp}} = (4/\pi^2)(gT)^2 N$ and $n_{\mathrm{cl}}^{\mathrm{ss}}$ is given by Eq. (4.52). Hence, we find the estimate

$$D_{\mathrm{cl}} = \frac{N}{\varepsilon \tau_{\mathrm{inj}}} \frac{4}{\pi^5} (gT)^4 (\omega_{\mathrm{r}} T)^2 \tag{4.79}$$

for the intrinsic linewidth of the classical FEl which takes the form

$$D_{\mathrm{cl}} = \frac{1}{\tau_{\mathrm{inj}}} \frac{1}{\epsilon} \frac{64 a_0^4 N_{\mathrm{W}}^6 \lambda_{\mathrm{W}}^4 r_{\mathrm{e}}^2 n_{\mathrm{e}}^2}{\pi \gamma_0^6 N} \tag{4.80}$$

in the laboratory frame according to Tab. A.1 in App. A.3. We note that D_{cl} is independent of $\hbar$ and thus can be interpreted as a classical quantity.

4.6 Summary

In this chapter we have studied the statistical properties of the radiation from a classical FEL employing the Wigner representation for electron and laser field. This approach leads to a Fokker–Planck equation, Eq. (4.23), for the laser dynamics which includes drift as well as fluctuations. In contrast to many existing models, we consider a rigorous quantum theory in which quantum effects are not included by hand and which does not rely on single-photon processes as in standard perturbation theory.

Moreover, we exactly identify the steps in our calculations, where we (i) enter the classical regime, Eq. (4.9), defined by the conditions $\omega_{\mathrm{r}} T \ll 1$ and $\Delta p \gg \hbar k$, and where we (ii) make the small-signal approximation, Eq. (4.18), given by the constraint $\kappa |a_{\mathrm{L}}| \ll 1$. This stands in contrast to the first-order recoil approximation of Refs. [35, 100], where both approximations are performed in a single step, as can be seen from Eq. (4.2).

However, we recover the results of the existing literature for (i) the steady-state photon statistics, Eq. (4.43), and (ii) for the intrinsic linewidth, Eq. (4.78), of an FEL oscillator in the classical limit. Most remarkably is the fact, Eq. (4.63), that the photon statistics of a classical FEL is broadened in comparison to a coherent state as well as to an ordinary laser.

5 The Quantum Regime of the FEL

In the preceding chapters we have considered the situation, where the quantum mechanical recoil of the electron is negligible, or, where it becomes more and more important, but still is a *small quantity* leading only to quantum mechanical *corrections* to the classical formulas. Now we turn to the opposite case, where the recoil *dominates* the dynamics which is known as the *quantum regime* of the FEL or simply 'Quantum FEL' [2, 3, 4, 18, 25, 26, 27, 28, 87, 88, 106, 107, 108, 109, 110, 111].

Many ideas and discussions in this chapter are based on Ref. [4]. There, we have defined the Quantum FEL as the limit where the infinite momentum ladder characterizing the electron dynamics in the FEL reduces to an effective two-level system. In this context, we have employed in this article the asymptotic method of averaging [36] to derive the conditions for entering the quantum regime and to find analytic expressions for the time evolution in this limit.

In this thesis we follow a similar but slightly different path: instead of the standard method of averaging [36, 59] we use the canonical variant of this method, developed in Ref. [37]. For this purpose, we first have to rewrite the FEL Hamiltonian with the help of projection operators for the momentum of the electron. By this procedure, we identify the two frequency scales governing the dynamics of the FEL: (i) the coupling $g\sqrt{n}$ between the electron and the fields and (ii) the discrete recoil $q \equiv 2\hbar k$ of the electron characterized by the recoil frequency ω_{r}.

When the quantum mechanical recoil is dominating we are in the *deep* quantum regime, where the electron jumps between the two resonant momentum levels $p = q/2$ and $p = -q/2$. Analogously to Ref. [4] we obtain two conditions for the Quantum FEL which are connected to (i) a small value of the *quantum parameter* α, defined, Eq. (3.4), as the ratio of the coupling strength and the recoil frequency, and (ii) to a small initial *momentum spread* of the electrons when compared to the recoil q in analogy to our discussions in Chap. 3. We proceed by calculating higher-order corrections to this 'hard' quantum limit and find that these corrections scale with powers of α. Hence, we are allowed to neglect higher-order contributions for decreasing values of α.

By also considering resonances different from the fundamental one at $p = q/2$ we add another aspect to the discussion of the quantum regime untouched upon in Ref. [4]. With the help of our asymptotic method we can explain the behavior of the electron for these 'higher' resonances and derive analytic expressions for the time evolution in contrast to the numerical approach in Ref. [112]. These resonances also show a two-level behavior, but the dynamics occurs on much longer time scales when compared to the fundamental one.

5.1 Rewriting the Hamiltonian

For the time being we restrict ourselves to the low-gain regime. That is why we consider the single-electron case, $N = 1$, where the quantized Hamiltonian, Eq. (A.41), reads

$$\hat{H} = \frac{\hat{p}^2}{2m} + \hbar g \left(\hat{a}_\mathrm{L}\, \mathrm{e}^{i2k\hat{z}} + \hat{a}_\mathrm{L}^\dagger\, \mathrm{e}^{-i2k\hat{z}} \right) . \tag{5.1}$$

In order to obtain the quantum regime of the FEL it is not necessary to quantize the light field, which is characterized by the photon annihilation $\hat{a}_\mathrm{L}$ and creation operator $\hat{a}_\mathrm{L}^\dagger$. As we have shown in Chapter 3 quantum effects, indeed, arise since position $\hat{z}$ and momentum $\hat{p}$ do not commute in quantum mechanics. However, in the further course of this thesis we derive expressions for the photon statistics and the intrinsic linewidth of the Quantum FEL making a fully quantized theory necessary in analogy to our procedure for the classical FEL in Chap. 4.

Applying the Hamiltonian, Eq. (5.1), on the state $|n, p\rangle$ consisting of a Fock state with photon number n and a momentum eigenstate of the electron with momentum p we obtain

$$\hat{a}_\mathrm{L}^\dagger\, \mathrm{e}^{-i2k\hat{z}}\, |n, p\rangle = \sqrt{n+1}\, |n+1, p-q\rangle \ , \tag{5.2}$$

that is a photon is *emitted* into the field while the electron *recoils* by $q \equiv 2\hbar k$ as well as the other way round, yielding $|n-1, p+q\rangle$, where a photon is *absorbed* and the electron *gains* the momentum q. By repeating this procedure several times we recognize that the electron is allowed to occupy only momenta which are separated by integer multiples of q. Hence, for a given initial momentum the electron dynamics can be described by a discrete momentum ladder, as argued in Ref. [4], which is connected to the corresponding number of emitted or absorbed photons.

Thus, it is convenient to use the 'scattering basis'

$$|\mu\rangle \equiv |n+\mu, p-\mu q\rangle \ , \tag{5.3}$$

introduced in Ref. [113]. This basis is characterized by the single parameter μ which indicates the number of emitted or absorbed photons and at the same time the change of the electron momentum as multiple of the recoil q.

In Ref. [4] a three-term recursion relation for the expansion coefficients

$$c_\mu \equiv \langle n+\mu, p-\mu q | \Psi(\tau) \rangle \tag{5.4}$$

of the total state vector was derived. This three-term relation was then asymptotically solved with the help of the method of averaging [36] and we identified the quantum regime as the lowest order of the resulting asymptotic expansion.

In this thesis we take a slightly different route: With the help of the method of *canonical* averaging [37] we derive an asymptotic expansion in operator form and then solve the corresponding equations of motion. Although this procedure gives results equivalent to the ordinary method [4] we find it convenient to work with this alternative form of the method in this thesis, because of two reasons: (i) We show in Chap. 7 that the Heisenberg picture and thus an operator formalism is more suitable when we consider a many-electron theory, where

involved superposition states are created which are similar to Dicke states [114] in the field of superradiance and amplified spontaneous emission. (ii) By obtaining explicit expressions for an effective Hamiltonian we straightforwardly identify the underlying physical processes.

In the following we treat the momentum of the electron as a discrete variable, since this discreteness is induced by the dynamics, according to Eq. (5.2). However, we restore the continuous nature of momentum in the next chapter when we expand the initial state in momentum eigenstates which we separately evolve in time before we weight them with the initial distribution and integrate over all momenta. This procedure is only reasonable when the initial momentum distribution does not cover more than one step of the momentum ladder leading to the condition $\Delta p < q$. However, since we show later that this constraint is also necessary to operate a Quantum FEL we argue that we are allowed to follow this procedure.

The method of averaging is based on the occurrence of two distinct frequency scales in the dynamics. However, the form of the Hamiltonian, Eq. (5.1), is not convenient to recognize these frequencies and we have to rewrite it in a more suitable form to make this dependence visible. That is why we introduce the projection operator

$$\hat{\sigma}_{\mu,\nu} \equiv |p - \mu q\rangle \langle p - \nu q| \tag{5.5}$$

for the electron momentum, where we have assumed that the initial state of the electron is given by a momentum eigenstate with eigenvalue p. Thus, the operator $\hat{\sigma}_{\mu,\nu}$ describes the transition from $p - \nu q$ to $p - \mu q$ on the discrete momentum ladder.

The commutator between two of these operators reads

$$[\hat{\sigma}_{\mu,\nu}, \hat{\sigma}_{\rho,\eta}] = \delta_{\nu,\rho}\hat{\sigma}_{\mu,\eta} - \delta_{\eta,\mu}\hat{\sigma}_{\rho,\nu}\,, \tag{5.6}$$

where we have used Kronecker deltas for discrete states instead of Dirac delta functions for continuous ones while

$$\hat{\sigma}_{\mu,\nu}\hat{\sigma}_{\rho,\eta} = \delta_{\nu,\rho}\hat{\sigma}_{\mu,\eta} \tag{5.7}$$

gives their product. We note that this last property constitutes a crucial difference of single-electron and many-electron model. As we show in Chap. 7 a commutation relation analogous to Eq. (5.6) can be found in the many-particle theory, however, a relation analogous to Eq. (5.7) cannot be formulated in this case. While the commutation relation, Eq. (5.6), can always be derived if the identity in Eq. (5.7) holds true, the opposite direction is not necessarily allowed, since additional terms in the product of Eq. (5.7) can emerge which cancel due to the minus sign in the commutator, Eq. (5.6).

With the help of the completeness relation for discrete eigenstates any operator

$$\hat{\mathcal{O}} = \mathbb{1}\hat{\mathcal{O}}\mathbb{1} = \sum_{\mu,\nu} \langle p - \mu q| \hat{\mathcal{O}} |p - \nu q\rangle \hat{\sigma}_{\mu,\nu} \tag{5.8}$$

describing the electron dynamics can be written in terms of the projection operators $\hat{\sigma}_{\mu,\nu}$. We evaluate the corresponding matrix element $\langle p - \mu q| \hat{\mathcal{O}} |p - \nu q\rangle$ in Eq. (5.8) for the contributions of the Hamiltonian in Eq. (5.1) by using the identities $\hat{p}^2 |p\rangle = p^2 |p\rangle$ and

$\mathrm{e}^{\pm i2k\hat{z}}\,|p\rangle = |p \pm q\rangle$. Thus, we arrive at the expressions

$$\begin{cases} \hat{p}^2 = \sum\limits_{\mu} (p-\mu q)^2\, \hat{\sigma}_{\mu,\mu} \\ \mathrm{e}^{i2k\hat{z}} = \sum\limits_{\mu} \hat{\sigma}_{\mu,\mu+1} \\ \mathrm{e}^{-i2k\hat{z}} = \sum\limits_{\mu} \hat{\sigma}_{\mu+1,\mu} \end{cases} \tag{5.9}$$

for the kinetic energy term and the momentum-shift operators, $\hat{p}^2$ and $\mathrm{e}^{\pm i2k\hat{z}}$, respectively. Hence, we cast the Hamiltonian, Eq. (5.1), into the form

$$\hat{H} = \sum_{\mu} \frac{(p-\mu q)^2}{2m} \hat{\sigma}_{\mu,\mu} + \hbar g \left(\hat{a}_{\mathrm{L}} \sum_{\mu} \hat{\sigma}_{\mu,\mu+1} + \hat{a}_{\mathrm{L}}^{\dagger} \sum_{\mu} \hat{\sigma}_{\mu+1,\mu} \right) , \tag{5.10}$$

where the momentum of the electron does not appear explicitly as an operator but as the c-number $p - \mu q$ over which is summed.
The next step that leads us naturally to the identification of the different time scales of the FEL dynamics is the transformation from the Schrödinger to the interaction picture. With the usual definition [40] of an operator in this picture we obtain the transformed projection operators

$$\begin{cases} \hat{\sigma}_{\mu+1,\mu} \to \hat{\sigma}_{\mu+1,\mu}\, \mathrm{e}^{-ikt[2p-(2\mu+1)q]/m} \\ \hat{\sigma}_{\mu,\mu+1} \to \hat{\sigma}_{\mu,\mu+1}\, \mathrm{e}^{ikt[2p-(2\mu+1)q]/m} \end{cases} , \tag{5.11}$$

where we have used the Baker–Campbell–Hausdorff theorem, Eq. (3.16), and the commutation relation, Eq. (5.6), for the projection operators. This procedure leads us to the Hamiltonian

$$\hat{H}_{\mathrm{I}}(t) = \hbar g \left(\hat{a}_{\mathrm{L}} \sum_{\mu} \mathrm{e}^{i\omega_{\mathrm{r}} t\left[\frac{p}{q/2} - (2\mu+1)\right]} \hat{\sigma}_{\mu,\mu+1} + \hat{a}_{\mathrm{L}}^{\dagger} \sum_{\mu} \mathrm{e}^{-i\omega_{\mathrm{r}} t\left[\frac{p}{q/2} - (2\mu+1)\right]} \hat{\sigma}_{\mu+1,\mu} \right) \tag{5.12}$$

in the interaction picture with the recoil frequency $\omega_{\mathrm{r}} \equiv q^2/(2m\hbar)$ according to Eq. (3.2). Finally, we recognize which two frequencies govern the FEL dynamics: on the one hand there is the coupling strength g and one the other hand we have to consider the recoil frequency ω_{r}, since the summands in Eq. (5.12) oscillate with multiples of this frequency. However, besides the ratio of these two quantities the initial momentum p of the electron is also of importance in our following discussion.

5.2 Two-level approximation

The initial momentum p of the electron has not been determined, yet. When we consider the phases

$$\pm i\omega_{\mathrm{r}} t \left[\frac{p}{q/2} - (2\mu+1) \right] \tag{5.13}$$

of the Hamiltonian, Eq. (5.12), resonances appear when the initial momentum p of the electron is a multiple integer of $q/2$. For the time being we just consider the 'lowest' or 'fundamental' resonance, that is $p \sim q/2$.

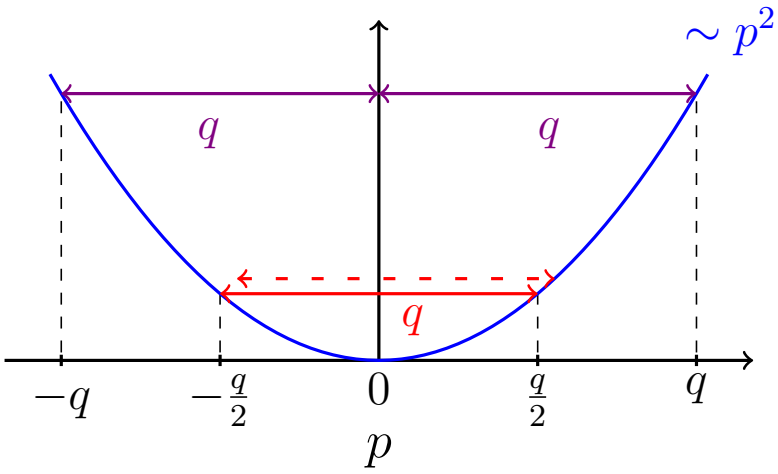

Figure 5.1: Resonances in the Quantum FEL as consequence of energy-momentum conservation: Only processes are resonant which are separated in momentum by multiples of the recoil q and at the same time lie on the parabola proportional to p^2 which correspond to conservation of energy. Due to these requirements resonances just appear at momenta which are integer multiples of $q/2$, that is $p = mq/2$. The dashed line correspond to an off-resonant process since energy and momentum are not totally conserved and thus we expect that it is suppressed.

The physical meaning for this resonance [4] is shown in Fig. 5.1, where the parabola p^2 corresponding to kinetic energy versus momentum p is shown. The processes which conserves, both, energy *and* momentum, under the condition of discrete momentum steps of the size of the recoil q, are indicated by horizontal arrows. We obtain that energy-momentum conservation allows only momenta which are integer multiples of $q/2$ in analogy to Eq. (5.13). Moreover, by assuming that in the quantum limit single-photon processes dominate we deduce that transitions including resonances higher than the fundamental one, $p = q/2$, are suppressed since they correspond to multiphoton transitions as visualized in Fig. 5.1. However, we come back to this aspect at the end of this chapter, where we rigorously prove this last statement and derive that these multiphoton processes occur on a longer characteristic time scale.

Introducing the dimensionless variables

$$\begin{cases} \tau \equiv \omega_{\mathrm{r}} t \\ \varepsilon \equiv g/\omega_{\mathrm{r}} \\ \Delta \equiv p/(q/2) - 1 \end{cases} \tag{5.14}$$

which are more suitable for the quantum regime as the ones, defined by Eq. (2.34) in Chap. 2 for the classical FEL, we obtain the expression

$$\hat{H}_{\mathrm{I}}(\tau) = \varepsilon \left(\hat{a}_{\mathrm{L}} \, \mathrm{e}^{i\Delta\tau} \sum_{\mu} \mathrm{e}^{-i2\mu\tau} \, \hat{\sigma}_{\mu,\mu+1} + \hat{a}_{\mathrm{L}}^{\dagger} \, \mathrm{e}^{-i\Delta\tau} \sum_{\mu} \mathrm{e}^{i2\mu\tau} \, \hat{\sigma}_{\mu+1,\mu} \right) \tag{5.15}$$

for the Hamiltonian, Eq. (5.12). We further write this expression as a Fourier series

$$\hat{H}_{\mathrm{I}}(\tau) \equiv \varepsilon \sum_{\mu} \hat{\mathcal{H}}_{\mu}(\tau)\, \mathrm{e}^{i2\mu\tau}\,, \tag{5.16}$$

where we have identified the terms

$$\begin{cases} \hat{\mathcal{H}}_0(\tau) \equiv \hat{a}_{\mathrm{L}}\, \mathrm{e}^{i\Delta\tau}\, \hat{\sigma}_{0,1} + \hat{a}_{\mathrm{L}}^{\dagger}\, \mathrm{e}^{-i\Delta\tau}\, \hat{\sigma}_{1,0} \\ \hat{\mathcal{H}}_{\mu}(\tau) \equiv \hat{a}_{\mathrm{L}}\, \mathrm{e}^{i\Delta\tau}\, \hat{\sigma}_{-\mu,-\mu+1} + \hat{a}_{\mathrm{L}}^{\dagger}\, \mathrm{e}^{-i\Delta\tau}\, \hat{\sigma}_{\mu+1,\mu} \end{cases} \tag{5.17}$$

as the individual Fourier components. We emphasize that we have not made any approximation, yet. However, the Hamiltonian, Eq. (5.16), is now in a form that is suitable for the asymptotic method of canonical averaging [37].

However, to apply this method, two conditions have to be satisfied. For an asymptotic expansion to converge we require the expansion parameter to be small. For our method of choice [37] this condition is given by

$$\alpha_n \equiv \varepsilon\sqrt{n+1} = \frac{g\sqrt{n+1}}{\omega_{\mathrm{r}}} \ll 1\,, \tag{5.18}$$

where we have defined the *quantum parameter* α_n in analogy to Ref. [4]. By inspection of Eq. (5.18) we obtain that α_n is the ratio of two frequencies: the coupling strength $g\sqrt{n+1}$ and the recoil frequency ω_{r}. As already predicted in Chap. 3 we now explicitly see that quantum mechanics becomes important when the recoil exceeds the coupling strength, Eq. (3.4), leading to a value of α_n that is less than unity. We *define* this limit as the quantum regime of the FEL in accordance with Ref. [4]. In this article we, moreover, established the connection to the analogue parameter $\bar{\rho}$ of Ref. [3] which reads $\alpha = \bar{\rho}^{3/2}/\sqrt{2}$.

The method of averaging is based on the fact that rapid oscillations have only a small influence on the dynamics. We can naively understand this argument by realizing that the integration of the Schrödinger equations brings the large frequencies corresponding to these rapid oscillations into the denominator and hence these contributions are suppressed [40]. Similarly, one could argue that for $\alpha_n \ll 1$ the coupling $g\sqrt{n}$ defines the dominant time scale, while the integration over time washes out the rapid oscillations with ω_{r}.

This clear separation of slowly and rapidly varying terms leads to the second condition for the method of averaging: The Fourier components $\hat{\mathcal{H}}_{\mu}(\tau)$ have to be slowly varying in time and by inspection of Eq. (5.17) we demand a small deviation [4]

$$\Delta \equiv \frac{p}{q/2} - 1 \ll 1 \tag{5.19}$$

of the initial momentum from the resonant momentum $p = q/2$. A process which starts from a momentum close to but not equal to $q/2$ is indicated in Fig. 5.1 by the dashed line. We expect that this transition is suppressed for an increasing value of Δ since energy and momentum are not conserved any longer.

Considering the Hamiltonian, Eq. (5.16), we recognize that the only contribution without rapid oscillations is the component with $\mu = 0$. Hence, in the lowest approximation, which corresponds to the *deep* quantum regime, the dynamics is governed by the effective

Hamiltonian

$$\hat{H}_{\text{eff}} \cong \varepsilon \hat{\mathcal{H}}_0(\tau) = \varepsilon \left(\hat{a}_{\text{L}} \, \mathrm{e}^{i\Delta\tau} \, \hat{\sigma}_{0,1} + \hat{a}_{\text{L}}^\dagger \, \mathrm{e}^{-i\Delta\tau} \, \hat{\sigma}_{1,0} \right) , \tag{5.20}$$

where we have recalled the definition, Eq. (5.17), of $\hat{\mathcal{H}}_0$.

The Hamiltonian in Eq. (5.20) is analogous to the Jaynes–Cummings Hamiltonian [32, 40] which describes the interaction of a two-level atom with a quantized mode of the radiation field. The projection operators $\hat{\sigma}_{0,1}$ and $\hat{\sigma}_{1,0}$ for the electron momentum correspond to the atomic ladder operators $\hat{\sigma}$ and $\hat{\sigma}^\dagger$, respectively, in the notation of Ref. [40]. Additionally, we have to deal with a detuning Δ which leads to the time-dependence of the Hamiltonian, Eq. (5.20).

We remove this time-dependence with the help of the transformation

$$|\tilde{\Psi}(t)\rangle \equiv \mathrm{e}^{-i\Delta\tau\hat{\sigma}_z/2} \, |\Psi(\tau)\rangle \ , \tag{5.21}$$

where we have defined $\hat{\sigma}_z \equiv \hat{\sigma}_{0,0} - \hat{\sigma}_{1,1}$ by recognizing the analogy to Pauli spin matrices. Using the Baker–Campbell–Hausdorff formula, Eq. (3.16), and the commutation relation, Eq. (5.6), for the $\hat{\sigma}_{\mu,\nu}$ we arrive at the transformed Hamiltonian

$$\tilde{H}_{\text{eff}} = \frac{\Delta}{2}\hat{\sigma}_z + \varepsilon \left(\hat{a}_{\text{L}}\hat{\sigma}_{0,1} + \hat{a}_{\text{L}}^\dagger\hat{\sigma}_{1,0} \right) \tag{5.22}$$

which is now independent of time.

In analogy to Eq. (5.4) we expand the state $|\tilde{\Psi}\rangle$ in terms of the scattering basis leading to the expansion coefficients

$$\tilde{c}_\mu(\tau) \equiv \langle n+\mu, p-\mu q|\Psi(\tau)\rangle \tag{5.23}$$

for which we introduce the vector notation $\tilde{\boldsymbol{c}} = (\tilde{c}_0, \tilde{c}_1)^{\text{T}}$. From the Schrödinger equation for the transformed state vector $|\tilde{\Psi}\rangle$, characterized by the Hamiltonian $\tilde{H}_{\text{eff}}$, Eq. (5.22), we derive the system of coupled differential equations [4]

$$i\frac{\mathrm{d}}{\mathrm{d}\tau}\tilde{\boldsymbol{c}} = \begin{pmatrix} \frac{\Delta}{2} & \alpha_n \\ \alpha_n & -\frac{\Delta}{2} \end{pmatrix} \tilde{\boldsymbol{c}} \tag{5.24}$$

governing the dynamics of $\tilde{\boldsymbol{c}}$.

Solving Eq. (5.24) is now straightforward: First, we insert the ansatz $\sim \mathrm{e}^{-i\lambda\tau}$ into Eq. (5.24) and obtain

$$\lambda_\pm = \pm\sqrt{\alpha_n^2 + \frac{\Delta^2}{4}} \tag{5.25}$$

for λ. In terms of the time t we thus find the solution [4]

$$\tilde{\boldsymbol{c}}(t) = \left[\cos\Omega_n t \begin{pmatrix} 1 & 0 \\ 0 & 1 \end{pmatrix} - i\frac{\omega_{\text{r}}}{\Omega_n} \sin\Omega_n t \begin{pmatrix} \Delta/2 & \alpha_n \\ \alpha_n & \Delta/2 \end{pmatrix} \right] \tilde{\boldsymbol{c}}(0) \tag{5.26}$$

for arbitrary initial conditions $\tilde{\boldsymbol{c}}(0)$. The amplitudes of Eq. (5.26) describe detuned Rabi oscillations with

$$\Omega_n \equiv \sqrt{g^2(n+1) + \left(\frac{\Delta}{2}\right)^2 \omega_{\text{r}}^2} \, . \tag{5.27}$$

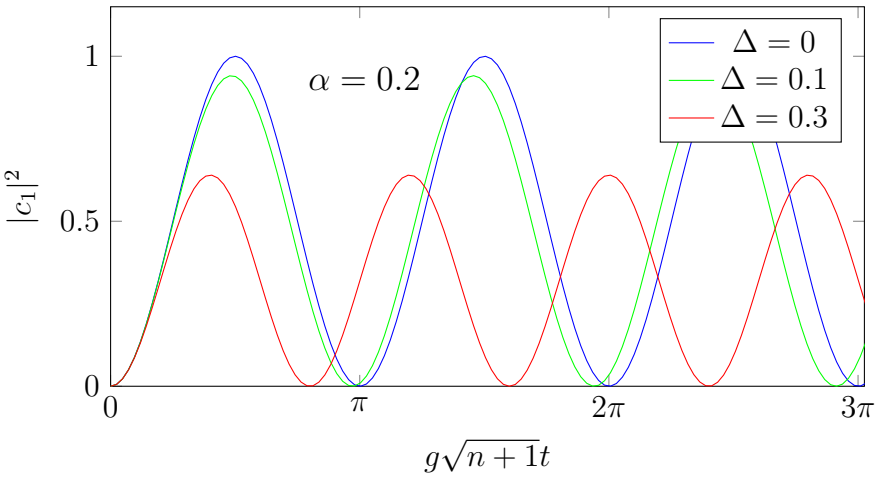

Figure 5.2: Detuned Rabi oscillations in the deep quantum regime of the FEL: We have drawn the probability $|c_1|^2$, Eq. (5.29) , for single-photon emission as a function of the dimensionless time $g\sqrt{n+1}t$ for the resonant case, $\Delta = 0$, (blue line) and for two nonzero values of the detuning, that is $\Delta = 0.1$ (green line) and $\Delta = 0.3$ (red line). We observe that for increasing values of the detuning Δ the Rabi frequency as well as the maximum probability decreases. This behavior is known from ordinary two-level atoms [58].

denoting the Rabi frequency.

Initially, the momentum of the electron is close to the excited state $p = q/2$ of the two-level system which corresponds to the initial condition $c_\mu(0) = \delta_{\mu,0}$. Hence, we find the probabilities

$$|c_0(t)|^2 = \cos^2 \Omega_n t + \frac{(\Delta/2)^2 \omega_r^2}{\Omega_n^2} \sin^2 \Omega_n t \tag{5.28}$$

and

$$|c_1(t)|^2 = \frac{g^2(n+1)}{\Omega_n^2} \sin^2 \Omega_n t \tag{5.29}$$

for the electron to occupy excited and ground state, $p \sim q/2$ and $p \sim -q/2$, respectively, at time t. The back transformation from $\tilde{c}_\mu$ to c_μ leading to the expressions in Eqs. (5.28) and (5.29) has been straightforward since the additional phase factors cancel when we calculate the modulus square of the amplitudes.

The probability $|c_1|^2$ for the electron to be in the ground state $-q/2$, corresponding to the emission of a single photon, is shown in Fig. 5.2 as a function of time for different values of the deviation Δ from resonance. We obtain that a higher value of Δ, indeed, suppresses the probability for emitting a photon and increases the Rabi frequency in analogy to ordinary two-level atoms [58].

In conclusion, we have defined the quantum regime as the limit where the electron dynamics is given by a two-level system consisting of the excited state $q/2$ and the ground state $-q/2$. We have achieved this identification in the framework of the asymptotic method of averaging which is valid under the conditions in Eqs. (5.18) and (5.19).

We want to stress that Eq. (5.19) for the deviation Δ from resonance is *not* a condition for the width Δp of the initial momentum distribution for the electrons. When we assume a broad distribution only the electrons with momenta close to resonant ones, that is multiples of $q/2$, experience an effect due to the interaction while the momenta of the other electrons are unchanged. In atomic diffraction [115, 116, 117] this effect is known as *velocity selectivity*. However, while the resonance $p = q/2$ corresponds to photon emission and hence positive gain its counterpart $p = -q/2$ gives rise to photon absorption, according to Fig. 5.1, and thus negative gain. When the initial momentum distribution covers both resonances, both effects, emission and absorption occur at the same time and the gain averages to zero. Hence, we require a small width [4, 108]

$$\Delta p < q \tag{5.30}$$

of the initial momentum distribution for the electrons, that is a small energy spread of the electron beam. Again, a small momentum spread is crucial to obtain quantum effects in the FEL dynamics similar to our investigations of the classical-quantum transition in Chap. 3.

5.3 Higher-order corrections

Up to now, we have only considered the lowest order of our asymptotic expansion. However, to prove that the dynamics of the FEL really reduces to a two-level behavior for $\alpha_n \ll 1$ we have to calculate the higher-order corrections to the Rabi oscillations given by the probabilities, Eqs. (5.28) and (5.29), in the framework of the method of canonical averaging [37]. The details of this derivation can be found in App. D while we sketch in the following only the basic ideas. For the sake of simplicity we restrict ourselves to the resonant case, that is $\Delta = 0$. In principle, however, we could have assumed any value of Δ which can be written as a power of ε.

As mentioned before the method of averaging [36, 59] is based on the idea that the dynamics represented by a Hamiltonian of the form of Eq. (5.16) consists of slowly varying and rapidly varying terms. Hence, we assume that the state vector

$$|\Psi(\tau)\rangle \equiv \mathrm{e}^{-\hat{F}(\tau)}\,|\Phi(\tau)\rangle \tag{5.31}$$

can also be separated into a slowly varying part, given by $|\Phi\rangle$, and a rapidly varying one, denoted by $\hat{F}(\tau)$. For the transformed state vector we derive the Schrödinger equation, Eq. (D.46),

$$i\frac{\mathrm{d}}{\mathrm{d}\tau}\,|\Phi(\tau)\rangle = \hat{H}_{\mathrm{eff}}\,|\Phi(\tau)\rangle \tag{5.32}$$

governed by the effective Hamiltonian $\hat{H}_{\mathrm{eff}}$.

For $\varepsilon \left\|\hat{H}\right\| \ll 1$ [37] we expand, both, the rapidly varying contribution

$$\hat{F}(\tau) = \varepsilon\hat{F}^{(1)}(\tau) + \varepsilon^2\hat{F}^{(2)}(\tau) + \varepsilon^3\hat{F}^{(3)}(\tau) + ... \tag{5.33}$$

as well as the effective Hamiltonian

$$\hat{H}_{\mathrm{eff}} = \varepsilon\hat{H}^{(1)}_{\mathrm{eff}} + \varepsilon^2\hat{H}^{(2)}_{\mathrm{eff}} + \varepsilon^3\hat{H}^{(3)}_{\mathrm{eff}} + ... \tag{5.34}$$

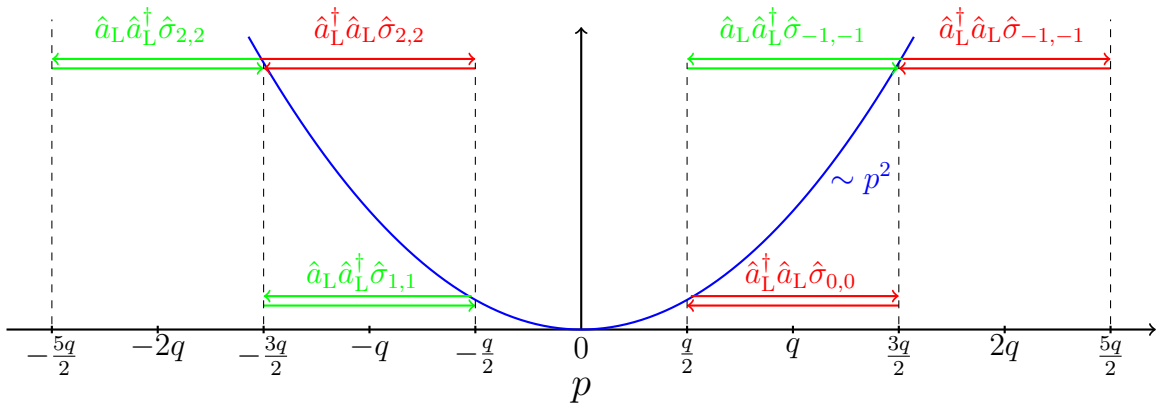

Figure 5.3: Resonant two-photon transitions corresponding to the effective Hamiltonian $H_\mathrm{eff}^{(2)}$, Eq. (5.36), of second order. In these processes a photon is emitted and then a second one is absorbed (green arrows), or the other way round (red arrows), such that the final momentum of the electron equals the initial one. We note that the two-photon transition from $q/2$ via $-q/2$ back to $q/2$ (as well as from $-q/2$ via $q/2$ to $-q/2$) is excluded from $H_\mathrm{eff}^{(2)}$ since the corresponding single-photon processes, from $q/2$ to $-q/2$ and from $-q/2$ to $q/2$, are resonant and already included in the first-order Hamiltonian $H_\mathrm{eff}^{(1)}$, Eq. (5.35).

in powers of ε. In an iterative manner (for a detailed description see App. D), we then determine $\hat{F}$ and $\hat{H}_\mathrm{eff}$ order by order in such a way that $\hat{H}_\mathrm{eff}$ is *independent* of time. The Schrödinger equation, Eq. (5.32), with the corresponding expression for $\hat{H}_\mathrm{eff}$ is then solved exactly. This procedure ensures that $\hat{F}$ does not contain secular terms which eventually would lead to an unphysical growth [59] in the solution of the Schrödinger equation.

The lowest order of the asymptotic expansion is identical to the two-level approximation of the preceding section for resonance, $\Delta = 0$. Hence, we consider the effective Hamiltonian

$$\hat{H}_\mathrm{eff}^{(1)} = \hat{a}_\mathrm{L}\hat{\sigma}_{0,1} + \hat{a}_\mathrm{L}^\dagger\hat{\sigma}_{1,0} \tag{5.35}$$

while we completely neglect rapid oscillations given by $\hat{F}$. The higher orders of $\hat{H}_\mathrm{eff}$ give rise to a frequency shift, and $\hat{F}$ is responsible for corrections to the amplitude.

Let us first consider the higher-order contributions of the effective Hamiltonian. According to Eq. (D.38) we obtain

$$\hat{H}_\mathrm{eff}^{(2)} = -\frac{1}{2}\hat{a}_\mathrm{L}\hat{a}_\mathrm{L}^\dagger\hat{\sigma}_{1,1} - \frac{1}{2}\hat{a}_\mathrm{L}^\dagger\hat{a}_\mathrm{L}\hat{\sigma}_{0,0} - \hat{a}_\mathrm{L}\hat{a}_\mathrm{L}^\dagger\sum_{\nu\neq 0,1}\frac{1}{2\nu}\hat{\sigma}_{\nu,\nu} + \hat{a}_\mathrm{L}^\dagger\hat{a}_\mathrm{L}\sum_{\nu\neq 0,1}\frac{1}{2(\nu-1)}\hat{\sigma}_{\nu,\nu} \tag{5.36}$$

in second order of ε. This Hamiltonian describes the resonant two-photon processes, shown in Fig. 5.3, where one photon is emitted and one absorbed and thus the momentum of the electron after interaction is the same as before. However, the effect of this second-order Hamiltonian cancels when we calculate the frequency corrections and thus we have to go the next higher order.

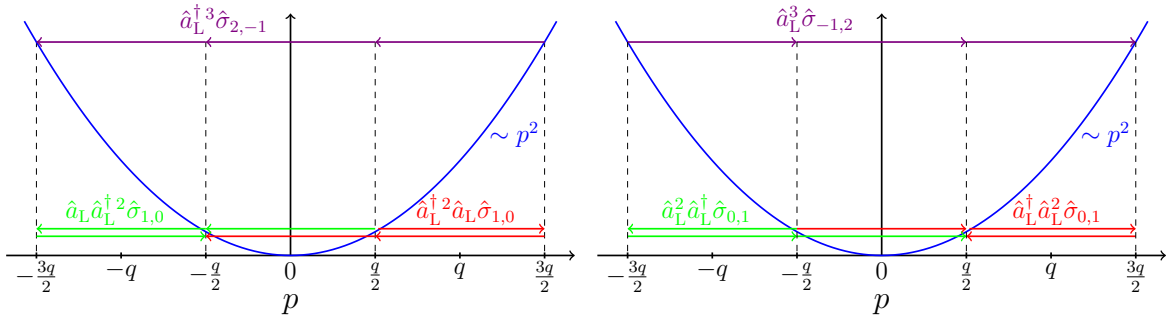

Figure 5.4: Resonant three-photon transitions corresponding to the effective Hamiltonian $H_{\mathrm{eff}}^{(3)}$, Eq. (5.37), of third order. We obtain (i) three-photon process from $q/2$ to $-q/2$ (and the other way round) where the electron occupies an intermediate level, either $3q/2$ (red arrows) or $-3q/2$ (green arrows), and (ii) transitions from $3q/2$ to $-3q/2$ and from $-3q/2$ to $3q/2$ (purple arrows). Resonant processes between $q/2$ and $-q/2$ where no intermediate level is involved, that is alternating photon emission and absorption, are excluded from $H_{\mathrm{eff}}^{(3)}$ but correspond to the dynamics due to the first-order contribution $\hat{H}_{\mathrm{eff}}^{(1)}$, Eq. (5.35).

The third-order contribution, Eq. (D.40),

$$\hat{H}_{\mathrm{eff}}^{(3)} = -\frac{1}{8}\left(\hat{a}_{\mathrm{L}}^{\dagger}\hat{a}_{\mathrm{L}}^{2} + \hat{a}_{\mathrm{L}}^{2}\hat{a}_{\mathrm{L}}^{\dagger}\right)\hat{\sigma}_{0,1} - \frac{1}{8}\left(\hat{a}_{\mathrm{L}}\hat{a}_{\mathrm{L}}^{\dagger\,2} + \hat{a}_{\mathrm{L}}^{\dagger\,2}\hat{a}_{\mathrm{L}}\right)\hat{\sigma}_{1,0} + \frac{1}{4}\hat{a}_{\mathrm{L}}^{3}\hat{\sigma}_{-1,2} + \frac{1}{4}\hat{a}_{\mathrm{L}}^{\dagger\,3}\hat{\sigma}_{2,-1} \tag{5.37}$$

of the effective Hamiltonian describes the resonant three-photon processes as shown in Fig. 5.4. On the one hand there are the transitions between the momenta $p = q/2$ and $p = -q/2$, but now with an additional intermediate level. On the other hand we obtain processes corresponding to a second two-level system consisting of the momenta $p = 3q/2$ and $p = -3q/2$. At first sight these momenta are not involved in the interaction when we consider a resonant electron with $p = q/2$. However, due to the transformation, Eq. (5.31), from $|\Psi\rangle$ to $|\Phi\rangle$ a mixing occurs in the initial state making a transition to the momenta $p = 3q/2$ and $p = -3q/2$ possible. Since $\hat{F}$, Eq. (5.33), is an expansion in powers of ε we expect that the amplitudes of these processes are suppressed with powers of α_n.

Introducing the expansion coefficients

$$d_\mu(\tau) \equiv \langle n+\mu, p-\mu q|\Phi(\tau)\rangle \tag{5.38}$$

of the slowly varying state $|\Phi\rangle$ and projecting on the Schrödinger equation, Eq. (5.32), for the effective Hamiltonian, Eq. (5.34), with the contributions Eqs. (5.35), (5.36) and (5.37) up to third order yields the coupled differential equations [4]

$$i\frac{\mathrm{d}}{\mathrm{d}\tau}\boldsymbol{d} = \begin{pmatrix} \frac{\alpha_n^2}{4} & 0 & 0 & \frac{1}{4}\alpha_{n-1}\alpha_n\alpha_{n+1} \\ 0 & -\frac{\alpha_{n-1}^2}{2} & \alpha_n\left(1-\frac{\alpha_n^2}{4}\right) & 0 \\ 0 & \alpha_n\left(1-\frac{\alpha_n^2}{4}\right) & -\frac{\alpha_{n+1}^2}{2} & 0 \\ \frac{1}{4}\alpha_{n-1}\alpha_n\alpha_{n+1} & 0 & 0 & \frac{\alpha_n^2}{4} \end{pmatrix}\boldsymbol{d}\,, \tag{5.39}$$

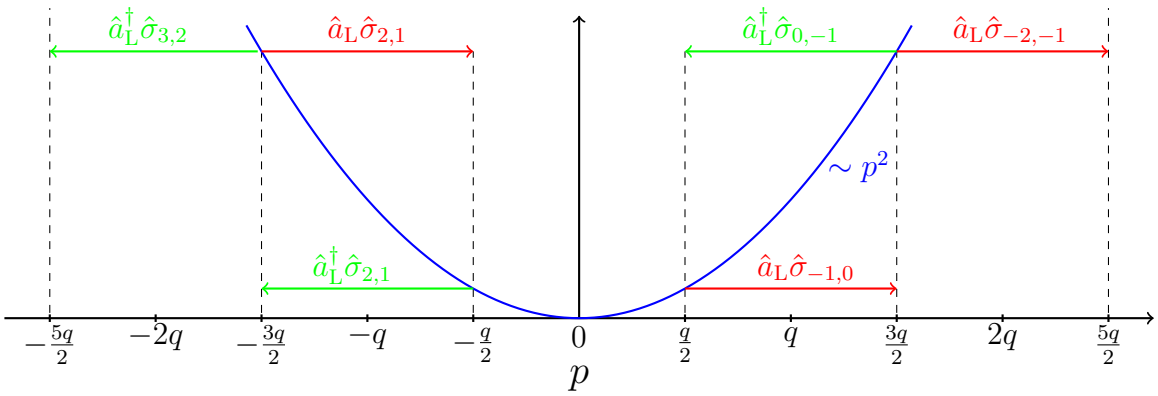

Figure 5.5: Non-resonant single-photon transitions according to the rapidly varying contribution $\hat{F}^{(1)}(\tau)$ of the dynamics. We note that the resonant processes involving $q/2$ and $-q/2$ are missing from $\hat{F}^{(1)}$ since they correspond to the slowly varying part of the dynamics due to $\hat{H}_{\mathrm{eff}}^{(1)}$, Eq. (5.35).

where we have used the vector notation $\boldsymbol{d} \equiv (d_{-1}, d_0, d_1, d_2)^{\mathrm{T}}$.

The differential equations in Eq. (5.39) can be straightforwardly solved and according to Eqs. (D.51) and (D.52) the solution [4] reads

$$\boldsymbol{d}(\tau) = U(\tau)\boldsymbol{d}(0) \tag{5.40}$$

with

$$U \equiv \begin{pmatrix} \mathrm{e}^{-\frac{i\alpha^2\tau}{4}}\cos\left(\frac{\alpha^3}{4}\tau\right) & 0 & 0 & \frac{1}{i}\,\mathrm{e}^{-\frac{i\alpha^2\tau}{4}}\sin\left(\frac{\alpha^3}{4}\tau\right) \\ 0 & \mathrm{e}^{\frac{i\alpha^2\tau}{2}}\cos\left[\left(\alpha-\frac{\alpha^3}{4}\right)\tau\right] & \frac{1}{i}\,\mathrm{e}^{\frac{i\alpha^2\tau}{2}}\sin\left[\left(\alpha-\frac{\alpha^3}{4}\right)\tau\right] & 0 \\ 0 & \frac{1}{i}\,\mathrm{e}^{\frac{i\alpha^2\tau}{2}}\sin\left[\left(\alpha-\frac{\alpha^3}{4}\right)\tau\right] & \mathrm{e}^{\frac{i\alpha^2\tau}{2}}\cos\left[\left(\alpha-\frac{\alpha^3}{4}\right)\tau\right] & 0 \\ \frac{1}{i}\,\mathrm{e}^{-\frac{i\alpha^2\tau}{4}}\sin\left(\frac{\alpha^3}{4}\tau\right) & 0 & 0 & \mathrm{e}^{-\frac{i\alpha^2\tau}{4}}\cos\left(\frac{\alpha^3}{4}\tau\right) \end{pmatrix}. \tag{5.41}$$

Here, we have made the approximation

$$\alpha_{n-1} \cong \alpha_n \cong \alpha_{n+1} \equiv \alpha \tag{5.42}$$

for a high photon number $n \gg 1$ which considerably simplifies the expression in Eq. (5.41). For the states $p = q/2$ and $p = -q/2$ we obtain the Rabi oscillations already derived in the preceding section with an additional frequency shift that scales with α^3. Moreover, we find oscillations for $p = 3q/2$ and $p = -3q/2$ with the frequency $\alpha^3/4$. Hence, the dynamics of this second two-level system occurs on a much longer time scale than the time evolution of the fundamental one.

While the slowly varying contributions of the dynamics represent *resonant* transitions which can be deduced from Figs. 5.1, 5.3 and 5.4 the rapid-varying ones describe *non–resonant*

processes. For example, the first-order term, Eq. (D.37),

$$\hat{F}^{(1)}(\tau) = -\hat{a}_{\mathrm{L}} \sum_{\mu\neq 0} \frac{\mathrm{e}^{-i2\mu\tau}}{\mu} \hat{\sigma}_{\mu,\mu+1} + \hat{a}_{\mathrm{L}}^{\dagger} \sum_{\mu\neq 0} \frac{\mathrm{e}^{i2\mu\tau}}{\mu} \hat{\sigma}_{\mu+1,\mu} \tag{5.43}$$

includes all non-resonant single-photon transitions which is apparent from the exclusion of the only resonant one between $\mu = 0$ and $\mu = 1$ from the summation and from Fig. 5.5, where the underlying processes of $\hat{F}^{(1)}$ are visualized. Similarly, we obtain from Eq. (D.39) that

$$\begin{aligned} \hat{F}^{(2)}(\tau) =& \hat{a}_{\mathrm{L}}^{2} \left[\frac{1}{4} \left(\hat{\sigma}_{-1,1}\, \mathrm{e}^{i2\tau} - \hat{\sigma}_{0,2}\, \mathrm{e}^{-i2\tau} \right) + \frac{1}{2} \sum_{\mu\neq 0,-1} \frac{\mathrm{e}^{-i2(2\mu+1)\tau}}{4\mu(\mu+1)(2\mu+1)} \hat{\sigma}_{\mu,\mu+2} \right] \\ & - \hat{a}_{\mathrm{L}}^{\dagger\,2} \left[\frac{1}{4} \left(\hat{\sigma}_{1,-1}\, \mathrm{e}^{-i2\tau} - \hat{\sigma}_{2,0}\, \mathrm{e}^{i2\tau} \right) + \frac{1}{2} \sum_{\mu\neq 0,-1} \frac{\mathrm{e}^{i2(2\mu+1)\tau}}{4\mu(\mu+1)(2\mu+1)} \hat{\sigma}_{\mu+2,\mu} \right] , \end{aligned} \tag{5.44}$$

only contains two-photon processes which are non-resonant.

To obtain the transition-probabilities we first transform the initial state $|\Psi(0)\rangle$ to $|\Phi(0)\rangle = \exp\left\{\hat{F}(0)\right\} |\Psi(0)\rangle$, according to Eq. (5.31), and obtain the initial condition for $\boldsymbol{d} = \boldsymbol{d}(0)$. The solution for $|\Phi(\tau)\rangle$, Eq. (5.40) , in terms of $\boldsymbol{d}(\tau)$ is then back-transformed via Eq. (5.31) to an expression for $|\Psi(\tau)\rangle$ with the corresponding expansion coefficients c_μ, Eq. (5.4). At the end we calculate the modulus square of the amplitudes and keep only terms up to the order we desire. The explicit details of this procedure are presented in App. D. We note that we have to go to the second order in α for the corrections to the amplitudes since these contributions cancel in first order.

Here, we present the resulting probabilities [4]

$$\begin{aligned} |c_1(\tau)|^2 =& \sin^2\left[(\Omega_n - \chi)\, t\right] - \frac{\alpha^2}{2} \sin\left[(\Omega_n - \chi)\, t\right] \\ & \times \left\{ \sin\left[(\Omega_n - \chi)\, t\right] - \sin(\chi t) \cos\left[2\omega_{\mathrm{r}} t \left(1 + \frac{3\alpha^2}{8} \right) \right] \right\} \end{aligned} \tag{5.45}$$

and

$$\begin{aligned} |c_2(\tau)|^2 =& \frac{\alpha^2}{4} \Big\{ \sin^2\left[(\Omega_n - \chi)\, t\right] + \sin^2(\chi t) \\ & - 2 \sin(\chi t) \sin\left[(\Omega_n - \chi)\, t\right] \cos\left[2\omega_{\mathrm{r}} t \left(1 + \frac{3\alpha^2}{8} \right) \right] \Big\} \end{aligned} \tag{5.46}$$

for single-photon emission, from Eq. (D.65), and for two-photon emission, Eq. (D.66), respectively. As before, we have considered the original variables and have introduced the Rabi frequency $\Omega_n \equiv g\sqrt{n+1}$ for zero detuning, according to Eq. (5.27), as well as the shift

$$\chi \equiv \frac{\alpha^2}{4} \Omega_n \tag{5.47}$$

due to higher orders. While $|c_1|^2$ corresponds to the ground state $p = -q/2$ of the two-level system defining the Quantum FEL, $|c_2|^2$ gives the probability for the electron to occupy the momentum $p = -3q/2$ and thus goes beyond the two-level approximation.

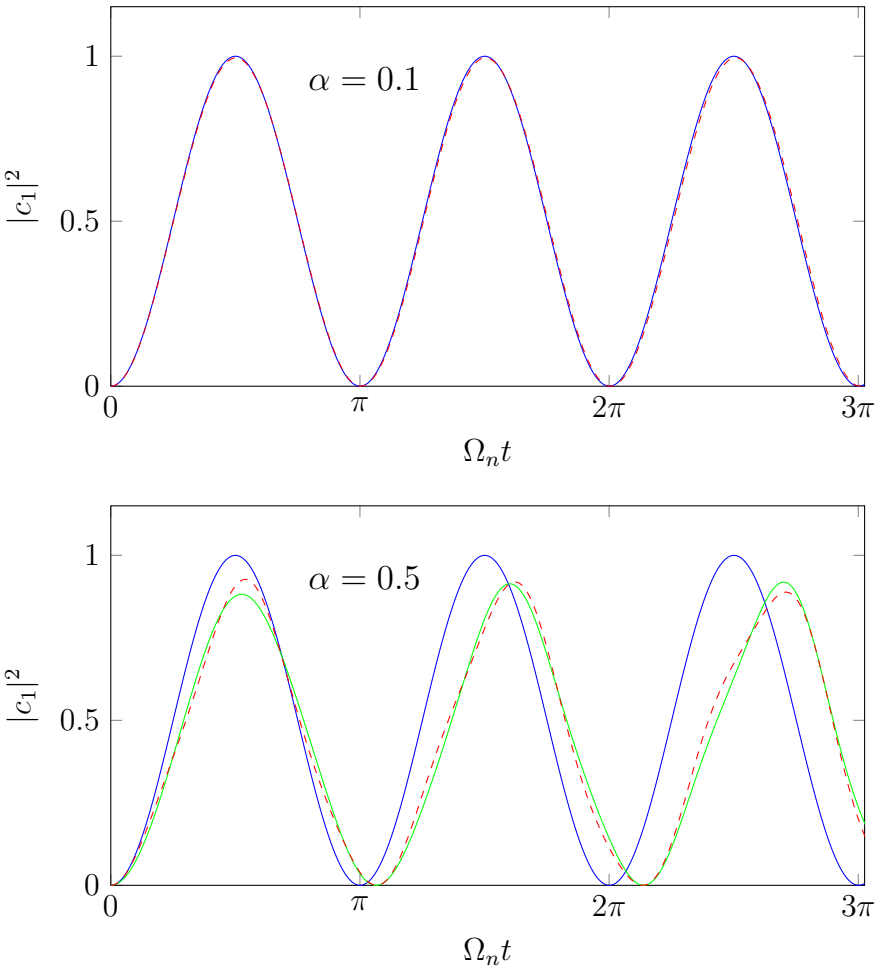

Figure 5.6: Probability $|c_1|^2$ for the electron to occupy the momentum level $-q/2$ in the Quantum FEL corresponding to single-photon emission as a function of the dimensionless time $\Omega_n T$, where Ω_n denotes the Rabi frequency, Eq. (5.27), for $\Delta = 0$. We compare the two-level approximation (blue line), Eq. (5.48), as well as the solution of third order (green line), Eq. (5.45), of the method of averaging to the numerical solution of Eq. (5.49) (red dashed line) for $\alpha = 0.1$ (above) and $\alpha = 0.5$ (below), respectively. For the deep quantum regime, $\alpha = 0.1$, the two-level approximation agrees very well with the simulation while for $\alpha = 0.5$ the numerical solution shifts in frequency compared to the zeroth-order solution and its amplitude is modulated. Hence, the two-level approximation is not accurate for this latter case. However, the third-order solution shows the correct behavior also for $\alpha = 0.5$.

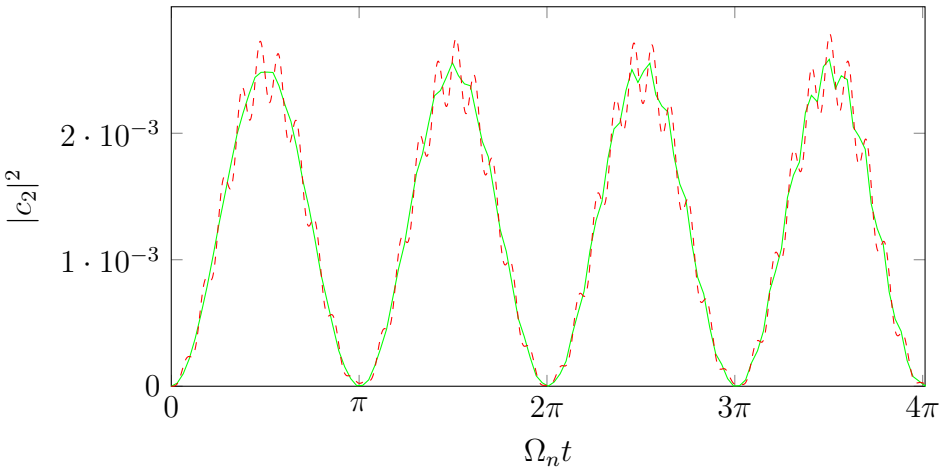

Figure 5.7: Probability $|c_2|^2$ for the electron to occupy the momentum level $-3q/2$ corresponding to two-photon emission in the Quantum FEL with $\alpha = 0.1$ as function of the dimensionless time $\Omega_n T$ where Ω_n denotes the Rabi frequency, Eq. (5.27), for $\Delta = 0$. We obtain that the analytic solution, Eq. (5.46), of third order of the method of averaging (green line) agrees rather well with the numerical simulation (red dashed line) of Eq. (5.49). Moreover, we observe an oscillation of the probability with the Rabi frequency Ω_n and small wiggles on top corresponding to rapidly varying corrections of the amplitude. Most importantly, however, the magnitude of the two-photon emission is suppressed with α^2 in comparison to single-photon emission in Fig. 5.6.

By inspection of $|c_1|^2$ in Eq. (5.45) we recognize that the first term, the amplitude of which is independent of α, contains the shift χ in the Rabi frequency which scales with α^2, according to Eq. (5.47). The amplitude of the second term scales quadratic with α and the time dependency is characterized by rapid oscillations with the frequency $2\omega_\mathrm{r}$. For $\alpha \to 0$ the probability $|c_1|^2$ in Eq. (5.45) reduces to

$$|c_1|^2 = \sin^2 \Omega_n t \tag{5.48}$$

which is identical to the result of the two-level approximation, Eq. (5.29), for zero detuning $\Delta = 0$.

The probability $|c_2|^2$ for two-photon emission, Eq. (5.46), is proportional to α^2. Hence, two-photon emission corresponding to the transition to the momentum $p = -3q/2$ is suppressed in the quantum regime due to $\alpha \ll 1$.

Similarly, by using Eqs. (D.64) and (D.67) in App. D we deduce that for $\alpha \ll 1$ the probability $|c_0|^2$ for the electron to have momentum $p = q/2$ reduces to the expression, Eq. (5.28) with $\Delta = 0$, in the two-level approximation while the probability $|c_{-1}|^2$ for the electron to have momentum $p = 3q/2$ is suppressed by α^2. Moreover, since other transitions occur at even higher orders of the method of averaging we assume that they are suppressed with the corresponding order of α. Hence, the deep quantum regime of the FEL is indeed characterized by the two momentum levels $q/2$ and $-q/2$.

This fact is even more pronounced in Figs. 5.6 and 5.7, where we show the probabilities $|c_1|^2$, Eq. (5.45), and $|c_2|^2$, Eq. (5.46), for single-photon and two-photon emission, respectively, as a function of time t and compare them to a numerical solution. These figures correspond to Figs. 6 and 7 of Ref. [4] where graphs for $|c_0|^2$ and $|c_{-1}|^2$ are presented.
The numerical solution is derived from the three-term recursion relation

$$i\frac{\mathrm{d}c_\mu(t)}{\mathrm{d}\tau} = \left(\frac{p}{q/2} - \mu\right)^2 c_\mu(t) + g\sqrt{n+\mu+1}\, c_{\mu+1}(t) + g\sqrt{n+\mu}\, c_{\mu-1}(t) \tag{5.49}$$

with $p = q/2$. This relation arises from the Schrödinger equation with the Hamiltonian, Eq. (5.10), in the Schrödinger picture. For the initial photon number we assume the value $n = 1000$ and we truncate the recurrence relation, Eq. (5.49), at $\mu = -49$ and $\mu = 50$ in analogy to Ref. [4]. The solution is then obtained by diagonalizing a 100×100 tridiagonal matrix.
For $\alpha = 0.1$ we observe from Fig. 5.6 that the two-level approximation, Eq. (5.29), already gives an accurate expression for $|c_1|^2$. Increasing the value of the quantum parameter to $\alpha = 0.5$ gives us corrections in the amplitude as well a shift in the Rabi frequency. Indeed, the two-level approximation, Eq. (5.29), deviates from the numerically computed curve. However, already the solution, Eq. (5.45), of the next higher order is in very good agreement with the numerical solution.
In Fig. 5.7 we have shown the result for $|c_2|^2$, Eq. (5.46), of the method of averaging in comparison to the numerical solution with $\alpha = 0.1$. Indeed, both curves match. Moreover, we obtain that the two-photon process described by this probability is strongly suppressed when compared to the single-photon emission, Eq. (5.45), as we have already expected from the discussion above. The 'wiggles' on top the oscillations in Fig. 5.7 emerge from the rapid oscillations in the Hamiltonian, Eq. (5.12).
In conclusion, we have proven that for the resonance $p = q/2$ the identification of the Quantum FEL with a two-level system for the momentum of the electron is justified. Corrections to the simple Rabi oscillations of the deep quantum regime, presented in the preceding section, scale with higher orders of the quantum parameter α, in the amplitude as well as in the frequency, and hence can be neglected for $\alpha \ll 1$. However, we have not yet discussed the situation for other resonances apart from $p = q/2$.

5.4 Higher resonances

The Hamiltonian, Eq. (5.12), shows resonances for integer multiples of $q/2$. Up to now we have just considered the first resonance, $p = q/2$, where the dynamics of the FEL in the quantum regime, $\alpha \ll 1$, is analogous to a two-level system. In the following we discuss which effects occur for other resonant momenta.

5.4.1 Second resonance

First, we turn to the next resonance, that is $p = q$. From Eq. (5.12) we obtain the Hamiltonian

$$\hat{H}_\mathrm{I}(\tau) = \varepsilon\left(\hat{a}_\mathrm{L}\sum_\mu \mathrm{e}^{-i2(\mu-1/2)\tau}\,\hat{\sigma}_{\mu,\mu+1} + \hat{a}_\mathrm{L}^\dagger\sum_\mu \mathrm{e}^{i2(\mu-1/2)\tau}\,\hat{\sigma}_{\mu+1,u}\right). \tag{5.50}$$

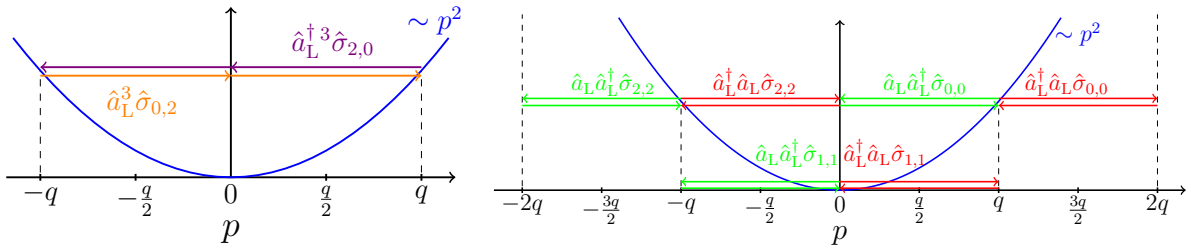

Figure 5.8: Resonant two-photon processes for the second resonance $p = q$ according to the effective Hamiltonian $\hat{H}_{\mathrm{eff}}^{(2)}$, Eq. (5.53) . The left-hand side shows the transition from q to $-q$ (purple arrows) and the vice-versa process (red arrows). On the right-hand side processes are presented where the final momentum of the electron equals the initial one either by first emitting and then absorbing a photon (green arrows) or the reverse process (red arrows).

To bring $\hat{H}_{\mathrm{I}}$ into the desired form of the Fourier series in Eq. (5.16) we change the summation index μ to k according to $k = \mu - 1/2$. We note that we do not sum over integer numbers but over odd multiples of $1/2$. This change of summation indices corresponds to the fact that we have shifted the discrete momentum ladder from *odd* multiples of $q/2$ to *even* multiples of $q/2$. Thus, we arrive at

$$\hat{H}_{\mathrm{I}} = \varepsilon \sum_{k} \hat{\mathcal{H}}_k \, \mathrm{e}^{i2k\tau} \,, \tag{5.51}$$

where we have defined the components

$$\begin{cases} \hat{\mathcal{H}}_0 & \equiv 0 \\ \hat{\mathcal{H}}_k & \equiv \hat{a}_{\mathrm{L}} \hat{\sigma}_{-k+\frac{1}{2},-k+\frac{3}{2}} + \hat{a}_{\mathrm{L}}^{\dagger} \hat{\sigma}_{k+\frac{3}{2},k+\frac{1}{2}} \,. \end{cases} \tag{5.52}$$

The Hamiltonian, Eq. (5.51) is now in a suitable form to apply the method of canonical averaging. In the following we just sketch this calculation the details of which are presented in App. D.

Since the first order of the effective Hamiltonian $\hat{H}_{\mathrm{eff}}^{(1)} = \hat{\mathcal{H}}_0$ vanishes according to Eq. (5.52) we go to the next higher order in the method of averaging. In App. D we obtain, Eq. (D.75), the expression

$$\hat{H}_{\mathrm{eff}}^{(2)} = \hat{a}_{\mathrm{L}}^{2} \hat{\sigma}_{0,2} + \hat{a}_{\mathrm{L}}^{\dagger\,2} \hat{\sigma}_{2,0} - \hat{a}_{\mathrm{L}} \hat{a}_{\mathrm{L}}^{\dagger} \sum_{\mu} \frac{1}{2\mu - 1} \hat{\sigma}_{\mu,\mu} + \hat{a}_{\mathrm{L}}^{\dagger} \hat{a}_{\mathrm{L}} \sum_{\mu} \frac{1}{2\mu - 3} \hat{\sigma}_{\mu,\mu} \tag{5.53}$$

in second order for the effective Hamiltonian. We can understand the form of this Hamiltonian with the help of Fig. 5.8. In this figure we show the resonant processes for $p = q$. On the one hand Eq. (5.53) describes a two-level system consisting of the momentum levels $p = q$ and $p = -q$ and on the other hand it contains two-photon processes, where the final momentum is identical to the initial one but with an additional intermediate level. In contrast to the fundamental resonance $p = q/2$, there are no resonant single-photon transitions. For $p = q$ we require at least two photons, that is two discrete momentum steps, to obtain conservation of energy and momentum.

In analogy to the first resonance we consider the expansion coefficients d_μ, Eq. (5.38), of $|\Phi\rangle$ in the scattering basis. From the Schrödinger equation, Eq. (5.32), we arrive at, Eq. (D.79),

$$i\frac{\mathrm{d}}{\mathrm{d}\tau}\boldsymbol{d} = \begin{pmatrix} \eta_n & 0 & \alpha_n\alpha_{n+1} \\ 0 & -3\eta_n & 0 \\ \alpha_n\alpha_{n+1} & 0 & \eta_n \end{pmatrix} \boldsymbol{d} \tag{5.54}$$

for the dynamics of the d_μ. Here, we have introduced the abbreviation

$$\eta_n \equiv \alpha_n^2 - \frac{\alpha_{n-1}^2}{3} \tag{5.55}$$

and have employed the vector notation $\boldsymbol{d} \equiv (d_0, d_1, d_2)^{\mathrm{T}}$.

The differential equation Eq. (5.54) can be straightforwardly solved and we thus obtain, Eq. (D.83),

$$\boldsymbol{d}(\tau) = \begin{pmatrix} \mathrm{e}^{-i\eta_n\tau}\cos(\alpha_n\alpha_{n+1}\tau) & 0 & -i\,\mathrm{e}^{-i\eta_n\tau}\sin(\alpha_n\alpha_{n+1}\tau) \\ 0 & \mathrm{e}^{i3\eta_n\tau} & 0 \\ -i\,\mathrm{e}^{-i\eta_n\tau}\sin(\alpha_n\alpha_{n+1}\tau) & 0 & \mathrm{e}^{-i\eta_n\tau}\cos(\alpha_n\alpha_{n+1}\tau) \end{pmatrix} \boldsymbol{d}(0) \tag{5.56}$$

which describes Rabi oscillations between the momentum levels $p = q$ and $p = -q$.

To obtain the transition probabilities $|c_\mu|^2$ we first have to determine the initial conditions for d_μ via the transformation Eq. (5.31) and under the assumption that the electron initially is at resonance, that is $c_\mu(0) = \delta_{\mu,0}$, before we apply Eq. (5.56). Then, we have to transform back to the original state, according to Eq. (5.31), where rapid oscillations come into play due to non-resonant processes. Finally, we take the modulus square of the amplitudes c_μ and keep terms up to second order in α_n. This procedure was already explained for the first resonance in the preceding section and is shown in detail in App. D.

When we assume a large photon number, that is $n \gg 1$, we set $\alpha_n \cong \alpha$ and make the identifications

$$\eta_n\tau \cong \frac{2}{3}\alpha^2\omega_{\mathrm{r}}t \tag{5.57}$$

as well as

$$\alpha_n\alpha_{n+1}\tau \cong \alpha\Omega_n t\,, \tag{5.58}$$

where we have returned to the original variables and have recalled the definition $\Omega_n \equiv g\sqrt{n+1}$ of Rabi frequency for the first resonance. The expression in Eq. (5.58) displays the Rabi frequency for the two-level system consisting of $p = q$ and $p = -q$ and is suppressed for $\alpha \ll 1$ in comparison to Ω_n characterizing the fundamental resonance $p = q/2$. Hence, the time evolution of the system at the second resonance $p = q$ occurs on a much longer time scale than in the case of the first resonance.

For example, we obtain the probability, Eq. (D.94),

$$|c_2|^2 = \sin^2(\alpha\Omega_n t) - 2\alpha^2\sin(\alpha\Omega_n t)\left\{\sin\left[\omega_{\mathrm{r}}t\left(1+\frac{3}{8}\alpha^2\right)\right] + \frac{10}{9}\sin(\alpha\Omega_n t)\right\} \tag{5.59}$$

for the electron to possess the momentum $p = -q$ which corresponds to the emission of two photons. When we let $\alpha \to 0$ we find

$$|c_2|^2 = \sin^2(\alpha\Omega_n t), \tag{5.60}$$

that is an oscillation between the momentum levels q and $-q$ with Rabi frequency $\alpha\Omega_n$. We emphasize that in Eq. (5.59) we have only considered corrections in the amplitude and not in the frequency. However, since corrections in the Rabi frequency emerge due to higher orders of the effective Hamiltonian we assume that they scale with higher orders of α and hence can be neglected for $\alpha \ll 1$.

In Fig. 5.9 we compare the asymptotic solutions, Eqs. (5.59) and (5.60), to the numerical solution of Eq. (5.49). For $\alpha = 0.1$ the frequency shift is negligible but increases for $\alpha = 0.5$. Moreover, we find that the oscillation of Eq. (5.60) occurs on a longer time scale when compared to Eq. (5.45) and Fig. 5.6 for the first resonance, due to $\alpha\Omega_n \ll \Omega_n$. The wiggles on top of the oscillations again correspond to rapid oscillations with frequency ω_r.

For the non-resonant transition from $p = q$ to $p = 0$, where a single photon is emitted, we obtain

$$|c_1|^2 = 2\alpha^2\left(1 - \cos\left[\omega_\mathrm{r} t\left(1 + \frac{5}{3}\alpha^2\right)\right]\right) \tag{5.61}$$

according to Eq. (D.94). Hence, the probability of this process is suppressed with α^2 in comparison to the resonant one, that is $|c_2|^2$, which we can also deduce from Fig. 5.4.1, where the analytic result, Eq. (5.61), is compared to the numerical one.

In Ref. [112] a numerical analysis of Eq. (5.49) for different resonances was presented, with results that are in accordance with our analytic expressions. The authors concluded that, besides the case of the fundamental resonance at $p = q/2$, the Quantum FEL does not show a two-level behavior. Moreover, they argued that the occurrence of higher resonances only emerges in a fully-quantized theory, where the motion of the electron as well as the laser field are quantized.

We disagree with these conclusions of Ref. [112]. Indeed, we have as well considered a quantized laser field and to talk about emission or absorption of 'photons' is very illustrative. However, as we have discussed in Chap. 3 it is the discrete motion of the *electron* that is responsible for quantum effects in the FEL. We would have found the same resonances if we have considered a classical laser field, which we have implicitly done by taking the limit $n \gg 1$ at the end of our calculations. It is just important that the *discrete momentum steps* simultaneously conserve energy and momentum of the electron which is for example illustrated in Fig. 5.1.

Moreover, we still identify the dynamics of the electron at a higher resonance with a two-level system, as we have shown for the example of the momentum levels $p = q$ and $p = -q$. However, the electron now has to take two discrete steps on the momentum ladder instead of just one step which leads to Rabi oscillations which are slower as in the case of $p = q/2$.

5.4.2 Third and higher resonances

The situation for other resonances is very similar. Without going into detail we sketch in the following the situation of the 'third resonance', that is $p = 3q/2$. According to Eq. (5.12) the

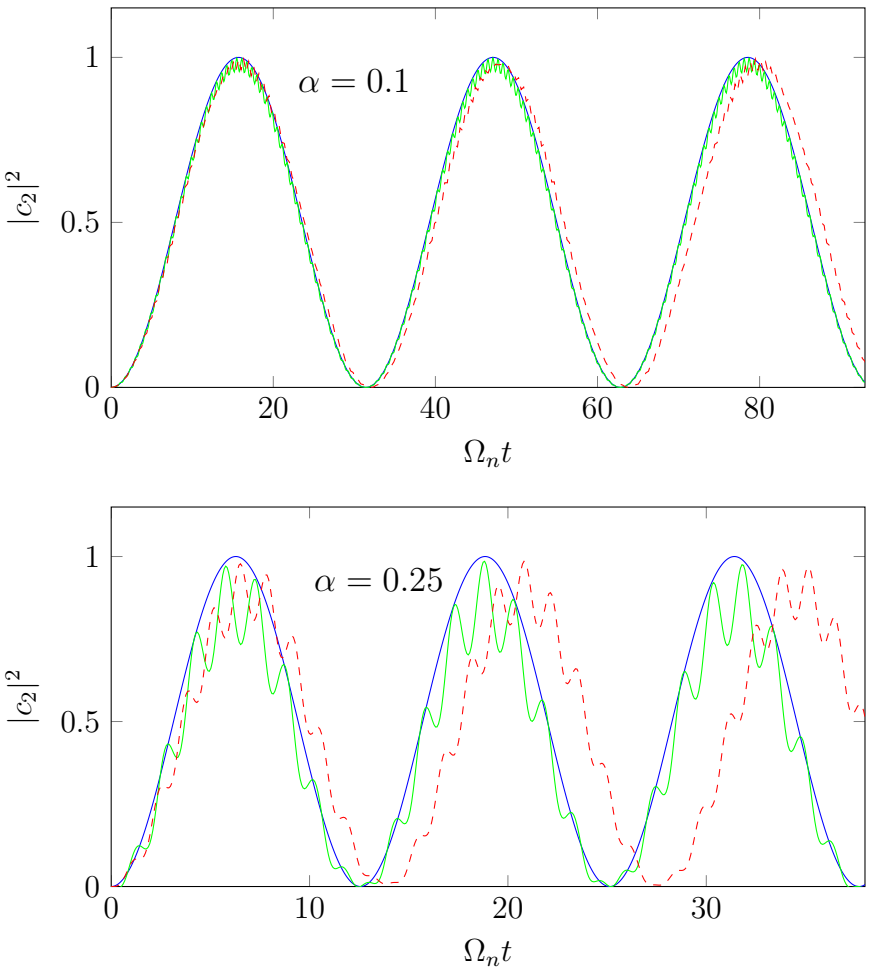

Figure 5.9: Probability $|c_2|^2$ for the electron to occupy the momentum level $p = -q$, corresponding to two-photon emission, for the second resonance $p = q$ as a function of the dimensionless time $\Omega_n t$ with Ω_n, Eq. (5.27), denoting the fundamental Rabi frequency for $\Delta = 0$. We compare the analytic solution in lowest order (blue line), Eq. (5.60), and the one of next higher order (green line), Eq. (5.59), from the method of averaging to the numerical simulation (red, dashed line) of Eq. (5.49) for two different values of α, that is $\alpha = 0.1$ (above) and $\alpha = 0.25$ (below), respectively. We observe that for the former case our analytic solution agrees very well with numerics. Increasing α, however, leads to a discrepancy in the frequency while the higher order of the method of averaging seems to predict at least the correct behavior of the amplitudes in form of the wiggles on top. For a better match of the frequency we would have to consider higher orders of the effective Hamiltonian $\hat{H}_{\text{eff}}$. For both values of α we obtain that the dynamics occurs on a much longer time scale in comparison to the fundamental resonance at $p = q/2$.

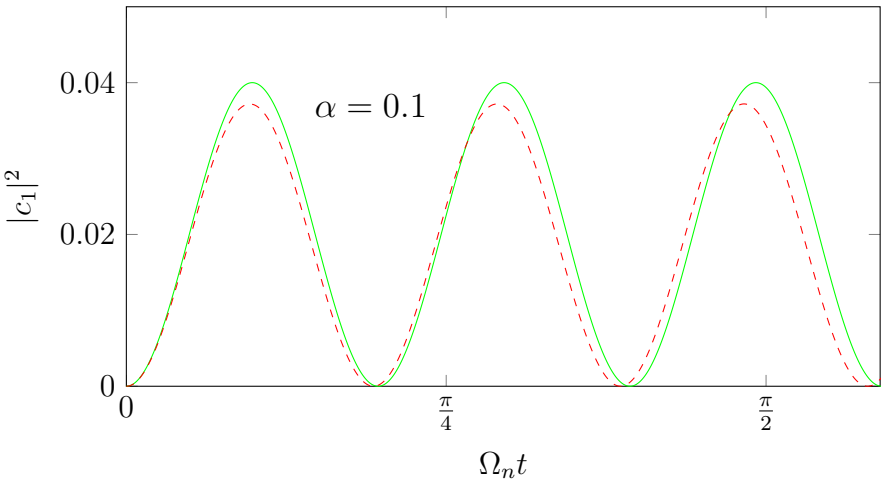

Figure 5.10: Probability $|c_1|^2$ for the electron to occupy the momentum level $p = 0$, corresponding to single-photon emission, for the second resonance $p = q$ as a function of the dimensionless time $\Omega_n t$ with Ω_n, Eq. (5.27), denoting the fundamental Rabi frequency for $\Delta = 0$. For our choice of the quantum parameter, that is $\alpha = 0.1$, the solution (green line), Eq. (5.61), from the method of averaging agrees rather well with the simulation (red, dashed line) of Eq. (5.49). We observe that the amplitude of this non-resonant process is suppressed with $\alpha^2 \ll 1$ while the oscillations occur on the small time scale, described by the recoil frequency ω_r.

phases of the Hamiltonian read

$$\pm i\tau \left(\frac{p}{q/2} - (2\mu + 1) \right) = \mp 2i\tau(\mu - 1)\,, \tag{5.62}$$

where we have set $p = 3q/2$.

From Eq. (5.12) we immediately obtain the resonant contribution

$$\hat{H}^{(1)}_\mathrm{eff} = \hat{a}_\mathrm{L}\hat{\sigma}_{1,2} + \hat{a}^\dagger_\mathrm{L}\hat{\sigma}_{2,1} \tag{5.63}$$

which we have identified as the effective Hamiltonian in first order. This Hamiltonian describes the two level-system consisting of $p = q/2$ and $p = -q/2$ like in the case of the first resonance. However, for the initial momentum $p = 3q/2$, that is $c_\mu(0) = \delta_{\mu,0}$, we do not obtain this transition, at least for the lowest order in the amplitude, since here the slowly varying part coincides with the total dynamics.

In analogy to Fig. 5.1 we deduce that the processes of lowest order are given by the transitions from $p = 3q/2$ to $p = -3q/2$, where three photons are emitted and the vice-versa process, where three photons are absorbed. Due to Eqs. (5.12) and (5.62) we can describe the absorption of three photons by

$$\hat{a}^3_\mathrm{L}\, \mathrm{e}^{-2i\tau(\mu+\nu+\rho-3)}\, \hat{\sigma}_{\mu,-\mu+1}\hat{\sigma}_{\nu,-\nu+1}\hat{\sigma}_{\rho,-\rho+1} = \delta_{\nu,\mu+1}\delta_{\rho,\mu+2}\, \hat{a}^3_\mathrm{L}\, \mathrm{e}^{-6i\mu\tau}\, \hat{\sigma}_{\mu,-\mu+3}\,, \tag{5.64}$$

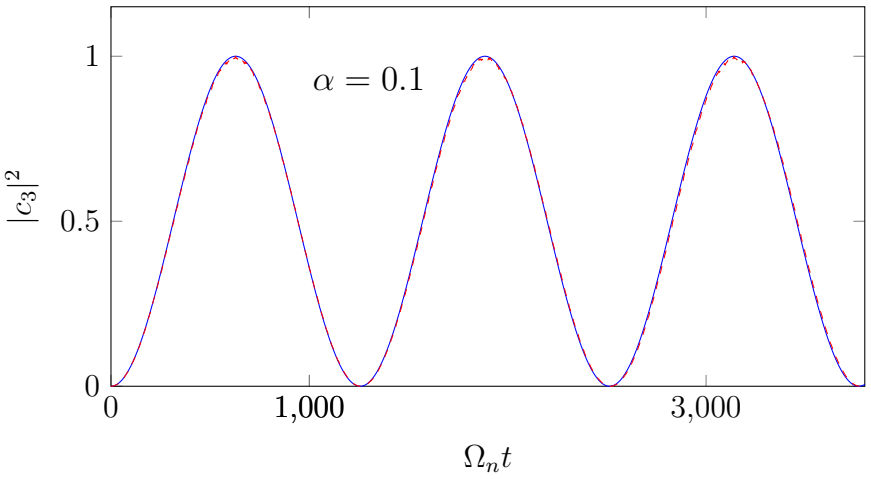

Figure 5.11: Probability $|c_3|^2$ for the electron to occupy the momentum level $p = -3q/2$, corresponding to three-photon emission, for the third resonance $p = 3q/2$ as a function of the dimensionless time $\Omega_n t$ with Ω_n, Eq. (5.27), denoting the fundamental Rabi frequency for $\Delta = 0$. For our choice of the quantum parameter, that is $\alpha = 0.1$, the lowest-order solution (blue line), Eq. (5.67), from the method of averaging agrees very well with the numerical solution (red, dashed line) of Eq. (5.49). However, this transition occurs on a much longer time scale than resonant processes of the first resonance $p = q/2$, Fig. 5.6, as well as the ones of the second resonance, Fig. 5.9.

where we have used Eq. (5.7). By setting $\mu = 0$ we arrive at the resonant contribution

$$\delta_{\nu,1}\delta_{\rho,2}\,\hat{a}_{\mathrm{L}}^{3}\hat{\sigma}_{0,3} \tag{5.65}$$

which is the expression we would have expected for this kind of process.

With the help of Eq. (D.26) we find that the effective Hamiltonian in third order is of the form

$$\hat{H}_{\mathrm{eff}} \sim \frac{\varepsilon^3}{4}\left(\hat{a}_{\mathrm{L}}^{3}\hat{\sigma}_{0,3} + \hat{a}_{\mathrm{L}}^{\dagger\,3}\hat{\sigma}_{3,0}\right) . \tag{5.66}$$

We are only interested in the leading term of our expansion, that is third order in the slowly varying part and zeroth order in the rapidly varying contribution.

Solving the Scrödinger equation, Eq. (5.32), with the Hamiltonian in Eq. (5.66) we finally obtain the probabilities

$$\begin{cases} |c_0(t)|^2 &= \cos^2\left(\frac{\alpha^2}{4}\Omega_n t\right) \\ |c_3(t)|^2 &= \cos^2\left(\frac{\alpha^2}{4}\Omega_n t\right) \end{cases} \tag{5.67}$$

for the electron to occupy the momentum levels $p = 3q/2$ and $p = -3q/2$, respectively. These probabilities describe Rabi oscillations with Rabi frequencies that are suppressed with α^2 in comparison to the first resonance $p = q/2$ and thus are much slower. In Fig. 5.11 we compare our analytical solution Eq. (5.67) with the numerical one and find excellent agreement for $\alpha = 0.1$.

We can even go a step further by assuming arbitrary multiples of $q/2$, that is $p = mq/2$. Due to our preceding discussions we assume that for $\alpha \ll 1$ the dynamics for the mth resonance is dictated by combinations of operators of the form $\varepsilon^m \hat{a}_{\mathrm{L}}^m \hat{\sigma}_{0,m}$ and the Hermitian conjugate. Hence, we assume for $m \ll n$ that the transition probabilities involving the momentum levels $p = mq/2$ and $p = -mq/2$ describe Rabi oscillations with Rabi frequencies

$$\Omega_n^{(m)} \propto \alpha^{m-1} \Omega_n \tag{5.68}$$

that are suppressed with the corresponding power of α. Thus, the oscillations occur on a much slower time scale than for the fundamental resonance, $p = q/2$.

5.5 Summary

In conclusion, we have defined the quantum regime of the FEL as the limit, where the electron dynamics reduces to a two-level system of two resonant momenta in accordance with Ref. [4]. For this purpose, we have made use of the method of canonical averaging [37] with the help of which we have identified the underlying transitions on the discrete momentum ladder which can be straightforwardly interpreted in terms of energy-momentum conservation.
When the conditions on the quantum parameter, Eq. (5.18), and on the initial momentum spread, Eq. (5.30), are both fulfilled the time evolution of the electron is characterized by Rabi oscillations. For the fundamental resonance $p = q/2$ the probability oscillates between $q/2$ and $-q/2$, Fig. 5.6. Non-resonant transitions, for example from $q/2$ to $-3q/2$, are suppressed with powers of α according to Fig. 5.7. Processes involving higher resonances, for example from q to $-q$, on the other hand are also described by Rabi oscillations between probability zero and one. However, these oscillations occur on a much longer time scale as the dynamics of the fundamental resonance and, hence, are also suppressed.
In this context, we have discussed the statements of Ref. [112] that these higher-resonances (i) arise due to a quantized laser field and (ii) do not show a two-level behavior. We disagreed with both statements due to the insight into the underlying processes of the Quantum FEL gained from our analytic approach in this chapter.

6 The Quantum FEL Oscillator

After investigating the emergence of the quantum regime of the FEL in the preceding chapter we now turn to the properties of an FEL oscillator operating in this limit. We expect the realization of a Quantum FEL for very short wavelenghts, that is X-rays, where up to now no high-qualtity mirrors exist. However, there already exist the first ideas [118] to construct cavities also for this part of the spectrum eventually leading to the realization of an X-ray FEL oscillator in the classical regime. Hence, we go one step further and propose a 'Quantum FEL oscillator'.
Due to the analogy with the one-atom maser [38, 39, 40, 119, 120] the calculation of features like (i) gain, (ii) steady-state photon statistics, and (iii) intrinsic linewidth is straightforward. To bring our results for the Quantum FEL into ab broader context we compare them with the corresponding quantities of its classical counterpart derived in Chap. 4. We note that our studies on the radiation properties in this chapter are based on Refs. [121, 122].
In principle, the gain in the quantum and in the classical regime can both take on arbitrary high values – at least within the boundaries of our low-gain theory. However, for the gain to be high enough to surpass cavity losses we show in this chapter that the experimental requirements on wiggler length and electron energy are more strict for the Quantum FEL than for the classical FEL.
The most striking feature of an FEL oscillator in the quantum regime is the possibility of obtaining Poissonian or sub-Poissonian photon statistics which follows from the analogy to the one-atom maser [40]. This fact was already pointed out in Ref. [26] and demonstrated with the help of standard perturbation theory for short times. Moreover, by comparing the width of the photon distribution to the corresponding quantity in the classical regime, Chap. 4, we show that the broadening of the latter distribution does not exist in the quantum case. Hence, the coherence properties of a Quantum FEL oscillator are closer to an ordinary laser [22] than the ones of a classical FEL.
In contrast, the intrinsic linewidth does not show significantly enhanced properties since in both regimes a high steady-state intensity stabilizes the phase fluctuations in the oscillator configuration. We emphasize that this statement is not in conflict with the results of Ref. [3] of a narrowed linewidth since there a SASE FEL was considered without a stabilizing cavity.
At the end of this chapter we investigate the influence of a nonzero momentum spread of the electron beam which differs from the approach in Ref. [27] since we here study the effect on the radiation properties and not on the final momentum distribution of the electrons. In this context, we derive conditions to efficiently operate a Quantum FEL oscillator which are more limiting than the fundamental constraint $\Delta p < q$ for the quantum regime to emerge.

6.1 Gain in the Quantum FEL

In the following we first calculate the gain of a low-gain Quantum FEL with the help of the results of the preceding chapter. For that we consider the diagonal elements of the

density operator for the laser field in photon number representation. To better understand the physical meaning of our results we then investigate the limits of a small and a maximized signal, respectively, and compare them to the corresponding quantities, Chap. 2, in the classical regime. Finally, we take higher-order corrections to the gain into account when we leave the deep quantum regime.

6.1.1 Diagonal elements of the density matrix

In the preceding chapter we have assumed for the sake of simplicity that the laser field initially is given by a Fock state. Instead, we now explicitly calculate the properties of this field and thus we first assume a more general state. For this purpose, we write the state vector corresponding to the laser field as a superposition of photon number states with coefficients $c_n(t)$ which translates to the initial condition

$$|\Psi(t)\rangle = \left(\int_0^q \mathrm{d}p\, \phi(p)\, |p\rangle\right) \otimes \sum_n c_n(t)\, |n\rangle \tag{6.1}$$

for the state vector $|\Psi\rangle$ of the total system at time t right before the electrons enter the wiggler. Since electrons and laser field should be uncorrelated before interaction the state in Eq. (6.1) constitutes a product of subsystems. Moreover, we have assumed that the electrons are characterized by the initial momentum distribution $|\phi(p)|^2$ which is sharply peaked around $p = q/2$, according to Eqs. (5.19) and (5.30).

After the interaction the state has evolved

$$|\Psi(t+T)\rangle = \int \mathrm{d}p \sum_n c_n(p, t+T)\, |n, p\rangle + \int \mathrm{d}p \sum_n c_{n+1}(p-q, t+T)\, |n+1, p-q\rangle \tag{6.2}$$

during an interaction time T. Since we consider the quantum regime the state vector is a superposition of excited $|p\rangle$ and ground state $|p-q\rangle$ of the two-level system described in the preceding chapter.

To derive the properties of the radiation field at a time t' with $t \leq t' < t+T$ it is sufficient to consider the reduced density operator

$$\hat{\rho}_{\mathrm{L}}(t') \equiv \mathrm{Tr}_{\mathrm{el}}\{|\Psi(t')\rangle \langle\Psi(t')|\} \equiv \sum_{n',n''} \rho_{n',n''}(t')\, |n'\rangle \langle n''| \tag{6.3}$$

for the laser field, which emerges by taking the partial trace $\mathrm{Tr}_{\mathrm{el}}$ over the subsystem of the electron. In contrast to our discussions about the radiation field of the classical FEL in Chapter 4, where we have used the Wigner representation, we now have chosen the photon number representation of $\hat{\rho}_{\mathrm{L}}$ with matrix elements $\rho_{n',n''}$.

We omit the details of the derivation of the radiation properties and instead refer to App. E.1. In the following we summarize the main steps of our procedure. First, we calculate the change of the diagonal elements $\rho_{n,n}(t)$ during the interaction of the laser field with a single electron bunch. However, to obtain steady-state in an oscillator configuration we require the subsequent interaction of many electron bunches. We incorporate multiple bunches with the

help of a *coarse-grained derivative* [22]

$$\dot{\rho}_{n,n}(t) \cong \frac{N}{\tau_{\mathrm{inj}}} \left[\rho_{n,n}(t+T) - \rho_{n,n}(t)\right] - \frac{\omega_{\mathrm{L}}}{Q} n \rho_{n,n}(t) + \frac{\omega_{\mathrm{L}}}{Q}(n+1)\rho_{n+1,n+1}(t)\,, \tag{6.4}$$

where the discrete change of $\rho_{n,n}$ due to interaction is approximated by the continuous limit. Here, we have defined the injection time τ_{inj} of the bunches in analogy to Eq. (4.21) in Chap. 4. Moreover, we have introduced the damping of the field due to a cavity with quality Q [22], according to Eq. (E.9), and have multiplied the change of $\rho_{n,n}$ caused by a single electron with the number N of electrons in a bunch. This procedure is justified when we consider the low-gain regime, where collective effects are neglected [21].
The gain of a laser describes the amplification of the field. That is why we calculate the expectation value

$$\langle \hat{n}(t) \rangle \equiv \sum n \rho_{n,n}(t) \tag{6.5}$$

of the photon number that corresponds to the intensity of the field. For the Quantum FEL we obtain from Eqs. (E.10) and (6.5) the relation

$$\frac{\mathrm{d}}{\mathrm{d}t} \langle \hat{n}(t) \rangle = 2 \frac{1}{\tau_{\mathrm{inj}}} \left\langle G_{\hat{n}(t)}(\hat{n}(t)+1) \right\rangle - \frac{\omega_{\mathrm{L}}}{Q} \langle \hat{n}(t) \rangle \ , \tag{6.6}$$

where we have defined the gain, Eq. (E.8),

$$G_n \equiv \frac{1}{2}(gT)^2 N \int \mathrm{d}p \, \mathrm{sinc}^2 \Omega_n T \, |\phi(p)|^2 \tag{6.7}$$

and have recalled the Rabi frequency Ω_n from Eq. (5.27). The factor of two in Eq. (6.6) appears, since we want to connect Eq. (6.7) to our usual definition of the gain, Eq. (2.18), which describes the change of the *amplitude* of the field rather than of its *intensity*.
When the photon statistics is strongly peaked around its mean value [40], that is $\rho_{n,n}(t) \cong \delta(n - \langle \hat{n} \rangle)$, we find

$$\frac{\mathrm{d}}{\mathrm{d}t} \langle \hat{n}(t) \rangle \cong 2 G_{\langle \hat{n} \rangle} \langle \hat{n}(t) \rangle - \frac{\omega_{\mathrm{L}}}{Q} \langle \hat{n}(t) \rangle \ , \tag{6.8}$$

which for suitable $G_{\langle \hat{n} \rangle}$ leads to an increasing photon number, and therefore to amplification. We note that a semiclassical theory, where the laser field is treated classically but the two-level behavior of the electron is taken into account, would lead to the same result for the gain. However, to calculate the photon statistics and the intrinsic linewidth of a Quantum FEL oscillator we require a quantized laser field.

6.1.2 Small-signal and strong-signal gain

To analyze the physical meaning for our result of the gain we investigate in the following the limits of a small and a strong signal, respectively.

Small signal

Similar to ordinary laser theory [22] we define the small-signal regime of the Quantum FEL as the limit where the change of intensity scales at most quadratically with the initial intensity.

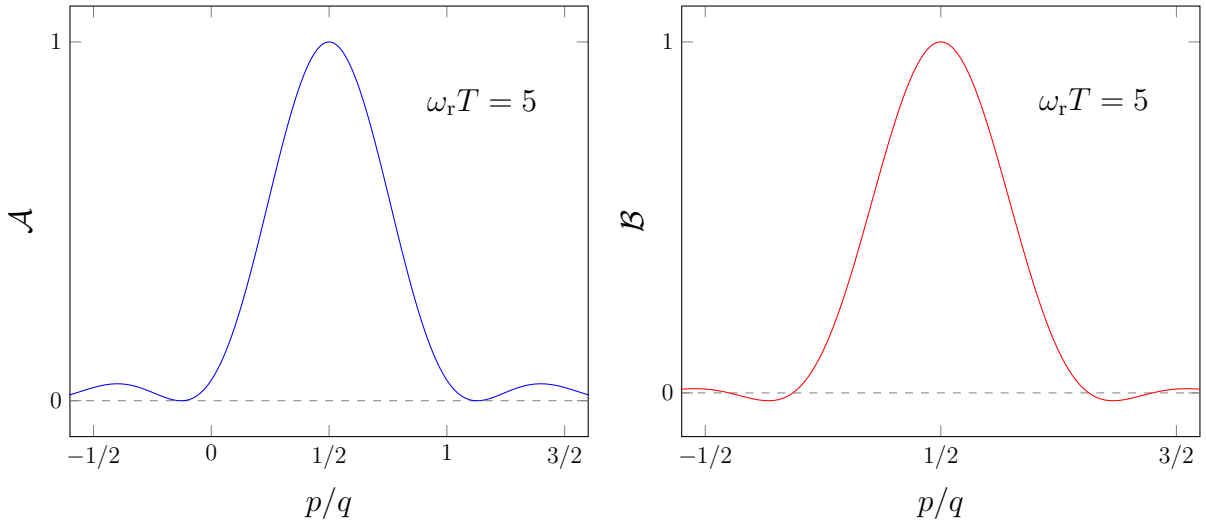

Figure 6.1: Characteristic functions $\mathcal{A}$ (left) for linear gain and $\mathcal{B}$(right) for self saturation, Eq. (6.11), in the small-signal regime, $gt\sqrt{n} \ll 1$, as functions of the momentum p of the electron for $\omega_r T = 5$. Both functions are maximized at $p = q/2$, that is exact resonance.

Hence, we perform the expansion

$$\begin{aligned} G_n(n+1) &\cong \left(G_n(n+1)\right)|_{\xi=0} + \frac{\partial}{\partial \xi}\left(G_n(n+1)\right)|_{\xi=0}\,\xi + \ldots \\ &\cong g_1 n - g_2 n^2 \end{aligned} \tag{6.9}$$

in powers of $\xi \equiv gT\sqrt{n+1}$, where we have used Eq. (6.7). The truncation of this series converges for $\xi \ll 1$.

In the second line of Eq. (6.9) we have defined

$$\begin{cases} g_1 & \equiv \frac{1}{2}(gT)^2 N \int \mathrm{d}p\, |\phi(p)|^2\, \mathcal{A}(p) \\ g_2 & \equiv \frac{1}{6}(gT)^4 N \int \mathrm{d}p\, |\phi(p)|^2\, \mathcal{B}(p)\,, \end{cases} \tag{6.10}$$

with the characteristic functions

$$\begin{cases} \mathcal{A}(p) & \equiv \mathrm{sinc}^2\left[\Delta(\omega_r T)/2\right] \\ \mathcal{B}(p) & \equiv \frac{3}{2}\frac{1-\cos\left[\Delta(\omega_r T)\right]-\Delta(\omega_r T)\sin\left[\Delta(\omega_r T)\right]/2}{\left[\Delta(\omega_r T)/2\right]^4}\,. \end{cases} \tag{6.11}$$

For a positive value of g_1 the laser field is amplified and thus g_1 corresponds to the *linear gain*. On the other hand the negative sign in Eq. (6.9) leads to a sustained field for a positive g_2, which we therefore identify as the *self-saturation* coefficient [22]. We note that ordinary perturbation theory, used in Refs. [4, 26] would lead to analogous results as presented here, since perturbation theory implies the short-time limit $gT\sqrt{n} \ll 1$ from the beginning.

In contrast to the classical case, where the maxima of the characteristic functions for gain and self saturation differ, $\mathcal{A}$ and $\mathcal{B}$ for the Quantum FEL are both maximized at resonance

$p = q/2$ according to Fig. 6.1. For $|\phi(p)|^2 = \delta(p - q/2)$, that is a momentum eigenstate with eigenvalue $p = q/2$, we obtain the maximum gain

$$g_1 \cong \frac{1}{2}(gT)^2 N \equiv G_{\max} \tag{6.12}$$

while

$$g_2 \cong \frac{(gT)^4 N}{6} \tag{6.13}$$

gives the self saturation for this particular initial condition.
We have to ensure that the Quantum FEL (i) is in the low-gain regime and (ii) operates above threshold. For a low gain we require that the change of photon number, which is maximized by $2G_{\max}$, is much smaller than unity, that is

$$(gT)^2 N \ll 1\,, \tag{6.14}$$

which describes the limit of a short wiggler similar to the constraint in Eq. (2.79) for the classical FEL.
We are above threshold if

$$\frac{\omega \tau_{\text{inj}}}{Q} < (gT)^2 N \tag{6.15}$$

is satisfied. This inequality gives us a lower limit for the quality Q of the cavity.

Strong signal

By studying Fig. 5.2 we recognize that the probability for photon emission oscillates between zero and one, at least in the resonant case, $\Delta = 0$. For $\Omega_n T = \pi/2$ this probability reaches its maximum. Hence, we define the strong-signal regime of the Quantum FEL with the help of the condition $gT\sqrt{n+1} \equiv \pi/2$.
From Eq. (6.7) we derive the strong-signal gain

$$G_{\text{str}} \cong \frac{N}{2n} \int \mathrm{d}p\, |\phi(p)|^2\, \mathcal{S}^2_{\pi/2} \tag{6.16}$$

with

$$\mathcal{S}^2_{\pi/2} \equiv \frac{\pi^2}{4} \mathrm{sinc}^2 \left[\frac{\pi}{2} \sqrt{1 + \left[\frac{\Delta(\omega_{\text{r}} T)}{\pi} \right]^2} \right] \tag{6.17}$$

as the characteristic function in this limit.
Similar to the small-signal regime the gain is maximized at resonance, $p = q/2$, yielding

$$G_{\max} = \frac{N}{2n} \tag{6.18}$$

which we could have already deduced from the fact that the probability for photon emission is unity and hence each electron indeed has emitted one photon. We recognize from Eq. (6.18) that the gain is suppressed for high photon numbers. However, the *absolute* intensity change is maximized which justifies the term 'strong-signal' regime.

When we demand for a low gain we require $N << n$, that is the photon number is higher than the number of electrons, which certainly cannot be obtained in the first passages of electron bunches if the field starts from vacuum. Hence, to achieve the strong-signal limit, $gT\sqrt{n} = \pi/2$, we need many passages of electrons before saturation occurs. Alternatively, we can also achieve saturation by a single passage of electrons when we consider the high-gain regime as we later show in Chap. 7.

6.1.3 Comparison to classical gain

We are now in the position to compare the gain of the Quantum FEL to the one of the classical FEL. Therefore, we first consider the small-signal limit before we turn to the strong-signal case. In this context we discuss differences with respect to structure as well as to magnitude.

Small signal

The gain in the quantum regime is characterized by a sharp resonance which occurs at $p = q/2$ and describes photon emission and thus positive gain. In Refs. [26, 4] also absorption and negative gain was discussed which gave rise to the second resonance $p = -q/2$. By subtracting absorption from emission we find the characteristic function

$$\mathcal{A}_{\mathrm{q}}(p) \equiv \mathcal{A}(p) - \mathcal{A}(-p)\,, \tag{6.19}$$

where we have used, that according to Refs. [4, 26] absorption is characterized by $\mathcal{A}(-p)$ with $\mathcal{A}$ defined in Eq. (6.11). We have discussed this difference of two sinc^2-functions in Eq. (6.19) already in Chap. 3, Eq. (3.31), for the transition from classical to quantum physics. However, in contrast to Chap. 3 it is now admissible to use results of first-order perturbation theory since in the quantum regime single-photon processes prevail.
The gain of the classical FEL, however, is described by the smooth function $\mathcal{A}_{\mathrm{cl}}$, Eq. (4.29), of the Doppler parameter $\wp \equiv 2kpT/m$. In Fig. 6.2 we display both functions, $\mathcal{A}_{\mathrm{q}}$ and $\mathcal{A}_{\mathrm{cl}}$, and obtain, as expected, separated peaks in the quantum regime and a continuous curve for the classical regime.
Moreover, the maximum of $\mathcal{A}_{\mathrm{cl}}$ occurs at $\wp \cong \pi$, which is independent of $\hbar$, while the maximum in the quantum regime is located at $p = \hbar k$. These 'resonances' correspond to two different processes: in the classical case we observe the emission of many photons washing out the discreteness of the electron dynamics as discussed in Chap. 3. In contrast, the Quantum FEL is characterized by single-photon processes and the electron occupies only two levels of the momentum ladder.
A naive comparison of the magnitude of g_1, Eq. (6.12), in the quantum regime and

$$g_1^{\mathrm{cl}} \equiv G_{\mathrm{cl}}^{(1)} = \frac{8}{\pi^3}\omega_{\mathrm{r}} T (gT)^2 N \tag{6.20}$$

in the classical regime, obtained from Eq. (4.24), yields

$$\frac{g_1}{g_1^{\mathrm{cl}}} \cong \frac{\pi^3}{16}\frac{1}{\omega_{\mathrm{r}} T} \ll 1\,. \tag{6.21}$$

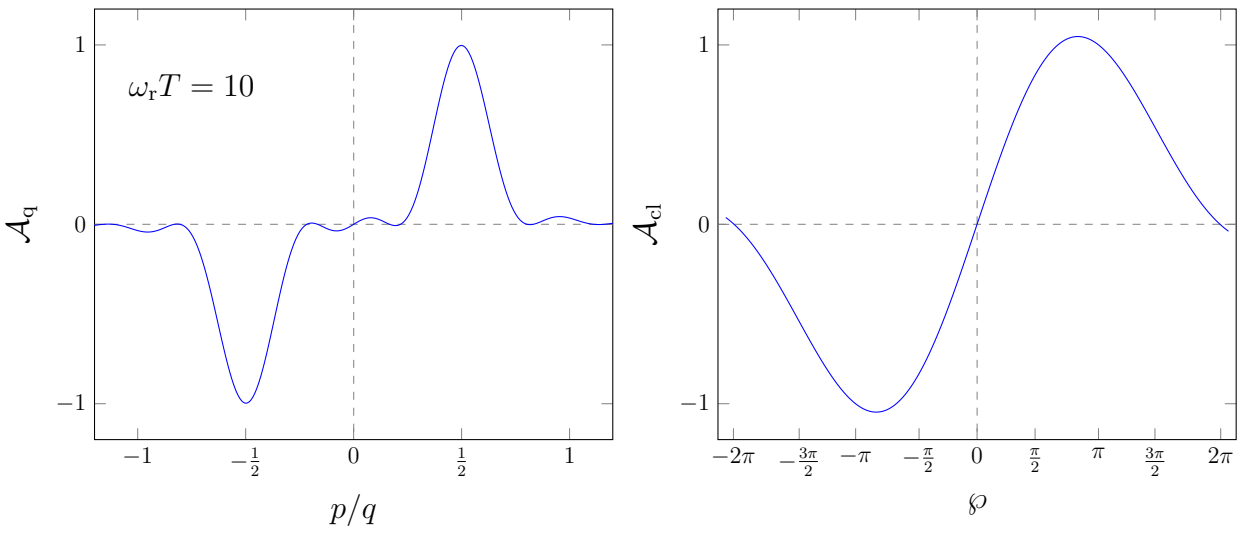

Figure 6.2: Comparison of the characteristic functions for the small-signal gain in the quantum and in the classical regime of the FEL. On the left-hand side $\mathcal{A}_q$, Eq. (6.11) with Eq. (6.19), for the Quantum FEL with $\omega_r T = 10$, is plotted as a function of p/q and displays two sharp peaks at $p = \pm q/2$. On the right-hand side we have drawn the smooth function $\mathcal{A}_{cl}$, Eq. (4.29), for the classical FEL depending on the Doppler parameter $\wp \equiv 2kpT/m$.

Since $\omega_r T \gg 1$ in the quantum regime, the gain of a Quantum FEL is much smaller than *predicted* by the classical theory. Although we identify this difference as a quantum effect, we cannot deduce from Eq. (6.21) that the gain of the Quantum FEL is always smaller than the one of the classical FEL. Each quantity g_1 and g_1^{cl} is only valid in the respective regime of consideration and g_1 as well as g_1^{cl} can in principle take on *any value*, at least within the limits of the low-gain approximation.
However, for amplification the gain in the classical as well as in the quantum regime should satisfy the respective threshold condition.Thus, the gain should be still smaller but of the order of unity, which we denote as $2G_{max} \lesssim 1$, in order to avoid unrealistic high values of the quality Q of the cavity.
To show the experimental limitiations implied by a moderately low gain, we cast the condition $2G_{max} \lesssim 1$ in terms of the laboratory frame, App. A, and arrive at the constraint [122]

$$L \lesssim \frac{2\gamma_0^2}{\sqrt{\pi}} \frac{\sqrt{\lambda_C / r_e}}{a_0 \sqrt{1 + a_0^2}} \frac{1}{\sqrt{\lambda_W n_e}} \tag{6.22}$$

for the length L of the wiggler, where we have introduced the relativistic factor γ_0, Eq. (A.47), of the electron, the wiggler wavelength λ_W, the wiggler parameter a_0, Eq. (A.30), and the electron density $n_e \equiv N/V$ as well as the Compton wavelength λ_C, Eq. (A.50), of the electron and the classical electron radius r_e, Eq. (A.51). On the other hand, we find for the classical regime the condition

$$L \lesssim \frac{(2\pi)^{1/3}}{4} \frac{\gamma_0 \lambda_W^{1/3}}{(r_e a_0^2 n_e)^{1/3}} \tag{6.23}$$

which is derived from $2g_1^{\mathrm{cl}} \lesssim 1$ in analogy to Eq. (6.22).
By comparing Eq. (6.22) with Eq. (6.23) we identify the difficulties that arise in the quantum regime: the required wiggler length scales *quadratically* with the energy γ_0 of the electrons and thus increases with increasing energy and also *increases* with a decreasing wiggler wavelength λ_{W}. In contrast, L is only *linear* in γ_0 and *decreases* for a smaller λ_{W}. Moreover, the condition $\omega_{\mathrm{r}} T \gg 1$ of a large recoil can be rewritten to [122]

$$16\pi\gamma_0 \frac{L}{1+a_0^2} \frac{\lambda_{\mathrm{C}}}{\lambda_{\mathrm{W}}^2} \gg 1\,, \tag{6.24}$$

according to Tab. A.2, which means that we need a high γ_0 and a small λ_{W} to be in the quantum regime leading, however, to a large L according to Eq. (6.22). In contrast for small γ_0 and large λ_{W} we are in the classical regime and do not have to concern about this issue due to Eq. (6.23).
In principle, both, quantum and classical gain can be high enough to satisfy the respective threshold condition. However, the experimental realization of a Quantum FEL above threshold is more challenging as in the classical case. We emphasize that this discussion concerns only the low-gain limit. Nevertheless, we find a similar behavior in Chap. 7 for the high-gain Quantum FEL.
Before we proceed, we note the peculiarity that the gain g_1^{cl}, Eq. (6.20), in the classical regime scales with T^3 [51], while the corresponding quantity g_1, Eq. (6.12), in the quantum regime just depends on T^2.

Strong signal

In the following we compare the strong-signal gain of a Quantum FEL with the saturated gain in the classical regime [51]. According to Eq. (2.68) we estimate the magnitude of the latter quantity by

$$G_{\mathrm{cl}} \cong \alpha_n \frac{N}{2n}\,, \tag{6.25}$$

where we have used the relation $\kappa = 4\omega_{\mathrm{r}} T g T$, have identified the dimensionless intensity $n \equiv |a_{\mathrm{L}}|^2$ as the mean number of photons in the laser field and have recalled the definition, Eq. (5.18), of the quantum parameter α_n.
Since $\alpha_n \gg 1$ in the classical regime the gain of a classical FEL is higher than in the quantum regime with $G \sim N/n$, Eq. (6.18). We identify multiphoton processes in the classical case opposing single-photon transitions in the quantum regime as origin for this difference. However, by setting $\alpha_n \ll 1$ in Eq. (6.25) we obtain that the classical formula would underestimates the gain of the Quantum FEL in contrast to the small-signal case, where the classical result overestimates the one in the quantum regime. Moreover, we note that G_{cl} scales with $n^{-3/4}$ while the gain in the quantum regime is proportional to n^{-1}.

6.1.4 Higher-order corrections

To conclude our discussion regarding the gain of a Quantum FEL we consider higher-order corrections to the deep quantum regime in the framework of the method of averaging. In the following we restrict ourselves to the resonant case $p = q/2$.

Additional to the excited and ground state, $|p\rangle$ and $|p-q/2\rangle$, respectively, of the fundamental two-level system in the deep quantum regime we have to consider, according to Eqs. (D.67) and (D.66), the momentum levels $|p+q/2\rangle$ and $|p-3q/2\rangle$. Hence, the evolved state reads

$$|\Psi(t+T)\rangle = \sum_{\mu=-1}^{2} c_\mu(t+T)\,|n+\mu, p-\mu q\rangle\ , \tag{6.26}$$

where we have recalled the notation $c_\mu \equiv c_{n+\mu}(p-\mu q)$ from Chap. 5.

Calculating the diagonal elements $\rho_{n,n}$ of the reduced density matrix of the laser field and using Eq. (6.26), we find for the change in the mean photon number $\langle\hat{n}\rangle$ the expression

$$\langle\hat{n}(t+T)\rangle - \langle\hat{n}(t)\rangle \cong N \sum_{\mu=-1}^{2} \mu|c_\mu(t+T)|^2\,. \tag{6.27}$$

which emerges due to the interaction with a single electron bunch.

In the limit of a sharply peaked photon statistics, with mean value $n \gg 1$, we obtain

$$\langle\hat{n}(t+T)\rangle - \langle\hat{n}(t)\rangle \cong \delta n^{(0)}(T) + \alpha^2 \delta n^{(2)}(T)\,, \tag{6.28}$$

with a contribution in zeroth order given by

$$\delta n^{(0)}(T) \equiv N \sin^2\left[(\Omega_n - \chi)T\right] \tag{6.29}$$

and one in second order which reads

$$\begin{aligned}\delta n^{(2)}(T) \equiv -\frac{N}{4}\Big(&\cos^2\left[(\Omega_n-\chi)T\right] + \cos^2(\chi T) - 2\sin^2(\chi T) \\ &-2\cos\Omega_n T\cos\left[2\omega_{\mathrm{r}}T\left(1+\frac{3}{8}\alpha^2\right)\right]\Big)\ .\end{aligned} \tag{6.30}$$

We have derived this result with the help of Eqs. (D.65), (D.67) and (D.66) and have recalled the definitions $\Omega_n \equiv gT\sqrt{n+1}$ for $\Delta = 0$ and $\chi \equiv (\alpha^2/4)\Omega_n$, Eqs. (5.27) and (5.47), respectively. We note that for $\alpha \to 0$ the result for the change in photon number, Eq. (6.28), reduces to the corresponding expression, Eq. (6.8), of the deep quantum regime without cavity damping.

In Fig. 6.3 we have drawn the change of mean photon number in the Quantum FEL as a function of time, according to Eq. (6.28) for $\alpha = 0.2$ and $\alpha = 0.4$, respectively, and have compared the resulting curve with the zeroth-order solution, Eq. (6.8). For increasing α the higher-order solution is more accurate than the lowest-order one since it incorporates a frequency shift as well as a modulation in amplitude up to the order of α^2. We, further, obtain that in contrast to the deep quantum regime a negative change of intensity becomes possible due to the absorption transition from $q/2$ to $3q/2$ which becomes more prominent for increasing α. Moreover, for increasing α each electron emits on average at most slightly less than one photon. A possible explanation for this effect is that the resonance shifts away from $p = q/2$ when we leave the deep quantum regime. Hence, we expect a maximized gain for a slightly different value of the momentum p than $q/2$.

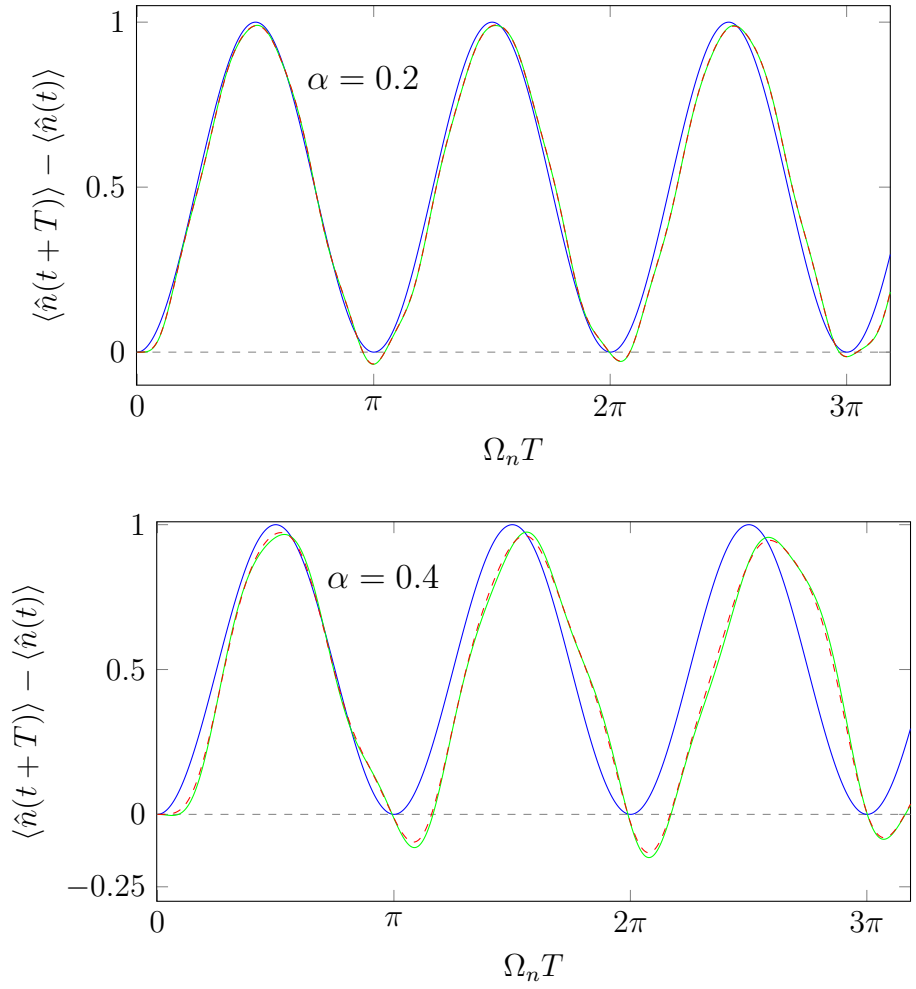

Figure 6.3: Change of mean photon number $\langle \hat{n}(t+T)\rangle - \langle \hat{n}(t)\rangle$ in a Quantum FEL at resonance, $p = q/2$, due to a single electron, $N = 1$, as a function of the dimensionless time $\Omega_n T$ with Ω_n, Eq. (5.27), denoting the Rabi frequency and T being the interaction time. We have compared the zeroth-order solution, Eq. (6.8), (blue line) as well as the higher-order solution, Eq. (6.28), (green line) of the method of averaging with the numerical simulation of Eq. (5.49) (red, dashed line) for two different values of α, that is $\alpha = 0.2$ (above) and $\alpha = 0.4$ (below). While for growing α the zeroth-order solution deviates from the exact one in frequency and in amplitude the higher-order result fits very well with numerics. We note that the change of the mean photon number can become negative since for increasing values of α absorption processes become more important. Moreover, the maximum gain is decreased and we interpret this effect as originating from a shift of resonance away from $p = q/2$.

6.2 Steady-state photon statistics

After investigating amplification in the quantum regime of the FEL we now turn to the statistical properties of a Quantum FEL oscillator. With the help of detailed balance [22] and a Gaussian approximation [39] we derive an explicit expression for the steady-state photon statistics. After that we compare mean value and variance of this distribution with the corresponding quantities derived in Chap. 4 for the classical FEL. At the end of this section we briefly discuss the influence of higher orders from the method of averaging on the photon statistics.

6.2.1 Detailed balance and Gaussian approximation

For steady state we require for the diagonal elements

$$\dot{\rho}_{n,n} = 0\,, \tag{6.31}$$

which means that we have to set the right-hand side of Eq. (6.4) to zero. Moreover, by employing the principle of *detailed balance* [22] we obtain

$$(gT)^2 Nn \left(\int \mathrm{d}p\, \mathrm{sinc}^2 \Omega_{n-1} T \left|\phi(p)\right|^2 \right) \rho_{n-1,n-1} - \frac{\omega_\mathrm{L}}{Q} n \rho_{n,n} = 0\,. \tag{6.32}$$

In this context, detailed balance means that *each line* of the three-term relation for $\rho_{n,n}$, explicitly given in Eq. (E.10), equals to zero, corresponding to a vanishing probability flow between two adjacent levels [22].

The expression in Eq. (6.32) is equivalent to the recurrence relation

$$\rho_{n,n} = \Lambda_n \rho_{n-1,n-1} \tag{6.33}$$

with

$$\Lambda_n \equiv \frac{2G_{n-1}}{\omega_\mathrm{L}\tau_\mathrm{inj}/Q} \tag{6.34}$$

which represents the ratio of gain G_{n-1}, Eq. (6.7), and losses. Since the dependency of Λ_n on the photon number n is rather complicated, as apparent from Eq. (6.7), the iteration of Eq. (6.33) does not yield a closed, analytic expression.

However, when the photon statistics is characterized by a single dominating peak a *Gaussian approximation* provides us with a simple expression for $\rho_{n,n}$. This approximation is discussed in detail in App. E.2 and results in the expression, Eq. (E.19),

$$\rho^\mathrm{ss}_{n,n} = \mathcal{N} \exp\left[-\frac{(n - n^\mathrm{ss})^2}{2\Delta n^2} \right] \tag{6.35}$$

for the steady-state photon statistics. This function is normalized such that the integral with respect to n from zero to infinity is equal to unity, determining the normalization constant $\mathcal{N}$.

In short, the derivation yielding Eq. (6.35) is based on a Taylor expansion in second order around the maximum n^{ss}. This maximum can be found from the relation

$$\Lambda_{n^{\mathrm{ss}}} \equiv \frac{2G_{n-1}n/\tau_{\mathrm{inj}}}{n\omega_{\mathrm{L}}/Q} = 1\,. \tag{6.36}$$

An expression analogous to Eq. (6.36) for the steady-state intensity also emerges when we set $\mathrm{d}\langle\hat{n}\rangle/\mathrm{d}t = 0$ in Eq. (6.8). Thus, our result, Eq. (6.36), is consistent with the one of a semiclassical laser theory [22, 56].

A quantity which cannot be described by a semiclassical theory is the variance Δn^2 of the photon statistics which in the Gaussian approximation is given by

$$\Delta n^2 \equiv -\left(\left.\frac{\mathrm{d}\Lambda_n}{\mathrm{d}n}\right|_{n=n^{\mathrm{ss}}}\right)^{-1} \tag{6.37}$$

according to Eq. (E.20).

With the help of Eq. (6.34) we obtain the explicit expression

$$\Delta n^2 = \left[\frac{(gT)^2N}{\omega_{\mathrm{L}}\tau_{\mathrm{inj}}/Q}\left(\int\mathrm{d}p\,\mathrm{sinc}^2\Omega_{n^{\mathrm{ss}}-1}T\,\left(1-\frac{\cos\Omega_{n^{\mathrm{ss}}-1}T}{\mathrm{sinc}\Omega_{n^{\mathrm{ss}}-1}T}\right)\frac{g^2}{\Omega^2_{n^{\mathrm{ss}}-1}}|\phi(p)|^2\right)\right]^{-1} \tag{6.38}$$

which simplifies considerably to

$$\Delta n^2 = \left[\left(1-\frac{\cos\left(gT\sqrt{n^{\mathrm{ss}}}\right)}{\mathrm{sinc}\left(gT\sqrt{n^{\mathrm{ss}}}\right)}\right)\frac{1}{n^{\mathrm{ss}}}\right]^{-1} \tag{6.39}$$

by assuming exact resonance, that is $|\phi(p)|^2 = \delta(p-q/2)$. Moreover, we have used the identity $\Lambda_{n^{\mathrm{ss}}} = 1$ valid for steady state according to Eq. (6.36).

In Fig. 6.4 we have drawn the photon statistics $\rho_{n,n}$ as a function of n exemplified by the strong-signal case $gT\sqrt{n^{\mathrm{ss}}} = \pi/2$ at exact resonance $p = q/2$. We obtain that our approximation, Eq. (6.35), agrees very well with the numeric result which is derived by an iteration of Eq. (6.33).

To bring our results for the Quantum FEL into a broader context we first recall that the photon statistics of a coherent state [40] corresponds to a Poisson distribution, which means that its mean value is equal to its variance. When the variance exceeds the mean value we speak of a super-Poissonian statistics, which is for example given in the case of an ordinary laser [22, 105], while the opposite case is called sub-Poissonian, which for example can be observed in a one-atom maser [38, 39].

That is why we we define the normalized variance [40]

$$\sigma^2 \equiv \frac{\Delta n^2}{n^{\mathrm{ss}}} \tag{6.40}$$

as the ratio of variance Δn^2 and mean photon number n^{ss} in analogy to the definition, Eq. (4.60), in Chap. 4. In the case of a Poisson statistics we have $\sigma^2 = 1$ while we obtain $\sigma^2 > 1$ and $\sigma^2 < 1$ for a super- and a sub-Poissonian statistics, respectively.

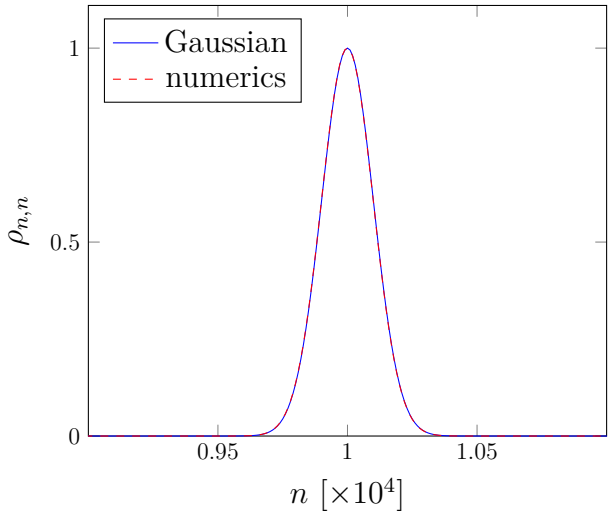

Figure 6.4: Comparison of the Gaussian approximation for $\rho_{n,n}$, Eq. (6.35), with the numerical solution of Eq. (6.33), both as functions of n and both in the strong-signal regime $gT = \sqrt{n^{\mathrm{ss}}} = \pi/2$ for resonance $p = q/2$. For the parameters $gT = \frac{\pi}{2} \cdot 10^{-2}$, $N = 1000$ and $\omega_{\mathrm{L}}\tau_{\mathrm{inj}}/Q = 0.1$ we find that both curves agree.

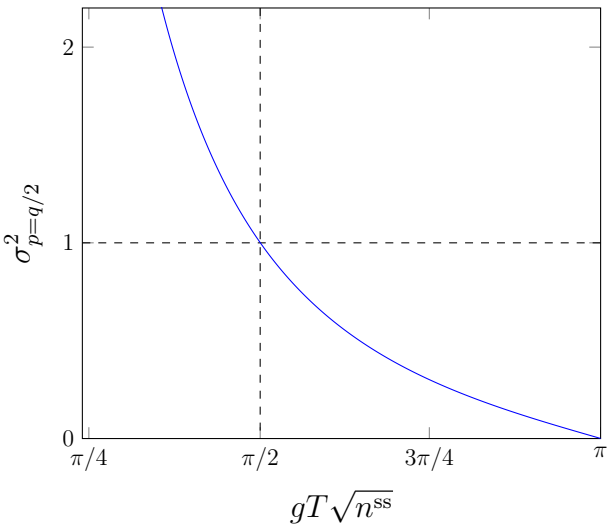

Figure 6.5: The normalized variance $\sigma^2_{p=q/2}$, Eq. (6.41), as a function of $gT\sqrt{n^{\mathrm{ss}}}$ for a momentum eigenstate of the electron at resonance $p = q/2$. For $gT\sqrt{n^{\mathrm{ss}}} < \pi/2$ we obtain a super-Poissonian behavior, $\sigma^2 > 1$, while for $gT\sqrt{n^{\mathrm{ss}}} > \pi/2$ the statistics is sub-Poissonian, $\sigma^2 < 1$.

For the Quantum FEL we derive with the help of Eq. (6.39) the expression

$$\sigma^2_{p=q/2} = \frac{1}{1 - \left(gT\sqrt{n^{\rm ss}}\right)\cot\left(gT\sqrt{n^{\rm ss}}\right)} \tag{6.41}$$

which is only a function of $gT\sqrt{n^{\rm ss}}$ since we have assumed exact resonance, $p = q/2$. We postpone the discussion of the influence from a nonzero momentum spread on σ^2 to the end of this chapter.
In Fig. 6.5 the normalized variance $\sigma^2_{p=q/2}$ is drawn versus $gT\sqrt{n^{\rm ss}}$. For $gT\sqrt{n^{\rm ss}} < \pi/2$, and in particular in the small signal limit, $gT\sqrt{n^{\rm ss}} << 1$, the statistics is super-Poissonian, with $\sigma^2_{p=q/2} > 1$, in analogy to a conventional laser. However, for $gT\sqrt{n^{\rm ss}} = \pi/2$, which we have defined as the strong-signal limit, the situation changes and we obtain $\sigma^2_{p=q/2} = 1$, that is a Poisson distribution. For increasing values of $gT\sqrt{n^{\rm ss}}$ we even find a sub-Poissonian behavior with $\sigma^2_{p=q/2} < 1$.
Since the Quantum FEL is analogous to the one-atom maser these results are not surprising [40]. We emphasize that, according to Ref. [39], we have to restrict ourselves to situations where the condition

$$\frac{gT\sqrt{N}}{\sqrt{\omega_{\rm L}\tau_{\rm inj}/Q}} < \frac{3}{2}\pi\,, \tag{6.42}$$

is satisfied since otherwise the Gaussian approximation, Eq. (6.35), could break down.

6.2.2 Comparison to classical FEL

For the classical regime there exists no an analytic expression for the photon statistics beyond the small-signal limit. Hence, we also restrict ourselves to this limit for the Quantum FEL when we compare quantum with classical regime. In Fig. 6.6 we have displayed the photon statistics of the Quantum FEL in the small-signal limit and observe that employing the Gaussian approximation and the small-signal approximation yields correct results when we take the numerical solution of Eq. (6.33) as a reference.

Mean photon number

From Eq. (6.9), valid for a small signal, that is $gT\sqrt{n^{\rm ss}} \ll 1$, we obtain

$$\Lambda_{n^{\rm ss}} \cong \frac{2g_1 - 2g_2 n^{\rm ss}}{\omega_{\rm L}\tau_{\rm inj}/Q} = 1 \tag{6.43}$$

for the steady-state condition, Eq. (6.36). Solving Eq. (6.43) for $n^{\rm ss}$ yields

$$n^{\rm ss} = \epsilon\frac{g_1}{g_2}\,, \tag{6.44}$$

where we have defined

$$\epsilon \equiv \frac{g_1 - \frac{1}{2}\frac{\omega_{\rm L}\tau_{\rm inj}}{Q}}{g_1} \tag{6.45}$$

as the relative deviation from threshold in analogy to Eq. (4.48).

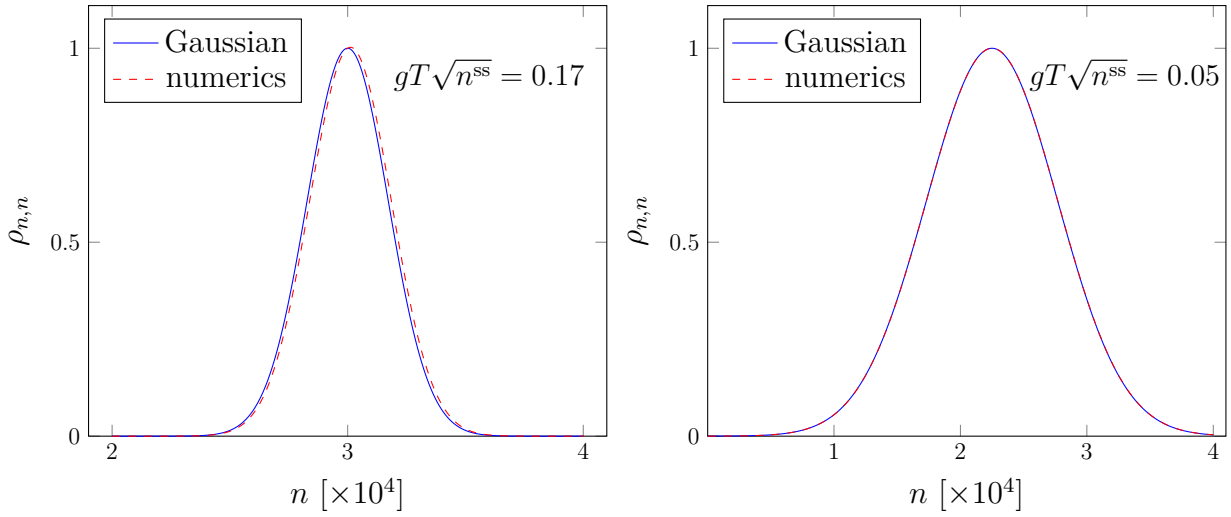

Figure 6.6: The steady-state photon statistics $\rho_{n,n}$ of the Quantum FEL in the small-signal limit as a function of the photon number n. On the left-hand side we have chosen the parameters $gT = 10^{-3}$, $N = 10^5$ and $\epsilon = 0.01$ leading to the steady-state photon number $n^{\mathrm{ss}} = 3 \cdot 10^4$ according to Eq. (6.46) and hence to $gT\sqrt{n^{\mathrm{ss}}} = 0.17$. The corresponding quantities on the right-hand side are given by $gT = \frac{1}{3} \cdot 10^{-3}$, $N = 9 \cdot 10^5$ and $\epsilon = \frac{25}{3} \cdot 10^{-5}$ yielding $n^{\mathrm{ss}} = 2.25 \cdot 10^4$ and $gT\sqrt{n^{\mathrm{ss}}} = 0.05$. For the case $gT\sqrt{n^{\mathrm{ss}}} = 0.05$ on the right-hand side the analytic solution, Eq. (6.35), together with Eqs. (6.46) and (6.54) which represent the small-signal approximation, is closer to the numerical simulation of the recurrence relation Eq. (6.33) as for the case $gT\sqrt{n^{\mathrm{ss}}} = 0.17$ on the left, which we identify as a higher-order effect form the expansion in powers of $\xi \equiv gT\sqrt{n^{\mathrm{ss}}} \ll 1$.

The structure of Eq. (6.36) is the same as of its classical counterpart Eq. (4.44). However, the explicit expression for gain g_1 and self saturation g_2 differ for the quantum and the classical regime. For the former one we find from Eqs. (6.12) and (6.13)

$$n^{\mathrm{ss}} = \frac{3\epsilon}{(gT)^2}\,, \tag{6.46}$$

where we have estimated the magnitude of g_1 and g_2 by their value at resonance $p = q/2$, Eqs. (6.12) and (6.13). To be above threshold we require $0 < \epsilon < 1$. The small-signal condition, $gT\sqrt{n^{\mathrm{ss}}} \ll 1$, translates with the help of Eq. (6.46) to $\epsilon \ll 1$.
After recalling Eq. (4.52)

$$n_{\mathrm{cl}}^{\mathrm{ss}} = \epsilon\frac{\pi^3}{2}\frac{1}{(\omega_{\mathrm{r}}T)^2}\frac{1}{(gT)^2} \tag{6.47}$$

for the classical FEL, as well as the identity $\kappa = 4(\omega_{\mathrm{r}}T)gT$, we make the comparison

$$\frac{n^{\mathrm{ss}}}{n_{\mathrm{cl}}^{\mathrm{ss}}} = \frac{6}{\pi^3}\omega_{\mathrm{r}}T \gg 1 \tag{6.48}$$

for the steady-state intensity in the quantum and in the classical regime. Since $\omega_{\mathrm{r}}T \gg 1$ for the Quantum FEL the photon number n^{ss} in the quantum regime exceeds the one predicted by the classical theory.
Following the arguments of Sec. 6.1 we consider another way of comparing classical and quantum regime. For this purpose, we rewrite the expressions for the steady-state photon number in terms of the respective maximum gain G_{max}, Eq. (6.12), and $G_{\mathrm{max}}^{\mathrm{cl}}$, Eq. (6.20). By this procedure we obtain

$$n^{\mathrm{ss}} = \frac{6\epsilon N}{G_{\mathrm{max}}} \tag{6.49}$$

and

$$n_{\mathrm{cl}}^{\mathrm{ss}} = \frac{1}{\omega_{\mathrm{r}}T}\frac{16\epsilon N}{G_{\mathrm{max}}^{\mathrm{cl}}}\,, \tag{6.50}$$

respectively.
Comparing the expressions Eqs. (6.50) and (6.49) makes of course only sense, if G_{max} and $G_{\mathrm{max}}^{\mathrm{cl}}$ are of the same order of magnitude, despite of the experimental difficulties which we have identified in Sec. 6.1. Moreover, we assume the same number N of electrons for both regimes. Due to $\omega_{\mathrm{r}}T \ll 1$ we obtain that the steady-state photon number of a classical FEL, Eq. (6.50) is larger than the corresponding quantity, Eq. (6.49), in the quantum regime.
Indeed, we cannot derive an analytic solution for the photon statistics of the classical FEL beyond the small-signal limit. However, in the following we at least determine the mean intensity of a classical FEL in a completely classical theory by equating cavity losses with the saturated FEL gain, Eq. (2.68), in analogy to Eq. (6.36). By this procedure we obtain the relation

$$n_{\mathrm{cl}}^{\mathrm{ss}} = \frac{(2gT)^{4/3}N^{4/3}}{\omega_{\mathrm{L}}\tau_{\mathrm{inj}}/Q} = \sqrt{\alpha_n}\frac{N}{\omega_{\mathrm{L}}\tau_{\mathrm{inj}}/Q} \tag{6.51}$$

for the dimensionless intensity $n \equiv |a_{\mathrm{L}}|^2$ at steady state, where we have used in the second step the identity $\kappa \equiv 4(\omega_{\mathrm{r}}T)gT$. We note that the proportionality of the intensity on $N^{4/3}$ is similar to the classical high-gain FEL, Eq. (2.81).

In contrast, since in the quantum regime each electron maximally emits one photon, Eq. (6.18), the mean photon number reads

$$n^{\mathrm{ss}} = \frac{N}{\omega_{\mathrm{L}}\tau_{\mathrm{inj}}/Q} \tag{6.52}$$

in the strong-signal regime of a Quantum FEL oscillator. Due to $\alpha_n \gg 1$ in the classical regime we expect from Eq. (6.51) a higher intensity in this limit when compared to the Quantum FEL. However, since for $\alpha_n \ll 1$ the relation in Eq. (6.52) is valid, and not the one in Eq. (6.51), we deduce that the steady-state intensity in the quantum regime is larger than predicted from a classical theory.

Variance

Having discussed the mean value of the photon statistics in the quantum and classical regime we finally turn to the variance of the corresponding statistics in the small-signal regime. For this purpose, we consider the normalized variance σ^2, Eq. (6.41), of the Quantum FEL in the limit $\xi \equiv gT\sqrt{n^{\mathrm{ss}}} \ll 1$. Expanding [121]

$$1 - \xi\cot\xi \cong \frac{1}{3}\xi^2\,, \tag{6.53}$$

the denominator in Eq. (6.41) in powers of ξ and using Eq. (6.46) yields the expression

$$\sigma^2 \cong \frac{1}{\epsilon} \tag{6.54}$$

for the normalized variance of the photon statistics of a Quantum FEL. As already predicted, this statistics shows a super-Poissonian behavior in the small-signal regime, due to $\epsilon \ll 1$.

According to Eq. (4.63) the normalized variance for a classical FEL is given by the expression

$$\sigma_{\mathrm{cl}}^2 \cong \frac{\pi}{4\omega_{\mathrm{r}}T}\frac{1}{\epsilon} \tag{6.55}$$

which also describes a super-Poissonian statistics. However, due to $\omega_{\mathrm{r}}T \ll 1$ in the classical limit, the statistics is always broader than the one of a Quantum FEL characterized by the expression in Eq. (6.54). In Fig. 6.7 we have contrasted a Poisson statistics with the photon statistics $\rho_{n,n}$, Eq. (6.35) together with Eqs. (6.44) and (6.54), in the quantum regime and the Wigner function W_{L}, Eq. (4.43) together with Eqs. (4.44) and (4.45), in the classical regime. Indeed, we obtain that $\rho_{n,n}$ is closer to a Poisson distribution than W_{L} and thus more similar to a coherent state.

When we assume that the broadening of the photon distribution in the classical FEL is also present beyond the small-signal limit, which is supported by the numerical analysis in Ref. [13], we identify the Poissonian or sub-Poissonian statistics, according to Fig. 6.5, as unique feature of the quantum regime. We emphasize that we have considered the situation at steady state. In Ref. [100] the squeezing of an initial Fock state of the laser field in a classical FEL was reported. However, this effect emerges for negative gain, where no steady state can be realized.

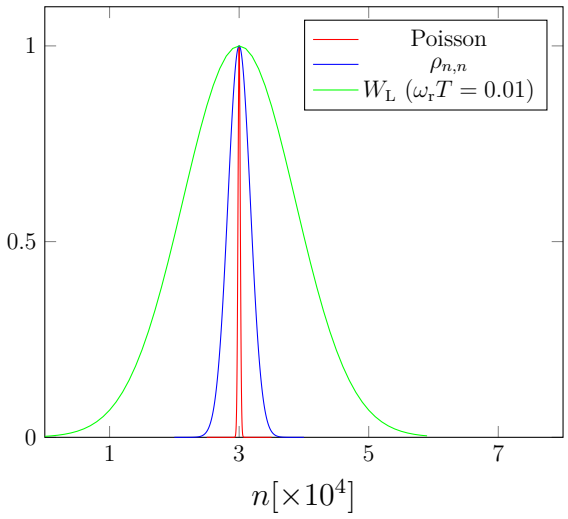

Figure 6.7: Photon statistics $\rho_{n,n}$ of the Quantum FEL, Eq. (6.35), as well as the Wigner function W_{L}, Eq. (4.43), for the laser field in the classical regime with $\omega_{\mathrm{r}}T = 0.01$, compared to a Poisson distribution, all as functions of n. To visualize the differences we have chosen the parameters such that all distribution have the same mean value at $n^{\mathrm{ss}} = 3 \cdot 10^4$ and we have normalized the functions to unity. Both, $\rho_{n,n}$ and W_{L}, deviate by $\epsilon = 0.01$ from threshold. As predicted by Eqs. (6.54) and (6.55) the width of the distribution in the quantum regime is much smaller than the one in the classical regime and hence closer to a Poisson distribution.

6.2.3 Higher-order corrections

To conclude our studies on the photon statistics of a Quantum FEL oscillator we provide a short discussion of higher-order effects in the framework of the method of averaging. For increasing α_n transitions outside the two-level system, consisting of $|q/2\rangle$ and $|-q/2\rangle$, become important. In second order of α_n we have to include single-photon absorption as well as two-photon emission, corresponding to the final electron momenta $p = 3q/2$ and $p = -3q/2$, respectively, according to Chap. 5. The detailed calculations for this problem can be found in App. E.3.

Hence, we have four levels which leads to a recursion relation, Eq. (E.29), for the photon statistics $\rho_{n,n}$ at steady state with four different terms instead of the three-term recurrence relation, Eq. (E.10), for the deep quantum regime. In this case we do not expect to solve this recurrence relation in a closed analytic way with the help of a detailed balance condition. However, in Ref. [123] an approximate approach was presented to obtain steady-state solutions without detailed balance.

The method in Ref. [123] is based on the assumption [124] that the ratio

$$R_n \equiv \frac{\rho_{n+1,n+1}}{\rho_{n,n}} \tag{6.56}$$

of two subsequent coefficients is a slowly varying function on the photon number n, that is $R_n \cong R_{n-1} \cong R_{n-2} \equiv R$. By this procedure, we derive in App. E.3 a quadratic equation for R which can be easily solved yielding two solutions $R_\pm = R_\pm(n)$. The photon statistics is

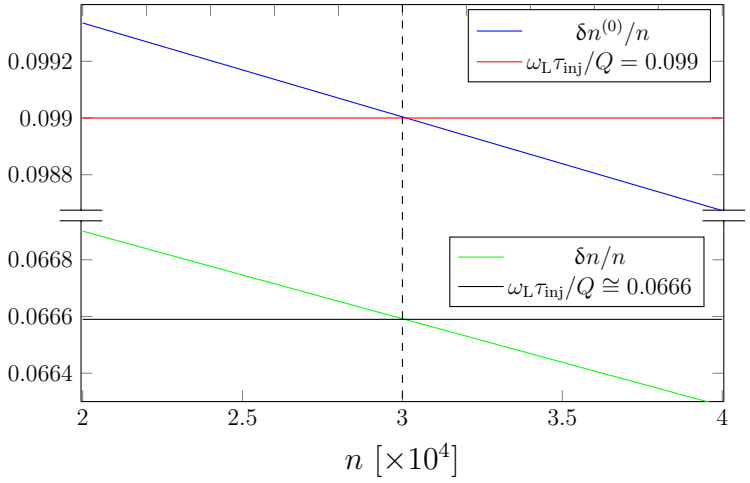

Figure 6.8: Steady-state condition in zeroth order, Eq. (6.36), (up) and in second order, Eq. (6.58), (below) of the method of averaging. We have drawn the change $\delta n^{(0)}$, Eq. (6.29), and δn, Eq. (6.28) , respectively, divided by n as function of n (blue and green line, respectively). The point of intersection with the red and black line, respectively, corresponding to the loss parameter $\omega_{\mathrm{L}}\tau_{\mathrm{inj}}/Q$, gives us the steady-state photon number for which we have fixed the value $n^{\mathrm{ss}} = 3 \cdot 10^4$. With the choice of parameters $gT = 0.001$, $N = 10^5$ and $\omega_{\mathrm{r}}T = \sqrt{3}$, leading to $\alpha_{n^{\mathrm{ss}}} = 0.1$, we obtain the required values $\omega_{\mathrm{L}}\tau_{\mathrm{inj}}/Q \cong 0.099$ and $\omega_{\mathrm{L}}\tau_{\mathrm{inj}}/Q \cong 0.066$ for steady state in zeroth and second order, respectively. Since for both cases the loss parameter itself is of the order of $\alpha_{n^{\mathrm{ss}}}$ the relative difference between the two values for $\omega_{\mathrm{L}}\tau_{\mathrm{inj}}/Q$ is also of this order of magnitude. We note that the nonlinear function $\delta n/n$ seems to be linear in n since our parameters correspond to the small-signal regime, where the nonlinear contributions of δn are small.

then calculated by iteration according to

$$\rho_{n,n} = \rho_{0,0} \prod_{n'=1}^{n} R_+(n') \tag{6.57}$$

where R_+ is the positive branch of the solution. We note that for $\alpha_n \to 0$ it follows that $R_+ \to \Lambda_n$, according to the results in App. E.3. Therefore, Eq. (6.57) correctly reduces to the corresponding relation, Eq. (E.13), of the two-level approximation.

In analogy to the deep quantum regime, Eq. (6.36), we calculate the mean photon number by setting $R = 1$ in the quadratic equation, Eq. (E.34). According to App. E.3 we obtain the relation, Eq. (E.39),

$$\frac{\omega}{Q} n^{\mathrm{ss}} = \delta n^{(0)}(n^{\mathrm{ss}}) + \alpha_{n^{\mathrm{ss}}}^2 \delta n^{(2)}(n^{\mathrm{ss}}) \tag{6.58}$$

with $\delta n^{(0)}$ and $\delta n^{(2)}$ defined in Eqs. (6.29) and (6.30), respectively. We could have already expected the form of Eq. (6.58) by simply equating the change of the mean photon number $\langle \hat{n}(t+T) \rangle - \langle \hat{n}(t) \rangle$, Eq. (6.28), with the losses $\omega_{\mathrm{L}} \langle \hat{n} \rangle / Q$ in analogy to semiclassical laser theory [22].

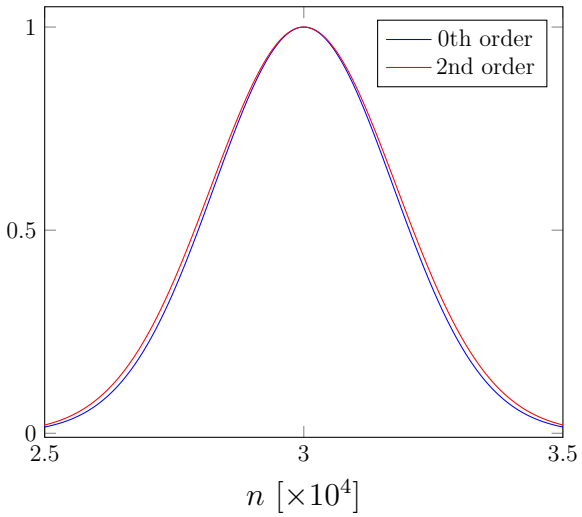

Figure 6.9: Steady-state photon statistics $\rho_{n,n}$ of a Quantum FEL oscillator normalized to unity as a function of the photon number n in zeroth order (blue line) and in second order (red line) of the method of averaging, respectively. We have chosen the parameters such that the mean photon number for both cases is at $n^{\mathrm{ss}} = 3 \cdot 10^4$ and that $\alpha_{n^{\mathrm{ss}}} = 0.1$ in accordance with Fig. 6.8. The two curves follow from numerical iteration of Eq. (E.13) with Λ_n from Eq. (6.34) and Eq. (6.57) with $R_+(n)$ from Eq. (E.35), respectively. We observe that the photon distribution is slightly broadened when we include the effects of higher orders in $\alpha_{n^{\mathrm{ss}}}$.

In Fig. 6.8 we have visualized the steady-state condition, Eq. (6.58), for zeroth and second order of the method of averaging, respectively. Surprisingly, we observe a rather high difference in the required value for the loss parameter $\omega_{\mathrm{L}}\tau_{\mathrm{inj}}/Q$ to establish in both cases the same mean photon number, even for $\alpha_{n^{\mathrm{ss}}} = 0.1$. We identify the fact that the loss parameter itself, $\omega_{\mathrm{L}}\tau_{\mathrm{inj}}/Q = 0.099$ and $\omega_{\mathrm{L}}\tau_{\mathrm{inj}}/Q = 0.066$, respectively, is of the order of $\alpha_{n^{\mathrm{ss}}}$ as the origin of this difference. Moreover, the relative deviation of the second-order value from the zeroth order one is at about 0.3 which again is of the order of $\alpha_{n^{\mathrm{ss}}}$. However, the value 0.3 for this deviation is still much smaller than unity and we assume that we are allowed to truncate our asymptotic expansion after the second order which is not guaranteed when we further increase $\alpha_{n^{\mathrm{ss}}}$. We note that a more thorough investigation of the influence of higher orders on the steady-state condition would be an interesting topic of future research.

The effect of including higher orders of $\alpha_{n^{\mathrm{ss}}}$ on the mean photon number is rather large. In contrast, the width of the photon statistics is not affected very much when we are beyond the two-level approximation which is illustrated in Fig. 6.9, where we have drawn $\rho_{n,n}$ as a function of n for zeroth and for second order of the method of averaging, respectively. We have chosen the parameters such that both distributions possess the same mean value n^{ss} and we obtain the value $\alpha_{n^{\mathrm{ss}}} = 0.1$ for the quantum parameter. However, we observe a slight broadening due to higher orders which is in accordance with the natural expectation that the width of the distribution in Fig. 6.9 is in between the small value, Eq. (6.54), of the two-level approximation and the high value, Eq. (6.55), for the classical FEL.

6.3 Intrinsic linewidth

In contrast to gain and photon statistics which rely on the diagonal elements of the density matrix, we have to consider off-diagonal elements to compute the linewidth. Again, we compare the results of our calculations for the Quantum FEL with the classical regime.

6.3.1 Off-diagonal elements

The linewidth of a laser can be connected to the decay, or rather the fluctuations, of the electric field. The expectation value of this quantity is proportional to [22]

$$\langle \hat{a}_{\mathrm{L}}(t) \rangle \equiv \mathrm{Tr}\left\{ \hat{\rho}(t) \hat{a}_{\mathrm{L}} \right\} = \sum_{n=0}^{\infty} \sqrt{n+1}\, \rho_{n+1,n}\,, \tag{6.59}$$

that is the expectation value of the photon annihilation operator $\hat{a}_{\mathrm{L}}$. Instead of the diagonal elements $\rho_{n,n}$ in the preceding sections we now have to consider the off-diagonal elements $\rho_{n+1,n}$ of the reduced density matrix according to Eq. (6.59). We note that a more suitable quantity than $\langle \hat{a}(t) \rangle$ to describe fluctuations of the electric field is given by the correlation function $\langle \hat{a}_{\mathrm{L}}^{\dagger}(t+\tau) \hat{a}_{\mathrm{L}} \rangle$ which was employed in Chap. 4. However, both approaches yield the same results for the micromaser [40, 120, 125, 126] as well as for the ordinary laser [22, 127]. Hence, we proceed by considering the decay of $\langle \hat{a}(t) \rangle$ due to the simplicity of this procedure [40].
Above threshold the steady-state photon statistics is peaked around a nearly constant photon number $n^{\mathrm{ss}} \gg 1$. Hence, we write for the change of $\langle \hat{a}_{\mathrm{L}} \rangle$ in time

$$\frac{\mathrm{d}}{\mathrm{d}t} \langle \hat{a}_{\mathrm{L}}(t) \rangle = \sum_{n=0}^{\infty} \sqrt{n+1} \dot{\rho}_{n+1,n}(t) \cong \sqrt{n^{\mathrm{ss}}+1} \sum_{n=0}^{\infty} \dot{\rho}_{n+1,n}(t)\,, \tag{6.60}$$

which means that we simply have to determine the corresponding change $\dot{\rho}_{n,n+1}$ of the off-diagonal elements. While the modulus of $\langle \hat{a}_{\mathrm{L}} \rangle$ given by $\sqrt{\langle \hat{n} \rangle} \cong \sqrt{n^{\mathrm{ss}}}$, is constant for steady state its *phase* fluctuates due to spontaneous emission, which is the reason for the linewidth of a laser [22], as discussed in Chap. 4.
In the following we just sketch the derivation of the linewidth and refer to App. E.4 for details. In analogy to our procedure for the photon statistics, Eq. (6.4), we use for the off-diagonal elements a coarse-grained derivative and obtain

$$\begin{aligned} \dot{\rho}_{n+1,n}(t) \cong \frac{N}{\tau_{\mathrm{inj}}} \left[\rho_{n+1,n}(t+T) - \rho_{n+1,n}(t) \right] - \frac{\omega_{\mathrm{L}}}{Q} \left(n + \frac{1}{2} \right) \rho_{n+1,n}(t) \\ + \frac{\omega_{\mathrm{L}}}{Q} \sqrt{(n+1)(n+2)}\, \rho_{n+2,n+1}(t)\,, \end{aligned} \tag{6.61}$$

where we have added cavity losses in accordance with Ref. [22].
Employing the explicit expression, Eq. (E.42), for the time-evolved off-diagonal element on the right-hand side of Eq. (6.61), inserting the result into Eq. (6.62), and shifting the summation indices as described in App. E.4 yields

$$\frac{\mathrm{d}}{\mathrm{d}t} \langle \hat{a}_{\mathrm{L}}(t) \rangle = -\sqrt{n^{\mathrm{ss}}+1} \sum_{n=0}^{\infty} \mu_n \rho_{n+1,n}(t) \tag{6.62}$$

with μ_n defined in Eq. (E.47).

When μ_n is a slowly varying function of n [40, 120] we can make the approximation

$$\frac{\mathrm{d}}{\mathrm{d}t}\langle\hat{a}_{\mathrm{L}}(t)\rangle \cong -\mu_{n^{\mathrm{ss}}}\langle\hat{a}_{\mathrm{L}}(t)\rangle \tag{6.63}$$

yielding a closed differential equation for $\langle\hat{a}_{\mathrm{L}}\rangle$ Again, we have considered a sharp photon statistics giving rise to $\langle\mu_n\rangle \cong \mu_{n^{\mathrm{ss}}}$.

To solve Eq. (6.63) we make the ansatz

$$\langle\hat{a}_{\mathrm{L}}(t)\rangle = \mathrm{e}^{(-D+iL)\frac{t}{2}}\langle\hat{a}_L(0)\rangle \tag{6.64}$$

from which we immediately identify D as the linewidth of the laser field. This comes from the fact that the Fourier transformation of $\langle\hat{a}_{\mathrm{L}}\rangle$ yields a Lorentzian spectrum, characterized by the width D [22].

With the help of Eq. (6.64) we obtain

$$D = 2\mathrm{Re}\left(\mu_{n^{\mathrm{ss}}}\right) \tag{6.65}$$

for the real part of the exponent, which translates to the explicit expression

$$\begin{aligned} D = \frac{2N}{\tau_{\mathrm{inj}}}\int\mathrm{d}p|\phi(p)|^2\,(1 - \cos\Omega_{n^{\mathrm{ss}}}T\cos\Omega_{n^{\mathrm{ss}}+1}T \\ -\frac{g^2\sqrt{(n^{\mathrm{ss}}+1)(n^{\mathrm{ss}}+2)}+\Delta^2(\omega_{\mathrm{r}}T)^2/4}{\Omega_{n^{\mathrm{ss}}}\Omega_{n^{\mathrm{ss}}+1}}\sin\Omega_{n^{\mathrm{ss}}}T\sin\Omega_{n^{\mathrm{ss}}+1}T\Bigg) \\ +2\frac{\omega_{\mathrm{L}}}{Q}\left[\left(n^{\mathrm{ss}}+\frac{1}{2}\right)-\sqrt{n^{\mathrm{ss}}(n^{\mathrm{ss}}+1)}\right] \end{aligned} \tag{6.66}$$

with the help of Eqs. (E.43) and (E.47) derived in App. E.4.

The expression for D in Eq. (6.66) is rather cumbersome. However, due to $n^{\mathrm{ss}} \gg 1$ we can make an expansion in terms of $1/n^{\mathrm{ss}} \ll 1$ which is discussed in detail in App. E.5. With the help of Eqs. (E.48), (E.48), (E.51), and (E.52) we finally arrive at

$$D \cong 4\frac{N}{\tau_{\mathrm{inj}}}\int\mathrm{d}p\,|\phi(p)|^2\sin^2\left[\frac{g^2}{4\Omega_{n^{\mathrm{ss}}}}\right] - \frac{(gT)^2N}{4\tau_{\mathrm{inj}}n^{\mathrm{ss}}}\int\mathrm{d}p\,|\phi(p)|^2\frac{\Delta^2\omega_{\mathrm{r}}^2}{4\Omega_{n^{\mathrm{ss}}}^2}\mathrm{sinc}^2\Omega_{n^{\mathrm{ss}}}T + \frac{\omega_{\mathrm{L}}}{Q}\frac{1}{4n^{\mathrm{ss}}} \tag{6.67}$$

for the linewidth in the Quantum FEL. We could have expected the form of the first and the third term in Eq. (6.67) from the solution [40] for the linewidth of a one-atom maser. The second term, however, is solely due to off-resonant contributions in the momentum distribution $|\phi(p)|^2$ of the electron.

6.3.2 Comparison to classical FEL

To compare the linewidth of a Quantum FEL to the one of a classical FEL we again consider the small-signal regime. For $gT\sqrt{n^{\mathrm{ss}}} \ll 1$ the expression in Eq. (6.66) translates to

$$\begin{aligned} D \cong \frac{N}{\tau_{\mathrm{inj}}} \left(gT\sqrt{n^{\mathrm{ss}}+2} - gT\sqrt{n^{\mathrm{ss}}+1}\right)^2 \int \mathrm{d}p |\phi(p)|^2 \mathcal{A}(p) \\ -2\frac{\omega_{\mathrm{L}}}{Q}\left[\left(n^{\mathrm{ss}}+\frac{1}{2}\right) - \sqrt{n^{\mathrm{ss}}(n^{\mathrm{ss}}+1)}\right], \end{aligned} \tag{6.68}$$

where we have recalled the characteristic function $\mathcal{A}$ for the small-signal gain from Eq. (6.11). The expression in Eq. (6.68) considerably simplifies to

$$D \cong \frac{1}{\tau_{\mathrm{inj}}} \frac{1}{4n^{\mathrm{ss}}} \left[(gT)^2 N \int \mathrm{d}p |\phi(p)|^2 \mathcal{A}(p) + \frac{\omega}{Q}\right]. \tag{6.69}$$

by an expansion in powers of $1/n^{\mathrm{ss}} \ll 1$. A similar result for the linewidth of a Quantum FEL was derived in Ref. [26] in terms of perturbation theory for short times. We note that a high photon number in the resonator leads to a small linewidth and thus suppresses fluctuations of the field.

To estimate the magnitude of D we consider resonance, $p = q/2$, and arrive at

$$D \cong \frac{N}{6\varepsilon\tau_{\mathrm{inj}}}(gT)^4, \tag{6.70}$$

where we have used Eq. (6.43) as well as Eq. (6.13), and have neglected a contribution with $\varepsilon/2 \ll 1$.

Again, we first make the naive comparison of D, Eq. (6.70), to its classical counterpart

$$D_{\mathrm{cl}} = \frac{2}{\pi^2}\frac{N}{\tau_{\mathrm{inj}}}\frac{(gT)^2}{2n_{\mathrm{cl}}^{\mathrm{ss}}} \tag{6.71}$$

according to Eq. (4.79) and obtain

$$\frac{D}{D_{\mathrm{cl}}} = \frac{\pi^5}{24}\frac{1}{(\omega_{\mathrm{r}}T)^2} \ll 1, \tag{6.72}$$

due to $\omega_{\mathrm{r}}T \gg 1$ in the quantum regime.

The more reasonable way of comparing the intrinsic linewidth of the quantum and classical regime emerges when we rewrite the expressions in Eqs. (6.70) and (6.71) with the help of the maximum gain in the corresponding regime. By this procedure we find

$$D = \frac{1}{\tau_{\mathrm{inj}}}\frac{\left(G_{\max}\right)^2}{6\varepsilon N} \tag{6.73}$$

and

$$D_{\mathrm{cl}} = \frac{1}{\tau_{\mathrm{inj}}}\frac{\pi}{64}\frac{\left(G_{\max}^{\mathrm{cl}}\right)^2}{\varepsilon N}. \tag{6.74}$$

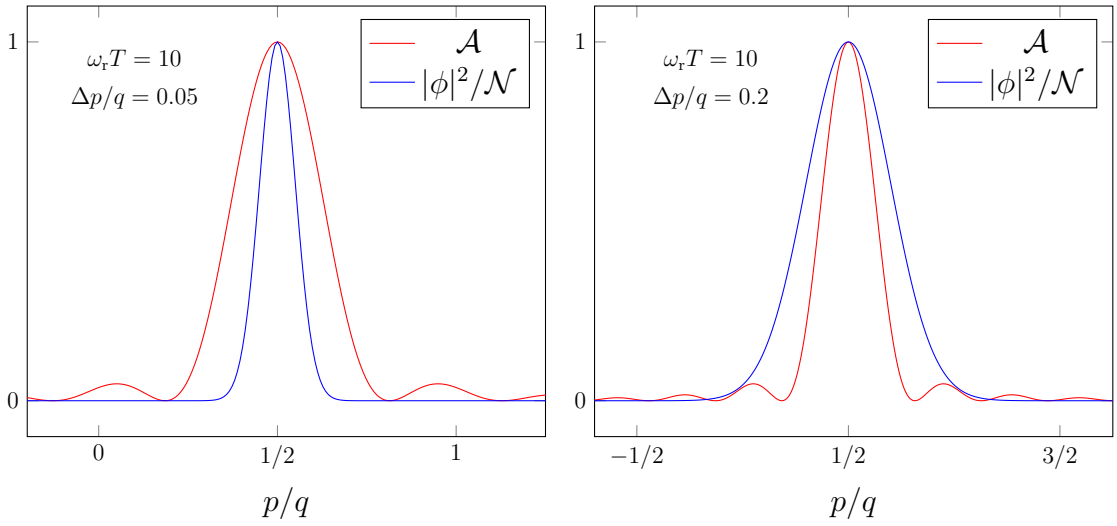

Figure 6.10: Characteristic function $\mathcal{A}$, Eq. (6.11), for linear gain in the small-signal regime and the rescaled initial momentum distribution $|\phi|^2/\mathcal{N}$, Eq. (6.75), plotted against the momentum p of the electron. While for both cases we have chosen $\omega_r T = 10$ on the left-hand side the width is $\Delta p = 0.05\, q$ and on the right-hand side it is $\Delta p = 0.2\, q$. In the latter case Δp exceeds the width of $\mathcal{A}$ and we expect a decreased gain.

Despite a different numerical pre-factor the order of magnitude of D and of D_{cl} is the same, at least under the condition that $G_{\max}$ and $G^{\mathrm{cl}}_{\max}$ are comparable.

In contrast to a Quantum SASE FEL [25] we do not find the beneficial effect of a narrower linewidth when compared to the classical FEL. In an FEL oscillator the cavity stores and stabilizes the field, leading to small field fluctuations – in the quantum as well as in the classical regime.

6.4 Velocity selectivity

In Chap. 5 we have required that the momentum spread of the electrons Δp has to be smaller than the recoil q, that is $\Delta p < q$, since otherwise absorption cancels with emission. This condition corresponds to population inversion in an atomic laser. However, we did not yet consider the connection between Δp and the width of a resonance which is described by the corresponding characteristic function.

In the following we show how an increasing momentum spread reduces the gain in the Quanum FEL and we derive conditions for the momentum spread which are even more limiting than $\Delta p < q$. Moreover, we study the effect of Δp on the steady-state photon statistics. We note that a first approach on this topic is given in Ref. [27], however, without explicitly studying the influence of Δp on the radiation properties of the Quantum FEL.

6.4.1 Gain

In the following discussion we again distinguish between the small-signal and the strong-signal limit.

Small signal

The gain of a Quantum FEL is described by the characteristic function $\mathcal{A}$ *and* by the initial momentum distribution $|\phi(p)|^2$. It is the product of both quantities integrated over p, which gives us the total value for the gain, according to Eq. (6.10).
If the momentum distribution of the electron is described by the Gaussian

$$|\phi(p)|^2 = \frac{1}{\sqrt{2\pi}\Delta p}\, \mathrm{e}^{-\frac{(p-q/2)^2}{2\Delta p^2}} \tag{6.75}$$

centered around the resonant momentum $p = q/2$, its width is characterized by the standard deviation Δp. However, when this width is *larger* than the one of the characteristic function $\mathcal{A}$, as on the right-hand side of Fig. 6.10, the wings of $|\phi(p)|^2$ do not contribute to the integral in Eq. (6.10). Hence, the gain is reduced compared to its maximal value, Eq. (6.12). In order to have a gain large enough to be above threshold, we require the opposite case, where Δp is *smaller* than the width of $\mathcal{A}$ which is shown on the left-hand side of Fig. 6.10.
To quantify this intuitive argument we have to estimate the typical width of the characteristic function for the gain. Therefore, we require that the argument of $\mathcal{A}$, Eq. (6.11),

$$\frac{\Delta(\omega_\mathrm{r} T)}{2} = \omega_\mathrm{r} T \left(\frac{p}{q} - \frac{1}{2}\right) \tag{6.76}$$

maximally is of the order of unity, that is $\Delta(\omega_\mathrm{r} T)/2 \sim \mathcal{O}(1)$.
Hence, we deduce from Eq. (6.76) the condition

$$\Delta p < \frac{1}{\omega_\mathrm{r} T}\, q \tag{6.77}$$

for the initial momentum spread Δp of the electron. Satisfying Eq. (6.77) ensures that the gain of the Quantum FEL is close to its maximum and eventually above threshold.
Indeed, we obtain in Fig. (6.11), where g_1, Eq. (6.10), is drawn as a function of $\Delta p/q$, that for small widths fulfilling the condition in Eq. (6.77) the gain still possesses a relatively large value. Increasing Δp, however, eventually leads to very small values of g_1. We emphasize that, due to $\omega_\mathrm{r} T \gg 1$, Eq. (6.77) is an even stronger condition on the quality of the electron beam than $\Delta p < q$, Eq. (5.30).

Strong signal

Having discussed the small-signal limit we now turn to the case of a strong signal, that is $gT\sqrt{n+1} = \pi/2$ which is characterized by $\mathcal{S}^2_{\pi/2}$, Eq. (6.17). Similar to the small-signal case

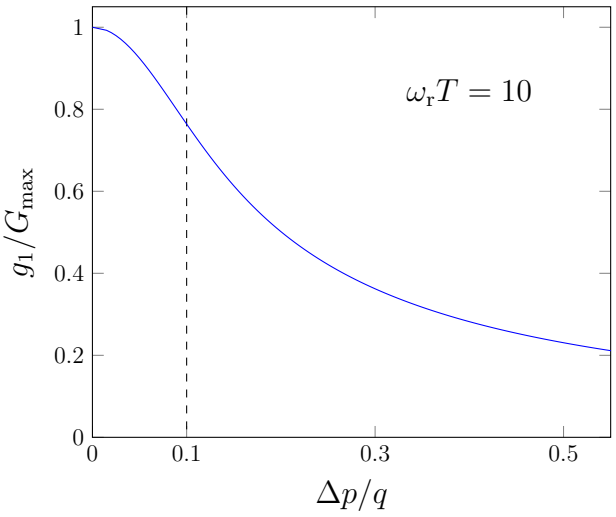

Figure 6.11: Linear gain g_1, Eq. (6.10), of a Quantum FEL normalized to the maximum gain $G_{\max}$, Eq. (6.12), as a function of the width Δp of the initial momentum distribution $|\phi(p)|^2$, Eq. (6.75), for $\omega_r T = 10$. As expected from Eq. (6.77) the gain is still relatively high for $\Delta p/q < 0.1$ (indicated by the dashed horizontal line) but decreases for higher values of Δp.

we consider the argument

$$gT\sqrt{n+1}\sqrt{1+\left(\frac{\Delta(\omega_r T)/2}{gT\sqrt{n+1}}\right)^2} \sim \mathcal{O}(1) \tag{6.78}$$

of the characteristic function $\mathcal{S}^2_{\pi/2}$ for which we again demand that it is maximally of the order of unity. Moreover, we cast the term in parentheses into the form

$$\frac{\Delta(\omega_r T)}{2gT\sqrt{n+1}} = \frac{1}{\alpha}\left(\frac{p}{q} - \frac{1}{2}\right) , \tag{6.79}$$

where we have used the definitions of Δ and α, Eqs. (5.19) and (5.18), respectively.
The comparison with the width Δp of the momentum distribution for the electrons yields the constraint

$$\Delta p < \frac{\alpha}{\pi/2}\, q \tag{6.80}$$

to efficiently operate a Quantum FEL in the strong-signal regime $gT\sqrt{n+1} = \pi/2$. Again, we obtain a stronger requirement than $\Delta p < q$, Eq. (5.30), since we consider the quantum regime, where $\alpha \ll 1$.
In Fig. 6.12, where the strong-signal gain G_{str}, Eq. (6.16), is drawn versus the momentum spread Δp we obtain a similar behavior as for the small-signal regime, Fig. 6.11. For widths satisfying Eq. (6.80) the gain is still relatively large while it decreases for increasing Δp
Hence, we require a very small momentum spread to operate a Quantum FEL oscillator in an efficient manner. Broadening this spread leads to a decreased value for the gain and thus it becomes more difficult for the gain to overcome threshold. This problem is less important

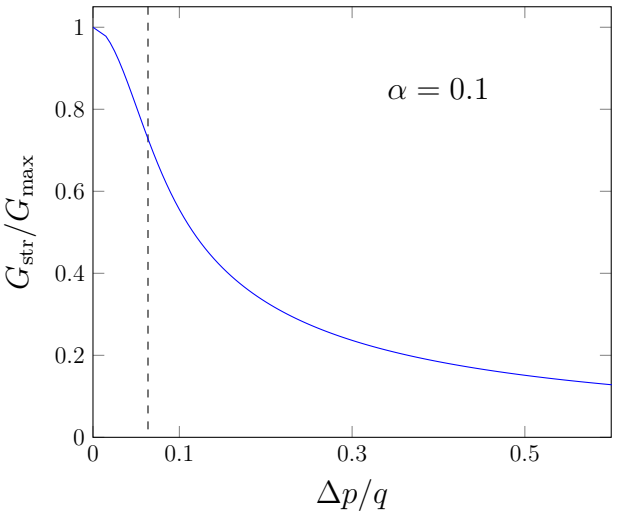

Figure 6.12: The strong-signal gain gain G_{str}, Eq. (6.16) normalized to the maximum gain G_{max}, Eq. (6.18), as a function of the width Δp of the initial momentum distribution $|\phi(p)|^2$, Eq. (6.75), for $\alpha = 0.1$. The dashed vertical line indicates the upper bound of the inequality, Eq. (6.80), characterizing the width Δp up to which the gain is till close to its maximal value.

in the classical regime since the characteristic functions are broad functions in contrast to the sharp resonances in the quantum regime.

6.4.2 Photon statistics

The steady-state photon statistics of the Quantum FEL in the Gaussian approximation, Eq. (6.35), is characterized by two quantities: the mean value n^{ss} and the variance Δn^2. In the following we investigate the influence of a nonzero momentum spread Δp on these two quantities.

For the steady-state photon number we only consider the small-signal case as an example with n^{ss} given by Eq. (6.44). In the following discussion we assume that the deviation ϵ from threshold is fixed since else one would eventually be below threshold with $\epsilon < 0$. Hence, we just consider the ratio of g_1 and g_2, both given in Eq. (6.10).

We have drawn this ratio in Fig. 6.13 as a function of the momentum spread Δp where we have assume that the momentum distribution $|\phi(p)|^2$ is a Gaussian and given by Eq. (6.75). We obtain that the effect of a growing Δp is relatively small and the value of n^{ss} varies rather slowly.

However, to be above threshold we still have to consider cavity losses. For a fixed value of ϵ we deduce from its definition, Eq. (6.45),

$$\frac{\omega_{\mathrm{L}}\tau_{\mathrm{inj}}}{Q} = (1-\epsilon)g_1\,, \tag{6.81}$$

that is the required magnitude of $\omega_{\mathrm{L}}\tau_{\mathrm{inj}}/Q$ is proportional to the gain g_1. The gain, however, decreases for increasing values of Δp according to Fig. 6.11 and so does $\omega_{\mathrm{L}}\tau_{\mathrm{inj}}/Q$. Despite the small direct influence of the momentum spread on the steady-state intensity, shown in

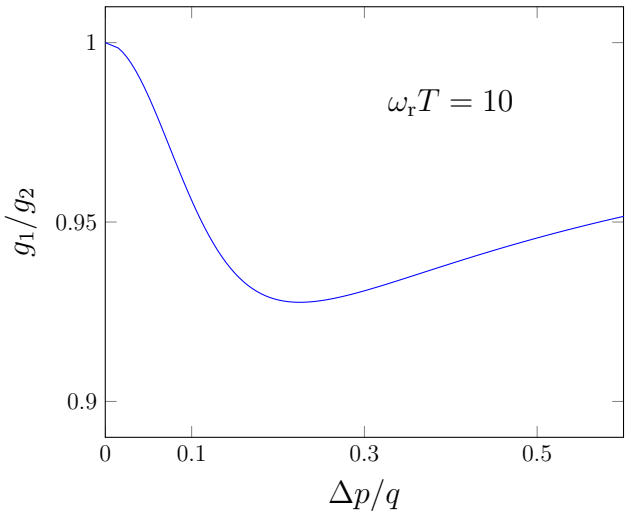

Figure 6.13: The ratio of linear gain g_1 and self saturation g_2, given by Eq. (6.10) in the small-signal regime as a function of the width Δp of the momentum distribution $|\phi(p)|^2$, Eq. (6.75).

Fig. 6.13, the experimental situation is thus more involved for an increasing momentum spread, since the required quality of the cavity also increases.

Regarding the influence of the momentum spread on the variance of the photon statistics we just discuss the example of a strong signal, that is $gT\sqrt{n^{\mathrm{ss}}} = \pi/2$. With the help of Eqs. (6.39) and (6.40) we obtain the expression

$$\sigma^2 = \frac{\int \mathrm{d}p\, |\phi(p)|^2\, \mathcal{S}^2_{\pi/2}}{\int \mathrm{d}p\, \frac{|\phi(p)|^2}{1+[\Delta(\omega_r T)/\pi]^2}\, \mathcal{S}^2_{\pi/2} - \int \mathrm{d}p\, \frac{|\phi(p)|^2}{1+[\Delta(\omega_r T)/\pi]^2} \mathcal{S}_{\pi/2} \cos\left[\frac{\pi}{2}\sqrt{1+\left[\frac{\Delta(\omega_r T)}{\pi}\right]^2}\right]} \tag{6.82}$$

for the normalized variance σ^2, where we have recalled the definition Eq. (6.17), for the characteristic function $\mathcal{S}^2_{\pi/2}$ of the strong-signal gain. According to Fig. 6.14, where σ^2, Eq. (6.82), is plotted versus Δp, the influence of the momentum spread on σ^2 is very small. In conclusion, we have found that a broad momentum distribution of the electron reduces the gain of the FEL. In this context, we have formulated conditions, Eqs. (6.77) and (6.80), for Δp which are even stronger than the fundamental requirement $\Delta p < q$. Thus, for a broader distribution it is more difficult to reach steady state. In principle, however, this can be achieved by increasing the quality Q of the cavity leading to a statistical behavior of the radiation field which differs just slightly from the one due to a small momentum spread of the electrons.

6.5 Summary

In this chapter we have studied radiation properties of a Quantum FEL oscillator and have compared them to the corresponding properties for a classical FEL. With the help of the

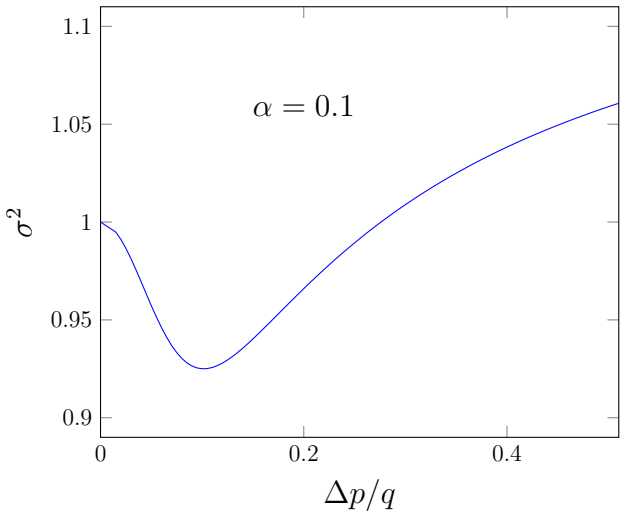

Figure 6.14: Normalized variance σ^2, Eq. (6.82), for the strong-signal case, $gT\sqrt{n^{\rm ss}} = \pi/2$ and for $\alpha = 0.1$, as function of the width Δp of the initial momentum distribution $|\phi(p)|^2$ of the electron, Eq. (6.75). The effect of increasing values for Δp on σ^2 is relatively small.

photon number representation we have derived explicit expressions for gain, steady-state photon statistics and intrinsic linewidth.
The experimental requirements to obtain a value for the gain which is high enough to surpass threshold are more strict than in the classical regime. In particular, we need a high electron energy to be in the quantum regime as well as a very long wiggler for a reasonable high gain. However, when we overcome these obstacles we are rewarded with the outstanding statistical properties of the radiation which we have identified by the possibility of a Poissonian or sub-Poissonian photon statistics. In Fig. 6.7 we have illustrated that the photon distribution of a Quantum FEL in the small-signal limit is always smaller than the corresponding distribution in the classical regime and thus closer to a coherent state. In contrast to the results [25] for a Quantum SASE FEL, a Quantum FEL oscillator does not possess a narrowed linewidth in comparison to its classical counterpart since in both regimes a high photon number reduces fluctuations of the phase.
At the end of this chapter we have investigated the effect of a nonzero momentum spread of the electron beam on the properties of an FEL in the quantum regime. We have obtained that the initial momentum spread has to be even lower than the limit $\Delta p < q$ in order to efficiently operate a Quantum FEL.

7 The High-Gain Quantum FEL

A large part of the existing literature on the Quantum FEL, for example Refs. [2, 3, 25, 88, 109], does not concern the low-gain but instead the high-gain regime. A high recoil, required to reach the quantum regime, corresponds to a short laser wavelength for which the experimental realization of a resonator might be very involved. Hence, it is quite reasonable to consider a Quantum FEL in the SASE mode, where a high gain in a single passage of electrons is necessary.

To apply our ideas and methods also to the high-gain regime we first have to develop a suitable many-electron model in analogy to the classical case discussed in Chap. 2. We do this by generalizing the concept of projection operators for the electron momentum introduced in Chap. 5 to *collective* projection operators and by employing the Heisenberg picture.

Similar to the single-electron case, Chap. 5, the deep quantum regime of the many-electron description corresponds to a two-level behavior of the momentum states of the electrons. However, the system now is analogous to the mutual interaction of many two-level systems with the radiation field, that is to the Dicke model [114] instead of to the Jaynes–Cummings model [32] in Chap. 5. As a result we obtain exponential gain for short times while for longer times the field saturates when each electron has roughly emitted one photon.

At the end of this chapter we study higher-order corrections to the deep quantum regime in the framework of the method of averaging [37]. By this procedure, we establish the connection to the theory in Refs. [2, 3, 25] and derive analytic expressions for the numerical results of these references. Some topics in this chapter were already presented in the proceedings of the FEL conference 2014 in Basel [31].

7.1 Many-electron model

In the classical regime of the FEL, studied in Chap. 2, the transition from a low to a high gain occurs when the collective effects due to the mutual interaction of the electrons with the laser field are not negligible any longer. Hence, we expect this behavior for the Quantum FEL, too.

In the collective description the equations of motion are not decoupled and we have to deal with the many-particle Hamiltonian

$$\hat{H} = \sum_{j=1}^{N} \frac{\hat{p}_j^2}{2m} + \hbar g \left(\hat{a}_\mathrm{L} \sum_{j=1}^{N} \mathrm{e}^{i2k\hat{z}_j} + \hat{a}_\mathrm{L}^\dagger \sum_{j=1}^{N} \mathrm{e}^{-i2k\hat{z}_j} \right) \tag{7.1}$$

describing the interaction of N electrons with a single laser mode. We note that this Hamiltonian describes distinguishable particles despite the fermionic nature of indistinguishable electrons. According to Ref. [3] this approach is justified for reasonable parameters of realistic electron beams. In short, the argument in Ref. [3] is based on the claim that the number N

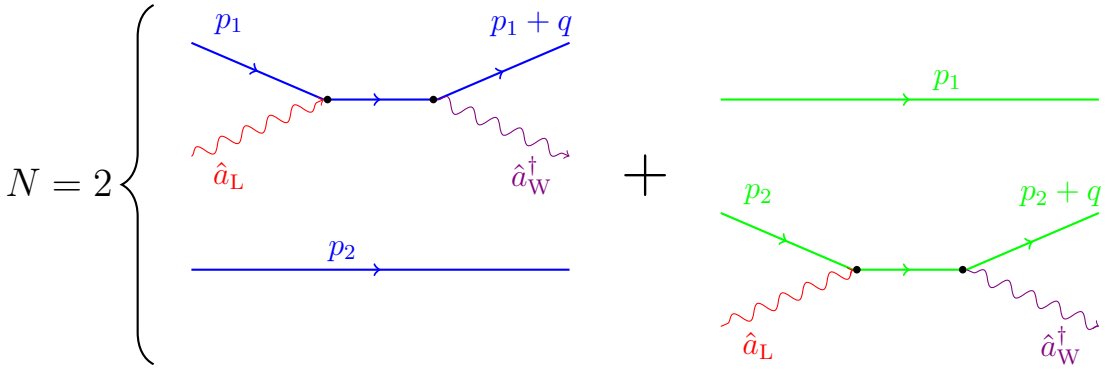

Figure 7.1: Creation of an entangled state for $N = 2$ electrons in Eq. (7.2). On the left-hand side the first electron absorbs a photon and changes its momentum from p_1 to $p_1 + q$, while the second electron does not interact with the field and maintains its initial momentum p_2. On the right-hand side the other possible path is sketched with the final momenta p_1 and $p_2 + q$. Due to the superposition principle in quantum mechanics we have to add up these two paths to arrive at the total state of the evolved system.

of electrons in a bunch has to be smaller than the phase space volume of the bunch in units of $\hbar$.

The difference between the single-electron and the many-particle model becomes most obvious when we consider the action of the Hamiltonian, Eq. (7.1), on a quantum state. As discussed in Chap. 5, the system in the single-electron case can always be described by the single quantum number μ which simultaneously indicates the number of scattered photons and the number of discrete momentum steps of the electron. Hence, we have expanded the total state vector in terms of the scattering basis $|\mu\rangle \equiv |n + \mu, p - \mu q\rangle$.

However, we cannot carry out this procedure when we deal with many electrons. For example, we obtain in the case $N = 2$ terms of the form

$$\hat{a}_\mathrm{L} \left(\mathrm{e}^{i2k\hat{z}_1} + \mathrm{e}^{i2k\hat{z}_2} \right) |n, p_1, p_2\rangle = \sqrt{n}\, |n-1\rangle \left(|p_1 + q, p_2\rangle + |p_1, p_2 + q\rangle \right) \tag{7.2}$$

which is an entangled state. We can understand the behavior described by Eq. (7.2) with the help of Fig. 7.1. When a single photon is absorbed from the laser field the system can follow two different paths: Either the first electron, with initial momentum p_1, absorbs the photon and increases its momentum by the recoil q while the second electron does not interact with the field and maintains its initial momentum p_2, or the second electron is scattered while the first one does not feel any effect of the interaction. Since these paths correspond to quantum mechanical states we have to superimpose them and arrive at the expression in Eq. (7.2).

For an arbitrary number N of electrons we find the expression

$$\hat{a}_\mathrm{L} \sum_{j=1}^{N} \mathrm{e}^{i2k\hat{z}_j} |n, p_1, p_2, ..., p_N\rangle = \sqrt{n}\, |n-1\rangle \sum_{j=1}^{N} |p_1, ..., p_j + q, ..., p_N\rangle \ , \tag{7.3}$$

where the electron part is similar to a Dicke state [114] from the field of superradiance and amplified spontaneous emission. However, in contrast to Dicke states where the atoms can

only occupy a ground and an excited state, multiphoton processes in the FEL cause the electrons to occupy in general more than just two momentum levels. This feature eventually leads to expressions which are even more involved than the one in Eq. (7.3).

To avoid tedious calculations with these entangled states we do in the following not consider the dynamics of states in the Schrödinger picture but instead the evolution of time-dependent operators in the Heisenberg picture. Since we are not interested in the detailed behavior of every single electron but in their total effect on the radiation field we treat the electrons in a collective way. To this end, we introduce the *collective* projection operators

$$\hat{\Upsilon}_{\mu,\nu} \equiv \sum_{j=1}^{N} \hat{\sigma}_{\mu,\nu}^{(j)} = \sum_{j=1}^{N} |p-\mu q\rangle^{(j)} \langle p-\nu q| \tag{7.4}$$

for the electrons where we have recalled the definition, Eq. (5.5), of the projection operator $\hat{\sigma}_{\mu,\nu}$ for a single electron with μ and ν denoting integer numbers. The definition, Eq. (7.4), is reasonable when we assume that every electron initially possesses the same momentum, that is $p_j = p_k \equiv p$ for any j and k. This statement implies that the initial state of the electrons is given by a product $|p, p, ..., p\rangle$ of momentum eigenstates each with the same eigenvalue p.

The algebra of the collective projection operator is described by the commutation relation

$$\left[\hat{\Upsilon}_{\mu,\nu}, \hat{\Upsilon}_{\rho,\eta}\right] = \delta_{\nu,\rho}\hat{\Upsilon}_{\mu,\eta} - \delta_{\eta,\mu}\hat{\Upsilon}_{\rho,\nu} \tag{7.5}$$

which is analogous to the one, Eq. (5.6), valid for a single electron. This analogy emerges since operators for different electrons commute, that is $\left[\hat{\sigma}_{\mu,\nu}^{(j)}, \hat{\sigma}_{\rho,\lambda}^{(k)}\right] = 0$ for $j \neq k$.

However, there exists an important difference to the single-electron case. The product of two projection operators

$$\hat{\Upsilon}_{\mu,\nu}\hat{\Upsilon}_{\rho,\eta} \neq \delta_{\nu,\rho}\hat{\Upsilon}_{\mu,\eta} \tag{7.6}$$

does not equal to a single projection operator in contrast to Eq. (5.7). For one electron the action of the projection operator $\hat{\sigma}_{\mu,\nu}$ on a state shifts the momentum of the electron and applying an additional projection operator results in an additional shift. In contrast, a collective operator $\hat{\Upsilon}_{\mu,\nu}$ creates an entangled state in analogy to Eq. (7.3), where the shift for a specific electron occurs with a certain probability and we cannot speak of a definite momentum shift of the electron. The second operator now has to act on this entangled state and again the momentum of each electron is shifted only with a certain probability. For example, we obtain for $N = 2$ the expression

$$\hat{\Upsilon}_{1,0}\hat{\Upsilon}_{1,0}\,|p,p\rangle = \hat{\Upsilon}_{1,0}\left(|p-q,p\rangle + |p,p-q\rangle\right) = 2\,|p-q,p-q\rangle \tag{7.7}$$

while the corresponding product $\hat{\sigma}_{1,0}\hat{\sigma}_{1,0}\,|p\rangle = 0$ for $N = 1$ is zero, due to Eq. (5.7).

We proceed by rewriting the Hamiltonian Eq. (7.1) in terms of the collective operators $\hat{\Upsilon}_{\mu,\nu}$ and arrive at the expressions

$$\begin{cases} \sum\limits_{j=1}^{N} \hat{p}_j^2 = \sum\limits_{\mu} (p - \mu q)^2 \, \hat{\Upsilon}_{\mu,\mu} \\ \sum\limits_{j=1}^{N} \mathrm{e}^{i2k\hat{z}_j} = \sum\limits_{\mu} \hat{\Upsilon}_{\mu,\mu+1} \\ \sum\limits_{j=1}^{N} \mathrm{e}^{-i2k\hat{z}} = \sum\limits_{\mu} \hat{\Upsilon}_{\mu+1,\mu} \end{cases} \tag{7.8}$$

which are analogous to the ones, Eq. (5.9), in the single-electron description. We note that we do not sum over the different electrons any longer since they are described by the collective operators. Instead, we now sum over different momenta which are not operators but numbers and discrete multiples of the recoil q.

The Hamiltonian $\hat{H} \equiv \hat{H}_0 + \hat{H}_1$ resulting from Eq. (7.8) can be split into two parts, that is a a contribution

$$\hat{H}_0 \equiv \sum_{\mu} \left(\Delta + \frac{1}{2} - \mu \right)^2 \hat{\Upsilon}_{\mu,\mu} \tag{7.9}$$

for the free time evolution and a term

$$\hat{H}_1 \equiv \varepsilon \left(\hat{a}_{\mathrm{L}} \sum_{\mu} \hat{\Upsilon}_{\mu,\mu+1} + \hat{a}_{\mathrm{L}}^{\dagger} \sum_{\mu} \hat{\Upsilon}_{\mu+1,\mu} \right) \tag{7.10}$$

describing the interaction. For that purpose, we have used the dimensionless variables introduced in Eq. (5.14).

The equation of motion for a Heisenberg operator $\hat{\mathcal{O}}$ then reads

$$i \frac{\mathrm{d}}{\mathrm{d}\tau} \hat{\mathcal{O}}(\tau) = \left[\hat{\mathcal{O}}(\tau), \hat{H} \right] = \left[\hat{\mathcal{O}}(\tau), \hat{H}_0 \right] + \left[\hat{\mathcal{O}}(\tau), \hat{H}_1 \right] . \tag{7.11}$$

We note that the expectation value of the observable $\hat{\mathcal{O}}$ has to be calculated via the relation

$$\langle \hat{\mathcal{O}} \rangle = \langle \Psi(0) | \, \hat{\mathcal{O}}(\tau) \, | \Psi(0) \rangle \tag{7.12}$$

with respect to the initial state vector $|\Psi(0)\rangle$.

In analogy to the single-particle model in Chap. 5, we want to remove the contribution, $\hat{H}_0$, of free time evolution and thus we perform the transformation

$$\hat{\mathcal{O}}'(\tau) \equiv \mathrm{e}^{-i\hat{H}_0\tau} \, \hat{\mathcal{O}} \, \mathrm{e}^{i\hat{H}_0\tau} \qquad |\Psi'(\tau)\rangle \equiv \mathrm{e}^{-i\hat{H}_0\tau} \, |\Psi(0)\rangle \tag{7.13}$$

leading due to Eq. (7.12) to the relation

$$\langle \hat{\mathcal{O}} \rangle = \langle \Psi'(\tau) | \, \hat{\mathcal{O}}'(\tau) \, | \Psi'(\tau) \rangle \tag{7.14}$$

for the expectation value of $\hat{\mathcal{O}}$ where the state vector is now time-dependent as well.

According to Eq. (7.13) we arrive at the transformed equation of motion

$$i\frac{\mathrm{d}}{\mathrm{d}\tau}\hat{\mathcal{O}}'(\tau) = \left[\hat{\mathcal{O}}'(\tau), \hat{H}'(\tau)\right] \tag{7.15}$$

for $\hat{\mathcal{O}}'$ with [82]

$$\hat{H}'(\tau) \equiv \mathrm{e}^{-i\hat{H}_0\tau}\,\hat{H}_1\,\mathrm{e}^{i\hat{H}_0\tau} \tag{7.16}$$

as the Hamiltonian in the rotating frame. With the help of the Baker–Campbell–Hausdorff formula, Eq. (B.13), and the commutation relations, Eq. (7.5), we obtain the explicit expression

$$\hat{H}'(\tau) = \varepsilon\left(\hat{a}_\mathrm{L}\,\mathrm{e}^{-i\Delta\tau}\sum_\mu \mathrm{e}^{i2\mu\tau}\,\hat{\Upsilon}_{\mu,\mu+1} + \hat{a}_\mathrm{L}^\dagger\,\mathrm{e}^{i\Delta\tau}\sum_\mu \mathrm{e}^{-i2\mu\tau}\,\hat{\Upsilon}_{\mu+1,\mu}\right) \tag{7.17}$$

for $\hat{H}'$ which allows us to identify the different time scales of the dynamics in analogy to $\hat{H}_\mathrm{I}$, Eq. (5.12), in Chap. 5.
Before we proceed, we note that it is convenient to perform a second transformation

$$\bar{\mathcal{O}}(\tau) \equiv \mathrm{e}^{-i\Delta\tau\hat{n}}\,\hat{\mathcal{O}}'(\tau)\,\mathrm{e}^{i\Delta\tau\hat{n}} \qquad \bar{H}(\tau) \equiv \mathrm{e}^{-i\Delta\tau\hat{n}}\,\hat{H}'(\tau)\,\mathrm{e}^{i\Delta\tau\hat{n}} \qquad |\bar{\Psi}(\tau)\rangle \equiv \mathrm{e}^{-i\Delta\tau\hat{n}}\,|\Psi'(\tau)\rangle \tag{7.18}$$

in order to eliminate the explicit dependence on the 'slow' time scale given by the relative deviation $\Delta \equiv (p - q/2)/(q/2)$ from resonance $p = q/2$. Hence, we finally obtain the Hamiltonian

$$\bar{H}(\tau) = \varepsilon\left(\hat{a}_\mathrm{L}\sum_\mu \mathrm{e}^{i2\mu\tau}\,\hat{\Upsilon}_{\mu,\mu+1} + \hat{a}_\mathrm{L}^\dagger\sum_\mu \mathrm{e}^{-i2\mu\tau}\,\hat{\Upsilon}_{\mu+1,\mu}\right) - \Delta\hat{n} \tag{7.19}$$

governing the dynamics of the FEL.
Our main focus lies on the quantum regime of the FEL, where the oscillations with multiples of the recoil frequency ω_r, that is with $\mu\tau$ in Eq. (7.19), are rapid due to a large recoil q, and hence can be neglected. In this limit, we expect that the method of averaging is again a suitable technique to calculate the properties of a Quantum FEL. To apply this method we rewrite the Hamiltonian as

$$\bar{H}(\tau) \equiv \varepsilon\sum_\mu \hat{\mathcal{H}}_\mu(\tau)\,\mathrm{e}^{i2\mu\tau} \tag{7.20}$$

with

$$\begin{cases}\hat{\mathcal{H}}_0(\tau) \equiv \hat{a}_\mathrm{L}\hat{\Upsilon}_{0,1} + \hat{a}_\mathrm{L}^\dagger\hat{\Upsilon}_{1,0} - \frac{\Delta}{\varepsilon}\hat{n} \\ \hat{\mathcal{H}}_\mu(\tau) \equiv \hat{a}_\mathrm{L}\hat{\Upsilon}_{\mu,\mu+1} + \hat{a}_\mathrm{L}^\dagger\hat{\Upsilon}_{-\mu+1,-\mu}\end{cases} \tag{7.21}$$

in analogy to Eqs. (5.16) and (5.17) in the low-gain regime. We emphasize that the inclusion of the term proportional to Δ in $\hat{\mathcal{H}}_0$ in Eq. (7.21) which emerges due to the transformation, Eq. (7.18), is only reasonable in this context when Δ is of the order of ε and $\hat{n}$ initially is small.

7.2 Deep quantum regime

In the following we investigate the high-gain FEL in the deep quantum regime. Just like in the low-gain limit, we obtain a two-level behavior for the momentum states of the electrons. However, the suitable analogy is now the Dicke model [114], where many two-level atoms

interact with a quantized mode of the radiation field rather than the Jaynes–Cummings model [32] which is restricted to a single atom. For short times we obtain exponential gain, similar to the classical case, justifying the term *high-gain Quantum FEL*. Moreover, we study the dynamics for longer times and obtain conditions for a maximized signal depending on the wiggler length and on the momenta of the electrons.

7.2.1 Dicke Hamiltonian

In the preceding section we have cast the FEL Hamiltonian into a suitable form, Eq. (7.20), for the method of averaging. To apply this method we require $\varepsilon \left|\hat{\mathcal{H}}_\mu\right| \ll 1$ [37]. This translates to the condition

$$\alpha_N \equiv \varepsilon\sqrt{N} \equiv \frac{g\sqrt{N}}{\omega_\mathrm{r}} \ll 1 \tag{7.22}$$

for the quantum parameter α_N, where we have made the estimation $\left|\hat{\mathcal{H}}_\mu\right| \sim \sqrt{N}$. Moreover, we demand $\Delta \ll 1$ in analogy to the single-electron case, Eq. (5.19).

In lowest order of the method of averaging the effective Hamiltonian, $\hat{H}_\mathrm{eff} \equiv \varepsilon \hat{H}^{(1)}_\mathrm{eff}$, is given by

$$\hat{H}_\mathrm{eff} \cong \varepsilon \hat{\mathcal{H}}_0(\tau) = \varepsilon \left(\hat{a}_\mathrm{L} \hat{\Upsilon}_{0,1} + \hat{a}_\mathrm{L}^\dagger \hat{\Upsilon}_{1,0}\right) - \Delta\hat{n} \tag{7.23}$$

which is the only slowly varying component of the Hamiltonian, Eq. (7.19). Since we discard all rapidly oscillating contributions we have performed a rotating-wave-like approximation [40].

From Eq. (7.23), we recognize that, just like in the single-particle case, Chap. 5, the deep quantum regime is the limit where the electron dynamics is characterized by two momentum levels, which are given by p and $p - q$. However, despite the similar form of Eq. (5.20) and Eq. (7.23) both Hamiltonians describe different situations and thus lead to different dynamics. Due to the corresponding algebras we expect a richer behavior in the collective case compared to the single-particle model. While we have identified Eq. (5.20) with the Jaynes–Cummings Hamiltonian, the expression in Eq. (7.23) is analogous to the Dicke Hamiltonian with detuning, describing the *simultaneous* interaction of N two-level atoms with a quantized mode of the radiation field [114].

As discussed in the preceding section we work with Heisenberg operators to avoid lengthy calculations with Schrödinger state vectors. The time evolution of an operator $\hat{\mathcal{O}}$ emerges by solving the Heisenberg equation of motion

$$i\frac{\mathrm{d}}{\mathrm{d}\tau}\hat{\mathcal{O}}(\tau) = \left[\hat{\mathcal{O}}(\tau), \hat{H}_\mathrm{eff}\right] . \tag{7.24}$$

Now, we obtain why it is favorable in the Heisenberg picture to use *canonical* averaging [37] instead of the ordinary method [36]. This way we have found an explicit expression for the effective Hamiltonian, Eq. (7.23), in operator form in contrast to the usual averaging technique.

Inserting Eq. (7.23) into Eq. (7.24) and employing the commutation relation, Eq. (7.5), yields the system of differential equations

$$\begin{aligned} i\frac{\mathrm{d}}{\mathrm{d}\tau}\hat{\Upsilon}_{1,0} &= -\varepsilon\hat{a}_{\mathrm{L}}\hat{\Upsilon}_z \\ i\frac{\mathrm{d}}{\mathrm{d}\tau}\hat{\Upsilon}_z &= 2\varepsilon\left(\hat{a}_{\mathrm{L}}\hat{\Upsilon}_{0,1} - \hat{a}_{\mathrm{L}}^\dagger\hat{\Upsilon}_{1,0}\right) \\ i\frac{\mathrm{d}}{\mathrm{d}\tau}\hat{a}_{\mathrm{L}} &= -\Delta\hat{a}_{\mathrm{L}} + \varepsilon\hat{\Upsilon}_{1,0}\,, \end{aligned} \tag{7.25}$$

where we have defined

$$\hat{\Upsilon}_z \equiv \hat{\Upsilon}_{0,0} - \hat{\Upsilon}_{1,1} \tag{7.26}$$

in analogy to $\hat{\sigma}_z$ in Chap. 5. In contrast to the single-electron case, where we have obtained an exact solution of the Schrödinger equation in the deep quantum regime, Eq. (7.25) represents a set of nonlinear coupled differential equations and cannot be solved in an analytic way [128]. That is why we have to search for suitable approximations or stick to a numeric solution.

We note that the analogy of the Quantum FEL and the Dicke model was also pointed out in Ref. [129] employing a different approach. The author uses a formalism in second quantization developed in Ref. [89] and obtains for the quantum regime a Hamiltonian which is trilinear in bosonic ladder operators, analogously to a parametric amplifier [130, 131]. With the help of the Schwinger representation of angular momentum [132] we can write

$$\hat{a}_{\mathrm{L}}^\dagger\hat{\Upsilon}_{1,0} = \hat{a}_{\mathrm{L}}^\dagger\hat{b}_1^\dagger\hat{b}_0\,, \tag{7.27}$$

where $\hat{b}_1^\dagger$ as well as $\hat{b}_0$ fulfill bosonic commutation relations and we recognize that our Hamiltonian, Eq. (7.23), for the Quantum FEL is analogus to the one in Ref. [129].

Although a sketch of a proof employing ordinary perturbation theory is presented in Ref. [129] to connect the Quantum FEL to the Dicke Hamiltonian, a rigorous proof is missing. We close this gap in Sec. 7.3 by calculating higher-order corrections of the method of averaging in the exponential gain regime and obtain that these corrections scale with powers of $\alpha_N \ll 1$. Moreover, we study the effect of a nonzero deviation Δ from resonance $p = q/2$ in Eq. (7.23), to derive a gain function and thus we are able to establish the connection to Ref. [25].

7.2.2 Exponential gain for short times

For short times the set of Heisenberg equations of motion, Eq. (7.25), can be solved in the so-called *parametric approximation* [128]. For this purpose, we first rescale the operators in Eq. (7.25) as

$$\begin{cases} \tilde{\Upsilon}_{1,0} & \equiv \frac{1}{\sqrt{N}}\hat{\Upsilon}_{1,0} \\ \tilde{\Upsilon}_z & \equiv \frac{1}{N}\hat{\Upsilon}_z \\ \tilde{a}_{\mathrm{L}} & \equiv \hat{a}_{\mathrm{L}} \end{cases} \tag{7.28}$$

and arrive at

$$\begin{aligned} i\frac{\mathrm{d}}{\mathrm{d}\tau}\tilde{\Upsilon}_{1,0} &= -\alpha_N \tilde{a}_\mathrm{L}\tilde{\Upsilon}_z \\ i\frac{\mathrm{d}}{\mathrm{d}\tau}\tilde{\Upsilon}_z &= \frac{\alpha_N}{N/2}\left(\tilde{a}_\mathrm{L}\tilde{\Upsilon}_{0,1} - \tilde{a}_\mathrm{L}^\dagger\tilde{\Upsilon}_{1,0}\right) \\ i\frac{\mathrm{d}}{\mathrm{d}\tau}\tilde{a}_\mathrm{L} &= -\Delta\tilde{a}_\mathrm{L} + \alpha_N\tilde{\Upsilon}_{1,0}\,, \end{aligned} \tag{7.29}$$

where the quantum parameter α_N appears in a rather natural way.

To apply the parametric approximation we first consider the initial state

$$|\Psi(0)\rangle = |n\rangle \otimes |p,p,...,p\rangle \quad \rightarrow \quad |\bar{\Psi}(\tau)\rangle = \mathrm{e}^{-i\Delta n\tau}\,\mathrm{e}^{-iN(\Delta+1/2)^2\tau}\,|n\rangle \otimes |p,p,...,p\rangle \tag{7.30}$$

of the total system, where each electron possesses the same momentum p. Moreover, we have assumed that the laser field initially is described by a photon number state with a photon number n which is much smaller than the number N of electrons, that is $n \ll N$. When we consider a SASE FEL the radiation starts from vacuum and we have to set $n = 0$. We note that, due to the transformations Eqs. (7.13) and (7.18), additional phase factors have emerged which, however, cancel when we calculate expectation values.

The operator $\hat{\Upsilon}_z$ is similar to an inversion operator for electrons in the excited state p and the ground state $p-q$ and its expectation value is bounded by $-N < \langle\hat{\Upsilon}_z(0)\rangle < N$. For the initial state, Eq. (7.30), where every electron occupies the excited state p this expectation value reaches its maximum and we find $\langle\hat{\Upsilon}_z(0)\rangle = N$ or alternatively $\langle\tilde{\Upsilon}_z(0)\rangle = 1$.

For short times, where only comparably few electrons switch to the ground state, we assume that $\tilde{\Upsilon}_z$ is approximately constant and thus we replace the operator $\tilde{\Upsilon}_z$ in Eq. (7.29) by its mean value, that is $\tilde{\Upsilon}_z \cong \langle\tilde{\Upsilon}_z(0)\rangle = 1$. Hence, we obtain the linearized equations

$$i\frac{\mathrm{d}}{\mathrm{d}\tau}\begin{pmatrix}\tilde{\Upsilon}_{1,0}\\ \tilde{a}_\mathrm{L}\end{pmatrix} = \begin{pmatrix}0 & -\alpha_N\\ \alpha_N & -\Delta\end{pmatrix}\begin{pmatrix}\tilde{\Upsilon}_{1,0}\\ \tilde{a}_\mathrm{L}\end{pmatrix} \tag{7.31}$$

which are analogous to the equations of motion of the quantum mechanical parametric amplifier [130].

We solve Eq. (7.31) with the ansatz $\sim \mathrm{e}^{-i\lambda\tau}$ yielding

$$\lambda_\pm = -\frac{\Delta}{2} \pm i\alpha_N\sqrt{1-\varkappa^2/4} \equiv -\frac{\Delta}{2} \pm i\alpha_N\,\vartheta(\Delta)\,. \tag{7.32}$$

with $\Delta \equiv \varkappa\alpha_N$ being small, that is $\varkappa \sim \mathcal{O}(1)$. We note the occurrence of a nonzero imaginary part of the frequency in Eq. (7.32). This contribution arises due to different signs of the off-diagonal elements in Eq. (7.31) which stands in contrast to the dynamical equations, Eq. (5.24), of the single-electron electron case, where the off-diagonal elements are both positive. Instead of Rabi oscillations we observe *exponential gain per pass* in the many-electron case, due to the nonzero imaginary part in Eq. (7.32). Hence, it is really possible to realize a high-gain FEL in the quantum regime.

The solution, Eq. (7.32), yields the time evolution of the laser field operator

$$\begin{aligned}\tilde{a}_{\mathrm{L}}(\tau)\,\mathrm{e}^{-i\Delta\tau/2} =& \frac{1}{i\vartheta(\Delta)}\sinh\left[\alpha_N\tau\vartheta(\Delta)\right]\tilde{\Upsilon}_{1,0}(0) \\ &+\left(\cosh\left[\alpha_N\tau\vartheta(\Delta)\right]-\frac{\Delta/(2\alpha_N)}{i\vartheta(\Delta)}\sinh\left[\alpha_N\tau\vartheta(\Delta)\right]\right)\tilde{a}_{\mathrm{L}}(0)\end{aligned} \tag{7.33}$$

which depends on the values of $\tilde{a}_{\mathrm{L}}$ and $\tilde{\Upsilon}_{1,0}$ at time $\tau = 0$.

Mean photon number

To calculate the gain of the Quantum FEL we consider the expectation value of the photon number operator $\hat{n} = \hat{a}_{\mathrm{L}}^{\dagger}\hat{a}_{\mathrm{L}}$. With the help of Eq. (7.33) we arrive at

$$\begin{aligned}\langle\hat{n}(\tau)\rangle =& \frac{1}{\vartheta(\Delta)^2}\sinh^2\left[g\tau\sqrt{N}\vartheta(\Delta)\right] \\ &+\left(\cosh^2\left[\alpha_N\tau\vartheta(\Delta)\right]+\frac{\Delta^2/(2\alpha_N)^2}{\vartheta(\Delta)^2}\sinh^2\left[\alpha_N\tau\vartheta(\Delta)\right]\right)\langle\hat{n}(0)\rangle\ ,\end{aligned} \tag{7.34}$$

where we have used that the expectation values $\langle\tilde{a}_{\mathrm{L}}^{\dagger}(0)\tilde{\Upsilon}_{1,0}(0)\rangle = \langle\tilde{\Upsilon}_{0,1}(0)\tilde{a}_{\mathrm{L}}(0)\rangle = 0$ vanish due to our choice, Eq. (7.30), for the initial state of electrons and laser field.
In the derivation of Eq. (7.34) we have to calculate also the expectation $\langle\tilde{\Upsilon}_{0,1}(0)\tilde{\Upsilon}_{1,0}(0)\rangle$ which requires a little more effort. For this purpose, we write

$$\langle\tilde{\Upsilon}_{0,1}(0)\tilde{\Upsilon}_{1,0}(0)\rangle = \frac{1}{N}\sum_j\langle p,p,...,p|\underbrace{\hat{\sigma}_{0,1}^{(j)}\hat{\sigma}_{1,0}^{(j)}}_{=\hat{\sigma}_{0,0}^{(j)}}|p,p,...,p\rangle + \frac{1}{N}\sum_{j\neq k}\langle p,p,...,p|\,\hat{\sigma}_{0,1}^{(j)}\hat{\sigma}_{1,0}^{(k)}\,|p,p,...,p\rangle\ , \tag{7.35}$$

where we have recalled the definition, Eq. (7.4), of the collective procjection operators and the relation Eq. (5.7) for products of single-electron operators. By applying the operators on the state $|p,p,...,p\rangle$

$$\langle\tilde{\Upsilon}_{0,1}(0)\tilde{\Upsilon}_{1,0}(0)\rangle = 1 + \frac{1}{N}\sum_{j\neq k}\underbrace{\langle p,...,(p-q)_j,...,p|p,...,(p-q)_k,...,p\rangle}_{=0} = 1 \tag{7.36}$$

we realize that only the first term in Eq. (7.36) gives a contribution to the expectation value while each scalar product in the second term vanishes since the momentum eigenstates are orthogonal.
The examination of Eq. (7.34) reveals that the time evolution of $\langle\hat{n}\rangle$ consists of two contributions: While the second term depends on the initial photon number $\langle\hat{n}(0)\rangle$, the first term is independent of this quantity. Hence, the photon number changes, even if the field starts from vacuum, that is $\langle\hat{n}(0)\rangle = 0$, which is the case for a SASE FEL. For this situation we derive from Eq. (7.34) the expression

$$\langle\hat{n}(T)\rangle = \frac{1}{1-\left(\Delta/(2\alpha_N)\right)^2}\sinh^2\left[gT\sqrt{N}\sqrt{1-\left(\frac{\Delta}{2\alpha_N}\right)^2}\right], \tag{7.37}$$

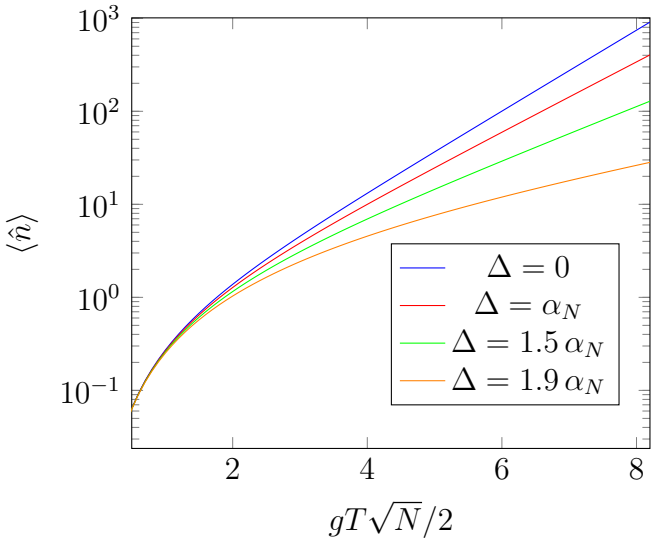

Figure 7.2: Mean value $\langle n\rangle$ of the photon number as function of the dimensionless time $gT\sqrt{N}/2$ for four different values of the deviation Δ from resonance ranging from $\Delta = 0$ to $\Delta = 1.9$. The logarithmic scale reveals an exponential growth of the photon number. Moreover, we obtain that the growth rate is maximized at resonance, $\Delta = 0$, while it strongly decreases for increasing values of Δ.

where we have transformed back to the original variables and have introduced the interaction time T. We note that Eq. (7.37) describes an exponentially growing photon number, which constitutes, besides the start-up from vacuum, one of the two necessary ingredients for a SASE FEL [21].

Gain function

In Fig. 7.2 we plot the photon number $\langle\hat{n}\rangle$, Eq. (7.37), as a function of time for different values of Δ. While the growth rate is small for a large deviation from resonance it is maximized for exact resonance $p = q/2$.
Since the imaginary part of λ, Eq. (7.32), that is

$$\mathrm{Im}\lambda = \alpha_N\sqrt{1 - \frac{\varkappa^2}{4}} \tag{7.38}$$

is responsible for the exponential growth of the photon number we identify the dependency of $\mathrm{Im}\lambda$ on the initial momentum p via $\Delta \equiv \varkappa\alpha_N$ as the gain function of the high-gain Quantum FEL in analogy to the classical case, studied in Chap. 2.
We have drawn this function, Eq. (7.38), on the right-hand side of Fig. 7.3 and obtain that the gain is maximized at resonance $p = q/2$ as already expected from Fig. 7.2. This behavior stands in contrast to the corresponding function in the classical case, shown on the left-hand side of Fig. 7.3, which has its maximum at $p = 0$. Moreover, the broad curve of the classical FEL covers multiples of the recoil q while the gain function of the Quantum FEL is very sharp.

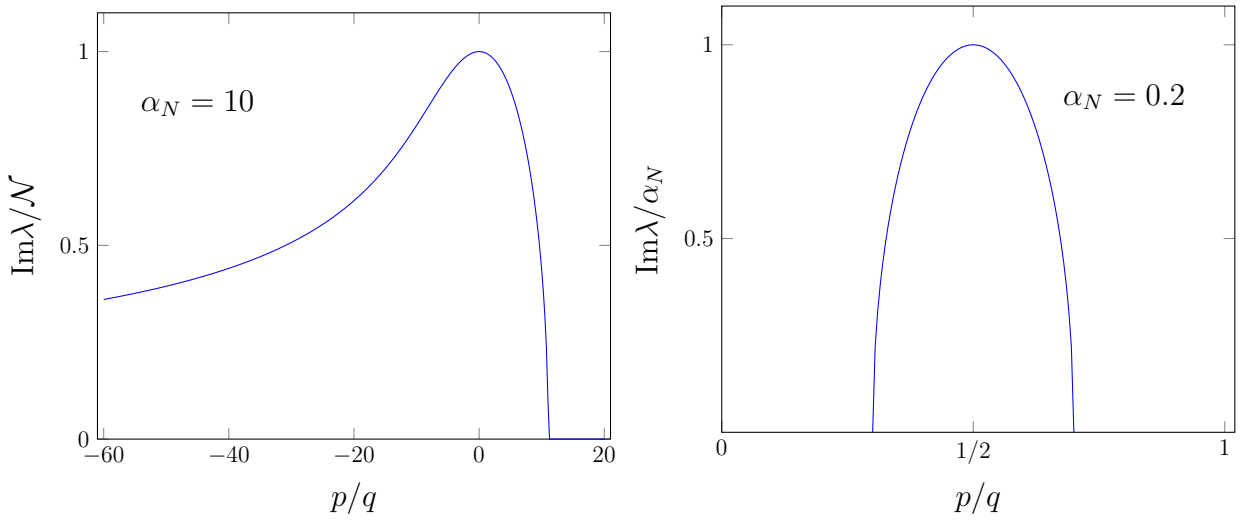

Figure 7.3: Comparison of the gain functions, that is Imλ over the initial momentum p, for the classical (left) and the Quantum FEL (right) in the high-gain regime. While in the classical regime, $\alpha_N = 10$, the numerical solution of Eq. (2.76) yields the momentum for the maximum at $p = 0$, the gain of the Quantum FEL, $\alpha_N = 0.2$, is maximized at $p = q/2$, according to Eq. (7.38). Moreover, the function in the classical case is broad and covers multiples of the recoil q, which stands in contrast to the quantum regime characterized by a sharp resonance.

In Ref. [25] a numerical approach revealed a similar structure of the gain function of a high-gain Quantum FEL. In contrast, we have found a very simple analytic expression, Eq. (7.38), for this gain function due to the identification of the effective electron dynamics with a two-level system. At the end of this chapter we come back to this aspect when we consider higher-order corrections to the deep quantum regime.

Gain length

The growth of the photon number $\langle\hat{n}\rangle$ at resonance $\Delta = 0$ is proportional to $\exp\left(2gT\sqrt{N}\right)$. Therefore, we can define the gain length in accordance with the classical FEL theory [48] in Chap. 2 as

$$L_g \equiv \frac{c}{2g\sqrt{N}}\,, \tag{7.39}$$

where we have set $L \cong cT$. The naive comparison with the corresponding classical quantity L_g^{cl}, Eq. (2.78), yields

$$\frac{L_g}{L_g^{\mathrm{cl}}} = \frac{\sqrt{3}}{2^{2/3}}\frac{1}{\alpha_N^{1/3}} \gg 1\,, \tag{7.40}$$

that is the gain length of a Quantum FEL is much larger than expected from a classical theory.

In order to clarify the experimental implications imposed by the expression in Eq. (7.39) for the gain length of a Quantum FEL we write L_g in the following in terms of the laboratory

frame. By this procedure we arrive at

$$L_g = \frac{\gamma_0^2}{\sqrt{\pi}} \frac{\sqrt{\lambda_\mathrm{C}/r_\mathrm{e}}}{a_0\sqrt{1+a_0^2}} \frac{1}{\sqrt{\lambda_\mathrm{W} n_\mathrm{e}}}\,, \tag{7.41}$$

according to Tab. A.2. For the quantum regime we additionally require [4]

$$\alpha_N = \frac{1}{\gamma_0^3} \frac{a_0(1+a_0^2)^{3/2}\sqrt{r_e n_e}}{32\sqrt{\pi}} \frac{\lambda_\mathrm{W}^{5/2}}{\lambda_\mathrm{C}^{3/2}} \ll 1\,, \tag{7.42}$$

as well as $\Delta p < q$, which translates to [28]

$$\frac{\Delta\gamma_0}{\gamma_0} < \frac{4\gamma_0}{1+a_0^2}\frac{\lambda_\mathrm{C}}{\lambda_\mathrm{W}} \tag{7.43}$$

in the laboratory frame.
To achieve a small value for α_N we need, according to Eq. (7.42), a high energy γ_0 and a small wiggler wavelength λ_W which makes it moreover easier to satisfy the condition, Eq. (7.43). However, L_g scales with γ_0^2, that is, a high energy leads to an increasing gain length and eventually to an unfeasible wiggler length. This problem does not arise in this form for the classical case since the classical gain length [48]

$$L_g^\mathrm{cl} = \frac{1}{\sqrt{3}} \frac{\gamma_0 \lambda_\mathrm{W}^{1/3}}{2\pi^{2/3}(r_e a_0^2 n_e)^{1/3}}\,, \tag{7.44}$$

which we have recalled from Tab. A.1, scales only linearly in γ_0 and the constraints Eqs. (7.42) and (7.43) do not have to be satisfied. We note that the present discussion about wiggler lengths and experimental requirements in the quantum and in the classical regime is very similar to the one in Chap. 6 for the low-gain FEL.

Variance of photon number

Having investigated the gain of a high-gain Quantum FEL we now briefly study the statistical behavior of the radiation. In analogy to the low-gain regime, Chap. 6, we introduce the dimensionless variance

$$\sigma^2(T) \equiv \frac{\langle \hat{n}^2(T)\rangle - \langle \hat{n}(T)\rangle^2}{\langle \hat{n}(T)\rangle} \tag{7.45}$$

as the ratio of the variance and the mean value of the photon number $\hat{n}$.
When we start from vacuum, that is $\langle \hat{n}(0)\rangle = 0$, we obtain the expression

$$\sigma^2(T) = \cosh^2\left[gT\sqrt{N}\sqrt{1-\varkappa^2/4}\right] + \frac{\varkappa/2}{1-\varkappa^2/4}\sinh^2\left[gT\sqrt{N}\sqrt{1-\varkappa^2/4}\right], \tag{7.46}$$

where we have inserted the solution for $\hat{a}_\mathrm{L}$, Eq. (7.33), into the definition, Eq. (7.45), and have caluclated the expectation values with respect to the initial state, Eq. (7.30). We note that the expression in Eq. (7.46) emerges from a contribution with $\hat{a}_\mathrm{L}(0)\hat{a}_\mathrm{L}^\dagger(0) = \hat{n}(0) + 1$

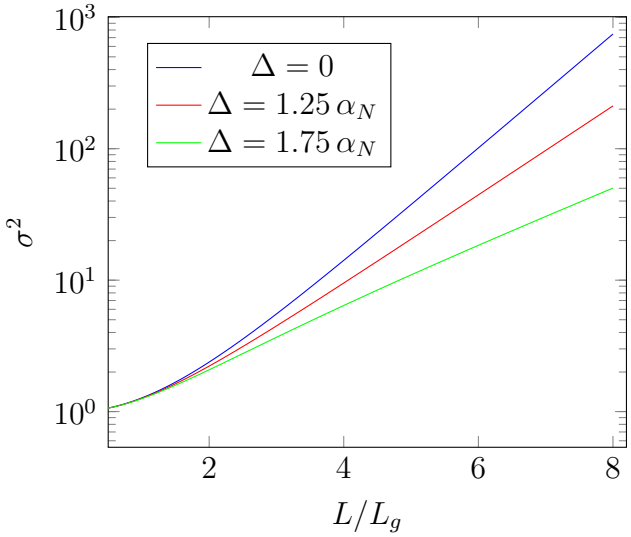

Figure 7.4: Normalized variance σ^2, Eq. (7.46), of the photon number for a high-gain Quantum FEL in the exponential gain regime and for start-up from vacuum, $\langle \hat{n}(0) \rangle = 0$, as a function of the wiggler length L. We observe an exponential growth of σ^2, that is, the super-Poissonian character of the radiation increases along the wiggler. Moreover, we investigate the influence for nonzero values of the deviation Δ from resonance, by comparing the resonant case $\Delta = 0$ to two off-resonant situations with $\Delta = 1.25\,\alpha_N$ and $\Delta = 1.75\,\alpha_N$, respectively. Indeed, the growth of σ^2 slows down for higher values of Δ, but so does the growth of the photon number $\langle \hat{n} \rangle$ according to Fig. 7.2.

which results in a nonzero expectation value, even for $\langle \hat{n}(0) \rangle = 0$. Moreover, we deal with a term proportional to $\langle \hat{\Upsilon}_{0,1} \hat{\Upsilon}_{1,0} \hat{\Upsilon}_{0,1} \hat{\Upsilon}_{1,0} \rangle_0 = N^2$, which can be calculated analogously to $\langle \hat{\Upsilon}_{0,1} \hat{\Upsilon}_{1,0} \rangle$ in Eq. (7.35). This term proportional to N^2 cancels with the contribution from $\langle \hat{n}(T) \rangle^2$ in the definition, Eq. (7.45), of σ^2.

In Fig. 7.4 we have drawn the normalized variance σ^2 as a function of the length L of the wiggler. We obtain that σ^2 exponentially grows with L and is of the order of $\langle \hat{n} \rangle$. Hence, the radiation from the high-gain Quantum FEL due to a single passage of the electrons shows a chaotic behavior [130].

For increasing deviation Δ from resonance the growth of σ^2 becomes more slowly. However, so does the growth of the mean photon number $\langle \hat{n} \rangle$ according to Fig. 7.2. Indeed, we obtain with the help of Eqs. (7.34) and (7.46) the asymptotic behavior

$$\frac{\sigma^2(T)}{\langle \hat{n}(T) \rangle} = \coth^2 \left[gT\sqrt{N}\sqrt{1 - \varkappa^2/4} \right] + \frac{\varkappa^2}{4} \frac{1}{\sinh^2 \left[gT\sqrt{N}\sqrt{1 - \varkappa^2/4} \right]} \to 1 \tag{7.47}$$

for large T. Hence, the dimensionless variance σ^2 is always of the order of the mean value $\langle \hat{n} \rangle$, no matter how large the deviation from resonance is, and thus the light field can always be considered as chaotic.

Validity of parametric approximation

Before we turn to the time evolution of the Quantum FEL for longer times we emphasize that the linearization of the Heisenberg equations, Eq. (7.29), is only valid for short times. Physically, it is clear that an infinite growth of the photon number violates energy conservation. In our approximation we have neglected that the electrons do not just emit but also absorb photons from the field. Hence, we expect a saturation of the growth for longer times and eventually an oscillatory behavior in rough analogy to the Rabi oscillations in Chap. 5.
We assume that our approximation breaks down when the number n of photons in the field is of the order of the number N of electrons, which means that a great fraction of the electrons has emitted a photon. Equivalently, our linearization procedure is valid as long as we can consider the operator $\tilde{\Upsilon}_z$ as a constant. To understand the dynamics of $\tilde{\Upsilon}_z$ it is convenient to use the Schwinger representation [132]. With the help of Eqs. (7.27) and (7.29) we obtain

$$\frac{\mathrm{d}}{\mathrm{d}\tau}\tilde{\Upsilon}_z \sim \frac{\alpha_N}{N^{3/2}}\hat{a}_\mathrm{L}\hat{b}_0^\dagger\hat{b}_1\,, \tag{7.48}$$

where $\hat{b}_0^\dagger$ and $\hat{b}_1$ describe an effective population of the excited p and the ground state $p-q/2$, respectively [128].
For short times only few photons have been emitted and the population of the laser mode and of the ground state of the electrons is small, that is $\hat{a}_\mathrm{L}, \hat{b}_1 \sim \mathcal{O}(1)$. On the other hand, nearly all electrons are in the excited state yielding $\hat{b}_0^\dagger \sim \sqrt{N}$. From Eq. (7.48) we obtain the scaling $\mathrm{d}\tilde{\Upsilon}_z/\mathrm{d}\tau \sim \alpha_N/N$, while the change of $\tilde{a}_\mathrm{L}$ and $\tilde{\Upsilon}_{1,0}$ scales with α_N according to Eq. (7.29). Hence, the dynamics of $\tilde{\Upsilon}_z$ occurs with a rate that is suppressed with $1/N$ when compared to $\tilde{a}_\mathrm{L}$ and $\tilde{\Upsilon}_{1,0}$ which justifies our assumption to treat $\tilde{\Upsilon}_z$ as a constant.
Time evolution leads to a growth of the photon number, Eq. (7.37), and more electrons switch to the ground state. At some point in time the number of excitations in the laser mode and in the ground state becomes comparable with the number of excitations in the excited state, that is $\hat{a}_\mathrm{L}, \hat{b}_1, \hat{b}_0^\dagger \sim \sqrt{N}$. From Eq. (7.48) we deduce $\mathrm{d}\tilde{\Upsilon}_z/\mathrm{d}\tau \sim \alpha_N$, which means that the dynamics of $\tilde{\Upsilon}_z$ now occurs on the same time scale as the one of $\tilde{a}_\mathrm{L}$ and $\tilde{\Upsilon}_{1,0}$, respectively, and we cannot approximate $\tilde{\Upsilon}_z$ as constant any longer. This analysis supports our expectation that the linearization of Eq. (7.29) is valid only as long as the condition $\langle\hat{n}(\tau)\rangle \ll N$ is satisfied.

7.2.3 Long-time behavior

In order to study the dynamics of the high-gain Quantum FEL beyond the short-time limit we apply two approaches in the following: (i) an analytic approach which gives us estimates for gain and saturation of the FEL and (ii) a numerical one which confirms at least the order of magnitude and the qualitative behavior derived from the analytic model. In this context, we study the maximum intensity and the wiggler length corresponding to the first local maximum as well as the influence of a deviation from resonance.

Analytic approach

Despite several approaches [128, 133, 134, 135, 136] in the literature the equations of motion corresponding to the Dicke Hamiltonian cannot be solved in an analytic way, especially for

our situation of interest, where the radiation field starts from vacuum and all two-level atoms occupy the excited state. However, there exists an approximate solution which gives us, at least qualitatively, the correct behavior for the dynamics. The derivation of this solution, which we present in the following, is based on the ideas developed in Refs. [128] and [135]. In addition to these approaches, we include off-resonant situations, that is nonzero values for Δ.

Again, we focus on the time evolution of the photon number of the laser field described by the operator $\hat{n} = \hat{a}_{\mathrm{L}}^{\dagger}\hat{a}_{\mathrm{L}}$. When we differentiate $\hat{n}$ with respect to time τ and take care of the correct operator ordering we obtain the relation

$$\frac{\mathrm{d}}{\mathrm{d}\tau}\hat{n} = i\varepsilon\left(\hat{a}_{\mathrm{L}}\hat{\Upsilon}_{0,1} - \hat{a}_{\mathrm{L}}^{\dagger}\hat{\Upsilon}_{1,0}\right) = -\frac{1}{2}\frac{\mathrm{d}}{\mathrm{d}\tau}\hat{\Upsilon}_{z}\,, \tag{7.49}$$

where we have used Eq. (7.25). Hence, we define the operator

$$\hat{B} \equiv \hat{n} + \frac{1}{2}\hat{\Upsilon}_{z} = \mathrm{const} \tag{7.50}$$

which is a constant of motion. Another constant operator is given by

$$\hat{A} \equiv \left(\hat{\Upsilon}_{0,1}\hat{\Upsilon}_{1,0} + \hat{\Upsilon}_{1,0}\hat{\Upsilon}_{0,1}\right) + \frac{1}{2}\hat{\Upsilon}_{z}^{2} = \mathrm{const} \tag{7.51}$$

which can be verified by differentiating $\hat{\Upsilon}_{0,1}\hat{\Upsilon}_{1,0} + \hat{\Upsilon}_{1,0}\hat{\Upsilon}_{1,0}$ with respect to time τ and applying Eq. (7.25). We note that $\hat{A}$ and $\hat{B}$ commute, that is $\left[\hat{A},\hat{B}\right] = 0$. Due to the time-independence of $\hat{H}_{\mathrm{eff}}$, Eq. (7.23), this Hamiltonian itself constitutes a third constant of motion.

By a further differentiation with respect to time τ and with the help of the constants of motion $\hat{A}$, $\hat{B}$ and $\hat{H}_{\mathrm{eff}}$ we can decouple the dynamics of $\hat{n}$ from the other time-dependent operators. The resulting equation of motion for $\hat{n}$ reads

$$\frac{\mathrm{d}^2\hat{n}}{\mathrm{d}\tau^2} = -2\varepsilon^2\left[3\hat{n}^2 - 2\left(2\hat{B} - \left(\frac{\Delta}{2\varepsilon}\right)^2 - \frac{1}{2}\right)\hat{n} - \left(\frac{1}{2}\hat{A} + \hat{B} - \hat{B}^2 - \frac{\Delta}{2\varepsilon}\hat{H}_{\mathrm{eff}}^{(1)}\right)\right]\,, \tag{7.52}$$

where we have used Eq. (7.25) as well as the definitions Eqs. (7.23) , (7.51) and (7.50) of $\hat{H}_{\mathrm{eff}} \equiv \varepsilon\hat{H}_{\mathrm{eff}}^{(1)}$, $\hat{A}$ and $\hat{B}$, respectively.

Although Eq. (7.52) only depends on $\hat{n}$ it is nevertheless a nonlinear differential equation for operators instead of numbers. Hence, we cannot find an analytic solution for Eq. (7.52) since it is nontrivial to obtain the correct operator ordering. For example, $\hat{n}$ and $\mathrm{d}\hat{n}/\mathrm{d}\tau$ do not necessarily commute with each other. However, by replacing the operators by numbers we might get a rough estimate for the dynamics of the Quantum FEL.

Hence, we set the operators $\hat{n}$, $\hat{A}$, $\hat{B}$, and $\hat{H}_{\mathrm{eff}}^{(1)}$ in Eq. (7.52) equal to their corresponding expectation values. Multiplying the resulting c-number equation with $2\mathrm{d}n/\mathrm{d}\tau$ and integrating by parts yields the first-order differential equation

$$\left(\frac{\mathrm{d}n}{\mathrm{d}\tau}\right)^2 = -4\varepsilon^2 n\left[n^2 - \left(B - \left(\frac{\Delta}{2\varepsilon}\right)^2 - \frac{1}{2}\right)n - \left(\frac{A}{2} + B - B^2 - \frac{\Delta}{2\varepsilon}H_{\mathrm{eff}}^{(1)}\right)\right]\,, \tag{7.53}$$

where we have introduced the abbreviations $n \equiv \langle \hat{n} \rangle$, $A \equiv \langle \hat{A} \rangle$, $B \equiv \langle \hat{B} \rangle$ and $H_{\text{eff}}^{(1)} \equiv \langle \hat{H}_{\text{eff}}^{(1)} \rangle$. In addition, we have assumed that the laser field starts at vacuum, that is $n(0) = 0$, and have assumed that the change of the photon number n with time τ initially as well is equal to zero, that is $(\mathrm{d}n/\mathrm{d}\tau)_{\tau=0} = 0$. The second assumption is justified since the short-time solution, Eq. (7.37), also shows this feature. We emphasize that this derivation is analogous to the one presented in Ref. [128] for the Dicke model except that there the authors used the Schwinger representation leading to different constants A and B and hence to a slightly different form of Eq. (7.53). Moreover, they did not consider a nonzero deviation Δ from resonance.

Since A, B, and $H_{\text{eff}}^{(1)}$ are constants of motion their magnitude does not change with respect to their corresponding initial value. For the initial condition Eq. (7.30) we straightforwardly calculate the expectation values at time $\tau = 0$ yielding the expressions

$$A = \langle \hat{A}(0) \rangle = N + \frac{N^2}{2}\,, \tag{7.54}$$

$$B = \langle \hat{B}(0) \rangle = \frac{N}{2}\,, \tag{7.55}$$

and

$$H_{\text{eff}}^{(1)} = \langle \hat{H}_{\text{eff}}(0) \rangle = 0\,, \tag{7.56}$$

where we have used Eq. (7.36) to compute the value of A in Eq. (7.54). Inserting Eqs. (7.54), (7.55) and (7.56) into Eq. (7.53) and factorizing finally leads us to

$$\left(\frac{\mathrm{d}n}{\mathrm{d}\tau}\right)^2 = 4\varepsilon^2 n(n_+ - n)(n + n_-) \tag{7.57}$$

with

$$n_\pm \equiv \pm\frac{N}{2}\left(1 - \frac{\varkappa^2}{4}\right) \mp \frac{1}{4} + \frac{N}{2}\left(1 - \frac{\varkappa^2}{4}\right)\sqrt{1 + \frac{1}{N}\frac{3 + \varkappa^2/4}{1 - \varkappa^2/4} + \frac{1}{4N^2}\frac{1}{1 - \varkappa^2/4}} \tag{7.58}$$

as the roots of the right-hand side of Eq. (7.57).

By setting $\mathrm{d}n/\mathrm{d}\tau = 0$ in Eq. (7.57) we identify the maximum photon number

$$n_{\max} = n_+ \cong N\left(1 - \frac{\varkappa^2}{4}\right)\,, \tag{7.59}$$

where we have assumed that $N \gg 1$. For resonance, $\Delta = 0$, we obtain $n^{\max} = N$, that is each electron has emitted exactly one photon into the field. According to Eq. (7.59) the value of this maximum decreases when we have a nonzero deviation Δ from resonance. The other two solutions of $\mathrm{d}n/\mathrm{d}\tau = 0$, which are $n = 0$ and $n = -n_- \cong -(1 - \varkappa^2/4)^{-1}$, correspond to the initial condition and to an unphysical negative photon number, respectively. The differential equation, Eq. (7.57), can be recast as an elliptic integral

$$2\alpha_N \tau = \int_0^{n/N} \frac{\mathrm{d}y}{\sqrt{(n_+/N - y)y(y + n_-/N)}} \tag{7.60}$$

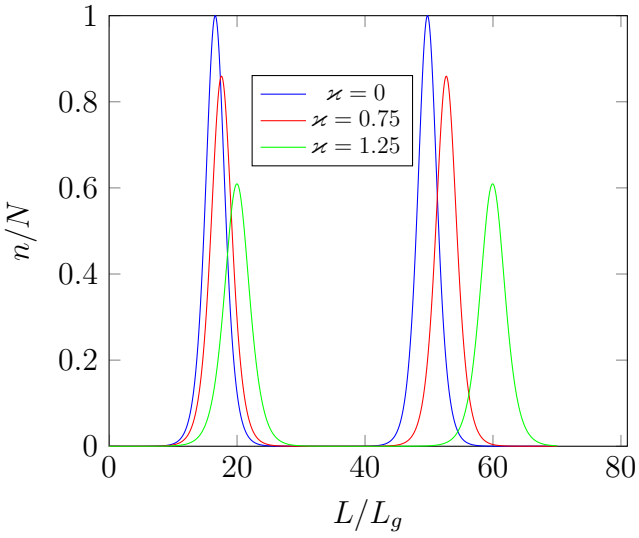

Figure 7.5: Number n of photons in the laser field as a function of the length L of the wiggler in multiples of the gain length L_g, Eq. (7.39), according to the approximation in Eq. (7.61), for three different values of the deviation $\Delta \equiv \varkappa\alpha_N$ from resonance and with $N = 10^6$ electrons in the bunch. For exact resonance the maximum photon number $n_{\max}$ equals the electron number N. For off-resonant situations $n_{\max}$ is smaller than N as predicted by Eq. (7.59). Moreover, the length $L_{\max}$, corresponding to the first maximum, increases with Δ.

which we solve in terms of Jacobian elliptic functions [128, 135, 137]. In App. F we derive for $N \gg 1$ the expression

$$n(T) \cong N\left(1-\frac{\varkappa^2}{4}\right)\mathrm{cn}^2\left[gT\sqrt{N}\sqrt{1-\frac{\varkappa^2}{4}}-K,k\right], \tag{7.61}$$

where cn denotes an elliptic function with modulus

$$k \equiv \left(1+\frac{1}{N}\frac{1}{(1-\varkappa^2/4)^2}\right)^{-1/2} \tag{7.62}$$

while

$$K \equiv K(k) \equiv \int_0^{\pi/2}\frac{\mathrm{d}y}{\sqrt{1-k^2\sin^2 y}} \tag{7.63}$$

represents a complete elliptic integral of the first kind [137].

The square of the elliptic function cn oscillates between $\mathrm{cn}^2(-K)=0$ and $\mathrm{cn}^2(0)=1$ [137] and thus we obtain the expected behavior for the photon number n: The field starts from vacuum $n(0)=0$ and undergoes an exponential growth, Eq. (7.37), for short times [135]. For longer times this growth saturates leading to a local maximum with $n_{\max} = N(1-\varkappa^2/4)$, which is already predicted in Eq. (7.59). This behavior is illustrated in Fig. 7.5, where we have shown the estimation, Eq. (7.61), of n as a function of the wiggler length L. For increasing

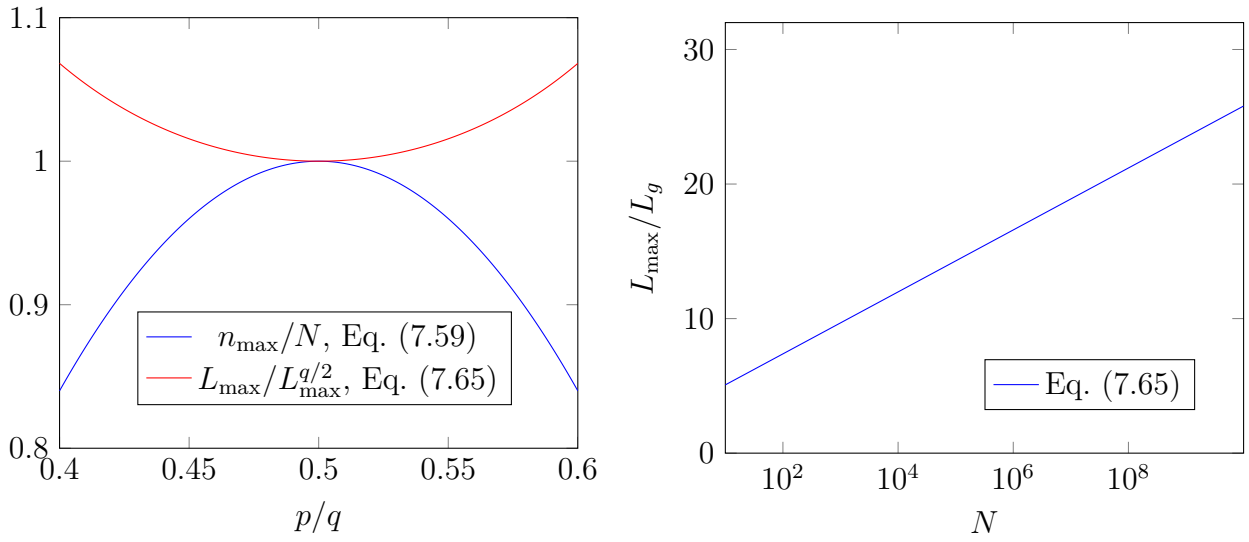

Figure 7.6: Left-hand side: the position $L_{\max}$ (red line) and magnitude $n_{\max}$ of the first maximum of the photon number n, Eq. (7.61), according to Eqs. (7.65) and (7.59) as functions of the initial momentum p of the electrons. We observe that $L_{\max}$ increases and that $n_{\max}$ decreases when we increase the deviation from resonance $p = q/2$. We have already expected this behavior from the inspection of Fig. 7.5. Right-hand side: the position $L_{\max}$, Eq. (7.65), of the first maximum as a function of the number N of electrons. We observe a logarithmic growth of $L_{\max}$ reaching values between 20 and 30 times the gain length L_g for more realistic numbers N of electrons.

values of the deviation Δ from resonance the maximum $n_{\max}$ of the photon number decreases while its position $L_{\max}$ along the wiggler axis increases.
The first maximum of Eq. (7.61) is obtained for

$$gT_{\max}\sqrt{N+1}\sqrt{1-\frac{\varkappa^2}{4}} = K \cong \ln\left[4\sqrt{N}\left(1-\frac{\varkappa^2}{4}\right)\right]. \tag{7.64}$$

The approximation in the second step is valid for $k \to 1$, Eq. (F.5), [137] which, according to Eq. (7.62), is satisfied for a high number $N \gg 1$ of electrons and a low-to-moderate value of the deviation $\varkappa < 2\sqrt{1-N^{-1/2}}$ from resonance. In terms of the gain length L_g, Eq. (7.39), we thus obtain the expression

$$\frac{L_{\max}}{L_g} \cong \frac{1}{\sqrt{1-\frac{\varkappa^2}{4}}}\left[\ln N + 4\ln 2 + 2\ln\left(1-\frac{\varkappa^2}{4}\right)\right] \tag{7.65}$$

for the length $L_{\max}$ of the wiggler for which this first maximum of the photon number occurs. Besides the dependency on the electron number N, $L_{\max}$ is a function of the deviation $\Delta = \varkappa\alpha_N$ from resonance.
On the left-hand side of Fig. 7.6 we have illustrated the dependency of the maximum photon number $n_{\max}$ and of its position $L_{\max}$ along the wiggler axis on the initial momentum p of

the electrons, according to Eqs. (7.59) and (7.65), respectively. Indeed, we find that $n_{\max}$ is maximized and $L_{\max}$ is minimized at resonance $p = q/2$, as already expected from the inspection of Fig. 7.5. On the right-hand side of Fig. 7.6 we have shown the dependency of $L_{\max}$ on N which is logarithmic according to Eq. (7.65). For a realistic number $N \sim 10^9$ of electrons the position of this maximum is at about 20 to 30 gain lengths L_g.

Interpreting the dimensionless intensity, Eq. (2.81), of the saturated classical FEL in the high-gain limit as maximum photon number, we obtain the expression

$$n_{\max}^{\mathrm{cl}} \cong \frac{2^{1/3}\alpha_N^{2/3}}{3} N \tag{7.66}$$

in terms of the quantum parameter α_N, Eq. (7.22). Due to $\alpha_N \gg 1$ we find that in the classical FEL an electron emits *many* photons which stands in contrast to the Quantum FEL where maximally *one* photon is emitted by an electron. However, if we let $\alpha_N \ll 1$ in Eq. (7.66) we recognize that the classical theory would underestimate the maximum photon number in the quantum regime which is given by $n_{\max} = N$. We moreover note that the direct proportionality of $n_{\max}$ to N in the quantum regime is a further difference to the classical regime, where the maximum intensity scales with $N^{4/3}$.

The position of the maximum intensity for the classical FEL is in Chap. 2 estimated by $L_{\max}^{\mathrm{cl}} \cong 4\pi\sqrt{3}L_g^{\mathrm{cl}}$ which is of the order of 10 to 20 gain lengths [73]. This behavior is similar to the Quantum FEL by the inspection of the right-hand side of Fig. 7.6. However, the explicit expressions for the gain length in the respective regimes differ.

We end this discussion by noting that it is questionable to talk about 'photon numbers' since we have switched to a kind of a semi-classical theory when we replaced the operators by numbers. Moreover, the classical number $n_{\max}^{\mathrm{cl}}$ is derived in a complete classical theory, where the term 'photon' is not admissible. Instead, we should talk about 'dimensionless intensities'. However, the picture of photons is very helpful in the context of a comparison between quantum and classical regime of the FEL which justifies our choice of words.

Numerical approach

In order to verify the estimates, we have derived in the preceding section in an analytic manner, we proceed to solve the dynamics of the deep quantum regime numerically. For this purpose, we rewrite the Schrödinger equation corresponding to the effective Hamiltonian, Eq. (7.23), into a suitable form in analogy to Ref. [134]. Then, we straightforwardly solve the resulting system of differential equations like in Ref. [138].

By considering the commutation relation, Eq. (7.5), for $\hat{\Upsilon}_{0,1}$, $\hat{\Upsilon}_{1,0}$ and $\hat{\Upsilon}_z$, yielding for example $\left[\hat{\Upsilon}_{0,1}, \hat{\Upsilon}_{1,0}\right] = \hat{\Upsilon}_z$, we recognize that this operators algebra is equivalent to the one for angular momentum [114, 134]. Indeed, we make the identifications

$$\begin{cases} \hat{J}_+ &= \hat{\Upsilon}_{0,1} \\ \hat{J}_- &= \hat{\Upsilon}_{1,0} \\ \hat{J}_z &= \frac{1}{2}\hat{\Upsilon}_z\,, \end{cases} \tag{7.67}$$

where $\hat{J}_+$ and $\hat{J}_-$ denote ladder operators while $\hat{J}_z$ represents the angular momentum in z-direction [139]. Moreover, we obtain that the constant of motion $\hat{A}$, defined in Eq. (7.51), corresponds to the total angular momentum $\hat{\boldsymbol{J}}$, that is, $\hat{A} = \hat{\boldsymbol{J}}^2$.

To derive a suitable expression for the dynamics of the system we expand the state vector $|\Psi\rangle$ in terms of the basis $|n, m, r\rangle$, where $|n\rangle$ is a photon number state of the laser field while $|m, r\rangle$ correspond to the total angular momentum and its z-component fulfilling the relations [139]

$$\begin{cases} \hat{\boldsymbol{J}}^2 |m, r\rangle &= r(r+1)\,|m, r\rangle \\ \hat{J}_z\,|m, r\rangle &= m\,|m, r\rangle\ . \end{cases} \tag{7.68}$$

Since the total angular momentum $\hat{\boldsymbol{J}}^2$, as well as $\hat{B} = \hat{J}_z + \hat{n}$, Eq. (7.50), are conserved the dynamics is characterized by just a single quantum number. With the help of Eq. (7.68) we deduce from Eq. (7.54) as well as from Eq. (7.55) the relations $r = N/2$ as well as $m + n = N/2$, respectively. Hence, we write the total state

$$|\Psi(\tau)\rangle \equiv \sum_{n=0}^{N} c_n(\tau) \Big| n, \frac{N}{2} - n, \frac{N}{2} \Big\rangle \equiv \sum_{n=0}^{N} c_n(\tau)\,|n\rangle \tag{7.69}$$

in terms of the photon number n which varies between $n = 0$ and $n = N$ due to $-N/2 \leq m \leq N/2$. Here, c_n denotes the expansion coefficient corresponding to the basis state $|n\rangle \equiv |n, N/2 - n, N/2\rangle$.

The action of a ladder operator on a state $|n, m, r\rangle$ is described by the relation [139]

$$\hat{J}_\pm\,|m, r\rangle = \sqrt{(r \pm m + 1)(r \mp m)}\,|m \pm 1, r\rangle\ , \tag{7.70}$$

that is, by a shift of the magnetic quantum number m while preserving the total angular momentum r. Applying Eq. (7.70) to the Schrödinger equation with the Hamiltonian, Eq. (7.23), and the state in Eq. (7.69) yields the set of differential equations [134, 138]

$$i\frac{\mathrm{d}}{\mathrm{d}\tau} c_n(\tau) = \alpha_N \left(-\varkappa n\, c_n(\tau) + (n+1)\sqrt{1 - \frac{n}{N}}\, c_{n+1}(\tau) + n\sqrt{1 - \frac{n-1}{N}}\, c_{n-1}(\tau) \right) \tag{7.71}$$

which couples the expansion coefficients c_n in a trilinear manner. The initial condition of Eq. (7.71) is given by $c_n(0) = \delta_{n,0}$ which corresponds to the state $|0, N/2, N/2\rangle$.

For the time being we investigate the resonant case, $\Delta = 0$. In Fig. 7.7 we have drawn the mean photon number $\langle \hat{n} \rangle$ of the high-gain Quantum FEL as a function of the wiggler length L for $N = 10^3$ (left) and $N = 10^4$ (right) electrons, respectively. In both cases the value of the first maximum $n_{\max} \cong 0.8\,N$ emerging from the numerical solution of Eq. (7.71) is lower as predicted by the estimation from Eq. (7.59), that is $n_{\max} = N$. Moreover, we obtain that the second maximum is further suppressed compared to the complete revival predicted in the approximation, Eq. (7.61). When we compare the actual positions of these maxima with the estimated ones we also find a small shift.

In Fig. 7.8 we have presented the change of the maximum photon number $n_{\max}$ and the position $L_{\max}$ of this maximum when we vary the number N of electrons. The numerically computed curve for $L_{\max}$ is slightly higher than the estimated one, Eq. (7.65), but both

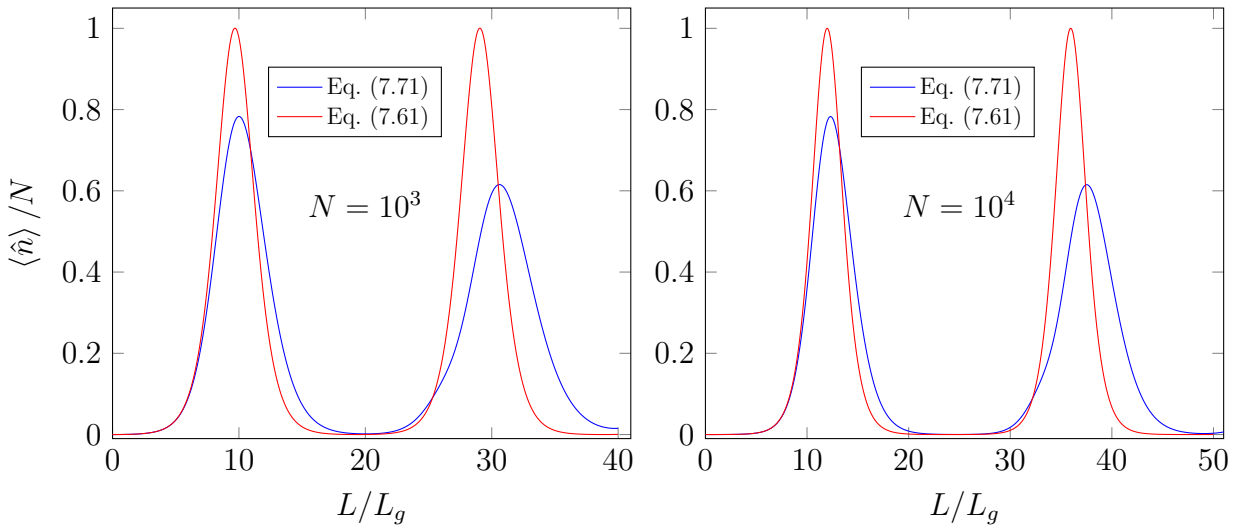

Figure 7.7: Comparison of numerics and analytic approximation: we have plotted the expectation value $\langle \hat{n} \rangle$ of the photon number in the high-gain Quantum FEL for resonance, $\Delta = 0$, against the wiggler length L for $N = 10^3$ (left) and $N = 10^4$ (right) electrons, respectively. The analytic solution (red line), Eq. (7.61), overestimates the maximum photon number which is in both cases at about $n_{\max} \cong 0.8\, N$, according to the numerical solution (blue line) of Eq. (7.71). Moreover, instead of a complete revival of the first maximum as predicted by Eq. (7.61) the height of the second peak is smaller than the first one. The estimated positions of the first maxima, Eq. (7.65), are also slightly shifted to the left in comparison to the exact ones.

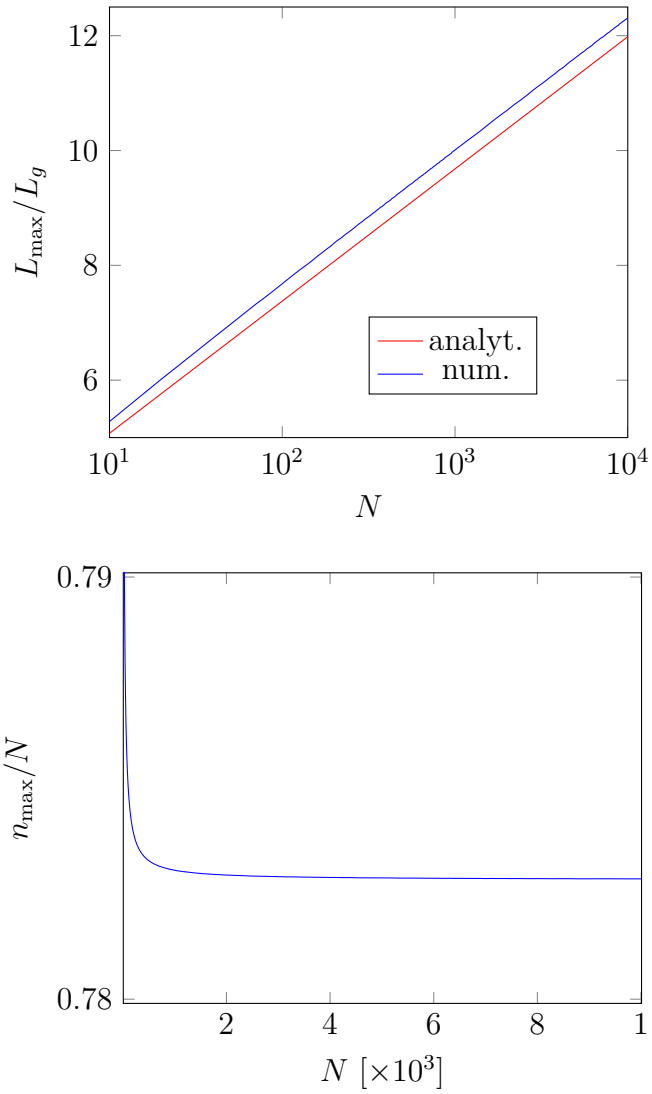

Figure 7.8: Above: we have drawn the position of the first maximum as a function of the electron number N for resonance, $\Delta = 0$, and compare the analytic approximation (red line), Eq. (7.65), to the numerical solution (blue line) of Eq. (7.71). Although the numerical curve lies slightly above the analytic one, the growth with N is very similar for both curves. Below: we have plotted the maximum number of photons $n_{\max}$ from the numerical simulation of Eq. (7.71) against the number N of electrons. The maximum photon number reaches the value $n_{\max} \cong 0.78\, N$ already for a small N which then approximately stays constant and thus is smaller than the corresponding value $n_{\max} = N$ from the analytic approach. We emphasize, that in both cases we have only considered values for the electron number up to $N = 10^4$.

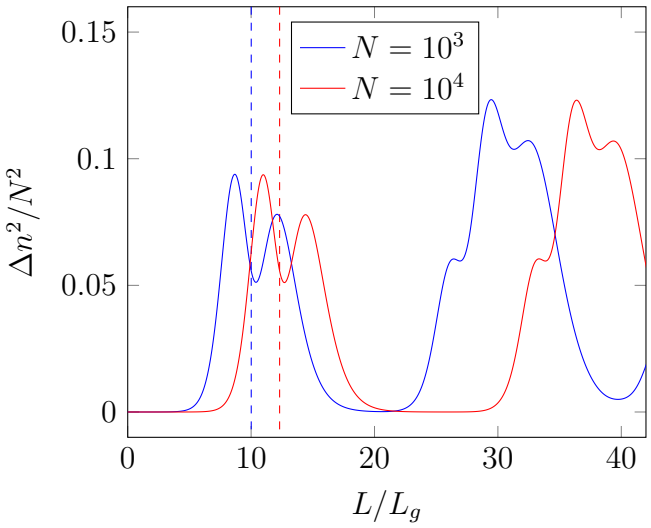

Figure 7.9: Numerical simulation of the variance Δn^2 of the photon number in a high-gain Quantum FEL for resonance $p = q/2$ as a function of the wiggler length L for $N = 1000$ (blue lines) and $N = 10000$ electrons in the bunch, respectively. We note that for increasing N the curve is shifted to the right similar to behavior of the mean photon number, Fig. 7.7, where $L_{\max}$ (dashed lines) increases for larger N. In both cases the variance maximally is about $\Delta n^2 \cong 0.1\, N^2$ and due to $n_{\max} \sim N$ we deduce a nearly chaotic behavior of the radiation field.

quantities behave very similarly with increasing N. The maximum photon number, on the other hand, reaches a constant value already for very low N. This number is given by $n_{\max} \cong 0.78\, N$ and thus is, at least, of the same order of magnitude as $n_{\max} = N$ from our analytic approach. We have only considered values for N up to $N = 10^4$ in Fig. 7.8 since the computational effort to diagonalize a $(N+1) \times (N+1)$ matrix increases drastically for higher values of N. Hence, we recognize the importance of our approximate analytic approach: since we obtain a matching of analytics and numerics for relatively low electron numbers we can expect that the analytic solution, Eq. (7.61), also correctly predicts the dynamics of the mean photon number for values of N inaccessible to numerics.

The numerical solution [138] of Eq. (7.71) gives us also the possibility to study the variance

$$\Delta n^2 \equiv \langle \hat{n}^2 \rangle - \langle \hat{n} \rangle^2 \tag{7.72}$$

of the photon number in the Quantum FEL for longer times. In Fig. 7.9 we have plotted Δn^2 against the length L of the wiggler for $N = 10^3$ and $N = 10^4$, respectively. We observe that, the approximate value $\Delta n^2 \cong 0.1\, N^2$ of the variance around saturation, $L_{\max} \cong 10\, L_g$. Hence, the variance Δn^2 is roughly of the same order of magnitude as the square of the mean value $\langle n \rangle^2 \cong N^2$ which is a feature of chaotic light [130] and thus the statistical behavior of the radiation is similar to the exponential gain regime.

We now turn to the more general situation of a nonzero detuning Δ from resonance. In Fig. 7.10 we have drawn the mean photon number $\langle \hat{n} \rangle$ of the Quantum FEL as a function of the wiggler length L for three different values of $\varkappa \equiv \Delta/\alpha_N$. Similar to the estimate in

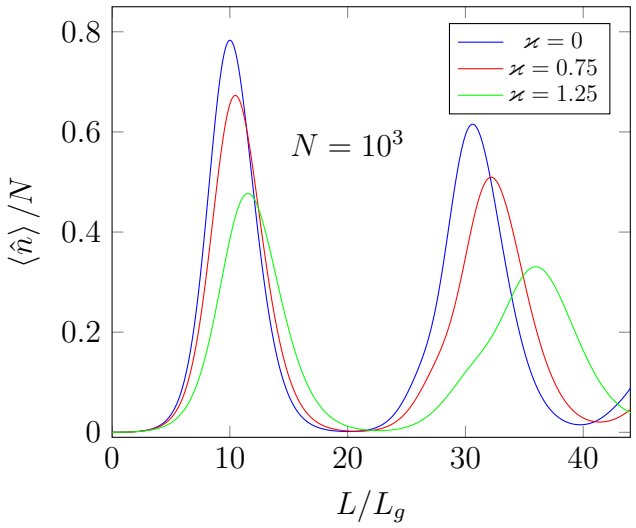

Figure 7.10: Mean photon number of the high-gain Quantum FEL as a function of the wiggler length L, according to the numerical solution of Eq. (7.71), for three different values of the deviation $\Delta = \kappa\alpha_N$ from resonance and with $N = 10^3$ electrons. In accordance with the analytic result, Fig. 7.5, the maximum photon number $n_{\max}$ decreases when we increase Δ while the position $L_{\max}$ of this maximum shifts towards the right. We emphasize, that the maximum photon number for resonance, Δ=0, is already reduced when compared to Fig. 7.5.

Fig. 7.5 the maximum photon number decreases for an increasing deviation Δ from resonance while its position $L_{\max}$ along the wiggler increases.

The position $L_{\max}$ and magnitude $n_{\max}$ of the first maximum of the photon number is displayed in Fig. (7.11) depending on the momentum p of the electrons. We observe that the numeric and the analytic approach show the same behavior when we increase the deviation from resonance $p = q/2$. However, the numeric and the analytic curves are normalized to their respective value at resonance which differ according to Fig. 7.7.

7.3 Higher-order corrections

In the following we study the higher-order corrections to the deep quantum regime in the exponential gain regime. The imaginary part of the frequency is responsible for the exponential growth and its dependency on the initial momentum p can be considered as the gain function of a high-gain FEL according to Chap. 2. Hence, we focus in the following discussion on this quantity.

Indeed, we obtain that the higher-order corrections scale with powers of α_N and thus reduce to the corresponding expression, Eq. (7.38), in the deep quantum regime for $\alpha_N \to 0$. Moreover, we connect our results to the existing literature [2, 3, 25] on the Quantum FEL and find excellent agreement.

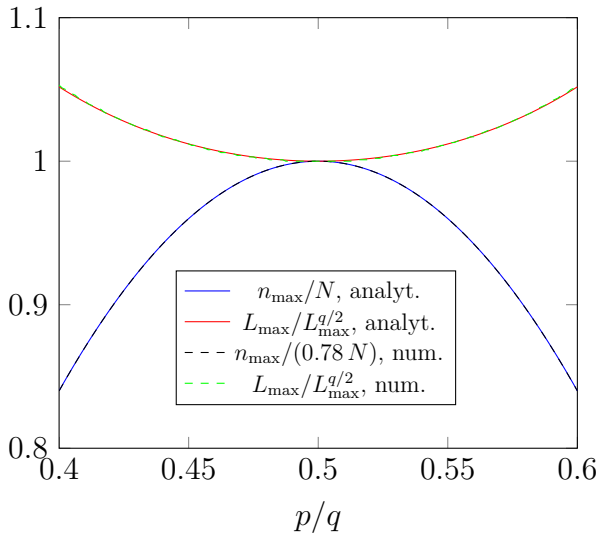

Figure 7.11: Position $L_{\max}$ and magnitude $n_{\max}$ of the first maximum of the mean photon number as a function of the initial momentum p of the electrons for $N = 10^3$. We observe that the numerical results (dashed lines) agree very well with the estimates from the analytic approach, Eqs. (7.65) and (7.59), respectively. We emphasize, however, that the numerical and the analytic curves are normalized to their respective value at resonance, $p = q/2$, which differ from each other.

7.3.1 Imaginary part

When we assume that Δ is small we identify

$$\hat{\mathcal{H}}_0 \equiv \hat{a}_{\mathrm{L}}\hat{\Upsilon}_{0,1} + \hat{a}_{\mathrm{L}}^\dagger\hat{\Upsilon}_{1,0} - \frac{\Delta}{\varepsilon}\hat{n}_{\mathrm{L}} \tag{7.73}$$

as the zeroth component of the Fourier decomposition, Eq. (7.20), of $\bar{H}$ while the other components are given by

$$\hat{\mathcal{H}}_\mu \equiv \hat{a}_{\mathrm{L}}\hat{\Upsilon}_{\mu,\mu+1} + \hat{a}_{\mathrm{L}}^\dagger\hat{\Upsilon}_{-\mu+1,-\mu} \tag{7.74}$$

in analogy to the single-electron case. We note that this procedure is only valid when the terms in Eq. (7.73) are of the same order of magnitude, that is $\Delta\hat{n}_{\mathrm{L}} \sim \alpha_N$. In principle, we could have chosen the magnitude of Δ proportional to any power of α_N, but we then had to modify our method.

Now we are in the position to derive the contributions of the effective Hamiltonian $\hat{H}_{\mathrm{eff}}$ order by order in the framework of the method of averaging which we show in detail in App. D. The time evolution of an observable $\hat{\mathcal{O}}$ up to third order in ε is then dictated by the Heisenberg equation of motion

$$i\frac{\mathrm{d}}{\mathrm{d}\tau}\hat{\mathcal{O}} = \varepsilon\left[\hat{\mathcal{O}}, \hat{H}_{\mathrm{eff}}^{(1)}\right] + \varepsilon^2\left[\hat{\mathcal{O}}, \hat{H}_{\mathrm{eff}}^{(2)}\right] + \varepsilon^3\left[\hat{\mathcal{O}}, \hat{H}_{\mathrm{eff}}^{(3)}\right], \tag{7.75}$$

where the first-order term $\hat{H}_{\rm eff}^{(1)}$ is identical to $\hat{\mathcal{H}}_0$ while the expressions in second and third order, $\hat{H}_{\rm eff}^{(2)}$ and $\hat{H}_{\rm eff}^{(3)}$, respectively, are given by the expressions in Eqs. (D.104) and (D.106), respectively.

In analogy to the deep quantum regime, we linearize the resulting equations of motions by setting $\hat{\Upsilon}_{0,0} \cong \langle \hat{\Upsilon}_{0,0}(0) \rangle = N$ and keeping only contributions which are linear in the 'small' quantities $\hat{a}_{\rm L} \cong \delta\hat{a}_{\rm L}$ and $\hat{\Upsilon}_{\mu,\nu} \cong \delta\hat{\Upsilon}_{\mu,\nu}$, except when $\mu = \nu = 0$. This procedure, which is discussed in more detail in App. D yields the linear system of differential equations

$$i\frac{\mathrm{d}}{\mathrm{d}\tau}\begin{pmatrix}\delta\tilde{\Upsilon}_{1,0}\\ \delta\tilde{a}_{\rm L}\end{pmatrix} = \begin{pmatrix}0 & -\alpha_N\left(1-\frac{\alpha_N^2}{8}\right)\\ \alpha_N\left(1-\frac{\alpha_N^2}{8}\right) & -\alpha_N\left(\varkappa+\frac{\alpha_N}{2}-\frac{\varkappa\alpha_N^2}{4}\right)\end{pmatrix}\begin{pmatrix}\delta\tilde{\Upsilon}_{1,0}\\ \delta\tilde{a}_{\rm L}\end{pmatrix}, \tag{7.76}$$

where we have introduced the rescaled operators

$$\begin{cases}\delta\tilde{\Upsilon}_{1,0} &= \frac{1}{\sqrt{N}}\delta\hat{\Upsilon}_{1,0}\\ \delta\tilde{a}_{\rm L} &= \delta\hat{a}_{\rm L}\end{cases} \tag{7.77}$$

in analogy to Eq. (7.28) in the deep quantum regime.

We solve Eq. (7.76) with the ansatz $\mathrm{e}^{-i\lambda\tau}$ and obtain for λ the expression, Eq. (D.117),

$$\lambda \cong -\frac{\varkappa\alpha_N}{2} - \frac{\alpha_N^2}{4} + \frac{\varkappa\alpha_N^3}{8} \pm i\alpha_N\sqrt{1-\frac{\varkappa^2}{4}}\left[1 - \frac{\varkappa/2}{1-\frac{\varkappa^2}{4}}\frac{\alpha_N}{4} - \frac{5-3\varkappa^2+\varkappa^4/2}{\left(1-\frac{\varkappa^2}{4}\right)^2}\frac{\alpha_N^2}{32}\right], \tag{7.78}$$

where we have assumed that the deviation $\Delta \equiv \varkappa\alpha_N$ from resonance is of the order of α_N with $\varkappa \sim \mathcal{O}(1)$. Indeed, we observe that Eq. (7.78) reduces to the corresponding expression, Eq. (7.32), in the deep quantum regime for $\alpha_N \to 0$. Hence, the dynamics of the quantum regime really turns to a two-level behavior when we decrease the value of the quantum parameter to $\alpha_N \ll 1$.

For the time being we restrict ourselves to the resonant case, that is $\Delta = 0$. When we set $\varkappa = 0$ in Eq. (7.78) we arrive at

$$\lambda_\pm \cong -\frac{\alpha_N^2}{4} \pm i\alpha_N\left(1-\frac{5}{32}\alpha_N^2\right) \tag{7.79}$$

which leads to

$$\langle\hat{n}(t)\rangle = \sinh^2\left[gT\sqrt{N}\left(1-\frac{5}{32}\alpha_N^2\right)\right] \tag{7.80}$$

for the time evolution of the mean photon number, when the field starts from vacuum, that is $\langle\hat{n}(0)\rangle = 0$.

In Fig. 7.12 we have compared the results for $\langle\hat{n}(t)\rangle$ of the deep quantum regime, Eq. (7.37) with $\Delta = 0$ and Eq. (7.80) including the lowest-order corrections. We observe that, for a fixed value of $gT\sqrt{N}$, the increase of the photon number, given by Eq. (7.80), is slower than predicted by the lowest-order approximation. In the next section we show that this effect emerges since for increasing values of α_N the momentum corresponding to a maximized gain deviates from the usual resonance at $p = q/2$.

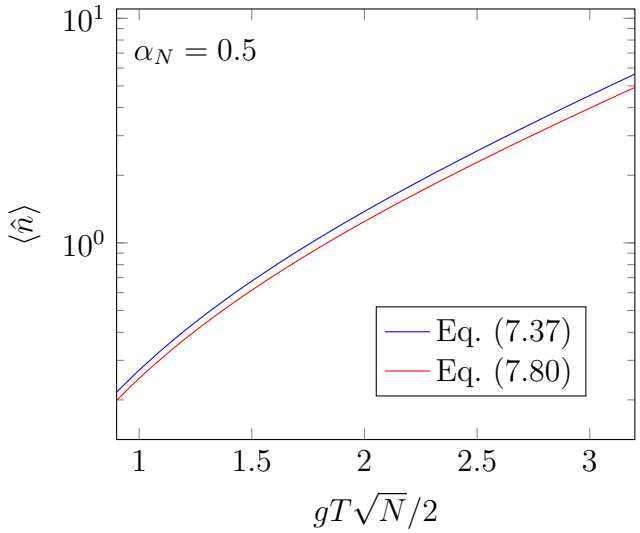

Figure 7.12: Mean photon number $\langle \hat{n} \rangle$ in the exponential gain regime of the high-gain Quantum FEL as a function of the dimensionless time $gT\sqrt{N}/2$ in the resonant case $\Delta = 0$ for $\alpha_N = 0.5$. We have drawn the solutions of first (blue line) and third order (red line), Eqs. (7.37) and (7.80), respectively. We observe that the growth rate slightly decreases when we take into account higher-order corrections.

7.3.2 Connection to existing literature

In the following we connect our theory of the high-gain Quantum FEL, based on the method of averaging, to the results of the existing literature on the Quantum FEL [25, 3, 2]. In this context, we include effects of a nonzero deviation Δ from resonance for different values of the quantum parameter α_N.

In contrast to our approach, in Ref. [25] the full set of equations was linearized first before the quantum regime was identified as one extreme limit of the solution. For this purpose, the authors introduced collective operators of the form

$$\begin{cases} \hat{B} & \equiv \frac{1}{\sqrt{N}} \sum_{j=1}^{N} \mathrm{e}^{-i2k\hat{z}_j} \\ \hat{P} & \equiv \frac{1}{\sqrt{N}} \sum_{j=1}^{N} \frac{1}{2} \left(\hat{p}_j \, \mathrm{e}^{-i2k\hat{z}_j} + \mathrm{e}^{-i2k\hat{z}_j} \, \hat{p}_j \right) \end{cases} \tag{7.81}$$

which correspond to the classical variables B and P, respectively, discussed in Chap. 2 and introduced in Eq. (2.71). The symmetric form of $\hat{P}$ was chosen since this form ensures that the resulting characteristic equation asymptotically yields the cubic equation, Eq. (2.76), of the classical case when we let $\alpha_N \to \infty$ [25].

We do not repeat the calculations of Ref. [25] but instead sketch an approach leading to the same results for the characteristic equation employing the collective projection operators $\hat{\Upsilon}_{\mu,\nu}$. In terms of these operators the Heisenberg equation of motion, Eq. (7.24), for the field

operator $\hat{a}_\mathrm{L}$ reads

$$i\frac{\mathrm{d}}{\mathrm{d}\tau}\hat{a}_\mathrm{L} = \varepsilon\sum_\mu \hat{\Upsilon}_{\mu+1,\mu} \tag{7.82}$$

where we have used Eqs. (7.9) and (7.10). Analogously, we obtain

$$i\frac{\mathrm{d}}{\mathrm{d}\tau}\hat{\Upsilon}_{\mu+1,\mu} = (\Delta-2\mu)\,\hat{\Upsilon}_{\mu+1,\mu} + \varepsilon\hat{a}_\mathrm{L}\left(\hat{\Upsilon}_{\mu+1,\mu+1}-\hat{\Upsilon}_{\mu,\mu}\right) + \varepsilon\hat{a}_\mathrm{L}^\dagger\left(\hat{\Upsilon}_{\mu+1,\mu-1}-\hat{\Upsilon}_{\mu+2,\mu}\right) \tag{7.83}$$

for the dynamics of $\hat{\Upsilon}_{\mu+1,\mu}$.
We can linearize the set of equations, Eqs. (7.82) and (7.83), by our usual procedure of approximating $\hat{\Upsilon}_{0,0}\approx N$ and keeping only terms which are linear in all other occurring operators. By inspection of the equation of motion for the laser field, Eq. (7.83), we observe that the only prominent contributions are the ones with $\mu=-1$ and $\mu=1$, that is, the operators $\hat{\Upsilon}_{0,-1}$ and $\hat{\Upsilon}_{1,0}$, respectively.
With the help of the transformation

$$\begin{cases}\bar{\Upsilon}_{1,0} & \equiv \frac{1}{\sqrt{N}}\hat{\Upsilon}_{1,0}\,\mathrm{e}^{i\tau(1+\Delta)}\\ \bar{\Upsilon}_{0,-1} & \equiv \frac{1}{\sqrt{N}}\hat{\Upsilon}_{0,-1}\,\mathrm{e}^{i\tau(1+\Delta)}\\ \bar{a}_\mathrm{L} & \equiv \hat{a}_\mathrm{L}\,\mathrm{e}^{i\tau(1+\Delta)}\end{cases} \tag{7.84}$$

we obtain the set of differential equations

$$i\frac{\mathrm{d}}{\mathrm{d}\tau}\begin{pmatrix}\bar{\Upsilon}_{1,0}\\ \bar{\Upsilon}_{0,-1}\\ \bar{a}_\mathrm{L}\end{pmatrix} = \begin{pmatrix}-1 & 0 & -\alpha_N\\ 0 & 1 & \alpha_N\\ \alpha_N & \alpha_N & -(1+\varkappa\alpha)\end{pmatrix}\begin{pmatrix}\bar{\Upsilon}_{1,0}\\ \bar{\Upsilon}_{0,-1}\\ \bar{a}_\mathrm{L}\end{pmatrix}. \tag{7.85}$$

Inserting the ansatz $\mathrm{e}^{-i\lambda\tau}$ we arrive at the characteristic equation

$$\left(\lambda^2-1\right)(\lambda+1+\varkappa\alpha_N)-2\alpha_N^2=0 \tag{7.86}$$

which is equivalent to the one in Ref. [25] besides a different scaling of the quantities.
In the limit $\alpha_N\gg 1$, Eq. (7.86) yields the correct classical result, that is Eq. (2.76), with the identity $\bar{\wp}/(\omega_\mathrm{r}T)=1+\varkappa\alpha_N$. This asymptotic behavior is similar to the low-gain and small-signal regime where considering only single-photon processes yields the correct classical result for $\hbar\to 0$, although many photons are scattered [81]. In the present case we again just include the transitions from p to $p-q$ and from p to $p+q$, represented in Eq. (7.86) by the operators $\hat{\Upsilon}_{1,0}$ and $\hat{\Upsilon}_{0,-1}$. However, in reality, the classical regime is characterized by continuous changes of the electron momentum of the order of large multiples of q.
However, we are interested in the quantum regime of the FEL, where $\alpha_N\ll 1$. In Fig. 7.13 we draw the positive imaginary part $\mathrm{Im}\lambda$, responsible for exponential gain, as a function of the initial momentum p for $\alpha_N=0.1$ and $\alpha_N=0.5$, respectively. In this figure we compare the analytic results of the deep quantum regime, Eq. (7.38), as well as

$$\mathrm{Im}\lambda = \alpha_N\sqrt{1-\frac{\varkappa^2}{4}}\left[1-\frac{\varkappa/2}{1-\frac{\varkappa^2}{4}}\frac{\alpha_N}{4}-\frac{5-3\varkappa^2+\varkappa^4/2}{\left(1-\frac{\varkappa^2}{4}\right)^2}\frac{\alpha_N^2}{32}\right] \tag{7.87}$$

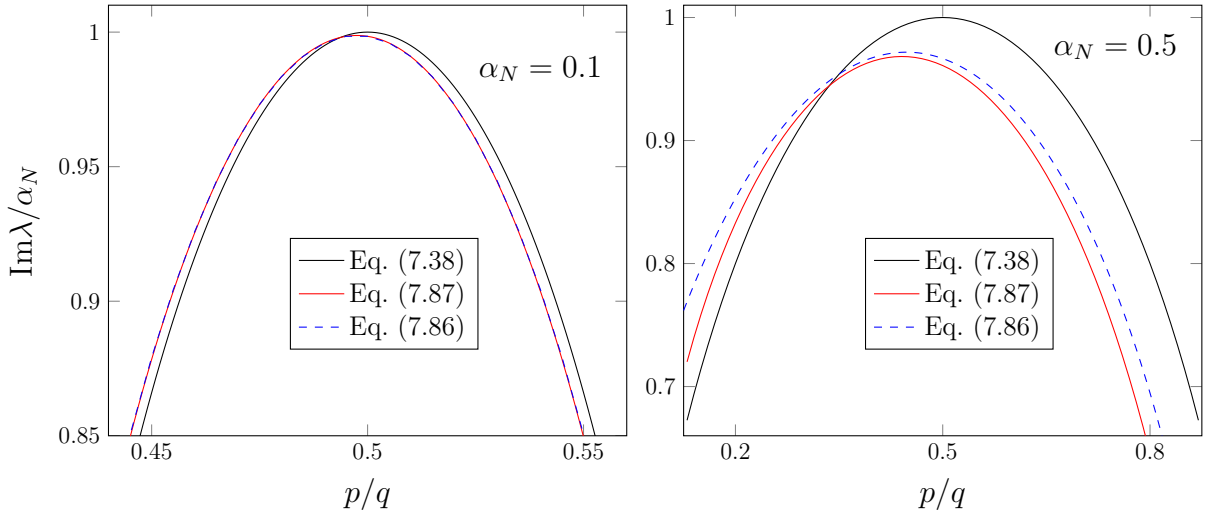

Figure 7.13: Positive imaginary part Imλ as a function of the initial momentum p of the electrons in the Quantum FEL for $\alpha_N = 0.1$ (left) and $\alpha_N = 0.5$ (right). We compare our analytic results Eqs. (7.38) and (7.87), up to first and up to third order in α_N, respectively, to the numerical solution of the cubic equation, Eq. (7.86), of Ref. [25]. We obtain good agreement of all three curves for the deep quantum regime $\alpha_N = 0.1$. For $\alpha_N = 0.5$, however, only the higher-order solution, Eq. (7.87), shows the same behavior as the results from Ref. [25]. Moreover, the maximum of the third-order solution deviates from the one $p = q/2$ and has moved in the direction of the classical resonance at $p = 0$.

from Eq. (7.78) including higher-order corrections, to the numerical solution of Eq. (7.86). The inspection of Fig. 7.13 leads to two important observations: (i) While the maximum gain for the deep quantum regime, Eq. (7.38), always occurs at $p = q/2$, the corresponding momentum of the higher-order solution, Eq. (7.87), moves to lower values when we increase α_N. This behavior indicates the beginning transition from the quantum resonance $p = q/2$ to the classical resonance $p = 0$.
(ii) For $\alpha_N = 0.1$ we obtain a good agreement between all three curves, with almost perfect matching of the higher-order result, Eq. (7.87), and the numerical solution of Eq. (7.86). When we increase the quantum parameter to $\alpha_N = 0.5$ the deep quantum regime does not give a perfectly accurate description. However, the higher-order result, Eq. (7.87), and the solution of the cubic equation, Eq. (7.86), agree very well, besides a slight deviation, which we interpret as an effect arising from even higher orders of α_N. Hence, our approach employing the method of averaging and the one of Ref. [25] lead to equivalent results.
In the following we also prove this connection of our results to the ones of Ref. [25], deduced from Fig. 7.13, in an analytic way. Since $\alpha_N \ll 1$ we are allowed to treat all contributions of the cubic equation Eq. (7.86) which include α_N as a perturbation. Hence, we can find an asymptotic solution for λ by iterating Eq. (7.86). We here just sketch the basic steps of this calculation and refer to App. G for a more detailed explanation of the underlying technique. First, we cast the cubic equation, Eq. (7.86), into the form, Eq. (G.4),

$$\lambda^{(n+1)} = -1 - \frac{\varkappa\alpha_N}{2} \pm \mathrm{i}\alpha_N \sqrt{\frac{2}{1-\lambda^{(n)}} - \frac{\varkappa^2}{4}}\,, \tag{7.88}$$

where we have related the solution $\lambda^{(n+1)}$ of $(n+1)$th order to the nth-order solution $\lambda^{(n)}$. Identifying $\lambda^{(0)} = -1$ we straightforwardly recognize that the imaginary part of the first-order solution $\lambda^{(1)}$ reproduces our result for the deep quantum regime, Eq. (7.38), that is $|\mathrm{Im}\lambda^{(1)}| = \alpha_N\sqrt{1-\varkappa^2/4}$. Moreover, when we proceed with the iteration of Eq. (7.86) up to third order in α_N we obtain that $\mathrm{Im}\lambda^{(3)}$ is identical to the corresponding expression, Eq. (7.87), of the method of averaging. We note that we would have found analogous results when we had expanded λ of Eq. (7.86) in powers of α_N and had solved the resulting equations order by order instead of employing the iteration procedure.
In conclusion, we have calculated higher-order corrections to the deep quantum regime of the high-gain FEL in the framework of the method of averaging. For $\alpha_N \to 0$ the resulting expressions reduce to the ones of the deep quantum regime, which proves that the Quantum FEL, defined by $\alpha_N \ll 1$, is analogous to a two-level system for the momenta of the electrons. On the other hand, increasing α_N to moderate values shifts the resonance from $p = q/2$ into direction of the classical resonance $p = 0$ according to Fig. 7.13. Finally, we have established the connection between our analytic results and the numerical ones of Ref. [25] in a graphical and in an analytic way, respectively.

7.4 Summary

In this chapter we have generalized our previous single-electron theory to the case where many electrons simultaneously interact with the laser field. Similarly to the classical case, this step has enabled us to develop a high-gain theory for the Quantum FEL. In the deep

quantum regime we have identified the FEL dynamics with the Dicke model describing the collective interaction of two-level atoms with a light field.
For short times we observe a possible start-up from vacuum and an exponentially growing photon number, Fig. 7.2, similar to the classical regime. However, the Quantum FEL is described by a sharp resonance at $p = q/2$ in contrast to the continuous gain curve of its classical counterpart, according to Fig. 7.3. Moreover, we have discussed the experimental obstacles to realize a high intensity in the quantum regime which are given by the constraints of a high electron energy and of a long wiggler due to Eqs. (7.41) and (7.42), respectively.
Saturation in a high-gain Quantum FEL occurs when each electron has emitted approximately one photon in contrast to the multiphoton processes of a classical FEL. In order to obtain this long-time behavior of the FEL dynamics we have employed an analytic approximation, Fig. 7.5, as well as a numerical solution, Fig. 7.7, of the equations of motion. Although the analytic solution slightly underestimates the maximum intensity both approaches qualitatively give the same results.
At the end of the chapter, we have considered higher-order corrections to the deep quantum regime in the exponential-gain limit by making use of the method of averaging. With the help of this procedure we could establish the connection to Ref. [25] which is illustrated in Fig. 7.13. Moreover, we have proven that both approaches lead to equivalent results by asymptotically solving the cubic equation, Eq. (7.86), from Ref. [25].

8 Conclusions and Outlook

After carefully studying the classical regime of the FEL and investigating the transition from classical to quantum we finally have discussed the emergence and the properties of the Quantum FEL, in a single-electron as well as in a many-electron description. To conclude this thesis, we first summarize our most important results before we give a brief outlook on possible extensions of our model and on consequential future subjects of research connected to the Quantum FEL.

8.1 Conclusions

We have devoted this thesis to the transition from classical to quantum in the FEL with special emphasis on the theory of the high-gain Quantum FEL. As a result, we have gained a lot of understanding of the *emergence* of quantum effects in the FEL and of the changed *properties* when we enter the quantum regime. In contrast to the continuous trajectories in the classical regime, the Quantum FEL is characterized by two resonant momentum levels and thus it is closely related to an ordinary atomic laser [22].

The 'true classical' limit of the FEL is achieved when the quantum mechanical recoil q is small *and* the momentum spread Δp of the electron beam is larger than the recoil, that is $\Delta p > q$. The importance of both constraints is illustrated in Figs. 3.6 and 3.7. There, we have studied the Wigner function of the electron which only reduces to the classical distribution function if we consider the correct classical limit. Increasing the recoil and decreasing the momentum spread, however, leads to quantum effects. We have presented the resulting quantum corrections to the FEL gain in Figs. 3.5 and 3.8.

With the help of these insights of the *classical limit* from a *quantum point of view* we have derived the Fokker–Planck equation, Eq. (4.34), for the laser field dynamics in a classical FEL oscillator. For the first time, we could include all aspects of the field dynamics, that is gain, self saturation, mode pulling and pushing, cavity losses, as well as fluctuations of amplitude and phase, in a single equation. Moreover, within this novel approach we could rederive the results for the steady-state photon statistics and the intrinsic linewidth of a classical FEL in a straightforward manner.

When we increase the recoil to the point, where it dominates the FEL dynamics, we enter the deep quantum regime which is characterized by a two-level behavior of the electrons. With the help of an operator formalism for the method of canonical averaging we have identified the underlying processes of the FEL dynamics as resonant transitions on a discrete momentum ladder, as illustrated for example in Figs. 5.1, 5.3 and 5.4. For a small value of the quantum parameter α, Eq. (5.18), corresponding to a high recoil, we indeed observe that non-resonant processes, Fig. 5.7, as well as multiphoton transitions, Fig. 5.9, are suppressed in comparison to the single-photon processes between the two resonant electron momenta. Moreover, we have derived the radiation properties of a Quantum FEL oscillator and have observed that

the photon statistics in a Quantum FEL is closer to the Poisson statistics of a coherent state than the broadened photon distribution in the classical regime, as illustrated in Fig. 6.7.
The most important result of this thesis, however, is the extension of our model for the Quantum FEL from a single-electron to a many-electron theory. With the concept of collective projection operators and by employing the method of averaging we have identified the quantum regime in the many-electron model as the *collective* interaction of many electrons with the laser field, with each of the electrons behaving like a two-level atom.
For short times we have solved the dynamics of the Quantum FEL with the help a parametric approximation, while we have employed an approximate approach based on Jacobian elliptic functions as well as numerical simulations for a long-time solution. After an exponential growth, Fig. 7.2, the laser intensity saturates, Fig. 7.7, when each electron has emitted on average one photon. Moreover, we have deduced the typical length scales to observe exponential growth, Eq. (7.39), as well as saturation, Eq. (7.65), respectively. We have observed that the wiggler length required for amplification is increased compared to its classical counterpart, which might be a challenging obstacle for the experimental realization of a Quantum FEL. Finally, we have discussed the gain function of the Quantum FEL and have demonstrated that our simple analytic expression, Eq. (7.38), is equivalent to the numerical results of earlier approaches, in a graphical, Fig. 7.13, and in an analytic way, respectively.
Despite the experimental obstacles concerning the energy spread of the electron beam and the wiggler length the construction of a Quantum FEL would lead to the observation of pure quantum effects and to a change of radiation properties. Moreover, the extension to a many-electron model enables us to realize a high-gain Quantum FEL without the need of a cavity in the X-ray regime.

8.2 Outlook

Although we have extended our model of the Quantum FEL to the collective interaction of many electrons with the fields our theory is still a simplified description which does not contain all possible influences on the FEL dynamics.
The most important step to develop a complete theory of a Quantum SASE FEL would be the unification of the many-electron model in the present thesis with the multi-mode approach in Refs. [27, 30]. In this context, one has to investigate the effects due to a 'photon cascade' [31]: for an electron in the excited state $p = q/2$ the only resonant transition is the one to $p = -q/2$ leading to the emission of a photon. In a multimode theory, however, besides the transition from $p = -q/2$ back to $p = q/2$, the electron can 'find' another resonant mode in which a second photon is emitted, which would eventually lead to a cascade of emission processes.
In addition, since there is no cavity in a SASE FEL we have to study the slippage [75] of the light over the electrons, and its influence on the operation of a Quantum SASE FEL. This way, we hope to establish the connection to the existing literature [107, 140] on this topic.
So far, we have only considered a one-dimensional model for the theory of the Quantum FEL. In the case of the classical FEL the one-dimensional theory [21] correctly describes the qualitative behavior, but a three-dimensional model [74] is necessary for a quantitative

analysis. Hence, we assume that we also have to take this step from one to three dimensions for the the theory of the Quantum FEL.

Moreover, by assuming that the recoil q has to be the dominating momentum scale, we expect that not only the momentum spread in the z-direction, but also the ones in the transverse directions x and y have to be smaller than the recoil, that is $\Delta p_j < q$ for $j = x, y, z$. As a consequence we would require that the volume V of an electron bunch is large enough that the phase space volume does not fall below $N\hbar^3$ yielding the necessary condition $n_{\mathrm{el}} < 1/\lambda_{\mathrm{L}}^3$ for the electron density n_{e}. Else, we cannot consider the electrons as distinguishable particles [3] and we would have to develop a theory for fermionic electrons in second quantization. However, we have to prove these qualitative arguments concerning a three-dimensional theory of the Quantum FEL in a rigorous way, which most likely can be achieved only by a numerical analysis similar to Ref. [88].

In Chap. 7 we have studied the indirect interaction of the electrons with each other via the laser field, but have neglected the effect of the direct interaction due to the Coulomb force between the electrons [20]. For a low electron density we are allowed to discard this space charge effect and similar to the classical case [48], Eq. (2.87), we expect that this procedure is allowed as long as $k_{\mathrm{p}} \ll L_g^{-1}$, where k_{p}, Eq. (2.88), is proportional to the electron density n_{e} and L_g, Eq. (7.39), denotes the gain length of the Quantum FEL. However, these assumptions again have to be verified by rigorous calculations.

Besides these elementary extensions of our model of the Quantum FEL, which are crucial for a possible experiment, there are several aspects presented in this thesis which can be developed further or studied in more detail. For example, we have only discussed the statistical properties of the radiation from a classical FEL in the low-gain regime. In order to compare the properties of a high-gain Quantum FEL, derived in Chap. 7, we have to develop a fully-quantized theory for the classical high-gain FEL. Some approaches already exist, for example in Ref. [141]. Moreover, one could extend our theory on the radiation properties in the low-gain limit in Chap. 4 to include quantum mechanical corrections by taking into account higher orders of the expansion in terms of the recoil.

In Chap. 3 we have investigated the transition from classical to quantum for a low-gain FEL in the small-signal limit. One could also study this transition for the saturated FEL. In Refs. [81, 51] this regime was treated by solving the Schrödinger equation, corresponding to the Hamiltonian of an anharmonic oscillator, and identifying the classical limit in the resulting dynamics. Since potentials higher than second order in position and momentum are generally considered as non-classical, we expect to also find quantum corrections to the classical regime of a saturated FEL. Moreover, it would be important to develop a fully quantized description for this regime in order to prove that the broadening of the photon statistics of a classical FEL is not just limited to the small-signal case.

We have only briefly discussed in Chap. 3 the topics of more realistic electron beams as well as the scattering of electron wave packets brought up in Refs. [92, 93]. We propose that our approach in phase space is well suited to gain more insight in these topics, for example by considering higher orders of our perturbative expansion.

It comes to no surprise that not only the classical regime of the FEL poses some open questions, but also the quantum regime: as discussed in Chap. 6 the effect of higher-order corrections to the deep quantum regime on the steady-state condition can be rather large.

This influence should be studied in more detail. Moreover, one can also include higher-order terms in the result for the intrinsic linewidth which would be a straightforward procedure.
An important extension of the many-electron model of the Quantum FEL in Chap. 7 would be achieved by allowing the electrons to possess different initial momenta. In this case, an approach with the help of collective projection operators would not be possible and numerics becomes necessary in order to really take the dynamics of each electron into account. However, this procedure would allow us to study the effect of a nonzero momentum spread of the electron beam on the emergence and properties of the high-gain Quantum FEL.
In conclusion, we have derived several crucial conditions and properties of the Quantum FEL within our very fundamental approach. To extend this model to more realistic situations it is very likely that in many cases extensive numerical computations become unavoidable. However, the analytic results and thoughts developed in this thesis could serve as a guideline for these future investigations.

A Classical and Quantum Theory in the Bambini–Renieri Frame

In this appendix we study the fundamental model of our approach towards the FEL: the classical as well as the quantized theory of the FEL in the co-moving Bambini–Renieri frame [61]. For this purpose, we first investigate the Lorentz transformation for (i) a laser wiggler and (ii) a magnetostatic wiggler which is in both cases constructed such that the frequencies of the laser field and the wiggler field coincide. Close to resonance the motion of an electron in this frame of reference is non-relativistic and we write down a simple Hamiltonian for this dynamics which corresponds to a mathematical pendulum. Moreover, we quantize the electron motion and the amplitude of the laser field which leads to a fully quantized Hamiltonian [101]. To conclude this appendix we present a list of important parameters in terms of the laboratory frame.

A.1 Lorentz transformation

In order to investigate the Lorentz transformation from the laboratory to the Bambini–Renieri frame we first introduce the concept of contra- and covariant four-vectors. Then, we turn to the explicit transformation for a laser wiggler and a magnetostatic wiggler, respectively.

A.1.1 Four-vectors

In the framework of special relativity space and time are treated on the same level. Hence, we define the four-vector [41]

$$x \equiv x^{\mu} \equiv (ct, x, y, z) \tag{A.1}$$

in Minkowski space where the time t is in the zeroth component while the spatial degrees of freedom x, y, z corresponding to Euclidian space are contained in the remaining three components. We note that the form, Eq. (A.1), of this four-vector is the contravariant one. In contrast, the covariant vector is defined as $x_{\mu} \equiv (ct, -x, -y, -z)$. The connection between these two forms arises by the Minkowski metric $g_{\mu,\nu} = \mathrm{diag}(1, -1, -1, -1)$ yielding $x_{\mu} = g_{\mu,\nu} x^{\nu}$. Here, we have employed the Einstein summation rule which means that we sum over indices which occur twice.
A scalar product of two four-vectors

$$\begin{aligned} x \cdot x \equiv x_{\mu} x^{\mu} &= g_{\mu,\nu} x^{\mu} x^{\nu} \\ &= (ct)^2 - x^2 - y^2 - z^2 \,, \end{aligned} \tag{A.2}$$

exemplified by the product of x with itself emerges when we multiply a contravariant with a covariant vector. When we change from an inertial frame I to another one I' a four-vector

transforms according to

$$(x')^\mu = \Lambda^\mu_\nu x^\nu \,, \tag{A.3}$$

where the Lorentz transformation Λ^μ_ν has to be chosen such that any scalar product is not affected [41].

When the frame I' is moving with a constant velocity $\boldsymbol{v} \equiv \beta c \boldsymbol{e}_z$ with respect to I along the z-direction we have to consider a Lorentz boost of the form [41]

$$\Lambda^\mu_\nu = \begin{pmatrix} \gamma & 0 & 0 & -\beta\gamma \\ 0 & 1 & 0 & 0 \\ 0 & 0 & 1 & 0 \\ -\beta\gamma & 0 & 0 & \gamma \end{pmatrix}, \tag{A.4}$$

where

$$\gamma \equiv \frac{1}{\sqrt{1-\beta^2}} \tag{A.5}$$

denotes the relativistic factor corresponding to v. With the help of Eqs. (A.3) and (A.4) we obtain the transformation rule

$$\begin{cases} (ct)' &= \gamma(ct - \beta z) \\ z' &= \gamma(-\beta ct + z) \end{cases} \tag{A.6}$$

while the coordinates perpendicular to the direction of the boost do not change due to the boost, that is $x' = x$ and $y' = y$. We emphasize that the four-vector, Eq. (A.1), is just an example for a four-vector. Other important examples, which also transform with Eq. (A.3), are given by four-wave vectors or four-momenta.

A.1.2 Laser wiggler

We model a laser wiggler or 'electromagnetic undulator' by a plane wave which *counterpropagates towards* the electrons while the laser field, that is the field which is amplified, is given by a plane wave which *copropagates with* the electrons.

Hence, we characterize the laser field by the four-wave vector

$$k^\mu_{\mathrm{L}} \equiv k_{\mathrm{L}}(1,0,0,1) \tag{A.7}$$

and the wiggler by

$$k^\mu_{\mathrm{W}} \equiv k_{\mathrm{W}}(1,0,0,-1) \tag{A.8}$$

with the respective wave numbers k_{L} and k_{W}. We note that the frequencies $\omega_{\mathrm{L}} \equiv k_{\mathrm{L}} c$ and $\omega_{\mathrm{W}} \equiv k_{\mathrm{W}} c$ appear in the zeroth component and the respective three-dimensional wave vectors are contained in the other components. We note that the scalar products $k_{\mathrm{L}} \cdot x = k_{\mathrm{L}}(ct - z)$ and $k_{\mathrm{W}} \cdot x = k_{\mathrm{W}}(ct + z)$ correspond to the phases of a plane wave in positive an one in negative z-direction, respectively. Moreover, the product of a four-wave vector with itself vanishes, that is $k_{\mathrm{L}} \cdot k_{\mathrm{L}} = k_{\mathrm{W}} \cdot k_{\mathrm{W}} = 0$.

When we change to a reference frame moving in the z-direction we obtain, according to Eqs. (A.3) and (A.4), the transformed wave vectors

$$(k'_{\mathrm{L}})^{\mu} = \gamma(1-\beta)k_{\mathrm{L}}(1,0,0,1) \tag{A.9}$$

and

$$(k'_{\mathrm{W}})^{\mu} = \gamma(1+\beta)k_{\mathrm{W}}(1,0,0,-1) \tag{A.10}$$

which are Doppler shifted in comparison to the laboratory frame. For relativistic velocities, that is $\beta \to 1$ we find the approximate expressions $(k'_{\mathrm{L}})^{\mu} \cong k_{\mathrm{L}}^{\mu}/(2\gamma)$ and $(k'_{\mathrm{W}})^{\mu} \cong (2\gamma)k_{\mathrm{W}}^{\mu}$, where we have used $1+\beta \cong 2$.

The Bambini–Renieri frame [61] is defined such that the frequencies coincide, that is

$$(k'_{\mathrm{L}})^0 = (k'_{\mathrm{W}})^0 \equiv k' \tag{A.11}$$

and with the help of the relation $k'^2 = (k'_{\mathrm{L}})^0(k'_{\mathrm{W}})^0$ we obtain the transformed wave number

$$k' = \sqrt{k_{\mathrm{L}}k_{\mathrm{W}}} \tag{A.12}$$

which is the geometric mean of k_{L} and k_{W} in the laboratory frame.

Moreover, by setting $(k'_{\mathrm{L}})^0 = (k'_{\mathrm{W}})^0$ in Eqs. (A.9) and (A.10) we obtain the expression

$$\beta_{\mathrm{BR}} = \frac{k_{\mathrm{L}} - k_{\mathrm{W}}}{k_{\mathrm{L}} + k_{\mathrm{W}}} \tag{A.13}$$

for the dimensionless velocity of the Bambini–Renieri frame compared to the laboratory frame and thus

$$\gamma_{\mathrm{BR}} = \frac{k_{\mathrm{L}} + k_{\mathrm{W}}}{2\sqrt{k_{\mathrm{L}}k_{\mathrm{W}}}} \tag{A.14}$$

for the corresponding relativistic factor. Moreover, we find the relation

$$2k' = \frac{1}{\gamma_{\mathrm{BR}}}(k_{\mathrm{L}} + k_{\mathrm{W}}) \tag{A.15}$$

with the help of Eqs. (A.12) and (A.14) .

Another important quantity is given by the relativistic four-momentum which reads

$$p^{\mu} = \gamma mc(1,0,0,\beta) \tag{A.16}$$

for a particle with rest mass m and the velocity βc in z-direction. The zeroth component gives us the energy of the particle while the remaining components display the momentum in the spatial directions. The scalar product of p with itself is a constant and connects via the relation $p \cdot p = m^2c^2$ to its mass. According to Eqs. (A.3) and (A.4) the Lorentz transformation of the four-momentum yields

$$\begin{cases} (p')^0 &= \gamma\gamma_{\mathrm{BR}}mc(1-\beta_{\mathrm{BR}}\beta) \\ (p')^3 &= \gamma\gamma_{\mathrm{BR}}mc(\beta-\beta_{\mathrm{BR}}) \end{cases} \tag{A.17}$$

while the momentum in the transverse directions remains zero.

For a particle which moves at a non-relativistic velocity in the Bambini–Renieri frame, that is $\gamma \cong \gamma_{\mathrm{BR}}$, the energy can be approximated by $p_0 \cong mc$ while the momentum $p' \equiv p'_z$ in z-direction reads

$$p' \cong \gamma^2 mc(\beta - \beta_{\mathrm{BR}}) \cong \frac{mc}{\gamma_{\mathrm{BR}}}(\gamma - \gamma_{\mathrm{BR}}) \tag{A.18}$$

in terms of the laboratory frame.

A.1.3 Magnetostatic wiggler

In contrast an electromagnetic undulator, we characterize a magnetostatic wiggler by the four-wave vector

$$k^{\mu}_{\mathrm{W}} \equiv k_{\mathrm{W}}(0, 0, 0, -1) \tag{A.19}$$

which does not possess a zeroth component and which corresponds to the time-independent phase $k_{\mathrm{W}} \cdot x = k_W z$. The transformed version of k^{μ}_{W} then reads

$$(k'_{\mathrm{W}})^{\mu} = \gamma k_{\mathrm{W}}(\beta, 0, 0, -1)\,, \tag{A.20}$$

where we have employed Eqs. (A.3) and (A.4).

In analogy to the laser wiggler we calculate the transformed wave number by setting $(k'_{\mathrm{L}})^0 = (k'_{\mathrm{W}})^0$ which leads to $k'^2 = (k'_{\mathrm{L}})^0 (k'_{\mathrm{W}})^0$. Hence, we obtain

$$k' \cong \frac{1}{\sqrt{2}} \sqrt{k_{\mathrm{L}} k_{\mathrm{W}}} \tag{A.21}$$

for the transformed wave number, where we have assumed $\beta \cong 1$ and thus $1 + \beta = 2$. As a result the expression in Eq. (A.21) differs by a factor $1/\sqrt{2}$ from the electromagnetic case, Eq. (A.12). By setting $(k'_{\mathrm{L}})^0 = (k'_{\mathrm{W}})^0$ in Eqs. (A.9) and (A.21) we, moreover, find the expressions

$$\beta_{\mathrm{BR}} = \frac{k_{\mathrm{L}}}{k_{\mathrm{L}} + k_{\mathrm{W}}} \tag{A.22}$$

for the velocity of the Bambini–Renieri frame and

$$\gamma_{\mathrm{BR}} = \frac{k_{\mathrm{L}} + k_{\mathrm{W}}}{\sqrt{2k_{\mathrm{L}} k_{\mathrm{W}} + k_{\mathrm{W}}^2}} \cong \frac{k_{\mathrm{L}} + k_{\mathrm{W}}}{\sqrt{2}\sqrt{k_{\mathrm{L}} k_{\mathrm{W}}}} \tag{A.23}$$

for the corresponding relativistic factor, where we have assumed that $k_{\mathrm{W}} \ll k_{\mathrm{L}}$. Although these expressions, Eqs. (A.22) and (A.23), differ from the corresponding ones, Eqs. (A.13) and (A.14), for the electromagnetic case we obtain the same relation for the wave number k' as in Eq. (A.15). For the sake of simplicity we omit in a large part of this thesis the prime labeling the quantities in the Bambini–Renieri frame except for the few cases, where we also consider quantities in the laboratory frame.

A.2 Hamiltonian & quantization

Having transformed to the Bambini–Renieri frame we now are in the position to derive our model for the dynamics in an FEL. By recognizing that the electron motion in the co-moving frame is non-relativistic we are allowed to make a Taylor expansion of the square root characterizing the energy of the system and we arrive at the classical Hamiltonian for the FEL within a one-dimensional single-mode model. Moreover, we quantize the electron motion as well as the laser field amplitudes in order to establish a quantum theory of the FEL.

A.2.1 Expansion of square root

The Hamiltonian of a classical particle with mass m_0 and charge e interacting with the electromagnetic field is given by [41]

$$H = c\sqrt{(\boldsymbol{p} - e\boldsymbol{A})^2 + m_0^2 c^2}\,, \tag{A.24}$$

where the field, characterized by its vector potential $\boldsymbol{A}$, connects via minimal coupling $\boldsymbol{p} \to \boldsymbol{p} - e\boldsymbol{A}$ to the momentum $\boldsymbol{p}$ of the electron.
In the case of an FEL the total field

$$\boldsymbol{A} \equiv \boldsymbol{A}_{\mathrm{L}}(z,t) + \boldsymbol{A}_{\mathrm{W}}(z,t) \tag{A.25}$$

consists of two modes, that is the laser field

$$\boldsymbol{A}_{\mathrm{L}}(z,t) \equiv \mathcal{A}_{\mathrm{L}} \left(a_{\mathrm{L}}\, \boldsymbol{e}\, \mathrm{e}^{-ik(ct-z)} + a_{\mathrm{L}}^*\, \boldsymbol{e}^*\, \mathrm{e}^{ik(ct-z)} \right) \tag{A.26}$$

and the wiggler

$$\boldsymbol{A}_{\mathrm{W}}(z,t) \equiv \mathcal{A}_{\mathrm{W}} \left(a_{\mathrm{W}}\, \boldsymbol{e}\, \mathrm{e}^{-i(ct+kz)} + a_{\mathrm{W}}^*\, \boldsymbol{e}^*\, \mathrm{e}^{ik(ct+z)} \right) \tag{A.27}$$

which are modeled as plane waves traveling in positive and negative z-direction, respectively, that is parallel to the wiggler axis. Since we consider the dynamics in the Bambini–Renieri frame the wave numbers of laser and wiggler coincide, that is $k_{\mathrm{L}} = k_{\mathrm{W}} \equiv k$. For both modes we have chosen circular polarization which leads to the relations $\boldsymbol{e}^2 = \boldsymbol{e}^{*2} = 0$ and $\boldsymbol{e} \cdot \boldsymbol{e}^* = 1$ for the polarization vectors $\boldsymbol{e}$ and $\boldsymbol{e}^*$. While $\mathcal{A}_{\mathrm{L}}$ and $\mathcal{A}_{\mathrm{W}}$ are constant a_{L} and a_{W} denote slowly varying dimensionless amplitudes of the fields. The free dynamics of these amplitudes which is already contained in the time-dependent phases, for example by $a_{\mathrm{L}} \to a_{\mathrm{L}}\, \mathrm{e}^{-ickt}$, is equivalent to the one of harmonic oscillators which follows by solving the Helmholtz equation in a cavity [40].
By inspection of Eq. (A.24) as well as of Eqs. (A.26) and (A.27) we obtain that the Hamiltonian is independent of the transverse directions x and y, that is $H \neq H(x,y)$. By means of the Hamiltonian equations of motion the momenta, p_x and p_y, conjugate to these directions are thus constant. Moreover, by injecting the electrons parallel to wiggler axis the transverse momenta $p_x = p_y = 0$ are always zero and we are left with a one-dimensional model characterized by the position z along the wiggler and its conjugate momentum $p \equiv p_z$.

By explicitly multiplying the single contributions in Eq. (A.24) we arrive at

$$H = c\sqrt{p^2 + e^2\boldsymbol{A}_{\mathrm{L}}^2 + 2e^2\boldsymbol{A}_{\mathrm{L}}(z,t)\cdot\boldsymbol{A}_{\mathrm{W}}(z,t) + e^2\boldsymbol{A}_{\mathrm{W}}^2 + m_0^2c^2}\,, \tag{A.28}$$

where no terms with $\boldsymbol{p}\cdot\boldsymbol{A}$ appear. Since the momentum of the electron is directed in longitudinal direction and the polarization of the fields is transverse we obtain $\boldsymbol{p}\cdot\boldsymbol{A} = 0$. While we neglect the contribution from $\boldsymbol{A}_{\mathrm{L}}^2$ due to its smallness we still have to consider the term with $\boldsymbol{A}_{\mathrm{W}}^2$. However, by assuming that the wiggler field is very strong and does not change due to the interaction with the electrons we treat it as constant, that is $a_{\mathrm{W}} \cong \text{const}$. Hence we incorporate the amplitude $\tilde{\mathcal{A}}_{\mathrm{W}} \equiv \mathcal{A}_{\mathrm{W}}|a_{\mathrm{W}}|$ of the wiggler into the effective mass, according to the relation

$$m^2c^2 \equiv m_0^2c^2 + e^2\boldsymbol{A}_{\mathrm{W}}^2 = m_0^2c^2 + 2e^2\tilde{\mathcal{A}}_W^2\,. \tag{A.29}$$

By introducing the dimensionless wiggler parameter [48]

$$a_0 \equiv \frac{\sqrt{2}e\tilde{A}_{\mathrm{W}}}{m_0c} \tag{A.30}$$

we obtain the simplified form

$$m = m_0\sqrt{1+a_0^2} \tag{A.31}$$

for this effective mass.

In the non-relativistic case we are allowed to perform the Taylor expansion

$$H \cong mc^2 + \frac{p^2}{2m} + \frac{e^2}{m}\boldsymbol{A}_{\mathrm{L}}(z,t)\cdot\boldsymbol{A}_{\mathrm{W}}(z,t) \tag{A.32}$$

of the square root in Eq. (A.28) in powers of $1/(mc)^2$. This approximation is just allowed when the motion of the electron is always non-relativistic resulting in the condition $p \ll mc$ for the momentum of the electron in the co-moving frame. The resonant initial momentum for the classical FEL fulfills this condition as discussed in Chap. 2. Moreover, we estimate the maximum momentum due to the interaction with the help of the interaction term $\frac{e^2}{m}|\boldsymbol{A}_{\mathrm{L}}(z,t)|\cdot|\boldsymbol{A}_{\mathrm{W}}(z,t)|$ and hence we demand for $e^2|\boldsymbol{A}_{\mathrm{L}}||\boldsymbol{A}_{\mathrm{W}}| \ll (mc)^2$ which is satisfied for reasonable strengths of the fields.

In the quantum regime of the FEL, however, the dynamics of the electrons is characterized by the recoil $q \equiv 2\hbar k$, according to Chap. 5, and we thus require $q \ll 2\hbar k$. This constraint translates to

$$\frac{q}{mc} \cong 4\gamma_0\frac{\lambda_{\mathrm{C}}}{\lambda_W}\frac{1}{1+a_0^2} \ll 1 \tag{A.33}$$

in the laboratory frame. Here, we have employed Eq. (A.15) as well as the resonance condition, Eq. (2.3), for the case of a laser wiggler and have used that $\gamma_{\mathrm{BR}}m \cong \gamma m_0$ according to Ref. [28]. Since the Compton wavelength $\lambda_{\mathrm{C}} \equiv (h/m_0c) \cong 2\cdot10^{-12}\,m$ is very small the condition, Eq. (A.33), is always fulfilled. Hence, we conclude that the non-relativistic approach, Eq. (A.32), in the Bambini–Renieri frame is always justified, in the classical as well as in the quantum regime.

To investigate the simultaneous interaction of N electrons we simply sum over each electron from $j = 1$ to N and arrive at the classical FEL Hamiltonian [61]

$$H = \sum_{j=1}^{N} \frac{p_j^2}{2m} + \frac{U_0}{2} \left(a_\mathrm{L} \sum_{j=1}^{N} \mathrm{e}^{i2kz_j} + a_\mathrm{L}^* \sum_{j=1}^{N} \mathrm{e}^{-i2kz_j} \right) \tag{A.34}$$

in the Bambini–Renieri frame, where we have explicitly calculated the product of $\boldsymbol{A}_\mathrm{L}$ and $\boldsymbol{A}_\mathrm{W}$ in Eq. (A.32). Moreover, we have defined

$$U_0 \equiv \frac{e^2 \mathcal{A}_\mathrm{L} \tilde{\mathcal{A}}_\mathrm{W}}{m} \tag{A.35}$$

as the height of the potential. We note that H is independent of time since the fields are circularly polarized. However, we can also assume other kinds of polarizations and effectively arrive at a Hamiltonian of the form of Eq. (A.34). The additional terms due to another choice of polarization represent rapid oscillations with 2ω which can be neglected.

The classical dynamics of the system is given by the Hamiltonian equations of motions

$$\begin{aligned} \dot{z}_j &= \frac{\partial H}{\partial p_j} = \frac{p_j}{m} \\ \dot{p}_j &= -\frac{\partial H}{\partial z_j} = \frac{U_0}{2i} \left(a_\mathrm{L}\, \mathrm{e}^{i2kz_j} - a_\mathrm{L}^*\, \mathrm{e}^{-i2kz_j} \right) \end{aligned} \tag{A.36}$$

for the electrons and

$$\dot{a}_\mathrm{L} = \{a_\mathrm{L}, H\} = -ig \sum_{j=1}^{N} \mathrm{e}^{-i2kz_j} \tag{A.37}$$

for the laser field. The Poisson brackets $\{.., ..\}$ from classical mechanics [142] can be calculated by the analogy of the field amplitude to a harmonic oscillator. We note that the frequency g is proportional to the potential height U_0 and its explicit form depends on the exact definitions of $\mathcal{A}_\mathrm{L}$ and a_L.

A.2.2 Quantization

We quantize electrons as well fields by substituting the positions and momenta of the electrons as well as the amplitudes of the fields by their operator versions which commute according to the relations

$$\begin{cases} [\hat{z}_j, \hat{p}_j] & = i\hbar \\ \left[\hat{a}_\mathrm{L}, \hat{a}_\mathrm{L}^\dagger\right] & = 1 \\ \left[\hat{a}_\mathrm{W}, \hat{a}_\mathrm{W}^\dagger\right] & = 1\,. \end{cases} \tag{A.38}$$

Since we have performed the quantization in the Schrödinger picture the fundamental operators are time-independent and we arrive at the expressions

$$\hat{\boldsymbol{A}}_\mathrm{L}(\hat{z}_j) \equiv \mathcal{A}_\mathrm{L} \left(\hat{a}_\mathrm{L}\, \boldsymbol{e}\, \mathrm{e}^{ik\hat{z}_j} + \hat{a}_\mathrm{L}^\dagger\, \boldsymbol{e}^*\, \mathrm{e}^{-ik\hat{z}_j} \right) \tag{A.39}$$

and

$$\hat{\boldsymbol{A}}_{\mathrm{W}}(\hat{z}_j) \equiv \mathcal{A}_{\mathrm{W}} \left(\hat{a}_{\mathrm{W}}\, \boldsymbol{e}\, \mathrm{e}^{-ik\hat{z}_j} + \hat{a}_{\mathrm{W}}^{\dagger}\, \boldsymbol{e}^{*}\, \mathrm{e}^{ik\hat{z}_j} \right) \tag{A.40}$$

for the quantized vector potentials of the laser and the wiggler field, respectively.
The many-electron Hamiltonian operator then reads in analogy to Eq. (A.34)

$$\hat{H} = \hbar\omega \hat{a}_{\mathrm{L}}^{\dagger}\hat{a}_{\mathrm{L}} + \hbar\omega \hat{a}_{\mathrm{W}}^{\dagger}\hat{a}_{\mathrm{W}} + \sum_{j=1}^{N} \frac{\hat{p}_j^2}{2m} + \hbar\tilde{g} \left(\hat{a}_{\mathrm{L}}\hat{a}_{\mathrm{W}}^{\dagger} \sum_{j=1}^{N} \mathrm{e}^{i2k\hat{z}_j} + \hat{a}_{\mathrm{L}}^{\dagger}\hat{a}_{\mathrm{W}} \sum_{j=1}^{N} \mathrm{e}^{-i2k\hat{z}_j} \right) , . \tag{A.41}$$

The first two terms in Eq. (A.41) correspond to the free dynamics of the laser field and the wiggler field, respectively, while

$$\tilde{g} \equiv \frac{e^2 \mathcal{A}_{\mathrm{L}} \mathcal{A}_{\mathrm{W}}}{\hbar m} \tag{A.42}$$

denotes the coupling constant of electrons and fields.
Similar to the classical case we incorporate the free motion of the fields into the phases and thus make the unitary transformation

$$\hat{H} \to \mathrm{e}^{-i\omega t \hat{a}_{\mathrm{L}}^{\dagger}\hat{a}_{\mathrm{L}}}\, \mathrm{e}^{-i\omega t \hat{a}_{\mathrm{W}}^{\dagger}\hat{a}_{\mathrm{W}}} \left(\hat{H} - \hbar\omega \hat{a}_{\mathrm{L}}^{\dagger}\hat{a}_{\mathrm{L}} - \hbar\omega \hat{a}_{\mathrm{W}}^{\dagger}\hat{a}_{\mathrm{W}} \right) \mathrm{e}^{i\omega t \hat{a}_{\mathrm{L}}^{\dagger}\hat{a}_{\mathrm{L}}}\, \mathrm{e}^{+i\omega t \hat{a}_{\mathrm{W}}^{\dagger}\hat{a}_{\mathrm{W}}} \tag{A.43}$$

which yields the relations $\hat{a}_{\mathrm{L}} \to \hat{a}_{\mathrm{L}}\, \mathrm{e}^{-i\omega t}$ and $\hat{a}_{\mathrm{W}}^{\dagger} \to \hat{a}_{\mathrm{W}}^{\dagger}\, \mathrm{e}^{-i\omega t}$ [40] for the corresponding field operators. We note that in the interaction part of the Hamiltonian, Eq. (A.41), just combinations of the form $\hat{a}_{\mathrm{L}}\hat{a}_{\mathrm{W}}^{\dagger}$ are present which stay unchanged during the transformation since the phases with different signs cancel. Hence, the transformed Hamiltonian is independent of time just like in the classical case.
Moreover, we assume that the wiggler field is strong an thus we neglect its depletion, that is $\hat{a}_{\mathrm{W}} \cong \sqrt{n_{\mathrm{W}}} = \text{const}$. Hence, we define the amplitude $\tilde{\mathcal{A}}_{\mathrm{W}} \equiv \mathcal{A}_{\mathrm{W}}\sqrt{n_{\mathrm{W}}}$ of the wiggler while the laser field is characterized by the vacuum amplitude [40]

$$\mathcal{A}_{\mathrm{L}} \equiv \sqrt{\frac{\hbar}{2\varepsilon_0 \omega_{\mathrm{L}} V}} \tag{A.44}$$

depending on quantities in the lab frame with ε_0 and V denoting the vacuum permittivity and the quantization volume, respectively.
Finally, we obtain the fully-quantized, many-particle Hamiltonian [101]

$$\hat{H} = \sum_{j=1}^{N} \frac{\hat{p}_j^2}{2m} + \hbar g \left(\hat{a}_{\mathrm{L}} \sum_{j=1}^{N} \mathrm{e}^{i2k\hat{z}_j} + \hat{a}_{\mathrm{L}}^{\dagger} \sum_{j=1}^{N} \mathrm{e}^{-i2k\hat{z}_j} \right) \tag{A.45}$$

in the Bambini–Renieri frame with

$$g \equiv \frac{e^2 \mathcal{A}_{\mathrm{L}} \tilde{\mathcal{A}}_{\mathrm{W}}}{\hbar m} \tag{A.46}$$

denoting the coupling constant. The dynamics of the system can either be obtained by the Schrödinger equation for a time-dependent state vector $|\Psi(t)\rangle$ or by Heisenberg equations of motion for time-dependent operators $\hat{\mathcal{O}}(t)$ in the Heisenberg picture. In both cases we characterize the FEL dynamics with the Hamiltonian in Eq. (A.45).

Table A.1: Important parameters for the classical FEL in the Bambini–Renieri frame (left) and in the laboratory frame (right).

	Bambini–Renieri frame	laboratory frame
g	g	$\frac{\sqrt{\pi}}{2}\frac{a_0 c}{\gamma_0}\sqrt{\frac{r_\mathrm{e}\lambda_\mathrm{W}}{\lambda_\mathrm{C} V}}$
L_g^cl	$\frac{cT'}{\sqrt{3}}\left[\frac{2}{gT'N\kappa}\right]^{1/3}$	$\frac{1}{\sqrt{3}}\frac{\gamma_0\lambda_\mathrm{W}^{1/3}}{2\pi^{2/3}(a_0^2 r_\mathrm{e} n_\mathrm{e})^{1/3}}$
${n'_\mathrm{cl}}^\mathrm{sat}\vert I_\mathrm{cl}^\mathrm{sat}$	$\left(\frac{2(gT')^2}{\kappa}\right)^{2/3} N^{4/3}$	$\frac{1}{6\pi^{1/3}} n_\mathrm{e}^{4/3} m_0 c^3 \lambda_\mathrm{W}^{2/3} r_\mathrm{e}^{1/3} a_0^{2/3}$
${n'_\mathrm{cl}}^\mathrm{ss}\vert I_\mathrm{cl}^\mathrm{ss}$	$\frac{\pi^3\epsilon}{2(\omega'_\mathrm{r}T')^2(gT')^2}$	$\frac{\epsilon\gamma_0^2\lambda_\mathrm{W}^2 m_0 c^3}{32 a_0^2 L^4 r_\mathrm{e}}$
D_cl	$\frac{4N}{\epsilon\tau_\mathrm{inj}\pi^5}(gT')^4(\omega'_\mathrm{r}T')^2$	$\frac{64}{\pi\epsilon\tau_\mathrm{inj}}\frac{r_\mathrm{e}^2 n_\mathrm{e}^2 a_0^4 L^6}{\gamma_0^6 N}$

A.3 Transformed parameters

In Tab. A.1 we have listed the most important parameters for the classical regime and in Tab. A.2 we have presented the corresponding quantities for the Quantum FEL in terms of the Bambini–Renieri frame (with prime) and of the laboratory frame (without prime), respectively. In the derivation of the transformed parameters we have made use of the prescriptions for the wave number k', Eq. (A.15), and the momentum p', Eq. (A.18), in a laser wiggler.

However, we have to be cautious when we perform this transformation: when an electron leaves the accelerator it is not characterized by the longitudinal dimensionless energy $\gamma \cong \gamma_\mathrm{BR}$ and the effective mass m, Eq. (A.31), but instead by the free energy γ_0 and bare mass m_0, as discussed for example in Refs. [28, 143]. By the relation $\gamma m \cong \gamma_0 m_0$ [28] we derive the connection

$$\gamma \cong \frac{\gamma_0}{\sqrt{1+a_0^2}} \tag{A.47}$$

of γ to γ_0. Moreover, we have to take time dilatation into account

$$T' = \frac{T}{\gamma} = \frac{T}{\gamma_0}\sqrt{1+a_0^2}\,, \tag{A.48}$$

where we have used Eq. (A.47) in the second step.

In an FEL with an electromagnetic undulator the wavelength λ_L of the laser field is connected via the resonance condition, Eq. (2.3),

$$\lambda_\mathrm{L} = \frac{\lambda_\mathrm{W}}{4\gamma^2} = \frac{\lambda_\mathrm{W}}{4\gamma_0^2}(1+a_0^2) \tag{A.49}$$

to the wiggler wavelength λ_W, the dimensionless electron energy γ_0, and the wiggler parameter a_0. In the derivation of Tabs. A.1 and A.2 we have always used Eq. (A.49) to express λ_L in

Table A.2: Important parameters for the Quantum FEL in the Bambini–Renieri frame (left) and in the laboratory frame (right).

	Bambini–Renieri frame	laboratory frame
$\omega_\mathrm{r} T$	$\dfrac{\hbar(2k')^2}{2m}T'$	$16\pi\gamma_0 \dfrac{L}{1+a_0^2}\dfrac{\lambda_\mathrm{C}}{\lambda_\mathrm{W}^2}$
α_N	$\dfrac{g\sqrt{N}}{\omega_\mathrm{r}'}$	$\dfrac{\sqrt{r_\mathrm{e} n_\mathrm{e}}}{32\gamma_0\sqrt{\pi}}\dfrac{\lambda_\mathrm{W}^{5/2}}{\lambda_\mathrm{C}^{3/2}} a_0(1+a_0^2)^{3/2}$
$\Delta p < q$	$\Delta p' < 2\hbar k'$	$\dfrac{\Delta\gamma_0}{\gamma_0} < \dfrac{4\gamma_0}{1+a_0^2}\dfrac{\lambda_\mathrm{C}}{\lambda_\mathrm{W}}$
L_g	$\dfrac{2c}{g\sqrt{N}}$	$\dfrac{\gamma_0^2}{\sqrt{\pi}a_0\sqrt{1+a_0^2}}\sqrt{\dfrac{\lambda_\mathrm{C}}{r_\mathrm{e}\lambda_\mathrm{W} n_\mathrm{e}}}$
$n'^{\mathrm{sat}}\big\vert I^{\mathrm{sat}}$	N	$\dfrac{4\gamma_0^2}{1+a_0^2}\dfrac{\lambda_\mathrm{C}}{\lambda_\mathrm{W}} n_\mathrm{e} m_0 c^3$
$n'^{\mathrm{ss}}\big\vert I^{\mathrm{ss}}$	$\dfrac{3\epsilon}{(gT')^2}$	$\dfrac{48\epsilon\gamma_0^6}{\pi a_0(1+a_0^2)^2}\dfrac{\lambda_\mathrm{C}^2}{\lambda_\mathrm{W}^2}\dfrac{m_0 c^3}{r_\mathrm{e} L^2}$
D	$\dfrac{N}{6\epsilon\tau_\mathrm{inj}}(gT')^4$	$\dfrac{\pi^2}{96\epsilon N\tau_\mathrm{inj}}\dfrac{\lambda_\mathrm{W}^2}{\lambda_\mathrm{C}^2} a_0(1+a_0^2)^2 L^4 r_\mathrm{e}^2 n_\mathrm{e}^2$

terms of these three quantities. Additionally, we have assumed that $k_\mathrm{L} \gg k_\mathrm{W}$, for a high value of γ_0 in Eq. (A.49), and we thus have made the approximation $(k_\mathrm{L} + k_\mathrm{W}) \cong k_\mathrm{L}$. Besides the explicit expressions Eqs. (A.30), (A.44), and (A.46) for the wiggler parameter a_0, the vacuum amplitude $\mathcal{A}_\mathrm{L}$, and the coupling constant g, respectively, we have also have made use of the Compton wavelength

$$\lambda_\mathrm{C} \equiv \frac{h}{m_0 c} \tag{A.50}$$

for the electron as well as the classical electron radius

$$r_\mathrm{e} \equiv \frac{e^2}{4\pi\varepsilon_0 m_0 c^2} \tag{A.51}$$

which are fundamental constants. Moreover, we have identified the ratio of the electron number N and the volume V with the particle density $n_\mathrm{e} \equiv N/V$ in the electron beam and have recalled the identity $\kappa \equiv 4(\omega_\mathrm{r}' T')(gT')$. Finally, we note that an intensity I is related by [13]

$$I \equiv \frac{\hbar\omega_\mathrm{L} c}{V}\langle\hat{n}\rangle \tag{A.52}$$

to the corresponding mean number of photons.

B Calculations in Heisenberg Picture

In this appendix we present the detailed calculations for the quantum corrections to the FEL gain in the Heisenberg picture discussed in Chap. 3. We begin with the treatment of various commutation relations which are helpful throughout these calculations. Then we search for the perturbative solution of the operator version, Eq. (3.11), of the pendulum equation for the electron motion. With this solution we are finally in the position to compute the classical gain and its quantum corrections.

B.1 Commutation relations

The main difference between classical position z and momentum p and their quantum versions $\hat{z}$ and $\hat{p}$ is that the latter ones are operators which do not commute, but instead behave according to the relation

$$[\hat{z}, \hat{p}] = i\hbar \tag{B.1}$$

which is the reason for quantum effects in the FEL. We emphasize that this relation is only valid for equal times, that is for $\hat{z}(t)$ and $\hat{p}(t)$.
Written in terms of the dimensionless variables

$$\begin{cases} \hat{\theta} & \equiv 2k\hat{z} \\ \hat{\wp} & \equiv \frac{2kT}{m}\hat{p} \end{cases} \tag{B.2}$$

introduced in Eq. (2.34) the commutation relation Eq. (B.1) transforms to

$$\left[\hat{\theta}, \hat{\wp}\right] = i2\omega_{\mathrm{r}}T\,, \tag{B.3}$$

where we have used the definition of the recoil frequency ω_{r} from Eq. (3.2).
Two very general identities for products of operators and for inverse operators read

$$\left[\hat{A}, \hat{B}\hat{C}\right] = \left[\hat{A}, \hat{B}\right]\hat{C} + \hat{B}\left[\hat{A}, \hat{C}\right] \tag{B.4}$$

and

$$\left[\hat{A}, \hat{B}^{-1}\right] = -\hat{B}^{-1}\left[\hat{A}, \hat{B}\right]\hat{B}^{-1}\,, \tag{B.5}$$

respectively, where $\hat{A}$, $\hat{B}$ and $\hat{C}$ denote arbitrary operators while $\hat{B}^{-1}$ is the inverse of $\hat{B}$, defined by $\hat{B}\hat{B}^{-1} = \hat{B}^{-1}\hat{B} = \mathbb{1}$. While the first relation, Eq. (B.4), can be proved in a straightforward way the second one, Eq. (B.5), needs a bit more effort: By inserting the unity operator and using Eq. (B.4) we obtain

$$\left[\hat{A}, \hat{B}^{-1}\underbrace{\hat{B}\hat{B}^{-1}}_{=\mathbb{1}}\hat{B}\right] = \left[\hat{A}, \hat{B}^{-1}\hat{B}^{-1}\right]\hat{B} + \hat{B}^{-2}\left[\hat{A}, \hat{B}\right]\,. \tag{B.6}$$

Employing Eq. (B.4) a second time yields

$$0 = \hat{B}^{-1}\left[\hat{A}, \hat{B}^{-1}\right]\hat{B} + \hat{B}^{-2}\left[\hat{A}, \hat{B}\right] \tag{B.7}$$

where we have subtracted $\left[\hat{A}, \hat{B}^{-1}\right]$ on both sides of the equation. The relation Eq. (B.5) is now obtained straightforwardly.

These general identities show to be helpful in the calculations presented in the following sections, for example for the commutator

$$\left[\hat{\theta}, \hat{\wp}^{-1}\right] = -i2\omega_{\mathrm{r}} T \hat{\wp}^{-2} \tag{B.8}$$

which follows directly from Eqs. (B.1) and (B.5) or for the relation

$$\left[\hat{\theta}, \hat{\wp}^{-2}\right] = -i4\omega_{\mathrm{r}} T \hat{\wp}^{-3}\,, \tag{B.9}$$

where we have additionally made use of Eq. (B.4).

In our investigations of the Heisenberg equations there frequently occur exponentials of the operators $\hat{\theta}$ and $\hat{\wp}$. Therefore, we need explicit expressions of commutators including these exponentials. Specifically we often make use of the identities

$$\left[\hat{\wp}, \mathrm{e}^{\pm i\hat{\theta}}\right] = \pm 2\omega_{\mathrm{r}} T\, \mathrm{e}^{\pm i\theta} \tag{B.10}$$

and

$$\left[\hat{\theta}, \mathrm{e}^{\pm i\hat{\wp}\tau}\right] = \mp 2\omega_{\mathrm{r}} T\tau\, \mathrm{e}^{\pm i\hat{\wp}\tau} = \mp 2\omega_{\mathrm{r}} T \hat{\wp}^{-1}\left(\hat{\wp}\tau\, \mathrm{e}^{\pm i\hat{\wp}\tau}\right) \tag{B.11}$$

which both emerge by expanding the corresponding exponential. The commutators $\left[\hat{\theta}, \hat{\wp}^{n}\right]$ and $\left[\hat{\wp}, \hat{\theta}^{n}\right]$, respectively, then are solved via induction and with the help of Eqs. (B.1) and (B.4). Using Eq. (B.11) we obtain for example the relation

$$\left[\hat{\theta}, \hat{\wp}^{-2}\, \mathrm{e}^{\pm i\hat{\wp}\tau}\right] = -2\omega_{\mathrm{r}} T \wp^{-3}\left(2\, \mathrm{e}^{\pm i\hat{\wp}\tau} \pm \hat{\wp}\tau\, \mathrm{e}^{\pm i\hat{\wp}\tau}\right)\,, \tag{B.12}$$

where we have additionally recalled Eqs. (B.4) and (B.9).

Another important property of operators is described by the Baker–Campbell–Hausdorff theorem [82]

$$\mathrm{e}^{\hat{A}}\, \hat{B}\, \mathrm{e}^{-\hat{A}} = \sum_{m}^{\infty} \frac{1}{m!}\left[\hat{A}, \hat{B}\right]_m \tag{B.13}$$

including the nested commutators

$$\left[\hat{A}, \hat{B}\right]_{m+1} \equiv \left[\hat{A}, \left[\hat{A}, \hat{B}\right]_m\right] \tag{B.14}$$

defined in a recursive way with

$$\left[\hat{A}, \hat{B}\right]_0 \equiv \hat{B} \tag{B.15}$$

for $m = 0$. We use this theorem to derive the identity

$$\mathrm{e}^{i\hat{\wp}\tau}\, \mathrm{e}^{\pm i\hat{\theta}} = \mathrm{e}^{\pm i2\omega_{\mathrm{r}} T\tau}\, \mathrm{e}^{\pm i\hat{\theta}}\, \mathrm{e}^{i\hat{\wp}\tau}\ . \tag{B.16}$$

We start the proof by rewriting Eq. (B.16) such that Eq. (B.13) can be applied yielding

$$\begin{aligned} \mathrm{e}^{i\hat{\wp}\tau}\,\mathrm{e}^{\pm i\hat{\theta}} &= \left(\mathrm{e}^{i\hat{\wp}\tau}\,\mathrm{e}^{\pm i\hat{\theta}}\,\mathrm{e}^{-i\hat{\wp}\tau}\right)\mathrm{e}^{i\hat{\wp}\tau} \\ &= \sum_{m}^{\infty} \frac{(i\tau)^m}{m!}\left[\hat{\wp},\mathrm{e}^{\pm i\hat{\theta}}\right]_m \mathrm{e}^{i\hat{\wp}\tau}\ . \end{aligned} \tag{B.17}$$

The commutator

$$\left[\hat{\wp},\mathrm{e}^{\pm i\hat{\theta}}\right] = (\pm 2\omega_\mathrm{r} T)^m\,\mathrm{e}^{\pm i\hat{\theta}} \tag{B.18}$$

is easily calculated via induction which brings us directly to Eq. (B.16). Moreover, we can derive

$$\mathrm{e}^{-i\hat{\wp}\tau}\,\mathrm{e}^{\pm i\hat{\theta}} = \mathrm{e}^{\mp i2\omega_\mathrm{r} T\tau}\,\mathrm{e}^{\pm i\hat{\theta}}\,\mathrm{e}^{-i\hat{\wp}\tau} \tag{B.19}$$

in an analogous way as shown for Eq. (B.16).
The alternative form [82]

$$\mathrm{e}^{\hat{A}+\hat{B}} = \mathrm{e}^{\hat{A}}\,\mathrm{e}^{\hat{B}}\,\mathrm{e}^{-\frac{1}{2}\left[\hat{A},\hat{B}\right]}\,\mathrm{e}^{\frac{1}{6}\left(2\left[\hat{B},\left[\hat{A},\hat{B}\right]\right]+\left[\hat{A},\left[\hat{A},\hat{B}\right]\right]\right)}\ldots \tag{B.20}$$

of the Baker–Campbell–Hausdorff formula is also very important for our following calculations. For example, we obtain the identity

$$\begin{aligned} \mathrm{e}^{\pm i\hat{\theta}\pm i\hat{\wp}\tau} &= \mathrm{e}^{\pm i\hat{\theta}}\,\mathrm{e}^{\pm i\hat{\wp}\tau}\,\mathrm{e}^{i\omega_\mathrm{r} T\tau} \\ &= \mathrm{e}^{\pm i\hat{\wp}\tau}\,\mathrm{e}^{\pm i\hat{\theta}}\,\mathrm{e}^{-i\omega_\mathrm{r} T\tau} \end{aligned} \tag{B.21}$$

which follows from Eqs. (B.1) and (B.20). We emphasize that this simple expression in Eq. (B.21) arises because the commutator of Eq. (B.1) is a *c*-number and all nested commutators are zero.

B.2 Perturbative solution

We proceed by explicitly performing the perturbative solution of the pendulum equation, Eq. (3.11), for the electron dynamics in the Heisenberg picture. We have to go to the third order of the expansion since the quantum corrections to the classical FEL gain cancel in second order.

B.2.1 Free motion

According to Chap. 3 we have to solve

$$\frac{\mathrm{d}^2}{\mathrm{d}\tau^2}\hat{\theta} = \frac{\kappa|a_\mathrm{L}|}{2}\left(\mathrm{e}^{i\hat{\theta}} - \mathrm{e}^{-i\hat{\theta}}\right)\ . \tag{B.22}$$

In the small-signal regime the right-hand side of Eq. (B.22) acts as a perturbation to the free motion. Hence, we expand the solution in powers of the coupling strength $\kappa|a_\mathrm{L}|$ which has to be a small parameter for this expansion to converge. Moreover, we demand that the quantum corrections are of the same order of the coupling, that is $\omega_\mathrm{r} T \sim \kappa|a_\mathrm{L}|$.

The zeroth order of our perturbative expansion is described by the free motion

$$\hat{\theta}^{(0)} = \hat{\theta}^{(\mathrm{in})} + \hat{\wp}^{(\mathrm{in})}\tau \tag{B.23}$$

of the electron, where $\hat{\theta}^{(\mathrm{in})}$ and $\hat{\wp}^{(\mathrm{in})}$ denote the operators for the dimensionless coordinate and momentum at time $\tau = 0$ prior to interaction.

B.2.2 First order

To find the next higher order for the solution of Eq. (B.22) we have to insert the zeroth-order term back into the pendulum equation, Eq. (B.22). During this procedure we encounter the expression

$$\mathrm{e}^{i\hat{\theta}^{(0)}} \cong \mathrm{e}^{i\hat{\theta}^{(\mathrm{in})}}\,\mathrm{e}^{i\hat{\wp}^{(\mathrm{in})}\tau} + \mathcal{O}(\omega_{\mathrm{r}}T)\,. \tag{B.24}$$

Due to the Baker–Campbell–Hausdorff relation, Eq. (B.20), we have to consider the exponential $\mathrm{e}^{i\omega_{\mathrm{r}}T\tau}$. However, when we expand this exponential in terms of $\omega_{\mathrm{r}}T$ we find that this procedure would lead to terms of higher order. Hence, for the first-order solution we can neglect these contributions.
The equation in first order reads

$$\frac{\mathrm{d}^2}{\mathrm{d}\tau^2}\hat{\theta}^{(1)} = \frac{\kappa|a_{\mathrm{L}}|}{2i}\left(\mathrm{e}^{i\hat{\theta}^{(\mathrm{in})}}\,\mathrm{e}^{i\hat{\wp}^{(\mathrm{in})}\tau} - \mathrm{e}^{-i\hat{\theta}^{(\mathrm{in})}}\,\mathrm{e}^{-i\hat{\wp}^{(\mathrm{in})}\tau}\right) \tag{B.25}$$

which we solve by a double integration with respect to time from 0 to τ. This procedure yields the expressions

$$\hat{\theta}^{(1)} = \frac{\kappa|a_{\mathrm{L}}|}{2}\left[\mathrm{e}^{i\hat{\theta}^{\mathrm{in}}}\,\hat{\wp}^{(\mathrm{in})-2}\mathfrak{h}_{+}^{(1)}(\hat{\wp}^{(\mathrm{in})}\tau) + \mathrm{e}^{-i\hat{\theta}^{\mathrm{in}}}\,\hat{\wp}^{(\mathrm{in})-2}\mathfrak{h}_{-}^{(1)}(\hat{\wp}^{(\mathrm{in})}\tau)\right]\,, \tag{B.26}$$

where we have defined

$$\begin{cases} \mathfrak{h}_{+}^{(1)}(\wp\tau) & \equiv -\frac{1}{i}\left(\mathrm{e}^{i\wp\tau} - 1\right) + \wp\tau \\ \mathfrak{h}_{-}^{(1)}(\wp\tau) & \equiv \frac{1}{i}\left(\mathrm{e}^{-i\wp\tau} - 1\right) + \wp\tau \end{cases} \tag{B.27}$$

as characteristic functions for positive and negative phase $i\hat{\theta}^{(\mathrm{in})}$, respectively.
We emphasize that we ordered the operators in the first-order solution, Eq. (B.26), in such a way that terms with $\hat{\theta}^{(\mathrm{in})}$ are left of the ones with $\hat{\wp}^{(\mathrm{in})}$. This ordering is helpful when we later calculate the gain.

B.2.3 Second order

The equation for second order arises by inserting the expressions $\hat{\theta}^{(0)}$ and $\hat{\theta}^{(1)}$, Eqs. (B.23) and (B.26), into the pendulum equation, Eq. (B.22), and by keeping only terms of second order. We obtain for the exponential

$$\begin{aligned} \mathrm{e}^{i\hat{\theta}^{(0)}+i\hat{\theta}^{(1)}} &\cong \mathrm{e}^{i\hat{\theta}^{(0)}}\,\mathrm{e}^{i\hat{\theta}^{(1)}}\,\mathrm{e}^{\frac{1}{2}\left[\hat{\theta}^{(0)},\hat{\theta}^{(1)}\right]} \\ &= \mathrm{e}^{i\hat{\theta}^{(\mathrm{in})}}\,\mathrm{e}^{i\hat{\wp}^{(\mathrm{in})}\tau}\,\mathrm{e}^{i\omega_{\mathrm{r}}T\tau}\,\mathrm{e}^{i\hat{\theta}^{(1)}} + \mathcal{O}\left[(\kappa|a_{\mathrm{L}}|)\cdot(\omega_{\mathrm{r}}T)\right]\,, \end{aligned} \tag{B.28}$$

where we have used in both steps the Baker–Campbell–Hausdorff theorem, Eq. (B.20). We note that commutator between $\hat{\theta}^{(0)}$ and $\hat{\theta}^{(1)}$ is of the order of $(\kappa|a_\mathrm{L}|)\cdot(\omega_\mathrm{r}T)$ and hence would lead to contributions of third order in the pendulum equation, Eq. (B.22). Hence, we neglect this term due to the Baker–Campbell–Hausdorff formula for the time being.

Next we perform a Taylor expansion of the exponentials in Eq. (B.28) which include first order quantities, namely $\theta^{(1)}$ and $\omega_\mathrm{r}T$. This procedure yields

$$\left(\mathrm{e}^{i\hat{\theta}}\right)^{(2)} \cong \mathrm{e}^{i\hat{\theta}^{(\mathrm{in})}}\,\mathrm{e}^{i\hat{\wp}^{(\mathrm{in})}\tau}\left[i\hat{\theta}^{(1)} + i(\omega_\mathrm{r}T)\tau\right] \tag{B.29}$$

for the contribution of $\mathrm{e}^{i\hat{\theta}}$ in the second order of our perturbative expansion.

After calculating the corresponding expression for $\mathrm{e}^{-i\hat{\theta}}$ in an analogous way we obtain from the pendulum equation, Eq. (B.22), the relation

$$\begin{aligned}\frac{\mathrm{d}^2}{\mathrm{d}\tau^2}\hat{\theta}^{(2)} =& \frac{\kappa^2|a_\mathrm{L}|^2}{4}\Big\{\hat{\wp}^{(\mathrm{in})-2}\left[\mathfrak{h}_-^{(1)}(\hat{\wp}^{(\mathrm{in})}\tau)\,\mathrm{e}^{i\hat{\wp}^{(\mathrm{in})}\tau} + \mathfrak{h}_+^{(1)}(\hat{\wp}^{(\mathrm{in})}\tau)\,\mathrm{e}^{-i\hat{\wp}^{(\mathrm{in})}\tau}\right]\\ &+ \mathrm{e}^{i2\hat{\theta}^{(\mathrm{in})}}\,\hat{\wp}^{(\mathrm{in})-2}\left[-i\mathfrak{h}_+^{(1)}(\hat{\wp}^{(\mathrm{in})}\tau)\,\mathrm{e}^{i\hat{\wp}^{(\mathrm{in})}\tau}\right] + \mathrm{e}^{-i2\hat{\theta}^{(\mathrm{in})}}\,\hat{\wp}^{(\mathrm{in})-2}\left[-i\mathfrak{h}_-^{(1)}(\hat{\wp}^{(\mathrm{in})}\tau)\,\mathrm{e}^{-i\hat{\wp}^{(\mathrm{in})}\tau}\right]\Big\}\\ &+ \omega_\mathrm{r}T\frac{\kappa|a_\mathrm{L}|}{2}\hat{\wp}^{(\mathrm{in})-1}\left[\mathrm{e}^{i\hat{\theta}^{(\mathrm{in})}}\left(\hat{\wp}^{(\mathrm{in})}\tau\,\mathrm{e}^{i\hat{\wp}^{(\mathrm{in})}\tau}\right) + \mathrm{e}^{-i\hat{\theta}^{(\mathrm{in})}}\left(-\hat{\wp}^{(\mathrm{in})}\tau\,\mathrm{e}^{-i\hat{\wp}^{(\mathrm{in})}\tau}\right)\right],\end{aligned} \tag{B.30}$$

where we have used Eqs. (B.26) and (B.29). We emphasize that we again have ordered the operators such that all terms with $\hat{\theta}^{(\mathrm{in})}$ are on the left. Due to this ordering there emerges an additional term since in Eq. (B.29) there is the exponential $\mathrm{e}^{i\hat{\wp}^{(\mathrm{in})}\tau}$ on the left of the $\mathrm{e}^{\pm i\hat{\theta}^{(\mathrm{in})}}$ of $\hat{\theta}^{(1)}$, Eq. (B.26). We bring this exponential with $\hat{\wp}^{(\mathrm{in})}$ to the right according to Eq. (B.16) and obtain corrections of the order of $\omega_\mathrm{r}T$. However, these corrections are higher than second order and we neglect them for the time being.

From Eq. (B.30) we deduce that $\hat{\theta}^{(2)}$ consists of a part proportional to $\kappa^2|a_\mathrm{L}|^2$ and one including $\omega_\mathrm{r}T$. While the first one is purely classical the latter one arises because the operators do not commute and hence is a quantum mechanical contribution. That is why we make the distinction

$$\hat{\theta}^{(2)} = \hat{\theta}^{(2)}_\mathrm{cl} + \hat{\theta}^{(2)}_\mathrm{qm} \tag{B.31}$$

between the classical $\hat{\theta}^{(2)}_\mathrm{cl}$ and the quantum part $\hat{\theta}^{(2)}_\mathrm{qm}$.

The classical contribution reads

$$\hat{\theta}^{(2)}_\mathrm{cl} \equiv \frac{\kappa|a_\mathrm{L}|^2}{4}\left[\hat{\wp}^{(\mathrm{in})-4}\mathfrak{h}_0^{(2)}(\hat{\wp}^{(\mathrm{in})}\tau) + \mathrm{e}^{2i\hat{\theta}^{(\mathrm{in})}}\,\hat{\wp}^{(\mathrm{in})-4}\mathfrak{h}_{+2}^{(2)}(\hat{\wp}^{(\mathrm{in})}\tau) + \mathrm{e}^{-2i\hat{\theta}^{(\mathrm{in})}}\,\hat{\wp}^{(\mathrm{in})-4}\mathfrak{h}_{-2}^{(2)}(\hat{\wp}^{(\mathrm{in})}\tau)\right], \tag{B.32}$$

where we have integrated twice over time and have introduced the characteristic functions

$$\begin{cases}\mathfrak{h}_0^{(2)}(\wp\tau) \equiv & \frac{3}{i}\left(\mathrm{e}^{i\wp\tau} - \mathrm{e}^{-i\wp\tau}\right) - \wp\tau(\mathrm{e}^{i\wp\tau} + \mathrm{e}^{-i\wp\tau}) - 4\wp\tau\\ \mathfrak{h}_{+2}^{(2)}(\wp\tau) \equiv & \frac{1}{4i}\,\mathrm{e}^{i2\wp\tau} + \frac{1}{i}\,\mathrm{e}^{i\wp\tau} - \frac{5}{4i} - \frac{1}{2}\wp\tau - \wp\tau\,\mathrm{e}^{i\wp\tau}\\ \mathfrak{h}_{-2}^{(2)}(\wp\tau) \equiv & -\frac{1}{4i}\,\mathrm{e}^{-i2\wp\tau} - \frac{1}{i}\,\mathrm{e}^{-i\wp\tau} + \frac{5}{4i} - \frac{1}{2}\wp\tau - \wp\tau\,\mathrm{e}^{-i\wp\tau}\end{cases} \tag{B.33}$$

for the term without dependency on $\hat{\theta}^{(\mathrm{in})}$ and for the ones with the phase factors $\mathrm{e}^{\pm 2i\hat{\theta}^{(\mathrm{in})}}$, respectively.

Similarly, we obtain

$$\hat{\theta}^{(2)}_{\mathrm{qm}} \equiv \omega_{\mathrm{r}} T \frac{\kappa|a_{\mathrm{L}}|}{2} \left(\mathrm{e}^{i\hat{\theta}^{(\mathrm{in})}} \, \hat{\wp}^{(\mathrm{in})-3} \mathfrak{q}^{(2)}_{+}(\hat{\wp}^{(\mathrm{in})}\tau) + \mathrm{e}^{-i\hat{\theta}^{(\mathrm{in})}} \, \hat{\wp}^{(\mathrm{in})-3} \mathfrak{q}^{(2)}_{-}(\hat{\wp}^{(\mathrm{in})}\tau) \right) \tag{B.34}$$

for the quantum corrections to $\hat{\theta}^{(2)}$ with

$$\begin{cases} \mathfrak{q}^{(2)}_{+}(\wp\tau) \equiv & \frac{2}{i}\,\mathrm{e}^{i\wp\tau} - \frac{2}{i} - \wp\tau\,\mathrm{e}^{i\wp\tau} - \wp\tau \\ \mathfrak{q}^{(2)}_{-}(\wp\tau) \equiv & \frac{2}{i}\,\mathrm{e}^{-i\wp\tau} - \frac{2}{i} + \wp\tau\,\mathrm{e}^{-i\wp\tau} + \wp\tau \end{cases} \tag{B.35}$$

for the terms with positive and negative phase $i\hat{\theta}^{(\mathrm{in})}$, respectively.
Since we have found quantum mechanical terms in the phase $\hat{\theta}$ we would naively assume that these corrections are sufficient to obtain quantum corrections to the gain. However, we later on show that these contributions cancel when we compute the gain. Therefore, we have to go to the next higher order of our perturbative treatment and eventually take care of saturation terms.

B.2.4 Third order

Analogous to the procedure in first and second order, for the third order we insert the expansion of $\hat{\theta}$ into the pendulum equation, Eq. (B.22), and keep only terms up to third order. This yields

$$\mathrm{e}^{i\hat{\theta}^{(0)}+i\hat{\theta}^{(1)}+\hat{\theta}^{(2)}} \cong \mathrm{e}^{i\theta^{(\mathrm{in})}} \, \mathrm{e}^{i\hat{\wp}^{(\mathrm{in})}\tau} \, \mathrm{e}^{i\omega_{\mathrm{r}}T\tau} \, \mathrm{e}^{i\hat{\theta}^{(1)}+\hat{\theta}^{(2)}} \, \mathrm{e}^{\frac{1}{2}\left[\hat{\theta}^{(0)},\hat{\theta}^{(1)}\right]}, \tag{B.36}$$

where we have used the Baker–Campbell–Hausdorff relation, Eq. (B.20), two times. In contrast to second order, the commutator between $\hat{\theta}^{(0)}$ and $\hat{\theta}^{(1)}$ does play a role here since it scales with $(\omega_{\mathrm{r}}T)\kappa|a_{\mathrm{L}}|$.
After expanding the exponentials in Eq. (B.36) we arrive at the third-order contribution

$$\begin{aligned} \left(\mathrm{e}^{i\hat{\theta}}\right)^{(3)} = & \, \mathrm{e}^{i\hat{\theta}^{(\mathrm{in})}} \, \mathrm{e}^{i\hat{\wp}^{(\mathrm{in})}\tau} \left[-\frac{1}{2} \left(\theta^{(1)2} \right)_{\mathrm{cl}} + i\hat{\theta}^{(2)}_{\mathrm{cl}} \right] \\ & + \mathrm{e}^{i\hat{\theta}^{(\mathrm{in})}} \, \mathrm{e}^{i\hat{\wp}^{(\mathrm{in})}\tau} \left(i\hat{\theta}^{(2)}_{\mathrm{qm}} + i\tilde{\theta}^{(1)} - \omega_{\mathrm{r}}T\tau\hat{\theta}^{(1)} + \frac{1}{2}\left[\hat{\theta}^{(0)},\hat{\theta}^{(1)}\right] - (\omega_{\mathrm{r}}T)^2\frac{\tau^2}{2} \right) \end{aligned} \tag{B.37}$$

of $\mathrm{e}^{i\hat{\theta}}$. The first line in Eq. (B.37) contains all classical terms. The subscript cl of the square of $\hat{\theta}^{(1)}$ is necessary because of the ordering of all $\hat{\theta}^{(\mathrm{in})}$ to the left. Quantum corrections due to this ordering emerges since $\hat{\theta}^{(\mathrm{in})}$ and $\hat{\wp}^{(\mathrm{in})}$ do not commute and thus they include an additional $\omega_{\mathrm{r}}T$. Hence, this quantum contribution is of fourth order and we can neglect it for the time being.
For the quantum mechanical terms in the second line of Eq. (B.37) we have to compute the commutator between $\hat{\theta}^{(0)}$ and $\hat{\theta}^{(1)}$. With the help of the identities Eqs. (B.8), (B.9), (B.10) and (B.12) as well as with the explicit expression, Eq. (B.26), for $\hat{\theta}^{(1)}$ we obtain

$$\frac{1}{2}\left[\hat{\theta}^{(0)},\hat{\theta}^{(1)}\right] = \omega_{\mathrm{r}}T\frac{\kappa|a_{\mathrm{L}}|}{2} \left(\mathrm{e}^{i\hat{\theta}^{(\mathrm{in})}} \, \hat{\wp}^{(\mathrm{in})-3} \mathfrak{K}_{+}(\hat{\wp}^{(\mathrm{in})}\tau) + \mathrm{e}^{-i\hat{\theta}^{(\mathrm{in})}} \, \hat{\wp}^{(\mathrm{in})-3} \mathfrak{K}_{-}(\hat{\wp}^{(\mathrm{in})}\tau) \right) \tag{B.38}$$

with

$$\begin{cases} \mathfrak{K}_+(\wp\tau) \equiv & 2\,\mathrm{e}^{i\wp\tau} - 2 + \frac{2}{i}\wp\tau + (\wp\tau)^2 \\ \mathfrak{K}_-(\wp\tau) \equiv & -2\,\mathrm{e}^{-i\wp\tau} + 2 + \frac{2}{i}\wp\tau - (\wp\tau)^2 \end{cases} \tag{B.39}$$

as characteristic functions for positive and negative phase, respectively.

The next term in Eq. (B.37) that we have to discuss is given by $\tilde{\theta}^{(1)}$. This term arises due to the ordering of $\mathrm{e}^{i\hat{\theta}^{(\mathrm{in})}}\,\mathrm{e}^{i\hat{\wp}^{(\mathrm{in})}\tau}\,\theta^{(1)}$ with respect to the operators $\hat{\theta}^{(\mathrm{in})}$ and $\hat{\wp}^{(\mathrm{in})}$ as discussed in the preceding section. When we put all operators with $\hat{\wp}^{(\mathrm{in})}$ to the left we arrive at

$$\begin{aligned} \mathrm{e}^{i\hat{\theta}^{(\mathrm{in})}}\,\mathrm{e}^{i\hat{\wp}^{(\mathrm{in})}\tau}\,\tilde{\theta}^{(1)} = \omega_{\mathrm{r}}T\frac{\kappa|a_{\mathrm{L}}|}{2}\Big\{ & \mathrm{e}^{i2\hat{\theta}^{(\mathrm{in})}}\,\hat{\wp}^{(\mathrm{in})-3}\left[-\frac{2}{i}\hat{\wp}^{(\mathrm{in})}\tau\mathfrak{h}_+^{(1)}(\hat{\wp}^{(\mathrm{in})}\tau)\,\mathrm{e}^{i\hat{\wp}^{(\mathrm{in})}\tau}\right] \\ & +\hat{\wp}^{(\mathrm{in})-3}\left[\frac{2}{i}\hat{\wp}^{(\mathrm{in})}\tau\mathfrak{h}_-^{(1)}(\hat{\wp}^{(\mathrm{in})}\tau)\,\mathrm{e}^{i\hat{\wp}^{(\mathrm{in})}\tau}\right]\Big\}\,, \end{aligned} \tag{B.40}$$

where we have recalled Eq. (B.16) and expanded the result in first order of $\omega_{\mathrm{r}}T$ and subtracted the zeroth order which is the classical term. In an analogous procedure we derive with the help of Eq. (B.19) the relation

$$\begin{aligned} \mathrm{e}^{-i\hat{\theta}^{(\mathrm{in})}}\,\mathrm{e}^{-i\hat{\wp}^{(\mathrm{in})}\tau}\,\tilde{\theta}^{(1)} = \omega_{\mathrm{r}}T\frac{\kappa|a_{\mathrm{L}}|}{2}\Big\{ & \hat{\wp}^{(\mathrm{in})-3}\left[\frac{2}{i}\hat{\wp}^{(\mathrm{in})}\tau\mathfrak{h}_+^{(1)}(\hat{\wp}^{(\mathrm{in})}\tau)\,\mathrm{e}^{-i\hat{\wp}^{(\mathrm{in})}\tau}\right] \\ & +\mathrm{e}^{-i2\hat{\theta}^{(\mathrm{in})}}\,\hat{\wp}^{(\mathrm{in})-3}\left[-\frac{2}{i}\hat{\wp}^{(\mathrm{in})}\tau\mathfrak{h}_-^{(1)}(\hat{\wp}^{(\mathrm{in})}\tau)\,\mathrm{e}^{-i\hat{\wp}^{(\mathrm{in})}\tau}\right]\Big\} \end{aligned} \tag{B.41}$$

which becomes important when we consider $\mathrm{e}^{-i\hat{\theta}}$. Hence, the first-order 'classical' quantity $\theta^{(1)}$ is responsible for the second order 'quantum' contribution $\tilde{\theta}^{(1)}$ due to the ordering of non-commuting operators. We also have to order the other quantities in Eq. (B.37) in such a way. However, theses corrections again include $\omega_{\mathrm{r}}T$ and become only important in the next higher orders of our expansion. Moreover, we note that the term $\omega_{\mathrm{r}}T\hat{\theta}^{(1)}$ appears in Eq. (B.37) which arises as a cross term originating from two different exponentials.

Due to the appearance of classical as well as quantum contributions in Eq. (B.37) we make the distinction

$$\hat{\theta}^{(3)} = \hat{\theta}^{(3)}_{\mathrm{cl}} + \hat{\theta}^{(3)}_{\mathrm{qm}} \tag{B.42}$$

similar to our procedure for $\hat{\theta}^{(2)}$.

We start with the discussion of the classical part $\hat{\theta}^{(3)}_{\mathrm{cl}}$. After calculating $(\mathrm{e}^{-i\hat{\theta}})^{(3)}$ in an analogous way that has led to Eq. (B.37), and by using the expressions, Eqs. (B.26) and (B.32), for $\hat{\theta}^{(1)}$ and $\hat{\theta}^{(1)}_{\mathrm{cl}}$, respectively, in the pendulum equation Eq. (B.22) we obtain

$$\begin{aligned} \frac{\mathrm{d}^2}{\mathrm{d}\tau^2}\hat{\theta}^{(3)}_{\mathrm{cl}} = \frac{\kappa^3|a_{\mathrm{L}}|^3}{8}\Big\{ & \mathrm{e}^{i\hat{\theta}^{(\mathrm{in})}}\,\hat{\wp}^{(\mathrm{in})-4}\Big[\mathfrak{h}_0^{(2)}(\hat{\wp}^{(\mathrm{in})}\tau)\,\mathrm{e}^{i\hat{\wp}^{(\mathrm{in})}\tau} + \mathfrak{h}_{+2}^{(2)}(\hat{\wp}^{(\mathrm{in})}\tau)\,\mathrm{e}^{-i\hat{\wp}^{(\mathrm{in})}\tau} \\ & -\frac{1}{i}\mathfrak{h}_+^{(1)}(\hat{\wp}^{(\mathrm{in})}\tau)\mathfrak{h}_-^{(1)}(\hat{\wp}^{(\mathrm{in})}\tau)\,\mathrm{e}^{i\hat{\wp}^{(\mathrm{in})}\tau} + \frac{1}{2i}\mathfrak{h}_+^{(1)2}(\hat{\wp}^{(\mathrm{in})}\tau)\,\mathrm{e}^{-i\hat{\wp}^{(\mathrm{in})}\tau}\Big] \\ & +\mathrm{e}^{i3\hat{\theta}^{(\mathrm{in})}}\,\hat{\wp}^{(\mathrm{in})-4}\left[\mathfrak{h}_{+2}^{(2)}(\hat{\wp}^{(\mathrm{in})}\tau)\,\mathrm{e}^{i\hat{\wp}^{(\mathrm{in})}\tau} - \frac{1}{2i}\mathfrak{h}_+^{(1)2}(\hat{\wp}^{(\mathrm{in})}\tau)\,\mathrm{e}^{i\hat{\wp}^{(\mathrm{in})}\tau}\right] + \mathrm{h.c.}\Big\} \end{aligned} \tag{B.43}$$

for the dynamics of $\hat{\theta}^{(3)}_{\mathrm{cl}}$.

When we integrate Eq. (B.43) over time τ we arrive at

$$\hat{\theta}^{(3)}_{\mathrm{cl}} = \frac{\kappa^3 |a_{\mathrm{L}}|^3}{8} \Big(\mathrm{e}^{i\hat{\theta}^{(\mathrm{in})}}\, \hat{\wp}^{(\mathrm{in})-6} \mathfrak{h}^{(3)}_{+}(\hat{\wp}^{(\mathrm{in})}\tau) + \mathrm{e}^{-i\hat{\theta}^{(\mathrm{in})}}\, \hat{\wp}^{(\mathrm{in})-6} \mathfrak{h}^{(3)}_{-}(\hat{\wp}^{(\mathrm{in})}\tau) + \mathrm{e}^{i3\hat{\theta}^{(\mathrm{in})}}\, \hat{\wp}^{(\mathrm{in})-6} \mathfrak{h}^{(3)}_{+3}(\hat{\wp}^{(\mathrm{in})}\tau) + \mathrm{e}^{-i3\hat{\theta}^{(\mathrm{in})}}\, \hat{\wp}^{(\mathrm{in})-6} \mathfrak{h}^{(3)}_{-3}(\hat{\wp}^{(\mathrm{in})}\tau) \Big) \,, \tag{B.44}$$

where we have defined the characteristic functions $\mathfrak{h}^{(3)}_{\pm}$ corresponding to phase factors $\mathrm{e}^{\pm i\hat{\theta}^{(\mathrm{in})}}$ and $\mathfrak{h}^{(3)}_{+3}$ corresponding to $\mathrm{e}^{\pm 3i\hat{\theta}^{(\mathrm{in})}}$. When we later calculate the gain only the terms for $\mathrm{e}^{\pm i\hat{\theta}^{(\mathrm{in})}}$ are of importance while for the other contributions the expectation value vanish. Hence, we restrict ourselves to the calculation of $\mathfrak{h}^{(3)}_{\pm}$ which yields

$$\mathfrak{h}^{(3)}_{+}(\wp\tau) \equiv \frac{1}{4} \Big(-\frac{6}{i}\,\mathrm{e}^{i2\wp\tau} - \frac{47}{i}\,\mathrm{e}^{i\wp\tau} + \frac{31}{i}\,\mathrm{e}^{-i\wp\tau} + \frac{22}{i} + 2\wp\tau\,\mathrm{e}^{i2\wp\tau} + 32\wp\tau\,\mathrm{e}^{i\wp\tau} + 14\wp\tau\,\mathrm{e}^{-i\wp\tau} + 42\wp\tau + \frac{4}{i}(\wp\tau)^2\,\mathrm{e}^{i\wp\tau} - \frac{2}{i}(\wp\tau)^2\,\mathrm{e}^{-\wp\tau} \Big) \tag{B.45}$$

while

$$\mathfrak{h}^{(3)}_{-}(\wp\tau) = \Big(\mathfrak{h}^{(3)}_{+}(\wp\tau) \Big)^{\dagger} \,. \tag{B.46}$$

We now proceed to the discussion of the quantum part $\hat{\theta}^{(3)}_{\mathrm{qm}}$. With the help of the expressions in Eqs. (B.26), (B.34), (B.38) and (B.40) as well as Eq. (B.37) and the pendulum equation (B.22) we obtain

$$\begin{aligned} \frac{\mathrm{d}^2}{\mathrm{d}\tau^2}\hat{\theta}^{(3)}_{\mathrm{qm}} =& \omega_{\mathrm{r}} T \frac{\kappa^2 |a_{\mathrm{L}}|^2}{4} \Bigg\{ \hat{\wp}^{(\mathrm{in})-3} \Bigg[\Bigg(\mathfrak{q}^{(2)}_{-} + \frac{\mathfrak{K}_{-}}{i} + \frac{\hat{\wp}^{(\mathrm{in})}\tau}{i}\mathfrak{h}^{(1)}_{-} \Bigg) \mathrm{e}^{i\hat{\wp}^{(\mathrm{in})}\tau} + \Bigg(\mathfrak{q}^{(2)}_{+} - \frac{\mathfrak{K}_{+}}{i} + \frac{\hat{\wp}^{(\mathrm{in})}\tau}{i}\mathfrak{h}^{(1)}_{+} \Bigg) \mathrm{e}^{-i\hat{\wp}^{(\mathrm{in})}\tau} \Bigg] \\ &+ \mathrm{e}^{i2\hat{\theta}^{(\mathrm{in})}} \hat{\wp}^{(\mathrm{in})-3} \Bigg(\mathfrak{q}^{(2)}_{+} + \frac{\mathfrak{K}_{+}}{i} - \frac{3\hat{\wp}^{(\mathrm{in})}\tau}{i}\mathfrak{h}^{(1)}_{+} \Bigg) \mathrm{e}^{i\hat{\wp}^{(\mathrm{in})}\tau} + \mathrm{e}^{-i2\hat{\theta}^{(\mathrm{in})}} \hat{\wp}^{(\mathrm{in})-3} \Bigg(\mathfrak{q}^{(2)}_{-} - \frac{\mathfrak{K}_{-}}{i} - \frac{3\hat{\wp}^{(\mathrm{in})}\tau}{i}\mathfrak{h}^{(1)}_{-} \Bigg) \mathrm{e}^{-i\hat{\wp}^{(\mathrm{in})}\tau} \Bigg\} \\ &+ (\omega_{\mathrm{r}} T)^2 \frac{\kappa |a_{\mathrm{L}}|}{2} \Bigg[\mathrm{e}^{i\hat{\theta}^{(\mathrm{in})}}\, \hat{\wp}^{(\mathrm{in})-2} \Bigg(-\frac{(\hat{\wp}^{(\mathrm{in})}\tau)^2}{2i}\,\mathrm{e}^{i\hat{\wp}^{(\mathrm{in})}\tau} \Bigg) + \mathrm{e}^{-i\hat{\theta}^{(\mathrm{in})}}\, \hat{\wp}^{(\mathrm{in})-2} \Bigg(\frac{(\hat{\wp}^{(\mathrm{in})}\tau)^2}{2i}\,\mathrm{e}^{-i\hat{\wp}^{(\mathrm{in})}\tau} \Bigg) \Bigg] \end{aligned} \tag{B.47}$$

which we again solve by integrating twice over time. For the sake of simplicity we have omitted in Eq. (B.47) the argument $\hat{\wp}^{(\mathrm{in})}\tau$ of the different characteristic functions.
Finally, we arrive the expression

$$\hat{\theta}^{(3)}_{\mathrm{qm}} = \omega_{\mathrm{r}} T \frac{\kappa^2 |a_{\mathrm{L}}|^2}{4} \Big(\hat{\wp}^{(\mathrm{in})-5} \mathfrak{q}^{(3)}_{0}(\hat{\wp}^{(\mathrm{in})}\tau) + \mathrm{e}^{i2\hat{\theta}^{(\mathrm{in})}}\, \hat{\wp}^{(\mathrm{in})-5} \mathfrak{q}^{(3)}_{+2}(\hat{\wp}^{(\mathrm{in})}\tau) + \mathrm{e}^{-i2\hat{\theta}^{(\mathrm{in})}}\, \hat{\wp}^{(\mathrm{in})-5} \mathfrak{q}^{(3)}_{-2}(\hat{\wp}^{(\mathrm{in})}\tau) \Big) + (\omega_{\mathrm{r}} T)^2 \frac{\kappa |a_{\mathrm{L}}|}{2} \Big(\mathrm{e}^{i\hat{\theta}^{(\mathrm{in})}}\, \hat{\wp}^{(\mathrm{in})-4} \mathfrak{q}^{(3)}_{+}(\hat{\wp}^{(\mathrm{in})}\tau) + \mathrm{e}^{-i\hat{\theta}^{(\mathrm{in})}}\, \hat{\wp}^{(\mathrm{in})-4} \mathfrak{q}^{(3)}_{-}(\hat{\wp}^{(\mathrm{in})}\tau) \Big) \,, \tag{B.48}$$

where we have defined

$$\begin{cases} \mathfrak{q}^{(3)}_{+}(\wp\tau) \equiv & -\frac{3}{i}\,(\mathrm{e}^{i\wp\tau} - 1) + 2\wp\tau\,\mathrm{e}^{i\wp\tau} + \wp\tau + \frac{1}{2i}(\wp\tau)^2\,\mathrm{e}^{i\wp\tau} \\ \mathfrak{q}^{(3)}_{-}(\wp\tau) \equiv & \frac{3}{i}\,(\mathrm{e}^{-i\wp\tau} - 1) + 2\wp\tau\,\mathrm{e}^{-i\wp\tau} + \wp\tau - \frac{1}{2i}(\wp\tau)^2\,\mathrm{e}^{-i\wp\tau} \end{cases} \tag{B.49}$$

which are the characteristic functions corresponding to $\mathrm{e}^{\pm i\hat{\theta}^{(\mathrm{in})}}$, respectively. Again we have refrained from explicitly writing down the characteristic functions $\mathfrak{q}^{(3)}_{0}$ and $\mathfrak{q}^{(3)}_{\pm 2}$ corresponding

to terms independent of $\hat{\theta}^{(\mathrm{in})}$ and depending on $\mathrm{e}^{\pm i2\hat{\theta}^{(\mathrm{in})}}$, respectively, since they do not contribute to the gain.

B.3 Calculation of gain

Having found a perturbative solution of the pendulum equation, Eq. (B.22), we are finally in the position to calculate the gain for the FEL by inserting this solution into Eq. (3.13) which describes the dynamics of the laser field during a single pass of electrons, and expand this expression up to third order. Besides classical gain and self saturation this procedure finally yields the quantum corrections to the gain.

B.3.1 Expansion

In Eq. (3.13) we have to consider the exponentials $\mathrm{e}^{\pm i\hat{\theta}}$. That is why we have to insert our perturbative expansion of $\hat{\theta}$ into these exponentials to calculate the change of the field amplitude $|a_\mathrm{L}|$ during a single pass of electrons. For the example of positive phase $i\hat{\theta}$ we obtain

$$\mathrm{e}^{i\hat{\theta}^{(0)}+i\hat{\theta}^{(1)}+i\hat{\theta}^{(2)}+i\hat{\theta}^{(3)}} \cong \mathrm{e}^{i\hat{\varphi}^{(\mathrm{in})}\tau}\,\mathrm{e}^{i\hat{\theta}^{(\mathrm{in})}}\,\mathrm{e}^{-i\omega_\mathrm{r}T\tau}\,\mathrm{e}^{i\hat{\theta}^{(1)}+i\hat{\theta}^{(2)}+i\hat{\theta}^{(3)}}\,\mathrm{e}^{\frac{1}{2}\left[\hat{\theta}^{(0)},\hat{\theta}^{(1)}\right]+\frac{1}{2}\left[\hat{\theta}^{(0)},\hat{\theta}^{(2)}\right]}\,\mathrm{e}^{-\frac{i}{6}\left[\hat{\theta}^{(0)},\left[\hat{\theta}^{(0)},\hat{\theta}^{(1)}\right]\right]}, \tag{B.50}$$

where we have considered terms up to third order and have made use of the Baker–Campbell–Hausdorff theorem, Eq. (B.20). We emphasize that the ordering is now a bit different from the preceding section, where we have put all terms with $\hat{\theta}^{(\mathrm{in})}$ to the left. Here, we have written the contribution from $\mathrm{e}^{i\hat{\theta}^{(0)}}$ such that $\mathrm{e}^{i\hat{\varphi}^{(\mathrm{in})}\tau}$ is on the left. However, all other contributions are ordered with $\hat{\theta}^{(\mathrm{in})}$ on the left. In this way the term $\mathrm{e}^{i\hat{\theta}^{(\mathrm{in})}}$ from $\hat{\theta}^{(0)}$ directly meets $\mathrm{e}^{-i\hat{\theta}^{(\mathrm{in})}}$ from the higher orders which gives unity and thus further ordering is unnecessary. These terms independent of $\hat{\theta}^{(\mathrm{in})}$ are responsible for the gain. By assuming a momentum eigenstate as initial condition for the electron, which has the feature of a uniform distribution in position, all expectation values with $\langle \mathrm{e}^{mi\hat{\theta}^{(\mathrm{in})}}\rangle = \langle p|p+mq\rangle$ are zero for $m \neq 0$.

We note that in Eq. (B.50) we had to take care of the nested commutator of $\theta^{(0)}$ with $[\hat{\theta}^{(0)},\hat{\theta}^{(1)}]$ which emerges from Eq. (B.20) and scales with $(\omega_\mathrm{r}T)^2\kappa|a_\mathrm{L}|$. Moreover, we have to consider the commutator of $\hat{\theta}^{(0)}$ with $\hat{\theta}^{(2)}$ which is also of third order.

Next, we perform a Taylor expansion of the exponentials in Eq. (B.50). While the zeroth order of this expansion is simply given by $\mathrm{e}^{i\hat{\varphi}^{(\mathrm{in})}\tau}\,\mathrm{e}^{i\hat{\theta}^{(\mathrm{in})}}$ we obtain

$$\left(\mathrm{e}^{i\hat{\theta}}\right)^{(1)}_\mathrm{cl} = \mathrm{e}^{i\hat{\varphi}^{(\mathrm{in})}\tau}\,\mathrm{e}^{i\hat{\theta}^{(\mathrm{in})}}\,i\hat{\theta}^{(\mathrm{in})} \tag{B.51}$$

and

$$\left(\mathrm{e}^{i\hat{\theta}}\right)^{(1)}_\mathrm{qm} = -i\omega_\mathrm{r}T\tau\,\mathrm{e}^{i\hat{\varphi}^{(\mathrm{in})}\tau}\,\mathrm{e}^{i\hat{\theta}^{(\mathrm{in})}} \tag{B.52}$$

for first order, where the first relation, Eq. (B.51), describes the classical part and the second one, Eq. (B.52), gives the quantum part. In contrast to the latter expression, the first one gives a nonzero contribution to the gain and is responsible for the classical gain of the FEL.

In second order we obtain

$$\left(\mathrm{e}^{i\hat{\theta}}\right)^{(2)}_{\mathrm{cl}} = \mathrm{e}^{i\hat{\wp}^{(\mathrm{in})}\tau}\,\mathrm{e}^{i\hat{\theta}^{(\mathrm{in})}}\left(i\hat{\theta}^{(2)}_{\mathrm{cl}} - \frac{1}{2}\left(\hat{\theta}^{(1)2}\right)_{\mathrm{cl}}\right) \tag{B.53}$$

for the classical part and

$$\left(\mathrm{e}^{i\hat{\theta}}\right)^{(2)}_{\mathrm{qm}} = \mathrm{e}^{i\hat{\wp}^{(\mathrm{in})}\tau}\,\mathrm{e}^{i\hat{\theta}^{(\mathrm{in})}}\left(i\hat{\theta}^{(2)}_{\mathrm{qm}} - \frac{(\omega_{\mathrm{r}}T)^2}{2}\tau^2 + \frac{1}{2}\left[\hat{\theta}^{(0)},\hat{\theta}^{(1)}\right] + \omega_{\mathrm{r}}T\hat{\theta}^{(1)}\tau\right) \tag{B.54}$$

for the quantum mechanical one. Both terms do not contribute to the dynamics of the laser field since there are no terms independent of $\hat{\theta}^{(\mathrm{in})}$.

We proceed by calculating the third order terms which read

$$\left(\mathrm{e}^{i\hat{\theta}}\right)^{(3)}_{\mathrm{cl}} = \mathrm{e}^{i\hat{\wp}^{(\mathrm{in})}\tau}\,\mathrm{e}^{i\hat{\theta}^{(\mathrm{in})}}\left(+i\hat{\theta}^{(3)} - \hat{\theta}^{(1)}\hat{\theta}^{(2)}_{\mathrm{cl}} - \frac{i}{6}\hat{\theta}^{(1)3}\right) \tag{B.55}$$

and

$$\begin{aligned}\left(\mathrm{e}^{i\hat{\theta}}\right)^{(3)}_{\mathrm{qm}} = \mathrm{e}^{i\hat{\wp}^{(\mathrm{in})}\tau}\,\mathrm{e}^{i\hat{\theta}^{(\mathrm{in})}}\Bigg(&\underline{i\hat{\theta}^{(3)}_{\mathrm{qm}}} - \frac{1}{2}\left(\hat{\theta}^{(1)2}\right)_{\mathrm{qm}} - \hat{\theta}^{(1)}\hat{\theta}^{(2)}_{\mathrm{qm}} + \frac{i}{6}(\omega_{\mathrm{r}}T)^3\tau^3 + \frac{1}{2}\left[\hat{\theta}^{(0)},\hat{\theta}^{(2)}_{\mathrm{cl}}\right]\\ &+\underline{\frac{1}{2}\left[\hat{\theta}^{(0)},\hat{\theta}^{(2)}_{\mathrm{qm}}\right]} - \underline{\frac{i}{6}\left[\hat{\theta}^{(0)},\left[\hat{\theta}^{(0)},\hat{\theta}^{(1)}\right]\right]} - \underline{\frac{(\omega_{\mathrm{r}}T)^2}{2}\tau^2 i\hat{\theta}^{(1)}} + i\hat{\theta}^{(1)}\frac{1}{2}\left[\hat{\theta}^{(0)},\hat{\theta}^{1}\right]\\ &+i\omega_{\mathrm{r}}T\tau\frac{1}{2}\left(\hat{\theta}^{(1)2}\right)_{\mathrm{cl}} + \omega_{\mathrm{r}}T\tau\hat{\theta}^{(2)}_{\mathrm{cl}} + \underline{\omega_{\mathrm{r}}T\tau\hat{\theta}^{(2)}_{\mathrm{qm}}} - \underline{i\omega_{\mathrm{r}}T\tau\frac{1}{2}\left[\hat{\theta}^{(0)},\hat{\theta}^{(1)}\right]}\Bigg)\,,\end{aligned} \tag{B.56}$$

where the classical term, Eq. (B.55), causes self saturation and the quantum mechanical part, Eq. (B.56), gives us the first nonzero quantum corrections to the classical gain. The underlined terms in Eq. (B.56) contain contributions which do not depend on $\hat{\theta}^{(\mathrm{in})}$ and therefore give rise to non-vanishing expectation values in the calculation of the gain. We note that in Eqs. (B.55) and (B.56) several cross terms occur which originate from the different exponentials and their expansions.

B.3.2 Classical gain

The dynamics of the laser field is given by the differential equation, Eq. (3.13),

$$\frac{\mathrm{d}}{\mathrm{d}\tau}|a_{\mathrm{L}}| = -\frac{gTN}{2i}\left\langle \mathrm{e}^{i\hat{\theta}} - \mathrm{e}^{-i\hat{\theta}}\right\rangle\,. \tag{B.57}$$

In our approach considering the low-gain and small-signal regime we insert the perturbative expressions for $\mathrm{e}^{\pm i\hat{\theta}}$, developed in the preceding section, into Eq. (B.57) take the expectation value and treat all $|a_{\mathrm{L}}|$ on the right-hand side as constant. Then, the gain follows from a straightforward integration over time t.

We assume that the initial state of the electron is given by the momentum eigenstate $|\bar{p}\rangle$ which corresponds to a sharp momentum and a uniform distribution in position. Hence, all contributions with $\mathrm{e}^{mi\hat{\theta}^{(\mathrm{in})}}$ with $m \neq 0$ vanish as already discussed.

With the help of Eq. (B.51) we arrive at

$$\left(\frac{\mathrm{d}}{\mathrm{d}\tau}|a_\mathrm{L}|\right)^{(1)}_\mathrm{cl} = -\kappa|a_\mathrm{L}|\frac{1}{4i\bar{\wp}^2}\left[\mathfrak{h}^{(1)}_-(\bar{\wp}\tau)\,\mathrm{e}^{i\bar{\wp}\tau} + \mathfrak{h}^{(1)}_+(\bar{\wp}\tau)\,\mathrm{e}^{-i\bar{\wp}\tau}\right] \tag{B.58}$$

for the dynamics of the laser field in first order. As stated in the preceding section the classical part is the only first-order contribution to the gain. By inserting the explicit expressions, Eq. (B.27) , for $\mathfrak{h}^{(1)}_\pm$, integrating over time from 0 to T and using the definition of the gain, Eq. (2.18), we obtain

$$G^{(1)}_\mathrm{cl} = gTN\kappa\frac{2}{\pi^3}\mathcal{A}(\bar{\wp})\,, \tag{B.59}$$

where we have defined

$$\mathcal{A}_\mathrm{cl}(\wp) \equiv \frac{\pi^3}{2}\frac{1-\cos\wp-\frac{\wp}{2}\sin\wp}{\wp^3}\,. \tag{B.60}$$

This result constitutes the Madey gain, Eq. (2.46), which we have already derived in Chapter 2. The second order, Eq. (B.53), of the expansion of $\mathrm{e}^{i\hat{\theta}}$ does not contribute to the gain since there are no terms which do not depend on $\hat{\theta}^{(\mathrm{in})}$ and the expectation value vanishes. Hence, we turn to the third order, Eq. (B.55), and obtain with the help of Eq. (B.57)

$$\begin{aligned}\left(\frac{\mathrm{d}}{\mathrm{d}\tau}|a_\mathrm{L}|\right)^{(3)}_\mathrm{cl} = &-\frac{gTN}{2}\frac{\kappa^3|a_\mathrm{L}|^3}{8}\frac{1}{\bar{\wp}^6}\left[\left(\mathfrak{h}^{(3)}_-\,\mathrm{e}^{i\bar{\wp}\tau}+\mathfrak{h}^{(3)}_+\,\mathrm{e}^{-i\bar{\wp}\tau}\right)+\left(-\mathfrak{h}^{(1)2}_-\mathfrak{h}^{(1)}_+\frac{\mathrm{e}^{i\bar{\wp}\tau}}{2}-\mathfrak{h}^{(1)2}_+\mathfrak{h}^{(1)}_-\frac{\mathrm{e}^{-i\bar{\wp}\tau}}{2}\right)\right.\\ &\left.+\left(-\frac{1}{i}\mathfrak{h}^{(1)}_+\mathfrak{h}^{(2)}_{-2}\,\mathrm{e}^{i\bar{\wp}\tau}+\frac{1}{i}\mathfrak{h}^{(1)}_-\mathfrak{h}^{(2)}_{+2}\,\mathrm{e}^{-i\bar{\wp}\tau}\right)+\left(-\frac{1}{i}\mathfrak{h}^{(1)}_-\mathfrak{h}^{(2)}_0\,\mathrm{e}^{i\bar{\wp}\tau}+\frac{1}{i}\mathfrak{h}^{(1)}_+\mathfrak{h}^{(2)}_0\,\mathrm{e}^{-i\bar{\wp}\tau}\right)\right]\end{aligned} \tag{B.61}$$

for the change of $|a_\mathrm{L}|$ in time. For the sake of simplicity we have omitted the argument $\bar{\wp}\tau$ of the different characteristic functions in Eq. (B.61). Using the explicit expressions, Eqs. (B.27) (B.33) and (B.45), (B.46), for the functions $\mathfrak{h}^{(1)}_\pm$, $\mathfrak{h}^{(2)}_{0,\pm2}$ and $\mathfrak{h}^{(3)}_\pm$, respectively, and integrating over time yields

$$G^{(3)}_\mathrm{cl} = -\frac{gTN}{4\pi^5}\kappa^3|a_\mathrm{L}|^2\mathcal{B}(\bar{\wp}) \tag{B.62}$$

with

$$\begin{aligned}\mathcal{B}(\wp) \equiv \frac{\pi^5}{\wp^7}\Big(&\frac{9}{2}\cos 2\wp+12\cos\wp-\frac{33}{2}+\frac{11}{4}\wp\sin 2\wp+\frac{53}{4}\wp\sin\wp\\ &-\frac{\wp^2}{2}\cos 2\wp-\frac{13}{4}\wp^2\cos\wp-\frac{\wp^2}{4}\sin\wp\Big)\,.\end{aligned} \tag{B.63}$$

Due to the negative sign in Eq. (B.62) and the dependency on $|a_\mathrm{L}|^2$ we can identify $G^{(3)}_\mathrm{cl}$ as the self saturation [22] of the classical FEL.

B.3.3 Quantum corrections

Finally, we are in the position to calculate the quantum corrections to the classical gain, given by Eqs. (B.59) and (B.62). In first order, Eq. (B.52), of our perturbative expansion there are no terms independent of $\hat{\theta}^{(\mathrm{in})}$ and hence the expectation value of $\mathrm{e}^{\pm i\hat{\theta}}$ vanishes.

The second order, Eq. (B.54), of the expansion, however, does not contribute to the gain due to another reason: When we insert Eq. (B.54) into Eq. (B.57) we obtain

$$\left(\frac{\mathrm{d}|a_\mathrm{L}|}{\mathrm{d}\tau}\right)^{(2)}_\mathrm{qm} = -\omega_\mathrm{r} T \frac{gTN}{2}\frac{\kappa^2|a_\mathrm{L}|^2}{4\bar{\wp}^3}\left[\left(\mathfrak{q}_-^{(2)} + \frac{\mathfrak{K}_-}{i} + \frac{\bar{\wp}\tau}{i}\mathfrak{h}_-^{(1)}\right)\mathrm{e}^{i\bar{\wp}\tau} + \left(\mathfrak{q}_+^{(2)} - \frac{\mathfrak{K}_+}{i} + \frac{\bar{\wp}\tau}{i}\mathfrak{h}_+^{(1)}\right)\mathrm{e}^{-i\bar{\wp}\tau}\right] \tag{B.64}$$

as quantum mechanical contribution to the laser dynamics in second order. However, by inspection of the explicit expressions Eqs. (B.27), (B.35) and (B.39) for the functions $\mathfrak{h}_\pm^{(1)}$, $\mathfrak{q}_\pm^{(2)}$ and $\mathfrak{K}_\pm$, respectively we find

$$\mathfrak{q}_-^{(2)} + \frac{\mathfrak{K}_-}{i} + \frac{\bar{\wp}\tau}{i}\mathfrak{h}_-^{(1)} = \mathfrak{q}_+^{(2)} - \frac{\mathfrak{K}_+}{i} + \frac{\bar{\wp}\tau}{i}\mathfrak{h}_+^{(1)} = 0 \tag{B.65}$$

that is the terms in second order cancel. Hence, there is no quantum correction to the gain in second order and we have to turn to the next higher order.
When we investigate the quantum mechanical terms, Eq. (B.56), of the third-order expansion of $\mathrm{e}^{i\hat{\theta}}$ we need an explicit expression for the commutator of $\hat{\theta}^{(0)}$ and $\hat{\theta}^{(2)}_\mathrm{qm}$, which reads

$$\frac{1}{2}\left[\hat{\theta}^{(0)}, \hat{\theta}^{(2)}_\mathrm{qm}\right] = \left(\mathrm{e}^{i\hat{\theta}^{(\mathrm{in})}}\,\hat{\wp}^{(\mathrm{in})-4}\mathfrak{L}_+(\hat{\wp}^{(\mathrm{in})}\tau) + \mathrm{e}^{-i\hat{\theta}^{(\mathrm{in})}}\,\hat{\wp}^{(\mathrm{in})-4}\mathfrak{L}_-(\hat{\wp}^{(\mathrm{in})}\tau)\right)\,. \tag{B.66}$$

with

$$\begin{cases}\mathfrak{L}_+(\wp\tau) \equiv & -6\,\mathrm{e}^{i\wp\tau} + 6 - \frac{2}{i}\wp\tau\,\mathrm{e}^{i\wp\tau} - \frac{4}{i}\wp\tau - (\wp\tau)^2 \\ \mathfrak{L}_-(\wp\tau) \equiv & -6\,\mathrm{e}^{-i\wp\tau} + 6 + \frac{2}{i}\wp\tau\,\mathrm{e}^{-i\wp\tau} + \frac{4}{i}\wp\tau - (\wp\tau)^2\,.\end{cases} \tag{B.67}$$

We have obtained this result by making use of the commutator relations Eqs. (B.1), (B.4), (B.8), (B.10) and (B.11).
Moreover, we calculate nested commutator

$$\frac{1}{6}\left[\hat{\theta}^{(0)}, \left[\hat{\theta}^{(0)}, \hat{\theta}^{(1)}\right]\right] = \left(\mathrm{e}^{i\hat{\theta}^{(\mathrm{in})}}\,\hat{\wp}^{(\mathrm{in})-4}\mathfrak{C}_+(\hat{\wp}^{(\mathrm{in})}\tau) + \mathrm{e}^{-i\hat{\theta}^{(\mathrm{in})}}\,\hat{\wp}^{(\mathrm{in})-4}\mathfrak{C}_-(\hat{\wp}^{(\mathrm{in})}\tau)\right) \tag{B.68}$$

analogously to the derivation of Eq. (B.66). Here, we have defined

$$\begin{cases}\mathfrak{C}_+(\wp\tau) \equiv & \frac{4}{i}\,\mathrm{e}^{i\wp\tau} - \frac{4}{i} - 4\wp\tau + \frac{2}{i}(\wp\tau)^2 + \frac{2}{3}(\wp\tau)^3 \\ \mathfrak{C}_-(\wp\tau) \equiv & -\frac{4}{i}\,\mathrm{e}^{-i\wp\tau} + \frac{4}{i} - 4\wp\tau - \frac{2}{i}(\wp\tau)^2 + \frac{2}{3}(\wp\tau)^3\end{cases} \tag{B.69}$$

as the characteristic functions for positive and negative phase $i\hat{\theta}^{(\mathrm{in})}$, respectively.
When we combine the expressions for the underlined terms of Eq. (B.56), namely Eqs. (B.26), (B.35), (B.38), (B.48), (B.66) and (B.68), and insert them into Eq. (B.57) we find

$$\begin{aligned}\left(\frac{\mathrm{d}}{\mathrm{d}\tau}|a_\mathrm{L}|\right)^{(3)}_\mathrm{qm} = -(\omega_\mathrm{r}T)^2\frac{gTN}{4}\frac{\kappa|a_\mathrm{L}|}{\bar{\wp}^4}\Bigg[&\left(\mathfrak{q}_-^{(3)}\,\mathrm{e}^{i\bar{\wp}\tau} + \mathfrak{q}_+^{(3)}\,\mathrm{e}^{-i\bar{\wp}\tau}\right) + \left(\frac{\mathfrak{K}_-}{i}\,\mathrm{e}^{i\bar{\wp}\tau} - \frac{\mathfrak{K}_+}{i}\,\mathrm{e}^{-i\bar{\wp}\tau}\right) \\ &+ \left(-\mathfrak{C}_-\,\mathrm{e}^{i\bar{\wp}\tau} - \mathfrak{C}_+\,\mathrm{e}^{-i\bar{\wp}\tau}\right) + \left(\frac{(\bar{\wp}\tau)^2}{2}\mathfrak{h}_-^{(1)}\,\mathrm{e}^{i\bar{\wp}\tau} + \frac{(\bar{\wp}\tau)^2}{2}\mathfrak{h}_+^{(1)}\,\mathrm{e}^{-i\bar{\wp}\tau}\right) \\ &+ \left(-\frac{\bar{\wp}\tau}{i}\mathfrak{q}_-^{(2)}\,\mathrm{e}^{i\bar{\wp}\tau} - \frac{\bar{\wp}\tau}{i}\mathfrak{q}_+^{(2)}\,\mathrm{e}^{-i\bar{\wp}\tau}\right) + \left(-\bar{\wp}\tau\mathfrak{K}_-\,\mathrm{e}^{i\bar{\wp}\tau} + \bar{\wp}\tau\mathfrak{K}_+\,\mathrm{e}^{-i\bar{\wp}\tau}\right)\Bigg]\end{aligned} \tag{B.70}$$

as quantum contribution of the dynamics of $|a_\mathrm{L}|$ in third order. With the help of the definitions Eqs. (B.27), (B.35), (B.39), (B.49), (B.66) and (B.68) for $\mathfrak{h}_\pm^{(1)}$, $\mathfrak{q}_\pm^{(2)}$, $\mathfrak{K}_\pm$, $\mathfrak{q}_\pm^{(3)}$, $\mathfrak{C}_\pm$ and $\mathfrak{L}_\pm$, respectively, Eq. (B.70) simplifies to

$$\left(\frac{\mathrm{d}|a_\mathrm{L}|}{\mathrm{d}\tau}\right)_\mathrm{qm}^{(3)} = -(\omega_\mathrm{r}T)^2\frac{gTN}{4}\frac{\kappa|a_\mathrm{L}|}{\bar{\wp}^4}\left(-2\sin\bar{\wp}\tau + 2\bar{\wp}\tau\cos\bar{\wp}\tau + (\bar{\wp}\tau)^2\sin\bar{\wp}\tau - \frac{(\bar{\wp}\tau)^3}{3}\sin\bar{\wp}\tau\right). \tag{B.71}$$

Integration over time from 0 to T straightforwardly yields the quantum correction

$$G_\mathrm{qm}^{(3)} = -(\omega_\mathrm{r}T)^2\frac{2gTN}{\pi^5}\kappa\mathcal{Q}(\bar{\wp}) \tag{B.72}$$

to the classical gain, where we have used the definition of the gain Eq. (2.18) and have defined

$$\mathcal{Q}(\wp) \equiv \frac{\pi^5}{4\wp^5}\left(4\cos\wp - 4 + 3\wp\sin\wp - \wp^2\cos\wp - \frac{\wp^3}{6}\sin\wp\right) \tag{B.73}$$

characterizing the dependency of the quantum corrections on the initial momentum $\bar{\wp}$. We note that Eq. (B.72) is independent of $|a_\mathrm{L}|$ and hence it is a correction to the linear gain $G_\mathrm{cl}^{(1)}$, Eq. (B.59).

C Operator Ordering and Wigner Function

This appendix about the Wigner function formalism for the FEL is structured in the following way: After introducing the Wigner distribution function and the Wigner–Weyl ordering for the semiclassical model in Chap. 3, where only the electrons are quantized, we generalize this description to a situation, Chap. 4, where, both, laser field and electrons are quantized. Then we eliminate the electron variables from the equation of motion in the classical limit and introduce cavity losses. The elimination procedure and the losses are the two ingredients to derive the Fokker–Planck equation, Chap. 4, governing the laser field dynamics of a classical FEL oscillator in the small-signal regime. At the end of this appendix, we derive the propagator corresponding to the phase diffusion of a classical FEL.

C.1 Wigner function for an electron

We first investigate the dynamics of the 'semiclassical' model of the FEL in Chapter 3, where the electron motion is quantized while the laser field is classical. The von Neumann equation

$$i\hbar\frac{\mathrm{d}}{\mathrm{d}t}\hat{\rho} = \left[\hat{H},\hat{\rho}\right] \tag{C.1}$$

describes the time evolution of the density operator $\hat{\rho}$. The Hamiltonian for our system of consideration reads

$$\hat{H} = \frac{\hat{p}^2}{2m} + \frac{U_0|a_\mathrm{L}|}{2}\left(\mathrm{e}^{i2k\hat{z}} + \mathrm{e}^{-i2k\hat{z}}\right) \tag{C.2}$$

according to Eq. (3.6).

In the following we consider the Wigner function W corresponding to $\hat{\rho}$ which is defined [82] as Fourier transform

$$W(z,p;t) \equiv \int\mathrm{d}\xi\int\mathrm{d}\zeta\,\mathrm{e}^{-iz\xi}\,\mathrm{e}^{-ip\zeta}\,\chi_{\hat{\rho}}(\xi,\zeta;t) \tag{C.3}$$

of the characteristic function

$$\chi_{\hat{\rho}}(\xi,\zeta;t) \equiv \mathrm{Tr}\left\{\hat{\mathcal{O}}\hat{\rho}\right\}. \tag{C.4}$$

The operator $\hat{\mathcal{O}}$ is given by [82]

$$\hat{\mathcal{O}} \equiv \mathrm{e}^{i\xi\hat{z}+i\zeta\hat{p}} \tag{C.5}$$

for the case of the Wigner representation. Hence, we transform from an operator to a c-number description, where we can interpret the variables z and p as position and momentum, respectively, of the electron.

When we apply the definition, Eq. (C.4), to the von Neumann equation, Eq. (C.1), with the Hamiltonian, Eq. (C.2), and cyclically permute the operators in the trace we obtain

$$\frac{\partial}{\partial t}\chi_{\hat{\rho}}(\xi,\zeta;t) = -\frac{i}{\hbar m}\,\mathrm{Tr}\left\{\left(\hat{\mathcal{O}}\frac{\hat{p}^2}{2} - \frac{\hat{p}^2}{2}\hat{\mathcal{O}}\right)\hat{\rho}(t)\right\} + \frac{U_0|a_\mathrm{L}|}{\hbar}\left[\mathrm{Tr}\left\{\frac{1}{2i}\left(\hat{\mathcal{O}}\,\mathrm{e}^{i2k\hat{z}} - \mathrm{e}^{-i2k\hat{z}}\,\hat{\mathcal{O}}\right)\hat{\rho}(t)\right\}\right. \\ \left. - \mathrm{Tr}\left\{\frac{1}{2i}\left(\mathrm{e}^{i2k\hat{z}}\,\hat{\mathcal{O}} - \hat{\mathcal{O}}\,\mathrm{e}^{-i2k\hat{z}}\right)\hat{\rho}(t)\right\}\right] \tag{C.6}$$

for the dynamics of $\chi_{\hat{\rho}}$.

Using the definition, Eq. (C.5), of $\hat{\mathcal{O}}$ as well as the commutation relation, Eq. (3.9), for $\hat{z}$ and $\hat{p}$ yields

$$\mathrm{Tr}\left\{\left(\hat{\mathcal{O}}\frac{\hat{p}^2}{2} - \frac{\hat{p}^2}{2}\hat{\mathcal{O}}\right)\hat{\rho}(t)\right\} = -\hbar\xi\frac{\partial}{\partial i\zeta}\chi_{\hat{\rho}}(\xi,\zeta;t)\,, \tag{C.7}$$

$$\mathrm{Tr}\left\{\frac{1}{2i}\left(\hat{\mathcal{O}}\,\mathrm{e}^{i2k\hat{z}} - \mathrm{e}^{-i2k\hat{z}}\,\hat{\mathcal{O}}\right)\hat{\rho}(t)\right\} = \frac{1}{2i}\,\mathrm{e}^{i\hbar k\zeta}\left[\chi_{\hat{\rho}}(\xi+2k,\zeta;t) - \chi_{\hat{\rho}}(\xi-2k,\zeta;t)\right]\,, \tag{C.8}$$

and

$$\mathrm{Tr}\left\{\frac{1}{2i}\left(\mathrm{e}^{i2k\hat{z}}\,\hat{\mathcal{O}} - \hat{\mathcal{O}}\,\mathrm{e}^{-i2k\hat{z}}\right)\hat{\rho}(t)\right\} = \frac{1}{2i}\,\mathrm{e}^{-i\hbar k\zeta}\left[\chi_{\hat{\rho}}(\xi+2k,\zeta;t) - \chi_{\hat{\rho}}(\xi-2k,\zeta;t)\right]\,. \tag{C.9}$$

Next, we perform the Fourier transformation according to Eq. (C.3) and obtain

$$\int\mathrm{d}\xi\int\mathrm{d}\zeta\,\mathrm{e}^{-iz\xi}\,\mathrm{e}^{-ip\zeta}\left(-\hbar\xi\frac{\partial}{\partial i\zeta}\chi_{\hat{\rho}}(\xi,\zeta;t)\right) = -\frac{p}{m}\frac{\partial}{\partial z}W(z,p;t)\,, \tag{C.10}$$

$$\int\mathrm{d}\xi\int\mathrm{d}\zeta\,\mathrm{e}^{-iz\xi}\,\mathrm{e}^{-ip\zeta}\left\{\frac{1}{2i}\,\mathrm{e}^{i\hbar k\zeta}\left[\chi_{\hat{\rho}}(\xi+2k,\zeta;t) - \chi_{\hat{\rho}}(\xi-2k,\zeta;t)\right]\right\} = \sin 2kz\,W(z,p-\hbar k;t)\,, \tag{C.11}$$

and

$$\int\mathrm{d}\xi\int\mathrm{d}\zeta\,\mathrm{e}^{-iz\xi}\,\mathrm{e}^{-ip\zeta}\left\{\frac{1}{2i}\,\mathrm{e}^{-i\hbar k\zeta}\left[\chi_{\hat{\rho}}(\xi+2k,\zeta;t) - \chi_{\hat{\rho}}(\xi-2k,\zeta;t)\right]\right\} = \sin 2kz\,W(z,p+\hbar k;t)\,. \tag{C.12}$$

Hence, we finally arrive at the Quantum Liouville equation

$$\left(\frac{\partial}{\partial t} + \frac{p}{m}\frac{\partial}{\partial z}\right)W(z,p;t) = -\frac{U_0|a_\mathrm{L}|}{\hbar}\sin 2kz\left[W(z,p+\hbar k;t) - W(z,p-\hbar k;t)\right] \tag{C.13}$$

which governs the dynamics of the Wigner function W for an electron in the FEL.

C.2 Wigner function for electron and laser field

In contrast to the preceding section we now derive the equation of motion for the Wigner function for the *combined* system of electron and quantized laser field in the FEL, which is the model in Chap. 4. We explicitly perform the operator ordering starting from the Hamiltonian, Eq. (4.3), and the density operator $\hat{\rho}$.

The time evolution of the density operator $\hat{\rho}$ for the electron and the laser field has to be calculated from the von Neumann equation, Eq. (C.1), where we have to use the Hamiltonian

$$\hat{H} = \frac{\hat{p}^2}{2m} + \hbar g \left(\hat{a}_\mathrm{L} \, \mathrm{e}^{i2k\hat{z}} + \hat{a}_\mathrm{L}^\dagger \, \mathrm{e}^{-i2k\hat{z}} \right) \tag{C.14}$$

governing the dynamics for the FEL.

The Wigner function $W(z, p, \alpha, \alpha^*; t)$ of the combined system is defined by the Fourier transform

$$W(z, p, \alpha, \alpha^*; t) \equiv \int \mathrm{d}\xi \int \mathrm{d}\zeta \int \mathrm{d}\beta \int \mathrm{d}\beta^* \, \mathrm{e}^{-iz\xi} \, \mathrm{e}^{-ip\zeta} \, \mathrm{e}^{-i\alpha\beta} \, \mathrm{e}^{-i\alpha^*\beta^*} \, \chi_{\hat{\rho}}(\xi, \zeta, \beta, \beta^*; t) \tag{C.15}$$

of the corresponding characteristic function $\chi_{\hat{\rho}}(\xi, \zeta, \beta, \beta^*; t)$ of the density operator. The variables z and p again play the role of electron position and momentum, respectively, while α and α^* can be interpreted as complex amplitudes of the laser field.

We obtain the characteristic function $\chi_{\hat{\rho}}$ by the ordering procedure

$$\chi_{\hat{\rho}} \equiv \mathrm{Tr} \left\{ \hat{\mathcal{O}} \hat{\rho} \right\} = \mathrm{Tr} \left\{ \hat{\mathcal{O}}_\mathrm{el} \hat{\mathcal{O}}_\mathrm{L} \hat{\rho} \right\} \tag{C.16}$$

from the density operator, where $\hat{\mathcal{O}}_\mathrm{el}$ and $\hat{\mathcal{O}}_\mathrm{L}$ are given by

$$\hat{\mathcal{O}}_\mathrm{el} \equiv \mathrm{e}^{i\xi\hat{z} + i\zeta\hat{p}} \tag{C.17}$$

and

$$\hat{\mathcal{O}}_\mathrm{L} \equiv \mathrm{e}^{i\beta\hat{a}_\mathrm{L} + i\beta^*\hat{a}_\mathrm{L}} \,, \tag{C.18}$$

respectively, for the particular choice of the Wigner representation [82].

We now transform the von Neumann equation, Eq. (C.1), for the Hamiltonian, Eq. (C.14), into this representation and arrive at

$$\begin{aligned} \frac{\partial}{\partial t} \chi_{\hat{\rho}}(\xi, \zeta, \beta, \beta^*, t) = &- \frac{i}{\hbar} \frac{1}{m} \mathrm{Tr} \left\{ \left(\hat{\mathcal{O}} \frac{\hat{p}^2}{2} - \frac{\hat{p}^2}{2} \hat{\mathcal{O}} \right) \hat{\rho} \right\} \\ &- \frac{i}{\hbar} U_0 \left(\mathrm{Tr} \left\{ \hat{\mathcal{O}} \hat{a}_\mathrm{L} \, \mathrm{e}^{i2k\hat{z}} \, \hat{\rho} \right\} - \mathrm{Tr} \left\{ \hat{a}_\mathrm{L} \, \mathrm{e}^{i2k\hat{z}} \, \hat{\mathcal{O}} \hat{\rho} \right\} \right) \\ &- \frac{i}{\hbar} U_0 \left(\mathrm{Tr} \left\{ \hat{\mathcal{O}} \hat{a}_\mathrm{L}^\dagger \, \mathrm{e}^{-i2k\hat{z}} \, \hat{\rho} \right\} - \mathrm{Tr} \left\{ \hat{a}_\mathrm{L}^\dagger \, \mathrm{e}^{-i2k\hat{z}} \, \hat{\mathcal{O}} \hat{\rho} \right\} \right) \,, \end{aligned} \tag{C.19}$$

where we have inserted the Hamiltonian, Eq. (C.14), into the von Neumann equation Eq. (C.1), have performed the operator ordering Eq. (C.16) and have made use of the possibility of permuting operators cyclically in traces.

Inserting the definitions, Eqs. (C.17) and (C.18), for $\hat{\mathcal{O}}_\mathrm{el}$ and $\hat{\mathcal{O}}_\mathrm{L}$, respectively, as well as utilizing the Baker–Campbell–Hausdorff theorem, Eq. (3.16), and the commutation relations $[\hat{z}, \hat{p}] = i\hbar$ and $[\hat{a}_\mathrm{L}, \hat{a}_\mathrm{L}^\dagger] = 1$ for the electron position $\hat{z}$ and momentum $\hat{p}$ and for photon annihilation $\hat{a}_\mathrm{L}$ and creation operator $\hat{a}_\mathrm{L}^\dagger$, respectively, we obtain the expressions

$$\mathrm{Tr} \left\{ \left(\hat{\mathcal{O}} \frac{\hat{p}^2}{2} - \frac{\hat{p}^2}{2} \hat{\mathcal{O}} \right) \hat{\rho} \right\} = -\hbar\xi \frac{\partial}{\partial i\zeta} \chi_{\hat{\rho}}(\xi, \zeta, \beta, \beta^*; t) \,, \tag{C.20}$$

$$\mathrm{Tr}\left\{\hat{\mathcal{O}}\hat{a}_\mathrm{L}\,\mathrm{e}^{i2k\hat{z}}\,\hat{\rho}\right\} = \left(\frac{\partial}{\partial i\beta} - \frac{i\beta^*}{2}\right)\mathrm{e}^{i\hbar k\zeta}\,\chi_{\hat{\rho}}(\xi+2k,\zeta,\beta,\beta^*;t)\,, \tag{C.21}$$

$$\mathrm{Tr}\left\{\hat{a}_\mathrm{L}\,\mathrm{e}^{i2k\hat{z}}\,\hat{\mathcal{O}}\hat{\rho}\right\} = \left(\frac{\partial}{\partial i\beta} + \frac{i\beta^*}{2}\right)\mathrm{e}^{-i\hbar k\zeta}\,\chi_{\hat{\rho}}(\xi+2k,\zeta,\beta,\beta^*;t)\,, \tag{C.22}$$

$$\mathrm{Tr}\left\{\hat{\mathcal{O}}\hat{a}_\mathrm{L}^\dagger\,\mathrm{e}^{-i2k\hat{z}}\,\hat{\rho}\right\} = \left(\frac{\partial}{\partial i\beta^*} + \frac{i\beta}{2}\right)\mathrm{e}^{-i\hbar k\zeta}\,\chi_{\hat{\rho}}(\xi-2k,\zeta,\beta,\beta^*;t)\,. \tag{C.23}$$

and

$$\mathrm{Tr}\left\{\hat{a}_\mathrm{L}^\dagger\,\mathrm{e}^{-i2k\hat{z}}\,\hat{\mathcal{O}}\hat{\rho}\right\} = \left(\frac{\partial}{\partial i\beta^*} - \frac{i\beta}{2}\right)\mathrm{e}^{i\hbar k\zeta}\,\chi_{\hat{\rho}}(\xi-2k,\zeta,\beta,\beta^*;t)\,. \tag{C.24}$$

The Fourier transforms of these expressions, Eqs. (C.20)–(C.24) read

$$\begin{aligned}\int\mathrm{d}\xi\int\mathrm{d}\zeta\int\mathrm{d}\beta\int\mathrm{d}\beta^*\,\mathrm{e}^{-iz\xi}\,\mathrm{e}^{-ip\zeta}\,\mathrm{e}^{-i\alpha\beta}\,\mathrm{e}^{-i\alpha^*\beta^*}\left(-\hbar\xi\frac{\partial}{\partial i\zeta}\chi_{\hat{\rho}}(\xi,\zeta,\beta,\beta^*;t)\right)\\ = -i\hbar p\frac{\partial}{\partial z}W(z,p,\alpha,\alpha^*;t)\,,\end{aligned} \tag{C.25}$$

$$\begin{aligned}\int\mathrm{d}\xi\int\mathrm{d}\zeta\int\mathrm{d}\beta\int\mathrm{d}\beta^*\,\mathrm{e}^{-iz\xi}\,\mathrm{e}^{-ip\zeta}\,\mathrm{e}^{-i\alpha\beta}\,\mathrm{e}^{-i\alpha^*\beta^*}\left[\left(\frac{\partial}{\partial i\beta} - \frac{i\beta^*}{2}\right)\mathrm{e}^{i\hbar k\zeta}\,\chi_{\hat{\rho}}(\xi+2k,\zeta,\beta,\beta^*;t)\right]\\ = \left(\alpha + \frac{1}{2}\frac{\partial}{\partial\alpha^*}\right)\mathrm{e}^{i2kz}\,W(z,p-\hbar k,\alpha,\alpha^*;t)\,,\end{aligned} \tag{C.26}$$

$$\begin{aligned}\int\mathrm{d}\xi\int\mathrm{d}\zeta\int\mathrm{d}\beta\int\mathrm{d}\beta^*\,\mathrm{e}^{-iz\xi}\,\mathrm{e}^{-ip\zeta}\,\mathrm{e}^{-i\alpha\beta}\,\mathrm{e}^{-i\alpha^*\beta^*}\left[\left(\frac{\partial}{\partial i\beta} + \frac{i\beta^*}{2}\right)\mathrm{e}^{-i\hbar k\zeta}\,\chi_{\hat{\rho}}(\xi+2k,\zeta,\beta,\beta^*;t)\right]\\ = \left(\alpha - \frac{1}{2}\frac{\partial}{\partial\alpha^*}\right)\mathrm{e}^{i2kz}\,W(z,p+\hbar k,\alpha,\alpha^*;t)\,,\end{aligned} \tag{C.27}$$

$$\begin{aligned}\int\mathrm{d}\xi\int\mathrm{d}\zeta\int\mathrm{d}\beta\int\mathrm{d}\beta^*\,\mathrm{e}^{-iz\xi}\,\mathrm{e}^{-ip\zeta}\,\mathrm{e}^{-i\alpha\beta}\,\mathrm{e}^{-i\alpha^*\beta^*}\left[\left(\frac{\partial}{\partial i\beta^*} + \frac{i\beta}{2}\right)\mathrm{e}^{-i\hbar k\zeta}\,\chi_{\hat{\rho}}(\xi-2k,\zeta,\beta,\beta^*;t)\right]\\ = \left(\alpha^* - \frac{1}{2}\frac{\partial}{\partial\alpha}\right)\mathrm{e}^{-i2kz}\,W(z,p+\hbar k,\alpha,\alpha^*;t)\,,\end{aligned} \tag{C.28}$$

and

$$\begin{aligned}\int\mathrm{d}\xi\int\mathrm{d}\zeta\int\mathrm{d}\beta\int\mathrm{d}\beta^*\,\mathrm{e}^{-iz\xi}\,\mathrm{e}^{-ip\zeta}\,\mathrm{e}^{-i\alpha\beta}\,\mathrm{e}^{-i\alpha^*\beta^*}\left[\left(\frac{\partial}{\partial i\beta^*} - \frac{i\beta}{2}\right)\mathrm{e}^{i\hbar k\zeta}\,\chi_{\hat{\rho}}(\xi-2k,\zeta,\beta,\beta^*;t)\right]\\ = \left(\alpha^* + \frac{1}{2}\frac{\partial}{\partial\alpha}\right)\mathrm{e}^{-i2kz}\,W(z,p-\hbar k,\alpha,\alpha^*;t)\,,\end{aligned} \tag{C.29}$$

where we have used the definition, Eq. (C.15), of the Wigner distribution function.

Finally, we arrive at the equation

$$\begin{aligned}\frac{\partial}{\partial t}W(z,p,\alpha,\alpha^*;t) = &-\frac{p}{m}\frac{\partial}{\partial z}W(z,p,\alpha,\alpha^*;t)\\ &-\frac{1}{i}\frac{2k\hbar g}{2\hbar k}\left(\alpha\,\mathrm{e}^{i2kz}-\alpha^*\,\mathrm{e}^{-i2kz}\right)\\ &\times\left[W(z,p+\hbar k,\alpha,\alpha^*;t)-W(z,p-\hbar k,\alpha,\alpha^*;t)\right]\\ &+\frac{1}{2i}\frac{2k\hbar g}{2\hbar k}\left(\frac{\partial}{\partial\alpha^*}\,\mathrm{e}^{i2kz}-\frac{\partial}{\partial\alpha}\,\mathrm{e}^{-i2kz}\right)\\ &\times\left[W(z,p+\hbar k,\alpha,\alpha^*;t)+W(z,p-\hbar k,\alpha,\alpha^*;t)\right]\end{aligned} \tag{C.30}$$

for the time evolution of the Wigner function.

C.3 Elimination of electron variables

We now present the detailed calculations to eliminate the electron variables from the Quantum Liouville equation, Eq. (4.11), in the classical limit of the FEL. Since we consider the low-gain small-signal regime we employ a perturbative approach before we average over positions and momenta of the electrons. For this purpose, we first outline our procedure before we derive the explicit expressions in second and fourth order, respectively.

C.3.1 Outline

The structure of the Liouville equation, Eq. (4.11), can be written as

$$\mathcal{L}_0 W = \mathcal{L}_1 W \tag{C.31}$$

where the free dynamics of the electron is given by

$$\mathcal{L}_0 \equiv \frac{\partial}{\partial\bar{\tau}} + \wp\frac{\partial}{\partial\theta} \tag{C.32}$$

while

$$\mathcal{L}_1 \equiv -\frac{1}{2i}\kappa\left[\alpha\,\mathrm{e}^{i\theta}-\alpha^*\,\mathrm{e}^{-i\theta}\right]\frac{\partial}{\partial_\wp} + \frac{1}{2i}\frac{\kappa}{2}\left[\frac{1}{\omega_\mathrm{r}T}\frac{\partial}{\partial\alpha^*}\,\mathrm{e}^{i\theta}-\frac{1}{\omega_\mathrm{r}T}\frac{\partial}{\partial\alpha}\,\mathrm{e}^{-i\theta}\right] \tag{C.33}$$

describes the interaction of electron and laser field.
By assuming that $\mathcal{L}_1$ just causes a small perturbation to the motion of the electron we write the Wigner function

$$W \cong W^{(0)} + W^{(1)} + W^{(2)} + \ldots \tag{C.34}$$

as an asymptotic expansion. When we insert this expansion into Eq. (C.31) we obtain

$$\begin{cases}\mathcal{L}_0 W^{(n)} &= \mathcal{L}_1 W^{(n-1)}\\ \mathcal{L}_0 W^{(0)} &= 0\end{cases} \tag{C.35}$$

which we have to solve order by order.

Before the electrons enter the wiggler, electron and laser field are uncorrelated leading to an initial Wigner function of the form

$$W(\wp, \alpha, \alpha^*; \tau) = \frac{1}{2\pi} g(\wp) W_{\mathrm{L}}(\alpha, \alpha^*; \tau)\,, \tag{C.36}$$

where $W_{\mathrm{L}}(\alpha, \alpha^*; \tau)$ denotes the Wigner function for the field while the electrons are distributed uniformly in position space and according to the function $g(\wp)$ in momentum space.
The zeroth-order solution of Eq. (C.35)

$$W^{(0)}(\theta, \wp, \alpha, \alpha^*; \bar{\tau}) = W(\theta - \wp(\bar{\tau} - \tau), \alpha, \alpha^*; \tau) = W(\wp, \alpha, \alpha^*; \tau) \tag{C.37}$$

displaces the argument corresponding to θ of the initial distribution by $\wp(\bar{\tau} - \tau)$ according to the classical trajectories of a free particle. Since the electrons are uniformly distributed in θ-direction according to Eq. (C.36) the zeroth-order solution equals the initial Wigner function.
For all higher-order contributions to $W^{(n)}$ the formal solution of Eq. (C.35) reads

$$W^{(n)}(\theta, \wp, \alpha, \alpha^*; \bar{\tau}) = \int_{\tau}^{\bar{\tau}} \mathrm{d}\tau' \int \mathrm{d}\theta'\, G_{\mathrm{free}}(\theta, \bar{\tau}; \theta', \tau') \left\{ \left[\mathcal{L}_1 W^{(n-1)} \right] (\theta', \wp'; \tau') \right\}\,, \tag{C.38}$$

where we have applied $\mathcal{L}_1$ on the solution $W^{(n-1)}$ of $(n-1)$th order and have propagated the resulting expression by the Green's function [65]

$$G_{\mathrm{free}}(\theta, \bar{\tau}; \theta', \tau') = \delta(\theta - \theta' - \wp(\bar{\tau} - \tau)) \tag{C.39}$$

for the free dynamics of the electron due to $\mathcal{L}_0$. To eliminate the electron variables from the Wigner function of the total system we simply integrate our result $W^{(n)}$ with respect to θ and to $\wp$ and arrive at

$$W_{\mathrm{L}}^{(n)}(\alpha, \alpha^*; \bar{\tau}) = \int \mathrm{d}\theta \int \mathrm{d}\wp\, W^{(n)}(\theta, \wp, \alpha, \alpha^*; \bar{\tau}) \tag{C.40}$$

for the reduced Wigner function for the subsystem of the laser field. By this procedure we straightforwardly identify $W_{\mathrm{L}}^{(0)} = W_{\mathrm{L}}(\alpha, \alpha^*; \tau)$ because electron and field are initially uncorrelated.
Since the operator $\mathcal{L}_1$ just contains terms with $\mathrm{e}^{i\theta}$ and $\mathrm{e}^{-i\theta}$ we obtain according to Eq. (C.38) a first-order solution of the form

$$W^{(1)} = w_+^{(1)}\, \mathrm{e}^{i\theta} + w_-^{(1)}\, \mathrm{e}^{-i\theta}\,, \tag{C.41}$$

where the $w_\pm^{(1)}$ are functions of $\wp$ and $\bar{\tau}$ but independent of θ. Due to the uniform distribution in θ the phase factors $\mathrm{e}^{i\theta}$ and $\mathrm{e}^{-i\theta}$ in Eq. (C.41) lead to a vanishing integral in Eq. (C.40) and hence the reduced Wigner function for the laser field does not possess a contribution of first order, that is $W_{\mathrm{L}}^{(1)} = 0$.
However, when we go to the solution in second order, that is

$$W^{(2)} = w_0^{(2)} + w_{+2}^{(2)}\, \mathrm{e}^{i2\theta} + w_{-2}^{(2)}\, \mathrm{e}^{-i2\theta} \tag{C.42}$$

we recognize the occurrence of a term independent of θ characterized by $w_0^{(2)}$. Applying $\mathcal{L}_1$ a second time leads to the contributions with $\mathrm{e}^{\pm i2\theta}$ but also to cross terms of the form $\mathrm{e}^{\pm i\theta}\,\mathrm{e}^{\mp i\theta} = 1$ responsible for $w_0^{(2)}$. Thus, we find, according to Eq. (C.40), the formal expression

$$W_{\mathrm{L}}^{(2)} = \int \mathrm{d}\wp\, w_0^{(2)} \tag{C.43}$$

for the reduced Wigner function in second order which is responsible for drift and diffusion in lowest order in the Fokker–Planck equation of the laser field.

In order to obtain saturation we even have to go higher orders of our perturbative approach. The third-order solution

$$W^{(3)} = w_+^{(3)}\,\mathrm{e}^{i\theta} + w_-^{(3)}\,\mathrm{e}^{-i\theta} + w_{+3}^{(3)}\,\mathrm{e}^{i3\theta} + w_{-3}^{(3)}\,\mathrm{e}^{-i3\theta} \tag{C.44}$$

is independent of θ and hence the reduced Wigner function vanishes for this order, that is $W_{\mathrm{L}}^{(3)} = 0$. However, when we consider the next higher order, cross terms, independent of θ, emerge when we apply $\mathcal{L}_1$ on terms including $\mathrm{e}^{i\theta}$ and $\mathrm{e}^{-i\theta}$. Therefore, we have to know $w_+^{(3)}$ and $w_-^{(3)}$ before we proceed. These terms arise from second-order contributions which are independent of θ, characterized by $w_0^{(2)}$, but also from ones that go with $\mathrm{e}^{\pm i2\theta}$ and thus we also have to consider $w_{+2}^{(2)}$ and $w_{-2}^{(2)}$.

The fourth-order solution then reads

$$W^{(4)} = w_0^{(4)} + w_{+2}^{(4)}\,\mathrm{e}^{i2\theta} + w_{-2}^{(4)}\,\mathrm{e}^{-i2\theta} + w_{+4}^{(4)}\,\mathrm{e}^{i4\theta} + w_{-4}^{(4)}\,\mathrm{e}^{-i4\theta} \tag{C.45}$$

and we obtain

$$W_{\mathrm{L}}^{(4)} = \int \mathrm{d}\wp\, w_0^{(4)} \tag{C.46}$$

for the reduced Wigner function in fourth order. These terms are responsible for higher-order contributions for drift and thus for self saturation of the laser.

C.3.2 Second order

Inserting the zeroth-order solution, Eq. (C.37), into Eq. (C.38) for $n = 1$, evaluating the delta function, Eq. (C.39), for θ' and performing the integration over time τ' yields the solution

$$\begin{aligned} W^{(1)}(\theta, \wp, \alpha, \alpha^*; \bar{\tau}) = \kappa \Bigg\{ & \frac{1}{2}\left[\alpha\,\mathrm{e}^{i\theta}\,\frac{1}{\wp} h_+^{(1)}(\wp, \bar{\tau}) + \alpha^*\,\mathrm{e}^{-i\theta}\,\frac{1}{\wp} h_-^{(1)}(\wp, \bar{\tau})\right] \frac{\partial}{\partial \wp} \\ & - \frac{1}{4}\left[\frac{1}{\omega_{\mathrm{r}} T}\frac{\partial}{\partial \alpha^*}\,\mathrm{e}^{i\theta}\, h_+^{(1)}(\wp, \bar{\tau}) + \frac{1}{\omega_{\mathrm{r}} T}\frac{\partial}{\partial \alpha}\,\mathrm{e}^{-i\theta}\, h_-^{(1)}(\wp, \bar{\tau})\right] \Bigg\} \frac{1}{2\pi} g(\wp) W_{\mathrm{L}}(\alpha, \alpha^*; \tau) \end{aligned} \tag{C.47}$$

in first order of κ with the coefficients

$$\begin{cases} h_+^{(1)}(\wp, \bar{\tau}) \equiv 1 - \mathrm{e}^{-i\wp(\bar{\tau} - \tau)} \\ h_-^{(1)}(\wp, \bar{\tau}) \equiv 1 - \mathrm{e}^{i\wp(\bar{\tau} - \tau)} \end{cases} \tag{C.48}$$

as functions of $\wp$ and τ.

For the second order we apply $\mathcal{L}_1$ on $W^{(1)}$, Eq. (C.47), and obtain four kind of contributions independent of θ: ones which depend on (i) $|\alpha|^2$, (ii) on $\alpha\dfrac{\partial}{\partial\alpha}$ or $\alpha^*\dfrac{\partial}{\partial\alpha^*}$, (iii) on $\dfrac{\partial}{\partial\alpha}\alpha$ or $\dfrac{\partial}{\partial\alpha^*}\alpha^*$ and (iv) on $\dfrac{\partial^2}{\partial\alpha\partial\alpha^*}$.

The terms (i) and (ii) do not contribute to $W_{\rm L}^{(2)}$, since the integration over momentum gives rise to expressions of the kind

$$\int \mathrm{d}\wp \frac{\partial}{\partial\wp} g(\wp) = g(\wp)|_{-\infty}^{\infty} = 0\,, \tag{C.49}$$

where we assumed that the momentum distribution $g(\wp)$ (as well as its derivative) vanishes at infinity.

For contributions of the type (iii) the integrations in Eq. (C.38) yield the expression

$$\left(w_0^{(2)}\right)_{\rm drift} = \frac{1}{2\pi}\frac{\kappa^2}{4}\frac{h_0^{(2)}(\wp,\bar\tau)}{\wp^2}\frac{\partial g(\wp)}{\partial\wp}\left(\frac{1}{\omega_{\rm r}T}\frac{\partial}{\partial\alpha}\alpha W_{\rm L}(\alpha,\alpha^*;\tau)\right) + \text{c.c.} \tag{C.50}$$

with

$$h_0^{(2)}(\wp,\bar\tau) \equiv \frac{1}{2}\left(\cos\left[\wp(\bar\tau-\tau)\right]-1\right) + \frac{i}{2}\left(\wp(\bar\tau-\tau) - \sin\left[\wp(\bar\tau-\tau)\right]\right)\,. \tag{C.51}$$

In the averaging process over the momenta according to the prescription, Eq. (C.43), we meet integrals of the form

$$\int \mathrm{d}\wp\, \frac{h_0^{(2)}(\wp,\bar\tau)}{\wp^2}\frac{\partial g(\wp)}{\partial\wp} = -\left.\frac{\partial}{\partial\wp}\left(\frac{h_0^{(2)}(\wp,\bar\tau)}{\wp^2}\right)\right|_{\wp=\bar\wp} \tag{C.52}$$

which we calculate by integration by parts and the assumption of a cold electron beam, that is $g(\wp) \cong \delta(\wp-\bar\wp)$.

Finally, we obtain the second-order contribution

$$\left(W_{\rm L}^{(2)}(\alpha,\alpha^*;\tau+1)\right)_{\rm drift} = -\frac{1}{N}\left(G_{\rm cl}^{(1)} + iM_{\rm cl}^{(1)}\right)\frac{\partial}{\partial\alpha}\alpha\, W_{\rm L}(\alpha,\alpha^*;\tau) + \text{c.c.} \tag{C.53}$$

of the reduced Wigner function corresponding to drift at time $\tau+1$, where

$$G_{\rm cl}^{(1)} \equiv (2/\pi^3) gTN\kappa\, \mathcal{A}_{\rm cl}(\bar\wp) \tag{C.54}$$

and

$$M_{\rm cl}^{(1)} \equiv \frac{gTN\kappa}{6}\mathcal{M}_{\rm cl}(\bar\wp) \tag{C.55}$$

denote the real and imaginary part of the drift coefficient, respectively, characterized by the momentum-dependent functions

$$\mathcal{A}_{\rm cl}(\wp) \equiv \frac{\pi^3}{2}\frac{1-\cos\wp-(\wp/2)\sin\wp}{\wp^3} \tag{C.56}$$

and

$$\mathcal{M}_{\mathrm{cl}}(\wp) \equiv 12\,\frac{\sin\wp - (\wp/2)(1+\cos\wp)}{\wp^3}\,, \tag{C.57}$$

respectively.

The terms of the kind (iv) give rise to the expression

$$\left(w_0^{(2)}\right)_{\mathrm{fluc}} = \frac{\kappa^2}{8}\frac{1-\cos\left[x(\bar{\tau}-\tau)\right]}{x^2}\frac{1}{2\pi}g(\wp)\frac{1}{(\omega_{\mathrm{r}}T)^2}\frac{\partial^2}{\partial\alpha\partial\alpha^*}W_{\mathrm{L}}(\alpha,\alpha^*;\tau) \tag{C.58}$$

due to Eq. (C.38) and averaging over momentum $\wp$, according to Eq. (C.43), yields

$$\left(W_{\mathrm{L}}^{(2)}(\alpha,\alpha^*;\tau+1)\right)_{\mathrm{fluc}} = \frac{1}{N}\delta n^{\mathrm{sp}}\frac{\partial^2}{\partial\alpha\partial\alpha^*}W_{\mathrm{L}}(\alpha,\alpha^*;\tau)\,. \tag{C.59}$$

Here, we have defined

$$\delta n^{\mathrm{sp}} \equiv (gT)^2 N\mathcal{S}(\bar{\wp}) \tag{C.60}$$

which equals the number of spontaneously emitted photons according to Chap. 4 with

$$\mathcal{S}(\wp) \equiv 2\frac{1-\cos\wp}{\wp^2} \tag{C.61}$$

denoting the corresponding characteristic function.

C.3.3 Fourth order

For nonzero contributions in fourth order of our perturbative expansion we require that there are no terms with $\partial/\partial\wp$ on the very left, since else integration by parts leads to vanishing expressions when $g(\wp)$ and its derivatives are zero for $\wp \to \pm\infty$ in analogy to Eq. (C.52). By inspection of $\mathcal{L}_1$, Eq. (C.33), thus only terms with $\partial/\partial\alpha$ and $\partial/\partial\alpha^*$, respectively, remain. Moreover, we just consider terms with $\dfrac{\partial}{\partial\alpha}\alpha|\alpha|^2$ and $\dfrac{\partial}{\partial\alpha^*}\alpha^*|\alpha|^2$ [22] since just these terms are responsible for self saturation, while other terms including more than one derivative with respect to α or α^* give higher-order corrections to the fluctuations.

For second order we thus have to consider an expression of the form

$$\tilde{W}^{(2)} = |\alpha|^2\tilde{w}_0^{(2)} + \alpha^2\,\mathrm{e}^{i2\theta}\,\tilde{w}_{+2}^{(2)} + \alpha^{*2}\,\mathrm{e}^{-i2\theta}\,\tilde{w}_{-2}^{(2)}\,, \tag{C.62}$$

where a tilde denotes the relevant terms in our present discussion. With the help of Eqs. (C.38), (C.39) and (C.47) we obtain

$$\begin{aligned}\tilde{w}_0^{(2)} = \frac{1}{2\pi}\frac{\kappa^2}{2}\Bigg[&\frac{\wp(\bar{\tau}-\tau)\sin\left[\wp(\bar{\tau}-\tau)\right] - 2\left(1-\cos\left[\wp(\bar{\tau}-\tau)\right]\right)}{\wp^3}\frac{\partial g(\wp)}{\partial\wp}\\ &+\frac{1-\cos\left[\wp(\bar{\tau}-\tau)\right]}{\wp^2}\frac{\partial^2 g(\wp)}{\partial\wp^2}\Bigg]W_{\mathrm{L}}(\alpha,\alpha^*;\tau)\end{aligned} \tag{C.63}$$

and

$$\tilde{w}_{+2}^{(2)} = \frac{1}{2\pi}\frac{\kappa^2}{4}\left[\frac{\frac{1}{2}\left(\mathrm{e}^{-i2\wp(\bar{\tau}-\tau)}-1\right)-\frac{1}{i}\wp(\bar{\tau}-\tau)\,\mathrm{e}^{-i\wp(\bar{\tau}-\tau)}}{\wp^3}\frac{\partial g(\wp)}{\partial\wp}\right.$$
$$\left.+\frac{\frac{1}{2}\,\mathrm{e}^{-i2\wp(\bar{\tau}-\tau)}-\mathrm{e}^{-i\wp(\bar{\tau}-\tau)}+\frac{1}{2}}{\wp^2}\frac{\partial^2 g(\wp)}{\partial\wp^2}\right] W_{\mathrm{L}}(\alpha,\alpha^*;\tau) \tag{C.64}$$

with $\tilde{w}_{-2}^{(2)} = \left(\tilde{w}_{+2}^{(2)}\right)^*$ for the coefficients in Eq. (C.62).
The relevant contribution in third order reads

$$\tilde{W}^{(3)} = \mathrm{e}^{i\theta}\,\alpha|\alpha|^2\tilde{w}_{+}^{(3)} + \mathrm{e}^{-i\theta}\,\alpha^*|\alpha|^2\tilde{w}_{-}^{(3)}\,. \tag{C.65}$$

In order to calculate the coefficients in Eq. (C.65) we first have to apply $\mathcal{L}_1$ on $\tilde{W}^{(2)}$ and arrive, due to Eqs. (C.33) and (C.62) at the expressions

$$\left(\mathcal{L}_1\tilde{w}^{(2)}\right)_+ = -\frac{\kappa}{2i}\alpha|\alpha|^2\left(\tilde{w}_0^{(2)}-\tilde{w}_{+2}^{(2)}\right) \tag{C.66}$$

and

$$\left(\mathcal{L}_1\tilde{w}^{(2)}\right)_- = \frac{\kappa}{2i}\alpha^*|\alpha|^2\left(\tilde{w}_0^{(2)}-\tilde{w}_{-2}^{(2)}\right)\,. \tag{C.67}$$

The solution, Eq. (C.38), in third order then leads to

$$\tilde{w}_{+}^{(3)} = \frac{1}{2\pi}\frac{\kappa^3}{4}\left[\frac{r_1(\wp,\bar{\tau})+is_1(\wp,\bar{\tau})}{\wp^5}\frac{\partial g(\wp)}{\partial\wp}+\frac{r_2(\wp,\bar{\tau})+is_2(\wp,\bar{\tau})}{\wp^4}\frac{\partial^2 g(\wp)}{\partial\wp^2}\right.$$
$$\left.+\frac{r_3(\wp,\bar{\tau})+is_3(\wp,\bar{\tau})}{\wp^3}\frac{\partial^3 g(\wp)}{\partial\wp^3}\right] W_{\mathrm{L}}(\alpha,\alpha^*;\tau) \tag{C.68}$$

with $\tilde{w}_{-}^{(3)} = \left(\tilde{w}_{+}^{(3)}\right)^*$.
The coefficients in Eq. (C.68) read

$$r_1(\wp,\bar{\tau}) \equiv -\frac{5}{4}\cos\left[2\wp(\bar{\tau}-\tau)\right]-4\cos\left[\wp(\bar{\tau}-\tau)\right]+\frac{21}{4}-\frac{1}{2}\wp(\bar{\tau}-\tau)\sin\left[2\wp(\bar{\tau}-\tau)\right]$$
$$-\frac{17}{4}\wp(\bar{\tau}-\tau)\sin\left[\wp(\bar{\tau}-\tau)\right]+\frac{3}{4}\wp^2(\bar{\tau}-\tau)^2\cos\left[\wp(\bar{\tau}-\tau)\right], \tag{C.69}$$

$$s_1(\wp,\bar{\tau}) \equiv \frac{5}{4}\sin\left[2\wp(\bar{\tau}-\tau)\right]-\frac{1}{4}\sin\left[\wp(\bar{\tau}-\tau)\right]-\frac{1}{2}\wp(\bar{\tau}-\tau)\cos\left[2\wp(\bar{\tau}-\tau)\right]$$
$$-\frac{7}{4}\wp(\bar{\tau}-\tau)\cos\left[\wp(\bar{\tau}-\tau)\right]-\frac{1}{4}\wp^2(\bar{\tau}-\tau)^2\sin\left[\wp(\bar{\tau}-\tau)\right], \tag{C.70}$$

$$r_2(\wp,\bar{\tau}) \equiv -\frac{3}{4}\cos\left[2\wp(\bar{\tau}-\tau)\right]+4\cos\left[\wp(\bar{\tau}-\tau)\right]-\frac{13}{4}-\frac{1}{2}\wp(\bar{\tau}-\tau)\sin\left[2\wp(\bar{\tau}-\tau)\right]$$
$$+\frac{3}{2}\wp(\bar{\tau}-\tau)\sin\left[\wp(\bar{\tau}-\tau)\right], \tag{C.71}$$

$$s_2(\wp,\bar{\tau}) \equiv \frac{3}{4}\sin\left[2\wp(\bar{\tau}-\tau)\right]-\frac{3}{2}\sin\left[\wp(\bar{\tau}-\tau)\right]-\frac{1}{2}\wp(\bar{\tau}-\tau)\cos\left[2\wp(\bar{\tau}-\tau)\right]$$
$$+\frac{1}{2}\wp(\bar{\tau}-\tau)\cos\left[\wp(\bar{\tau}-\tau)\right], \tag{C.72}$$

$$r_3(\wp,\bar{\tau}) \equiv \frac{1}{4}\cos\left[2\wp(\bar{\tau}-\tau)\right] - \cos\left[\wp(\bar{\tau}-\tau)\right] + \frac{3}{4}\,, \tag{C.73}$$

and

$$s_3(\wp,\bar{\tau}) \equiv -\frac{1}{4}\sin\left[2\wp(\bar{\tau}-\tau)\right] + \frac{1}{2}\sin\left[\wp(\bar{\tau}-\tau)\right] + \frac{3}{4} \tag{C.74}$$

which we have derived with the help of Eqs. (C.63), (C.64), (C.66) and (C.67).

The reduced Wigner function in fourth order can be written as

$$W_L^{(4)}(\alpha,\alpha^*;\tau+1) = \frac{\partial}{\partial\alpha}\alpha|\alpha^2|\,\varpi_{|\alpha|^2\alpha}^{(4)} + \frac{\partial}{\partial\alpha^*}\alpha^*|\alpha^2|\,\varpi_{|\alpha^*|^2\alpha}^{(4)} \tag{C.75}$$

with $\varpi_{|\alpha^*|^2\alpha}^{(4)} = \left(\varpi_{|\alpha|^2\alpha}^{(4)}\right)^*$ and has to be calculated by the integral

$$\varpi_{|\alpha^*|^2\alpha}^{(4)} = -\frac{\kappa}{4i}\frac{1}{\omega_\mathrm{r}T}\int\mathrm{d}\wp\int\mathrm{d}\theta\int\limits_{\tau}^{\tau+1}\mathrm{d}\bar{\tau}\,\tilde{w}_+^{(3)}(\wp,\bar{\tau}) \tag{C.76}$$

according to Eqs. (C.38) and (C.46). The averaging procedure over momentum $\wp$ yields

$$\int\mathrm{d}\wp\,\frac{r_1(\wp,\bar{\tau})+is_1(\wp,\bar{\tau})}{\wp^5}\frac{\partial g(\wp)}{\partial\wp} = -\frac{\partial}{\partial\wp}\left(\frac{r_1(\wp,\bar{\tau})+is_1(\wp,\bar{\tau})}{\wp^5}\right)\bigg|_{\wp=\bar{\wp}}\,, \tag{C.77}$$

$$\int\mathrm{d}\wp\,\frac{r_2(\wp,\bar{\tau})+is_2(\wp,\bar{\tau})}{\wp^4}\frac{\partial^2 g(\wp)}{\partial\wp^2} = \frac{\partial^2}{\partial\wp^2}\left(\frac{r_2(\wp,\bar{\tau})+is_2(\wp,\bar{\tau})}{\wp^4}\right)\bigg|_{\wp=\bar{\wp}} \tag{C.78}$$

and

$$\int\mathrm{d}\wp\,\frac{r_3(\wp,\bar{\tau})+is_3(\wp,\bar{\tau})}{\wp^3}\frac{\partial^3 g(\wp)}{\partial^3\wp} = -\frac{\partial^3}{\partial\wp^3}\left(\frac{r_3(\wp,\bar{\tau})+is_3(\wp,\bar{\tau})}{\wp^5}\right)\bigg|_{\wp=\bar{\wp}}\,, \tag{C.79}$$

respectively, where we have employed integration by parts and have again assumed a cold electron beam, that is $g(\wp) \cong \delta(\wp-\bar{\wp})$.

The final integration over time brings us to the contribution

$$W_\mathrm{L}^{(4)}(\alpha,\alpha^*;\tau+1) = \frac{1}{N}\left(G_\mathrm{cl}^{(3)} - iM_\mathrm{cl}^{(3)}\right)\frac{\partial}{\partial\alpha}\alpha|\alpha|^2 W_\mathrm{L}(\alpha,\alpha^*;t) \tag{C.80}$$

of the reduced Wigner function in fourth order, where we have introduced the coefficients

$$G_\mathrm{cl}^{(3)} \equiv \frac{gTN\kappa^3}{4\pi^5}\mathcal{B}_\mathrm{cl}(\bar{\wp}) \tag{C.81}$$

and

$$M_\mathrm{cl}^{(3)} \equiv \frac{gTN\kappa^3}{2\pi^6}\mathcal{R}_\mathrm{cl}(\bar{\wp}) \tag{C.82}$$

which are characterized by the functions

$$\mathcal{B}_{\mathrm{cl}}(\wp) \equiv \frac{\pi^5}{\wp^7}\left(\frac{9}{2}\cos 2\wp + 12\cos\wp - \frac{33}{2} + \frac{11}{4}\wp\sin 2\wp + \frac{53}{4}\wp\sin\wp - \frac{\wp^2}{2}\cos 2\wp - \frac{13}{4}\wp^2\cos\wp - \frac{\wp^3}{4}\sin\wp\right) \tag{C.83}$$

and

$$\mathcal{R}_{\mathrm{cl}}(\wp) \equiv \frac{\pi^6}{2\wp^7}\left(\frac{9}{2}\sin 2\wp + \frac{27}{2}\sin\wp - \frac{25}{4}\wp - \frac{11}{4}\wp\cos 2\wp - \frac{27}{2}\wp\cos\wp - \frac{\wp^2}{2}\sin 2\wp - \frac{13}{4}\wp^2\sin\wp + \frac{\wp^3}{4}\cos\wp\right), \tag{C.84}$$

respectively. Combining Eqs. (C.37), (C.53), (C.59) and (C.80) we obtain the expression

$$W_{\mathrm{L}}(\alpha,\alpha^*;\tau+1) - W_{\mathrm{L}}(\alpha,\alpha^*;\tau) = -\frac{1}{N}\frac{\partial}{\partial\alpha}\left\{\left[\left(G_{\mathrm{cl}}^{(1)} - G_{\mathrm{cl}}^{(3)}|\alpha|^2\right) + i\left(M_{\mathrm{cl}}^{(1)} + M_{\mathrm{cl}}^{(3)}|\alpha|^2\right)\right]\alpha\right\} \times W_{\mathrm{L}}(\alpha,\alpha^*;\tau) + \mathrm{c.c.} + \frac{1}{N}\delta n^{\mathrm{sp}}\frac{\partial^2}{\partial\alpha\partial\alpha^*}W_{\mathrm{L}}(\alpha,\alpha^*;\tau) \tag{C.85}$$

for the change of the reduced Wigner function of the laser field due to the interaction with a single electron.

C.4 Cavity losses

In this section we study the dynamics of the laser field due to cavity losses in the Wigner representation in analogy to Ref. [56], where the P-representation is employed. According to Ref. [22] the time evolution of a field in a cavity with quality Q is given by

$$\left(\frac{\partial\hat{\rho}(t)}{\partial t}\right)_{\mathrm{loss}} = \frac{\omega_{\mathrm{L}}}{2Q}\left(\left[\hat{a}_{\mathrm{L}}\hat{\rho}(t), a_{\mathrm{L}}^\dagger\right] + \left[\hat{a}_{\mathrm{L}}, \hat{\rho}(t)a_{\mathrm{L}}^\dagger\right]\right), \tag{C.86}$$

where we have set the number $\bar{n}$ of thermal photons to zero, $\bar{n} = 0$, for the sake of simplicity. The dynamics described by Eq. (C.86) arises when we couple the cavity to a reservoir, which for example can consist of harmonic oscillators [57] or of two-level atoms [22]. Moreover, we have to employ the Markoff approximation [57], where one assumes that the two-time correlations characterizing the bath decay very fast.

With the help of the definition $\chi_{\hat{\rho}} \equiv \mathrm{Tr}\left\{\hat{\mathcal{O}}_{\mathrm{L}}\hat{\rho}\right\}$ of the characteristic function $\chi_{\hat{\rho}}$ and by cyclically permuting the operators in the trace we arrive at

$$\left(\frac{\partial}{\partial t}\chi_{\hat{\rho}}(\beta,\beta^*,t)\right)_{\mathrm{loss}} = \frac{\omega_{\mathrm{L}}}{2Q}\,\mathrm{Tr}\left\{\left(2\hat{a}_{\mathrm{L}}^\dagger\hat{\mathcal{O}}_{\mathrm{L}}\hat{a}_{\mathrm{L}} - \hat{\mathcal{O}}_{\mathrm{L}}\hat{a}_{\mathrm{L}}^\dagger\hat{a}_{\mathrm{L}} - \hat{a}_{\mathrm{L}}^\dagger\hat{a}_{\mathrm{L}}\hat{\mathcal{O}}_{\mathrm{L}}\right)\hat{\rho}(t)\right\} \tag{C.87}$$

with the operator $\hat{\mathcal{O}}_\mathrm{L}$, Eq. (C.18), for Wigner–Weyl ordering. In a similar procedure as in Sec. C.2 we obtain that Eq. (C.87) is equivalent to

$$\left(\frac{\partial}{\partial t}\chi_{\hat{\rho}}(\beta,\beta^*,t)\right)_\mathrm{loss} = -\frac{\omega_\mathrm{L}}{2Q}\left[(i\beta^*)\frac{\partial}{\partial(i\beta^*)} + (i\beta)\frac{\partial}{\partial(i\beta)} + |\beta|^2\right]\chi_{\hat{\rho}}(\beta,\beta^*,t) \tag{C.88}$$

which is a closed equation for $\chi_{\hat{\rho}}$.
The Fourier transformation,

$$W_\mathrm{L}(\alpha,\alpha^*;t) \equiv \int \mathrm{d}^2\beta\ \mathrm{e}^{-i\alpha\beta}\,\mathrm{e}^{-i\alpha^*\beta^*}\,\chi_{\hat{\rho}}(\beta,\beta^*;t) \tag{C.89}$$

according to Eq. (C.15), yields the equation of motion

$$\left(\frac{\partial}{\partial t}W_\mathrm{L}(\alpha,\alpha^*;t)\right)_\mathrm{loss} = \frac{\omega_\mathrm{L}}{2Q}\left(\frac{\partial}{\partial\alpha}\alpha + \frac{\partial}{\partial\alpha^*}\alpha^*\right)W_\mathrm{L}(\alpha,\alpha^*;t) + \frac{\omega_\mathrm{L}}{2Q}\frac{\partial^2}{\partial\alpha\partial\alpha^*}W_\mathrm{L}(\alpha,\alpha^*;t) \tag{C.90}$$

for the Wigner function of the laser field due to cavity losses. We note the occurrence of drift, corresponding to an exponential decay of the field, as well as of fluctuations.

C.5 Phase diffusion

To conclude this appendix we derive the explicit form, Eq. (4.74), of the propagator for the diffusion of the laser phase φ in Chap. 4. Here, we follow the lines of Ref. [82] and solve the Fokker–Planck equation, Eq. (4.65),

$$\frac{\partial}{\partial t'}W_\mathrm{L}(\varphi,t';\varphi_0,t) = A_\varphi\frac{\partial}{\partial\varphi}W_\mathrm{L}(\varphi,t';\varphi_0,t) + \frac{1}{2}D_\mathrm{cl}\frac{\partial^2}{\partial\varphi^2}W_\mathrm{L}(\varphi,t';\varphi_0,t) \tag{C.91}$$

where only the phase φ of the amplitude $\alpha = \varrho\,\mathrm{e}^{-i\varphi}$ varies while the modulus ϱ is stabilized at its steady-state value. Moreover, we have introduced the drift coefficient A_φ, Eq. (4.66), as well as the Diffusion constant D_cl, Eq. (4.67).
According to Ref. [82] we make the ansatz

$$W_\mathrm{L}(\varphi,t';\varphi_0,t) = \sum_{n=-\infty}^{\infty} c_n(t')\,\mathrm{e}^{in\varphi} \tag{C.92}$$

and obtain after inserting this expression into Eq. (C.91) the differential equation

$$\dot{c}_n(t') = \left(inA_\mathrm{cl} - n^2\frac{D_\mathrm{cl}}{2}\right)c_n(t') \tag{C.93}$$

for the expansion coefficients c_n. The solution of Eq. (C.93) is simply given by the exponential

$$c_n(t') = c_n(t)\,\mathrm{e}^{inA_\mathrm{cl}(t'-t)}\,\mathrm{e}^{-n^2D_\mathrm{cl}(t'-t)/2}\ . \tag{C.94}$$

Initially, that is $t' = t$ the propagator should reduce to a Delta function which maps the phase φ to its initial values φ_0. With the choice $c_n(t) = \mathrm{e}^{-in\varphi_0}/(2\pi)$ as initial condition for

c_n we obtain the desired behavior, that is

$$W_{\mathrm{L}}(\varphi, t'; \varphi_0, t) \to \frac{1}{2\pi} \sum_{n=-\infty}^{\infty} \mathrm{e}^{in(\varphi-\varphi_0)} = \delta(\varphi - \varphi_0) \qquad \text{for} \quad t' \to t\,. \tag{C.95}$$

Hence, we arrive at the explicit expression

$$W_{\mathrm{L}}(\varphi, t'; \varphi_0, t) = \frac{1}{2\pi} \sum_{n=-\infty}^{\infty} \mathrm{e}^{in(\varphi-\varphi_0)}\, \mathrm{e}^{inA_\varphi(t'-t)}\, \mathrm{e}^{-n^2 D_{\mathrm{cl}}(t'-t)/2} \tag{C.96}$$

for the propagator of the Fokker-Planck equation, Eq. (C.91) .

D Method of Canonical Averaging

In this appendix we describe the method of canonical averaging according to Ref. [37] which is a special form of the Bogoliubov–Mitropolski method [36]. This variant has the advantage that it offers an effective Hamiltonian in operator form which is needed for our approach in the Heisenberg picture for the many-electron model of the FEL. We begin with the discussion of the general method before we apply it to the FEL, for (i) the single-electron model for different resonances as well as for (ii) the many-electron case.

D.1 Description of method

The method of averaging is suitable for systems with two different time scales [59]. In its canonical form [37] we first separate the state vector into a slowly and a rapidly varying term and thus obtain a transformed, effective, Hamiltonian for the slowly varying part. We have to make sure that this effective Hamiltonian is independent of time so that it really describes the slow part of the motion and secularly growing terms are absorbed into it. We achieve this by performing a perturbative treatment and obtain an expression for the effective Hamiltonian order by order.

D.1.1 Transformation of the Hamiltonian

The dynamics of a system described by a time-dependent Hamiltonian $\hat{H}(\tau)$ is predicted by the Schrödinger equation

$$i\frac{\mathrm{d}}{\mathrm{d}\tau}\,|\Psi(\tau)\rangle = \hat{H}(\tau)\,|\Psi(\tau)\rangle \tag{D.1}$$

for the state vector $|\Psi(\tau)\rangle$ of the system. We assume that the Hamiltonian is of the form

$$\hat{H}(\tau) \equiv \varepsilon \sum_{\mu} \hat{\mathcal{H}}_{\mu}\,\mathrm{e}^{i2\mu\tau}\,, \tag{D.2}$$

where $\varepsilon\|\hat{\mathcal{H}}_{\mu}\| \ll 1$ represents the slow time scale, while the rapid one is given by the oscillations with multiples of τ.
Since the Hamiltonian, Eq. (D.2), depends on two different time (or frequency) scales we make the separation ansatz

$$|\Psi(\tau)\rangle \equiv \mathrm{e}^{-\hat{F}(\tau)}\,|\Phi(\tau)\rangle \tag{D.3}$$

for the state $|\Psi(\tau)\rangle$. While $\hat{F}(\tau)$ is rapidly varying, $|\Phi(\tau)\rangle$ is slowly varying. With the help of the transformation, Eq. (D.3), and the Schrödinger equation, Eq. (D.1), we arrive at

$$i\frac{\mathrm{d}}{\mathrm{d}\tau}\,|\Phi(\tau)\rangle = \underbrace{\left(\left(i\frac{\mathrm{d}}{\mathrm{d}\tau}\,\mathrm{e}^{\hat{F}(\tau)}\right)\mathrm{e}^{-\hat{F}(\tau)} + \mathrm{e}^{\hat{F}(\tau)}\,\hat{H}(\tau)\,\mathrm{e}^{-\hat{F}(\tau)}\right)}_{\equiv\hat{H}_{\mathrm{eff}}}\,|\Phi(\tau)\rangle\,, \tag{D.4}$$

where the effective Hamiltonian $\hat{H}_{\text{eff}}$ governs the dynamics of $|\Phi(\tau)\rangle$. In contrast to the approach in Ref. [37] within the framework of the density operator $\hat{\rho}$ and the von Neumann equation, we develop the method for the state vector and the Schrödinger equation. However, both approaches are equivalent and in the rest of the derivation we closely follow the lines of Ref. [37].

While the second term of the effective Hamiltonian $\hat{H}_{\text{eff}}$ in Eq. (D.4) can be easily calculated with the help of the Baker–Campbell–Hausdorff formula, Eq. (B.13), the first one, including the derivative of a matrix exponential, needs a little more care. First, we write down the expansion

$$\frac{\mathrm{d}}{\mathrm{d}\tau} \exp\left\{\hat{F}(\tau)\right\} = \sum_{m}^{\infty} \frac{1}{m!} \left(\frac{\mathrm{d}}{\mathrm{d}\tau} \hat{F}^m(\tau)\right) . \tag{D.5}$$

Hence, we need an explicit expression for the derivative of $\hat{F}^m$ with respect to time τ for an arbitrary power m.

With the help of induction we prove in the following the identity

$$\frac{\mathrm{d}}{\mathrm{d}\tau} \hat{F}^m(\tau) = \sum_{j=0}^{m-1} \binom{m}{j+1} \left[\hat{F}(\tau), \frac{\mathrm{d}}{\mathrm{d}\tau} \hat{F}(\tau)\right]_j \left(\hat{F}(\tau)\right)^{m-(j+1)} , \tag{D.6}$$

where we have used the definition, Eqs. (B.14) and (B.15), of the mth commutator. For $m = 0$ and $m = 1$, the relation in Eq. (D.6) is easily verified. Performing the induction step $m \to m + 1$ we arrive at

$$\frac{\mathrm{d}}{\mathrm{d}\tau} \hat{F}^{m+1} = \left(\frac{\mathrm{d}\hat{F}}{\mathrm{d}\tau}\right) \hat{F}^m + \sum_{j=0}^{m-1} \binom{m}{j+1} \hat{F} \left[\hat{F}, \frac{\mathrm{d}\hat{F}}{\mathrm{d}\tau}\right]_j \hat{F}^{m-(j+1)} , \tag{D.7}$$

where we have already assumed that Eq. (D.6) is valid. When we order the expression in Eq. (D.7) such that all $\hat{F}$ are on the very right we obtain

$$\begin{aligned} \frac{\mathrm{d}}{\mathrm{d}\tau} \hat{F}^{m+1} = \left(\frac{\mathrm{d}\hat{F}}{\mathrm{d}\tau}\right) \hat{F}^m &+ \sum_{j=0}^{m-1} \binom{m}{j+1} \left[\hat{F}, \frac{\mathrm{d}\hat{F}}{\mathrm{d}\tau}\right]_j \hat{F}^{(m+1)-(j+1)} \\ &+ \sum_{j=0}^{m-1} \binom{m}{j+1} \left[\hat{F}, \frac{\mathrm{d}\hat{F}}{\mathrm{d}\tau}\right]_{j+1} \hat{F}^{m-(j+1)} . \end{aligned} \tag{D.8}$$

By shifting the summation indices appropriately the first sum in Eq. (D.8) can be cast into the form

$$\sum_{j=0}^{m-1} \binom{m}{j+1} \left[\hat{F}, \frac{\mathrm{d}\hat{F}}{\mathrm{d}\tau}\right]_{j+1} \hat{F}^{m-(j+1)} = \sum_{k=0}^{m-1} \binom{m}{k} \left[\hat{F}, \frac{\mathrm{d}\hat{F}}{\mathrm{d}\tau}\right]_k \hat{F}^{(m+1)-(k+1)} + \left[\hat{F}, \frac{\mathrm{d}\hat{F}}{\mathrm{d}\tau}\right]_m - \frac{\mathrm{d}\hat{F}}{\mathrm{d}\tau} \hat{F}^m \tag{D.9}$$

and with of the help of the fundamental relation [67]

$$\binom{m}{j} + \binom{m}{j+1} = \binom{m+1}{j+1} \tag{D.10}$$

for binomial coefficients we finally arrive at

$$\frac{\mathrm{d}}{\mathrm{d}\tau}\hat{F}^{m+1} = \sum_{j=0}^{m}\binom{m+1}{j+1}\left[\hat{F},\frac{\mathrm{d}\hat{F}}{\mathrm{d}\tau}\right]_j \hat{F}^{(m+1)-(j+1)} \tag{D.11}$$

which is according to Eq. (D.6) the desired expression for $m \to m+1$ and thus completes our proof.

Inserting the identity, Eq. (D.6), into the expansion, Eq. (D.5), yields

$$\begin{aligned}\frac{\mathrm{d}}{\mathrm{d}\tau}\,\mathrm{e}^{\hat{F}} &= \sum_{m=0}^{\infty}\sum_{j=0}^{m-1}\frac{1}{(j+1)!(m-(j+1))!}\left[\hat{F},\frac{\mathrm{d}\hat{F}}{\mathrm{d}\tau}\right]_j \hat{F}^{m-(j+1)} \\ &= \sum_{j=0}^{\infty}\frac{1}{(j+1)!}\left[\hat{F},\frac{\mathrm{d}}{\mathrm{d}\tau}\hat{F}\right]_j \sum_{k=0}^{\infty}\frac{\hat{F}^k}{k!}\,,\end{aligned} \tag{D.12}$$

where we have changed the summation in the second step according to $k \equiv m-(j+1)$ and have made use of the summation to infinity. Hence, we find

$$\frac{\mathrm{d}}{\mathrm{d}\tau}\,\mathrm{e}^{\hat{F}(\tau)} = \sum_{j=0}^{\infty}\frac{1}{(j+1)!}\left[\hat{F}(\tau),\frac{\mathrm{d}}{\mathrm{d}\tau}\hat{F}(\tau)\right]_j \mathrm{e}^{\hat{F}(\tau)} \tag{D.13}$$

for the derivative of $\exp\left\{\hat{F}\right\}$ with respect of time.

Finally, we obtain

$$\hat{H}_{\mathrm{eff}} = \sum_{j=0}^{\infty}\frac{1}{(j+1)!}\left[\hat{F}(\tau), i\frac{\mathrm{d}}{\mathrm{d}\tau}\hat{F}(\tau)\right]_j + \sum_{j=0}^{\infty}\frac{1}{j!}\left[\hat{F}(\tau),\hat{H}(\tau)\right]_j\,. \tag{D.14}$$

For the first term on the right-hand side of Eq. (D.4) we have used Eq. (D.13) and for the second one we have recalled the Baker–Campbell–Hausdorrf formula, Eq. (B.13).

D.1.2 Avoiding secular terms

In the ordinary perturbative treatment of the Schrödinger equation with a time-dependent Hamiltonian, described by Eq. (D.2), there occur terms independent of time either because of a nonzero component $\hat{\mathcal{H}}_0$ in Eq. (D.2) or in higher orders due to products of terms, where the rapidly varying phases cancel. An integration over time would lead to secular terms which grow with powers of τ and diverge for large times. To get rid of these terms we absorb them in the effective Hamiltonian

$$\hat{H}_{\mathrm{eff}} \neq \hat{H}_{\mathrm{eff}}(\tau) \tag{D.15}$$

which may not depend on time and which describes the slowly varying part of the dynamics.

In the following we pursue a perturbative approach to solve the dynamics, that is we expand the rapidly varying part

$$\hat{F}(\tau) = \varepsilon\hat{F}^{(1)}(\tau) + \varepsilon^2\hat{F}^{(2)}(\tau) + \varepsilon^3\hat{F}^{(3)}(\tau) + \ldots \tag{D.16}$$

and the effective Hamiltonian

$$\hat{H}_{\text{eff}} = \varepsilon \hat{H}_{\text{eff}}^{(1)} + \varepsilon^2 \hat{H}_{\text{eff}}^{(2)} + \varepsilon^3 \hat{H}_{\text{eff}}^{(3)} + ... \tag{D.17}$$

in powers of ε and write down the resulting expressions order by order with the condition that every order of $\hat{H}_{\text{eff}}$ is independent of time. We emphasize that although $\hat{H}_{\text{eff}}$, Eq. (D.17), itself is an asymptotic expansion we must not solve the equation of motion, Eq. (D.4), in a perturbative manner since this procedure would lead to the secular terms we wanted to avoid.

First order

Insertion of the expansions Eqs. (D.17) and (D.16) as well as of the original Hamiltonian, Eq. (D.2), into the effective Hamiltonian, Eq. (D.14), yields

$$\hat{H}_{\text{eff}}^{(1)} = \hat{\mathcal{H}}_0 + \underbrace{\left(i\frac{\mathrm{d}}{\mathrm{d}\tau}\hat{F}^{(1)}(\tau) + \sum_{\mu\neq 0} \hat{\mathcal{H}}_\mu \, \mathrm{e}^{i\mu\tau} \right)}_{=0} \tag{D.18}$$

where we have only considered terms of first order in ε. For $\hat{H}_{\text{eff}}^{(1)}$ to be time-independent the expression in parentheses has to vanish and we obtain

$$\hat{H}_{\text{eff}}^{(1)} = \hat{\mathcal{H}}_0 \tag{D.19}$$

for the effective Hamiltonian and

$$\hat{F}^{(1)}(\tau) = \sum_{\mu\neq 0} \frac{\mathrm{e}^{i2\mu\tau}}{2\mu} \hat{\mathcal{H}}_\mu \tag{D.20}$$

for the rapidly varying contribution in first order, where we have performed an integration over time for the latter quantity.

Second order

By the same procedure as for the first order we obtain the relation

$$\hat{H}_{\text{eff}}^{(2)} = i\frac{\mathrm{d}}{\mathrm{d}\tau}\hat{F}^{(2)}(\tau) + \frac{1}{2}\left[\hat{F}^{(1)}(\tau), \frac{\mathrm{d}}{\mathrm{d}\tau}\hat{F}^{(1)}(\tau)\right] + \left[\hat{F}^{(1)}(\tau), \sum_{\mu=0} \hat{\mathcal{H}}_\mu \, \mathrm{e}^{i\mu\tau}\right] \tag{D.21}$$

for the effective Hamiltonian in second order of ε which translates to

$$\hat{H}_{\text{eff}}^{(2)} = \frac{1}{2}\sum_{\nu\neq 0}\frac{1}{2\nu}\left[\hat{\mathcal{H}}_\nu, \hat{\mathcal{H}}_{-\nu}\right] + \underbrace{\left(i\frac{\mathrm{d}}{\mathrm{d}\tau}\hat{F}^{(2)}(\tau) + \frac{1}{2}\sum_{\substack{\mu,\nu\neq 0 \\ \mu+\nu\neq 0}} \frac{\mathrm{e}^{2i(\mu+\nu)\tau}}{2\mu}\left[\hat{\mathcal{H}}_\mu, \hat{\mathcal{H}}_\nu\right] + \sum_{\mu\neq 0}\frac{\mathrm{e}^{i2\mu\tau}}{2\mu}\left[\hat{\mathcal{H}}_\mu, \hat{\mathcal{H}}_0\right] \right)}_{=0} \tag{D.22}$$

after inserting the expressions Eqs. (D.19) and (D.20) for $\hat{H}_{\text{eff}}^{(1)}$ and $\hat{F}^{(1)}$, respectively. Again, the term in parentheses has to be zero to exclude all rapidly varying terms from $\hat{H}_{\text{eff}}$.

Hence, we find the results

$$\hat{H}_{\text{eff}}^{(2)} = \frac{1}{2}\sum_{\nu\neq 0}\frac{1}{2\nu}\left[\hat{\mathcal{H}}_{\nu},\hat{\mathcal{H}}_{-\nu}\right] \tag{D.23}$$

and

$$\hat{F}^{(2)}(\tau) = \frac{1}{2}\sum_{\substack{\mu,\rho\neq 0\\ \mu\neq\rho}}\frac{\mathrm{e}^{i2\rho\tau}}{4\mu\rho}\left[\hat{\mathcal{H}}_{\mu},\hat{\mathcal{H}}_{\rho-\mu}\right] + \sum_{\mu\neq 0}\frac{\mathrm{e}^{2i\mu\tau}}{4\mu^2}\left[\hat{\mathcal{H}}_{\mu},\hat{\mathcal{H}}_{0}\right] \tag{D.24}$$

for the second order of our asymptotic expansion. In the derivation of $\hat{F}^{(1)}$, Eq. (D.24), we have additionally integrated with respect to time τ and have changed the summation from ν to ρ according to the relation $\rho \equiv \mu + \nu$.

Third order

Collecting all third order terms in Eq. (D.14) we obtain

$$\begin{aligned}\hat{H}_{\text{eff}}^{(3)} = i\frac{\mathrm{d}}{\mathrm{d}\tau}\hat{F}^{(3)}(\tau) + \frac{1}{2}\left[\hat{F}^{(1)}(\tau), i\frac{\mathrm{d}}{\mathrm{d}\tau}\hat{F}^{(2)}(\tau)\right] + \frac{1}{2}\left[\hat{F}^{(2)}(\tau), i\frac{\mathrm{d}}{\mathrm{d}\tau}\hat{F}^{(1)}(\tau)\right]\\ +\frac{1}{6}\left[\hat{F}^{(1)}(\tau),\left[\hat{F}^{(1)}(\tau),\hat{F}^{(1)}(\tau)\right]\right] + \left[\hat{F}^{(1)}(\tau),\sum_{\mu=0}\hat{\mathcal{H}}_{\mu}\,\mathrm{e}^{2i\mu\tau}\right]\\ +\frac{1}{2}\left[\hat{F}^{(1)}(\tau),\left[\hat{F}^{(1)}(\tau),\sum_{\mu=0}\hat{\mathcal{H}}_{\mu}\,\mathrm{e}^{i2\mu\tau}\right]\right]\end{aligned} \tag{D.25}$$

for the third-order contribution $\hat{H}_{\text{eff}}^{(3)}$ of the effective Hamiltonian. In the following we omit the explicit expression for $\hat{F}^{(3)}$ and just derive the result of $\hat{H}_{\text{eff}}$. By inserting the identities Eqs. (D.20), and (D.24) for $\hat{F}^{(1)}$ and $\hat{F}^{(2)}$, respectively, into Eq. (D.25) we find after a lengthy but straightforward calculation the result

$$\hat{H}_{\text{eff}}^{(3)} = -\frac{1}{3}\sum_{\substack{\mu,\rho\neq 0\\ \mu+\rho\neq 0}}\frac{1}{4\mu(\mu+\rho)}\left[\hat{\mathcal{H}}_{-\mu-\rho},\left[\hat{\mathcal{H}}_{\mu},\hat{\mathcal{H}}_{\rho}\right]\right] - \frac{1}{2}\sum_{\mu\neq 0}\frac{1}{4\mu^2}\left[\hat{\mathcal{H}}_{\mu},\left[\hat{\mathcal{H}}_{-\mu},\hat{\mathcal{H}}_{0}\right]\right], \tag{D.26}$$

where we have assumed that all rapidly varying terms are absorbed in $\hat{F}^{(3)}$.

D.1.3 Heisenberg picture

The application of the canonical averaging in the Heisenberg picture is rather analogous to the procedure in the Schrödinger picture. That is why we highlight the differences of both approaches emerging due to a different sign in the von Neumann equation, Eq. (3.33), (which can be derived from the Schrödinger equation, Eq. (D.1)) and in the Heisenberg equation of motion, Eq. (3.10).
In analogy to Eq. (D.3) we perform the transformation

$$\hat{\mathcal{X}}(\tau) \equiv \mathrm{e}^{\hat{F}(\tau)}\,\hat{\mathcal{O}}\,\mathrm{e}^{-\hat{F}(\tau)} \tag{D.27}$$

of an operator $\hat{\mathcal{O}}$, with $\hat{\mathcal{X}}$ denoting the slowly varying part. With the help of the Heisenberg equation of motion, Eq. (3.10), we derive for this slowly varying part the dynamical equation

$$i\frac{\mathrm{d}}{\mathrm{d}\tau}\hat{\mathcal{X}}(\tau) = \left[\hat{\mathcal{X}}(\tau), \hat{H}_{\mathrm{eff}}\right] \tag{D.28}$$

governed by the effective Hamiltonian

$$\hat{H}_{\mathrm{eff}} \equiv \sum_{j=0}^{\infty} \frac{1}{(j+1)!}\left[\hat{F}(\tau), i\frac{\mathrm{d}}{\mathrm{d}\tau}\hat{F}(\tau)\right]_j - \sum_{j=0}^{\infty}\frac{1}{j!}\left[\hat{F}(\tau), \hat{H}(\tau)\right]_j \tag{D.29}$$

for which we demand $\hat{H}_{\mathrm{eff}} \neq \hat{H}_{\mathrm{eff}}(\tau)$. We note that $\hat{H}_{\mathrm{eff}}$ in Eq. (D.29) differs by a sign from the corresponding expression, Eq. (D.14), in the Schrödinger picture.
By making the asymptotic expansions, Eqs. (D.16) and (D.17), for $\hat{F}$ and $\hat{H}_{\mathrm{eff}}$, respectively, in powers of ε we derive how the expressions in the Heisenberg picture (subscript H) differ from the ones in the Schrödinger picture (subscript S). By this procedure we obtain

$$\begin{cases} \left(\hat{H}_{\mathrm{eff}}^{(1)}\right)_{\mathrm{H}} & = \left(\hat{H}_{\mathrm{eff}}^{(1)}\right)_{\mathrm{S}} \\ \left(\hat{F}^{(1)}(\tau)\right)_{\mathrm{H}} & = -\left(\hat{F}^{(1)}(\tau)\right)_{\mathrm{S}} \end{cases} \tag{D.30}$$

with $\left(\hat{H}_{\mathrm{eff}}^{(1)}\right)_{\mathrm{S}}$ and $\left(\hat{F}^{(1)}\right)_{\mathrm{S}}$ from Eqs. (D.19) and (D.20), respectively, as well as

$$\begin{cases} \left(\hat{H}_{\mathrm{eff}}^{(2)}\right)_{\mathrm{H}} & = -\left(\hat{H}_{\mathrm{eff}}^{(2)}\right)_{\mathrm{S}} \\ \left(\hat{F}^{(2)}(\tau)\right)_{\mathrm{H}} & = \left(\hat{F}^{(2)}(\tau)\right)_{\mathrm{S}} \end{cases} \tag{D.31}$$

with $\left(\hat{H}_{\mathrm{eff}}^{(1)}\right)_{\mathrm{S}}$ and $\left(\hat{F}^{(1)}\right)_{\mathrm{S}}$ from Eqs. (D.23) and (D.24), respectively, and

$$\left(\hat{H}_{\mathrm{eff}}^{(3)}\right)_{\mathrm{H}} = \left(\hat{H}_{\mathrm{eff}}^{(3)}\right)_{\mathrm{S}} \tag{D.32}$$

with $\left(\hat{H}_{\mathrm{eff}}^{(1)}\right)_{\mathrm{S}}$ from Eq. (D.26). Hence, the expressions for the effective Hamiltonian and the rapidly varying contributions differ in both pictures at most by a sign.

D.2 Averaging applied to the FEL

In the preceding section we have derived the general equations describing the method of canonical averaging. Now we apply them to the FEL for (i) the low-gain regime, that is the single-electron case and (ii) the high-gain regime, where we need a many-particle model. This procedure is crucial to obtain the quantum regime of the FEL as well as the corrections to it.

D.2.1 Single-electron model – first resonance

We begin our investigations for the FEL by applying the method of averaging to the single-electron model with the fundamental resonance, $p = q/2$. In this context we derive the higher-order contributions to the transition probabilities Eqs. (5.45) and (5.46) in the

framework of the method of canonical averaging. While we consider the slowly varying terms up to third order in α we calculate the contributions arising from the rapidly varying parts in second order of α. In both cases these are the lowest nonzero corrections to the two-level approximation.

We cast the single-particle Hamiltonian, Eq. (5.12), for the FEL into the form of Eq. (D.2), where the $\hat{\mathcal{H}}_\mu$ are given by

$$\begin{cases} \hat{\mathcal{H}}_0 \equiv & \hat{a}_\mathrm{L}\hat{\sigma}_{0,1} + \hat{a}_\mathrm{L}^\dagger\hat{\sigma}_{1,0} \\ \hat{\mathcal{H}}_\mu \equiv & \hat{a}_\mathrm{L}\hat{\sigma}_{-\mu,-\mu+1} + \hat{a}_\mathrm{L}^\dagger\hat{\sigma}_{\mu+1,\mu}\,, \qquad \mu \neq 0 \end{cases} \tag{D.33}$$

in accordance with Eqs. (5.16) and (5.17). Here, the operators $\hat{\sigma}_{\mu,\nu}$, defined in Eq. (5.5), denote the momentum projection operators fulfilling the commutation relation, Eq. (5.6),

$$[\hat{\sigma}_{\mu,\nu}, \hat{\sigma}_{\rho,\lambda}] = \delta_{\nu,\rho}\hat{\sigma}_{\mu,\lambda} - \delta_{\lambda,\mu}\hat{\sigma}_{\rho,\nu} \tag{D.34}$$

as well as the identity, Eq. (5.7),

$$\hat{\sigma}_{\mu,\nu}\hat{\sigma}_{\rho,\lambda} = \delta_{\nu,\rho}\hat{\sigma}_{\mu,\lambda} \tag{D.35}$$

with the latter one being only valid in the single-electron case. The annihilation $\hat{a}_\mathrm{L}$ and creation operator $\hat{a}_\mathrm{L}^\dagger$ for the laser field satisfy the relation $\left[\hat{a}_\mathrm{L}, \hat{a}_\mathrm{L}^\dagger\right] = 1$.

From now on, the procedure is straightforward: inserting the explicit expressions, Eq. (D.33), for $\hat{\mathcal{H}}_\mu$ into the identities for the effective Hamiltonian and the rapidly varying corrections derived in the preceding section and then use the commutation relations for the laser field and for the electron Eq. (D.34), together with Eq. (D.35) to obtain the final expressions for $\hat{H}_\mathrm{eff}$ and $\hat{F}$ up to third and second order in ε, respectively.

Then we search for the initial condition for $|\Phi\rangle$ according the transformation, Eq. (D.3), and solve the Schrödinger equation, Eq. (D.4), subject to this initial condition. To finally calculate the transition probabilities we have to transform back to the original state $|\Psi\rangle$ giving rise to rapidly varying contributions.

First order

With the help of Eqs. (D.19) and (D.20) we find the first-order contributions

$$\hat{H}_\mathrm{eff}^{(1)} \equiv \hat{\mathcal{H}}_0 = \hat{a}_\mathrm{L}\hat{\sigma}_{0,1} + \hat{a}_\mathrm{L}^\dagger\hat{\sigma}_{1,0} \tag{D.36}$$

and

$$\hat{F}^{(1)}(\tau) = -\hat{a}_\mathrm{L}\sum_{\mu\neq 0}\frac{\mathrm{e}^{-i2\mu\tau}}{2\mu}\hat{\sigma}_{\mu,\mu+1} + \hat{a}_\mathrm{L}^\dagger\sum_{\mu\neq 0}\frac{\mathrm{e}^{i2\mu\tau}}{2\mu}\hat{\sigma}_{\mu+1,\mu} \tag{D.37}$$

for the effective Hamiltonian and for the rapidly varying corrections, respectively. While $\hat{H}_\mathrm{eff}^{(1)}$ describes the resonant single-photon processes from excited p to ground state $p-q$ and vice versa, described by the operators $\hat{\sigma}_{1,0}$ and $\hat{\sigma}_{0,1}$, respectively, $\hat{F}^{(1)}$ includes all non-resonant single-photon transitions.

Second order

From Eqs. (D.23) and (D.24) we obtain in second order

$$\hat{H}_{\text{eff}}^{(2)} = -\frac{1}{2}\hat{a}_{\text{L}}\hat{a}_{\text{L}}^{\dagger}\hat{\sigma}_{1,1} - \frac{1}{2}\hat{a}_{\text{L}}^{\dagger}\hat{a}_{\text{L}}\hat{\sigma}_{0,0} - \hat{a}_{\text{L}}\hat{a}_{\text{L}}^{\dagger}\sum_{\nu\neq 0,1}\frac{1}{2\nu}\hat{\sigma}_{\nu,\nu} + \hat{a}_{\text{L}}^{\dagger}\hat{a}_{\text{L}}\sum_{\nu\neq 0,1}\frac{1}{2(\nu-1)}\hat{\sigma}_{\nu,\nu} \tag{D.38}$$

and

$$\begin{aligned}\hat{F}^{(2)}(\tau) =& \hat{a}_{\text{L}}^{2}\left[\frac{1}{4}\left(\hat{\sigma}_{-1,1}\,\mathrm{e}^{i2\tau} - \hat{\sigma}_{0,2}\,\mathrm{e}^{-i2\tau}\right) + \frac{1}{2}\sum_{\mu\neq 0,-1}\frac{\mathrm{e}^{-i2(2\mu+1)\tau}}{4\mu(\mu+1)(2\mu+1)}\hat{\sigma}_{\mu,\mu+2}\right] \\ & - \hat{a}_{\text{L}}^{\dagger\,2}\left[\frac{1}{4}\left(\hat{\sigma}_{1,-1}\,\mathrm{e}^{-i2\tau} - \hat{\sigma}_{2,0}\,\mathrm{e}^{i2\tau}\right) + \frac{1}{2}\sum_{\mu\neq 0,-1}\frac{\mathrm{e}^{i2(2\mu+1)\tau}}{4\mu(\mu+1)(2\mu+1)}\hat{\sigma}_{\mu+2,\mu}\right]\end{aligned} \tag{D.39}$$

for the effective Hamiltonian and the rapidly varying part, respectively. Two-photon transitions, where the electron momentum is the same before and after the interaction, are resonant and therefore contained in the effective Hamiltonian $\hat{H}_{\text{eff}}^{(2)}$. On the other hand, all other two-photon processes are non-resonant and appear in $\hat{F}^{(2)}$.

Third order

In third order we find for the effective Hamiltonian

$$\hat{H}_{\text{eff}}^{(3)} = -\frac{1}{8}\left(\hat{a}_{\text{L}}^{\dagger}\hat{a}_{\text{L}}^{2} + \hat{a}_{\text{L}}^{2}\hat{a}_{\text{L}}^{\dagger}\right)\hat{\sigma}_{0,1} - \frac{1}{8}\left(\hat{a}_{\text{L}}\hat{a}_{\text{L}}^{\dagger\,2} + \hat{a}_{\text{L}}^{\dagger\,2}\hat{a}_{\text{L}}\right)\hat{\sigma}_{1,0} + \frac{1}{4}\hat{a}_{\text{L}}^{3}\hat{\sigma}_{-1,2} + \frac{1}{4}\hat{a}_{\text{L}}^{\dagger\,3}\hat{\sigma}_{2,-1}\,, \tag{D.40}$$

where we have used Eq. (D.26). We note that besides three-photon transitions in the fundamental two-level system consisting of p and $p-q$ other three-photon processes appear for a two-level system with the momenta p and $p-3q$.

Initial conditions

When we write down the initial state $|\Psi(0)\rangle$ of the system in terms of the scattering basis $|n+\mu, p-\mu q\rangle$ we obtain

$$c_{\mu}(0) \equiv \langle n+\mu, p-\mu q|\Psi(0)\rangle = \delta_{\mu,0} \tag{D.41}$$

which simply means that we describe the electron initially by a momentum eigenstate with the resonant momentum $p = q/2$ and the laser field by a Fock state with the photon number n. The condition Eq. (D.41) can be brought into alternative form by defining the vector $\boldsymbol{c} \equiv (c_{-1}, c_0, c_1.c_2)^{\text{T}}$ and thus reads $\boldsymbol{c}(0) = (0,1,0,0)^{\text{T}}$. This notation will be convenient for our further investigations.

However, before solving the differential equation, dictated by the effective Hamiltonian, Eq. (D.17), we have to consider the initial condition for the slowly varying contribution $|\Phi\rangle$ and not of the total state vector $|\Psi\rangle$. Due to Eq. (D.3) we have to calculate

$$|\Phi(0)\rangle = \mathrm{e}^{\hat{F}(0)}\,|\Psi(0)\rangle \cong \left(\mathbb{1} + \varepsilon\hat{F}^{(1)}(0) + \varepsilon^{2}\frac{1}{2}\hat{F}^{(1)2} + \varepsilon^{2}\hat{F}^{(2)}(0)\right)|\psi(0)\rangle\,, \tag{D.42}$$

where we have used Eq. (D.5) and have expanded the exponential up to second order in ε. Defining the expansion coefficients

$$d_\mu(0) \equiv \langle n+\mu, p-\mu q|\Phi(0)\rangle \tag{D.43}$$

and inserting the expressions Eqs. (D.37) and (D.39) for $\hat{F}^1$ and $\hat{F}^{(2)}$, respectively, at $\tau = 0$ yields

$$d_\mu(0) = \left(1 - \frac{\alpha_{n-1}^2}{8}\right)\delta_{\mu,0} + \frac{\alpha_{n-1}}{2}\delta_{\mu,-1} + \frac{1}{4}\alpha_n\alpha_{n+1}\delta_{\mu,2} + \frac{1}{24}\alpha_{n-1}\alpha_{n-2}\delta_{\mu,-2} \tag{D.44}$$

or

$$\boldsymbol{d}(0) = \left(\frac{\alpha_{n-1}}{2}, 1 - \frac{\alpha_{n-1}^2}{8}, 0, \frac{1}{4}\alpha_n\alpha_{n+1}\right)^{\mathrm{T}} \tag{D.45}$$

in vector form. We note that this expression, Eq. (D.45), derived with the help of *canonical* averaging differs from the one derived in Eq. (D.6) of Ref. [4] which emerges in the standard method. This comes from the fact that the transformation, Eq. (D.1) in this reference is not an exponential like in Eq. (D.3), but a direct expansion in ε. However, both cases yield equivalent results, when, at the end, the back transformation to $|\Psi\rangle$ and c_μ is made.

Slowly varying terms

We now solve the Schrödinger equation

$$i\frac{\mathrm{d}}{\mathrm{d}\tau}|\Phi(\tau)\rangle = \hat{H}_{\mathrm{eff}}|\Phi(\tau)\rangle \tag{D.46}$$

for the slowly varying part $|\Phi\rangle$ of the state $|\Psi\rangle$ corresponding to the initial condition, Eq. (D.45). Applying the expansion Eq. (D.17), of $\hat{H}_{\mathrm{eff}}$ with the contributions $\hat{H}_{\mathrm{eff}}^{(1)}$, $\hat{H}_{\mathrm{eff}}^{(2)}$ and $\hat{H}_{\mathrm{eff}}^{(3)}$, from Eqs. (D.36), (D.38) and (D.40), respectively, we obtain two separate 'two-level systems': the first one is the usual one which consists of the levels $\mu = 0$ and $\mu = 1$, corresponding to the momenta $p = q/2$ and $p = -q/2$, respectively, while the other system is given by $\mu = -1$ and $\mu = 2$, that is $p = 3q/2$ and $p = -3q/2$, respectively.

For the fundamental two-level system we obtain the system of coupled differential equations

$$i\frac{\mathrm{d}}{\mathrm{d}\tau}\begin{pmatrix} d_0 \\ d_1 \end{pmatrix} = \begin{pmatrix} -\frac{\alpha_{n-1}^2}{2} & \alpha_n\left(1 - \frac{\alpha_n^2}{4}\right) \\ \alpha_n\left(1 - \frac{\alpha_n^2}{4}\right) & -\frac{\alpha_{n+1}^2}{2} \end{pmatrix}\begin{pmatrix} d_0 \\ d_1 \end{pmatrix} \tag{D.47}$$

where the second order contributions appear on the diagonal and effectively give just a global phase. That is why we need to include the third order contributions which appear on the off-diagonal and later can be identified as a shift of the Rabi frequency.

With the ansatz $\mathrm{e}^{-i\lambda\tau}$ we find from Eq. (D.47) the quadratic equation

$$\lambda^2 + \alpha_n^2\lambda - \alpha_n^2 + \left(\frac{\alpha_n^4}{2} + \frac{1}{4}\alpha_{n-1}^2\alpha_{n+1}^2\right) = 0 \tag{D.48}$$

which is solved by

$$\lambda_\pm \cong -\frac{\alpha_n^2}{2} \pm (\alpha_n - \chi_n) \tag{D.49}$$

with

$$\chi_n \equiv \frac{1}{8}\left(\alpha_n^3 + \frac{\alpha_{n-1}^2 \alpha_{n+1}^2}{\alpha_n}\right) \tag{D.50}$$

and we have neglected terms of fourth or higher order in α_n. The solution of Eq. (D.47) then reads

$$\begin{pmatrix} d_0(\tau) \\ d_1(\tau) \end{pmatrix} = \mathrm{e}^{i\alpha_n^2\tau/2} \begin{pmatrix} \cos\left[(\alpha_n - \chi_n)\,\tau\right] & -i\sin\left[(\alpha_n - \chi_n)\,\tau\right] \\ -i\sin\left[(\alpha_n - \chi_n)\,\tau\right] & \cos\left[(\alpha_n - \chi_n)\,\tau\right] \end{pmatrix} \begin{pmatrix} d_0(0) \\ d_1(0) \end{pmatrix}, \tag{D.51}$$

where we have not yet assumed specific initial conditions for d_0 and d_1.

The second two-level system evolves in time according to the differential equation

$$i\frac{\mathrm{d}}{\mathrm{d}\tau}\begin{pmatrix} d_{-1} \\ d_2 \end{pmatrix} = \begin{pmatrix} \frac{\alpha_n^2}{4} & \frac{1}{4}\alpha_{n-1}\alpha_n\alpha_{n+1} \\ \frac{1}{4}\alpha_{n-1}\alpha_n\alpha_{n+1} & \frac{\alpha_n^2}{4} \end{pmatrix} \begin{pmatrix} d_{-1} \\ d_2 \end{pmatrix} \tag{D.52}$$

which again can be solved with the ansatz $\sim \mathrm{e}^{-i\lambda\tau}$. From the resulting quadratic equation

$$\left(\lambda - \frac{\alpha_n^2}{4}\right)^2 - \left(\frac{1}{4}\alpha_{n-1}\alpha_n\alpha_{n+1}\right)^2 = 0 \tag{D.53}$$

we find

$$\lambda_\pm = \frac{\alpha_n^2}{4} \pm \frac{1}{4}\alpha_{n-1}\alpha_n\alpha_{n+1} \tag{D.54}$$

and hence

$$\begin{pmatrix} d_{-1}(\tau) \\ d_2(\tau) \end{pmatrix} = \mathrm{e}^{-i\alpha_n^2\tau/4} \begin{pmatrix} \cos\left(\frac{1}{4}\alpha_{n-1}\alpha_n\alpha_{n+1}\tau\right) & -i\sin\left(\frac{1}{4}\alpha_{n-1}\alpha_n\alpha_{n+1}\tau\right) \\ -i\sin\left(\frac{1}{4}\alpha_{n-1}\alpha_n\alpha_{n+1}\tau\right) & \cos\left(\frac{1}{4}\alpha_{n-1}\alpha_n\alpha_{n+1}\tau\right) \end{pmatrix} \begin{pmatrix} d_{-1}(0) \\ d_2(0) \end{pmatrix} \tag{D.55}$$

in analogy to Eq. (D.51).

Combining the expressions Eq. (D.51) and (D.52) and using the initial condition Eq. (D.45) we obtain

$$\begin{aligned} \boldsymbol{d}(\tau) = \mathrm{e}^{i\alpha_n^2\tau/2}\left(1 - \frac{\alpha_{n-1}^2}{8}\right)\begin{pmatrix} 0 \\ \cos\left[(\alpha_n - \chi_n)\,\tau\right] \\ -i\sin\left[(\alpha_n - \chi_n)\,\tau\right] \\ 0 \end{pmatrix} + \frac{\alpha_{n-1}}{2}\,\mathrm{e}^{-i\alpha_n^2\tau/4}\begin{pmatrix} \cos\left(\frac{1}{4}\alpha_{n-1}\alpha_n\alpha_{n+1}\tau\right) \\ 0 \\ 0 \\ -i\sin\left(\frac{1}{4}\alpha_{n-1}\alpha_n\alpha_{n+1}\tau\right) \end{pmatrix} \\ + \frac{1}{4}\alpha_n\alpha_{n+1}\,\mathrm{e}^{-i\alpha_n^2\tau/4}\begin{pmatrix} -i\sin\left(\frac{1}{4}\alpha_{n-1}\alpha_n\alpha_{n+1}\tau\right) \\ 0 \\ 0 \\ \cos\left(\frac{1}{4}\alpha_{n-1}\alpha_n\alpha_{n+1}\tau\right) \end{pmatrix} \end{aligned} \tag{D.56}$$

as the solution for the slowly-varying part. We note that the term in the second line of this equation, corresponding to the second-order corrections to d_{-1} and d_2, will later be of no importance when we calculate the transition probabilities, since they only result in terms of higher than second order in α. However, we have included this term in Eq. (D.56) for the sake of completeness.

In the following it is convenient to write $\boldsymbol{d}$, Eq. (D.56), as an expansion in α, that is

$$\boldsymbol{d}(\tau) \equiv \boldsymbol{d}^{(0)}(\tau) + \alpha \boldsymbol{d}^{(1)}(\tau) + \alpha^2 \boldsymbol{d}^{(2)}(\tau)\,, \tag{D.57}$$

where we have omitted the different indices of α, corresponding to different photon numbers, in order to simplify our notation.

Rapidly varying terms

To obtain the full solution for the state $|\Psi\rangle$ we have to consider the rapidly varying terms $\hat{F}(\tau)$ according to the transformation, Eq. (D.3). The arising corrections to the amplitude scale with powers of α.

From Eq. (D.3) and the expansion, Eq. (D.16), of $\hat{F}$ in powers of ε we obtain the evolved state

$$|\Psi(\tau)\rangle = \mathrm{e}^{-\hat{F}(\tau)}\,|\Phi(\tau)\rangle \cong \left(\mathbb{1} - \varepsilon\hat{F}^{(1)}(\tau) + \varepsilon^2\frac{1}{2}\hat{F}^{(1)2}(\tau) - \varepsilon^2\hat{F}^{(2)}(\tau)\right)|\Phi(\tau)\rangle\,, \tag{D.58}$$

where we have made a Taylor expansion of the exponential. We write this state again in terms of the coefficients

$$c_\mu(\tau) \equiv \langle n+\mu, p-\mu q|\Psi(\tau)\rangle \tag{D.59}$$

of the scattering basis.

For the excited, $\mu = 0$, and the ground state, $\mu = 1$, of the Quantum FEL we consider terms up to second order in α. Hence, we find with the help of Eqs. (D.37), (D.39), (D.56), (D.58), and (D.59) the expressions

$$c_0(\tau) = d_0^{(0)}(\tau) + \alpha^2\left(d_0^{(2)}(\tau) + \frac{1}{2}\,\mathrm{e}^{-i2\tau}\,d_{-1}^{(1)}(\tau) - \frac{1}{8}d_0^{(0)}(\tau)\right) \tag{D.60}$$

and

$$c_1(\tau) = d_1^{(0)}(\tau) + \alpha^2\left(d_1^{(2)}(\tau) + \frac{1}{2}\,\mathrm{e}^{-i2\tau}\,d_2^{(1)}(\tau) - \frac{1}{8}d_1^{(0)}(\tau)\right)\,. \tag{D.61}$$

When we later take the modulus square of theses amplitudes to calculate the probabilities we obtain that the cross term consisting of the contribution of zeroth and the one in second order scales with α^2. That is why we cannot neglect the second-order terms in Eqs. (D.60) and (D.61).

In contrast, according to Eq. (D.56), d_{-1} and d_2 have no zeroth-order contribution and thus neither have c_{-1} and c_2. Hence, we can restrict ourselves to the first order in α and arrive at

$$c_{-1}(\tau) = \alpha\left(d_{-1}^{(1)}(\tau) - \frac{1}{2}\,\mathrm{e}^{i2\tau}\,d_0^{(0)}(\tau)\right) \tag{D.62}$$

and

$$c_2(\tau) = \alpha \left(d_2^{(1)}(\tau) - \frac{1}{2} \mathrm{e}^{i2\tau} \, d_1^{(0)}(\tau) \right) , \tag{D.63}$$

where we have performed an analogous calculation like in the case of c_0 and c_1.

Probabilities

To obtain the probabilities characterizing the processes in the Quantum FEL we simply have to take the modulus square of the probability amplitudes c_μ. This procedure yields with the amplitudes in Eqs. (D.60) and (D.61) the expressions

$$\begin{aligned} |c_0(\tau)|^2 = &\left(1 - \frac{\alpha_{n-1}^2}{2}\right) \cos^2\left[(\alpha_n - \chi_n)\,\tau\right] \\ &+ \frac{\alpha_{n-1}^2}{2} \cos\left[\left(2 + \frac{3}{4}\alpha_n^2\right)\tau\right] \cos\left[(\alpha_n - \chi_n)\,\tau\right] \cos\left(\frac{1}{4}\alpha_{n-1}\alpha_n\alpha_{n+1}\tau\right) \end{aligned} \tag{D.64}$$

and

$$\begin{aligned} |c_1(\tau)|^2 = &\left(1 - \frac{\alpha_n^2}{2}\right) \sin^2\left[(\alpha_n - \chi_n)\,\tau\right] \\ &+ \frac{1}{2}\alpha_{n-1}\alpha_{n+1} \cos\left[\left(2 + \frac{3}{4}\alpha_n^2\right)\tau\right] \sin\left[(\alpha_n - \chi_n)\,\tau\right] \sin\left(\frac{1}{4}\alpha_{n-1}\alpha_n\alpha_{n+1}\tau\right) . \end{aligned} \tag{D.65}$$

While $|c_0|^2$ describes a process where the initial momentum $p = q/2$ is re-obtained at the end of the interaction, for $|c_1|^2$ the momentum has changed to $p = -q/2$.

The processes corresponding to a final momentum $p = 3q/2$ and $p = -3q/2$ are described by the probabilities

$$\begin{aligned} |c_{-1}(\tau)|^2 = \frac{\alpha_{n-1}^2}{4} \Big\{ &\cos^2\left[(\alpha_n - \chi_n)\,\tau\right] + \cos^2\left(\frac{1}{4}\alpha_{n-1}\alpha_n\alpha_{n+1}\tau\right) \\ &-2\cos\left[\left(2 + \frac{3}{4}\alpha_n^2\right)\tau\right] \cos\left[(\alpha_n - \chi_n)\,\tau\right] \cos\left(\frac{1}{4}\alpha_{n-1}\alpha_n\alpha_{n+1}\tau\right) \Big\} \end{aligned} \tag{D.66}$$

and

$$\begin{aligned} |c_2(\tau)|^2 = \frac{1}{4} \Big\{ &\alpha_{n+1}^2 \sin^2\left[(\alpha_n - \chi_n)\,\tau\right] + \alpha_{n-1}^2 \sin^2\left(\frac{1}{4}\alpha_{n-1}\alpha_n\alpha_{n+1}\tau\right) \\ &-2\alpha_{n-1}\alpha_{n+1} \cos\left[\left(2 + \frac{3}{4}\alpha_n^2\right)\tau\right] \sin\left[(\alpha_n - \chi_n)\,\tau\right] \sin\left(\frac{1}{4}\alpha_{n-1}\alpha_n\alpha_{n+1}\tau\right) \Big\} , \end{aligned} \tag{D.67}$$

respectively. Here, we have calculated the modulus square of the amplitudes given in Eqs.(D.63) and (D.62) and have used Eq. (D.56). We obtain that these 'two-photon' processes are suppressed with α^2 compared to 'single-photon' processes in Eqs. (D.64) and (D.65). Moreover, we note that the the sum of all probabilities gives unity which we should be expected for a unitary time evolution.

D.2.2 Single-electron model – second resonance

In the following we derive the transition probabilities for the FEL at the second resonance $p = q$ within the single-electron model. For this purpose, we again use the method of canonical averaging for which we consider contributions up to second order in frequency and up to second order in amplitude. We again find that for $\alpha \ll 1$ the dynamics reduces to the one of a two-level system which is, however, characterized by a decreased Rabi frequency when compared to the case of the first resonance $p = q/2$.
For $p = q$ the Hamiltonian, Eq. (5.12), is identical to

$$\hat{H}_\mathrm{I} = \varepsilon \left(\hat{a}_\mathrm{L} \sum_\mu \mathrm{e}^{-i2(\mu-1/2)\tau}\, \hat{\sigma}_{\mu,\mu+1} + \hat{a}_\mathrm{L}^\dagger \sum_\mu \mathrm{e}^{i2(\mu-1/2)\tau}\, \hat{\sigma}_{\mu+1,u} \right) . \tag{D.68}$$

To bring $\hat{H}_\mathrm{I}$ into the form of Eq. (D.2), which we need to perform canonical averaging, we change the summation index to $k \equiv \mu - 1/2$. We not that k covers the range

$$k = \ldots -\frac{3}{2}, -\frac{1}{2}, \frac{1}{2}, \frac{3}{2}, \ldots , \tag{D.69}$$

that is, k is an odd multiple of $1/2$. In our notation we stick in the following to Latin indices for this kind of summation while we use Greek letters for the usual summation over integer numbers.
Finally, we find the desired expression

$$\hat{H}_\mathrm{I} = \varepsilon \sum_k \hat{\mathcal{H}}_k\, \mathrm{e}^{i2k\tau} , \tag{D.70}$$

where

$$\begin{cases} \hat{\mathcal{H}}_0 & = 0 \\ \hat{\mathcal{H}}_k & = \hat{a}_\mathrm{L} \hat{\sigma}_{-k+\frac{1}{2},-k+\frac{3}{2}} + \hat{a}_\mathrm{L}^\dagger \hat{\sigma}_{k+\frac{3}{2},k+\frac{1}{2}} \end{cases} \tag{D.71}$$

give the single components.

First order

According to Eq. (D.71) the zeroth component $\hat{\mathcal{H}}_0$ is zero, and thus we have

$$\hat{H}_\mathrm{eff}^{(1)} = 0 . \tag{D.72}$$

Hence, we have to go to the next higher order of our perturbative expansion to find a nonzero contribution to the slowly varying part of the dynamics.
With the help of Eqs. (D.20) and (D.71) we find

$$\hat{F}^{(1)}(\tau) = -\hat{a}_\mathrm{L} \sum_\mu \frac{\mathrm{e}^{-i(2\mu-1)\tau}}{(2\mu-1)} \hat{\sigma}_{\mu,\mu+1} + \hat{a}_\mathrm{L}^\dagger \sum_\mu \frac{\mathrm{e}^{i(2\mu-1)\tau}}{(2\mu-1)} \hat{\sigma}_{\mu+1,\mu} \tag{D.73}$$

for the rapidly varying contribution, where we have returned to the summation over integer numbers.

Second Order

The second-order contribution, Eq. (D.23), of the effective Hamiltonian reads

$$\hat{H}_{\text{eff}}^{(2)} = \frac{1}{2}\sum_k \frac{1}{2k}\left[\hat{\mathcal{H}}_k, \hat{\mathcal{H}}_{-k}\right] \tag{D.74}$$

and by inserting the expression, Eq. (D.71), for $\hat{\mathcal{H}}_k$ we arrive at

$$\hat{H}_{\text{eff}}^{(2)} = \hat{a}_{\text{L}}^2\hat{\sigma}_{0,2} + \hat{a}_{\text{L}}^{\dagger\,2}\hat{\sigma}_{2,0} - \hat{a}_{\text{L}}\hat{a}_{\text{L}}^\dagger\sum_\mu \frac{1}{2\mu-1}\hat{\sigma}_{\mu,\mu} + \hat{a}_{\text{L}}^\dagger\hat{a}_{\text{L}}\sum_\mu \frac{1}{2\mu-3}\hat{\sigma}_{\mu,\mu}\,. \tag{D.75}$$

Hence, the slowly-varying dynamics at this order is described by a two-level system with the momenta $p = q$ and $p = -2q$, as apparent from the first two terms in Eq. (D.75).
According to Eq. (D.24) the rapidly varying part of the dynamics is given by

$$\hat{F}^{(2)}(\tau) = \frac{1}{2}\sum_{\nu\neq 0,k} \frac{\mathrm{e}^{i2\nu\tau}}{4k\nu}\left[\hat{\mathcal{H}}_k, \hat{\mathcal{H}}_{\nu-k}\right] \tag{D.76}$$

which yields

$$\hat{F}^{(2)} = \hat{a}_{\text{L}}^2\sum_{\mu\neq 0}\frac{\mathrm{e}^{-i4\mu\tau}}{4\mu(4\mu^2-1)}\hat{\sigma}_{\mu,\mu+2} - \hat{a}_{\text{L}}^{\dagger\,2}\sum_{\mu\neq 0}\frac{\mathrm{e}^{i4\mu\tau}}{4\mu(4\mu^2-1)}\hat{\sigma}_{\mu+2,\mu} \tag{D.77}$$

after inserting Eq. (D.71).
Having found explicit expressions for the effective Hamiltonian $\hat{H}_{\text{eff}}$ and for the rapidly varying contribution $\hat{F}(\tau)$ we are in the position to asymptotically solve the dynamics of the FEL for this resonance, that is $p = q$.

Initial conditions

We assume that the electron initially is described a momentum eigenstate with the resonant momentum $p = q$ while the laser field is given a Fock state with photon number n. This choice leads to the initial condition $c_\mu(0) = \delta_{\mu,0}$ in terms of the scattering basis, Eq. (5.4).
However, to solve the dynamics governed by the effective Hamiltonian $\hat{H}_{\text{eff}}$ we have to consider the initial condition for the transformed state vector $|\Phi\rangle$ rather than for $|\Psi\rangle$. In a procedure, analogous to the one described for the first resonance, $p = q/2$, we find the initial condition

$$d_\mu(0) = \left(1 - \frac{\alpha_n^2}{2} - \frac{\alpha_{n-1}^2}{18}\right)\delta_{\mu,0} - \alpha_n\delta_{\mu,1} + \frac{\alpha_{n-1}}{3}\delta_{\mu,-1} - \frac{1}{2}\alpha_n\alpha_{n+1}\delta_{\mu,2} - \frac{1}{120}\alpha_{n-1}\alpha_{n-2}\delta_{\mu,-2} \tag{D.78}$$

for the expansion coefficients d_μ of $|\Phi\rangle$ in the scattering basis, defined in Eq. (5.38).

Slowly varying terms

By projecting on the Schrödinger equation for $|\Phi\rangle$ with the effective Hamiltonian, Eq. (D.75), and introducing the vector notation $\boldsymbol{d} \equiv (d_{-1}, d_0, d_1, d_2)^{\text{T}}$ we find the system of coupled

differential equations

$$i\frac{\mathrm{d}}{\mathrm{d}\tau}\boldsymbol{d} = \begin{pmatrix} \frac{1}{5}\left(\alpha_n^2 - \frac{\alpha_{n-1}^2}{3}\right) & 0 & 0 & 0 \\ 0 & \alpha_n^2 - \frac{\alpha_{n-1}^2}{3} & 0 & \alpha_n\alpha_{n+1} \\ 0 & 0 & -3\left(\alpha_n^2 - \frac{\alpha_{n-1}^2}{3}\right) & 0 \\ 0 & \alpha_n\alpha_{n+1} & 0 & \alpha_n^2 - \frac{\alpha_{n-1}^2}{3} \end{pmatrix} \boldsymbol{d} \tag{D.79}$$

subject to the initial condition in Eq. (D.78). While the dynamics of the levels $\mu = -1$ and $\mu = 1$, corresponding to the momenta $p = 2q$ and $p = 0$, respectively, are decoupled, the two levels $\mu = 0$ and $\mu = 2$, that is $p = q$ and $p = -q$, respectively, are mixed.

We solve Eq. (D.79) with the ansatz $\mathrm{e}^{-i\lambda\tau}$. For the decoupled levels we straightforwardly find

$$\lambda_{-1} = \frac{1}{5}\left(\alpha_n^2 - \frac{\alpha_{n-1}^2}{3}\right) \equiv \frac{1}{5}\eta_n \tag{D.80}$$

and

$$\lambda_1 = -3\left(\alpha_n^2 - \frac{\alpha_{n-1}^2}{3}\right) \equiv -3\eta_n \tag{D.81}$$

for $\mu = -1$ and $\mu = 1$, respectively.

The eigenvalues of the coupling of $p = q$ and $p = -q$ are given by

$$\lambda_\pm = -\left(\alpha_n^2 - \frac{\alpha_{n-1}^2}{3}\right) \pm \alpha_n\alpha_{n+1} \equiv -\eta_n \pm \alpha_n\alpha_{n+1}\,, \tag{D.82}$$

where the second term can be identified with the Rabi frequency of this specific two-level system. In contrast to the first resonance $p = q/2$ where the Rabi frequency is linear in α, Eq. (D.49), the Rabi frequency in Eq. (D.82) scales now quadratically with α.

The solution of Eq. (D.79) then reads

$$\boldsymbol{d}(\tau) = \begin{pmatrix} \mathrm{e}^{-\frac{i\eta_n\tau}{5}} & 0 & 0 & 0 \\ 0 & \mathrm{e}^{-i\eta_n\tau}\cos\left(\alpha_n\alpha_{n+1}\tau\right) & 0 & -i\,\mathrm{e}^{-i\eta_n\tau}\sin\left(\alpha_n\alpha_{n+1}\tau\right) \\ 0 & 0 & \mathrm{e}^{i3\eta_n\tau} & 0 \\ 0 & -i\,\mathrm{e}^{-i\eta_n\tau}\sin\left(\alpha_n\alpha_{n+1}\tau\right) & 0 & \mathrm{e}^{-i\eta_n\tau}\cos\left(\alpha_n\alpha_{n+1}\tau\right) \end{pmatrix} \boldsymbol{d}(0) \tag{D.83}$$

for arbitrary initial conditions.

Inserting the initial condition Eq. (D.78) into Eq. (D.83) yields

$$d_\mu(\tau) = d_\mu^{(0)}(\tau) + \alpha d_\mu^{(1)}(\tau) + \alpha^2 d_\mu^{(2)}(\tau) \tag{D.84}$$

with the expressions in zeroth order

$$d_\mu^{(0)}(\tau) \equiv \mathrm{e}^{-i\eta_n\tau}\cos\left(\alpha_n\alpha_{n+1}\tau\right)\delta_{\mu,0} - i\,\mathrm{e}^{-i\eta_n\tau}\sin\left(\alpha_n\alpha_{n+1}\tau\right)\delta_{\mu,2}\,, \tag{D.85}$$

in first order

$$\alpha d_\mu^{(1)}(\tau) \equiv -\alpha_n\,\mathrm{e}^{i3\eta_n\tau}\,\delta_{\mu,1} + \frac{\alpha_{n-1}}{3}\,\mathrm{e}^{-\frac{i\eta_n\tau}{5}}\,\delta_{\mu,-1}\,, \tag{D.86}$$

and in second order of α

$$\begin{aligned}\alpha^2 d_\mu^{(2)}(\tau) \equiv & \,\mathrm{e}^{-i\eta_n\tau}\left[-\left(\frac{\alpha_n^2}{2}+\frac{\alpha_{n-1}^2}{18}\right)\cos\left(\alpha_n\alpha_{n+1}\tau\right)+\frac{i}{2}\alpha_n\alpha_{n+1}\sin\left(\alpha_n\alpha_{n+1}\tau\right)\right]\delta_{\mu,0}\\ & +\mathrm{e}^{-i\eta_n\tau}\left[i\left(\frac{\alpha_n^2}{2}+\frac{\alpha_{n-1}^2}{18}\right)\sin\left(\alpha_n\alpha_{n+1}\tau\right)-\frac{1}{2}\alpha_n\alpha_{n+1}\cos\left(\alpha_n\alpha_{n+1}\tau\right)\right]\delta_{\mu,2}\\ & -\frac{1}{120}\alpha_{n-1}\alpha_{n-2}\delta_{\mu,-2}\,,\end{aligned} \tag{D.87}$$

respectively. In analogy to our procedure for the first resonance, Eq. (D.57) , we have omitted in Eq. (D.84) the index of α indicating the respective photon number.

Rapidly varying terms

In order to obtain the full expressions for the probability amplitudes corresponding to the processes in the FEL we have to make the back transformation from $|\Phi\rangle$ with d_μ to $|\Psi\rangle$ with the coefficients c_μ, according to Eq. (D.3). This procedure yields rapid oscillations which arise from $\hat{F}(\tau)$.
In an analogous way as in the case of $p = q/2$ we find the amplitudes

$$c_0(\tau) = d_0^{(0)}(\tau) + \alpha^2\left(d_0^{(2)}(\tau) - d_1^{(1)}(\tau)\,\mathrm{e}^{i\tau} + \frac{1}{3}d_{-1}^{(1)}(\tau)\,\mathrm{e}^{-i3\tau} - \frac{1}{2}d_0^{(0)}(\tau) - \frac{1}{18}d_0^{(0)}(\tau) - \frac{1}{2}d_2^{(0)}(\tau)\right) \tag{D.88}$$

and

$$c_2(\tau) = d_2^{(0)}(\tau) + \alpha^2\left(d_2^{(2)}(\tau) - d_1^{(1)}(\tau)\,\mathrm{e}^{i\tau} - \frac{1}{2}d_0^{(0)}(\tau) - \frac{1}{18}d_2^{(0)}(\tau) - \frac{1}{2}d_2^{(0)}(\tau)\right) \tag{D.89}$$

for the two-level system of $p = q$ and $p = -q$, respectively. Moreover, we find the expressions

$$c_1(\tau) = \alpha\left[d_1^{(1)}(\tau) + \mathrm{e}^{-i\tau}\left(d_2^{(0)}(\tau) + d_0^{(0)}(\tau)\right)\right]\,, \tag{D.90}$$

as well as

$$c_{-1}(\tau) = \alpha\left[d_{-1}^{(1)}(\tau) + \frac{1}{3}d_0^{(0)}(\tau)\,\mathrm{e}^{3i\tau}\right] \tag{D.91}$$

and

$$c_3(\tau) = -\frac{\alpha}{3}d_2^{(0)}\,\mathrm{e}^{i3\tau} \tag{D.92}$$

corresponding to the momentum levels $p = 0$, $p = 2q$ and $p = 3q$, respectively, where we have used Eqs. (D.73), (D.77) and (D.84). In the derivation of these expressions for the probability amplitudes we have just kept terms in powers of α that are relevant when we calculate the transition probabilities up to second order in α by squaring the corresponding amplitude.

Probabilities

Taking the modulus square of the amplitudes Eqs. (D.88), (D.89), (D.90), (D.91) and (D.92), inserting the expressions, Eqs. (D.85), (D.86) (D.87) and neglecting all terms which are of higher than second order in α gives us the transition probabilities for the FEL at the second resonance $p = q$.

For the two-level system we find the probabilities

$$|c_0(\tau)|^2 = \cos^2(\alpha_n\alpha_{n+1}\tau) + 2\alpha_n^2\cos(\alpha_n\alpha_{n+1}\tau)\left\{\cos\left[\tau(1+4\eta_n)\right] - \cos(\alpha_n\alpha_{n+1}\tau)\right\} + \frac{2}{9}\alpha_{n-1}^2\cos(\alpha_n\alpha_{n+1}\tau)\left\{\cos\left[\tau\left(3-\frac{4}{5}\eta_n\right)\right] - \cos(\alpha_n\alpha_{n+1}\tau)\right\} \tag{D.93}$$

and

$$|c_2(\tau)|^2 = \sin^2(\alpha_n\alpha_{n+1}\tau) - \left(\alpha_n^2+\alpha_{n+1}^2\right)\sin^2(\alpha_n\alpha_{n+1}\tau) - \frac{1}{9}\left(\alpha_{n-1}^2+\alpha_{n+2}^2\right)\sin^2(\alpha_n\alpha_{n+1}\tau) - 2\alpha_n\alpha_{n+1}\sin(\alpha_n\alpha_{n+1}\tau)\sin\left[\tau(1+4\eta_n)\right] \tag{D.94}$$

for the electron to have the momentum $p = q$ and $p = -q$, respectively, corresponding to zero emitted or absorbed photons and the emission of two photons, respectively.
The non-resonant processes are described by the probabilities

$$|c_1(\tau)|^2 = \alpha_n^2\left[1+\cos^2(\alpha_n\alpha_{n+1}\tau) - 2\cos(\alpha_n\alpha_{n+1}\tau)\cos\left[\tau(1+4\eta_n)\right]\right] + \alpha_{n+1}^2\sin^2(\alpha_n\alpha_{n+1}\tau) + 2\alpha_n\alpha_{n+1}\sin(\alpha_n\alpha_{n+1}\tau)\sin\left[\tau(1+4\eta_n)\right], \tag{D.95}$$

as well as

$$|c_{-1}(\tau)|^2 = \frac{\alpha_{n-1}^2}{9}\left[1+\cos^2(\alpha_n\alpha_{n+1}\tau) - 2\cos(\alpha_n\alpha_{n+1}\tau)\right]\cos\left[\tau\left(3-\frac{4}{5}\eta_n\right)\right] \tag{D.96}$$

and

$$|c_3(\tau)|^2 = \frac{1}{9}\alpha_{n+2}^2\sin^2(\alpha_n\alpha_{n+1}\tau) \tag{D.97}$$

for the momentum of the electron to be $p = 0$, $p = 2q$ and $p = -2q$, respectively, corresponding to single-photon emission, single photon-absorption and two-photon emission, respectively.
Similar to the situation for the first resonance the probabilities for transitions 'outside' the two-level system are suppressed with α^2. We note that we did not calculate corrections higher-order corrections to the Rabi frequency $\alpha_n\alpha_{n+1}$ which would arise when we consider higher orders of the effective Hamiltonian $\hat{H}_{\text{eff}}$. However, these corrections would scale with higher powers of α and thus are small for $\alpha \ll 1$.

D.2.3 Many-electron model

In our treatment of the method of averaging for the many-electron model of the FEL we restrict ourselves to the first resonance $p = q/2$. According Chap. 7 the dynamics of the FEL for this situation is described by the Hamiltonian, Eq. (7.19),

$$\bar{H}(\tau) = \varepsilon\left(\hat{a}_{\text{L}}\sum_{\mu}\mathrm{e}^{i2\mu\tau}\,\hat{\Upsilon}_{\mu,\mu+1} + \hat{a}_{\text{L}}^{\dagger}\sum_{\mu}\mathrm{e}^{-i2\mu\tau}\,\hat{\Upsilon}_{\mu+1,\mu}\right) - \Delta\,\hat{n}_{\text{L}}\,, \tag{D.98}$$

where $\hat{\Upsilon}_{\mu,\mu+1}$ and $\hat{\Upsilon}_{\mu+1,\mu}$ now represent *collective* projection operators. Moreover, we assume that the deviation Δ from resonance $p = q/2$ is of the order of α_N, that is $\Delta \sim \alpha_N$. We note

that the sign in the phases of $\bar{H}$, Eq. (7.19), is reversed when compared to $\hat{H}_{\mathrm{I}}$, Eq. (5.15), from the approach employing the Schrödinger equation.
To apply the method of averaging we have to cast Eq. (D.98) into the form of Eq. (D.2). By this procedure we obtain the coefficients

$$\begin{cases} \hat{\mathcal{H}}_0 &= \hat{a}_{\mathrm{L}}\hat{\Upsilon}_{0,1} + \hat{a}_{\mathrm{L}}^\dagger\hat{\Upsilon}_{1,0} - \frac{\Delta}{\varepsilon}\,\hat{n} \\ \hat{\mathcal{H}}_\mu &= \hat{a}_{\mathrm{L}}\hat{\Upsilon}_{\mu,\mu+1} + \hat{a}_{\mathrm{L}}^\dagger\hat{\Upsilon}_{-\mu+1,-\mu} \end{cases} \tag{D.99}$$

which are analogue to the ones, Eq. (D.33), in the single-electron case, but with a reversed sign of the indices μ, that is $\mu \to -\mu$ for $\mu \neq 0$, emerging from the different signs in the phases of $\bar{H}$ and $\hat{H}_{\mathrm{I}}$. Despite the similar form of these coefficients, the different properties of the collective $\hat{\Upsilon}_{\mu,\nu}$ and the single-particle operators $\hat{\sigma}_{\mu,\nu}$ lead to a different dynamical behavior. Indeed, the commutation relation, Eq. (7.5),

$$\left[\hat{\Upsilon}_{\mu,\nu}, \hat{\Upsilon}_{\rho,\lambda}\right] = \delta_{\nu,\rho}\hat{\Upsilon}_{\mu,\lambda} - \delta_{\lambda,\mu}\hat{\Upsilon}_{\rho,\nu} \tag{D.100}$$

corresponds to Eq. (D.34) valid in the single-electron model, but the product, Eq. (7.6),

$$\hat{\Upsilon}_{\mu,\nu}\hat{\Upsilon}_{\rho,\lambda} \neq \delta_{\nu,\rho}\hat{\Upsilon}_{\mu,\lambda} \tag{D.101}$$

of two operators does not result in a closed expression, in contrast to Eq. (D.35), leading to different expressions for the method of averaging.

First order

With the help of Eqs. (D.19), (D.20), (D.30), and Eq. (D.99) we identify

$$\hat{H}_{\mathrm{eff}}^{(1)} = \hat{a}_{\mathrm{L}}\hat{\Upsilon}_{0,1} + \hat{a}_{\mathrm{L}}^\dagger\hat{\Upsilon}_{1,0} - \frac{\Delta}{\varepsilon}\,\hat{n} \tag{D.102}$$

and

$$\hat{F}^{(1)}(\tau) = -\hat{a}_{\mathrm{L}}\sum_{\mu\neq 0}\frac{\mathrm{e}^{i2\mu\tau}}{2\mu}\hat{\Upsilon}_{\mu,\mu+1} + \hat{a}_{\mathrm{L}}^\dagger\sum_{\mu\neq 0}\frac{\mathrm{e}^{-i2\mu\tau}}{2\mu}\hat{\Upsilon}_{\mu+1,\mu} \tag{D.103}$$

as the first-order contributions of the effective Hamiltonian and of the rapidly varying corrections, respectively. Since no products of operators occur in the first order of the method of averaging the resulting expressions, Eqs. (D.102) and (D.103), coincide for $\Delta = 0$ and for $\tau \to -\tau$ with the ones, Eqs. (D.36) and (D.39), in the single-particle case.

Second order

Application of Eqs. (D.23), (D.20), (D.31), and (D.99) yields the expressions

$$\begin{aligned} \hat{H}_{\mathrm{eff}}^{(2)} &= \frac{1}{2}\left(\hat{a}_{\mathrm{L}}^\dagger\hat{a}_{\mathrm{L}} + 1\right)\sum_{\mu\neq 0}\frac{1}{\mu}\left(\hat{\Upsilon}_{\mu+1,\mu+1} - \hat{\Upsilon}_{\mu,\mu}\right) - \sum_{\mu\neq 0}\frac{1}{\mu}\hat{\Upsilon}_{\mu+1,\mu}\hat{\Upsilon}_{\mu,\mu+1} \\ &= \frac{1}{2}\hat{a}_{\mathrm{L}}^\dagger\hat{a}_{\mathrm{L}}\sum_{\mu\neq 0}\frac{1}{\mu}\hat{\Upsilon}_{\mu+1,\mu+1} - \frac{1}{2}\left(\hat{a}_{\mathrm{L}}^\dagger\hat{a}_{\mathrm{L}} + 1\right)\sum_{\mu\neq 0}\frac{1}{\mu}\hat{\Upsilon}_{\mu,\mu} - \sum_{\mu\neq 0}\frac{1}{\mu}\left(\hat{\Upsilon}_{\mu+1,\mu}\hat{\Upsilon}_{\mu,\mu+1} - \hat{\Upsilon}_{\mu+1,\mu+1}\right) \end{aligned} \tag{D.104}$$

and

$$\begin{aligned}\hat{F}^{(2)}(\tau) =&\hat{a}_{\mathrm{L}}^{2}\left[\frac{1}{4}\left(\hat{\Upsilon}_{-1,1}\,\mathrm{e}^{-i2\tau}-\hat{\Upsilon}_{0,2}\,\mathrm{e}^{i2\tau}\right)+\frac{1}{2}\sum_{\mu\neq 0,-1}\frac{\mathrm{e}^{i2(2\mu+1)\tau}}{4\mu(\mu+1)(2\mu+1)}\hat{\Upsilon}_{\mu,\mu+2}\right]\\ &-\hat{a}_{\mathrm{L}}^{\dagger\,2}\left[\frac{1}{4}\left(\hat{\Upsilon}_{1,-1}\,\mathrm{e}^{i2\tau}-\hat{\Upsilon}_{2,0}\,\mathrm{e}^{-i2\tau}\right)+\frac{1}{2}\sum_{\mu\neq 0,-1}\frac{\mathrm{e}^{-i2(2\mu+1)\tau}}{4\mu(\mu+1)(2\mu+1)}\hat{\Upsilon}_{\mu+2,\mu}\right]\\ &+\sum_{\mu\neq 0}\frac{\mathrm{e}^{i2\mu\tau}}{4\mu^{2}}\hat{\Upsilon}_{\mu,\mu+1}\hat{\Upsilon}_{1,0}-\sum_{\mu\neq 0}\frac{\mathrm{e}^{-i2\mu\tau}}{4\mu^{2}}\hat{\Upsilon}_{\mu+1,\mu}\hat{\Upsilon}_{0,1}\\ &+\sum_{\substack{\mu,\rho\neq 0\\ \mu\neq\rho}}\frac{\mathrm{e}^{i2\rho\tau}}{4\mu\rho}\hat{\Upsilon}_{\mu,\mu+1}\hat{\Upsilon}_{\mu-\rho+1,\mu-\rho}-\sum_{\substack{\mu,\rho\neq 0\\ \mu\neq\rho}}\frac{\mathrm{e}^{-i2\rho\tau}}{4\mu\rho}\hat{\Upsilon}_{\mu+1,\mu}\hat{\Upsilon}_{\mu-\rho,\mu-\rho+1}\end{aligned}\tag{D.105}$$

for the effective Hamiltonian and the rapidly varying terms, respectively, in second order of the method of averaging.

Due to Eq. (D.101) the results, Eqs. (D.102) and (D.105) differ from the ones, Eqs. (D.38) and (D.39), in the single-electron description where we were allowed to apply Eq. (D.35) for products of projection operators. However, replacing the $\hat{\Upsilon}_{\mu,\nu}$ by $\hat{\sigma}_{\mu,\nu}$ and employing Eq. (D.35) in Eqs. (D.104) and (D.105) lead to the correct single-electron limit for $\Delta = 0$ and $\tau \to -\tau$.

Third order

In third order we derive from Eqs. (D.26), (D.32), and (D.99) the effective Hamiltonian

$$\begin{aligned}\hat{H}_{\mathrm{eff}}^{(3)} =&\frac{1}{4}\hat{a}_{\mathrm{L}}^{\dagger}\sum_{\substack{\mu\neq 0\\ \mu\neq -1}}\frac{1}{\mu(\mu+1)(2\mu+1)}\hat{\Upsilon}_{2\mu+1,2\mu+2}\hat{\Upsilon}_{\mu+2,\mu}\\ &+\frac{1}{4}\hat{a}_{\mathrm{L}}\sum_{\substack{\mu\neq 0\\ \mu\neq -1}}\frac{1}{\mu(\mu+1)(2\mu+1)}\hat{\Upsilon}_{2\mu+2,2\mu+1}\hat{\Upsilon}_{\mu,\mu+2}\\ &-\frac{1}{8}\hat{a}_{\mathrm{L}}^{\dagger}\sum_{\mu\neq 0}\frac{1}{\mu^{2}}\left(\hat{\Upsilon}_{\mu+1,\mu+1}-\hat{\Upsilon}_{\mu,\mu}\right)\hat{\Upsilon}_{1,0}-\frac{1}{8}\hat{a}_{\mathrm{L}}\sum_{\mu\neq 0}\frac{1}{\mu^{2}}\left(\hat{\Upsilon}_{\mu+1,\mu+1}-\hat{\Upsilon}_{\mu,\mu}\right)\hat{\Upsilon}_{0,1}\\ &+\frac{3}{8}\hat{a}_{\mathrm{L}}\left(\hat{\Upsilon}_{0,-1}\hat{\Upsilon}_{-1,1}-\hat{\Upsilon}_{0,2}\hat{\Upsilon}_{2,1}\right)+\frac{3}{8}\hat{a}_{\mathrm{L}}^{\dagger}\left(\hat{\Upsilon}_{1,-1}\hat{\Upsilon}_{-1,0}-\hat{\Upsilon}_{1,2}\hat{\Upsilon}_{2,0}\right)\\ &-\frac{1}{4}\hat{a}_{\mathrm{L}}^{\dagger}\left(\hat{a}_{\mathrm{L}}^{\dagger}\hat{a}_{\mathrm{L}}+\frac{3}{2}\right)\hat{\Upsilon}_{1,0}-\frac{1}{4}\left(\hat{a}_{\mathrm{L}}^{\dagger}\hat{a}_{\mathrm{L}}+\frac{1}{2}\right)\hat{a}_{\mathrm{L}}\hat{\Upsilon}_{0,1}+\frac{1}{4}\hat{a}_{\mathrm{L}}{}^{3}\hat{\Upsilon}_{-1,2}+\frac{1}{4}\hat{a}_{\mathrm{L}}^{\dagger\,3}\hat{\Upsilon}_{2,-1}\\ &+\frac{\Delta}{4\varepsilon}\left\{(\hat{n}_{\mathrm{L}}+1)\sum_{\mu\neq 0}\frac{1}{\mu^{2}}\left(\hat{\Upsilon}_{\mu+1,\mu+1}-\hat{\Upsilon}_{\mu,\mu}\right)-\sum_{\mu\neq 0}\frac{1}{\mu^{2}}\hat{\Upsilon}_{\mu+1,\mu}\hat{\Upsilon}_{\mu,\mu+1}\right\}\end{aligned}\tag{D.106}$$

which is very cumbersome when compared to the corresponding expression, Eq. (D.40) in the single-particle case. The replacement of the $\hat{\Upsilon}_{\mu,\nu}$ by $\hat{\sigma}_{\mu,\nu}$ and application of the product property Eq. (D.35), however, yields again the correct single-electron limit.

Linearization

Despite the lengthy expression, Eqs. (D.104) and (D.106) of the effective Hamiltonian in higher orders we can, indeed, find an analytic solution for the time evolution of the laser field, at least in the short-time limit. In analogy to the deep quantum regime in Chap. 7 we linearize the Heisenberg equations of motion by approximating $\hat{\Upsilon}_{0,0} \cong \langle \hat{\Upsilon}_{0,0}(0) \rangle = N$.

The equation of motion corresponding to the slowly varying part of the dynamics reads

$$i\frac{\mathrm{d}}{\mathrm{d}\tau}\hat{\mathcal{O}} = -\varepsilon\left[\hat{H}_{\mathrm{eff}}^{(1)}, \hat{\mathcal{O}}\right] - \varepsilon^2\left[\hat{H}_{\mathrm{eff}}^{(2)}, \hat{\mathcal{O}}\right] - \varepsilon^3\left[\hat{H}_{\mathrm{eff}}^{(3)}, \hat{\mathcal{O}}\right] + \ldots \tag{D.107}$$

where $\hat{\mathcal{O}}$ is an arbitrary operator. In first order we obtain with the help of Eq. (D.102) the expressions

$$\left[\hat{H}_{\mathrm{eff}}^{(1)}, \hat{\Upsilon}_{1,0}\right] = \hat{a}_{\mathrm{L}}\hat{\Upsilon}_z \cong N\hat{a}_{\mathrm{L}} \tag{D.108}$$

and

$$\left[\hat{H}_{\mathrm{eff}}^{(1)}, \hat{a}_{\mathrm{L}}\right] = -\hat{\Upsilon}_{1,0} + \frac{\Delta}{\varepsilon}\hat{a}_{\mathrm{L}} \tag{D.109}$$

for $\hat{\Upsilon}_{1,0}$ and $\hat{a}_{\mathrm{L}}$, respectively, leading to the linear set of equations, Eq. (7.31), of the deep quantum regime.

For second order we derive from Eq. (D.23) the relations

$$\left[\hat{H}_{\mathrm{eff}}^{(2)}, \hat{\Upsilon}_{1,0}\right] = -\frac{1}{2}\left(\hat{\Upsilon}_{-1,0}\hat{\Upsilon}_{1,-1} + \hat{\Upsilon}_{2,0}\hat{\Upsilon}_{1,2} - \hat{\Upsilon}_{1,0}\right) \cong \frac{1}{2}\hat{\Upsilon}_{1,0} \tag{D.110}$$

and

$$\left[\hat{H}_{\mathrm{eff}}^{(2)}, \hat{a}_{\mathrm{L}}\right] = -\frac{1}{2}\hat{a}_{\mathrm{L}}\sum_{\mu\neq 0}\frac{1}{\mu}\left(\hat{\Upsilon}_{\mu+1,\mu+1} - \hat{\Upsilon}_{\mu,\mu}\right) \cong \frac{1}{2}N\hat{a}_{\mathrm{L}}\,, \tag{D.111}$$

where we have set $\hat{\Upsilon}_{0,0} \cong N$. Moreover, we have treated $\hat{a}_{\mathrm{L}} \equiv \delta\hat{a}_{\mathrm{L}}$ and $\hat{\Upsilon}_{\mu,\nu} \equiv \delta\hat{\Upsilon}_{\mu,\nu}$, expect for $\mu = \nu = 0$, as small quantities. That is why we have neglected products like $\delta\hat{a}_{\mathrm{L}}\delta\hat{\Upsilon}_{\mu,\nu}$ and $\delta\hat{\Upsilon}_{\mu,\nu}\delta\hat{\Upsilon}_{\rho,\lambda}$ since they are of second order in our linearization scheme.

An analogous procedure yields with the help of Eq. (D.106) the third-order contributions

$$\begin{aligned}
\left[\hat{H}_{\mathrm{eff}}^{(3)}, \hat{\Upsilon}_{1,0}\right] =& -\frac{1}{8}\hat{a}_{\mathrm{L}}\left(\sum_{\mu\neq 0}\frac{1}{\mu^2}\hat{\Upsilon}_{\mu+1,\mu+1}\hat{\Upsilon}_z - \sum_{\mu\neq 0}\frac{1}{\mu^2}\hat{\Upsilon}_{\mu+1,\mu+1}\hat{\Upsilon}_z + 2\hat{\Upsilon}_z - 2\hat{\Upsilon}_{0,1}\hat{\Upsilon}_{1,0}\right) \\
&- \frac{3}{8}\hat{a}_{\mathrm{L}}\left(\hat{\Upsilon}_z + \hat{\Upsilon}_{1,-1}\hat{\Upsilon}_{-1,1} - \hat{\Upsilon}_{1,2}\hat{\Upsilon}_{2,1} + \hat{\Upsilon}_{0,-1}\hat{\Upsilon}_{-1,0} + \hat{\Upsilon}_{0,2}\hat{\Upsilon}_{2,0}\right) \\
&+ \frac{1}{4}\left(\hat{n}+2\right)\hat{a}_{\mathrm{L}}\hat{\Upsilon}_z + \frac{1}{4}\hat{a}_{\mathrm{L}}^{\dagger}\hat{\Upsilon}_{1,0}^2 + \frac{1}{24}\hat{a}_{\mathrm{L}}^{\dagger}\left(\hat{\Upsilon}_{-3,-2}\hat{\Upsilon}_{1,-2} + \hat{\Upsilon}_{3,4}\hat{\Upsilon}_{3,0}\right) \\
&- \frac{\Delta}{2\varepsilon}\left(\hat{n}+1\right)\hat{\Upsilon}_{1,0} + \frac{\Delta}{4\varepsilon}\left(\hat{\Upsilon}_{-1,0}\hat{\Upsilon}_{1,-1} - \hat{\Upsilon}_{2,0}\hat{\Upsilon}_{1,2} + \hat{\Upsilon}_{1,0}\right) \\
&\cong \frac{N}{8}\left(N+1\right)\hat{a}_{\mathrm{L}} - \frac{\Delta}{4\varepsilon}\hat{\Upsilon}_{1,0}
\end{aligned} \tag{D.112}$$

and

$$\begin{aligned}\left[\hat{H}_{\text{eff}}^{(3)},\hat{a}_{\text{L}}\right] =& -\frac{1}{4}\sum_{\substack{\mu\neq 0\\ \mu\neq -1}}\frac{1}{\mu(\mu+1)(2\mu+1)}\hat{\Upsilon}_{2\mu+1,2\mu+2}\hat{\Upsilon}_{\mu+2,\mu}\\ &-\frac{1}{8}\sum_{\mu\neq 0}\frac{1}{\mu^2}\left(\hat{\Upsilon}_{\mu,\mu}-\hat{\Upsilon}_{\mu+1,\mu+1}\right)\hat{\Upsilon}_{1,0}+\frac{1}{2}\hat{n}\hat{\Upsilon}_{1,0}+\frac{1}{4}\hat{a}_{\text{L}}^2\hat{\Upsilon}_{0,1}-\frac{3}{4}\hat{a}_{\text{L}}^{\dagger\,2}\hat{\Upsilon}_{2,-1}\\ &-\frac{\Delta}{4\varepsilon}\hat{a}_{\text{L}}\sum_{\mu\neq 0}\frac{1}{\mu^2}\left(\hat{\Upsilon}_{\mu+1,\mu+1}-\hat{\Upsilon}_{\mu,\mu}\right)\\ \cong&\frac{1}{8}\left(N+3\right)\hat{\Upsilon}_{1,0}-\frac{\Delta}{4\varepsilon}\hat{a}_{\text{L}}\end{aligned} \tag{D.113}$$

to the dynamics of $\hat{\Upsilon}_{1,0}$ and $\hat{a}_{\text{L}}$, respectively, in the short-time limit.
By rescaling the operators according to

$$\begin{cases}\tilde{\Upsilon}_{1,0} &= \frac{1}{\sqrt{N}}\hat{\Upsilon}_{1,0}\\ \tilde{a}_{\text{L}} &= \hat{a}_{\text{L}}\end{cases} \tag{D.114}$$

and inserting Eqs. (D.108) – (D.113) into the corresponding Heisenberg equation, Eq. (D.107), we finally arrive at the linearized equations of motion

$$i\frac{\mathrm{d}}{\mathrm{d}\tau}\begin{pmatrix}\tilde{\Upsilon}_{1,0}\\ \tilde{a}_{\text{L}}\end{pmatrix} = \begin{pmatrix}0 & -\alpha_N\left(1-\frac{\alpha_N^2}{8}\right)\\ +\alpha_N\left(1-\frac{\alpha_N^2}{8}\right) & -\alpha_N\left(\varkappa+\frac{\alpha_N}{2}-\frac{\varkappa\alpha_N^2}{4}\right)\end{pmatrix}\begin{pmatrix}\tilde{\Upsilon}_{1,0}\\ \tilde{a}_{\text{L}}\end{pmatrix} \tag{D.115}$$

for $\tilde{\Upsilon}_{1,0}$ and $\hat{a}_{\text{L}}$ in the quantum regime. Here, we have assumed that the deviation $\Delta\equiv\varkappa\alpha_N$ from resonance is of the order of α_N, that is $\varkappa\sim\mathcal{O}(1)$, and have made the approximation $N+3\cong N+1\cong N$ due to the high number N of electrons in the bunch. Moreover, we have neglected the term proportional to Δ in Eq. (D.112) since it would scale with α_N^3/N in Eq. (D.115) and thus is suppressed with $1/N$ in comparison to the other contributions of Eq. (D.115).
The ansatz $\sim \mathrm{e}^{-i\lambda\tau}$ yields the quadratic equation

$$\lambda^2+\alpha_N\left(\varkappa+\frac{\alpha_N}{2}-\frac{\varkappa\alpha_N^2}{4}\right)\lambda+\alpha^2\left(1-\frac{\alpha_N^2}{8}\right)^2=0 \tag{D.116}$$

which has the solutions

$$\begin{aligned}\lambda &\cong -\frac{\varkappa\alpha_N}{2}-\frac{\alpha_N^2}{4}+\frac{\kappa\alpha_N^3}{8}\pm i\alpha_N\sqrt{1-\frac{\varkappa^2}{4}-\frac{\varkappa\alpha_N}{4}-\frac{5\alpha_N^2}{4}+\frac{\varkappa^2\alpha_N^2}{8}}\\ &\cong -\frac{\varkappa\alpha_N}{2}-\frac{\alpha_N^2}{4}+\frac{\varkappa\alpha_N^3}{8}\pm i\alpha_N\sqrt{1-\frac{\varkappa^2}{4}}\left[1-\frac{\varkappa/2}{1-\frac{\varkappa^2}{4}}\frac{\alpha_N}{4}-\frac{5-3\varkappa^2+\varkappa^4/2}{\left(1-\frac{\varkappa^2}{4}\right)^2}\frac{\alpha_N^2}{32}\right],\end{aligned} \tag{D.117}$$

where we have expanded in the second step the square root up to second order in $\alpha_N\ll 1$. The imaginary part of the dimensionless frequency λ in Eq. (D.117) leads to exponential gain

in the Quantum FEL and includes the corrections to the deep quantum regime, Eq. (7.32), which scale with powers of α_N.

E Photon Number Representation

In this appendix we present the detailed calculations for the Quantum FEL oscillator, Chap. 6. In contrast to the Wigner representation for the classical FEL in Chap. 4 we here employ the photon number representation for the reduced density matrix of the laser field. First, we derive the equation of motion for the diagonal elements of this matrix leading to a recurrence relation for the steady-state photon statistics in the deep quantum regime. We solve this relation with the help of a Gaussian approximation [39]. After that, we incorporate higher-order corrections of the method of averaging with the help of an approach developed in Ref. [123] for situations without detailed balance. Finally, we consider the off-diagonal elements of the reduced density matrix which are crucial to calculate the intrinsic linewidth and we expand the occurring quantities in powers of $1/n \ll 1$.

E.1 Diagonal elements

We consider the elements

$$\rho_{n,m} \equiv \langle n|\mathrm{Tr}_{\mathrm{el}}\{\hat{\rho}\}|m\rangle \tag{E.1}$$

of the reduced density matrix $\hat{\rho}_{\mathrm{L}}$ for the laser field in photon number representation. For the reduced density operator we have to take the partial trace $\rho_{\mathrm{L}} \equiv \mathrm{Tr}_{\mathrm{el}}\{\hat{\rho}\}$ for the density operator of the total system $\hat{\rho}$ with respect to the electronic subsystem.

Similar to our considerations for the classical FEL in Chap. 4 and App. C we split the equation of motion

$$\dot{\rho}_{n,m} = \left(\frac{\partial \rho_{n,m}}{\partial t}\right)_{\mathrm{int}} + \left(\frac{\partial \rho_{n,m}}{\partial t}\right)_{\mathrm{loss}} \tag{E.2}$$

for the reduced density matrix into a contribution due to the interaction of electron and fields and one due to cavity losses.

The interaction term is approximated by a coarse-grained derivative [22]

$$\left(\frac{\partial \rho_{n,m}}{\partial t}\right)_{\mathrm{int}} \cong \frac{N}{\tau_{\mathrm{inj}}} \left[\rho_{n,m}(t+T) - \rho_{n,m}(t)\right] , \tag{E.3}$$

where τ_{inj} denotes the injection time of the electron bunches, each of them consisting of N electrons, and T being the interaction time of the electrons in the wiggler.

According to Eq. (6.1) the state vector of the combined system of electron and laser field prior to interaction can be described by the product

$$|\Psi(t)\rangle = \left(\int_0^q \mathrm{d}p\, \phi(p)\, |p\rangle\right) \otimes \sum_n c_n(t)\, |n\rangle \tag{E.4}$$

with c_n denoting the expansion coefficients for the laser field in the Fock basis and $\phi(p)$ describing the wave function of the electron in momentum representation which should be sharply peaked around $p = q/2$ in order to be in the quantum regime, Eq. (5.30). During the interaction of electron and fields the state evolves to $|\Psi(t+T)\rangle$ which is characterized by the expansion coefficients

$$\begin{aligned} c_n(p, t+T) &= \mathrm{e}^{-i\Delta\omega_\mathrm{r} T}\, \phi(p) \left(\cos\Omega_n T - i\frac{\Delta\omega_\mathrm{r}}{2\Omega_n} \sin\Omega_n T \right) c_n(t) \\ c_{n+1}(p-q; t+T) &= -\,i\,\mathrm{e}^{i\Delta\omega_\mathrm{r} T}\, \phi(p) \frac{gT\sqrt{n+1}}{\Omega_n} \sin\Omega_n T\, c_n(t) \end{aligned} \tag{E.5}$$

in the combined $|n, p\rangle$ basis, where p corresponds to the excited state, Eq. (5.28), and $p - q$ to the ground state, Eq. (5.28), of the two-level system in Chap. 5.

By making the identification $\hat{\rho} = |\Psi\rangle\langle\Psi|$ and using the initial state $|\Psi(t)\rangle$ in Eq. (E.4) we find the simple relation $\rho_{n,n} = |c_n(t)|^2$ for the diagonal elements, given by $n = m$ in Eq. (E.1), before interaction. After interaction, we obtain the expression

$$\rho_{n,n}(t+T) = \int \mathrm{d}p\, |c_n(p; t+T)|^2 + \int \mathrm{d}p\, |c_n(p-q; t+T)|^2 \tag{E.6}$$

which leads with the help of Eq. (E.5) and the coarse-grained derivative, Eq. (E.3), to

$$\left(\frac{\partial \rho_{n,n}(t)}{\partial t} \right)_\mathrm{int} = -(n+1)\frac{2G_n}{\tau_\mathrm{inj}} \rho_{n,n}(t) + n\frac{2G_{n-1}}{\tau_\mathrm{inj}} \rho_{n-1,n-1}(t)\,, \tag{E.7}$$

where we have defined

$$G_n \equiv \frac{1}{2}(gT)^2 N \int \mathrm{d}p\, \mathrm{sinc}^2 \Omega_n T\, |\phi(p)|^2 \tag{E.8}$$

as the gain of the Quantum FEL. The identification of G_n with the gain is verified in Chap. 6 by explicitly calculating the change of the mean photon number $\langle \hat{n} \rangle$ in time.

In App. C.4 we have introduced an equation of motion, Eq. (C.86), for the reduced density matrix $\hat{\rho}_\mathrm{L}$ due to the cavity losses. By projecting on the diagonal elements of Eq. (C.86), according to Eq. (E.1), we obtain

$$\left(\frac{\partial \rho_{n,n}(t)}{\partial t} \right)_\mathrm{loss} = -n\frac{\omega_\mathrm{L}}{Q} \rho_{n,n}(t) + (n+1)\frac{\omega_\mathrm{L}}{Q} \rho_{n+1,n+1}(t)\,. \tag{E.9}$$

Combining Eqs. (E.7) and (E.9) we finally arrive at the equation of motion

$$\begin{aligned} \dot{\rho}_{n,n}(t) = &-(n+1)\frac{2G_n}{\tau_\mathrm{inj}} \rho_{n,n}(t) + (n+1)\frac{\omega_L}{Q} \rho_{n+1,n+1} \\ &+ n\frac{2G_n}{\tau_\mathrm{inj}} \rho_{n-1,n-1}(t) - n\frac{\omega_\mathrm{L}}{Q} \rho_{n,n}(t) \end{aligned} \tag{E.10}$$

for the diagonal elements.

For steady state we require [22] $\dot{\rho}_{n,n} = 0$. Moreover, by employing detailed balance, which means that each line of Eq. (E.10) has to vanish separately, we obtain the recurrence relation

$$\rho_{n,n} = \Lambda_n \rho_{n-1,n-1} \,, \tag{E.11}$$

where the parameter

$$\Lambda_n \equiv \frac{2G_{n-1}}{\omega_\mathrm{L}\tau_\mathrm{inj}/Q} \tag{E.12}$$

constitutes the ratio of gain and losses.

E.2 Gaussian approximation

The recurrence relation, Eq. (E.11), is too complicated to find a closed analytic solution for the steady-state photon statistics $\rho_{n,n}$. However, if the distribution is peaked around a single dominant maximum we can approximate it by a Gaussian in analogy to the procedure in Ref. [39].

By iterating Eq. (E.11) we can write down its formal solution

$$\frac{\rho_{n,n}}{\rho_{0,0}} = \prod_{n'=1}^{n} \Lambda_{n'} = \exp\left(\sum_{n'=1}^{n} \ln \Lambda_{n'}\right). \tag{E.13}$$

When we assume that n is approximately continuous we obtain the expression

$$\frac{\rho_{n,n}}{\rho_{0,0}} \cong \mathrm{e}^{\mathcal{I}(n)} \tag{E.14}$$

with

$$\mathcal{I}(n) \equiv \int_1^n \mathrm{d}n' \, \ln \Lambda(n') \,, \tag{E.15}$$

where we have replaced the discrete summation in Eq. (E.13) by a continuous integration.

Simple considerations show that $\rho_{n,n}$ possesses an extreme value if $\Lambda_n = 1$. By differentiating $\rho_{n,n}$ with respect to n we observe that this derivative is always equal to zero if $\ln \Lambda_n = 0$ or $\Lambda_n = 1$. In the case, where the corresponding extreme value is a single dominating maximum of the photon statistics, we identify $n = n^\mathrm{ss}$ for which

$$\Lambda_{n^\mathrm{ss}} = 1. \tag{E.16}$$

as the mean photon number at steady state.

For a Gaussian we just require the second moment of the distribution and hence we expand $\mathcal{I}$, Eq. (E.15),

$$\mathcal{I}(n) \cong \int_1^{n^\mathrm{ss}} \mathrm{d}n' \, \ln \Lambda(n') + \ln \Lambda(n^\mathrm{ss}) \, (n - n^\mathrm{ss}) + \frac{1}{2} \frac{1}{\Lambda(n^\mathrm{ss})} \left.\frac{\mathrm{d}\Lambda(n)}{\mathrm{d}n}\right|_{n=n^\mathrm{ss}} (n - n^\mathrm{ss})^2 \tag{E.17}$$

up to to second order in powers of $(n - n^{\mathrm{ss}})$. Due to Eq. (E.16) the linear term is zero and we, thus, obtain the approximation

$$\mathcal{I}(n) \cong \mathcal{I}(n^{\mathrm{ss}}) + \frac{1}{2} \left.\frac{\mathrm{d}\Lambda(n)}{\mathrm{d}n}\right|_{n=n^{\mathrm{ss}}} (n - n^{\mathrm{ss}})^2 \tag{E.18}$$

for the integral $\mathcal{I}$.

With the help of Eqs. (E.14), (E.16) and (E.18) we finally obtain the Gaussian approximation

$$\rho_{n,n}^{\mathrm{ss}} \cong \mathcal{N} \exp\left[-\frac{(n - n^{\mathrm{ss}})^2}{2\Delta n^2}\right] \tag{E.19}$$

for the photon statistics, corresponding to the recurrence relation Eq. (E.11). The maximum of this distribution is at n^{ss}, Eq. (E.16), while the variance is given by

$$\Delta n^2 \equiv -\left(\left.\frac{\mathrm{d}\Lambda(n)}{\mathrm{d}n}\right|_{n=n^{\mathrm{ss}}}\right)^{-1}, \tag{E.20}$$

according to Eq. (E.18). We note that the normalization constant

$$\mathcal{N} \equiv \rho_{0,0}\, \mathrm{e}^{\mathcal{I}(n^{\mathrm{ss}})} \tag{E.21}$$

has to be calculated by integrating $\rho_{n,n}$ over n from one to infinity and setting the result equal to unity.

We again emphasize that the Gaussian approximation is only allowed when the photon statistics possesses a single dominant maximum. According to Ref. [39] this constraint is always satisfied if the condition

$$\frac{gT\sqrt{N}}{\sqrt{\omega_{\mathrm{L}}\tau_{\mathrm{inj}}/Q}} < \frac{3\pi}{2} \tag{E.22}$$

is fulfilled.

E.3 Photon statistics without detailed balance

When we leave the deep quantum regime and incorporate higher-order corrections due the method of averaging we additionally have to consider two-photon emission yielding the final momentum $p = -3q/2$ as well as single-photon absorption resulting in $p = 3q/2$ as discussed in Chap. 5. Instead of a three-term recurrence relation as in Eq. (E.10) we have to take four contributions into account. As a result we cannot solve the equation for the steady state with the help of detailed balance. However, in Ref. [123] an approach is sketched to observe an approximate steady-state photon statistics even without detailed balance.

For the sake of simplicity we misuse in the following notation and separate the coefficients

$$|c_{n+\mu}(p - \mu q; t + T)|^2 \to |c_{n+\mu}(p - \mu q; T)|^2 \rho_{n,n}(t) \tag{E.23}$$

in two parts, that is a contribution from interaction and the initial diagonal element $\rho_{n,n}(t)$ for the laser field which is given by $\rho_{n,n}(t) = |c_n(t)|^2$. Moreover, we restrict ourselves to exact resonance, $p = q/2$.

Similarly to the two-level case, Eq. (E.10), we obtain the equation of motion

$$\dot{\rho}_{n,n} = -\xi_0 \rho_{n,n} + \xi_{-1}\rho_{n-1,n-1} + \xi_1 \rho_{n+1,n+1} + \xi_{-2}\rho_{n-2,n-2} \tag{E.24}$$

for the diagonal elements including higher orders of the method of averaging. Here, we have defined

$$\xi_0 \equiv \frac{N}{\tau_{\text{inj}}}\left(1 - |c_n(p;T)|^2\right) - \frac{\omega_{\text{L}}}{Q}n\,, \tag{E.25}$$

$$\xi_{-1} \equiv \frac{N}{\tau_{\text{inj}}}|c_n(p-q;T)|^2\,, \tag{E.26}$$

$$\xi_1 \equiv \frac{\omega_{\text{L}}}{Q}(n+1) + |c_n(p+q;T)|^2\,, \tag{E.27}$$

and

$$\xi_{-2} \equiv |c_n(p-2q;T)|^2\,. \tag{E.28}$$

In addition to Eq. (E.10) for the deep quantum regime, a term proportional to $\rho_{n-2,n-2}$ appears in Eq. (E.24). For steady-state, $\dot{\rho}_{n,n} = 0$, Eq. (E.24) simplifies to

$$\xi_0 \rho_{n,n} = \xi_{-1}\rho_{n-1,n-1} + \xi_1 \rho_{n+1,n+1} + \xi_{-2}\rho_{n-2,n-2} \tag{E.29}$$

which is an algebraic equation.

Following Ref. [123] we rewrite Eq. (E.29) in terms of the ratio

$$R_n \equiv \frac{\rho_{n+1,n+1}}{\rho_{n,n}} \tag{E.30}$$

which yields

$$\xi_0 = \frac{\xi_{-1}}{R_{n-1}} + \xi_1 R_n + \frac{\xi_{-2}}{R_{n-1}R_{n-2}}\,. \tag{E.31}$$

According to Refs. [124, 123] R_n is a slowly varying function with respect to n and by approximating $R_n \cong R_{n-1} \cong R_{n-2} \equiv R$ we obtain the cubic equation

$$\xi_1 R^3 - \xi_0 R^2 + \xi_{-1} R + \xi_{-2} = 0 \tag{E.32}$$

which can be easily solved. Moreover, we set $n \cong n \pm 1 \cong n \pm 2$ in the expressions for the coefficients ξ_n, Eqs. (E.25), (E.26), (E.27), and (E.28), and arrive at

$$\xi_0 = \xi_1 + \xi_{-1} + \xi_{-2} \tag{E.33}$$

which corresponds to the conservation of probabilities.

By inspecting Eq. (E.32) we find with the help of Eq. (E.33) the solution $R = 1$ which, however, would lead to a distribution which cannot be normalized [123]. By polynomial long

division by $(R-1)$ we obtain the quadratic equation

$$\xi_1 R^2 - (\xi_{-1} + \xi_{-2})R - \xi_{-2} = 0\,, \tag{E.34}$$

where we have used Eq. (E.33). The roots of Eq. (E.34) are given by

$$R_\pm = -\frac{\xi_{-1}+\xi_{-2}}{2\xi_1} \pm \frac{\sqrt{(\xi_{-1}+\xi_{-2})^2 + 4\xi_1\xi_{-2}}}{2\xi_1}\,. \tag{E.35}$$

Since R_+ correctly reduces to Λ_n for $\alpha_n \to 0$ we discard R_- and use R_+ in the further course of our investigations. The definition of R_n in Eq. (E.30) gives us the prescription

$$\rho_{n+1,n+1} = R_+(n)\rho_{n,n} \tag{E.36}$$

to calculate the steady-state photon statistics including higher-order corrections. For example, this can be done by the numerical iteration of Eq. (E.36).

Alternatively, one can employ the Gaussian approximation introduced in the preceding section. There we have required for steady state, Eq. (E.16), that $\Lambda_n = 1$. Hence, we find the corresponding condition for the present approach when we set $R = 1$ in the quadratic equation Eq. (E.34). By this procedure we obtain

$$\xi_1 - \xi_{-1} - 2\xi_{-2} = 0 \tag{E.37}$$

which translates to

$$\frac{\omega_\mathrm{L}}{Q} n^\mathrm{ss} = \frac{N}{\tau_\mathrm{inj}} \sum_\mu |c_\mu(T)|^2 \tag{E.38}$$

when we use the definitions of the coefficients in Eqs. (E.25), (E.26), (E.27), and (E.28). By inserting the expression for the probabilities $|c_\mu|^2$, Eqs. (D.64), (D.65), (D.67) and (D.66) we finally arrive at

$$\frac{\omega}{Q} n^\mathrm{ss} = \delta n^{(0)}(n^\mathrm{ss}) + \alpha_n^2 \delta n^{(2)}(n^\mathrm{ss}) \tag{E.39}$$

with $\delta n^{(0)}$ and $\delta n^{(2)}$ introduced in Eqs. (6.29) and (6.30), respectively.

Moreover, we can find an expression for the variance Δn^2, in analogy to Eq. (E.20) for the two-level case, by differentiating Eq. (E.34) with respect to n. Thus, we obtain

$$\left(\frac{\mathrm{d}R}{\mathrm{d}n}\right)_{n=n^\mathrm{ss}} = -\left[(\xi_{-1}+3\xi_{-2})\big|_{n=n^\mathrm{ss}}\right]^{-1} \left[\frac{\mathrm{d}}{\mathrm{d}n}(\xi_1 - \xi_{-1} - 2\xi_{-2})\right]\Bigg|_{n=n^\mathrm{ss}} \tag{E.40}$$

and the inverse of this expression gives us the variance Δn^2 in accordance with Eq. (E.20).

E.4 Off-diagonal elements

In this section we derive in detail the intrinsic the linewidth D, Eq. (6.66), for an FEL in the deep quantum regime. Hence, we require knowledge about the off-diagonal elements $\rho_{n+1,n}$ of the reduced density matrix of the laser field.

Analogously to our procedure for the diagonal elements in Sec. E.1 we employ the expansion of the state $|\Psi(t+T)\rangle$ in the basis $|n,p\rangle$ and obtain with the coefficients in Eq. (E.5) the expression

$$\rho_{n+1,n}(t+T) = \int \mathrm{d}p\, c_{n+1}(p;t+T)c_n^*(p;t+T) + \int \mathrm{d}p\, c_{n+1}(p-q;t+T)c_n^*(p-q;t+T) \tag{E.41}$$

for the change of the off-diagonal elements during the interaction. Employing the coarse-grained derivative, Eq. (E.3), we arrive at the continuous change

$$\frac{\partial \rho_{n+1,n}(t)}{\partial t} = \frac{N}{\tau_{\mathrm{inj}}}\left[-\zeta_n \rho_{n+1,n}(t) + \chi_{n-1}\rho_{n,n-1}(t)\right] \tag{E.42}$$

with

$$\begin{cases} \mathrm{Re}\,(\zeta_n) & \equiv \int \mathrm{d}p\, |\phi(p)|^2 \left(1 - \cos\Omega_n T \cos\Omega_{n+1} T - \frac{\Delta^2}{4}\frac{(\omega_{\mathrm{r}}T)^2}{\Omega_n \Omega_{n+1}} \sin\Omega_n T \sin\Omega_{n+1} T\right) \\ \chi_{n-1} & \equiv \int \mathrm{d}p\, |\phi(p)|^2 \frac{g^2 T^2 \sqrt{n(n+1)}}{\Omega_{n-1}\Omega_n} \sin\Omega_{n-1} T \sin\Omega_n T\,. \end{cases} \tag{E.43}$$

Here, we have omitted the imaginary part of ζ_n since it is not of importance for the linewidth as it later turns out.

Projecting on the off-diagonal elements in Eq. (C.86) for the losses we find

$$\left(\frac{\partial \rho_{n+1,n}(t)}{\partial t}\right)_{\mathrm{loss}} = -\frac{\omega_{\mathrm{L}}}{Q}\left(n+\frac{1}{2}\right)\rho_{n+1,n}(t) + \frac{\omega_{\mathrm{L}}}{Q}\sqrt{(n+1)(n+2)}\,\rho_{n+2,n+1}(t) \tag{E.44}$$

and due to Eq. (E.2) we finally arrive at the equation of motion

$$\begin{aligned} \dot{\rho}_{n+1,n} =& \frac{N}{\tau_{\mathrm{inj}}}\left[-\zeta_n \rho_{n+1,n}(t) + \chi_{n-1}\rho_{n,n-1}(t)\right] \\ & - \frac{\omega_{\mathrm{L}}}{Q}\left(n+\frac{1}{2}\right)\rho_{n+1,n}(t) + \frac{\omega_{\mathrm{L}}}{Q}\sqrt{(n+1)(n+2)}\,\rho_{n+2,n+1}(t) \end{aligned} \tag{E.45}$$

for the off-diagonal elements.

According to Eq. (6.60) we have to sum over the $\dot{\rho}_{n+1,n}$ to calculate the linewidth. With the help of Eq. (E.45) we obtain the relation

$$\sum_n \dot{\rho}_{n+1,n} = \sum_n \mu_n \rho_{n+1,n} \tag{E.46}$$

where we have defined

$$\mu_n \equiv \frac{N}{\tau_{\mathrm{inj}}}\left[\zeta_n - \chi_n\right] + \frac{\omega}{Q}\left[\left(n+\frac{1}{2}\right) - \sqrt{n(n+1)}\right] \tag{E.47}$$

after appropriately shifting the summation indices. The real part of this parameter μ_n at steady state $n = n^{\mathrm{ss}}$ gives us then the intrinsic linewidth $D = 2\mathrm{Re}(\mu_n^{\mathrm{ss}})$ according to Eq. (6.65).

E.5 Expansion of square roots

In the following we present the details of the expansion in powers of $1/n$ which leads from Eq. (6.66) to the simplified expression in Eq. (6.67) for the intrinsic linewidth D of a Quantum FEL. For $n \gg 1$ we can expand [67] the square roots

$$\sqrt{n(n+1)} \cong n + \frac{1}{2} - \frac{1}{8n}\,, \tag{E.48}$$

and

$$\sqrt{(n+1)(n+2)} \cong n + \frac{3}{2} - \frac{1}{8n} \tag{E.49}$$

up to second order in $1/n$.
The approximation in Eq. (E.48) is important for the cavity losses and by inspection of Eq. (6.66) we observe that the terms with $n + 1/2$ cancel and only the contribution with $1/(8n)$ remains. With the help of the definition, Eq. (5.27), for the Rabi frequency Ω_n we obtain on the other hand that we require the second approximation, Eq. (E.49), for the contribution

$$g^2\sqrt{(n+1)(n+2)} + \frac{\Delta^2\omega_\mathrm{r}^2}{4} = \sqrt{\Omega_n^2\Omega_{n+1}^2 + g^2\frac{g\Delta^2\omega_\mathrm{r}^2}{2}\left[\sqrt{(n+1)(n+2)} - \left(n+\frac{3}{2}\right)\right]}\,. \tag{E.50}$$

Hence, we arrive at

$$g^2\sqrt{(n+1)(n+2)} + \frac{\Delta^2\omega_\mathrm{r}^2}{4} \cong \Omega_n\Omega_{n+1}\left[1 - \frac{\Delta^2}{4}\frac{g^2\omega_\mathrm{r}^2}{8(n+1)\Omega_n^2\Omega_{n+1}^2}\right]\,, \tag{E.51}$$

where the term in square brackets emerges from a further Taylor expansion due to $1/(\Omega_n^2\Omega_{n+1}^2) \ll 1$.
With the help of trigonometric relations [67] we, moreover, derive the relation

$$1 - \cos\Omega_n T\cos\Omega_{n+1}T - \sin\Omega_n T\sin\Omega_{n+1}T \cong 2\sin^2\left[\frac{g^2}{4\Omega_n}\right]\,, \tag{E.52}$$

where we have made the approximation

$$\Omega_{n+1} - \Omega_n \cong \frac{g^2}{2\Omega_n} \tag{E.53}$$

which can be straightforwardly derived for $1/n \ll 1$. The expression in Eq. (E.52) corresponds to the leading term of the intrinsic linewidth D in Eq. (6.67).

F Jacobian Elliptic Functions

In the investigation of the approximate long-time behavior of the high-gain Quantum FEL in Chap. 7 we have derived an elliptic integral, Eq. (7.60). This integral can be solved with the help of Jacobian ellitptic functions [137, 144]. Therefore, we devote this appendix to this kind of special functions. First, we summarize the definitions and properties of the elliptic functions before we apply these concepts on the solution of Eq. (7.60).

F.1 Properties

In the following we just briefly review Jacobian elliptic functions with emphasis on the properties required for solving Eq. (7.60). For a complete review on elliptic integrals and Jacobian functions we recommend Ref. [137]. An elliptic integral of the first kind is given by [137]

$$u = \int_0^{\varphi} \frac{\mathrm{d}\vartheta}{\sqrt{1 - k^2 \sin\vartheta}}\,, \tag{F.1}$$

where k is referred to as 'modulus' and satisfies $0 < k < 1$. It is convenient to introduce also the parameter

$$k' \equiv \sqrt{1 - k^2} \tag{F.2}$$

which we call complementary modulus.
Moreover, we can define the inverse functions of the elliptic integral, Eq. (F.1), as [137]

$$\begin{aligned} \mathrm{am}(u,k) &\equiv \varphi \\ \mathrm{sn}(u,k) &\equiv \sin\varphi \\ \mathrm{cn}(u,k) &\equiv \cos\varphi \\ \mathrm{dn}(u,k) &\equiv \sqrt{1 - k^2 \sin^2\varphi} \end{aligned} \tag{F.3}$$

which are the fundamental Jacobian elliptic functions. While am is sometimes called 'amplitude', sn, cn and dn are known as 'sine amplitude', 'cosine amplitude' and 'delta amplitude', respectively.
A special value for the argument u of the elliptic functions is given by the complete elliptic integral

$$K \equiv K(k) \equiv \int_0^{\pi/2} \frac{\mathrm{d}\vartheta}{\sqrt{1 - k^2 \sin\vartheta}} \tag{F.4}$$

and integer multiples of it. We note the asymptotics [137]

$$\lim_{k\to 1} K = \ln\frac{4}{k'} \tag{F.5}$$

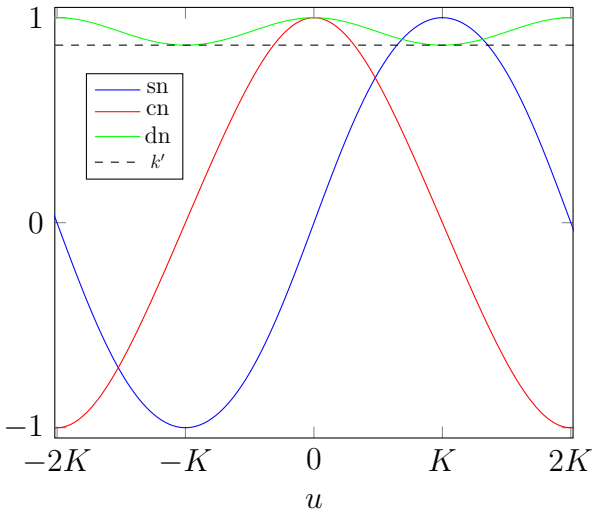

Figure F.1: Jacobian elliptic functions: We have drawn the sine amplitude sn (blue line), the cosine amplitude cn (red line) and the delta amplitude dn (red line) all as functions of the argument u in units of the complete elliptic integral K, Eq. (F.4). While sn and cn, both, are $4K$-periodic and vary between 0 and 1, dn shows $2K$-periodicity and just takes on values between k' (black, dashed line) and 1. Moreover, we observe that cn and dn, both, are even functions of u contrarily to sn which is point symmetric with respect to the origin.

for k approaching unity.

From Fig. F.1, where we have drawn the fundamental elliptic functions depending on the argument u, we obtain a similar behavior of sn and cn compared to the trigonometric functions sin and cos. Both Jacobian elliptic functions vary between 0 and 1, are $4K$-periodic and change their sign at odd integers of $2K$, that is for example $\mathrm{cn}(0,k) = 1$ while $\mathrm{cn}(2K,k) = -1$. Moreover, sn is an odd function while cn is an even one. We note that dn is an even, $2K$-periodic, function with values between k' and 1.

Another similarity to trigonometric functions arises by the identity [137]

$$\mathrm{sn}^2(u,k) + \mathrm{cn}^2(u,k) = 1 \tag{F.6}$$

which relates sn and cn in an analogous way as sine and cosine. Moreover, sn and dn are connected via

$$k^2\mathrm{sn}^2(u,k) + \mathrm{dn}^2(u,k) = 1\,. \tag{F.7}$$

We note that there are two more similar identities for these elliptic functions which we do not present here but can be found in Ref. [137].

Besides the four fundamental functions, Eq. (F.3), the various ratios of these quantities are also defined as Jacobian elliptic functions giving rise to the total number of twelve possible combinations. We only present here the ratio [137]

$$\mathrm{sd}(u,k) \equiv \frac{\mathrm{sn}(u,k)}{\mathrm{dn}(u,k)} \tag{F.8}$$

of sn and dn. It is connected via [137]

$$\mathrm{cn}(u+K,k) = -k'\mathrm{sd}(u,k) \tag{F.9}$$

to the cosine amplitude and the complementary modulus.
For our calculations we, moreover, need the relation [137]

$$\left[\frac{\mathrm{d}}{\mathrm{d}u}\mathrm{sn}(u,k)\right]^2 = \left(1-\mathrm{sn}^2(u,k)\right)\left(1-k^2\mathrm{sn}^2(u,k)\right) \tag{F.10}$$

for the derivative of the sine amplitude.

F.2 Solution of integral

In Chap. 7 we have derived the integral, Eq. (7.60),

$$2\alpha_N\tau = \int_0^{n/N} \frac{\mathrm{d}y}{\sqrt{(n_+/N-y)y(y+n_-/N)}} \tag{F.11}$$

for the dimensionless time τ as function of the photon number n. In the following we show how to express the photon number n in terms of a Jacobian elliptic function depending on τ. The roots of the denominator in Eq. (F.11) are given by, Eq. (7.58),

$$n_\pm \equiv \pm\frac{N}{2}\left(1-\frac{\varkappa^2}{4}\right) \mp \frac{1}{2} + \frac{N}{2}\left(1-\frac{\varkappa^2}{4}\right)\sqrt{1+\frac{1}{N}\frac{3+\varkappa^2/4}{1-\varkappa^2/4}+\frac{1}{4N^2}\frac{1}{1-\varkappa^2/4}}\,, \tag{F.12}$$

with $N \gg 1$ and $\kappa < 2$. Thus, we obtain that $n_+/N \geq n/N \geq 0 > -n_-/N$.
According to Ref. [137] we solve this integral by performing the substitution

$$\mathrm{sn}^2(u,k) = \frac{(n_+ + n_-)y}{n_+(y+n_-/N)} \equiv \frac{y}{k^2(y+n_-/N)}\,, \tag{F.13}$$

where we have defined in the second step the modulus

$$k^2 \equiv \frac{n_+}{n_+ + n_-}\,. \tag{F.14}$$

We note that

$$k'^2 \equiv \frac{n_-}{n_+ + n_-} \tag{F.15}$$

gives us the complementary modulus which is related by the simple connection

$$\frac{k^2}{k'^2} = \frac{n_+}{n_-} \tag{F.16}$$

to k.

With the help of this substitution, Eqs. (F.13) and (F.14), we obtain the relation

$$\frac{2\sqrt{N}\mathrm{d}u}{\sqrt{n_+ + n_-}} = \frac{\mathrm{d}y}{\sqrt{(n_+/N - y)y(y + n_-/N)}}\,, \tag{F.17}$$

where we have made use of the identity Eq. (F.10). The limits of the integration are given by

$$u(y = 0) = 0 \tag{F.18}$$

and

$$u(y = n/N) = \mathrm{sn}^{-1}\left[\sqrt{\frac{n}{k^2(n + n_-)}}, k\right] \tag{F.19}$$

which follow from $\mathrm{sn}(0, k) = 0$ and setting $y = n/N$ in Eq. (F.13), respectively.
Hence, we arrive at the equation

$$\frac{1}{1 + \frac{n_-}{n}} = k^2\mathrm{sn}^2\left[\alpha_N\tau\sqrt{\frac{n_+ + n_-}{N}}, k\right] \tag{F.20}$$

for the mean photon number n where we have solved for the argument of the inverse function in Eq. (F.19). With the help of Eqs. (F.7) and (F.8) we obtain the expression

$$n = n_+k'^2\mathrm{sd}^2\left[\alpha_N\tau\sqrt{\frac{n_+ + n_-}{N}}, k\right] \tag{F.21}$$

for the photon number. It is convenient to rewrite this result to

$$n = n_+\mathrm{cn}^2\left[\alpha_N\tau\sqrt{\frac{n_+ + n_-}{N}} - K, k\right]\,, \tag{F.22}$$

where we have employed Eqs. (F.16) and (F.9) and have made use of the periodicity and symmetry of cn.

G Iteration of Cubic Equation

In the following we present the detailed procedure to approximately solve the cubic equation, Eq. (7.86),

$$\left(\lambda^2 - 1\right)(\lambda + 1 + \varkappa\alpha_N) = 2\alpha_N^2 \tag{G.1}$$

of Ref. [3] in the limit $\alpha_N \ll 1$ with the help of the asymptotic method of iteration [145].

We note that for $\alpha_N = 0$ this equation has the roots $\lambda = -1$ and $\lambda = 1$ with the former one being degenerate. Since the root $\lambda = -1$ gives us a nonzero imaginary part in higher orders we first focus on this branch of the solution. In order to apply the iteration method it shows to be convenient to cast Eq. (G.1) into the symmetric form

$$\left(\lambda + 1 + \frac{\varkappa\alpha_N}{2}\right)^2 (\lambda - 1) - \frac{\varkappa^2\alpha_N^2}{4}(\lambda - 1) = 2\alpha_N^2 \tag{G.2}$$

which is still an exact relation.

We now proceed by taking the square root of Eq. (G.2) and solve the resulting expression for λ. Hence, we arrive at the recurrence relation

$$\lambda^{(n+1)} = -1 - \frac{\varkappa\alpha_N}{2} \pm \sqrt{\frac{2\alpha_N^2}{\lambda^{(n)} - 1} + \frac{\varkappa^2\alpha_N^2}{4}} \tag{G.3}$$

which connects the solution $\lambda^{(n+1)}$ of $(n+1)$th order in α_N with the nth order solution $\lambda^{(n)}$. Since the leading term of λ is given by $\lambda = -1$ we, moreover, recognize that the expression in the square root is negative and we write

$$\lambda^{(n+1)} = -1 - \frac{\varkappa\alpha_N}{2} \pm i\alpha_N\sqrt{\frac{2}{1 - \lambda^{(n)}} - \frac{\varkappa^2}{4}} \tag{G.4}$$

which means that λ possesses an imaginary part for higher orders in α_N.

We now iterate Eq. (G.4) by inserting the expression for $\lambda^{(n)}$ and keeping just terms of $(n+1)$th power of α_N to determine the result for $\lambda^{(n+1)}$. We start this procedure with the zeroth-order solution

$$\lambda^{(0)} = -1 \tag{G.5}$$

which leads with the help of Eq. (G.4) to

$$\lambda^{(1)} = -1 - \frac{\varkappa\alpha_N}{2} \pm i\alpha_N\sqrt{1 - \frac{\varkappa^2}{4}}\,, \tag{G.6}$$

where we just have considered terms linear in α_N.

Inserting this expression, Eq. (G.6), for $\lambda^{(1)}$ into the recurrence relation, Eq. (G.4), and performing a Taylor expansion up to α_N^2 leads to

$$\lambda^{(2)} = -\frac{\varkappa\alpha_N}{2} - \frac{\alpha_N^2}{4} \pm i\alpha_N\sqrt{1-\frac{\varkappa^2}{4}}\left[1 - \frac{\varkappa/2}{1-\frac{\varkappa^2}{4}}\frac{\alpha_N}{4}\right]. \tag{G.7}$$

By repeating this procedure for $\lambda^{(2)}$, Eq. (G.7), we finally arrive at

$$\lambda^{(3)} = -\frac{\varkappa\alpha_N}{2} - \frac{\alpha_N^2}{4} + \frac{\varkappa\alpha_N^3}{8} \pm i\alpha_N\sqrt{1-\frac{\varkappa^2}{4}}\left[1 - \frac{\kappa/2}{1-\frac{\varkappa^2}{4}}\frac{\alpha_N}{4} - \frac{5-3\varkappa^2+\varkappa^4/2}{\left(1-\frac{\varkappa^2}{4}\right)^2}\frac{\alpha_N^2}{32}\right] \tag{G.8}$$

where we have considered terms up to α_N^3.
For the sake of completeness we also discuss the third solution of Eq. (G.1) which corresponds in zeroth order to $\lambda = 1$. From Eq. (G.2) we obtain the recurrence relation

$$\lambda^{(n+1)} = 1 + \frac{2\alpha_N^2}{\left(\lambda^{(n)} + 1 + \varkappa\alpha_N/2\right)^2 - \varkappa^2\alpha_N^2/4}. \tag{G.9}$$

By inspection of this relation we recognize that the zeroth- and first-order solution coincide, that is

$$\lambda^{(0)} = \lambda^{(1)} = 1 \tag{G.10}$$

since there are no terms linear in α_N on the right-hand side of Eq. (G.9).
In second order, however, we obtain

$$\lambda^{(2)} = 1 + \frac{\alpha_N^2}{2} \tag{G.11}$$

and by substituting this expression into Eq. (G.9) and performing an expansion up to α_N^3 we finally arrive

$$\lambda^{(3)} = 1 + \frac{\alpha_N^2}{2} - \frac{\varkappa\alpha_N^3}{4} \tag{G.12}$$

for the third-order solution. We note that this solution of Eq. (G.1) is always real in contrast to the other two solutions, Eq. (G.8), which possess a nonzero imaginary part.

Bibliography

[1] M. Borenstein and W. E. Lamb. Classical laser. *Phys. Rev. A*, 5:1298 – 1311, 1972.

[2] C. B. Schroeder, C. Pellegrini, and P. Chen. Quantum effects in high-gain free-electron lasers. *Phys. Rev. E*, 64:056502, 2001.

[3] R. Bonifacio, N. Piovella, and G. R. M. Robb. The quantum free electron laser: A new source of coherent, short-wavelength radiation. *Fortschr. Phys.*, 57:1041 – 1051, 2009.

[4] P. Kling, E. Giese, R. Endrich, P. Preiss, R. Sauerbrey, and W. P. Schleich. What defines the quantum regime of the free-electron laser? *New J. Phys.*, 17:123019, 2015.

[5] J. M. J. Madey. Stimulated emission of bremsstrahlung in a periodic magnetic field. *J. Appl. Phys.*, 42:1906 – 1913, 1971.
J. M. J. Madey, H. A. Schwettman, and W. M. Fairbank. A free electron laser. *IEEE Transcr. Nucl. Sci.*, 20:980 – 983, 1973.

[6] J. M. J. Madey, M. O. Scully, and P. Sprangle. The free electron laser: conceptual history. *Phys. Scr.*, 91:083003, 2016.

[7] F. A. Hopf, P. Meystre, M. O. Scully, and W. H. Louisell. Classical theory of a free-electron laser. *Opt. Commun.*, 18:413 – 416, 1976.

[8] W. B. Colson. One-body electron dynamics in a free electron laser. *Phys. Lett. A*, 64: 190 – 192, 1977.

[9] A. Friedman, A. Gover, G. Kurizki, S. Ruschin, and A. Yariv. Spontaneous and stimulated emission from quasifree electrons. *Rev. Mod. Phys.*, 60:471 – 535, 1988.

[10] M. V. Fedorov. Free-electron lasers and multiphoton free-free transitions. *Prog. Quantum Electron.*, 7:73 – 116, 1981.

[11] W. Becker and J. K. McIver. Quantum descriptions of free-electron lasers. *Journal de Physique Colloques*, 44:289 – 311, 1983.

[12] W. Becker and M. S. Zubairy. Photon statistics of a free-electron laser. *Phys. Rev. A*, 25:2200 – 2207, 1982.

[13] J. Gea-Banacloche. Steady-state photon statistics of a free-electron laser. *Phys. Rev. A*, 33:1448 – 1450, 1986.

[14] W. Becker, J. Gea-Banacloche, and M. O. Scully. Intrinsic linewidth of a free-electron laser. *Phys. Rev. A*, 33:2174 – 2176, 1986.

[15] A. Gover, A. Amir, and L. R. Elias. Laser line broadening due to classical and quantum noise and the free-electron-laser linewidth. *Phys. Rev. A*, 35:164 – 172, 1987.

[16] M. Orszag. Free-electron-laser linewidth obtained from a master Fokker-Planck equation. *Phys. Rev. A*, 36:189 – 191, 1987.

[17] W. Becker and J. K. McIver. Madey's theorems for free-electron devices, spontaneous emission, and applications. *Z. Phys. D*, 7:353 – 372, 1988.

[18] E. M. Belenov, S. V. Grigor'ev, A. V. Nazarkin, and I. V. Smetanin. X-ray free-electron laser in quantum regime. *JETP*, 78:431 – 435, 1993.

[19] N. M. Kroll and W. A. McMullin. Stimulated emission from relativistic electrons passing through a spatially periodic transverse magnetic field. *Phys. Rev. A*, 17:300 – 308, 1978.

[20] P. Sprangle and R. A. Smith. Theory of free-electron lasers. *Phys. Rev. A*, 21:293 – 301, 1980.

[21] R. Bonifacio, C. Pellegrini, and L. M. Narducci. Collective instabilities and high-gain regime in a free electron laser. *Opt. Commun.*, 50:373 – 378, 1984.

[22] M. Sargent, M. O. Scully, and W. E. Lamb. *Laser Physics*. Addison-Wesley, Reading, Massachusetts, 1974.

[23] P. Emma, R. Akre, J. Arthur, R. Bionta, C. Bostedt, J. Bozek, A. Brachmann, P. Bucksbaum, R. Coffee, F.-J. Decker, et al. First lasing and operation of an ångstrom-wavelength free-electron laser. *Nature Photonics*, 4:641 – 647, 2010.

[24] C. Pellegrini. X-ray free-electron lasers: from dreams to reality. *Phys. Scr.*, 2016: 014004, 2017.

[25] R. Bonifacio, N. Piovella, G. R. M. Robb, and A. Schiavi. Quantum regime of free electron lasers starting from noise. *Phys. Rev. STAB*, 9:090701, 2006.

[26] P. Preiss. *Theory of the Quantum Free-Electron Laser*. PhD thesis, Universität Ulm, 2013.

[27] R. Endrich. *Spontaneous Emission in the Quantum Regime of the Free-Electron Laser*. PhD thesis, Universität Ulm, 2015.

[28] P. Kling, R. Sauerbrey, P. Preiss, E. Giese, R. Endrich, and W. P. Schleich. Quantum regime of a free-electron laser: relativistic approach. *Appl. Phys. B*, 123:9, 2017.

[29] P. Preiss, R. Sauerbrey, M. S. Zubairy, R. Endrich, E. Giese, P. Kling, M. Knobl, and W. P. Schleich. Theory of the Quantum FEL in a nuthsell. *Proceedings of the 34th International Free Electron Laser Conference, Nara, Japan*, pages 93 – 96, 2012.

[30] R. Endrich, E. Giese, P. Kling, R. Sauerbrey, and W. P. Schleich. Quantum FEL I: Multimode theory. *Proceedings of the 36th International Free Electron Laser Conference, Basel, Switzerland*, pages 353 – 357, 2014.

[31] P. Kling, R. Endrich, E. Giese, R. Sauerbrey, and W. P. Schleich. Quantum FEL II: Many-electron theory. *Proceedings of the 36th International Free Electron Laser Conference, Basel, Switzerland*, pages 348 – 352, 2014.

[32] E. T. Jaynes and F. W. Cummings. Comparison of quantum and semiclassical radiation theories with application to the beam maser. *Proc. IEEE*, 51:89 – 109, 1963.

[33] W. B. Case. Wigner functions and Weyl transforms for pedestrians. *Am. J. Phys.*, 76: 937 – 946, 2008.

[34] H. Risken. *The Fokker–Planck Equation – Methods of Solution and Applications*. Springer, Berlin, 1989.

[35] W. Becker and J. K. McIver. Many-particle quantum theory for a class of free-electron devices. *Phys. Rep.*, 154:205 – 245, 1987.

[36] N. N. Bogoliubov and Y. A. Mitropolsky. *Asymptotic Methods in the Theory of Non-Linear Oscillations*. Hindustan Publishing Corporation, Delhi, 1961.

[37] L. L. Buishvili, E. B. Volzhan, and M. G. Menabde. Higher approximations in the theory of the average Hamiltonian. *Theoretical and Mathematical Physics*, 46:166 – 173, 1981.

[38] D. Meschede, H. Walther, and G. Müller. One-atom maser. *Phys. Rev. Lett.*, 54:551 – 554, 1985.

[39] L. A. Lugiato, M. O. Scully, and H. Walther. Connection between microscopic and macroscopic maser theory. *Phys. Rev. A*, 36:740 – 743, 1987.

[40] W. P. Schleich. *Quantum Optics in Phase Space*. Wiley-VCH, Weinheim, 2001.

[41] J. D. Jackson. *Classical Electrodynamics*. Wiley, New York, 1999.

[42] W. Becker and J. K. McIver. Quantum theory of stimulated Čerenkov radiation. *Phys. Rev. A*, 25:956 – 963, 1982.

[43] W. Becker and J. K. McIver. Classical theory of stimulated Čerenkov radiation. *Phys. Rev. A*, 31:783 – 789, 1985.

[44] S. J. Smith and E. M. Purcell. Visible light from localized surface charges moving across a grating. *Phys. Rev.*, 92:1069, 1953.

[45] J. Schneider. Stimulated emission of radiation by relativistic electrons in a magnetic field. *Phys. Rev. Lett.*, 2:504 – 505, 1959.

[46] L. R. Elias, W. M. Fairbank, J. M. J. Madey, H. A. Schwettman, and T. I. Smith. Observation of stimulated emission of radiation by relativistic electrons in a spatially periodic transverse magnetic field. *Phys. Rev. Lett.*, 36:717 – 720, 1976.
D. A. G. Deacon, L. R. Elias, J. M. J. Madey, G. J. Ramian, H. A. Schwettman, and T. I. Smith. First operation of a free-electron laser. *Phys. Rev. Lett.*, 38:892 – 894, 1977.

[47] C. A. Brau. *Free-Electron Lasers*. Academic Press, San Diego, California, 1990.

[48] P. Schmüser, M. Dohlus, and J. Rossbach. *Ultraviolet and Soft X-Ray Free-Electron Lasers*. Springer, Heidelberg, 2008.

[49] `http://flash.desy.de`. Accessed: 20th June 2016.

[50] R. H. Pantell, G. Soncini, and H. E. Puthoff. Stimulated photon-electron scattering. *IEEE J. Quantum Electron.*, 4:905 – 907, 1968.
V. P. Sukhatme and P. A. Wolff. Stimulated Compton scattering as a radiation source – theoretical limitations. *J. Appl. Phys.*, 44:2331 – 2334, 1973.

[51] M. V. Fedorov. *Atomic and Free Electrons in a Strong Light Field*. World Scientific, Singapore, 1997.

[52] R. R. Schlicher, M. O. Scully, and H. Walther. Vorschlag für einen kompakten Freie-Elektronen Laser mit einem elektromagnetischen Undulator für den Infrarot- und weichen Röntgenbereich. Technical report, Max-Planck Institut für Quantenoptik, 1987.
J. Gea-Banacloche, G. T. Moore, R. R. Schlicher, M. O. Scully, and H. Walther. Soft X-ray free-electron laser with a laser undulator. *IEEE J. Quantum Electron.*, 23:1558 – 1570, 1987.
P. Sprangle, B. Hafizi, and J. R. Peñano. Laser-pumped coherent x-ray free-electron laser. *Phys. Rev. STAB*, 12:050702, 2009.
K. Steiniger, M. Bussmann, R. Pausch, T. Cowan, A. Irman, A. Jochmann, R. Sauerbrey, U. Schramm, and A. Debus. Optical free-electron lasers with traveling-wave Thomson-scattering. *J. Phys.*, 47:234011, 2014.

[53] A. Einstein. Zur Quantentheorie der Strahlung. *Phys. Z.*, 18:121 – 128, 1917.

[54] W. E. Lamb, W. P. Schleich, M. O. Scully, and C. H. Townes. Laser physics: Quantum controversy in action. *Rev. Mod. Phys.*, 71:263 – 273, 1999.
W. E. Lamb. Anti-photon. *Appl. Phys. B*, 60:77 – 84, 1995.

[55] W. E. Lamb. Theory of an optical maser. *Phys. Rev.*, 134:1429 – 1450, 1964.

[56] H. Haken. *Light, Volume 2: Laser Light Dynamics*. North-Holland Physics Publishing, Amsterdam, 1986.

[57] P. Meystre and M. Sargent. *Elements of Quantum Optics*. Springer, Berlin, 2007.

[58] L. Allen and J. H. Eberly. *Optical Resonance and Two-Level Atoms*. Dover Publications, Mineola, New York, 1987.

[59] A. H. Nayfeh. *Perturbation Methods*. Wiley, New York, 1973.

[60] C. M. Bender and S. A. Orszag. *Advanced Mathematical Methods for Scientists and Engineers*. McGraw-Hill, Singapore, 1978.

[61] A. Bambini and A. Renieri. The free electron laser: A single-particle classical model. *Lett. Nuovo Cimento*, 21:399 – 404, 1978.
A. Bambini, A. Renieri, and S. Stenholm. Classical theory of the free-electron laser in a moving frame. *Phys. Rev. A*, 19:2013 – 2025, 1979.

[62] R. Bonifacio, F. Casagrande, G. Cerchioni, L. de Salvo Souza, P. Pierini, and N. Piovella. Physics of the high-gain FEL and superradiance. *La Rivista del Nuovo Cimento*, 13:1 – 69, 1990.

[63] W. H. Louisell, J. F. Lam, D. A. Copeland, and W. B. Colson. "Exact" classical electron dynamic approach for a free-electron laser amplifier. *Phys. Rev. A*, 19:288 – 300, 1979.

[64] D. R. Nicholson. *Introduction to Plasma Theory*. Wiley, New York, 1983.

[65] P. Carruthers and F. Zachariasen. Quantum collision theory with phase-space distributions. *Rev. Mod. Phys.*, 55:245 – 260, 1983.

[66] M. V. Fedorov and J. K. McIver. Saturation in the classical theory of the free-electron laser. *Opt. Acta*, 26:1121 – 1124, 1979.

[67] I. P. Bronstein, H. Mühlig, G. Musiol, and K. A. Semendjajev. *Taschenbuch der Mathematik*. Harri Deutsch, 2006.

[68] A. M. Kondratenko and E. L. Saldin. Generation of coherent radiation by a relativistic electron beam in an ondulator. *Part. Acc.*, 10:207 – 216, 1980.

[69] Z. Huang and K.-J. Kim. Review of x-ray free-electron laser theory. *Phys. Rev. STAB*, 10:034801, 2007.

[70] C. Pellegrini, A. Marinelli, and S. Reiche. The physics of x-ray free-electron lasers. *Rev. Mod. Phys.*, 88:015006, 2016.

[71] C. W. Robertson and P. Sprangle. A review of free-electron lasers. *Phys. Fluids B*, 1:3 – 42, 1989.

[72] R. Bonifacio, F. Casagrande, and L. De Salvo Souza. Collective variable description of a free-electron laser. *Phys. Rev. A*, 33:2836 – 2839, 1986.

[73] G. Margaritondo and P. Rebernik Ribic. A simplified description of X-ray free-electron lasers. *J. Synchrotron Rad.*, 18:101 – 108, 2011.

[74] K.-J. Kim. Three-dimensional analysis of coherent amplification and self-amplified spontaneous emission in free-electron lasers. *Phys. Rev. Lett.*, 57:1871 – 1874, 1986.
K.-J. Kim. An analysis of self-amplified spontaneous emission. *Nucl. Instrum. & Methods A*, 250:396 – 403, 1986.

[75] R. Bonifacio, L. De Salvo, P. Pierini, N. Piovella, and C. Pellegrini. Spectrum, temporal structure, and fluctuations in a high-gain free-electron laser starting from noise. *Phys. Rev. Lett.*, 73:70 – 73, 1994.

[76] E. L. Saldin, E. A. Schneidmiller, and M. V. Yurkov. Statistical properties of the radiation from SASE FEL operating in the linear regime. *Nucl Instrum. & Methods A*, 407:291 – 295, 1998.

[77] R. Bonifacio, C. Maroli, and N. Piovella. Slippage and superradiance in the high-gain FEL: Linear theory. *Opt. Commun.*, 68:369 – 374, 1988.

[78] P. Sprangle, C.-M. Tang, and W. M. Manheimer. Nonlinear theory of free-electron lasers and efficiency enhancement. *Phys. Rev. A*, 21:302 – 318, 1980.

[79] W. H. Louisell, J. F. Lam, and D. A. Copeland. Effect of space charge on free-electron-laser gain. *Phys. Rev. A*, 18:655 – 658, 1978.

[80] J. B. Murphy, C. Pellegrini, and R. Bonifacio. Collective instability of a free electron laser including space charge and harmonics. *Opt. Commun.*, 53:197 – 202, 1985.
R. Bonifacio, F. Casagrande, and C. Pellegrini. Hamiltonian model of a free electron laser. *Opt. Commun.*, 61:55 – 60, 1987.

[81] M. V. Fedrov and J. K. McIver. Multiphoton stimulated Compton scattering. *Opt. Commun.*, 32:179 – 182, 1980.

[82] W. H. Lousiell. *Quantum Statistical Properties of Radiation*. John Wiley & Sons, Inc., New York, 1990.

[83] J. Gea-Banacloche. Quantum theory of the free-electron laser: Large gain, saturation, and photon statistics. *Phys. Rev. A*, 31:1607 – 1621, 1985.

[84] R. J. Glauber. Photon correlations. *Phys. Rev. Lett.*, 10:84 – 86, 1963.
E. C. G. Sudarshan. Equivalence of semiclassical and quantum mechanical descriptions of statistical light beams. *Phys. Rev. Lett.*, 10:277 – 279, 1963.

[85] K. Husimi. Some formal properties of the density matrix. *Proc. Phys. Math. Soc. Jap.*, 22:264 – 314, 1940.
Y. Kano. A new phase-space distribution function in the statistical theory of the electromagnetic field. *J. Math. Phys.*, 6:1913 – 1915, 1965.

[86] E. Wigner. On the quantum correction for thermodynamic equilibrium. *Phys. Rev.*, 40: 749 – 759, 1932.

[87] R. Bonifacio, M. M. Cola, N. Piovella, and G. R. M. Robb. A quantum model for collective recoil lasing. *EPL*, 69:55 – 60, 2005.

[88] N. Piovella, M. M. Cola, L. Volpe, A. Schiavi, and R. Bonifacio. Three-dimensional Wigner-function description of the quantum free-electron laser. *Phys. Rev. Lett.*, 100: 044801, 2008.

[89] G. Preparata. Quantum field theory of the free-electron laser. *Phys. Rev. A*, 38:233 – 237, 1988.

[90] R. Koekoek, P. A. Lesky, and R. F. Swarttouw. *Hypergeometric Orhtogonal Polynomials and Their q-Analogues*. Springer, Heidelberg, 2010.

[91] E. J. Heller. Wigner phase space method: Analysis for semiclassical applications. *J. Chem. Phys.*, 65:1289 – 1298, 1976.

[92] P. M. Anisimov. Quantum nature of electrons in classical X-ray FELs. *Proceedings of 37th International FEL Conference, Daejeon, Korea*, pages 338 – 341, 2015.

[93] A. Gover and Y. Pan. Stimulated radiation interaction of a single electron quantum wavepacket. *arXiv preprint arXiv:1702.06394*, 2017.

[94] H. Risken. Distribution- and correlation-functions for a laser amplitude. *Z. Phys.*, 186: 85 – 98, 1965.

[95] M. Lax and W. H. Louisell. Quantum noise IX: Quantum Fokker–Planck solution for laser noise. *IEEE Quantum Electron.*, 3:47 – 58, 1967.

[96] J. K. McIver and M. V. Fedorov. Quantum theory of stimulated processes in a free-electron laser in a strong field. *Sov. Phys. JETP*, 49:1012 – 1019, 1979.

[97] W. Becker and H. Mitter. Quantum theory of a free electron laser. *Z. Phys. B*, 35:399 – 404, 1979.

[98] W. Becker. Saturation behaviour of the free electron laser from barrier reflection. *Phys. Lett. A*, 74:66 – 68, 1979.
W. Becker. Quantum theory of a free electron laser for strong fields. *Z. Phys. B*, 38: 287 – 292, 1980.

[99] W. Becker. Multiphoton analysis of the free electron laser. *Opt. Commun.*, 33:69 – 74, 1980.

[100] W. Becker, M. O. Scully, and M. S. Zubairy. Generation of squeezed coherent states via a free-electron laser. *Phys. Rev. Lett.*, 48:475 – 477, 1982.

[101] W. Becker and J. K. McIver. Fully quantized many-particle theory of a free-electron laser. *Phys. Rev. A*, 27:1030 – 1043, 1983.

[102] I. Berson and J. Valdmanis. Electron in the field of two monochromatic electromagnetic waves. *J. Math. Phys.*, 14:1481 – 1484, 1973.

[103] H. Haken, H. Risken, and W. Weidlich. Quantum mechanical solutions of the laser masterequation III. Exact equation for a distribution function of macroscopic variables. *Z. Phys.*, 206:355 – 368, 1967.

[104] H. J. Carmichael. *Statistical Methods in Quantum Optics 1 – Master Equations and Fokker–Planck Equations*. Springer-Verlag, Berlin Heidelberg, 1998.

[105] M. O. Scully and W. E. Lamb. Quantum theory of an optical maser. I. General theory. *Phys. Rev.*, 159:208 – 226, 1967.

[106] R. Bonifacio. Quantum SASE FEL with laser wiggler. *Nucl. Instrum.& Methods A*, 546:634 – 638, 2005.

[107] R. Bonifacio, N. Piovella, G. R. M. Robb, and M. M. Cola. Propagation effects in the quantum description of collective recoil lasing. *Opt. Commun.*, 252:381 – 396, 2005.

[108] N. Piovella and R. Bonifacio. Inhomogeneous effects in the quantum free electron laser. *Nucl. Instrum. & Methods A*, 560:240 – 244, 2006.

[109] H. K. Avetissian and G. F. Mkrtchian. Nonlinear quantum regime of the x-ray Compton laser. *Phys. Rev. E*, 65:046505, 2002.
H. K. Avetissian and G. F. Mkrtchian. Quantum self-amplified spontaneous emission regime of the x-ray Compton laser. *Phys. Rev. STAB*, 10:030703, 2007.

[110] A. Serbeto, L. F. Monteiro, K. H. Tsui, and J. T. Mendonca. Quantum plasma fluid model for high-gain free-electron lasers. *Plasma Phys. Control. Fusion*, 51:124024, 2009.

[111] B. Eliasson and P. K. Shukla. Relativistic x-ray quantum free-electron lasers: a collective Klein–Gordon model. *Plasma Phys. Control. Fusion*, 54:124011, 2012.
B. Eliasson and P. K. Shukla. Relativistic x-ray free-electron lasers in the quantum regime. *Phys. Rev. E*, 85:065401, 2012.

[112] R. Bonifacio and H. Fares. A fully quantum theory of high-gain free-electron laser. *EPL*, 115:34004, 2016.

[113] F. Ciocci, G. Dattoli, A. Renieri, and A. Torre. About the mathematical aspects of the FEL and their relationship to quantum optics. *Phys. Rep.*, 141:1 – 50, 1986.

[114] R. H. Dicke. Coherence in spontaneous radiation processes. *Phys. Rev.*, 93:99 – 110, 1954.

[115] D. M. Giltner, R. W. McGowan, and S. A. Lee. Theoretical and experimental study of the Bragg scattering of atoms from a standing light wave. *Phys. Rev. A*, 52:3966 – 3972, 1995.

[116] S. S. Szigeti, J. E. Debs, J. J. Hope, N. P. Robins, and J. D. Close. Why momentum width matters for atom interferometry with Bragg pulses. *New J. Phys.*, 14:023009, 2012.

[117] E. Giese, A. Roura, G. Tackmann, E. M. Rasel, and W. P. Schleich. Double Bragg diffraction: A tool for atom optics. *Phys. Rev. A*, 88:053608, 2013.

[118] K.-J. Kim, Y. Shvyd'ko, and S. Reiche. A proposal for an X-ray free-electron laser oscillator with an energy-recovery linac. *Phys. Rev. Lett.*, 100:244802, 2008.
B. W. Adams and K.-J. Kim. X-ray comb generation from nuclear-resonance-stabilized x-ray free-electron laser oscillator for fundamental physics and precision metrology. *Phys. Rev. STAB*, 18:030711, 2015.

[119] P. Filipowicz, J. Javanainen, and P. Meystre. Theory of a microscopic maser. *Phys. Rev. A*, 34:3077 – 3087, 1986.

[120] M. O. Scully, H. Walther, G. S. Agarwal, T. Quang, and W. P. Schleich. Micromaser spectrum. *Phys. Rev. A*, 44:5992 – 5996, 1991.

[121] E. Giese, P. Kling, P. Preiss, R. Sauerbrey, and W. P. Schleich. A Quantum free-electron laser oscillator. *In preparation.*

[122] P. Kling, E. Giese, R. Endrich, P. Preiss, R. Sauerbrey, and W. P. Schleich. What distinguishes the quantum regime of the free-electron laser? *In preparation.*

[123] R. Görtz and D. F. Walls. Steady state solutions of master equations without detailed balance. *Z. Phys. B*, 25:423 – 427, 1976.

[124] R. Landauer. Fluctuations in bistable tunnel diode circuits. *J. Appl. Phys.*, 33:2209 – 2216, 1962.

[125] T. Quang, G. S. Agarwal, J. Bergou, M. O. Scully, H. Walther, K. Vogel, and W. P. Schleich. Calculation of the micromaser spectrum. I. Green's-function approach and approximate analytical techniques. *Phys. Rev. A*, 48:803 – 812, 1993.
K. Vogel, W. P. Schleich, M. O. Scully, and H. Walther. Calculation of the micromaser spectrum. II. Eigenvalue approach. *Phys. Rev. A*, 48:813 – 817, 1993.

[126] W. C. Schieve and R. R. McGowan. Phase distribution and linewidth in the micromaser. *Phys. Rev. A*, 48:2315 – 2323, 1993.

[127] M. O. Scully and W. E. Lamb. Quantum theory of an optical maser. II. Spectral profile. *Phys. Rev.*, 166:246 – 249, 1968.

[128] S. Kumar and C. L. Mehta. Theory of the interaction of a single-mode resonant radiation field with N two-level atoms. *Phys. Rev. A*, 21:1573 – 1586, 1980.

[129] R. Gaiba. *Quantum Aspects of the Free Electron Laser.* PhD thesis, Universität Hamburg, 2007.

[130] W. H. Louisell, A. Yariv, and A. E. Siegman. Quantum fluctuations and noise in parametric processes. I. *Phys. Rev.*, 124:1646 – 1654, 1961.

[131] B. R. Mollow and R. J. Glauber. Quantum theory of parametric amplification. I. *Phys. Rev.*, 160:1076 – 1096, 1967.
B. R. Mollow and R. J. Glauber. Quantum theory of parametric amplification. II. *Phys. Rev.*, 160:1097 – 1108, 1967.

[132] J. Schwinger. On Angular Momentum. Technical report, United States Atomic Energy Comission, 1952.

[133] M. Tavis and F. W. Cummings. Exact solution for an N-molecule-radiation field Hamiltonian. *Phys. Rev.*, 170:379 – 384, 1968.

[134] R. Bonifacio and G. Preparata. Quantum-mechanical description of coherent spontaneous emission. *Lett. Nuovo Cimento*, 1:887 – 893, 1969.
R. Bonifacio and G. Preparata. Coherent spontaneous emission. *Phys. Rev. A*, 2:336 – 347, 1970.

[135] R. Gambini. Parametric amplification with a trilinear Hamiltonian. *Phys. Rev. A*, 15: 1157 – 1168, 1977.

[136] S. Carusotto. Dynamics of processes with a trilinear boson Hamiltonian. *Phys. Rev. A*, 40:1848 – 1857, 1989.

[137] P. F. Byrd and M. D. Friedman. *Handbook of Elliptic Integrals for Engineers and Scientists*. Springer, Berlin, 1971.

[138] D. F. Walls and R. Barakat. Quantum-mechanical amplification and frequency conversion with a trilinear Hamiltonian. *Phys. Rev. A*, 1:446 – 453, 1970.

[139] C. Cohen-Tannoudji, B. Diu, and F. Laloë. *Quantum Mechanics, Volume One*. Wiley, Singapore, 1977.

[140] R. Bonifacio, N. Piovella, and G. R. M. Robb. Quantum theory of SASE FEL. *Nucl. Instrum.& Methods A*, 543:645 – 652, 2005.

[141] C. B. Schroeder. Photon statistics of the SASE FEL. *Nucl. Instrum. & Methods A*, 483:499 – 503, 2002.

[142] L. D. Landau and E. M. Lifschitz. *Lehrbuch der Theoretischen Physik, Band I, Mechanik*. Harri Deutsch, 1997.

[143] S. Varró. Intensity effects and absolute phase effects in nonlinear laser-matter interactions. In *Laser Pulse Phenomena and Applications*, chapter 12, pages 243 – 266. InTech, Rijeka, 2010.

[144] M. Abramowitz and I. A. Stegun. *Handbook of Mathematical Functions*. Dover Publications, Inc., New York, 1972.

[145] E. J. Jackson. *Perturbation Methods*. Cambridge Univeristy Press, Cambridge, 1991.

Danksagung

An erster Stelle möchte ich mich bei meinem Betreuer Prof. Wolfgang Schleich bedanken, der mir die Gelegenheit geboten hat, an diesem spannenden Thema zu forschen und die vorliegende Arbeit zu verfassen. Durch die gemeinsame Arbeit an Fachartikeln habe ich sehr viel von ihm gelernt und während Dienstreisen und der Teilnahme an Konferenzen, die er mir ermöglicht hat, konnte ich einen faszinierenden Einblick in die wissenschaftliche Welt erhalten.
Außerdem bedanke ich mich bei Prof. Peter Reineker für sein Interesse und die Bereitschaft, Zweitgutachter dieser Arbeit zu sein.
Weiterhin danke ich Prof. Roland Sauerbrey vom Helmholtz-Zentrum Dresden-Rossendorf, der die Finanzierung meiner Stelle ermöglicht hat und die treibende Kraft hinter der Kooperation zwischen dem Helmholtz-Zentrum Dresden-Rossendorf und der Universität Ulm darstellt.
Ganz besonders möchte ich mich bei meinem Kollegen Enno bedanken, der auch nach seiner Zeit in Ulm immer bereit war, um über Ideen und Entwürfe zu diskutieren und wichtige Ratschläge zu geben. Großer Dank gilt auch Paul, der mich erst für das Thema 'Quanten FEL' begeistert hat, und Rainer für die gemeinsame, ertragreiche Arbeit in unserer FEL-Arbeitsgruppe.
Im Allgemeinen will ich mich bei allen Kollegen im Institut für Quantenphysik bedanken. Sie waren dafür verantwortlich, dass die Arbeitsatmosphäre immer hervorragend war und ich jeden Tag gerne zur Arbeit gekommen bin. Im Besonderen bedanke ich mich bei Simon, Christian, Paul, Florian, Alexander und Fabio für die gemeinsame Zeit im Büro, in der es immer möglich war eine fachliche Diskussion zu führen oder wichtige Ratschläge zu bekommen.
Außerdem möchte ich mich bei Enno, Harry, Stephan, Christian, Alexander und Simon dafür bedanken, dass sie Teile der vorliegenden Arbeit Korrektur gelesen haben und somit einen wichtigen Beitrag zu deren Fertigstellung geleistet haben. Des Weiteren danke ich PD Maxim Efremov, von dem ich durch Diskussionen sowie durch den Besuch seiner Vorlesungen viel über die Anwendung asymptotischer Lösungsmethoden gelernt habe.
Weiterhin bedanke ich mich bei Dr. Petr Anisimov, Prof. William Case, Dr. Michael Bussmann, Dr. Alexander Debus, Prof. Ulrich Schramm, Klaus Steiniger und Prof. Sandor Varró für viele interessante und ertragreiche Diskussionen.
Großer Dank gilt auch Frau Wilma Fiebelkorn, Frau Petra Neumann und Frau Anne Varga für die Unterstützung in Verwaltungsfragen und bei der Organisation von Dienstreisen.
Zu guter Letzt möchte ich mich bei den Personen bedanken, die mir in meinem Privatleben Rückhalt gegeben haben. Zum einen sind hierbei meine Eltern zu nennen, die mich immer unterstützt haben und mir meine Studium ermöglicht haben. Zum anderen will ich mich bei meiner Freundin Vera bedanken, die mir durch ihr Verständnis und Vertrauen die Kraft gegeben hat, diese Arbeit zu vollenden.